# ABSTRACT


Title of Dissertation: CHARACTERIZATION OF DAMAGE IN MORTAR AND CONCRETE SPECIMENS DUE TO DELAYED ETTRINGITE FORMATION (DEF)

Jorgomai Ceesay, Doctor of Philosophy, 2007

Dissertation Directed By: Amde M. Amde, Professor
Department of Civil and Environmental Engineering



Delayed ettringite formation (DEF) in concrete and mortar systems has been associated with deleterious expansion leading to its premature deterioration. DEF causes a characteristic form of damage which is highly influenced by the cement chemistry, curing methods and exposure conditions. While the cement paste expands, the aggregate does not and cracks around these aggregates that usually form during curing, grow over time and eventually become filled with DEF at a later age. Therefore, considerable research work in preventing such deterioration is required to improve the durability of concrete structures.

In this research, mortar and concrete specimens were prepared with different potassium contents and different curing methods before subsequently subjecting them to different exposure conditions. Duggan Heat and Freeze-Thaw cycles were employed to initiate microcracks. Length and weight change measurements of the specimens were periodically monitored for the research duration. Also, the pH value,

Potassium ion [$K^+$], Sodium ion [$Na^+$] and Calcium ion [$Ca^{2+}$] concentrations of the storage solutions were monitored. A scanning electron microscope (SEM) equipped with high-energy dispersive analysis X-ray (EDAX) was used to identify mineral deposits present in the cavities, transition zones and cracks to determine the failure mechanism. Laser shearography, a nondestructive technique, was used to detect the onset of cracking and its subsequent propagation due to DEF.

The results showed that potassium content, curing methods and exposure conditions are the most important factors responsible for expansion associated with DEF. Increasing the potassium content leads to deleterious expansion associated with DEF and is accompanied by an increase in the weight of the specimen. Steam-cured concretes showed relatively larger expansions than the room temperature-cured concretes. The exposure condition of the mortar and concrete specimens is very critical to the re-formation of ettringite. Leaching of alkalis from the specimens into the storage solution increased the rate of expansion, and hence enhancing the formation of ettringite. Laser shearography image analysis showed that an increase in crack growth over time is essential for expansion due to DEF. Extensive microstructural investigations of the specimens revealed presence of DEF without any sign of Alkali-Silica Reaction (ASR).

# CHARACTERIZATION OF DAMAGE IN MORTAR AND CONCRETE SPECIMENS DUE TO DELAYED ETTRINGITE FORMATION (DEF)

By

Jorgomai Ceesay

Dissertation submitted to the Faculty of the Graduate School of the
University of Maryland, College Park, in partial fulfillment
of the requirements for the degree of
Doctor of Philosophy
2007

Advisory Committee:
Professor Amde M. Amde, Chair/Advisor
Professor Mohamad S. Aggour
Professor Donald W. Vannoy
Professor Chung C. Fu
Professor Sung W. Lee

# Dedication

This dissertation is dedicated to my late dad, Mr. Muhammadou O. J. Ceesay for his endless vision and belief in education.  May his soul rest in peace.

# Acknowledgements

I first thank my adviser, Professor Amde M. Amde, for his support, suggestions and guidance throughout the entire research.

Special thanks to Dr. Richard Livingston, Senior Physical Scientist at Turner-Fairbank Highway Research Center (FHWA) in McLean, Virginia for his knowledge and advice during the course of the research.

I am very grateful to Dr. Clay Ormsby, Research Chemist at FHWA, for his technical support and assistance in the SEM sample preparation and analysis.

Special thanks to Gary M. Mullings and Solomon Ben-Barka at National Ready Mixed Concrete Association Laboratory, College Park, Maryland for their assistance in sample preparations.

Thanks to LAFARGE – North America, Frederick, Maryland for their generous donation of the sand and coarse aggregate used in this research and Tom Horbaker, Field Technician, Quality Control, LAFARGE, for his help in providing technical information on the aggregates.

I also thank my fellow co-workers at Tuhin Basu and Associates, Inc. for their time and continuous support during the entire research.

Finally, I thank my wife, Mariama, Mum, family and friends for their encouragement, support and understanding.

Thank You.

# Table of Contents

# List of Tables

# List of Figures

# List of Abbreviations and Symbols

| | |
|---|---|
| Å | Angstrom $10^{-10}$ m |
| AH | Aluminum Hydroxide $Al(OH)_3$ |
| ASTM | American Society for Testing Materials |
| AFm | Monosulfate $C_3A.CaSO_4.12H_2O$ |
| Aft | Ettringite $C_3A.3CaSO_4.32H_2O$ |
| AAR | Alkali-Aggregate Reaction |
| ASR | Alkali-Silica Reaction |
| CH | Calcium Hydroxide $Ca(OH)_2$ |
| C-S-H | Calcium Silicate Hydrate |
| $C_3S$ | Tricalcium Silicate $3CaO.SiO_2$ Alite |
| $C_2S$ | Dicalcium Silicate $2CaO.SiO_2$ Belite |
| $C_3A$ | Tricalcium Aluminate $3CaO.Al_2O_3$ Aluminate |
| $C_4AF$ | Tetracalcium Aluminoferrite $4Ca.Al_2O_3.FeO_3$ Ferrite |
| DEF | Delayed Ettringite Formation |
| DSC | Differential Scanning Calorimetry |
| EDAX | Energy Dispersive Analysis X-ray |
| ESEM | Environmental Scanning Electron Microscopy |
| Exp. Cond. | Exposure Condition |
| Exp. Cond. 1 | Isothermal Water Bath, pH maintained at 12.5 (C1) |
| Exp. Cond. 2 | Plain Water at Room Temperature (C2) |
| Exp. Cond. 3 | Moist Air Chamber, R.H maintained at 97% (C3) |
| Exp. Cond. 4A | Field Conditions Steam-Cured (C4A) |

| | |
|---|---|
| Exp. Cond. 4B | Field Conditions Room Temperature-Cured (C4B) |
| FHWA | Federal Highway Administration |
| Fss | Ferrite Solid Solution |
| ISA | Internal Sulfate Attack |
| ISE | Ion Selective Electrode |
| $K_2O$ | Potassium Content |
| $KC_{23}S_{12}$ | Alkali Silicate |
| LAS | Laser Shearography |
| MDSHA | Maryland State Highway Administration |
| $NC_8A_3$ | Alkali Aluminate |
| mmol/l | Millimoles per Liter $10^{-3}$ moles/l |
| Phase One | Control Mortar Samples (P1) |
| Phase Two | Mortar Samples Made With 1.5% $K_2O$ (P2) |
| Phase Three | Control Concrete Samples (P3) |
| Phase Four | Concrete Samples Made With 1.5% $K_2O$ (P4) |
| pH | Acid Concentration Measurement |
| QXRD | Quantitative X-ray Diffraction |
| R.H | Relative Humidity |
| SEM | Scanning Electron Microscopy |
| TxDOT | Texas Department of Transportation |
| µm | Micrometer $10^{-6}$ m |
| UMD | University of Maryland at College Park |
| W/C | Water to cement ratio by weight |

| | |
|---|---|
| Wt. | Weight |
| X-ray CT | X-ray Computed Tomography |

# Chapter 1: Introduction

## *1.1 Background*

The premature deterioration of mortar and concrete in an infrastructure is very significant and is widely recognized in the world. Restoring, maintaining and replacement of these structures are very expensive, cause delays and hinder access. Therefore, there is an increasing demand to produce and specify more durable mortars and concretes, to be used in structures in aggressive environments, to satisfy the long-term economy and serviceability of the structures.

The deleterious reactions in mortar and concrete can be characterized as physical or chemical. Alkali silica reaction (ASR), sulfate attack, alkali-aggregate reaction (AAR), carbonation and delayed ettringite formation (DEF) include some of the chemical reactions in concrete, which lead to its premature deterioration. The occurrence of ASR and DEF are associated with expansion and cracks that may lead to deleterious effects. Based on comprehensive analysis of the literature, Day concluded that there appears to be a potential for delayed ettringite formation problems in North America, with the current cement production and concrete construction practices used especially in the Prestressed Industry (1992).

Extensive research studies have been carried out to study the influence on expansion and correlation with curing conditions, aggregate type and cement composition. According to Famy et al (2001), there is no direct correlation established between the amount of ettringite detected and expansion of the heat-cured mortars. Microcracking, late sulfate release and exposure to moisture have been

identified as essential characteristics for DEF. It seems that inhomogeneities in the microstructure of concrete are responsible for the microcracks which, when subjected to tensile stress from weathering and loading effects during the service, grow into macrocracks (Mehta, 2006). The late sulfate release (from cement or aggregate) would be available later to produce delayed deposition of ettringite in the pre-existing microcracks. Intermittent or continuous exposure to moisture causes swelling or crystal growth of ettringite leaching to crack openings and subsequent damage in the form of macrocracking. The Duggan Test Method is used to accelerate formation of microcracks in mortar and concrete specimens (Amde et al. 2005c, 2004a and 2003b).

Ettringite is a complex calcium sulfoaluminate hydrate, with the chemical formula $[Ca_6\ [Al\ (OH)_6\ ]_2.24H_2O].(SO_4)_3.2H_2O$ and is of practical importance in the technology of Portland cement. The curing temperature was shown to be the critical factor for expansion to occur in hardened concrete, cement paste and mortar (Skoblinskaya et al, 1975, Famy et al, 2001 and Petrov et al, 2006).

In this experimental study four different phases of mortar and concrete mixes are used to study the DEF and its associated deleterious expansions. Phase I mortar (control) has no additional potassium carbonate added to the mixing water to increase the potassium ($K_2O$) content, while Phase II mortar has a total of 1.5% $K_2O$ content by weight of cement. Phase III concrete (control) has no additional potassium carbonate, while Phase IV concrete with 1.5% $K_2O$ content by weight of cement added to batch mixes. Additional potassium carbonate was added to increase the alkali content of the mortar and concrete specimens. Adding potassium carbonate was preferable than using cement with varying and high potassium contents because

potassium in cement is present as potassium sulfate. Throughout the entire study the same batch of cement and aggregates was used and additional potassium carbonate was added in the mix water. The carbonate salt of potassium is used because it is the ultimate form in carbonated concrete. During the curing of concrete, the carbonate precipitates out in the form of calcium carbonate, as shown below:

$$K_2CO_3 + Ca^{2+} + 2OH^- \longrightarrow 2KOH + CaCO_3$$

The calcium and hydroxyl ions are products of the reaction of water and tricalcium silicate ($3CaO.SiO_2$), usually abbreviated as $C_3S$. Thus the end result is the formation of calcium carbonate ($CaCO_3$) and potassium hydroxide (KOH), which is the same as the normal form of potassium as potassium sulfate:

$$K_2SO_4 + Ca^{2+} + 2OH^- \longrightarrow 2KOH + CaSO_4$$

In most DEF studies, the heat-cured specimens are stored in water, following heating cycles to accelerate expansion and without monitoring the storage conditions. Research on the effect of curing conditions and cement composition relating to expansion has been extensive but very little work has been carried out on the influence of storage conditions after heat treatment. The monitoring of the storage conditions will also help in the understanding of DEF and predicting the amount of alkalis that are leached. Leaching is very substantial for mortars stored in water and less for those stored in 90–100% relative humidity (R.H) (Famy, 2001). In 2001, Famy et al. also estimated that more than 80% of the alkalis present in pore solution of the mortar specimens kept at 90$^o$C in humid air (90-100% R.H) were leached out. Based on a comprehensive literature review the following storage conditions were investigated in this research study:

Isothermal water bath, pH maintained at 12.5 (Saturated Limewater).

Plain water and monitored pH value.

Moist Air Chamber, R.H maintained at 97%.

Field conditions.

*1.2 Literature Review*

Heinz and Ludwig were the first to use the term "Delayed Ettringite Formation" (DEF) and they used the word "delayed" to suggest that the ettringite did not form at early hydration but some time later due to restriction. Also, the terms "secondary ettringite" and "delayed ettringite formation" are often interchangeable in most research publications. In 1992, Day emphasized that the term "Secondary Ettringite Formation (SEF)" is preferable because, he believes, primary ettringite forms as the sulphoaluminate settles shortly after and tends to disappear when sulfate ions in the pore solution become depleted. Day, in his literature analysis, further suggested that the term DEF is not accurate because "this term implies that conditions within the microstructure might be stable for the formation of ettringite but that ettringite does not form," which he believes is not true. Other researchers, like Fu and Beaudoin in (1996), suggested that both DEF and SEF occur in concretes and their respective occurrences were different. In this study, the term DEF is preferred over SEF because the term "secondary" may imply minor or less important.

The natural mineral ettringite was reported in 1847 to occur in limestone minerals in Lava at Ettringen and Mayen in the Rheinland (Dana, 1932). Ettringite was considered to be a mineral consisting of minute colorless hexagonal crystals.

Candlot's work published in 1890, first observed the compound now widely accepted as having a formula of $C_3A.3CaSO_4.32H_2O$. It also occurs naturally as a mineral ettringite that consists of a number of minerals having similar structures. In normal modern cement, ettringite forms due to the reaction between gypsum and tricalcium aluminate ($C_3A$). In Portland cement, the source of most of the sulfate is gypsum or other forms of calcium sulfate added to the clinker. The main purpose for this addition is to retard the quick setting of the Portland cement clinker that is due to the very high reactivity of $C_3A$. Calcium sulfate can occur as gypsum ($CaSO_4.2H_2O$), hemihydrate ($CaSO_4.1/2H_2O$) and anhydrate ($CaSO_4$). The gypsum dissolves relatively quickly in the water releasing a large amount of heat and decomposes to form hemihydrate. The addition of gypsum slows down the rapid reaction of $C_3A$ with water through the formation of ettringite coatings around the $C_3A$ (containing grains) (Scrivener and Pratt, 1984). The results obtained from most scanning electron microscopes (SEM) show that ettringite is normally a slender needle-like crystal with a prismatic hexagonal cross section (Schwiete, Ludwig and Jager 1966, Midgley and Pettifer 1971, Mehta 1973, Scrivener 1984, Famy, Scrivener et al 2001).

The action of alkalis, sodium and potassium, are believed to affect the solubilities of the reactants (e.g., tricalcium aluminate ($C_3A$), calcium hydroxide (CH), and gypsum) in the system and hence the concentration of the ions (e.g., hydroxide ion ($OH^-$), sulfate ion ($SO_4^{2-}$), calcium ion ($Ca^{2+}$), etc.). These alkalis in the Portland cement clinker are mainly from the clay components of the raw materials and from coal. The total amount, expressed as $Na_2O$ equivalent ($Na_2O + 0.64K_2O$), may range from 0.3 to 1.5 percent of the Portland cement clinker. Thus, alkali

compounds in the clinker can be divided into three groups (Diamond, 1976): (1) Alkali sulfates, $Na_2SO_4.2K_2SO_4$, $2CaSO4.K_2SO_4$, and $K_2SO_4$; (2) Alkali silicate, $KC_{23}S_{12}$; (3) Alkali aluminate $NC_8A_3$, and their respective solid solutions. Alkalis apparently can increase the solubility of ettringite and decrease the solubility of the CH (Wang et al, 1986 and Daerr, 1977). Basically, the presence of alkali suppresses the dissolution of CH but enhances the formation of ettringite. In 1989, Duggan and Scott proposed a method, referred to as the Duggan test to predict concrete's potential for ASR formation. They subsequently concluded that expansion of specimens subjected to the Duggan test is primarily a function of the amount and form of the sulfate in cement material rather than alkali-aggregate reaction (AAR).

In the production of precast concrete products, excessive heat curing at elevated temperatures above $70^oC$ is used to promote the development of strength at early ages and to allow for rapid production. Studies by Ronne and Sellevold, 1994 and Taylor, 1994, showed a lower strength development for concrete cured at high temperature than for concrete cured at normal room temperature. During recent years various studies have shown that Portland cement-based materials exposed to temperatures higher than approximately $70^oC$ will stop forming ettringite (AFt) and the already existing ettringite will decompose to hydrated calcium monosulphoaluminate (AFm), releasing sulfates to the pore solution (Ronne and Sellevold, 1994, and Taylor, 1994). At this high temperature, the sulfates released by the cement do not react completely with the tricalcium aluminate ($C_3A$), and therefore become available to the pore solution (Yang et al., 1996). Various researchers postulated that these available sulfates are trapped by physical adsorption on the

surfaces of the calcium silicate hydrate (C-S-H gel), whose hydration has been accelerated as a result of heat curing (Divet et al., 1998).

Various laboratory researches on the effect of heat-curing have been reported in the literature and it is now generally agreed that, when cured above a certain temperature, the paste, mortar, or concrete may develop DEF later when exposed to moisture conditions. Most studies outlined that the calcium sulphoaluminates hydrates (AFm) in paste, mortar or concrete are very unstable thermally. In 1941, Kalousek reported that monosulphate is a metastable phase in hardened cement. Later, Heinz and Ludwig (1989) and Klemmm and Adams (1990) confirmed that the monosulphate would form at steam-curing temperatures above 70$^{o}$C and then transform to ettringite at later stages. In 1988, Stadelman showed that ettringite diminishes at temperatures above 60$^{o}$C. Later, in 1999, Ronne and Hammer also concluded an apparent decrease of ettringite content in cement pastes interface zone cracks with an increase in temperatures from 20$^{o}$C to 85$^{o}$C using energy dispersive analysis X-ray (EDAX).

Some controversies concerning a critical curing temperature resulted in employing standards and guidelines. The Norwegian Standard specifies to keep the heat of hydration generated to below a maximum temperature of 65$^{o}$C (Ronne and Hammer, 1999) and the German Standard limits the maximum temperature of concrete during curing to 60$^{o}$C for externally exposed concrete (Scrivener, Damidot and Famy, 1999). When hydration-generated temperatures become a problem, the critical temperature will occur in the inner part of the concrete structure. The moisture content of lightweight aggregate prevents internal drying and may thus keep

the moisture above the critical level (Ronne and Hammer, 1999). Consequently, if the moisture content is sufficiently high it will enhance DEF. Again, Ronne and Hammer concluded that the initial curing of concrete at high temperatures might cause volume expansion due to DEF in both normal density and lightweight concrete. Another research by Petrov et al. also postulated that concretes made with a relatively moderate cement can develop a temperature as high as 72$^{o}$C at the center of massive elements, and that in such a case, it can be vulnerable to DEF and subsequent expansion (2006).

First documented in the early 1980's, laboratory research concluded that one of the factors responsible for DEF was the application of heat and excessive temperatures on the concrete during curing (Ghorah et al., 1980 and Sylla, 1988). Research studies on precast structures made of high strength concretes have been shown to be partly damaged due to loss of strength. Heinz and Taylor (1987) performed studies on the influence of ettringite in heat-cured mortar and concrete using PZ 55 ($C_3A$ at about 12% by wt. and $SO_3$ at 3.8% by wt.). They found that the damages are characterized by crack formation emerging from the edges as well as loss of bond between the cement paste and coarse aggregate. Heat treatments were carried out between the range of 20 and 100$^{o}$C and then the specimens were stored in water at 20$^{o}$C. Periodical measurements were taken to determine the length change and weight, as well as resonance frequency. Heinz's and Taylor's results show that temperatures above or equal to 75$^{o}$C lead to expansion linked with decreases of strength shown by the diminution of resonance frequencies and partly an over proportional increase in weight (1987). It follows that increasing temperatures lead to

increases of damage variables in the precast units. Their x-ray analysis of the heat-treated mortar specimens showed that increasing the temperature results in a decreasing amount of ettringite, seen in the basal spacing of 9.7 Å. Their results revealed that the monosulphate phase (AFm) immediately after 70$^{o}$C heat treatment increases only in the presence of the sulphoaluminate. The aluminate and sulphate ions get bound within the C-S-H gel, and later become available to form the AFt phase. They stored their specimens for almost 3 years and found that samples heat-cured at 80 – 100$^{o}$C contained nothing but ettringite while samples heat-cured at 20$^{o}$C had the AFt and AFm phases present as at the beginning of hydration. Heinz and Taylor also studied the influence of relative humidity (R.H) and found that the damage reaction became intensified with pre-storage at 60% R.H while being at relative humidity below or equal to 95% caused no expansion (1987).

Calcium silicate hydrate, or C-S-H, in cementitious materials is a phase related to natural calcium silicate hydrates such as tobermorite and jennite. In 1951, Kalousek and Adams believed that the depletion of ettringite at high temperatures can be attributed to the substitution of sulfate ions in the structure of the C-S-H gel, resulting in the loss of sulfate for the stability of ettringite and later confirmed by Odler (1980 and Odler et al., 1987). Kalousek also shows that the amount of missing $SO_3$ clearly increased with the rise of temperature from 24 to 82$^{o}$C (1951). He suggested that the missing $SO_3$ might be the source of ettringite and suspected it to be associated with the C-S-H gel structure. Furthermore, microanalysis studies by Scrivener and Taylor, 1993; Lewis, 1996; Lewis et al., 1994; and Lewis and

Scrivener, 1997 indicate that the rapid growth of C-S-H leads to the entrapment of sulfate and aluminate species in the gel structure.

In his studies, Lawrence uses about 55 different types of Portland cement to postulate the complex relationship between expansion and curing temperatures (1995). He cured the mortar bars at various initially elevated temperatures and subsequently stored them under water at 20$^{o}$C. Subsequent storage of specimens in water at 20$^{o}$C under 100% relative humidity was done to minimize the leaching of alkalis from the specimens. Siliceous sands, composed largely of quartz, were employed in preparing the specimens. Lawrence revealed that at curing temperatures of 60$^{o}$C or 65$^{o}$C none of the mortar bars exhibited significant expansion while at 75$^{o}$C only one of the 55 mortars shows expansion. He found that the critical temperature for expansion for his 55 different cements was between 65$^{o}$C and 70$^{o}$C. He concluded that expansion measurements on mortar bars after elevated temperature-curing show a complex pattern influenced by the composition of the cement and the detailed curing conditions imposed. Furthermore, Lawrence also reported that temperature curing leads to much reduced expansions, mirroring the chemical changes involving the possibility of ettringite formation after heat-curing. Ronne and Sellvold (1994) and Taylor (1994) demonstrated that ettringite would form later if sufficient amounts of moisture or humidity were available.

The implication of heat-curing in railroad tie degradation in other countries such as Finland (Eriksson and Tepponen, 1985, Eriksson and Tepponn, 1987), South Africa (Obercholster et al.,1992) and Australia (Shayan and Quick, 1992, Shayan, 1996) is controversial, as in most cases ASR was also present. Furthermore, research

by Shayan in 1996 found that deleterious expansions occurred only when reactive aggregates are used with curing temperatures of 75$^{o}$C. The expansion mechanism that occurs in mortars and concretes after curing at elevated temperatures is not yet understood and there still exist various uncertainties in its association with delayed ettringite formation.

*1.3 Research Approach*

Delayed ettringite formation (DEF) has been outlined by researchers as one of the major causes of premature deterioration of concrete structures potentially affecting the durability of concrete and is a growing concern in the industry. In the past decade many studies on DEF have paid much attention into the potential expansion of Portland cement cured at elevated temperatures. Extensive laboratory studies have been carried out to study the influence of DEF on expansion of mortar and concrete specimens and its correlation with curing conditions, aggregate type and cement composition. But no correlation has been established between the amount of ettringite detected and expansion of heat-cured mortars (Famy et al., 2001).

This experimental study was conducted in four phases. In Phases 1 and 2, mortar samples were mixed and stored in four different storage conditions. Phase 3 and 4 concrete samples were mixed and also consequently exposed to different storage conditions. All specimens were steam-cured except one (1) set subjected to field conditions and prepared throughout the entire study according to the UMD/FHWA modified sample preparation. The Duggan Heat Cycle was carried out after one week of casting the specimens. It took sixteen (16) days from casting to

storage of the specimens. At the end of the Duggan Cycle, the specimens were left outside at room temperature for two (2) days to cool before storing them in various exposure conditions. Phase 1 (mortar) and Phase 3 (concrete), with no additional potassium carbonate ($K_2CO_3$) added to the batch mixes served as the control. Phase 2 (mortar) and Phase 4 (concrete) has a 1.5% potassium content ($K_2O$) added in the batch mixes. After obtaining the results of the chemical analysis of the cement (shown in Chapter 4), the required amount of $K_2CO_3$ was calculated based on the potassium oxide ($K_2O$) content. Additional $K_2CO_3$ was added to accelerate the expansion rate and to enhance the formation of DEF.

In most DEF studies, the heat-cured specimens are stored in water following heating cycles to accelerate expansion and without monitoring the storage environments. Based on extensive literature review and previous work conducted at the University of Maryland (Amde et al 2005a, 2005b, 2005c, 2004a, 2003a, 2003b) and (Livingston et al 2002, 2001a, 2001b, 2000), the following exposure conditions were used in this study: Isothermal water bath, pH maintained at 12.5 (saturated limewater) and monitoring potassium and sodium concentration of storage solution; moist air chamber R.H at 97%, plain water and monitored the pH value, potassium, sodium and calcium concentration of the storage solution; and field conditions (no Duggan Heat Cycle). Also the influence of curing condition, Duggan Heat and Freeze-Thaw cycles on concrete were employed. Laboratory-prepared mortar and concrete samples exposed to field conditions were also studied. For detailed outlines of the exposure conditions, materials and test parameters, see Chapter 4.

The objectives of Phase 1 were to study the mechanism of DEF associated with exposure conditions in normal type III Portland cement while keeping all other parameters constant. Frederick sand and ASTM Portland Type III cement were used to study DEF throughout the entire research. The objectives of Phase 2 were to study increased potassium content ($K_2O$) and its association to DEF. Besides preparing mortar bars to study length change and weight change measurements, cubes were made to explore the influence of the different exposure conditions on compressive strength. In Phases 3 and 4, concrete was used to study the mechanism of DEF with its associated deleterious expansion. In Phase 3 (control), the objective was to study the influence of different exposure conditions, curing and heat treatment of concrete. The effect of an increase in potassium content ($K_2O$) and DEF is outlined with Phase 4 concrete.

In this study, DEF caused by internal sulfate attack (ISA) was investigated. ISA occurs in a sulfate-free environment due to the interaction of internal sulfate (from cement or gypsum contaminated aggregate) with calcium-aluminate hydrates of the cement.

### *1.4 Problem Statement*

Delayed ettringite formation is one form of what is termed as Internal Sulfate Attack (ISA). Sulfate attack involves a set of both chemical and physical processes. Sulfate attack is considered to be the cause of most expansions and disruption of concrete structures. It is also responsible for a decrease in the durability of the concrete by changing the chemical and microstructural nature of the cement paste and

thereby the mechanical properties of the concrete, leading to their premature deterioration. Concrete structures such as precast units, cladding panels, railway sleepers and ties have suffered damage due to delayed ettringite formation. Delayed ettringite formation deterioration has resulted in expensive rehabilitation and replacement of concrete structures in several countries and has led to substantial litigation in the state of California (Kasdan, 2003).

Since 1965, when Kennerly first demonstrated the problems related to DEF, various case studies have been reported, mainly attributed to DEF and excluding alkali-aggregate reaction (AAR) or external sulfate attack. Kennerly revealed that ettringite was found at the cold-joints in the Roxburgh Dam, Otago, New Zealand. He further outlined that the formation of ettringite was due to the variation of the calcium hydroxide (CH) concentration at different areas of the dam. Ettringite was found at the areas of high CH concentration because the solubility of ettringite is inversely proportional to the CH concentration in the solution.

In the 1980's, several instances of damage to concrete structures were reported as, apparently, mostly due to delayed ettringite formation. In most of the structures reported, DEF contributed a great deal to the deterioration including alkali-aggregate reaction (AAR) and chloride contamination. In the English Midlands, ettringite was found in the pores, voids, and at the aggregate surfaces in concrete bases. Also, substations in Western England and South Wales showed similar damage, with ettringite co-existing with gel from the alkali-aggregate reaction (Pettifer and Nixon, 1980). In the same year, Pettifer and Nixon detected ettringite in the concrete just four years after placement of the Pirow Street Bridge in Cape Town,

South Africa. In their research studies, Volkwein and Springenschmid (1981) often found needle-like ettringite crystals near the splashing zone of the concrete bridge deck. They further postulated that the rich chloride-contaminated bridge enhanced the formation of ettringite from the sulfate originating from the cement. Deterioration was also found in reinforced concrete of marine structures in Egypt. Ettringite existed in cracks of three out of the seven reinforced concrete structures (El-Sayed, 1987). Ettringite was found in the pores and cracks of precast concrete railway ties steam-cured at high temperatures (75-80$^{o}$C) using high early strength cement (Heinz, 1987, Tepponen, 1987). In Sweden, ettringite was found in the concrete of a swimming pool along with CH, calcite and gypsum, which had been leached to the surface. The damage to the concrete was due to a combination of alkali-silica reaction (ASR) and aggressive reaction of sulphates (Chandra and Bernston, 1988).

Lawrence et al., examined fifteen prestressed and reinforced concrete structures cast between 1963 and 1969 and found expansive cracking problems after fifteen years. They confirmed alkali-silica reaction and found ettringite around the aggregate grains (1990). In Strathclyde, Scotland, Maclead detected ettringite in the form of white spheres within the air-entrained voids of the concrete deck (1990).

A few years after installation of concrete railway ties on the east coast of the United States, Marusin diagnosis revealed DEF crystals in the cracks (Marusin, 1995). Again, in the U.S., the Texas Department of Transportation (TxDOT) found premature deterioration of 56 precast/prestressed concrete box beams which were to be used on highway bridges and stored at the fabrication site. The research team postulated that DEF was the primary distress mechanism, with little association with

ASR. Other cases studied by TxDOT include a parking garage in central Texas and cast-in-place concrete foundation piers for transmission of power line towers in Austin. The four-story parking garage, constructed in 1986-1987, showed substantial distress in the form of cracks with internal expansion reaction. Just after eight years of service, it was discovered that the cast-in-place concrete foundation piers exhibited premature deterioration, which was attributed to delayed ettringite formation (Lawrence et al., 1999).

In 2000, Brewer Stadium, Appalachian State University, Boone, North Carolina, reported that 375 of 860 precast units exhibited severe cracking and delamination leading to spalling. Fibrous crystallized ettringite was identified as filling the cracks and voids in the mortar and also in the paste between coarse and fine aggregate in the concrete. Due to significant defects in the precast element attributed to DEF, reconstruction of the stadium proved to be the economical alternative (Ozol, 2000).

### *1.5 Objectives and Scope of this Study*

1. Apply advanced material testing methods and analyze the complex process of expansive cracking associated with DEF in mortar and concrete systems;
2. Investigate the influence of exposure conditions in DEF pertaining to weight change, expansion/contraction and damage variables;

3. Study the potential of DEF in mortar and concrete specimens as a function of the amount of alkalis leached into the storage solution by water analysis;
4. Study DEF in mortar and concrete specimens exposed to field conditions;
5. Study the effect of potassium content ($K_2O$) on mortar and concrete expansion associated with DEF;
6. Investigate and explore the complexity of DEF using a Scanning Electron Microscope (SEM) equipped with energy dispersive X-ray (EDAX) at several stages;
7. Perform laser shearography (non-destructive testing) to analyze and evaluate premature cracking in concrete specimens subjected to different concrete treatments and exposure conditions;

*1.6 Structure of Thesis*

This thesis consists of 10 (ten) chapters. The first chapter gives a brief review of the literature and background information outlining the overall research. In Chapter 2, cement chemistry and its association to ettringite formation is presented. Chapter 3 deals with a comprehensive collection of literature review on delayed ettringite formation, accelerated test methods, and expansion theories. Experimental details such as sample preparation, test materials used and test methods are precisely given in Chapter 4. Chapter 5 presents the results of the mortar samples (control) while Chapter 6 provides a analysis of the results for the mortar samples with 1.5%

potassium content. Chapter 7 outlined the control concrete samples and Chapter 8 deals with concrete samples made with 1.5% potassium content ($k_2O$). Chapter 9 provides a comprehensive analysis and discussion of the results presented in Chapters 5 through 8. Finally, Chapter 10 provides the conclusions and recommendations for future research work.

# Chapter 2: Chemistry of Cement and Ettringite Formation

## *2.1 Introduction*

Portland cement is one of the most widely used and most important materials used in the construction industry today. Cement is the key ingredient used in concrete, mortar, plaster, stucco, and grout.

Portland cement is defined, according to ASTM C150, as a hydraulic cement, one that sets or hardens when mixed with water. Particles of the cement take up water, forming a gel cementing the particles together through a process known as hydration. Cement is produced by pulverizing clinker consisting of hydraulic silicates, usually containing one or more of the forms of calcium sulfate as an interground addition (Derucher et al, 1998). The main minerals required in the production of Portland cement are lime (CaO) about 60–65 %, silica ($SiO_2$) about 20 – 25%, alumina ($Al_2O_3$) and iron oxide ($Fe_2O_3$) about 7–12% (Atkins, 1997).

Eight types of Portland cements are recognized by the ASTM under ASTM C150; type (I, IA, II, IIA, III, IIIA, IV, and V). Type I and II are normal cements used generally in most situations calling for Portland cement. Type III, or high early strength, is used when early strength is required as in precast and prestressed concrete. This cement is obtained by finer grinding and by better burning so that the dicalcium silicate ($2CaO.SiO_2$) is less and the tricalcium silicate is greater ($3CaO.SiO_2$).

Damages associated with delayed ettringite formation have been mainly with precast concrete made of high early strength cement (Lawrence, 1993, and Fu et al., 1996).

*2.2 Portland Cement Composition*

In the manufacture of Portland cement, the raw materials, limestone and clay are ground up, mixed to produce the desired proportion of minerals and burned in a large kiln. The temperature of the kiln reaches about 1450$^{o}$C (Taylor, 1997). This drives off water and gases, and then produces new chemical compositions in particles called clinker. The clinker is subsequently ground with about 5 percent gypsum (to control rate of hardening) and is then ready for use as Portland cement.

The cement compounds produced are: tricalcium silicate ($3CaO.SiO_2$), dicalcium silicate ($2CaO.SiO_2$), tricalcium aluminate ($3CaO.Al_2O_3$) and tetracalcium aluminoferrite ($4CaO.Al_2O_3.Fe_2O_3$). They are the major phases in cement and usually abbreviated as $C_3S$, $C_2S$, $C_3A$, and $C_4AF$ respectively. The relative amounts of these chemicals in the final product depend on the desired properties such as rate of hardening, amount of heat of hydration and resistance to sulfate attack. Hardening results from the chemical reactions between major phases and water. Hydration reactions of aluminates influence the various types of setting behavior and those of the silicates influence the strength development of mortar and concrete. Chemists normally denote these major phases in cement as: elite ($C_3S$), belite ($C_2S$), aluminate ($C_3A$) and ferrite ($C_4AF$). Several other phases such as alkali sulfates and calcium oxide are present in minor amounts.

Alite is tricalcium silicates ($3CaO.SiO_2$ or $C_3A$) modified in composition and crystal structure by ionic substitutions such as $Mg^{2+}$, $Al^{3+}$ and $Fe^{3+}$ (Taylor 1997). Elite is the most important constituent and constitutes 50–70% of normal Portland cement clinker. The chemical reaction for elite ($C_3S$) with water is:

$$2C_3S + 6H_2O \longrightarrow 3CaO.2SiO_2.3H_2O + 3Ca(OH)_2$$

The product, $3CaO.2SiO_2.3H_2O$, is calcium silicate hydrate or tobermorite, which gives concrete its strength.

Belite is dicalcium silicate ($2CaO.SiO_2$ or $C_2S$) and constitutes about 15 – 30% of normal Portland cement clinkers. It reacts with water relatively slowly and contributes little to strength during the first 28 days. It is a major phase that contributes later to the development of the strength.

Aluminate is tricalcium aluminate ($3CaO.Al_2O_3$ or $C_3A$) and constitutes about 5-10% of most Portland cement clinkers. Their compositions, and sometimes its structure, are significantly modified by foreign ionic substitutions such as $Si^{4+}$, $Fe^{3+}$, $Na^+$ and $K^+$. It reacts very rapidly with water and can cause undesirably rapid setting if no set-controlling agent is added.

Ferrite is tetracalcium aluminoferrite ($4CaO.Al_2O_3.Fe_2O_3$ or $C_4AF$) and constitutes 5-15% of normal Portland cement clinkers. It is substantially modified in composition by variation in Al/Fe ratio and substitutions of foreign ions.

Alite and belite react with water to form calcium silicate hydrate (C-S-H) and calcium hydroxide (CH). Calcium silicate hydrate is commonly called C-S-H because it does not have a fixed stoichiometric composition. The aluminate phase reacts with gypsum in the presence of water and yields ettringite.

*2.3 Portland Cement Hydration*

The hydration of Portland cement is the chemical reaction between the cement clinker components, calcium sulfate and water and is responsible for the setting and hardening of mortar and concrete. The setting process is a consequence of changes from a concentrated suspension of flocculated particles to a viscoelastic skeletal solid capable of supporting an applied stress (Gartner et al., 2002). The development of the solid skeleton is known as hardening and leads to the ultimate mechanical properties and durability of the mortar or concrete.

During the earliest stage of hydration, a series of rapid reactions begin which involve mainly clinker interstitial phases (i.e., aluminates and aluminoferrites, alkali sulfates, and free lime), plus calcium sulfates (gypsum, hemihydrate and/or anhydrite) that have been interground into the cement (Gartner et al., 2002). After several hours, definite shells of hydration products, mostly C-S-H, CH, ettringite needles or thin calcium monosulfate (AFm Phase) plates are sometimes present in the shells (Diamond, 1987). This layer of ettringite or AFt phase is often poorly crystalline and difficult to detect by X-ray diffraction (XRD) (Gartner, 2002 and Taylor, 1997). The AFt phase contains lots of sulfate, which comes from the rapidly soluble sources such as alkali sulphates, hemihydrate and gypsum. The continued formation of AFt and AFm phases can influence the workability, but the C-S-H formation leads to the onset of normal set concrete.

Although cement paste shrinks due to drying, hydration continues for years if water is available. The hydration products are found around the grains and prevent the access of water to the unhydrated particles, which impede the late hydration (Azzam,

2002). This causes a continuous strength increase due to porosity, but at an ever-diminishing rate (Gartner, 2002).

*2.3.1 Hydration of Calcium Silicate*

The main product of Portland cement, $3CaO.2SiO_2.3H_2O$, is calcium silicate hydrate or tobermorite gel, C-S-H, which constitutes 50 to 60% of the hydration cement paste and is the most important in determining the properties of the paste. The C-S-H quality and composition gives concrete its strength.

The C-S-H is not a well-defined compound and the C/S ratio varies between 1.5 to 2.0 (Mehta, 1993). The internal structure of the C-S-H remains unsolved due to its indefinite stoichiometry. The hydrations of silicates are accelerated in the presence of sulfate ions in the solution. Various observations indicate that absorption of sulfate ions ($SO_4^{2-}$) by the C-S-H plays an important part in the mechanism of expansion and formation of ettringite (Older 1980, 1987, Fu et al. 1994, Scrivener 1992, 1993, Lawrence 1990, Lewis 1994, 1996, 1997 and Taylor, 1997). After storage of specimens, sulfate is released from the lighter inner C-S-H gel at a rate that is affected by the hydroxide concentration of the pore fluid, which depends on the hydroxide solution of the storage solution (Famy, 2001). Basically, the higher the hydroxide concentration, the lower the rate of sulfate release and expansion. Also, the leaching of alkalis increases the rate at which sulfate is released from the C-S-H and causes an increase in the pH level of the storage solution. Therefore, limiting alkali leaching slows down sulfate release and, in turn, retards the expansion process leading to the formation of DEF (Famy, 2001).

*2.3.2 Calcium Hydroxide*

Calcium hydroxide, $Ca(OH)_2$ crystals are another major product formed during Portland cement hydration, and it constitutes 20 - 25% of the volume of solids in the hydrated paste. Unlike C-S-H, calcium hydroxide (CH) has a definite stoichiometry and an adverse effect on the chemical durability of acidity solutions. The dissolution of CH is greatly suppressed in the presence of alkalis, and this enhances the formation of ettringite. Also, the presence of CH increases expansion (Cohen and Richards, 1982, Mehta, 1973).

*2.3.3 Hydration of Aluminates*

Several hydraulic calcium aluminates can occur in the $CaO\text{-}Al_2O_3$ system; however, tricalcium aluminate ($C_3A$) is the principal aluminate compound in Portland cement clinker. Calcium ferrites usually are not formed in ordinary Portland cement clinker; instead, calcium ferroaluminates that belong to the $C_2A\text{-}C_2F$ ferrite solid solution (fss) are formed and correspond approximately to $C_4AF$.

The reaction of $C_3A$ and water is very rapid and the addition of gypsum slows down the reaction. This retardation is attributed to the formation of ettringite coatings around the $C_3A$ containing grains (Collepardi et al, 1987, Scrivener and Pratt, 1984). Reaction of $C_3A$ with water in the presence of sulfate may produce calcium aluminate hydrate, $3CaO.Al_2O_3.3(CaSO_4).32H_2O$ (ettringite) or $3(3CaO.Al_2O_3.(CaSO_4).12H_2O)$ (monosulfate) depending on the concentration of the aluminate and sulfate ions in the solution.

In solutions saturated with calcium and hydroxyl ions, the former crystallizes as short prismatic needles referred to as high-sulfate or ettringite and usually is termed as the AFt phase. The hydration reaction in the presence of sulfate is:

$$3CaO.Al_2O_3 + 3(CaSO_4.2H_2O) + 26H_2O \longrightarrow 3CaO.Al_2O_3.3(CaSO_4).32H_2O$$

Ettringite forms immediately after mixing and acts as a skeleton, providing the principal source of early stage strength. This ettringite may be very unstable, react with more $C_3A$, and be converted into monosulfate. The monosulfate (AFm phase) is also called low-sulfate and crystallizes as thin hexagonal plates. The chemical reaction for monosulfate is:

$$3CaO.Al_2O_3 .3(CaSO_4).32H_2O + 2(3CaO.Al_2O_3).32H_2O + 4H_2O \longrightarrow 3(3CaO.Al_2O_3.(CaSO_4).12H_2O)$$

*2.4 Heat of Hydration*

The compounds of Portland cement are none equilibrium products of high-temperature reactions and these compounds react with water to acquire stable low-energy states (Mehta, 1993). The hydration reactions involve the release of energy in the form of heat. The total amount of heat liberated and the rates of heat liberation from hydration of the individual compounds can be used as indices of their reactivity. Also, the heat of hydration characterizes the setting and hardening behavior of cements and can be used for predicting temperature rise in concrete paste.

For typical Portland cement, approximately 50 percent of the potential heat is liberated within the first 3 days and 90 percent within the first 3 months of hydration. It should be noted that, as the percentage of $C_3A$ and $C_3S$ increases, the heat of

hydration increases. From analyses of heat of hydration of various cements by Verbeck and Foster in 1950, they computed the individual rates of heat evolution due to the four principal compounds in Portland cement. They concluded that the total heats of hydration at a given age and under given conditions are due to the additive percentage contents of $C_3S$, $C_2S$, $C_3A$ and $C_4AF$ present in the cement.

*2.5 Heat Treatment of Mortar and Concrete*

The heat treatment method was used to accelerate the strengthening of the mortar and concrete specimens. Similar heat treatment programs have been used in the prestressed/precasted industry for the production of concrete box beams and railway sleepers to obtain high strength within short periods of time. Figure 2.1 shows the heat treatment program used. To prevent over drying and shrinkage the exposed parts of the specimens were covered with aluminum foil throughout the heat treatment program. Most DEF cases were associated with the use of high heat treatment such as this. Various researches found that the curing method plays an important role in DEF formation and its associated deleterious expansion but is not the primary factor. In 1999, Stark and Bollmann found that ettringite also occurs in no-heat treated concrete, which is exposed only to normal climatic conditions.

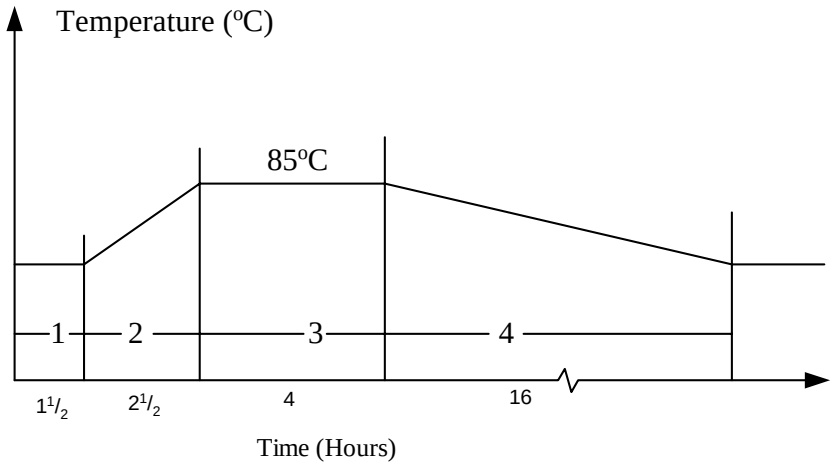


1 – The Presetting time

2 – Heating

3 – Heat (Steam) Curing at 85°C

4 – Cooling, overnight

Figure 2.1: Heat Treatment Program (Adapted from Azzam, 2002)

*2.5.1 Effect of Heat Treatment on the Stability and Formation of Ettringite*

Heat treatment is used in the production of precast concrete to promote the early strength development and to allow rapid production. In 1954, Powers et al revealed that the maximum curing temperature used may be in the range of 40 to 100°C (10 to 21°F), although the optimum temperature is in the range of 65 to 85°C (150 to 175°F). The heat treatment affects the stability and formation of ettringite, and absorption of sulfate ions.

Ettringite is not entirely stable; it may lose water or decompose under certain conditions. Ettringite as a crystal has 32 water molecules, which easily dehydrate upon heating in dry conditions. Parameters such as relative humidity, the pH value of

storage solutions, and the concentration of the sulfate ions in solutions affect the stability of ettringite.

In 1963, Lieber concluded that ettringite was stable in water up to 90$^{o}$C. A similar study by Mehta revealed that ettringite was only stable up to 66$^{o}$C if heated dry but started to decompose at 93$^{o}$C (1969). Other researchers' results were controversial, as when Satava and Veprek investigated the stability of ettringite in saturated steam and found that ettringite did not decompose even at 110$^{o}$C (1975). In 1985, Ghorab et al studied the stability of ettringite in relation to its solubility in pure water at 30$^{o}$C, 60$^{o}$C and 100$^{o}$C. They found that ettringite was stable up to two weeks of stirring in water at 60$^{o}$C. When stirred in pure water at 100$^{o}$C, after one hour the ettringite decomposes to monosulfate (AFm phase). Sylla in 1988 examined the stability of ettringite at various temperatures and his results suggested that the stability of ettringite in cementitious systems is not only related to the curing temperature but also to the maturity of the system at the time it is heat-cured. He showed that if specimens were pre-cured for several hours at room temperature, some of the ettringite persists even at 80$^{o}$C heat-curing, and in the specimens that were not pre-cured, no ettringite was found after heat-curing at 80$^{o}$C.

Many researchers suggested that the stability of ettringite in cementitious systems might be related not only to the curing temperature but also to the hydration of the Portland cement (Sylla, 1988, Kalousek and Adam, 1951, Fu et al, 1944 and 1995). It was reported that, during heat curing, sulfate and aluminate ions may get adsorbed by the C-S-H gel. The applied high heat curing temperature destroys ettringite. Ettringite decomposition during heat curing is closely related to the

adsorbing of sulfate and aluminate ions but not to the instability nature of ettringite (Heinz and Ludwig, 1987). Fu, Xie, Gu and Beadoin, in 1994 and 1995, reported that the C-S-H gel will adsorb sulfate ions faster at high temperature and sulfate adsorbed at high temperature is desorbed more slowly than that adsorbed at normal temperature. They further concluded that the slower release of sulfate ions from an internal sulfate source might be an important condition for delayed ettringite formation in high temperature-cured cementitious systems.

In 1996, Lewis performed microanalyses on C-S-H of heat-cured cementitious systems in his investigation of delayed ettringite formations. His findings revealed that the sulfur-calcium ratio of C-S-H was high after high temperature heat curing, but decreased with the curing age. Yang et al also confirmed Lewis's results (1995 and 1996). Divet et al found that C-S-H has a high capacity of adsorbing $SO_4^{2-}$ ions, which depends on the pH level of the pore solution of the cementitious system and on the temperature (1998). They also found that the adsorption of $SO_4^{2-}$ ions by the C-S-H gel increases as the pH and temperature increases.

It is believed by many researchers that ettringite formation depends mainly on the exposure conditions (Lawrence, Dalziel and Hobbs, 1990 and Famy et al., 2001). The expansion and cracking of cementitious systems subjected to heat treatment above $70^oC$ and subsequently immersed in wet or moist conditions contributed to delayed ettringite formation (Heinz, 1986, Heinz and Ludwig, 1986, Lawrence, 1990, 1995, Sylla, 1988 and Ronne, 1999).

*2.5.2 Effect of Heat Treatment on the Mechanical Strength of Mortar and Concrete*

The influence of heat treatment on the compression and bending strengths of mortar and concrete has been researched and well-documented by Chamberline, Brewer and Shideler, 1952, Klieger, 1958, Hanson, 1963, Farsky, 1971, and Ronne and Sellevold, 1994. In 1971, Farsky investigated the delayed period influences on the properties of steam-cured mortar specimens. Portland cement was used in making the mortar specimens, beams 4 x 4 x 16 cm. Investigations of various delay periods were performed, ranging from 30 minutes to 7 hours 30 minutes. Samples were then subjected to heat in a steam chamber maintained at $70^{o}$C. A set of specimens was tested in bending and compression immediately after heating. The next series were tested after twenty-four hours of hardening. Another two series were tested at the end of 28 days hardening, one of them after curing in humid atmosphere and the other after curing in water. Farsky's results revealed that curing in water has no considerable influence on the 28-day compressive strength, but results in an increase of about 10 to 15 percent in the bending strength.

The compressive strength decreases as a result of the rapid temperature rise during pretreatment of mortar and concrete specimens (Saul, 1951). The precast concrete industries use accelerated hardening of concrete (AHC) methods, which include delay period, soaking time, temperature and all other technological aspects of concrete in its condensed state. Various investigators suggest an optimum delay period of $1^{1}/_{2}$ hours, and they found that a shorter delay period results in a decrease in compressive strength of about 70 to 75 percent (Farsky et al., 1971).

*2.5.3 Effect of Heat Treatment on Cement Chemistry and Microstructure*

The utilization of heat-curing in the precast industry to accelerate the hardening of the concrete, in order to achieve high early strength, and provide rapid production has been very successful. The high temperature used may change the composition of the hydration cement, and thereby alter the microstructure of the cementitious system.

Investigation by Idorn on the effect of hydration temperature on the hydration of Portland cement revealed that, at high temperatures, smaller amounts of hydrated aluminate, ferrite or sulfoaluminate phases will be formed, and the ratio of ettringite to monosulfate will be reduced (1968). A similar research by Odler et al showed that the C-S-H formed at elevated temperatures has a lower water content and higher Ca/Si ratio (1987). Odler et al also revealed that the amount of foreign ions ($Al^{3+}$, $Fe^{3+}$, $SO_4^{2-}$) incorporated in the C-S-H phase increases with a rise in hydration temperature. They finally concluded that the decrease in compressive strength at elevated temperatures was due to the increase in porosity. In 1996, a report from Kjellsen also confirmed that the Ca/Si ratio of the outer product in heat-cured concrete was significantly higher than that in the concrete that was continuously cured at room temperature. Other researchers obtained similar results (Oztekin, 1984, and Bentur and Berger, 1979).

Escalante-Garcia and Sharp postulated that high-temperature curing increases the rate of heat of hydration of all the main phases in Portland cement at early ages (1998). However, the ultimate degree of hydration was reduced by high-curing temperature. In 1992, Kjellsen and Detwiler found similar results, and they

concluded that the ultimate degree of hydration, evaluated by means of the non-evaporable water content, tended to increase with a rise in hydration temperature. From their research work, Verbeck and Helmuth suggested that the curing temperature at elevated temperatures results in a non-uniform distribution of the hydration product within the microstructure of the cement paste, with a high concentration of hydration product built up around the hydrating grains, which subsequently retards the hydration process (1968).

In 1996, Kjellsen studied the effect of heat curing and post-heat curing regimes on the microstructure and C-S-H composition of high performance concrete. He stored the concrete samples under different conditions and found that the heat-cured high performance concrete showed a higher content of hollow shell pores at later ages than a continuously cured sample at room temperature. He also noticed a significant amount of CH formed in hollow shells in the concrete cured at room temperature. He postulated that this may be one of the reasons for the apparently hollow shell porosity and for the low Ca/Si ratio of the outer product in the room temperature-cured concrete.

Other effects of heat-curing at high temperatures may lead to the concrete paste in the vicinity of aggregates tending to be more porous and having more ettringite rods and CH crystals than the bulk paste (Mouret et al., 1999). They compared their images obtained from SEM and an environmental scanning electron microscope (ESEM), and pointed out that the drying procedure in the SEM sample preparation may cause microcracking in the paste and induce gaps between paste and aggregate.

Scrivener studied the effect of heat treatment on the inner product C-S-H, and revealed the “two tone” feature of the inner hydration product in the cement pastes (1992). She heat-cured specimens at 80$^{o}$C and subsequently stored them in water at 20$^{o}$C. She observed that the “two tone” comprised a brighter outer band, considered to be formed at 80$^{o}$C, and a darker inner band, considered to be formed due to storage at 20$^{o}$C. She also reported that the darker inner band increases in thickness as hydration of the cement paste proceeds. Later, Diamond et al, presented SEM images of polished samples from room-temperature-cured cement paste showing the “two tone” feature. They further revealed that the “two tone” feature can occur in both heat-cured and room temperature-cured concrete (1998).

# Chapter 3: Delayed Ettringite Formation (DEF)

## *3.1 Introduction*

Delayed Ettringite Formation (DEF) has been considered as one of the potential destructive reactions affecting the durability of concrete. Frost action, corrosion of steel reinforcement and ASR had been outlined to be the other causes of deterioration in concrete (Mehta, 2006). DEF can be defined as formation of ettringite in paste mortar, or concrete by a process beginning after hardening is substantially complete and in which there exists no external sulfate source. Ettringite can cause damage that may be apparent only after a period of months or years. The first reactions to occur, when Portland cement concrete is cured under ambient conditions, are associated with tricalcium aluminate ($C_3A$) and its reaction with sulfate ions in the pore solution to form ettringite. Ettringite that forms early is almost certainly a product of recrystallization. The later formation of ettringite after the concrete has hardened is the potential host for destruction and the cause of final deterioration of the concrete.

The potential for deterioration of Portland cement concrete due to DEF has been recognized in the precast industry since Heinz et al reported cases related to high temperature (>75$^{o}$C) steam-cured concrete (Heinz and Ludwig, 1987, Heinz, Ludwig and Rudiger, 1989). They argued that delayed expansion in concrete was due to the transformation of metastable monosulphate into ettringite when steam-curing was subsequently followed by normal temperature-moist curing at later stages. Various

researchers confirmed this phenomenon (Siedel et al., 1993 and Grabowski et al., 1992).

In the presence of gypsum and lime, Portland cement hydration produces reaction products of tricalcium aluminate that include both monosulphate and tetracalcium aluminate hydrates. These hydrated aluminates are essential components of formation of ettringite at later stages. The source of $SO_3$-bearing materials in the presence of aluminate phases appears to be very critical for DEF. Sulfate attacks on concrete have been widely investigated by many researchers. Delayed ettringite formation occurrences have been reported with cements associated with high sulfate content (4 – 5% $SO_3$), usually high clinker sulfate (Diamond, 1996). Late discovery of DEF may be associated with changes in the cement composition, which has taken place in the last several decades. Reports of representative American cement analyses and their respective clinkers were typically less than 0.5% and the total cement sulfate contents were usually less than 2% (Lerch and Ford, 1948). Recent cements and clinker sulfate levels of 3% or more and total sulfate levels of 4 – 5% are common (Diamond, 1996). Other factors reported to influence DEF include cement type, fines and composition, concrete curing and exposure conditions. All these factors contribute to the damage associated with DEF and deterioration effects on concrete structures.

### *3.2 Damage Caused by DEF*

In the past two decades, expansion has been associated with internal deleterious expansive reaction, known as ettrringite formation in hardened concrete.

Ettringite was reported as the possible damage to the concrete structure of the Roxburgh Dam, Otago, New Zealand (Kennerley, 1965). Ettringite was found in the cold-joints of the dam.

Several causes of damage to concrete structures have been reported, most apparently due to DEF. In the English Midlands, ettringite was found in the pores, voids and at the aggregate surfaces in the concrete bases (Pettifer and Nixon, 1980). Pettifer and Nixon also detected ettringite in the concrete of the Pirow Street Bridge in South Africa.

In the U.S. concrete railway ties on the East Coast were diagnosed as revealing delayed ettringite crystals in the cracks (Maurusin, 1995). Also, in Texas, precast concrete box beams awaiting installation on a highway bridge exhibited significant expansion map cracking attributed to DEF. Petrographic analysis of the damaged structures showed DEF in the cement paste and cracks of the precast box beams. Other structures in Texas also identified damage due to DEF such as cast-in-place concrete foundation piers and parking garages (Lawrence et al., 1999).

Ettringite is usually found in structures such as railway ties, precast/prestress concrete, walls and stairways of parking garages, cast-in-place foundation piers, cladding panels and foundation slabs, and transmission pole footings (Mielenz, 1995, Chandra et al, 1988, Oberholster, 1992, Ozol, 2002, Schlorholtz, 1993 and 1995, and Vitousova, 1991). Expansions due to ettringite (gel-like material) are typically characterized by map cracks. SEM and X-ray analyses are commonly used to identify the chemical composition of ettringite. Exploration of the physical conditions for DEF and DEF-induced expansion would be ideal ways to examine this gel-like

material. Basically, researching the different conditions for DEF would probably lead to better understanding of the complex expansive mechanism. Consequently, this would help in providing appropriate practical test methods to assess potential for DEF-related expansion and suitable preventive measures.

### *3.3 Condition for DEF*

Various researches have been carried out to explore the complexity and conditions necessary for DEF and its associated expansion. Hypotheses and holistic perspectives that were exposed in order to satisfactorily address the necessary conditions for enhanced delayed ettringite formation were based on three (3) essential elements (Collepardi, 1999). The essential elements were the late sulfate release (from cement or aggregate), the pre-existing microcracks caused during manufacturing or any other initiated mechanism. Also, the intermittent or continuous exposure to environmental water or saturated air causing swelling or crystal growth of ettringite leading to crack opening, and subsequent damage in the form of macrocracking. Other researchers also believe that high temperature is an essential factor for DEF (Heinz and Ludwig, 1986, 1987, Heinz et al., 1989, Taylor, 1993, Ghorab et al., 1980 and Ludwig, 1991).

#### *3.3.1 Sulfate in Cement and Cement Clinker*

Modern cements such as Portland cement are manufactured in kilns that burn sulfur-rich fuels or organic residues which can incorporate huge amount of sulfate (up to about 2.5%) in the clinker (Miller and Tang, 1996). Particularly in the precasted/prestressed production of concrete ties, there was significant increase in the

incidence of internal sulfate attack (ISA)-related DEF in the last two decades. This may be related to the use of high-sulfur fuels and organic residues in the clinker sulfate. Different fuels are used in the manufacturing process such as gaseous or liquid hydrocarbons, as well as solid small-particle coals, depending on the cheapest available fuels. The sulfur content of these fuels can change and cause unwitting variations of sulfate incorporated in the clinker phase of the cement.

According to Hime, some of the sulfur in the clinker phase is present as relatively slow soluble sulfate (1996). They are unavailable for the early ettringite formation but would later be available to produce delayed ettringite formation. These sulfates enter into the solution, after hardening of the concrete, and react with $C_4AH$ and water to form ettringite. Delayed deposit of ettringite into these cracks expands causing the concrete to crack and deteriorate. Many researchers have attributed DEF to the sulfur in the clinker phase of the Portland cement (Hime 1996, Gress and Mielenz et al., 1995).

### *3.3.2 Presence of Microcracks*

The pre-existence of microcracks is considered essential to damage associated with DEF. Concrete and mortar cracking can be promoted by other mechanisms that cause microcracks, which then promote the ettringite deposition into pre-existing microcracks. These mechanisms include curing at high temperatures, localized high stress in prestressed structures, freeze-thaw cycles, ASR with microcracks around aggregate particles, dynamic loads, and fatigue stresses (Fu et al., 1996, Shayan,

1995, Oberholster et al., 1992 and Tepponen and Eriksson, 1987 and Collepardi, 1999).

Fu et al studied the significance of pre-existing cracks on nucleation of secondary ettringite in steam-cured cement paste (1994). They mechanically induced microcracks in their cement paste specimens, and witnessed their respective expansions under different curing conditions. They concluded that nucleation of ettringite crystals in cement pastes will occur preferentially under conditions of super saturation in cracked tip zones rather than on plane solid surfaces. They also postulated that high-temperature steam-curing followed by high-temperature drying is a favorable condition for deterioration by secondary ettringite formation, and those larger, pre-existing cracks are caused by high expansion due to secondary ettringite formation.

Fu and Beaudoin investigated the influence of microcracking on delayed ettringite formation in cementitious systems (1996). Different treatments, such as high-temperature curing, loading and freezing/thawing were applied after 24 hours to induce microcracks. They found that mortar and concrete bars that were cured at elevated temperatures (85$^{o}$C for concrete, 95$^{o}$C for mortar) and subsequently treated with high-temperature drying showed significant expansion. All other specimens did not show any significant cracks after 250 days of storage. They revealed that the pre-existing microcracks are a precursor for delayed ettringite formation.

*3.3.3 Exposure to Moisture*

The intermittent or continuous exposure to water or humid air is reported to be one of the essentials for delayed ettringite formation to occur. The presence of water filling the pore system of concrete is essential for the migration of reactant ions, such as $SO_4^{2-}$, $Al(OH)_4^-$ and $Ca^{2+}$, up to microcracks where ettringite deposition can occur. Field experience indicates that concrete ties exposed to rain and sun alternative actions are more severely damaged by Internal Sulfate Attack (ISA) than those exposed to rain but in permanent shadow conditions (Collepradi, 1999 and Thaulow et al, 1996). This different behavior could be attributed to the important role played by the degree of super saturation in favoring the deposition of ettringite formation.

Heniz and Ludwig investigated the mechanism of secondary ettringite formation in mortars and concretes subjected to heat treatment (1987). Their results relating to the moisture conditions essential to optimize the conditions for DEF revealed that expansion could be avoided if the concrete was exposed in an environment below 59% R.H. The concrete specimens with similar constituents subjected to similar heat treatment regimes showed severe deterioration when placed in a saturated atmosphere and stored at humidities above 60% for four months.

Microcracked concrete ties, with the same cement source and concrete composition, showed DEF in wet concrete structures while the same microcracked concrete ties, when protected from contact with water do not show any ettringite (Mielenz et al., 1995 and Shayan, 1995). This confirms the important role played by water in the migration of reactant ions from the cement paste up to the site of

microcracks and then resulting in the deposition of ettringite crystals into the microcracks and the subsequent crack opening.

### *3.3.4 High-Temperature Curing*

The issue of high-temperature curing as one of the critical elements for DEF is controversial. Some researchers believed that high curing temperatures (> 70$^{o}$C) are required for delayed ettringite formation (Taylor, 1997 and Lawrence, 1998). High temperature curing has been attributed to increase expansion due to DEF (Ghorab et al., 1980 and Lawrence, 1995). In 1995, Lawrence examined the expansion behavior of 55 Portland cements with a curing temperature range of 65 to 100$^{o}$C. He found that the critical curing temperature for DEF is between 65 and 70$^{o}$C. He also revealed that great extensions of high-temperature curing periods resulted in much reduced expansions.

High-temperature curing (above 70$^{o}$C) may dissolve ettringite in the pore liquid of the hardened concrete (Day, 1992). Also, Heinz et al suggested that, at elevated temperatures, primary ettringite is broken down to monosulfate (1987). Later, when the concrete is exposed to moisture at normal temperatures, the monosulfate is reconverted to ettringite. Hypothesis presented by Petrov et al. revealed that the rise in concrete temperature above 70$^{o}$C caused only by heat of cement hydration can create conditions for DEF especially in massive concrete elements (2006).

Other researchers present alternative hypotheses for the breakdown of primary ettringite at elevated temperatures. Fu and Beaudoin revealed that, at temperatures

above 65$^{o}$C, calcium silicate hydrate (C-S-H) absorbs sulfate very quickly from gypsum, reducing the amount available for ettringite formation (1996). Later on, when the temperature of the C-S-H is returned to normal, sulfate is slowly released through the pore solution, enhancing DEF.

According to other researchers, DEF may occur in concrete whether steam-cured or not (Collepardi, 1999, Mielenz et al., 1995, Maursin, 1995, Diamond, 1996 and Hime, 1996). They believed that DEF occurs even in non-steam-cured concrete specimens at temperatures much lower than 70$^{o}$C that are insufficient to cause thermal decomposition of the "normal" ettringite. This does not conform to the hypothesis that suggested that DEF is necessarily caused by thermal decomposition of ettringite at high temperatures (above 70$^{o}$C).

### *3.4 The Morphology of Ettringite*

The morphology and crystal size of ettringite varies with the different conditions under which it forms. Many SEM studies outlined that ettringite is normally formed as slender, needle-like crystals with a prismatic hexagonal cross section (Schwiet et al., 1966, Midgley and Pettifer, 1971, Mehta, 1973, Mehta and Hu, 1978). Its crystal size depends on the w/c ratio, that is, the availability of sufficient space (Mehta, 1969). Cohen et al also revealed that the particle size of Al-bearing agents also affects the size of ettringite (1985). The ettringite crystals will be smaller in the presence of calcium hydroxide (Possetti et al., 1982).

The form and shape of ettringite is relevant to studies of the mechanism of expansion. According to Lerch et al, synthetic ettringite consists of long needles,

which often are sphere-like (1929). Mehta reported the presence of spherule ettringite (1976). In 1983, Mehta noted that ettringite has two types of morphology, depending upon the conditions under which it forms. In low hydroxyl ion concentration, large lath-like crystals 10-100μm long and several μm thick are formed in solution. The other type forms in high hydroxyl ion concentrations, which is the normal situation for concrete, and are small rods 1-2μm long and 0.1-0.2μm thick. Ogawa and Roy found that, during the heat of hydration, the ettringite is formed as very small irregular particles around the Al-bearing particles in the early stages, and then changes to long needle-like crystals (1982). Though different sizes and forms have been reported, the chemical composition of all of them remains the same.

### *3.5 Detecting DEF*

Early ettringite formation which occurs immediately (within hours) in a plastic fresh concrete does not produce any damaging expansion and is associated with the regulation setting of Portland cement during hydration. Delayed ettringite formation (DEF) occurs at later ages, and the related heterogeneous expansion in very rigid hardened concrete can produce cracking and spalling. The internal cracking is accompanied by ring cracking around the aggregates particles where ettringite is usually found.

Extensive experience of various researchers suggested that DEF should be studied using a scanning electron microscopy (SEM) equipped with an energy-dispersive X-ray analyzer and using the secondary electron mode (Hime and Marusin,

1999). Cut sections from the studied sample are coated with carbon to permit easy analysis (Marusin, 1993 and 1995, Livingston et al. 2002, Amde et al. 2003b). A step-stair EDAX pattern of the chemical elemental analysis of ettringite (Ca, S, Al) is characteristic of DEF. Each element is identified on the spectrum by the position of its peak, and the computer calculates quantitative analysis by weight of each element. The chemical composition of ettringite is 6 calcium to 3 sulfur to 2 aluminum.

### *3.6 Alkali-Silica Reaction and DEF*

Many ASR (Alkali-Silica Reaction)-damaged structures undergo healing and filling of cracks, while DEF usually leads to widening of cracks, loss of prestress and the consequent failure of structure (Hime and Marusin, 1999). Therefore, it is very necessary to distinguish between ASR and DEF in order to be able to develop methods to mitigate or to prevent such occurrences in the future.

Many researchers have speculated that ASR was often a precursor of DEF in deteriorating concrete structures (Mielenz et al., 1995, Johansen et al., 1993 and Shayan and Quick, 1992). Shayan and Quick investigated the cause of extensive cracking in precast prestressed sleepers in Australia (1992). They found that, in the badly-cracked sleepers, there was a simultaneous presence of large amounts of AAR (Alkali-Aggregate Reaction) gel and of ettringite crystals. They postulated that the formation of the AAR gel products weakened the cement paste causing initial cracking and the formation of delayed ettringite which may involve the release of $OH^-$ ions and enhance AAR.

Other researchers also reported the simultaneous presence of DEF and ASR (Oberholster et al., 1992, Johansen et al., 1993 and Marusin, 1993). It was reported that high-temperature steam-curing could induce immediate ASR for some reactive aggregates (Diamond and Ong, 1994). The ASR-induced cracking facilitated the formation of delayed ettringite and the combined effect is more serious for the deterioration of the concrete.

However, investigations carried out by other researchers showed that DEF can take place in cement pastes without the occurrence of ASR (Older et al., 1996, Yang et al., 1996).

### *3.7 Stability of Ettringite*

The commonly accepted view that ettringite is more stable in sulfate solutions and lime water than in distilled water, and that monosulfate in solutions containing calcium sulfate, sodium sulfate, calcium chloride and sodium chloride may transform to ettringite is based on the work of Lerch et al (1929). Many researchers believe that many factors affect the stability of ettringite such as chemical composition of cement or the type of aggregates, alkali, carbonation and temperature.

#### *3.7.1 The Chemical Stability of Ettringite*

Many researchers have studied the effect of cement constituents on the stability of both ettringite and monosulphate (Mehta, 1969, Jones, 1939, Hampson and Bailey, 1982 and Zhang et al., 1980). In 1969, Mehta found that monosulphate might exist along with ettringite only if the solution surrounding it has a lower

concentration of sulphate than is usually required for the existence of ettringite. The three conditions necessary for the stability of monosulphate in aqueous solution are high calcium content (CaO), low sulphate content ($CaSO_4$), and high temperature (Jones, 1939, Kalousek, 1941, Heinz and Ludwig, 1987).

Zhang et al. reported that, according to the solubility product method, the solubility product of ettringite ($1.0x10^{-40}$) is much lower than that of monosulphate ($1.7x10^{-28}$), indicating that, under ambient temperature, ettringite is more stable than monosulphate in cement solution (1980). Therefore, monosulphate has the natural tendency to convert to ettringite. Hampson and Bailey reported the effect of pH value of the pore solution on the morphology of sulphoaluminates. At pH 11.5 to 11.8, sulphoaluminate forms as ettringite crystals and precipitates from the solution. At pH 12.5 to 12.8, the material is non-crystalline with composition similar to ettringite (1982).

### *3.7.2 Effect of Temperature on the Stability of Ettringite*

Many researchers have reported that calcium sulphoaluminates are thermally unstable phases (Kalousek, 1941, Heinz and Ludwig, 1989 and Daerr, 1977 and Klemm and Adams, 1990). Calcium sulphoaluminates transform from one state to the other with changes of the curing temperature, during which the sulphate groups and water molecules are re-arranged in the structures.

Curing temperature affects the size and stability of ettringite. At curing temperature of $60^oC$, ettringite x-ray peaks were noted only after 15 minutes (Hekal, 1986). At curing temperature above $60^oC$, ettringite loses more of its water molecules as the curing temperature increases. The water molecules drop from 32 to

18 at 70.5°C (Daerr, 1977). Abo-Elnein and Hekal reported that the loss of ettringite water molecules depends on its hydration temperature (1988). They concluded that as the hydration temperature increases, ettringite becomes stable, and water content reduction would be less.

Many researches have been carried out concerning a critical temperature resulting in the unstable ettringite-monosulphate transformation. In 1972, Mehta postulated that ettringite can be found in cement paste subjected to a 65°C drying condition and that the decomposition starts when dried at 93°C. In a moist environment at 93°C, ettringite poses no apparent decomposition but decomposes when exposed to saturated steam at 149°C. Research by Satava and Veprek also reported similar results that ettringite can exist stably in aqueous solution up to 93°C (1975).

Kalousek postulated a transformation of sulphoaluminates; he believed that the depletion of ettringite at high temperature could be attributed to the substitution of sulphate ions in the structure of the C-S-H gel (1965). Research on cement pastes showed that the amount of the missing $SO_3$ clearly increases as curing temperature increases. Kalousek suggested that the missing sulfate ion ($SO_3^-$) might be the source of delayed ettringite formation and is associated with the C-S-H gel structure. Ghorab et al concluded that the instability of ettringite at higher curing temperatures might be associated with its higher solubility (1980 and 1985).

*3.7.3 Effect of Alkalis on the Stability of Ettringite*

The presence of alkalis is believed to affect the solubilities of the reactants (e.g., $C_3A$, CH and $CSH_2$) in the $C_3A - CSH_2 - CH - H_2O$ system and hence the concentrations of the dissolved ions (e.g., $OH^-$, $SO_4^{2-}$, $Ca^{2+}$, etc.). The alkalis apparently could increase the formation of ettringite and decrease the solubility of calcium hydroxide (CH) (Daerr 1977, Wang et al., 1986 and Way et al., 1989). The pH of the pore solution depends on the alkali level and the higher the level the higher the pH. Ettringite can form in alkaline solution at pH of 13.3 at normal temperatures and at alkaline concentrations as low as 0.08 M. At high temperature ($60^oC$) or higher alkaline concentration (0.2 to 1.0 M), ettringite quickly decomposes while monosulphate appears to be more stable (Ghorab et al., 1985 and 1986).

*3.7.4 Effect of $CO_2$ on the Stability of Ettringite*

The effect of $CO_2$ on ettringite-related systems has been widely researched. Taylor revealed that carbonation during ettringite formation results in the formation of thaumasite ($\{Ca_6.[Si(OH)_6].24H_2O\}.[(SO_4)_2].[(CO_3)_2]\}$), and can cause the deterioration of concrete (1997). The formation of thaumasite may occur with all sulfate salts if high relative humidity and low temperature ($< 4^oC$) conditions exist (Pauri and Collepardi, 1989). It involves ettringite-like expansions and can cause cracking and deterioration of concrete (Hunter, 1989 and Lachaud, 1979). In 1988, Sylla found some evidence indicating that expansion can be attributed to both ettringite and thaumasite. He steam-cured his specimens at $80^oC$ and then stored

them at 5°C in the presence of $CO_2$. He found a high content of thaumasite with ettringite.

Seligmann and Greening first revealed the carbonation of monosulphate to produce ettringite and hemicarbonate (1964). Later Kuzel et al indicated that $CO_2$ acted as a catalyst to provide a favorable environment in the Portland cement for monosulphate transformation to ettringite (1989 and 1996). Various researchers have showed that ettringite converts to monosulphate only in cases where the Portland cement contains less than 0.5% $CO_2$ and the instability of monosulphate in the presence of $CO_2$ leads to its late formation (Kuzel, 1993 and 1996, Kuzel et al., 1991 and 1993).

### *3.8 Mitigating Techniques to Reduce Deterioration due to Ettringite Formation*

Siliceous materials can be used in Portland cement products to reduce or eliminate deterioration due to DEF (Fu, 1996). Different siliceous materials have different characteristics with respect to the reduction of the deleterious expansion. Fu analyzed the effect of some mineral additives on the expansion of mortars containing a DEF-suspect cement. Other researchers such as Amde et al. have use Class F fly ash and mix water conditioner to migitate DEF in concrete (2005b). The mineral additives included ground granulated blast furnace slag (GGBFS), Class F fly ash, Class C fly ash, silica fume and natural zeolite. Since microcracking plays an important role in the expansion from DEF, natural wollastonite was also used to control microcracking. The results of these tests yielded the following conclusions:

1. Class F fly ash and GGBFS were most effective mineral additives for eliminating expansion in Portland cement mortars resulting from DEF. Class F fly ash, when used to replace a portion of the cement, decreased the ettringite formation and the expansion.
2. Silicia fume was also good for reducing deleterious expansion but has an adverse effect on the workability of the cement product.
3. The expansion of the cement mortar due to DEF was greatly decreased by using wollastonite microfiber (Fu, 1996)

Other authors and agencies recognized the fact that an important factor in preventing DEF-induced deterioration is related to cement composition. Clinker with lower sulfate content can significantly reduce the risk of DEF-induced damage. Collepardi noted that the risk of DEF-related damage significantly increases with high strength (high $C_3S$ and $C_3A$) Portland cements, especially Type III cements (1999). Some agencies have set a maximum temperature threshold (between 140$^oF$ and 160$^oF$) on either the concrete or the steam used during accelerated curing to help prevent the development of DEF.

Research is currently under way in using external chemical treatments, such as sealers in mitigating DEF. Research projects done by the Iowa and Texas Departments of Transportation (TxDOT) within the past few years used external treatments in the form of sealers and crystal growth inhibitors in reducing DEF and its associated deleterious expansions. In 2001, Cody used commercial crystal inhibitors commonly used to prevent crystallization in industrial processes, such as water

treatment plants and boilers, for mitigating DEF in cores from in-service bridges. Cody also prepared laboratory specimens with the in-service bridge cores which were treated with different crystal inhibitors and subsequently subjected to different storage conditions. He found that two phosphate inhibitors, Dequest 2060S and Dequest 2010, were the most effective in reducing the ettringite growth. He finally concluded that there is a direct link between ettringite growth and concrete expansion since the only known effect of the commercial inhibitors is to reduce crystal growth.

In another similar research project, for TxDOT (2004a-c), Klinger experimented with surface treatments impermeable to water but permeable to water vapor for mitigating concrete deterioration. He tested twenty-three (23) different combinations of mitigating techniques composed of silane, siloxane, linseed oil, polyurethane, and high-molecular-weight methacrylate (HWM)-based solutions. Concrete prisms 3" x 3" x 11.25" with gage studs installed at the ends and cured at 23$^{o}$C and 95% relative humidity were used for the research project. The study concluded that Silane combined with either TxDOT Apperance Coat Paint or Opaque Concrete Sealer were the most effective in mitigating concrete deterioration caused by delayed ettringite formation or alkali-silica reaction.

### *3.9 Expansion Mechanisms due to Ettringite Formation*

The expansion mechanism due to ettringite formation is a very controversial issue. The main controversial issue over the DEF mechanism has been whether the gaps or air voids at the paste-aggregate interface, usually filled with ettringite crystals, are the cause of the expansion or a result of expansion. The theories of

ettringite formation and its associated expansion have been classified into two particular mechanisms - the topochemical reaction with directional growth theory and the uniform paste expansion theory. For ettringite formation and expansion, both mechanisms require an alkaline environment saturated with CH. Day suggested that both expansion mechanisms are active depending on the predominant environmental conditions at particular times (1992).

### *3.9.1 Topochemical Reaction with Directional Growth Theory*

In 1983, Cohen summarized a number of different theories and models developed to explain the formation of ettringite and its associated expansion mechanisms. He did classify them into two groups, crystal growth and the swelling theory. The crystal growth group suggested that expansion was caused by the growth of ettringite crystals on the surface of some cement particles in solution, a topochemical reaction approach. A topochemical reaction is a solid-state hydration mechanism whereby the product forms at the surface of the solid interface and grows in a direction perpendicular to the solid interface.

The presence of calcium hydroxide (CH) affects the properties of ettringite. Cohen also reviewed the effects of CH on the mode of ettringite formation (1983). If CH is present in solution, ettringite particles were thought to be small in size and to behave as colloidal particles, thus causing expansion. If CH is absent in solution, ettringite particles were considered to be larger in size. The magnitude of expansion does not depend on the amount of ettringite, but upon the size of the crystals formed. This implies that a small number of large crystals can produce more large cracks than

a large number of small crystals (Cohen, 1982 and 1983, Heinz and Ludwig, 1986, 1987, Sylla, 1988, Lawrence, 1990 and 1993, Diamond and Ong, 1994 and Maurusin, 1993).

Deng and Tang believed that expansion is the result of ettringite crystals forming on the surfaces of the Al-bearing particles in the surface (1994). They proposed that in highly-alkaline pore solutions, the diffusion of aluminum hydroxide (AH) from the Al-bearing particles into the bulk of the pore solution is slow due to low concentrations of AH ions between the interface of the Al-bearing particles and the pore solution, and the bulk pore solution. The near-interface solution and the wet surfaces of the hydrating Al-bearing grains will rapidly become highly supersaturated with ettringite. The high super saturation will lead consequently to a large nucleation rate, and thus to the formation of many crystallizing crystals around or close to the Al-bearing grains. Due to the limited space around the Al-bearing particles, the growth of these ettringite crystals will introduce high pressure on the surroundings, and a large expansion may be consequently expected. In a pore solution of low alkalinity, owing to the relatively low concentration of $OH^-$ ions and low mobility of $Ca^{2+}$ and $SO_4^{2-}$ ions, the dissolved AH ions might diffuse into bulk solution before many nuclei of ettringite crystals can be formed. The near-interface solution around the Al-bearing grains will not be a favored place for the nucleation of ettringite crystals. Therefore, ettringite crystals formed in pore solutions of low alkalinity will cause little or even no expansion.

Xie and Beaudoin suggested that the expansion caused by internal sulfate attack is a process in which chemical energy is converted into mechanical work to

overcome the cohesion system. The expansive forces result from the crystallization pressure which is again a result of the interaction between the solid products of a chemical reaction and cement paste. The two necessary conditions proposed for the crystallization pressure to occur are: a confined crystal growth of solid product and an "activity product" of reactants in the pore solution greater than the "solubility product" of the solid product under atmospheric pressure.

Many arguments have been suggested against the crystal growth hypothesis. If the growth of ettringite is due surely to the aggregate grains on the surface, the cracks would be uniform, but ettringite crystals growth is usually random and with associated heterogeneous cracks. Many researchers supported the hypothesis of a uniform paste expansion. They believed that the ettringite-filled gaps around the aggregate in expanded mortar and concrete at the transition zone, aggregate-paste or steel paste zones are the cause of expansion (Heinz and Ludwig, 1987 and Fu et al, 1993 and 1994).

### *3.9.2 The Uniform Paste Theory*

In this hypothesis, expansion is attributed to water-adsorption and swelling characteristic of ettringite gel which forms by a through-solution mechanism. These gel-like particles have a large specific surface area analogous to the C-S-H gel, and they adsorb water, resulting in overall expansion (Mehta, 1983). Small ettringite crystals of colloidal size formed in a saturated CH environment pose a negative surface charge. The large surface area combined with the negative charge results in the attraction of a large amount of water. Tests on disks of pure ettringite confirmed

the theory (Mehta, 1983). The disk adsorbs large quantities of water and large swelling strains occur. The X-ray diffraction patterns of the ettringite before and after show no substantial change in the chemical composition. Many other researchers support Mehta's results (Seligman and Greening, 1964, Stefania, 1982, Sagrera, 1972 and Johansen, Thaulow and Skalny, 1993)

Sagrera mixed paste cylinders containing either calcium sulphate or sodium sulphate. He measured volume change and the quantity of ettringite in the pastes using X-ray diffraction (1972). He found that a huge amount of ettringite forms before there is any volume increase. Mather argues that the detailed formation of ettringite is of less importance than the fundamental mechanism involved in the process (1984). The ettringite attempted to form in a confined space producing very high forces of about 169,000 ft-lb (Mather, 1984).

### *3.10 Rapid Test For Predicting Expansion Due to Ettringite Formation*

A rapid test method (Duggan Test) was used to determine the potential of expansion due to delayed ettringite formation. In 1989, Duggan and Scott first used this method to measure the potential of concrete for damage due to ASR but found that the expansion of concrete is related more to ettringite formation in the concrete matrix than the silica gel. Grabowski reported apparent expansion in the concrete samples after severe heat-drying/re-wetting cycles used to simulate certain severe conditions relevant to the performance of railway sleepers (1992). On the basis of his investigation, Garbowski argued that the Duggan Test showed that all tested concrete sleepers were potentially subject to deleterious expansion.

The Duggan Test Method involves taking a minimum of five concrete cylinder cores from an existing structure or laboratory prisms or cylinders. The cores (25 mm in diameter) should be parallel and smooth. The heat treatment cycles include three cycles; the first two cycles include one day in a dry heat oven at 82$^{o}$C, then allowing them to cool for about one (1) hour and soaking for one (1) day in water at 21$^{o}$C. The third cycle includes three (3) days in the oven at 82$^{o}$C, then allowing the samples to cool down. Before immersing the cores in distilled water, measurements of the samples are taken to be used as the zero datum from which other readings are taken, and then the cores are stored in water. Length measurements are recorded at intervals of three (3) days over a period of 20 days. A pass/fail criterion of 0.05% at 21 days is defined. Many researchers revealed that the first 20 days expansion of the concrete subjected to the Duggan Test Method is caused by DEF (Abo El-Enein, 1984, Gillott, 1989 & 1990, Attiogbe, 1990 and Wells, 1990).

Criticisms of the Duggan Test Method have been: the collection of samples, the size of samples, lack of correlation studies between the results and field concrete, and the severe heat cycles procedures (Fu et al., 1993 and 1996, Livingston et al., 2001b). However, in this research, modifications have been made by increasing the sample size, the use of gage studs to facilitate length measurements, and the addition of potassium carbonate to accelerate expansion of the specimens.

# Chapter 4: Sample Preparation, Materials, and Test Methods

## *4.1 Introduction*

This chapter details the procedures followed in the preparation of the mortar and concrete specimens. The materials used and corresponding specifications are outlined. The various test methods and test procedures are also detailed and explained. Water to cement ratio was 0.5 for all the batches in the entire research. For the mortar specimens, a sand to cement ratio of 2.5 was used. The specimens were subjected to either Duggan Heat or Freeze-Thaw cycles one week after casting.

## *4.2 Experimental*

This research study was divided into four phases. The mixing and casting of the mortar specimens were done according to ASTM C109-99 and ASTM C305-99 (ASTM 2001). The specimens also were cured according to ASTM C192-00 (ASTM 2001). The Duggan Test Method was modified by using mortar and concrete specimens with end gage steel studs instead of concrete cores to facilitate length-change measurements.

Phase 1 mortar specimens were used as a control with no varying parameters. All specimens were steam-cured and then de-molded after 24 hours of casting except one set of specimens exposed to field conditions. Then, the specimens were stored under water at room temperature for six (6) days before subjecting them to the Duggan Heat Cycle. After the Duggan heat cycle and then allowing the specimens to

cool for two (2) days, the specimens were measured for length change (zero reading) and weight-change. Then they were stored in their respective storage conditions.

Phase 2 mortar specimens were cured and prepared similar to Phase 1, but with additional potassium carbonate ($K_2CO_3$) added to the mixing water. The total potassium ($K_2O$) content of all the batch mixes in Phase 2 was adjusted to 1.5% ($K_2O$) by weight of cement to accelerate the expansion and DEF. Again, after the Duggan Cycle, the specimens were stored in the different storage conditions. The specimens and the storage conditions were monitored throughout the entire research study.

Phase 3 concrete specimens were used as control with no varying parameters. Two different concrete treatments conditions (steam-cured and freeze-thaw cycles) were employed before subsequently storing the specimens in the different exposure conditions.

Phase 4 concrete specimens were cured the same as in phase 3, but with an additional potassium carbonate ($K_2CO_3$) added to the mixing water to accelerate the expansion. The total potassium ($K_2O$) content of all the batch mixes was adjusted to 1.5%.

### *4.2.1 UMD/FHWA Modified Samples Preparation*

Two types of mortar specimens were prepared in this research study: 2" cubes and 1"x1"x11.25" mortar bars. The concrete specimens include 4" x 8" cylinders and 3" x 3" x 11.25" prisms. The 2" mortar cubes and 4" x 8" concrete cylinders were used for compressive strength-testing, the mortar bars and concrete prisms were used

for expansion measurements, weight-change measurements, X-ray computed tomography (X-ray CT), scanning electron microscope (SEM) and laser shearography (LAS). The samples were prepared in accordance with ASTM C109-99 and C305-99. The prisms and bars were each equipped with two steel gage studs at each end to monitor the length change of the specimens periodically, instead of drilled cores suggested by Duggan.

### *4.2.2 Duggan Heat Cycle*

The Duggan heat cycle consists of three cycles as shown in figure 4.1. The first two cycles include subjecting the specimens to one (1) day in a dry oven at 82$^{o}$C followed by about $1^{1}/_{2}$ hour cooling and one (1) day soaking in water at room temperature. In the third cycle, the specimens are left in the oven for three (3) days at 82$^{o}$C. At the end of the third cycle, the specimens are allowed to cool for two (2) days at room temperature in the laboratory. Length change measurements were recorded at 3-5 days periodically, up to 100 days, and once weekly afterwards to monitor the expansion of the specimens. The heat-treatment (Duggan Heat Cycle) was used to initiate microcracks.

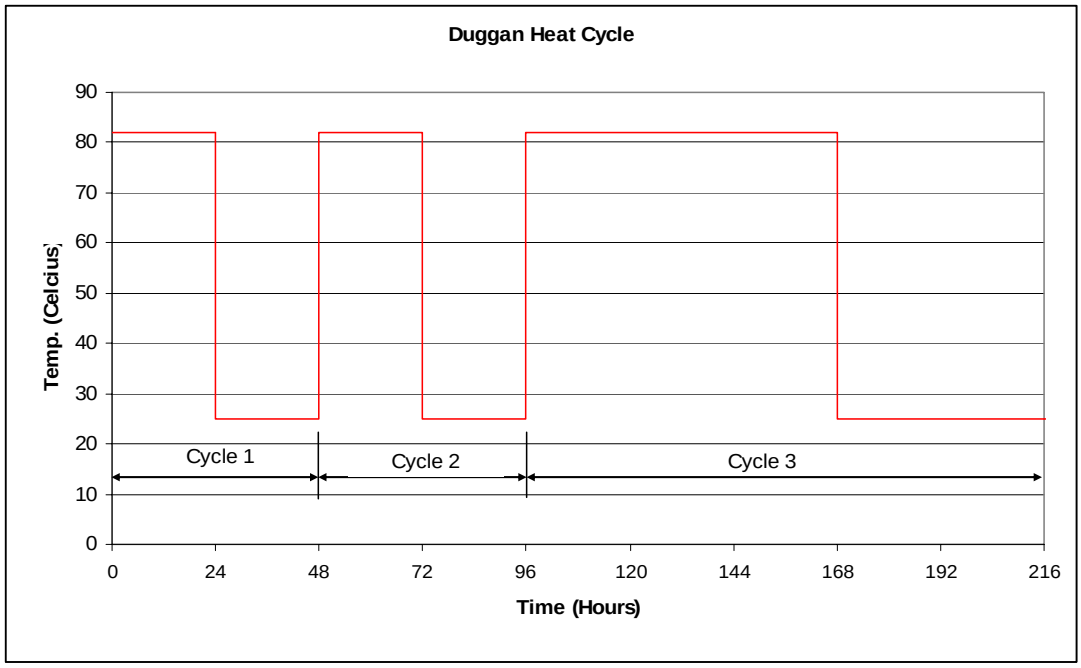


Figure 4.1: Duggan Heat Cycle for Mortar and Concrete Specimens

*4.2.3 Freeze-Thaw Cycles*

The Freeze-Thaw cycles employed took nine (9) days to complete. Then, the concrete specimens were stored in storage condition 1 (saturated calcium hydroxide solution) for the duration of the research study. The Freeze-Thaw cycles were employed to initiate microcracks in the concrete specimens. Figure 4.2 below shows the Freeze-Thaw cycles used for the pretreatment of the concrete specimens.

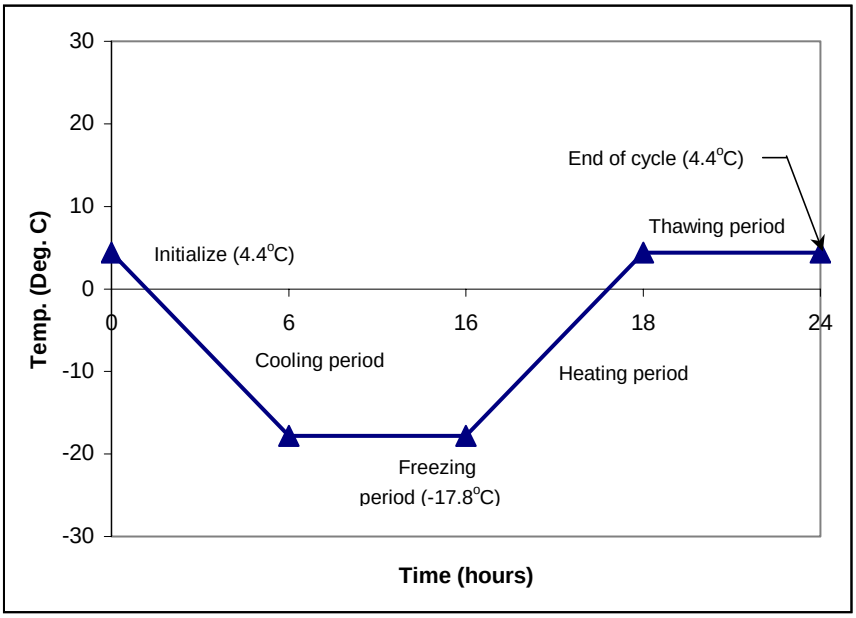


Figure 4.2: Freeze-Thaw Cycles for Concrete Specimens

## *4.3 Material*

### *4.3.1 Mortar Molds*

A steel mold with two compartments (1"x1"x11.25") with provisions for stainless steel gage studs and an effective gage length of 10 inches was used. The length change measurement was monitored in accordance with ASTM C490-90 (ASTM 2003). Brass molds with three compartments (2" cubes) were used to prepare for the compressive strength testing.

### *4.3.2 Concrete Molds*

Prism molds (3" x 3" x 11.25") with provision for stainless steel gage studs and an effective gage length of 10 inches were used. The length-change measurement was monitored in accordance with ASTM C490-90 (ASTM 2003). 4"

x 8" PVC cylinder molds were used to prepare for the compressive strength testing. The molds conformed to ASTM C470 specifications.

### *4.3.3 Cement*

Portland cement type III was used throughout the entire research. Type III cement was chosen because it has been identified as a potential cause of DEF. Its relatively high sulfate content, fineness and higher heat of hydration favors ettringite formation. The chemical analysis of the cement used in this research study is provided in Tables 4.1. The chemical analysis of the cement was measured by a commercial laboratory using X-ray fluorescence spectrometry.

Table 4.1: The Chemical Composition of Type III Portland Cement

| Chemical Analysis of Cement | |
|---|---|
| Analyze | Weight % |
| $SiO_2$ | 19.88 |
| $Al_2O_3$ | 5.03 |
| $Fe_2O_3$ | 2.79 |
| CaO | 61.79 |
| MgO | 2.51 |
| $SO_3$ | 3.89 |
| $Na_2O$ | 0.31 |
| $K_2O$ | 0.82 |
| $TiO_2$ | 0.21 |
| $P_2O_5$ | 0.17 |
| $Mn_2O_3$ | 0.07 |
| SrO | 0.20 |
| $Cr_2O_3$ | < .01 |
| ZnO | 0.02 |
| L.I.O (950$^o$C) | 2.01 |
| Total | 99.67 |
| Alkalis as $Na_2O$ | 0.85 |
| Calculated Compounds per ASTM C150-02 | |
| $C_3S$ | 51 |
| $C_2S$ | 18 |
| $C_3A$ | 9 |
| $C_4AF$ | 8 |
| ss($C_4AF + C_2F$) | -- |

*4.3.4 Sand*

Manufactured Frederick Stone Sand conforming to ASTM C33-99a was used throughout the research. The Frederick Sand was obtained from the Frederick Quarry, Frederick, Maryland. The Frederick Sand used had moisture absorption of 1.0% and a specific gravity of 2.69. According to the Maryland State Highway Administration, the potential alkali reactivity of the sand using ASTM C1260 is 0.09% and is considered intermediate reactive. The technical information about the Frederick Sand is given in Table 4.2.

Table 4.2: Technical Information Sheet for Frederick Sand

| **LAFARGE Frederick Quarry, Maryland Manufactured ASTM C33 Stone Sand Technical Information Sheet** | | |
|---|---|---|
| Rock Type: | Carbonate | Calcitic Limestone |
| Color: | Light to dark gray | |
| Average Gradation | Analysis | |
| ASTM C136 | % Passing | |
| 3/8 (in) | 100 | |
| #4 | 98.3 | |
| #8 | 86.6 | |
| #16 | 53.9 | |
| #30 | 29.4 | |
| #50 | 16.9 | |
| #100 | 6.2 | |
| #200 | 3.4 | |
| Specific Gravity (SG) | 2.69 | |
| Absorption | 1.0% | |
| Alkali reactivity of aggregate (ASTM C1260) | 0.09% expansion | |
| Soundness | 1.2% Loss | |
| Unit weight, dry rodded | 109#/CF | |
| Los Angeles Abrasion | 22.0% Loss | |
| Deleterious Substances - 200 Wash | 3.6% Dust of Fracture | |

*4.3.5 Coarse Aggregate*

Limestone aggregate of one-inch maximum diameter was used throughout the entire research. The aggregate had a dry rodded weight of 102.3 lb/ft$^3$, specific gravity of 2.72 and moisture absorption of 3%. The technical information about this coarse aggregate is given in Table 4.3.

Table 4.3: Technical Information Sheet for Coarse Aggregate

| **RGI Frederick Quarry ASTM # 57 Stone<br>Technical Information Sheet** | | | |
|---|---|---|---|
| Rock Type: | Carbonate | | Calcitic Limestone |
| Color: | Light to dark gray | | |
| Average Gradation | Dry Analysis | | Wet Analysis |
| ASTM C136 | % Passing | | % Passing |
| 1 (in) | 0 | | 100 |
| 3/4 (in) | 7.3 | | 93.5 |
| 1/2 (in) | 48.6 | | 39.1 |
| 3/8 (in) | 26 | | 15.3 |
| # 4 | 15.1 | | 3.7 |
| # 8 | 1.9 | | 1.1 |
| Pan | 1.1 | | 1.1 |
| | Bulk | SSD | Apparent |
| Specific Gravity (AASHTO T85) | 2.712 | 2.75 | 2.74 |
| Absorption (ASTM C127) | 0.3% | | |
| 200 Wash (ASTM C 117) | 1.5% | | |
| Polish Value (MSMT 411) | 7 | | |
| British Pendulum Number (ASTM D 411) | 26 | | |
| Alkali Silica Reactivity (MSMT 212 / ASTM C1260) | 0.09% expansion | | |
| L.A Abrasion (AASHTO T96 / ASTM C131) | 26% wear | | |
| Sodium Sulfate Soundness (AASHTO T104) | 0.1 % loss | | |
| Unit weight, dry rodded (AASHTO T19) | 95.7#/CF | | |
| MOHs Hardness | 4.0 | | |
| Sand equivalency (AASHTO T176) | 94% | | |
| Fractured faces (PMT 621) | 100% | | |

*4.3.6 Potassium Carbonate*

Anhydrous granular reagent grade potassium carbonate ($K_2CO_3$) was used. Potassium carbonate was added to the mixing water to increase the potassium content of the mix.

*4.3.7 Potassium Sulfate*

Potassium sulfate ($K_2SO_4$), white fine crystals, was used as a means of establishing an atmosphere of 97% relative humidity (R.H) for one of the storage conditions. The solubility of potassium sulfate at 20$^{o}$C is 111 grams per liter (Dean, 1999).

*4.3.8 Calcium Hydroxide (Hydrated Lime)*

Hydrated lime, chemically known as calcium hydroxide, $Ca(OH)_2$, or caustic lime, a white powder, was used to provide a required storage condition. The hydrated lime was dissolved in water at room temperature to produce a saturated solution with a pH of 12.5.

*4.4 Storage Conditions*

A plastic rack was built to hold the mortar specimens in the storage containers. The storage containers were 5-gallon plastic buckets. The racks can hold as many as 12 bars and 12 cubes. The concrete specimens were also in 5-gallon plastic buckets. Based on past research, four particular storage conditions were chosen to study their influence on DEF in mortar and concrete specimens.

*4.4.1 Isothermal Water Bath, pH maintained at 12.5 (Exp. Cond. 1)*

This storage condition is obtained by having a saturated solution of calcium hydroxide, $Ca(OH)_2$, and water at room temperature. This makes a 12.5 pH value of the aqueous solution, and the specimens are totally immersed throughout the research. The storage solution was periodically monitored for alkalis concentration using ion selective electrodes.

*4.4.2 Plain Water at Room Temperature (Exp. Cond. 2)*

Ordinary tap water at room temperature was used. The specimens were stored under water at room temperature and were periodically removed for measurements. The water was also monitored for pH value, alkalis and calcium concentrations.

*4.4.3 Moist Air Chamber, R.H maintained at 97% (Exp. Cond. 3)*

A saturated solution of potassium sulfate, $K_2SO_4$, was used to establish a R.H of 97%. About two (2) liters of water at 25$^{o}$C were mixed with 240 grams of $K_2SO_4$, and then poured into the plastic bucket. The specimens were arranged in a rack and placed in the bucket. The bucket was then covered airtight with a plastic lid, and was opened only during removal of specimens for measurements. All procedures per ASTM E104-85 were followed to maintain constant relative humidity using aqueous solutions.

*4.4.4 Field Conditions (Exp. Cond. 4)*

The specimens were either steam-cured (C4A) or room temperature-cured (C4B) prior to storing them outside exposed to atmospheric conditions throughout. Figure 4.3 shows the mortar specimens under field conditions.

Figure 4.3: Mortar Specimens Exposed to Field Conditions

*4.5 Samples Preparation*

The mortar specimens were prepared in the laboratory as per ASTM C192-00, standard practice for making and curing test specimens in the laboratory. To limit the number of varying parameters, no admixtures were used. Adding only 0.68 % potassium carbonate by weight of cement in the mixing water was utilized in phase batches, which increased the potassium level of the cement to 1.5% $K_2O$. All mortar batches were mixed according to ASTM C305-99. The mortar specimens were

mixed in an electrically driven mixer. Mortar bars (1" x 1" x 11.25"), were used for length and weight-change measurements, and 2" cubes were used for compressive strength-testing. The concrete specimens were 3" x 3" x 11.25" prisms, for length, weight change measurements scanning electron microscope (SEM), and laser shearography (non-destructive testing). For compressive strength tests, 4" x 8" concrete cylinders were prepared. The exposed parts of the specimens were covered with aluminum foil to prevent drying and shrinkage. They were then subjected to either steam-curing in the oven or cured at room temperature for 24 hours. Then, the specimens were kept for six (6) days before exposing them to either Duggan or Freeze and Thaw cycles. The total number of mortar specimens prepared is shown in Table 4.4. Table 4.45 gives the total number of concrete samples prepared during the entire research.

Table 4.4: Total Number of Mortar Samples Prepared

| Total Number of Mortar Samples Prepared | | |
|---|---|---|
| | Phase I | Phase II |
| 1" x 1" x 11.25" Bars | 54 | 54 |
| 2" Cubes | 76 | 76 |

Table 4.5: Total Number of Concrete Samples Prepared

| Total Number of Concrete Samples Prepared | | |
|---|---|---|
| | Phase III | Phase IV |
| 3" x 3" x 11.25" Prisms | 63 | 63 |
| 4" x 8" cylinders | 86 | 86 |

*4.5.1 Phase One*

In this phase, five (5) sets of mortar batches were prepared. All the mix materials and proportions were kept the same. The chemical analysis of the cement indicated 0.82% potassium content ($K_2O$). The cement was used as the control throughout Phase 1 batches without changing the potassium content. The mixing proportions of each batch are shown in Table 4.6. Specimens were then prepared by the modified sample preparation method.

Table 4.6: Mixing Proportions for Each Batch of Mortar Specimens

| | Phase 1 | | | | | Phase 2 | | | | |
|---|---|---|---|---|---|---|---|---|---|---|
| Mix | I | II | III | IV | V | I | II | III | IV | V |
| Water (mL) | 1150 | 1150 | 1150 | 1546 | 1546 | 1150 | 1150 | 1150 | 1546 | 1546 |
| Cement (g) | 2300 | 2300 | 2300 | 3091 | 3091 | 2300 | 2300 | 2300 | 3091 | 3091 |
| F. Agg. (g) | 5750 | 5750 | 5750 | 7728 | 7728 | 5750 | 5750 | 5750 | 7728 | 7728 |
| Add. P. Carbonate by weight of cement (g) | - | - | - | - | - | 20 | 20 | 20 | 27 | 27 |

**NOTE:** 1mL = 0.0022 lb $H_2O$ & 1g = 0.0022 lb mass

For batches I, II, III & IV the exposed parts of the specimens were covered with aluminum foil. Then, the specimens, while in steel molds, were placed in a water bath in an oven and the temperature raised to 85$^{o}$C for two (2) hours and then maintained at 85$^{o}$C for four (4) hours. After four (4) hours, the oven was turned off and the specimens allowed to cool overnight. The specimens were then stored under water at room temperature for six (6) days. After storage under water, batch IV was stored outside the laboratory under field conditions while batches I, II and III were subjected to the Duggan Heat Cycle. For batch V, the mortar specimens were cured

inside the laboratory for 24 hours. Then the specimens were de-molded and stored under water for six (6) days before being subjected to field conditions. All specimens were marked with different codes to reflect their phase and exposure conditions respectively. The specimens were coded with the date stored; the expression P1C3.1 was used for P1 – phase one, C3 – exposure condition 3 (maintained at a RH of 97%) and 1 – the sample number as shown in Figure 4.4. Initial weight and length change measurements were recorded for each batch prior to storing them.

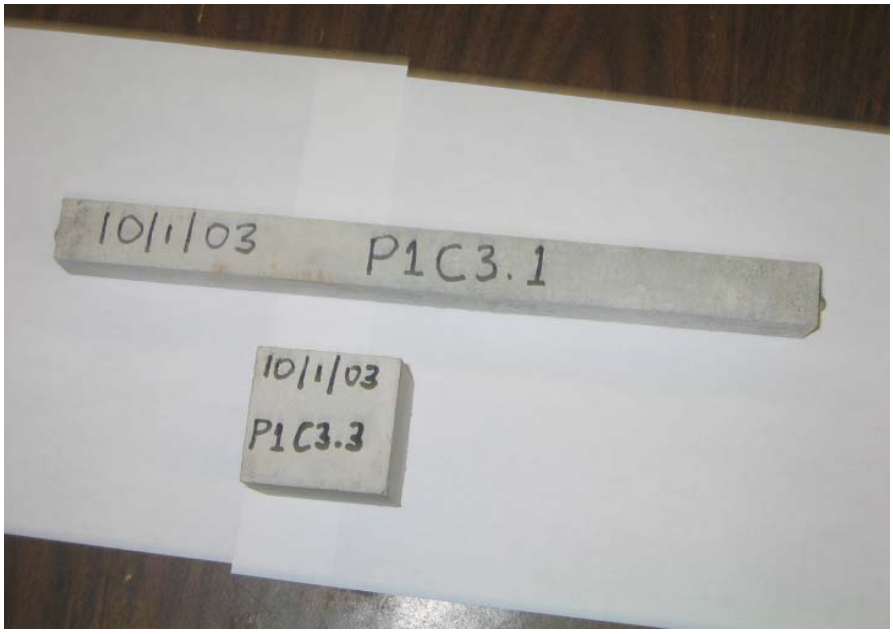


Figure 4.4: Identification of Specimens

Table 4.7: Batches and Exposure Conditions

| **PHASE 1 / PHASE 2** | | | | |
|---|---|---|---|---|
| MIX I | MIX II | MIX III | MIX IV | MIX V |
| EXP. COND. 1 | EXP. COND. 2 | EXP. COND. 3 | EXP. COND. 4A | EXP. COND. 4B |
| BARS: 10<br>CUBES: 12 | BARS: 10<br>CUBES: 12 | BARS: 10<br>CUBES: 12 | BARS: 10<br>CUBES: 15 | BARS: 10<br>CUBES: 15 |

*4.5.2 Phase Two*

All batches in phase 2 were prepared with a potassium content ($K_2O$) level of 1.5%. Additionally, 0.68% potassium carbonate by weight of cement was added to the mixing water to achieve the desired 1.5% $K_2O$. Again, all the mixing materials and proportions remained unaltered, while only the potassium content of the cement was increased. The mixing proportions of each batch are shown in Table 4.6. Again, all batch mixes were identically prepared and cured similar to phase 1 and stored. Table 4.7 provides the mortar batches and exposure conditions chart. The specimens were similarly numbered using different codes to reflect their phase and exposure conditions. Initial weight and length-change measurements were recorded for each batch before storing.

*4.5.3 Phase Three*

Five concrete batches were prepared. All the mix materials and proportions were kept the same and stored in different storage conditions. Additional concrete batches were cast to postulate the effect of curing conditions on expansion due to DEF. The mixing proportions for each concrete batch are shown in Table 4.8. Table 4.9 provides the concrete batches and exposure conditions chart. The specimens were prepared according to the modified method and were either initially steam-cured or cured at room temperature before subjected to Duggan Cycle or Freeze-Thaw cycles. The exposed parts of the specimens were covered with aluminum foil. Then, while in steel molds, they were placed in water batch in an oven and the temperature raised to 85$^{o}$C for two (2) hours and then maintained at 85$^{o}$C for four (4) hours. After four (4)

hours, the oven was turned off and the specimens allowed to cool overnight. The specimens were then stored under water at room temperature for six (6) days. After storage under water, the specimens were subjected to Duggan or Freeze-Thaw cycles. Initial weight and length measurements were recorded for each batch before storing.

### *4.5.4 Phase Four*

Again, all batches were mixed and prepared similar to phase 3. Only the potassium content ($k_2O$) level was increased to 1.5%. Again, additional concrete batches were mixed to compare curing conditions and its influence on DEF and associated damages variables. The mixing proportions for each concrete batch are shown in Table 4.8.

Table 4.8: Mixing Proportions for Each Batch of Concrete Mix

| | PHASE 3 | | | | | | PHASE 4 | | | | | |
|---|---|---|---|---|---|---|---|---|---|---|---|---|
| Mix | I | II | III | IV | V | VI | I | II | III | IV | V | VI |
| Water (lb) | 30.0 | 30.0 | 30.0 | 33.8 | 33.8 | 48.8 | 30.0 | 30.0 | 30.0 | 33.8 | 33.8 | 48.8 |
| Cement (lb) | 60.0 | 60.0 | 60.0 | 67.5 | 67.5 | 97.6 | 60.0 | 60.0 | 60.0 | 67.5 | 67.5 | 97.6 |
| C. Aggregate (lb) | 129.2 | 129.2 | 129.2 | 145.4 | 145.4 | 210.0 | 129.2 | 129.2 | 129.2 | 145.4 | 145.4 | 210.0 |
| F. Aggregate (lb) | 59.3 | 59.3 | 59.3 | 88.9 | 88.9 | 128.4 | 59.3 | 59.3 | 59.3 | 88.9 | 88.9 | 128.4 |
| Added P. Carbonate by wt. of cement (lb) | - | - | - | - | - | - | 0.52 | 0.52 | 0.52 | 0.58 | 0.58 | 1.14 |

Table 4.9: Concrete Batches and Exposure Conditions

| **PHASE 3 / PHASE 4** | | | | | |
|---|---|---|---|---|---|
| MIX I | MIX II | MIX III | MIX IV | MIX V | MIX VI |
| EXP. COND. 1 | EXP. COND. 2 | EXP. COND. 3 | EXP. COND. 4A | EXP. COND. 4B | EXP. COND. 1 |
| PRISMS: 10<br>CYLD: 12 | PRISMS: 10<br>CYLD: 12 | PRISMS: 10<br>CYLD: 12 | PRISMS: 12<br>CYLD: 15 | PRISMS: 12<br>CYLD: 15 | PRISMS: 24<br>CYLD: 25 |

*4.6 Test Procedures*

*4.6.1 Compressive Strength*

2" mortar cubes were tested to determine their compressive strength according to ASTM C109 "Standard Test Method for Compressive Strength of Hydraulic Cement Mortars (Using 2-in or [50 mm] Cube Specimens." Three (3) cubes from each exposure condition were tested at different stages to determine the compressive strength. Again, 4" x 8" concrete cylinders were tested according to ASTM C39-99 "Standard Specification for Compressive Strength of Cylinders." Again, three (3) concrete cylinders were tested to determine the compressive-strength from each storage condition at each stage. Figure 4.5 shows the compressive strength testing machine used to test the mortar and concrete specimens.

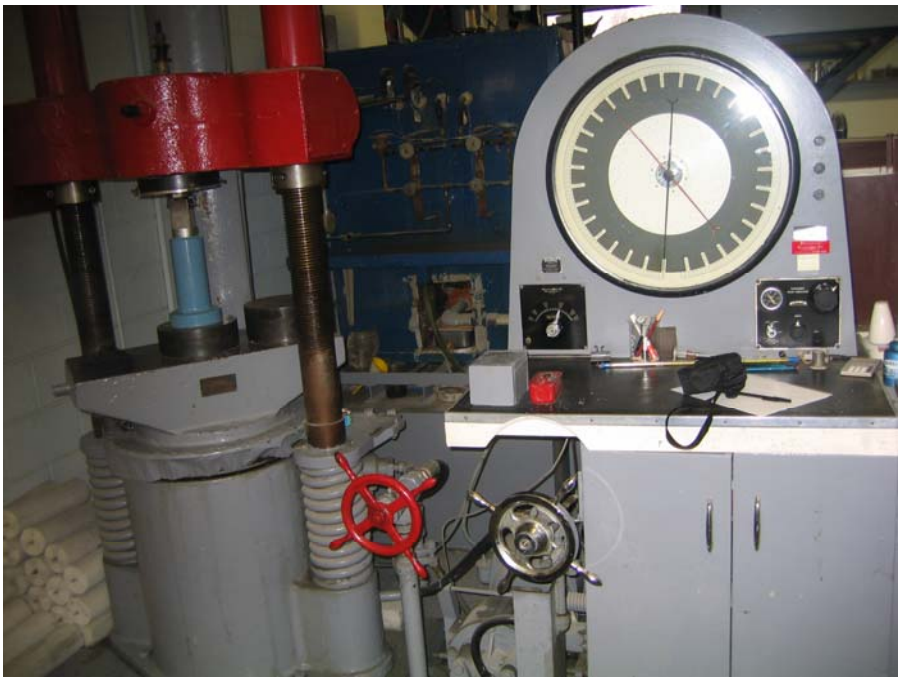

Figure 4.5: Compressive Strength Testing Machine

*4.6.2 Expansion Measurements*

The mortar specimens were prepared according to ASTM C109-99 and C305-99. The mortar and concrete specimens were prepared and measurements of their length-change were monitored in accordance with ASTM C490-00. Initial length-change measurements were recorded immediately after the completion of the Duggan Heat or Freeze-Thaw cycles, and before storing the specimens in their respective storage conditions. Five (5) mortar and concrete prisms were used to measure the length-change at intervals of 3 to 5 days for 200 days and periodically afterwards. The measurements were recorded, then the expansion of each bar calculated and the average expansion of each set calculated.

A standard length comparator equipped with a digital indicator and a reference invar bar were used to measure the length-change of the specimens. The digital indication was graduated to read in 0.0001-in. units and it was accurate within 0.0001 in. in any 0.0010-in range. All length-change measurements were done in a $70^{o}$C room. Prior to each measurement, the digital indicator was calibrated using the reference invar bar.

The mortar bars were all measured with the marked date part always positioned up as required by ASTM C490-00 for accurately obtaining comparator readings. Figure 4.6 shows a mortar bar carefully positioned to measured the length-change with a digital comparator.


Figure 4.6: Comparator Setup for Length Change Measurements

*4.6.3 Weight Change Measurements*

The specimens were blotted surface dry (wiped with an absorbent paper towel until all visible films of water were removed) at the time of weight measurement. The weight change measurements reflect not only weight changes during cement hydration but also different extents of contributions from other weight change mechanisms. The weight changes of the specimens during exposure were calculated in percentages using the equation below.

$$\text{Weight change (\%)} = [(W-W_0)/W_0] \times 100$$

Where:

W = weight of specimen at the age of measurement

$W_0$ = initial weight of specimen

A digital weighing scale was used for the weight change measurement. A set of five (5) concrete and mortar prisms was used for each exposure condition during weight-change measurements. The weight-change of each prism was calculated and then the average weight-change for each set was calculated. Figure 4.7 shows the digital scale used to monitor weight-change of the mortar bars.


Figure 4.7: Weighing Mortar Bars

*4.7 Water Analysis*

Water analysis was performed for storage conditions 1 and 2 using ion selective electron (ISE) and a bench top meter. Potassium, sodium and calcium ion selective electrodes were used to measure their respective concentrations in the storage solution at intervals of two (2) weeks to a month.

About 100ml of each sample was taken periodically, from each storage solution, in order to perform water analysis. The samples were analyzed and the results recorded. After collecting samples for measurement, water at room temperature was added and mixed to maintain saturation in exposure condition 1. As needed, distilled water was topped up for exposure condition 2 to ensure the specimens remained totally submerged. Prior to any analysis, the ISE was calibrated with known standardized ISE solutions, and the bench top recorded the electrode potential in millivolts. For an accurate and precise ISE, the electrode potential should be in the range 54 to 60 mV (Thermo Orion, 2001). Figure 4.8 shows water analysis performed using an ISE and a bench top meter.


Figure 4.8: ISE and Bench Top Meter Setup for Water Analysis

*4.8 Petrography Analysis for Identifying DEF*

Visual techniques were used by many researchers in the past two decades for identifying materials present in cracks and cavities of deteriorating mortar and concrete to determine the failure mechanism. These include scanning electron microscopes (SEM) equipped with energy dispersive analyzer x-ray (EDAX), differential scanning calorimetry (DSC), quantitative X-ray diffraction (QXRD), and X-ray computed tomography (X-ray CT). The SEM and EDAX are very powerful tools for studying the microstructural characteristics of solid substances. Its high resolution and versatility make it possible to precisely examine the microstructure and to identify the material.

Many researchers have used SEM and EDAX to distinguish between DEF and ASR gel distress mechanisms (Maursin, 1994, 1995, Hime, 1996). Also, Maursin reported that SEM petrography analyses were essential in differentiating between alkali-silica and DEF morphologies, and the EDAX provides the elemental analysis. In this research study, SEM equipped with EDAX and X-ray CT, were used as identification techniques for examining the microstructure of the mortar specimens.

*4.8.1 Scanning Electron Microscopy (SEM) and X-ray Analyzer (EDAX)*

The specimen in a scanning electron microscope is bombarded by a beam of high-speed electrons with an accelerating voltage of 10 to 20 kV aimed directly at the specimen. Three major types of signals are produced as a result of the interaction between the electron beam and the surface of the specimen. These signals are backscattered electrons, secondary electrons, and X-ray photos. Those signals can be

used to characterize the specimen. The electron micrographs obtained by using high-energy backscattered electrons reflect differences in the atomic numbers and can distinguish among the particles based on the variation in brightness of the topography image of the specimen. The electron micrographs that are obtained by using low-energy secondary electrons are capable of showing the morphology of the microstructure in two or three dimensions. X-ray radiation produces the elemental compositions as quantitative analyses printed on a chart by weight percent of elements. Each element is identified on a spectrum by the position of its peak.

Preparation of samples for SEM analysis is very important in diagnosis of the mortar or concrete failure mechanism. Different researchers use various methods of sample preparation for SEM. In 1986, Grattan-Bellow used polished concrete sections while Shayan 1989 used broken sections. Some used thin sections, such as Shayan 1992, while others used fractured surface samples, as did Shayan 1992 and Oberholster 1992. The fractured-sample preparation method appears to be the best for SEM diagnosis for DEF distress mechanism in concrete and mortar specimens (Marusin, 1995, Oberholster, 1992 and Amde et al., 2005a, 2004a and 2003b).

Fractured-surface samples were used in this research program. From each sample two (2) specimens were collected, an interior and exterior, to analyze the microstructure of the sample qualitatively. The fractured samples, 1-1.5 cm in diameter, were glued to carbon stubs with carbon paint prior to the scanning electron microscope (SEM) examination of specimens. The samples were dried in a vacuum oven at about $55^{o}$C, and then coated with a thin layer of carbon. The coating was done by thermal evaporation using a hummer 10.2 sputtering system with a CEA 2.2

carbon evaporation accessory. The carbon layer minimizes the charging effects. Static charges on the surface appear as bright spots in the SEM image. Carbon was used because it does not affect results since SEM is configured to ignore carbon in its elemental analysis, and has no interfering X-ray florescence. Figure 4.9 shows a scanning electron microscopy (SEM) and x-ray analyzer (EDAX setup.

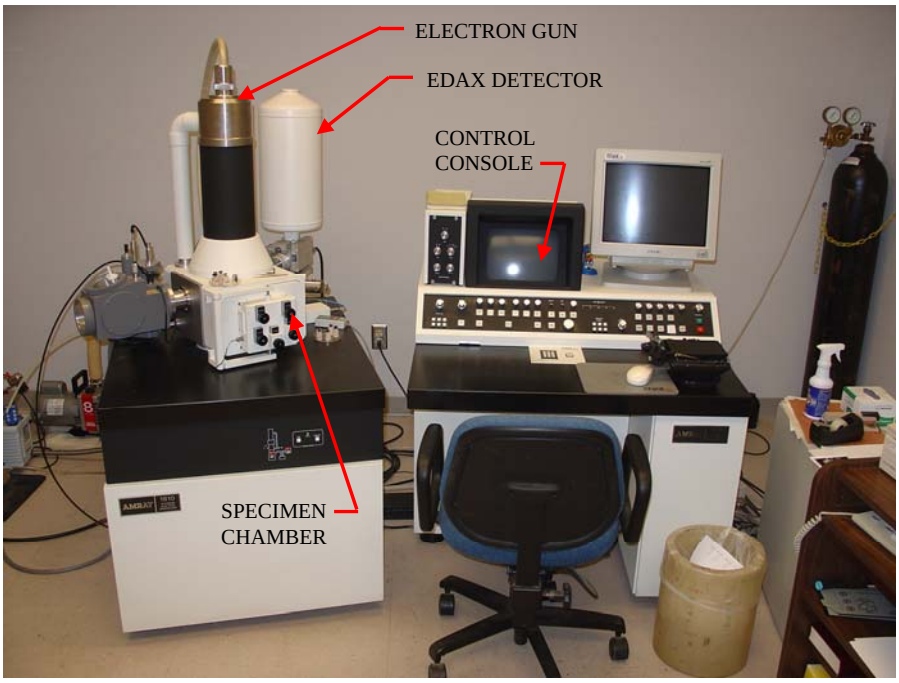


Figure 4.9: Scanning Electron Microscopy (SEM) and X-ray Analyzer (EDAX)

*4.8.2 X-ray Computed Tomography (X-ray CT)*

The X-ray computed tomography (X-ray CT) is a nondestructive method used to study the internal and external cracking patterns of solid substances. An industrial X-ray CT system with 420 kV photons and a 512 channel digital detector (BIR, 1998) were used to acquire images of the mortar specimens. Horizontal slices of 0.5 mm

were captured for every 0.4 mm and the data saved, while the 20% overlap ensures that all internal structure is captured. The data was then reconstructed using a back project reconstruction algorithm to generate TIF files format. The captured image consisted of 256 levels of gray intensity corresponding to different densities within the specimen.

Direct planar X-rays pass through the specimens along several different paths and directions producing sets of CT images. The intensity of the X-rays is measured after it passes through the specimens. The scan of each slice is complete after collecting the intensity measurement for a full rotation of the specimen. The specimen was then shifted vertically to generate another slice image, and the entire procedure was repeated in order to generate additional slice images. The X-ray CT captured the aggregate distribution, cavities, and interior cracks of the specimen. A schematic representation of the X-ray CT system is shown in Figure 4.10.

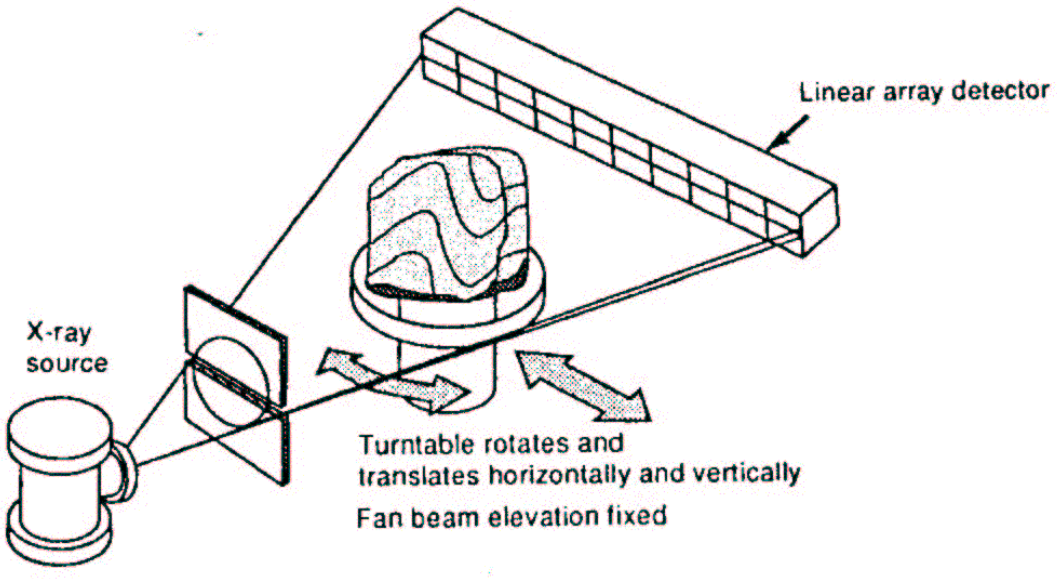


Figure 4.10: Systematic Representation of a Computed Tomographic System (After R. A. Ketcham, C. Denison and W. D. Carlson 1997)

*4.9 Laser Shearography (LAS)*

Electron laser shearography is a non-destructive technique that uses laser speckles as the carrier of deformation or displacement information for a tested object's surface, and records the speckle interference field by image-shearing camera. A shearing element is implemented in between the camera so that a pair of laterally sheared images of the object is generated in the same plane, and hence the method is called shearography. The effect of shearography is to match a point on the image into two points in the image. Conversely, this is equivalent to bringing two separate points on the object surface to meet in the same plane. The two overlapped portions of the sheared images interfere and produce a speckle pattern. When the object is deformed, the speckle pattern is slightly modified. Comparing the two speckle patterns (stressed and unstressed) produces a fringe pattern which depicts the relative displacement of two neighboring points. Since the magnitude of shearing is small, the fringe pattern approximately represents the derivative of displacement with respect to the shearing direction. This differs from holography which depicts displacement rather than its derivative. This difference from holography results in shearography being much less sensitive to external vibration interference, and hence much more suitable for production and field environments. A setup for laser shearography is given in figure 4.11.

Figure 4.11: Laser Shearography Setup

Laser shearography processes require that the materials under examination be stressed to reveal the defects. The stressing can take many forms, the optimum being the one which differentiates defects from the parent material, and has the ability to find the minimum defects standard. Figure 4.12 shows a schematic diagram of the laser shearography method and a view of concrete after slightly heating the specimen by $10^{o}$C. Note that these were pre-existing, and not generated by heating of the specimen. Similar results were observed using bending, instead of thermal stressing. This demonstrates that it is feasible to apply laser shearography to characterize microcracking in concrete both in the laboratory and in the field. Since the images are already produced in digital form, image analysis software can be readily applied

to identify cracks, and quantify them in terms of density, aspect ratio, area, crack mouth opening displacement (CMOD), size (length) and preferred orientation.

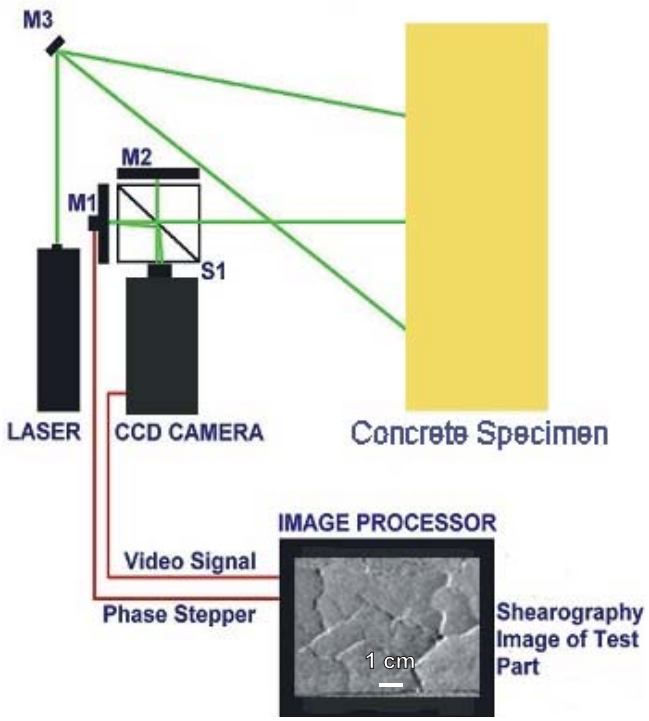


Figure 4.12: Schematic Diagram of Laser Shearography Method and View of Concrete Specimen After Slight Heating

The laser shearography images were analyzed using Image-Pro Plus version 5 for the Microsoft Windows operating system. Image-Pro Plus provides technologically advanced analysis techniques which allow the user to acquire and enhance image data from a camera, microscope, scanners, etc., before analyzing. Image-Pro Plus reads and writes image data in all standard images file formats including TIF, JPEG, BMP and TGA. The laser shearography images are imported for processing using automated image analysis algorithms to extract statistics about

the cracks such as width, length and preferred orientation. This also involves histogram stretching and an edge detection algorithm to highlight the cracks.

Concrete prisms - 3" x 3" x 11.25" were prepared and then cured under different conditions. Laser shearography tests were done after curing, at around 100 days and at 300 days of storage in water with pH maintained at 12.5 and relative humidity (R.H 97%). Another four (4) sets of concrete prisms were subjected either to heat-cured (Duggan Cycle) or Freeze-Thaw Cycle before subsequently being stored in isothermal water, pH maintained at 12.5 (limewater). Laser shearography work was done before and after the curing of the specimens to determine surface crack density. Statistical analysis of the collected image data will help in the detection of cracking, quantify crack growth over time and observation of crack patterns due to delayed ettringite formation.

# Chapter 5: Mortar Samples (Control) and DEF

## *5.1 Introduction*

The potential for deterioration of Portland cement concrete and mortar due to DEF has been widely recognized in the precast industry. In this study, five (5) sets of mortar samples were prepared according to the Modified Sample Preparation Method. The deleterious effect due to DEF was monitored for the mortar specimens stored in four (4) different conditions. Frederick Sand (manufactured sand) was used in all the batch mixes and, according to the Maryland State Highway Administration (MDSHA); the ASR result is 0.09%. The MDSHA classified the Frederick Sand to be of medium reactivity. Most of the specimens were steam-cured and then stored under water. They were then subjected to the Duggan Heat Cycle after one week to accelerate formation of microcracks. Expansion and weight change measurements were monitored for about two (2) years.

Early measurements of the compressive strength of the mortar samples were performed after 28 days for each exposure condition. Compressive strength tests were later performed after one (1) year and $1^1/_2$ year of storage (i.e., from the end of the heat cycle). Three (3) cubes were tested from each exposure condition and the average result used. Scanning electron microscope (SEM) with X-ray analysis and X-ray computed tomography (X-ray CT) studies were performed on the expanded mortar specimens. The objectives were to study the effect of using a manufactured fine aggregate and different exposure conditions on leaching of ions, weight changes, DEF, and its associated deleterious expansions. Expansions, weight-change, water

analysis of storage solutions, SEM with EDAX, and X-ray CT results are presented and discussed in this chapter.

*5.2 Influence of Exposure Conditions*

Four (4) different storage conditions were employed in this research study. After the Duggan heat cycle, the samples were stored in their respective exposure conditions and monitored for weight-change, expansion, leaching of ions, SEM with EDAX and X-ray CT. Expansion and weight changes were monitored periodically. Expansion values at 21 days were compared to the threshold value of 0.05% expansion that was suggested by Duggan as pass/fail criteria. It should be noted that the expansion and expansion rate are affected by specimen size (Fu, 1996). Therefore, the Duggan threshold value is only considered as a suitable criterion for determining the DEF potential in Portland cement products. Other researchers considered expansion up to 0.1% to be insignificant and a final degree of expansion over 0.1% as significant (Kelham, 1999 and Shimada, 2005). Heinz and Ludwig reported that storage in water or nearly saturated air is a necessary condition for the DEF-related expansion to occur. They suggested that ettringite reformation, owing to its water-rich composition, requires a sufficient supply of water from external sources. SEM with EDAX and X-ray CT studies were performed to reveal the presence of ettringite in different forms in the cracks and air voids. No ASR was found in any of the examined samples.

*5.3. Mortar Samples Subjected to Duggan Heat Cycle Test Results*

The first three (3) batch mixes were all subjected to the Duggan heat cycle after one (1) week of casting. The experimental results are discussed and analyses for the different exposure conditions are presented.

*5.3.1 Expansion Results*

*5.3.1.1 Length Change Measurements*

From each exposure condition, five (5) mortar bars were used for each expansion measurement and the average expansion recorded. The expansions were measured according to ASTM C-490. The initial length measurements were taken after the Duggan heat cycle after two (2) days of cooling and before storage under the respective exposure conditions. Afterwards, expansion readings were then collected at specific intervals afterwards. This continued for two years. Specimens measured from all three exposure conditions showed expansion within three (3) days after the end of the Duggan heat cycle. Expansion values at 21 days were compared to the threshold value of 0.05% expansion suggested by Duggan as pass/fail criteria for concrete. Expansion values and rates of the mortar bars (control samples) are shown in Figures 5.1 through 5.4.

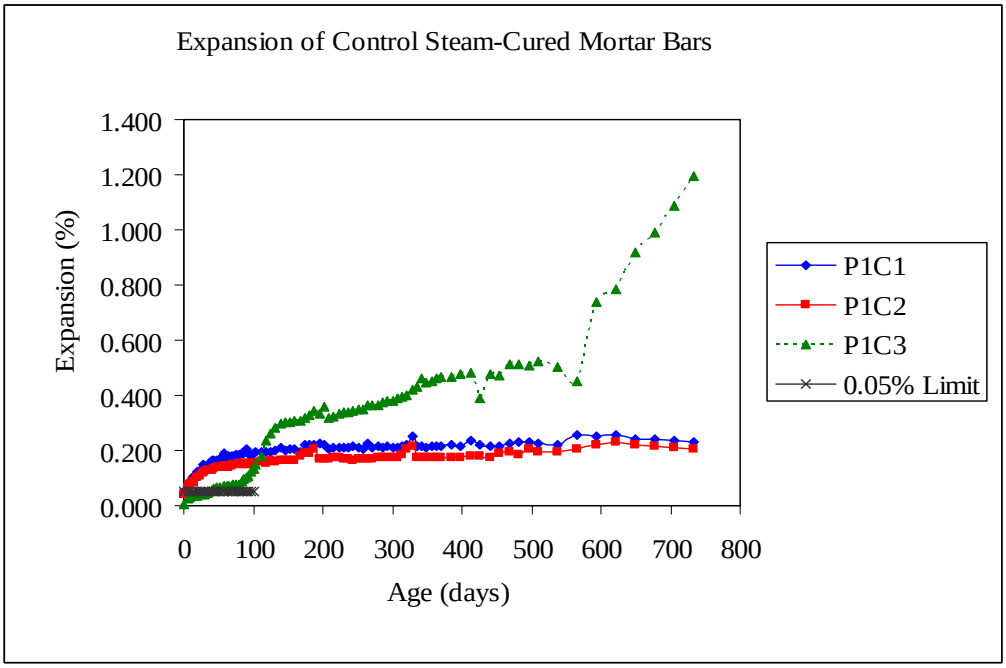


Figure 5.1: Expansion of Mortar Bars Subjected to Duggan Heat Cycle and Stored Under Different Exposure Conditions

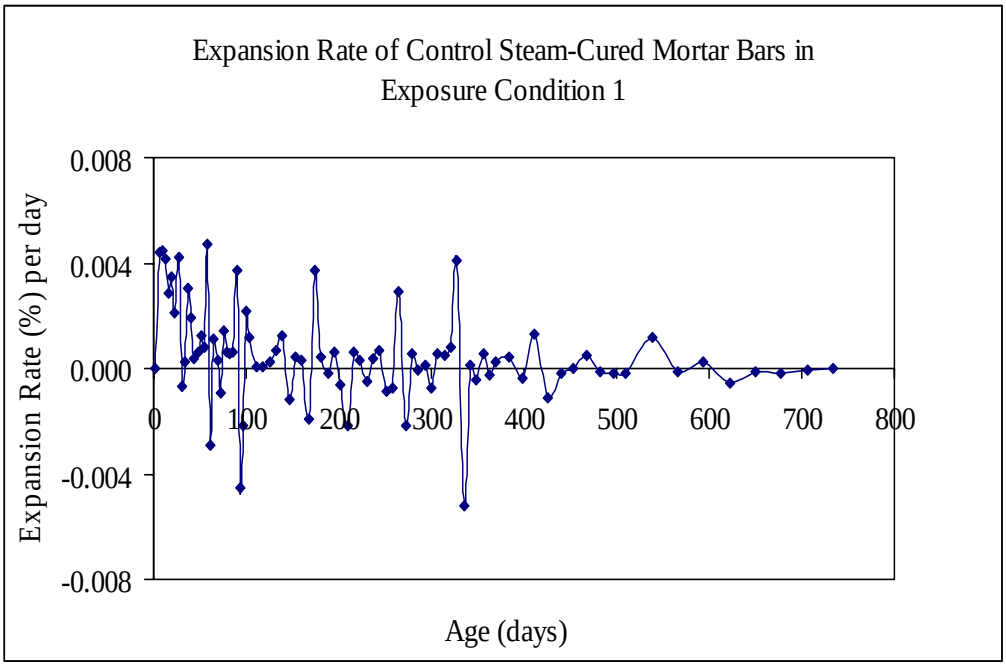


Figure 5.2: Expansion Rate of Mortar Bars Subjected to Duggan Heat Cycle and Stored in Isothermal Water Bath, pH maintained at 12.5 - limewater

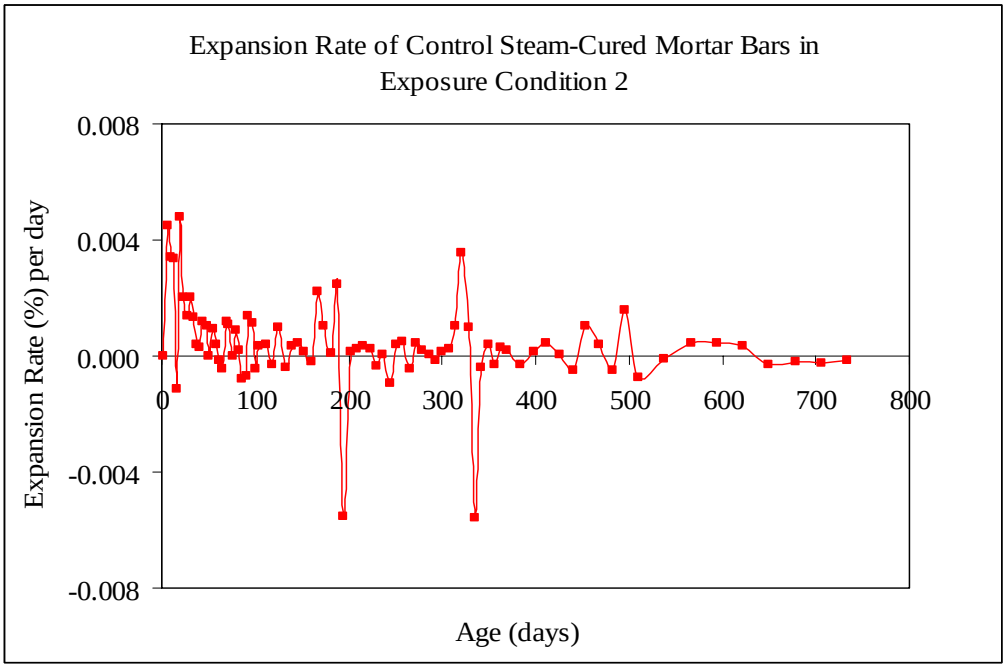


Figure 5.3: Expansion Rate of Mortar Bars Subjected to Duggan Heat Cycle and Stored in Plain Water at Room Temperature

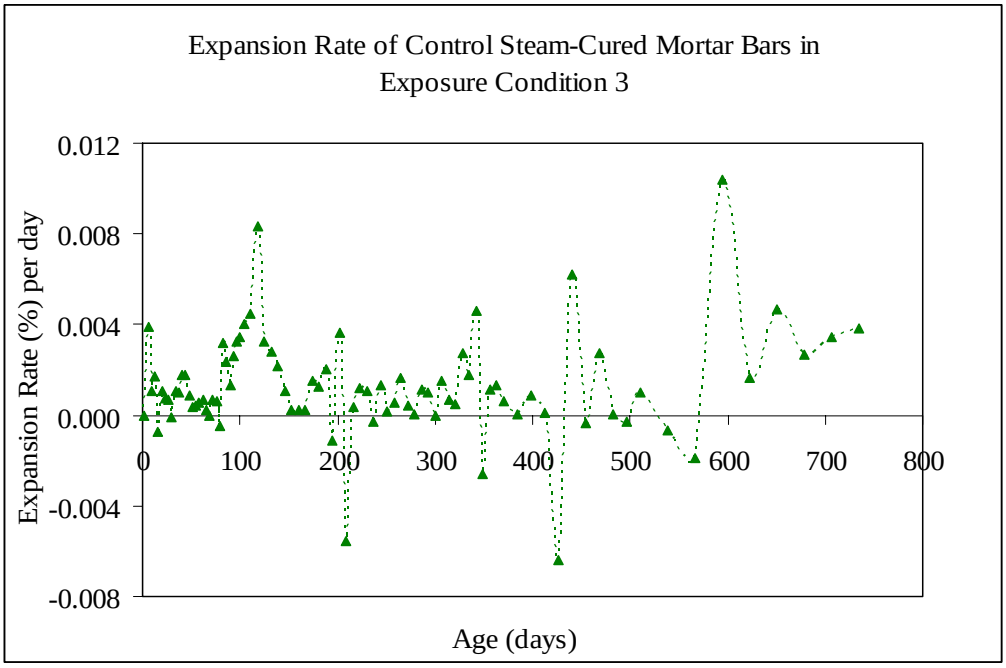


Figure 5.4: Expansion Rate of Mortar Bars Subjected to Duggan Heat Cycle and Stored in Moist Air Chamber, R.H maintained at 97%

The expansion at 21 days was about 0.132% for exposure condition 1, 0.104% for exposure condition 2 and 0.038% for exposure condition 3 (relative humidity of 97%). Expansion values of the mortar samples stored in exposure conditions 1 and 2 exceed the Duggan threshold value of 0.05% after 21 days. The differences observed in the expansive behavior are fully attributed to the different exposure conditions. These expansion results suggest that the mortar samples subjected to exposure conditions 1 and 2 have the potential for deterioration due to DEF. Just 100 days of storage in exposure condition 3 after the Duggan heat cycle, cracks started as isolated vertical or horizontal hairline cracks that later developed into pattern cracking as expansion progressed. The expansion is associated with the availability of water which also facilitates the formation of ettringite. Once the expansion takes place, the weakened mortar microstructure is likely to have low resistance to the expansion pressure, and the preexisting cracks may easily propagate to promote severe expansion (Shimada, 2005). The totally submerged mortar bars simply expanded monotonically, while the expansion of the mortar bars in relative humidity of 97% is delayed to 120 days. After 120 days, the mortar bars in relative humidity of 97% exhibited faster expansion rate which may be attributed to an increase in moisture condensation in the pores. Similar results were found by Shimada (2005). In the relative humidity of 97%, the potassium continually extracts moisture which reacts to form more ettringite. This is known as the potassium hygroscopic effect. There is constant leached of potassium from the mortar bars stored in exposure conditions 1 and 2.

Figure 5.5 shows damaged mortar bar ends in exposure condition 3. The damaged mortar ends can be attributed to the localized expansion due to a greater availability of moisture along the container walls of exposure condition 3 (Shimada, 2005). About 90% of the final expansion took place during the first 100 days of storage in exposure condition 1 (limewater) and 2 (plain water) after the Duggan heat cycle. The expansions at 700 days were 0.234%, 0.208% and 1.087% for mortar bars in exposure conditions 1, 2, and 3 respectively. It can be seen that the expansion results for mortar specimens stored in exposure conditions 1 and 2 showed similar expansion rates and seem to level off by 200 days. The highest expansion rates exhibited by mortar specimens were 0.0047%, 0.00485 and 0.5016% per day for exposure conditions 1, 2 and 3 respectively. Mortar specimens in exposure condition 3 observed the highest expansion rate, and showed higher expansion values.

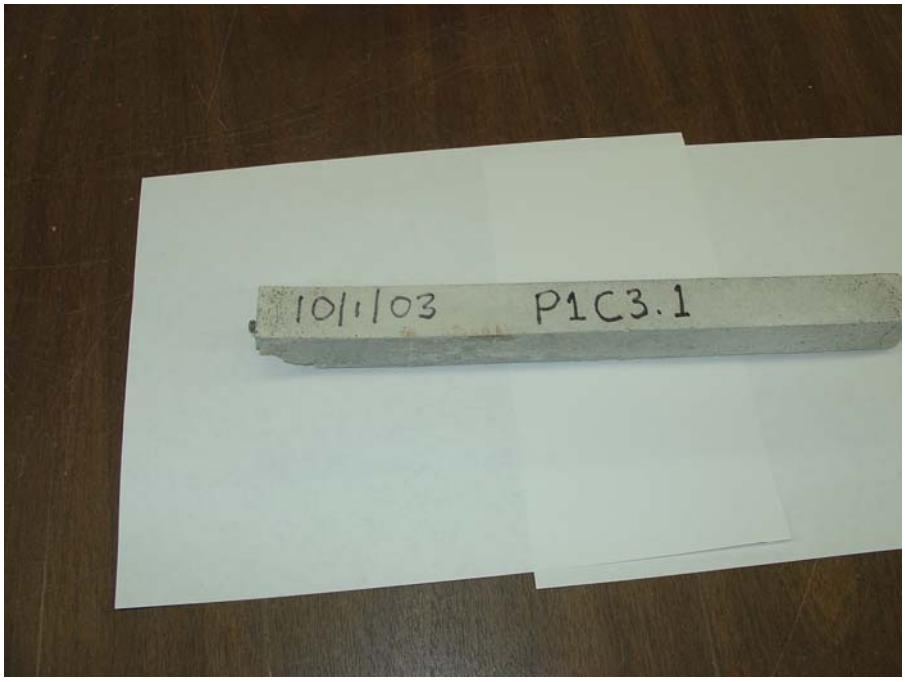


Figure 5.5: Damage Mortar Bar Stored in Relative Humidity at 97%

*5.3.1.2 Curve-Fitting Analysis*

For detailed characterization of the expansive behavior, the mean expansion data for the samples are plotted as a function of time and curve-fitted to numerical equations. The curve fitting analysis is for numerical representation and does represent any physical or chemical behaviors. Linear fits for each individual exposure condition are analyzed and plotted in Figures 5.6 through 5.8. Table 5.1 provides the results used for the best fit of the experimental data.

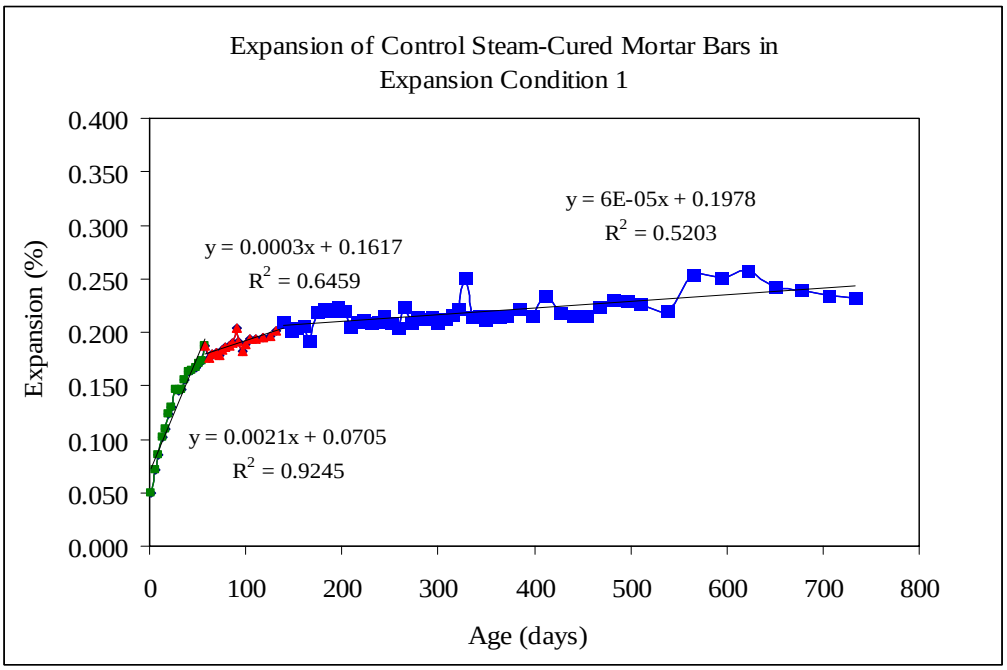


Figure 5.6: Expansion of Mortar Bars Subjected to Duggan Heat Cycle and Stored in Isothermal Water Bath, pH maintained at 12.5 – limewater (Regression Curves)

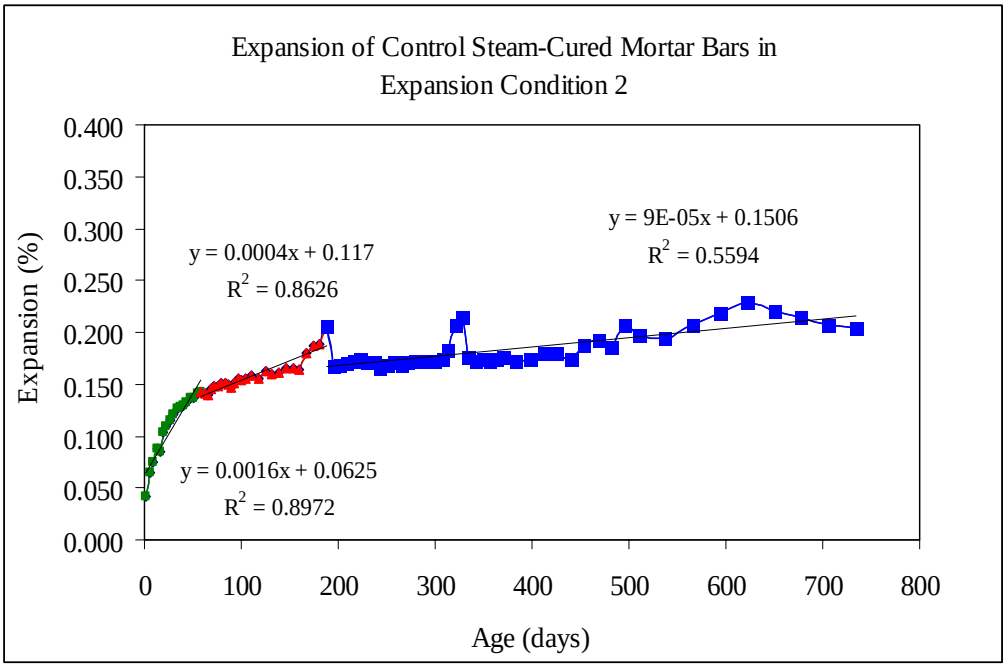


Figure 5.7: Expansion of Mortar Bars Subjected to Duggan Heat Cycle and Stored in Plain Water at Room Temperature (Regression Curves)

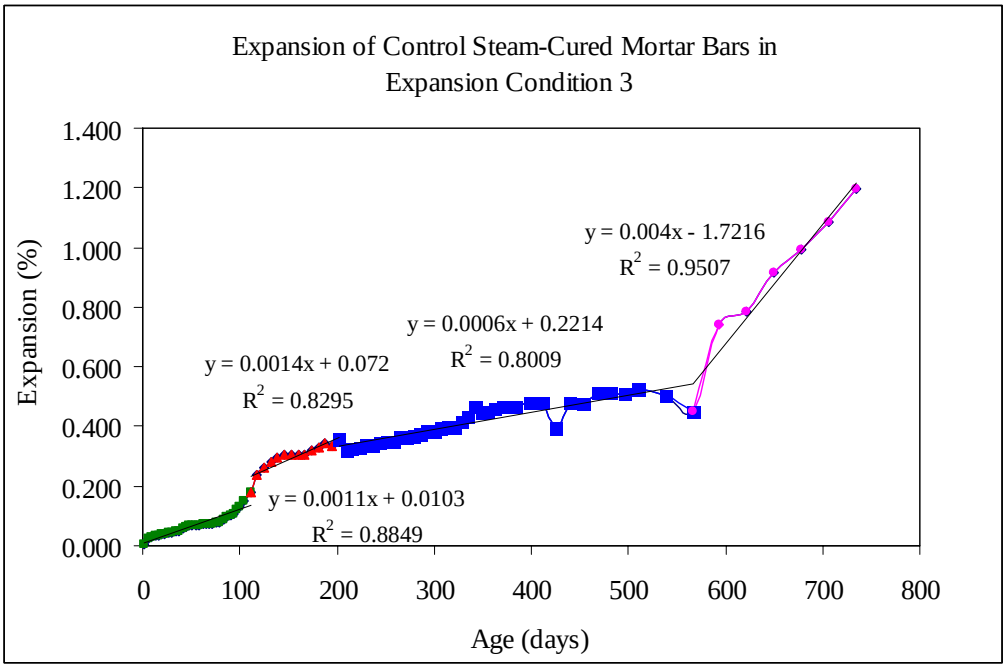


Figure 5.8: Expansion of Mortar Bars Subjected to Duggan Heat Cycle and Stored in a Moist Air Chamber, R.H maintained at 97% (Regression Curves)

Table 5.1: Linear Equations for Expansion vs. Age of Steam-Cured Mortar Bars Stored Under Different Exposure Conditions

| Phase 1 (Mortar Control Samples - Subjected to Duggan Heat Cycle) | | | | | |
|---|---|---|---|---|---|
| | | | | | |
| Exp. Cond. 1 | Maximum Expansion 0.26% | Curve 1 | Day 1 - 58 | y = 0.0021x + 0.0705 | $R^2$ = 0.9245 |
| | | Curve 2 | Day 58 - 139 | y = 0.0003x + 0.1617 | $R^2$ = 0.6459 |
| | | Curve 3 | Day 139 - 734 | y = 6E_05x + 0.1978 | $R^2$ = 0.5203 |
| | | | | | |
| Exp. Cond. 2 | Maximum Expansion 0.23% | Curve 1 | Day 1 - 58 | y = 0.0016x + 0.0625 | $R^2$ = 0.8972 |
| | | Curve 2 | Day 58 - 188 | y = 0.0004x + 0.117 | $R^2$ = 0.8626 |
| | | Curve 3 | Day 188 - 734 | y = 9E_05x + 0.1506 | $R^2$ = 0.5594 |
| | | | | | |
| Exp. Cond. 3 | Maximum Expansion 1.20% | Curve 1 | Day 1 - 111 | y = 0.0011x + 0.0103 | $R^2$ = 0.8849 |
| | | Curve 2 | Day 111 - 202 | y = 0.0014x + 0.072 | $R^2$ = 0.8295 |
| | | Curve 3 | Day 202 - 566 | y = 0.0039x + 1.087 | $R^2$ = 0.8009 |
| | | Curve 4 | Day 566 - 734 | y = 0.0004x - 1.7216 | $R^2$ = 0.9507 |

The best correlation coefficient for mortar specimens in exposure conditions 1 and 2 was obtained by using 3 linear regression curves to give the best fit for the expansion data results. For the mortar specimens stored in exposure condition 3 (R.H of 97%), four (4) linear regression curves were used to analyze the expansion data. The expansion data results yield good correlation coefficients for the first 200 days after the Duggan heat cycle. This can be used to predict the effect of mortar test parameters on expansive behavior using the same materials, mixing proportions and test methods. Any difference in expansion behaviors of the mortar bars is attributed to the difference exposure conditions.

### *5.3.2 Weight Change Results*

#### *5.3.2.1 Weight Change Measurements*

The formation of ettringite involves the uptake of water, which results in permanent weight gain of the specimen. The weight gain during the early stage of storage is mostly determined by the cement hydration behavior, leading not only to ettringite formation but also to the formation of various hydrated phases (Shimada, 2005). The weight change of mortar specimens is shown in Figure 5.9 under different exposure conditions. Mortar specimens stored in exposure condition 3 showed rapid varying increases in weight change and did not stabilize throughout the entire research. This can be attributed to be weight gain through formation of ettringite and hydration of unhydrated cement particles.

After just one (1) day of storage, specimens in exposure conditions 1 and 2 showed very significant weight changes reaching about 10%. This might be attributed to the uptake of water by the mortar specimens after Duggan heat cycle leading to relatively weight gain. Mortar specimens in exposure condition 3 (R.H maintained at 97%) showed less significant weight gain of about 2%. Both exposure conditions 1 and 2 showed similar weight change patterns. A significant jump in weight-gain occurred between 37 and 41 days by mortar specimens in exposure condition 3. This can be attributed to the sudden weight gain associated with the formation of ettringite which has a water-rich composition. The specimens exhibited an average weight gain of 3.84% during that interval.

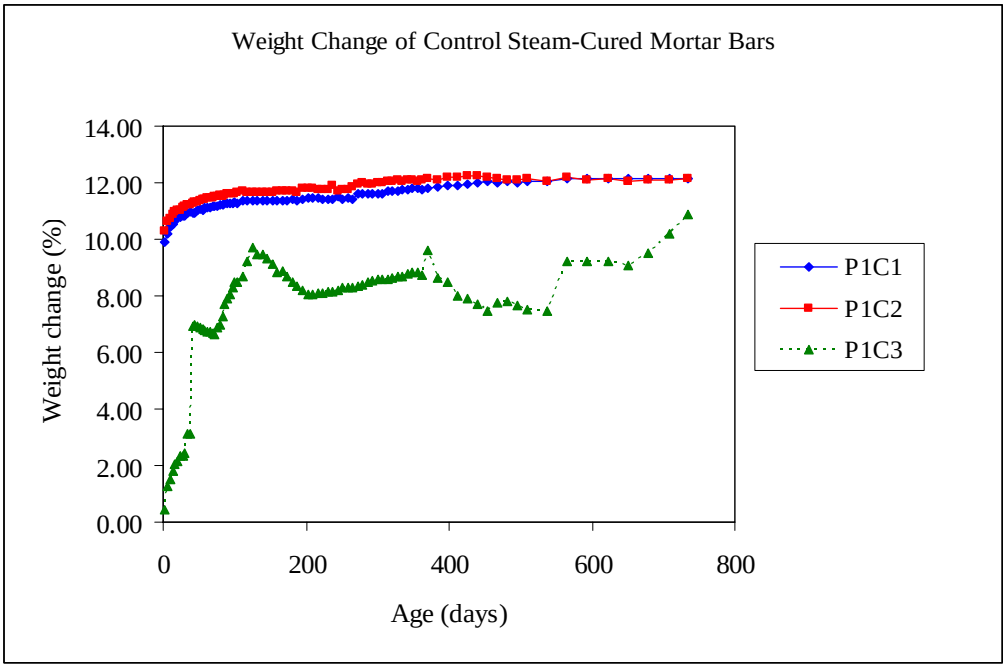


Figure 5.9: Weight Change of Mortar Bars Subjected to Duggan Heat Cycle and Stored Under Different Exposure Conditions

Both exposure conditions 1 and 2 show similar weight change patterns. From 1 day to 100 days, the weights of the mortar specimens showed significant increases in all three exposure conditions. The weight changes at 100 days were 11.31% for exposure condition 1, 11.61% for exposure condition 2, and 8.31% for exposure condition 3. From 100 days on, the weight change seems to level off for the mortar bars in exposure conditions 1 and 2. As noted earlier, 90% of the expansion values of the mortar bars in exposure conditions 1 and 2 were observed during the first 100 days. Therefore, no significant weight gain after 100 days can be attributed to lack of serve paste expansion which introduces various structural defects. These structural defects are filled with the storage solution which results in an increase in weight gain.

Mortar bars in exposure conditions 1, 2 and 3 showed maximum weight changes of 12.16%, 12.23% and 10.87% respectively.

*5.3.2.2 Curve-Fitting Analysis*

Linear regressions were employed to obtain the best fit for the experimental data. Two linear regression curves were used to best fit the weight change data of the mortar bars. Figures 5.10, 5.11 and 5.12 show the linear regression curves, while Table 5.2 provides the regression equations used for the data analysis.

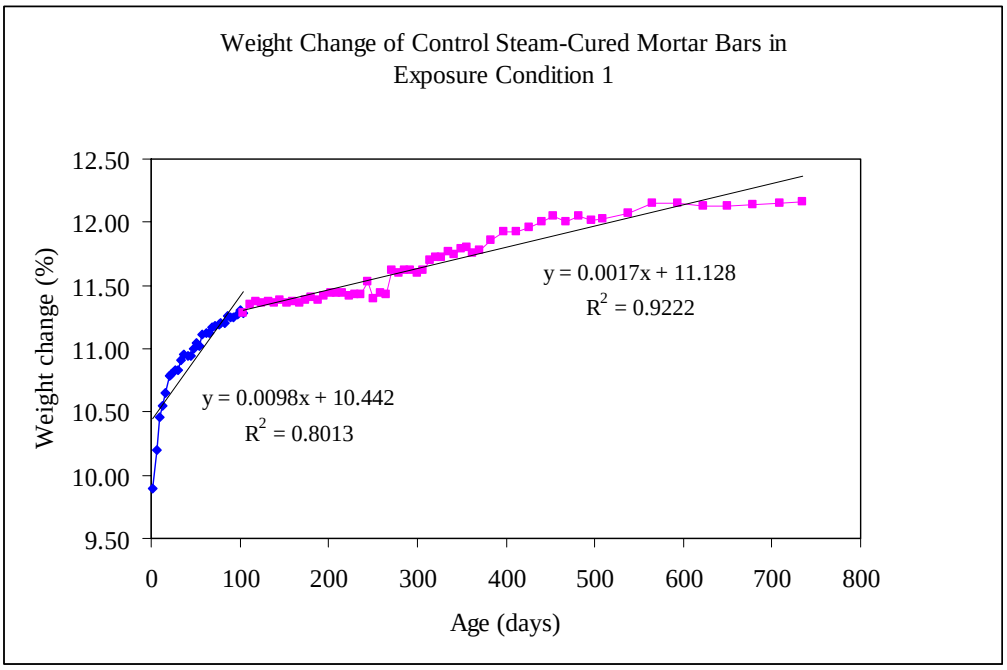


Figure 5.10: Weight Change of Mortar Bars Subjected to Duggan Heat Cycle and Stored in Isothermal Water Bath, pH maintained at 12.5 - limewater (Regression Curves)

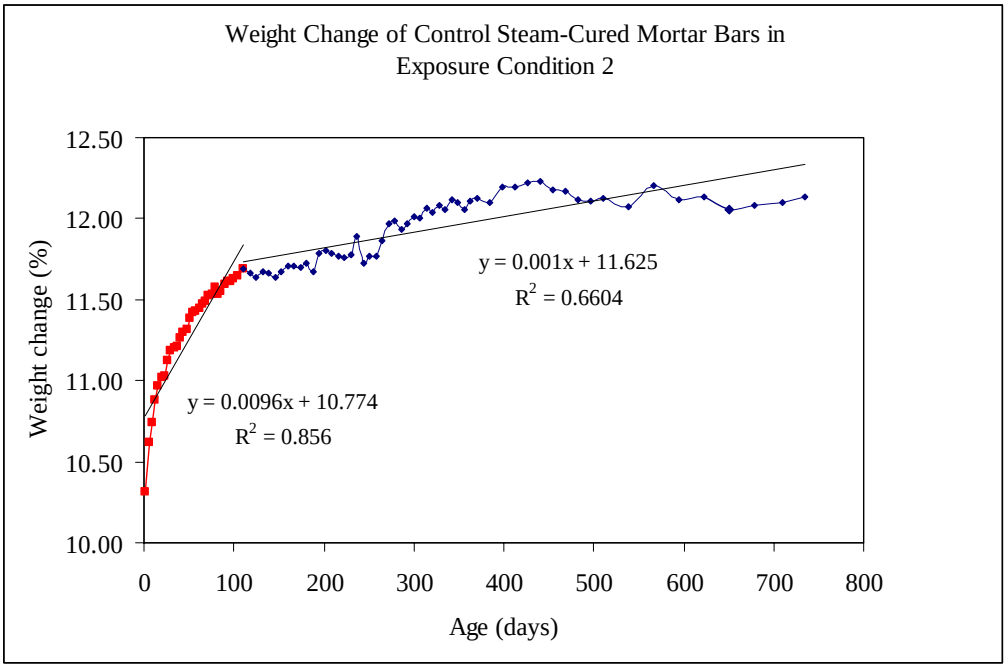


Figure 5.11: Weight Change of Mortar Bars Subjected to Duggan Heat Cycle and Stored in Plain Water at Room Temperature (Regression Curves)

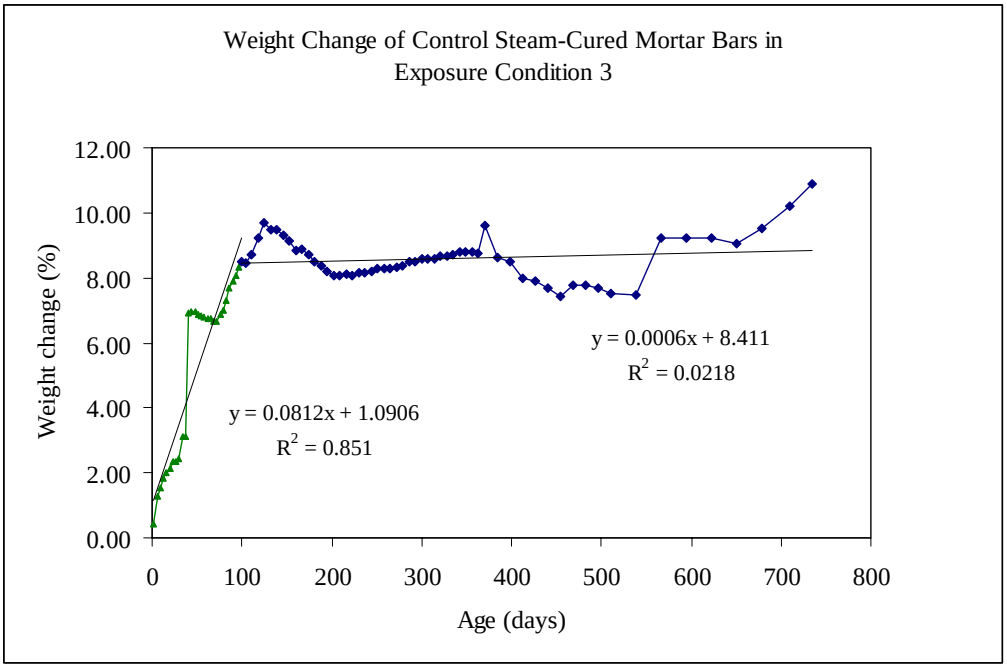


Figure 5.12: Weight Change of Mortar Bars Subjected to Duggan Heat Cycle and Stored in a Moist Air Chamber, R.H maintained at 97% (Regression Curves)

Table 5.2: Linear Equations for Weight Change vs. Age of Steam-Cured Mortar Bars Stored Under Different Exposure Conditions

| Phase 1 (Mortar Control Samples - Subjected to Duggan Heat Cycle) | | | | | |
|---|---|---|---|---|---|
| | | | | | |
| Exp. Cond. 1 | Max. 12.16% | Curve 1 | Day 1 - 104 | y = 0.0098x + 10.442 | $R^2$ = 0.8013 |
| | | Curve 2 | Day 104 - 734 | y = 0.0017x + 11.128 | $R^2$ = 0.9222 |
| | | | | | |
| Exp. Cond. 2 | Max. 12.23% | Curve 1 | Day 1 - 111 | y = 0.0096x + 10.774 | $R^2$ = 0.856 |
| | | Curve 2 | Day 111 - 734 | y = 0.0001x + 11.625 | $R^2$ = 0.6604 |
| | | | | | |
| Exp. Cond. 3 | Max. 10.87% | Curve 1 | Day 1 - 100 | y = 0.0812x + 1.0906 | $R^2$ = 0.851 |
| | | Curve 2 | Day 100 - 734 | y = 0.0006x + 8.411 | $R^2$ = 0.0218 |

*5.3.3 Expansion and Weight Change*

Expansion and weight change measurements were monitored to investigate for any correlation of expansion of mortar bars resulting in formation and growth of ettringite. Grattan-Bellew et al concluded that a linear correlation exists between mass change and expansion over the period from 17 to 59 days (1998). A model was developed by Shimada based on the assumption that any extra volume created by paste expansion is filled with storage solution, under which the mortar specimens are fully submerged (2005). Shimada's model suggests a linear relationship exists between the weight-change and the degree of expansion. Figure 5.13 shows the results of expansion and weight changes under the different exposure conditions.

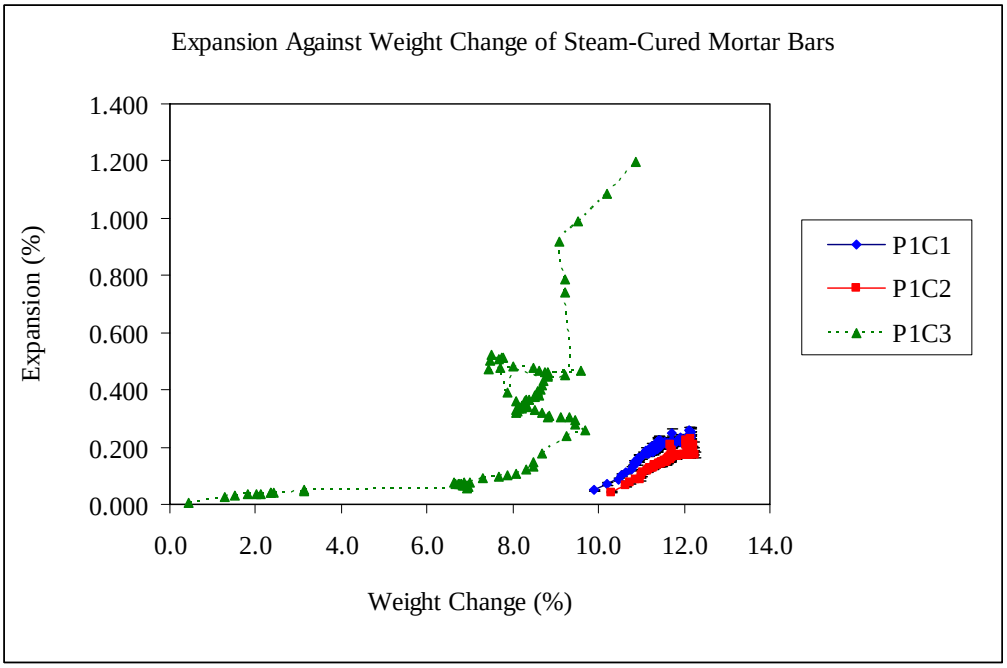


Figure 5.13: Expansion Against Weight Change of Mortar Bars Subjected to Duggan Heat Cycle and Stored Under Different Exposure Conditions

From the scatter plots of the results, linear regression curves were applied to obtain correlation between the expansion and weight changes of the mortar specimens stored under different exposure conditions. Figures 5.14, 5.15 and 5.16 show the linear curves of the control mortar bars' results for the different exposure conditions. Table 5.3 shows the regression equations for the different exposure conditions. Analysis of the results revealed a high positive linear correlation exists between expansion and weight-change of the mortar samples for the first 100 days. However, it can be speculated that observed significant weight-change might be due to ettringite formation and trapping of water in the cracks in the mortar during the expansion process. Other researchers such as Zhang et al. also observed expansion of mortar bars due to formation of ettringite accompanied by significant weight gain (1999).

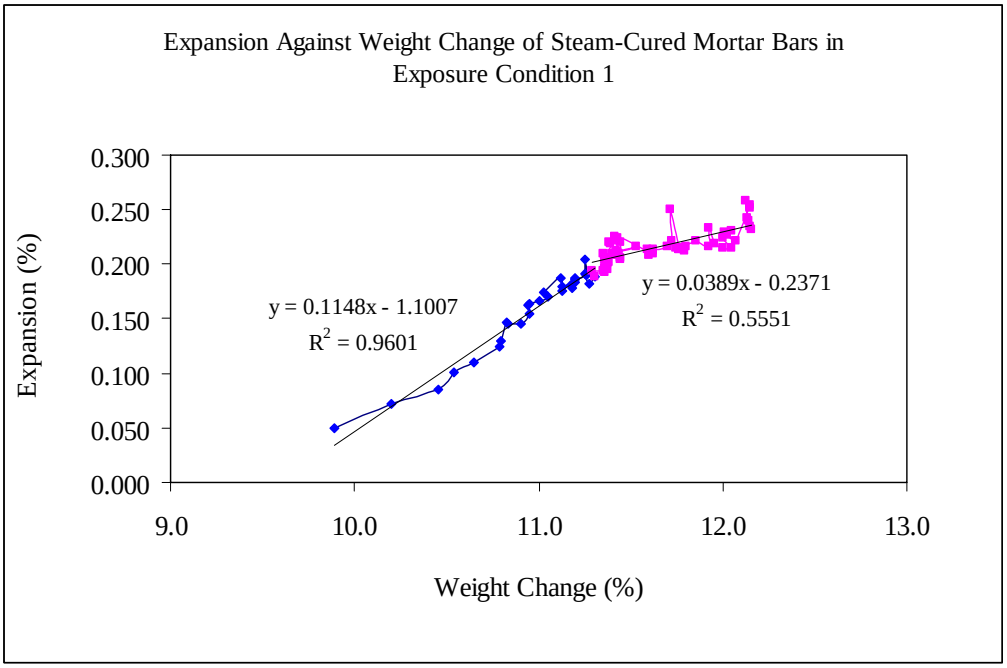


Figure 5.14: Expansion Against Weight Change of Mortar Bars Subjected to Duggan Heat Cycle and Stored in Isothermal Water Bath, pH maintained at 12.5 – limewater (Regression Curves)

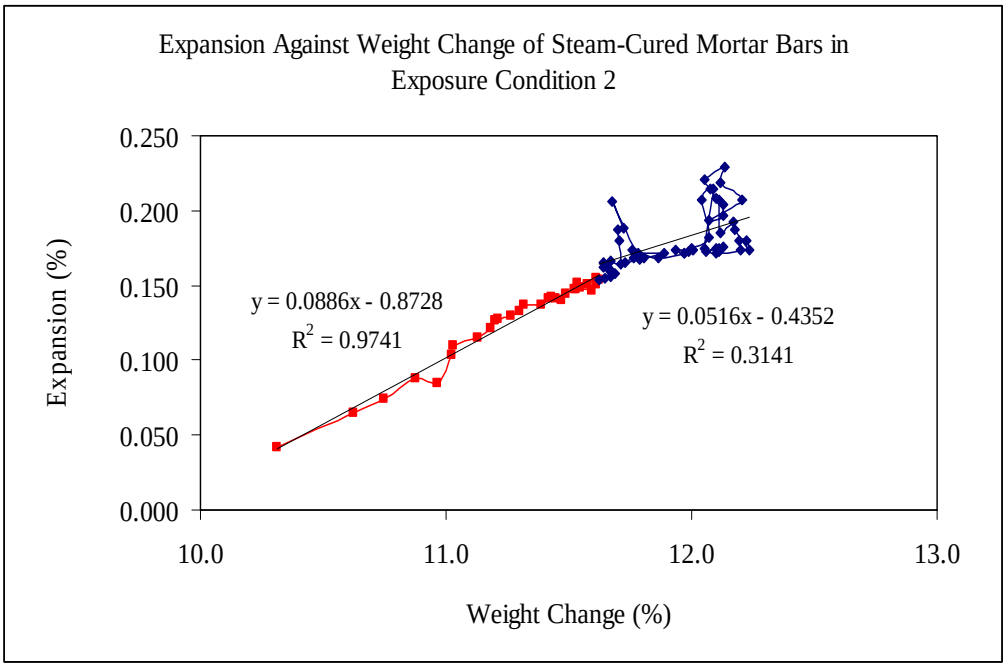


Figure 5.15: Expansion Against Weight-Change of Mortar Bars Subjected to Duggan Heat Cycle and Stored in Plain Water at Room Temperature (Regression Curves)

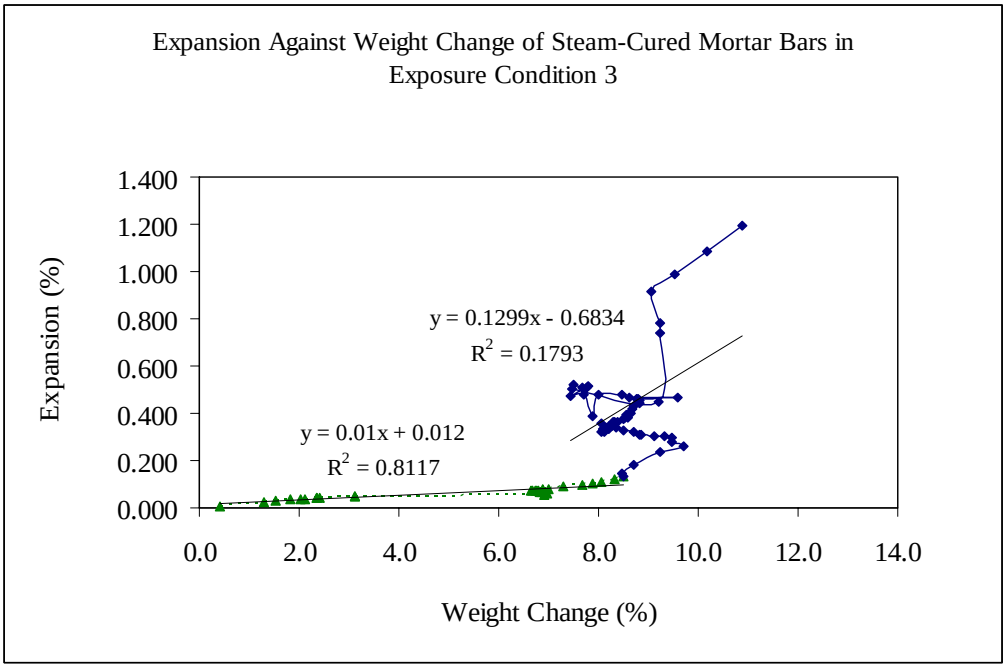


Figure 5.16: Expansion Against Weight Change of Mortar Bars Subjected to Duggan Heat Cycle and Stored in a Moist Air Chamber, R.H maintained at 97% (Regression Curves)

Table 5.3: Linear Equations for Expansion vs. Weight Change of Steam-Cured Mortar Bars Stored Under Different Exposure Conditions

| Phase 1 (Mortar Control Samples - Subjected to Duggan Heat Cycle) | | | | |
|---|---|---|---|---|
| | | | | |
| Exp. Cond. 1 | Curve 1 | Day 1 - 100 | y = 0.1148x - 1.1007 | $R^2$ = 0.9601 |
| | Curve 2 | Day 100 - 734 | y = 0.0389x - 0.2371 | $R^2$ = 0.5551 |
| | | | | |
| Exp. Cond. 2 | Curve 1 | Day 1 - 100 | y = 0.0886x - 0.8728 | $R^2$ = 0.9741 |
| | Curve 2 | Day 100 - 734 | y = 0.0516x + 0.4352 | $R^2$ = 0.3141 |
| | | | | |
| Exp. Cond. 3 | Curve 1 | Day 1 - 100 | y = 0.01x + 0.012 | $R^2$ = 0.8117 |
| | Curve 2 | Day 100 - 734 | y = 0.1299x - 0.6834 | $R^2$ = 0.1793 |
| | | | | |

*5.3.4 Compressive Strength Results*

The compressive strength results of the heat-cured mortar specimens subjected to Duggan heat cycle and then stored under different exposure conditions is shown in figure 5.17. The mortar cubes were surface dried with paper towel before testing. The compressive strength of the mortar cubes were 5745 psi, 5475 psi and 6072 psi after 28 days of storage in exposure conditions 1, 2 and 3 respectively. A 25% increase in strength was observed at 365 days after storage. The expansion values after 365 days were less than 0.5% and do not cause significant damage to the mortar microstructure to warrant a loss in strength. In 1999, Zhang concluded that the later age strength of the mortar specimens increased after early heating, and the magnitude of increase is higher at higher heating temperatures. These results suggest that the compressive strength is adversely affected by the different exposure conditions. Table 5.4 gives the calculated averages and standard deviation (Std) of the compressive strength results. The mortar samples in relative humidity of 97% (Exp. Cond. 3) exhibit the highest compressive strength.

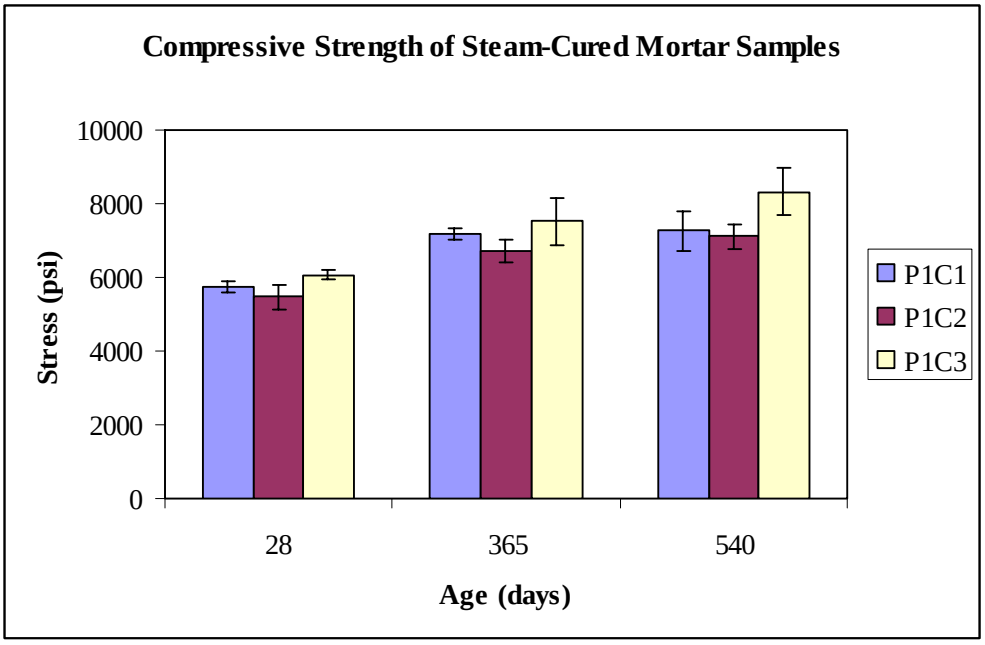


Figure 5.17: Compressive Strength Chart of Mortar Samples Subjected to Duggan Heat Cycle and Stored Under Different Exposure Conditions

Table 5.4: Compressive Strength of Mortar Samples Subjected to Duggan Heat Cycle and Stored Under Different Exposure Conditions

| | Average Compressive Strength (psi) | | |
|---|---|---|---|
| | 28 Days | 365 Days | 540 Days |
| | Std | Std | Std |
| P1C1 | 5745 | 7188 | 7267 |
| | 155 | 140 | 546 |
| P1C2 | 5475 | 6708 | 7125 |
| | 334 | 315 | 331 |
| P1C3 | 6072 | 7517 | 8333 |
| | 145 | 649 | 641 |

*5.4 Field Samples (No Duggan Heat Cycle)*

Two batches of mortar were mixed and subjected to atmospheric conditions outside the laboratory. The first batch (P1C4A) was steam-cured at 85$^{o}$C, then subsequently stored in water for six (6) days and stored outside the laboratory. The second batch (P1C4B) was cured in the laboratory at room temperature for 24 hours and then stored under water for six (6) days prior to exposure to field conditions. None of the batch mixes were subjected to the Duggan heat cycle. All other parameters such as mix proportion and cement type were unaltered.

*5.4.1 Length Change Results*

Figures 5.18 and 5.19 shows change in length and shrinkage rate of the mortar bars prepared in the laboratory and then exposed to field conditions. Different curing conditions were used for each set of mortar samples. For the research duration, both mortar samples showed shrinkage. Steam-cured mortar samples exhibited lower shrinkage values than those cured at room temperature. The maximum shrinkage rate of the mortar bars were 0.0090% and 0.0083% per day for steam-cured and room temperature cured respectively. Visual examination showed no cracks in the mortar samples stored under field conditions.

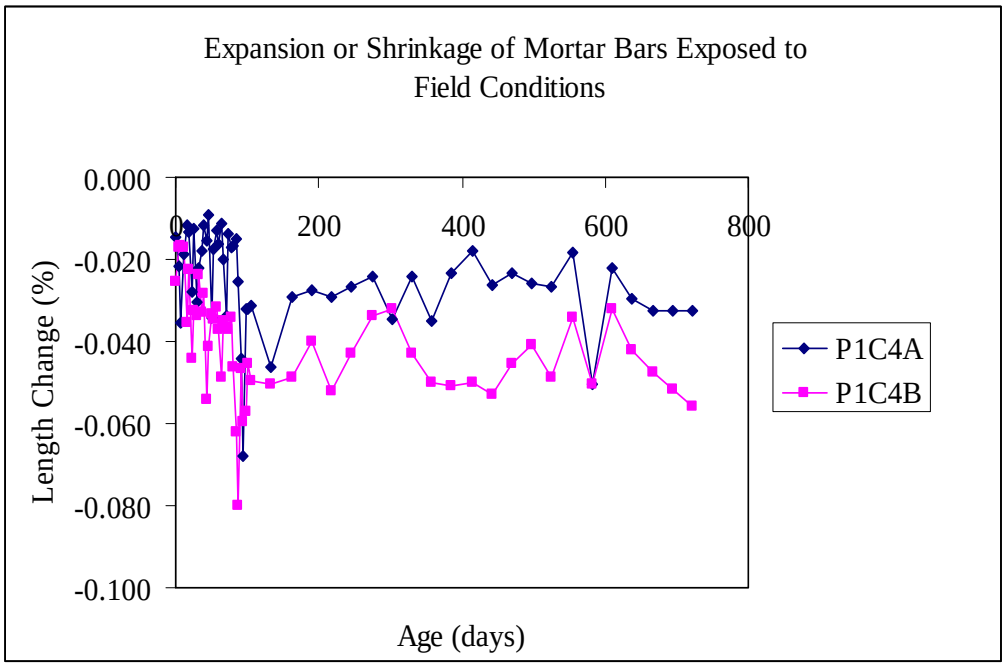


Figure 5.18: Length Change of Mortar Bars Exposed to Field Conditions

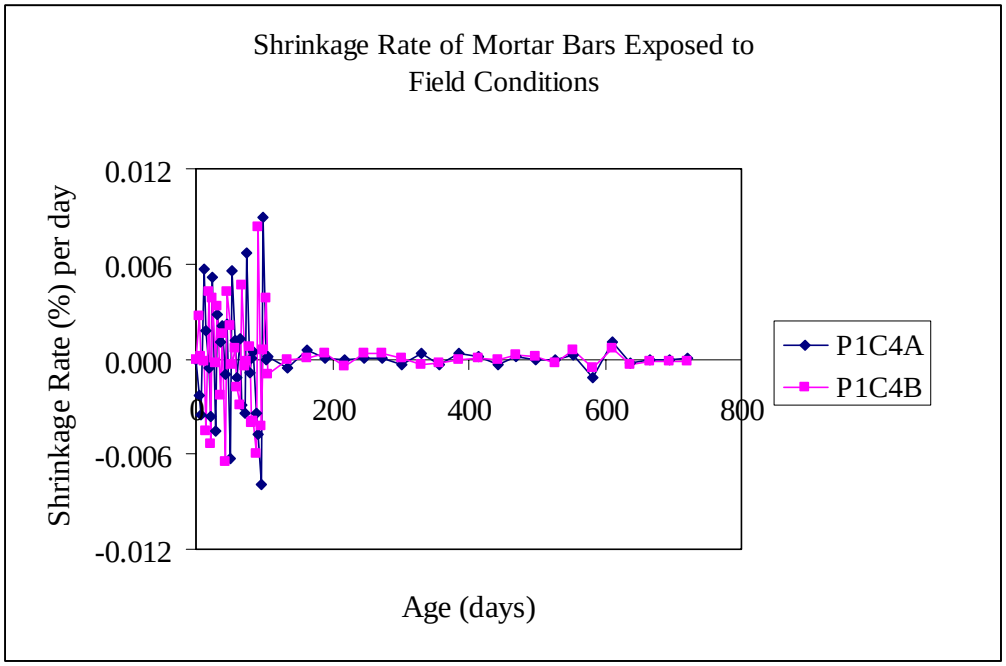


Figure 5.19: Shrinkage Rate of Mortar Bars Exposed to Field Conditions

The linear regression curves of the field-exposed mortar samples are shown in figures 5.20 and 5.21. Table 5.5 illustrates the linear equations for the best fit to the experimental data. None of the regression analysis performed could be regarded as a best fit to the data. The experimental data points exhibit little or no correlation between shrinkage and time (duration of exposure) for the mortar samples exposed to field conditions.

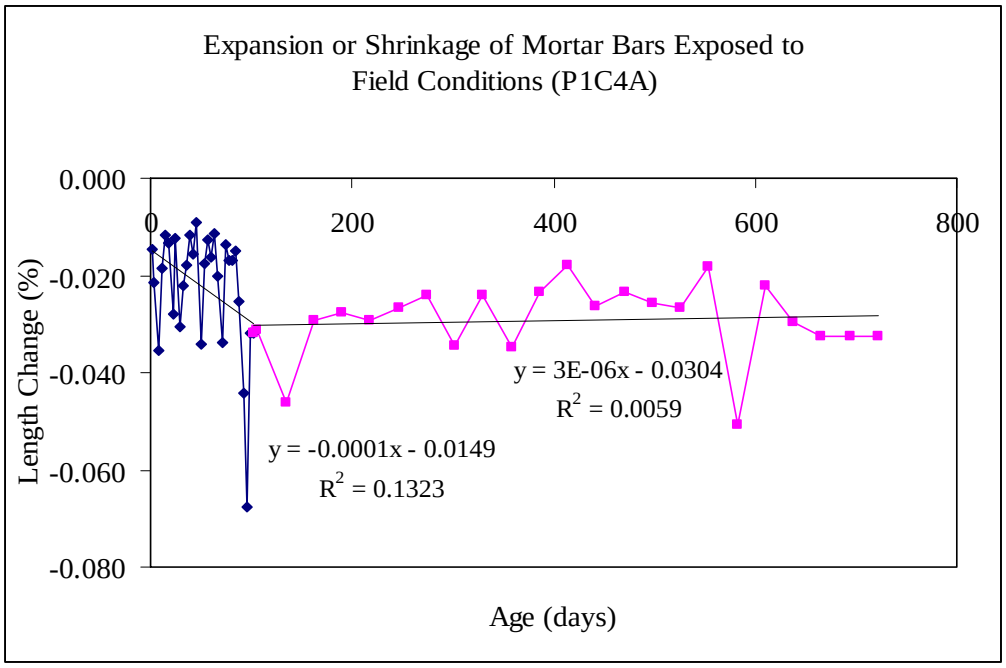


Figure 5.20: Length Change vs. Age of Steam-Cured Mortar Bars and Stored Under Field Conditions (C4A) (Regression Curves)

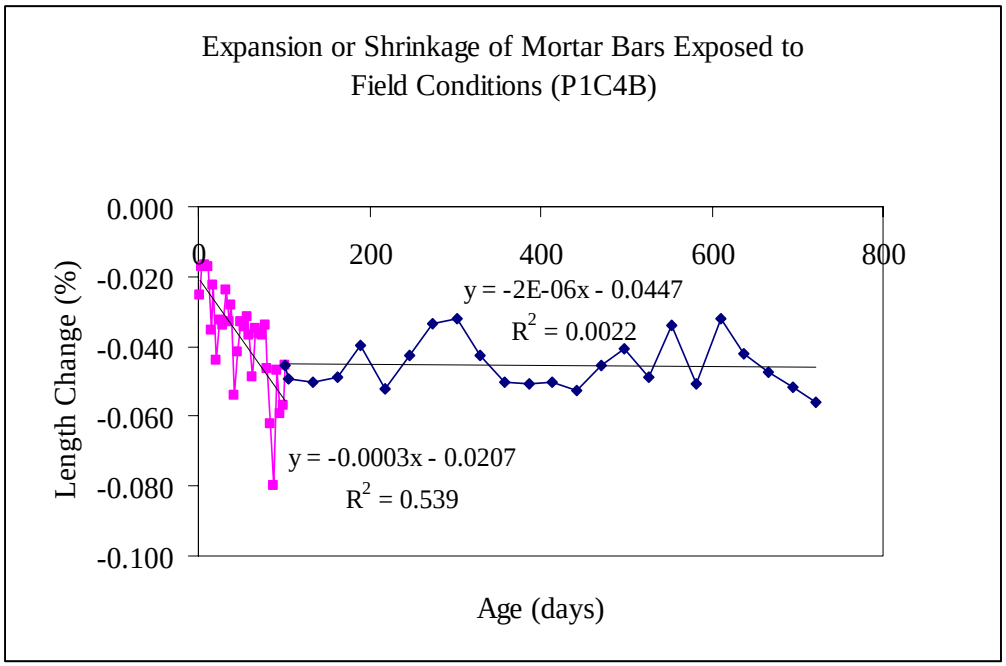


Figure 5.21: Length Change vs. Age of Room Temperature-Cured Mortar Bars and Stored Under Field Conditions (C4B) (Regression Curves)

Table 5.5: Linear Equations for Length Change vs. Age of Mortar Bars Stored Under Field Conditions

| Phase 1 (Mortar Control Samples Exposed to Field Conditions) | | | | |
|---|---|---|---|---|
| | | | | |
| Exp. Cond. 4A | Curve 1 | Day 1 - 100 | y = -0.0001x - 0.0149 | $R^2$ = 0.1323 |
| | Curve 2 | Day 100 - 722 | y = 3E-06x - 0.0304 | $R^2$ = 0.0059 |
| | | | | |
| Exp. Cond. 4B | Curve 1 | Day 1 - 100 | y = -0.0003x - 0.0207 | $R^2$ = 0.539 |
| | Curve 2 | Day 100 - 722 | y = -2E-06x - 0.0447 | $R^2$ = 0.0022 |
| | | | | |

*5.4.2 Weight Change Results*

Weight-change measurements of the mortar samples were monitored for both sets. Figure 5.22 shows the weight-change results for the field-exposed mortar samples. Mortar samples in exposure condition 4B exhibit a higher weight-change than those in exposure condition 4A. Both sets of mortar samples show a decrease in weight of the mortar samples for the entire research period. It seems that the weight fluctuates throughout with no defined pattern. This can be attributed to the various environmental changes such as temperature, humidity, etc. occurring in the field.

Figure 5.23 and 5.24 illustrate the regression curves for the best fit for the data. From the linear and polynomial equations provided in Table 5.6, there exists little or no correlation between weight-change and time (duration of exposure). The fluctuation of the weight-change of the mortar samples shows the influence of the constantly changing atmospheric conditions outside.

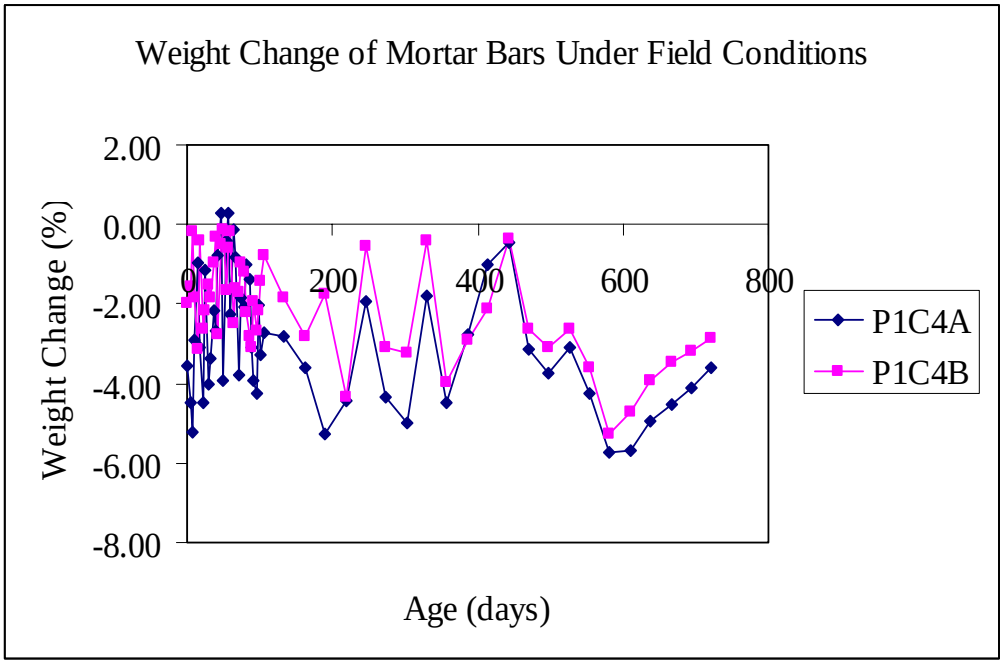


Figure 5.22: Weight Change of Mortar Samples Exposed to Field Conditions

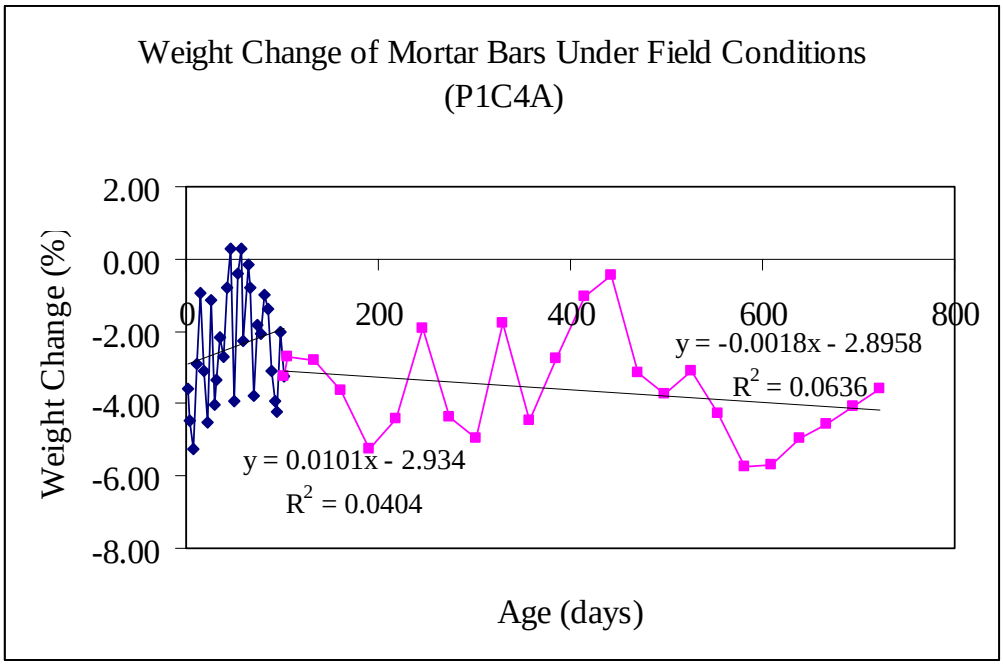


Figure 5.23: Weight Change vs. Age of Steam-Cured Mortar Bars and Stored Under Field Conditions (C4A) (Regression Curves)

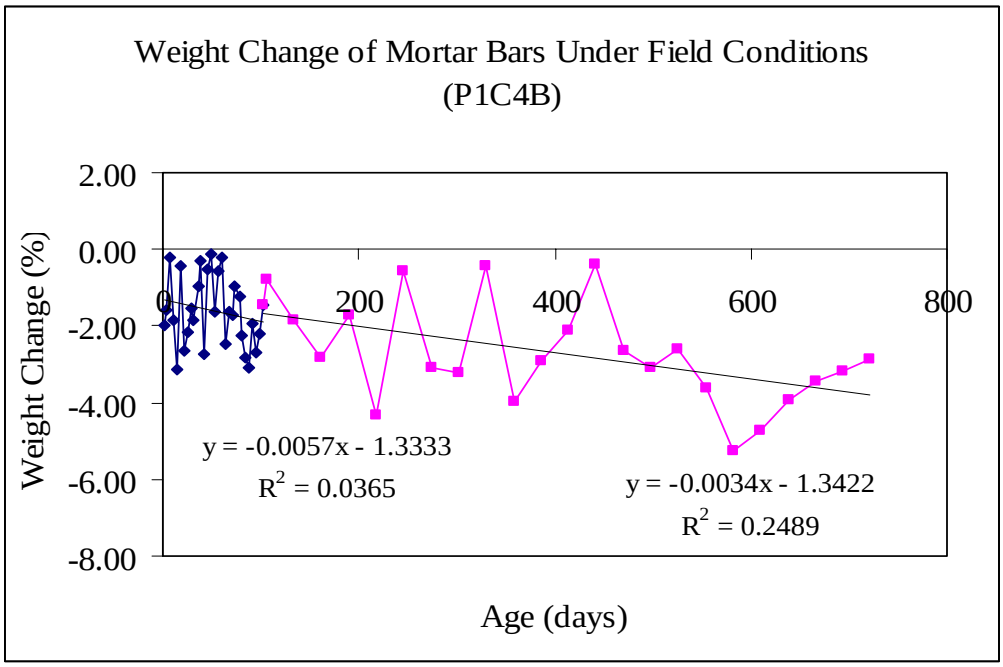


Figure 5.24: Weight Change vs. Age of Room Temperature-Cured Mortar Bars and Stored Under Field Conditions (C4B) (Regression Curves)

Table 5.6: Linear Equations for Weight Change vs. Age of Mortar Bars Stored Under Field Conditions

| Phase 1 (Mortar Control Samples - Subjected to Duggan Heat Cycle) | | | | |
|---|---|---|---|---|
| Exp. Cond. 4A | Curve 1 | Day 1 - 100 | y = 0.0101x - 2.934 | $R^2$ = 0.0404 |
| | Curve 2 | Day 100 - 722 | y = -0.0018x -2.8958 | $R^2$ = 0.0636 |
| Exp. Cond. 4B | Curve 1 | Day 1 - 100 | y = -0.0057x - 1.3333 | $R^2$ = 0.0365 |
| | Curve 2 | Day 100 - 722 | y = -0.0034x - 1.3422 | $R^2$ = 0.2489 |

*5.4.3 Compressive Strength Results*

The mortar specimens steam-cured at 85°C exhibited an average compressive strength of 6280 psi at 28 days, while the room temperature cured mortar specimens exhibited an average compressive strength of 6996 psi at 28 days. There is a 35% increase in strength of the mortar specimens tested at a later age. Figure 5.25 shows the effect of curing on the strength of the field exposure mortar specimens. The room temperature-cured mortar specimens have even higher compressive strengths than those steam-cured at 85°C. The increased in compressive strength can be due to the non-existence of severe expansion or observed structural defects which would warrant a loss in strength. Table 5.8 shows the compressive strength results of the mortar samples subjected to field conditions.

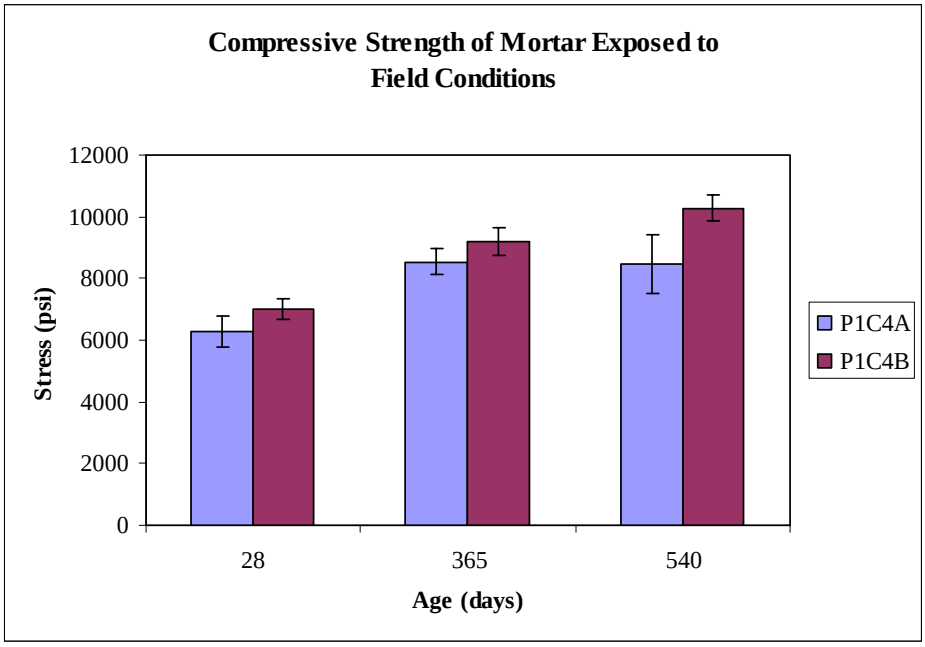


Figure 5.25: Compressive Strength Chart of Mortar Samples Subjected to Field Conditions

Table 5.7: Compressive Strength of Mortar Samples Stored Under Field Conditions

| | Average Compressive Strength (psi) | | |
|---|---|---|---|
| | 28 Days | 365 Days | 540 Days |
| | Std | Std | Std |
| P1C4A | 6280 | 8525 | 8467 |
| | 516 | 421 | 972 |
| P1C4B | 6996 | 9200 | 10283 |
| | 343 | 436 | 413 |

*5.5 Water Analysis of Storage Solutions*

Water analysis was performed using ion selective electrodes (ISE) and an ISE meter to obtain readings of the ion concentrations in the storage solutions of the respective exposure conditions. Potassium ($K^+$), Sodium ($Na^+$) and Calcium ($Ca^{2+}$) ion concentrations in the storage solutions were monitored periodically for depletion of alkali content. Also the pH values were monitored for exposure condition 2 to predict their effects on DEF. Analyzing the results of these selected variances may help in understanding the influence of the storage conditions after the heat treatment.

*5.5.1 Water Analysis of Exposure Condition 1*

Mortar samples stored in isothermal water bath, with pH maintained at 12.5 (exposure condition 1), were monitored for leaching of $Na^+$ (sodium) and $K^+$ (potassium) into the storage solution. The highest concentration of leached alkalis [$Na^+ + K^+$] was about 175 mmol/l for the duration of the research. The measured $Na^+$ and $K^+$ concentrations in the storage solution increased with time for the storage period. Similar results were confirmed by Famy et al in their research study of

storage conditions on dimensional changes of heat-cured mortars (2001). Ettringite does not exist without loss of alkali in normal cementations materials and can be stable in very high pH environment (Damidot and Glasser, 2005). The presence of alkalis also greatly suppressed the dissolution of calcium hydroxide (CH) but enhanced the formation of ettringite (Fu et al. 1996). Figure 5.26 shows the alkalis' concentration against age for the mortar samples in exposure condition 1.

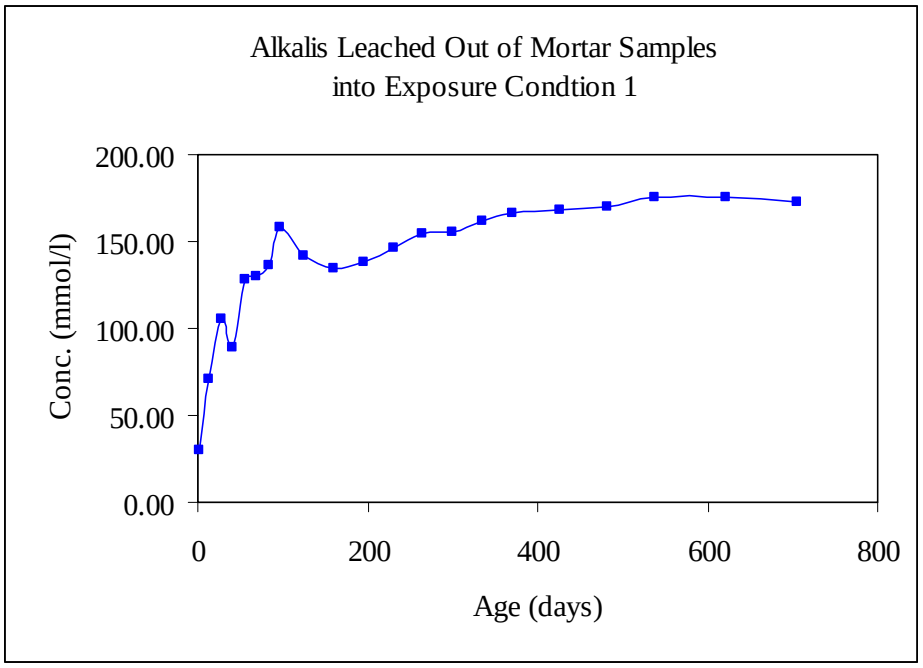


Figure 5.26: Alkalis Leaching from Mortar Samples Stored in Isothermal Water Bath, pH maintained at 12.5 - limewater

*5.5.2 Water Analysis of Exposure Condition 2*

Mortar samples stored in exposure condition 2 (plain water at room temperature) were monitored for pH value, $Na^{+}$, $K^{+}$ and $Ca^{2+}$ ion concentrations.

*5.5.2.1 Amount of Alkalis*

Again, the amount of alkalis leached increased with time for the mortar samples stored in exposure condition 2. For the mortar samples stored in exposure condition 2 (plain water) about most of the alkalis are leached out during the first 100 days of storage. Famy et al. estimated that about 80% of the $K^+$ and 60% of the $Na^+$ were leached into the water for the first 10 days of storage (2001). Figure 5.27 illustrates the change in alkalis concentration leached out of the mortar samples over time.

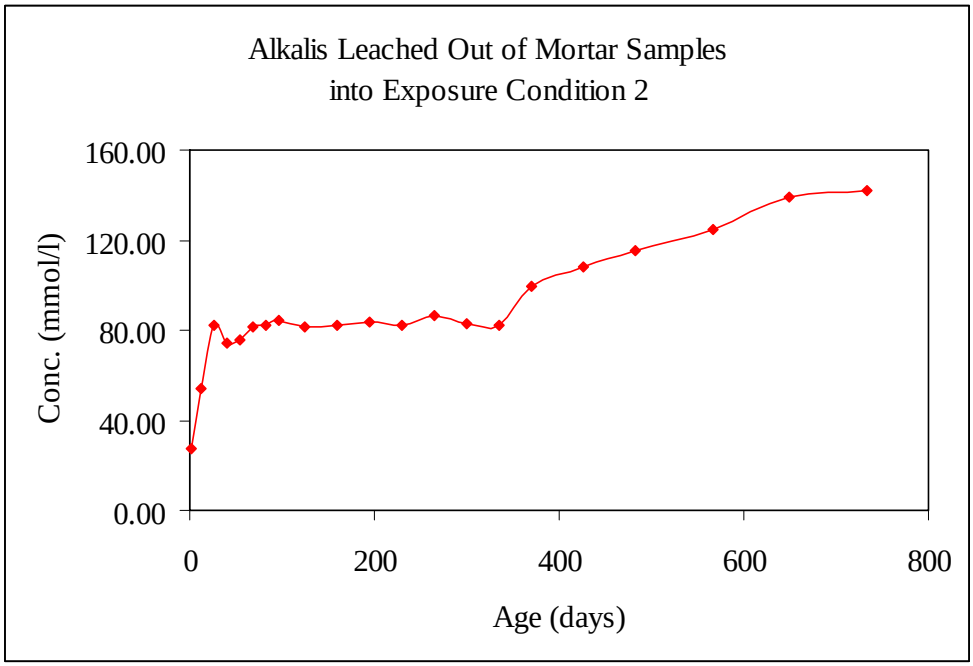


Figure 5.27: Alkalis Leaching from Mortar Samples Stored in Plain Water at Room Temperature

*5.5.3.2 pH Value*

The pH value of the storage solution ranged from 8.57 to 12.23 for the research duration. The pH value has effects on the morphology of ettringite. A decrease in pH of the mortar system due to alkali leaching may favor the conversion from monosulfate to renewed ettringite (Shimada, 2005). Hampson and Bailey concluded that at pH 11.5 to 11.8, sulphoaluminate forms as ettringite crystals and, at pH 12.5 to 12.8, some non-crystalline materials might form with a composition similar to ettringite (1982). Ettringite was able to form in alkaline solution at pH of 13.3 at normal temperatures and at alkali concentration as low as 0.08M (Fu et al. 1999).

*5.5.2.3 Calcium Concentration*

Various researchers have mentioned that calcium is essential to the ASR process (Chatterji et al. 1987, Diamond 1989, Struble 1987 and Kilgour 1988). They also illustrated that the presence of $Ca(OH)_2$ seems to be essential for sodium and other ions to penetrate into the reacting grain inside the concrete microstructure. The formation of the reaction gel can take place without deleterious expansion of concrete or mortar depending on the amount and availability of the $Ca^{2+}$ ion. Figure 5.28 gives the calcium concentration of the storage solution for exposure condition 2. The highly alkaline pore solution depressed the calcium being leached out into the solution to negligible concentrations. However, the formation of ettringite may also significantly affect the calcium being into the storage solution. The drastic increase in calcium

observed after 300 days can be attributed to renewed ettringite formation. The calcium concentration seems to reach a plateau after 400 days of storage in water.

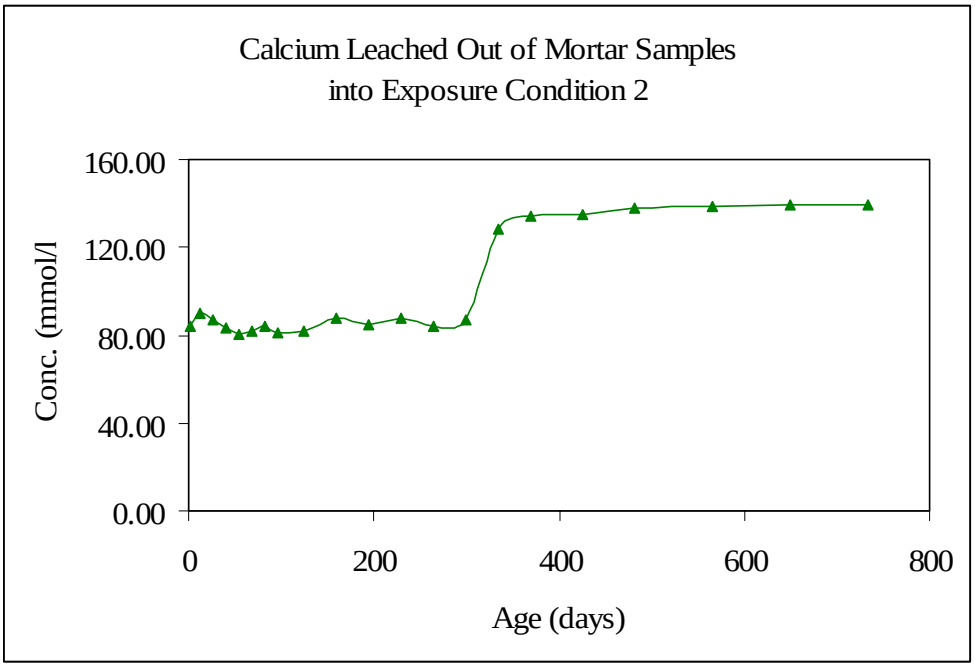


Figure 5.28: Calcium Leached from Mortar Samples Stored in Plain Water at Room Temperature

*5.6 Microstructure Analysis Using SEM and EDAX*

A scanning electron microscope (SEM) equipped with energy dispersive analysis X-ray (EDAX) testing was used on the samples to determine the chemical composition of the deposits within the microstructure. The samples were prepared as a fractured surface and then coated with carbon. Exposure condition influence on the ettringite shape and size was also noted during the SEM examinations.

*5.6.1 Mortar Samples in Exposure Condition 1*

At 40 days of storage in water, pH maintained at 12.5 (Exp. Cond. 1), SEM examination showed plenty of bubble-like needles of ettringite and patches of calcium hydroxide (CH) filling the air voids and cracks. Ettringite crystals (clusters) (> 10μm) were precipitated into the air voids and cracks within the microstructure of the mortar sample. At this early stage, well-developed and concentrated needle-like crystals completely filled voids and cracks. Figure 5.29 shows the SEM micrograph and EDAX analysis of the ettringite crystals forming at air void and cracks. Notice, also, that figure 5.29 was captured at a magnification (935x), with 20,000 volts applied to the filament to generate electrons. The EDAX analysis, a graph of intensity against x-ray energy, revealed ettringite having a chemical composition of Al = 5.51% wt., Si = 0.82% wt., S = 12.39% wt., and Ca = 77.57% wt., as shown in figures 5.29 and 5.30. The SEM/EDAX criteria for ettringite are based on: 1) Morphology 2.) Chemical composition ratio of Ca: S: Al (6: 4 (3): 2) varies due to experimental errors and isomorphous substitutions. In general, experimental errors for ettringite can occur because of lack of a plane sample surface or less than ideal orientation (sample should be 30 degrees to electron beam for maximum signal. Also, isomorphous substitution of elements can take such as Al for Si.

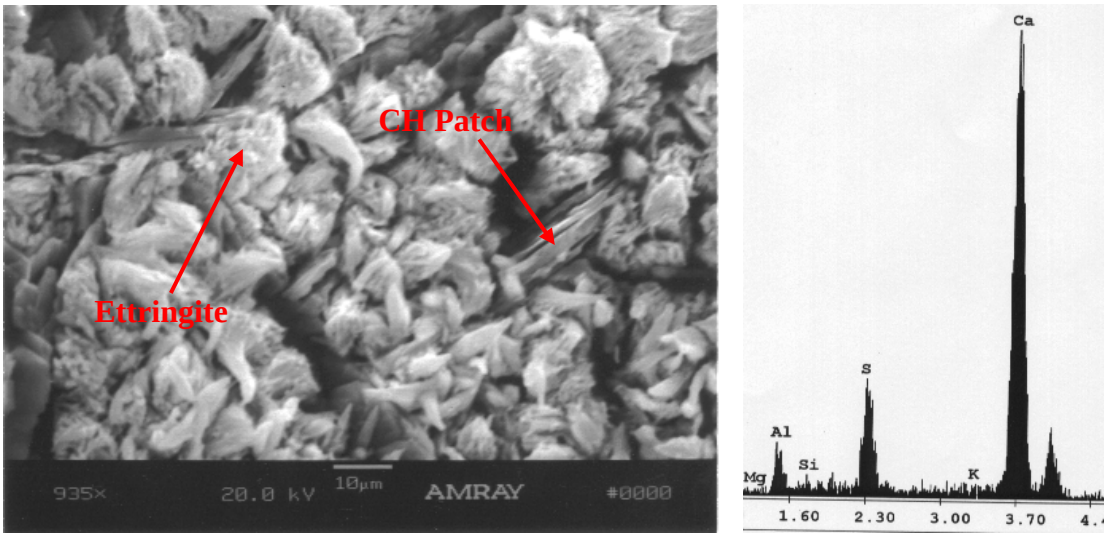


Figure 5.29: SEM and EDAX Analysis of Mortar Specimen in Exposure Condition 1 at Age of 40 Days, Showing Clusters of Ettringite Crystals and Patches of Calcium Hydroxide (CH)

EDAX ZAF Quantification (Standardless)
Element Normalized
SEC Table : Default

| Element | Wt % | At % | K-Ratio | Z | A | F |
|---|---|---|---|---|---|---|
| MgK | 0.59 | 0.91 | 0.0027 | 1.0255 | 0.4465 | 1.0050 |
| AlK | 5.51 | 7.73 | 0.0325 | 0.9951 | 0.5874 | 1.0078 |
| SiK | 0.82 | 1.11 | 0.0057 | 1.0238 | 0.6675 | 1.0140 |
| S K | 12.39 | 14.61 | 0.1108 | 1.0200 | 0.8503 | 1.0312 |
| K K | 1.08 | 1.04 | 0.0109 | 0.9770 | 0.9203 | 1.1275 |
| CaK | 77.57 | 73.21 | 0.7327 | 0.9992 | 0.9448 | 1.0006 |
| FeK | 2.04 | 1.38 | 0.0170 | 0.9108 | 0.9151 | 1.0000 |
| Total | 100.00 | 100.00 | | | | |

Figure 5.30: EDAX of the Elemental Analysis of Massive Deposits as Shown in Figure 5.28

SEM investigations at 100 days revealed clusters of ettringite needles filling cavities within the microstructure of the specimen as shown in Figure 5.31. The clusters became more distinct and can be predominantly identified from the SEM

micrograph and EDAX elemental composition analysis. The clusters of the ettringite needles (>100 μm) filled the cavities; the EDAX analysis of the ettringite layer showed a chemical composition of Al = 5.74% wt., Si = 3.57% wt., S = 13.75% wt., and Ca = 72.95% wt. Also in figure 5.24, the EDAX analysis shows two (2) peaks for Ca are due to the intensity of the X-rays and originated from the different electronic shell transitions.

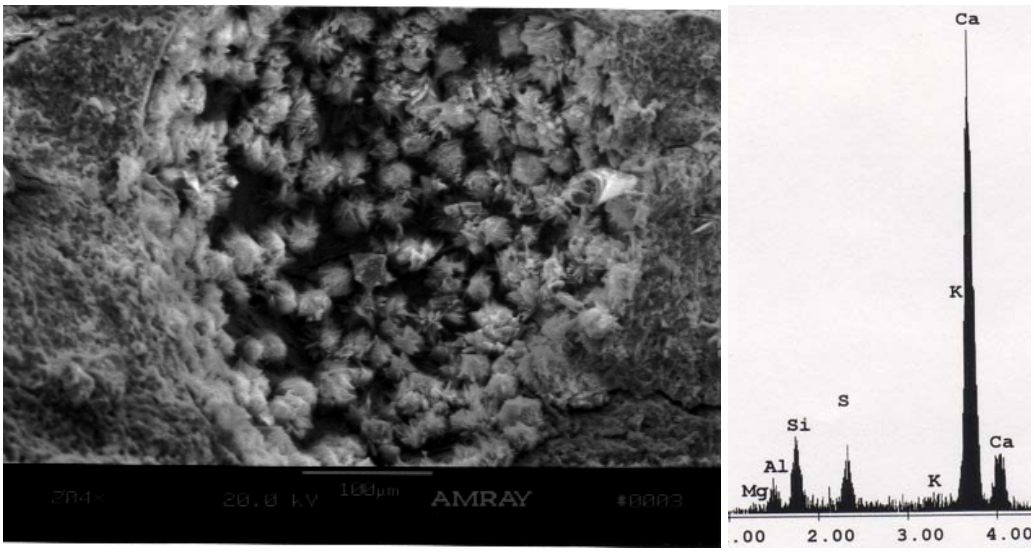


Figure 5.31: SEM and EDAX Analysis of Mortar Specimen in Exposure Condition 1 at Age of 100 Days, Showing Clusters of Ettringite Needles Filling Cavities

Figure 5.32 shows the 240 days' SEM results of the mortar specimen in exposure condition 1. An abundance of ettringite spherical balls was found completely filling the cavities and air voids. The EDAX analysis of the ettringite showed a chemical composition of Al = 6.07% wt., Si = 0.95% wt., S = 16.75% wt., and Ca = 76.51% wt.

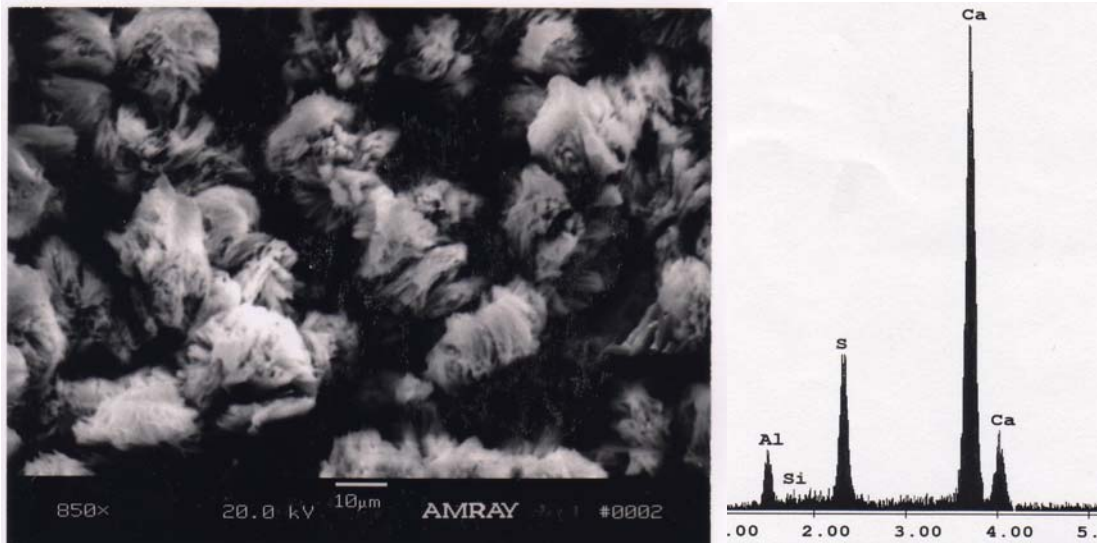


Figure 5.32: SEM and EDAX Analysis of Mortar Specimen in Exposure Condition 1 at Age of 240 Days, Showing Spherical Ettringite Balls Filling Cavities and Air Voids

The SEM examinations at 540 days reveal lots of ettringite needle-like crystals covering the entire specimens. Most of the ettringite was found in voids and aggregate pull-outs of the mortar specimens. This discovery suggested that ettrringite undergoes physical transition from crystal balls into needle-like crystals as time proceeded. SEM and EDAX analysis of the mortar specimens is shown in figure 5.33. The EDAX analysis of the ettringite needle-like crystals showed a chemical composition of Al = 4.06% wt., Si = 5.70% wt., S = 7.24% wt., and Ca = 81.74% wt.

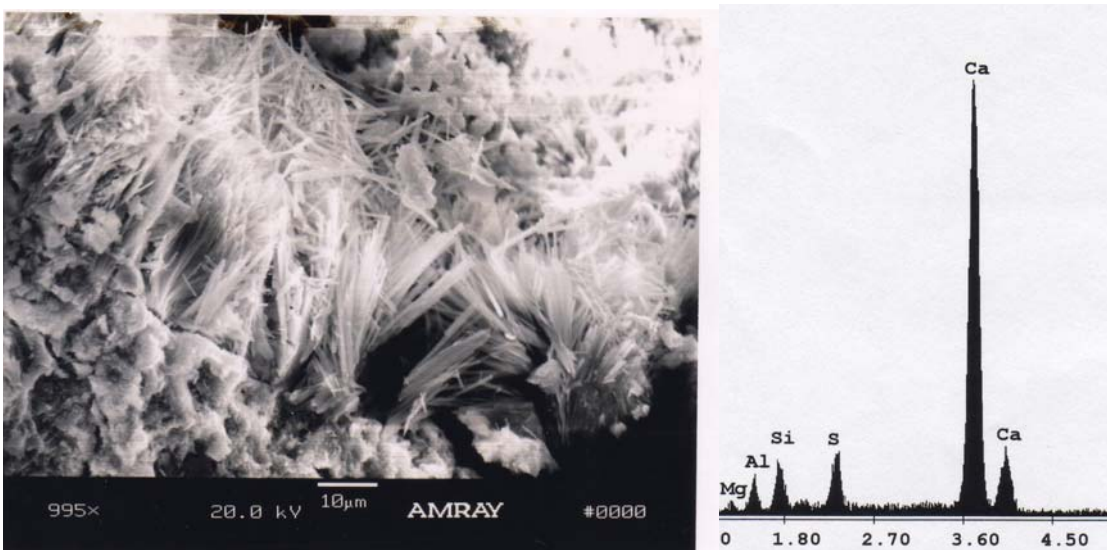


Figure 5.33: SEM and EDAX Analysis of Mortar Specimen in Exposure Condition 1 at Age of 540 Days, Showing Ettringite Needle-Like Crystals Filling Air Voids and Aggregate Pull-Outs

*5.6.2 Mortar Samples in Exposure Condition 2*

Mortar samples were prepared and stored in water for 40 days after the Duggan heat cycle before SEM examination. SEM and EDAX were used to determine or detect the chemical composition of deposits in the cracks and air voids within the microstructure of the specimen. Ettringite spherical balls were found filling the air voids and cavities of the specimens. A crack rim found around the sand aggregate was observed, and was partially filled with DEF as shown in Figures 5.34 and 5.35. The EDAX results indicate that the crack rim has a chemical composition of Al = 5.50% wt., Si = 7.30% wt., S = 9.57% wt., and Ca = 72.79% wt., which is characteristic of DEF.

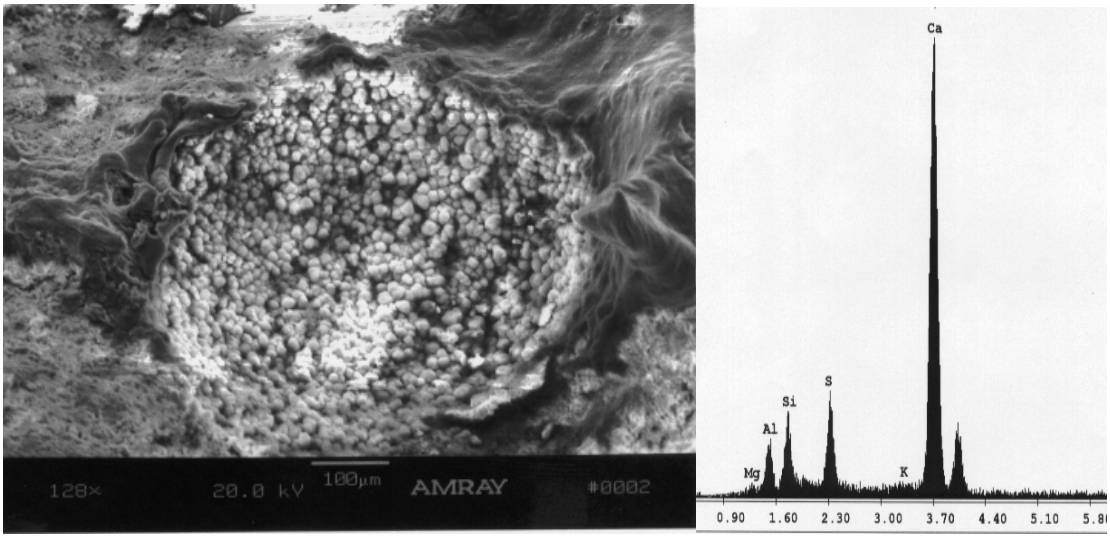


Figure 5.34: SEM and EDAX Analysis of Mortar Specimen in Exposure Condition 2 at Age of 40 Days, Showing Ettringite Balls Filling a Cavity

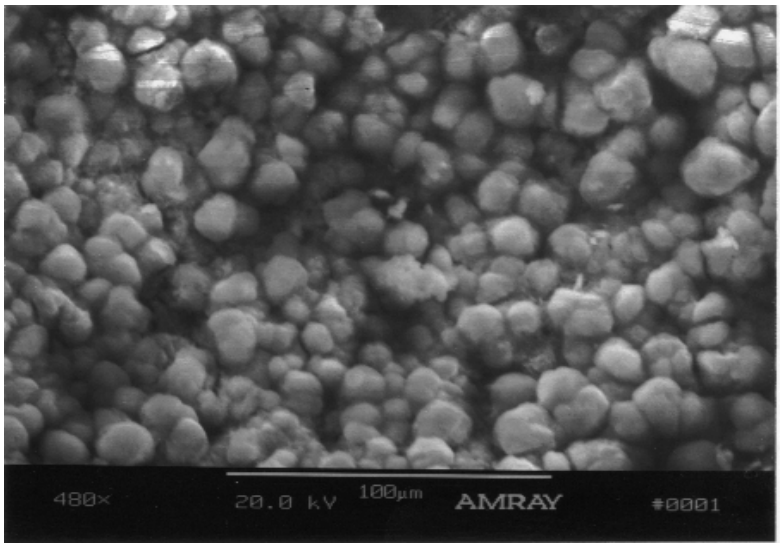


Figure 5.35: SEM of Mortar Specimen in Exposure Condition 2 at a Higher Magnification

SEM results at 100 days show ettringite balls in various locations in the examined mortar specimens. Figure 5.36 shows ettringite balls filling an aggregate pullout. The EDAX elemental mapping of these balls matched with ettringite having a chemical composition of Al = 4.95% wt., Si = 3.82% wt., S = 10.69% wt., and Ca = 76.41% wt.

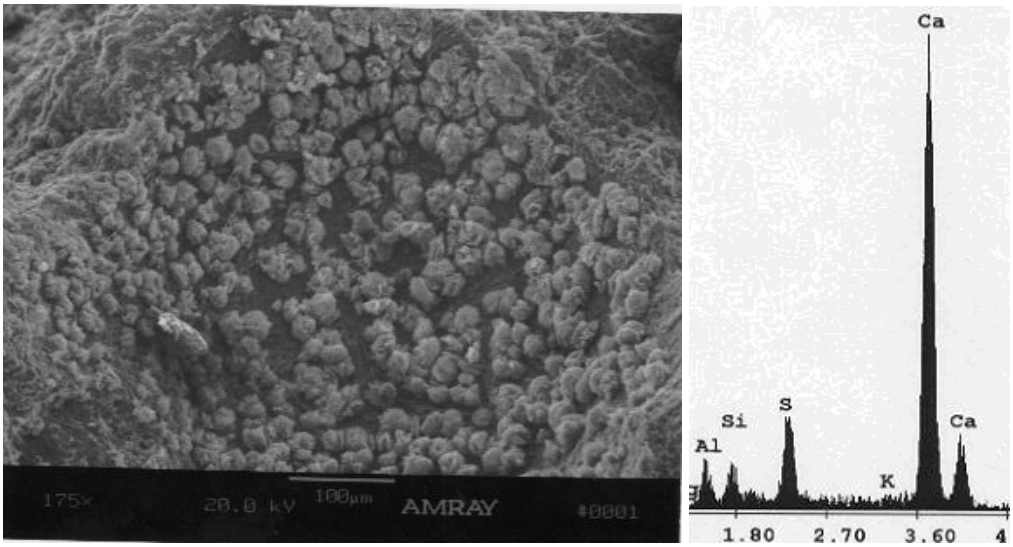


Figure 5.36: SEM and EDAX Analysis of Mortar Specimen in Exposure Condition 2 at Age of 100 Days, Showing Ettringite Balls Filling an Aggregate Pull-Out

At 240 days, ettringite needle-like crystals (>10µm) were found completely filling the cavities of the specimens. Ettringite in cracks through the paste and around aggregate particles was observed. Some of the cracking occurred during the sample preparation. However, the cracks containing ettringite clearly occurred during the test. Figure 5.37 shows the SEM and EDAX analysis of ettringite needle-like crystals within the cement paste matrix. EDAX elemental mapping of these needle-like

crystals matched with ettringite having a chemical composition of Al = 2.73% wt., Si = 2.08% wt., S = 4.48% wt., and Ca = 90.71% wt.

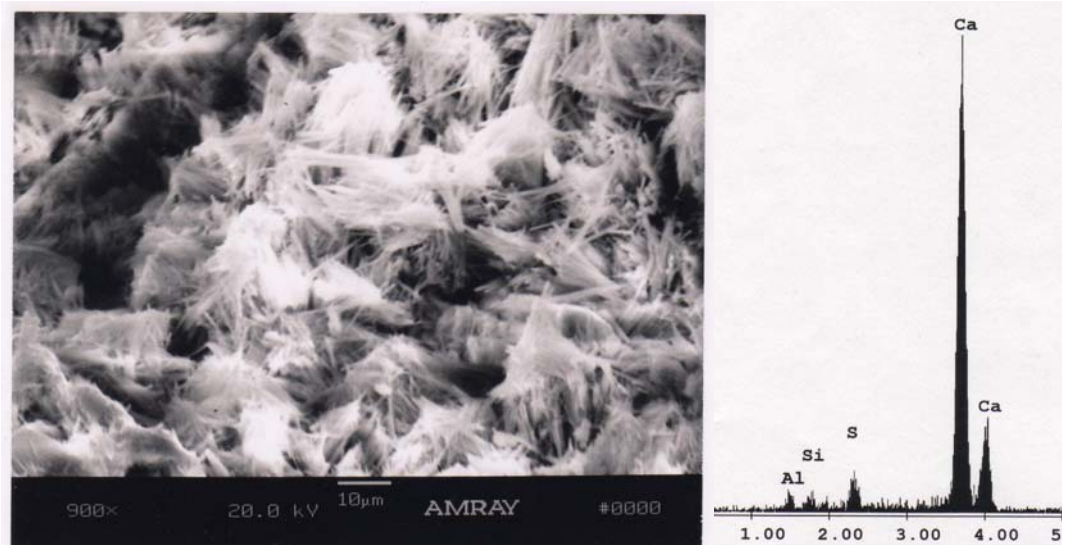


Figure 5.37: SEM and EDAX Analysis of Mortar Specimens in Exposure Condition 2 at Age of 240 Days, Showing Ettringite Needle-Like Crystals Filling the Cavities

SEM examination at 540 days showed clusters of ettringite needle-like crystals throughout the test mortar specimen especially within the cavities. This observation was confirmed by using EDAX analysis as ettringite, shown in figure 5.38. The EDAX results indicate that the cavities have a chemical composition of Al = 3.42% wt., Si = 10.96% wt., S = 3.25% wt., and Ca = 76.75% wt., which is characteristic of DEF. The morphology of ettringite varies with the different conditions under which it forms. Many SEM studies outlined that ettringite is normally formed as slender, needle-like crystals with prismatic hexagonal cross section (Schwiet et al, 1966, Midgley and Pettifer, 1971, Mehta, 1973, Mehta and Hu,

1978). The alkali content also affects the solubility of ettringite. Bailey concluded that the pH value of the pore solution affects the morphology of sulphoaluminates which transforms into ettringite at later stages (1982). The form and crystal size of ettringite can also be attributed to the expansion values and ever changing expansion rate of the mortar specimens.

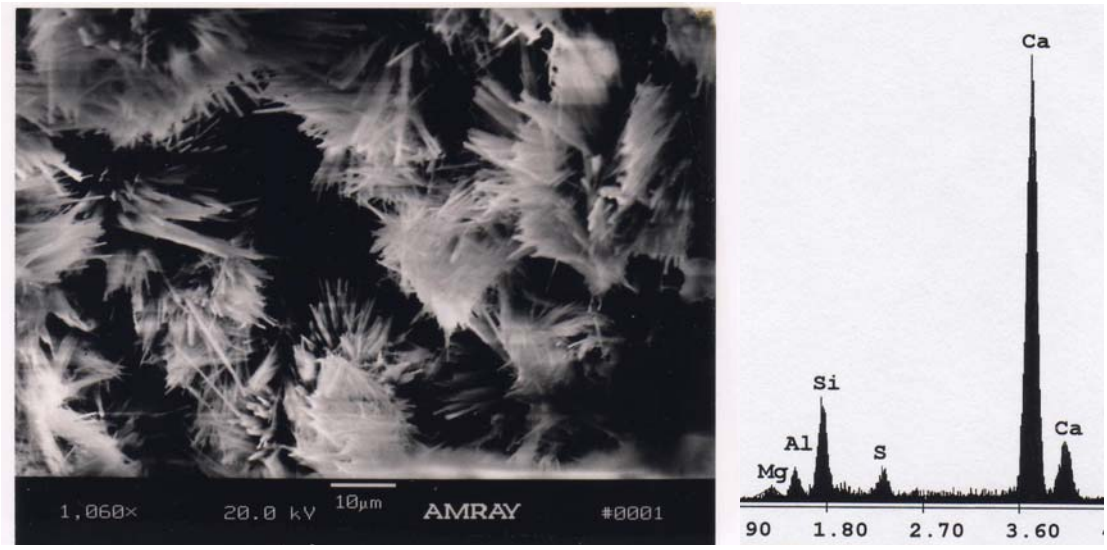


Figure 5.38: SEM and EDAX Analysis of Mortar Specimens in Exposure Condition 2 at Age of 540 Days, Showing Ettringite Needle-Like Crystals Filling the Cavities

*5.6.3 Mortar Samples in Exposure Conditions 3*

At 40 days, SEM and EDAX analysis of the specimens in exposure condition 3 show lots of ettringite needles in the air voids and cavities. The EDAX analysis indicates that the ettringite within the cavity of microstructure of the specimen has a chemical composition of Al = 1.51% wt., Si = 6.64% wt., S = 2.68% wt., and Ca = 86.76% wt. Also some calcium hydroxide (CH) crystals are found as shown in Figure 5.39.

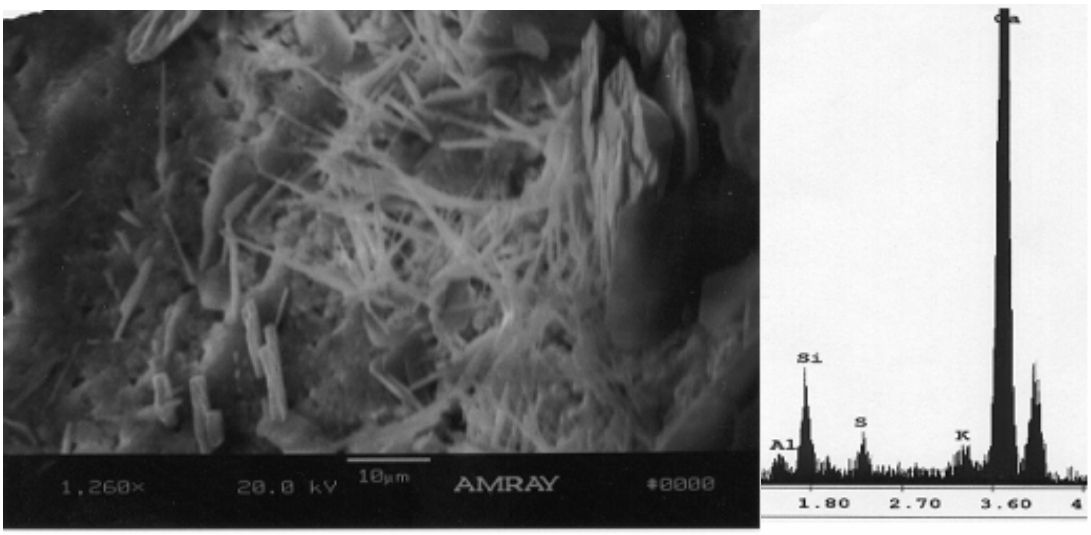


Figure 5.39: SEM and EDAX Analysis of Mortar Specimens in Exposure Condition 3 at Age of 40 Days, Showing Ettringite Needles and CH Crystals Filling a Cavity

Results of the specimen examinations at 100 days reveal no ettringite found from the SEM micrograph or any detected by EDAX. Only cement paste, C-S-H gel and calcium hydroxide (CH) were determined by the EDAX elemental composition analysis within the specimen's microstructure.

Figure 5.40 shows the SEM and EDAX results after 240 days storage in exposure condition 3. Lots of spherical ettringite balls were discovered at several locations of the mortar specimen. The EDAX results were consistent with the ettringite composition.

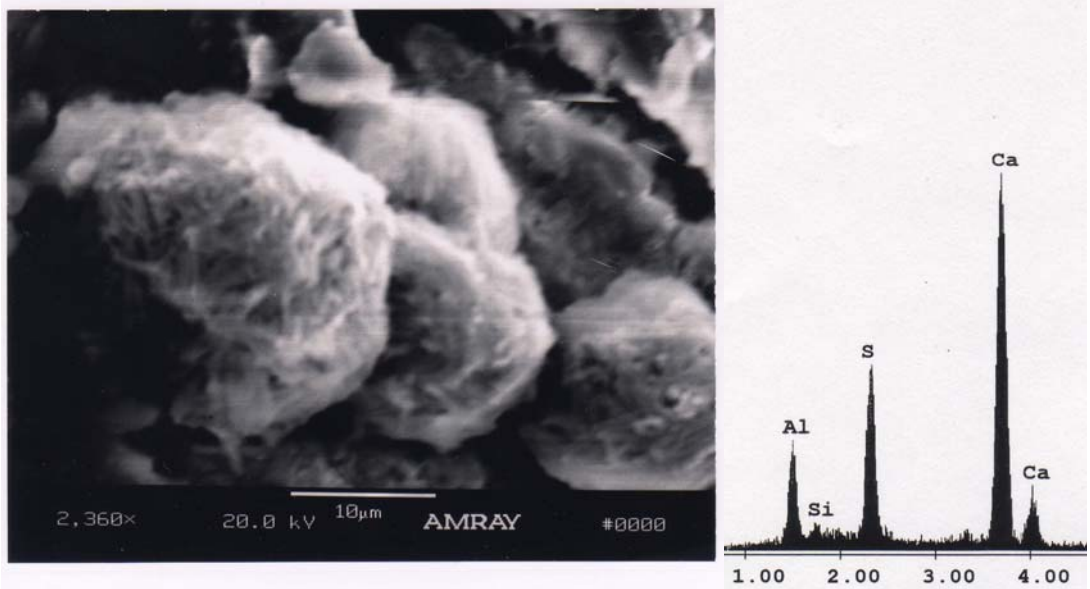


Figure 5.40: SEM and EDAX Analysis of Mortar Specimen in Exposure Condition 3 at Age of 240 Days, Showing Spherical Ettringite Balls Filling the Cavities

At 540 days, the SEM results revealed lots of well-developed ettringite crystals filling cavities and air voids of the specimen. The ettringite formation has changed over time from needle to well-developed crystals. The ettringite crystals were hexagonally shaped at closer examination under higher magnification of the SEM micrograph. The EDAX analysis confirmed the deposits in the cavities and air voids to be ettringite, as shown in figure 5.41.

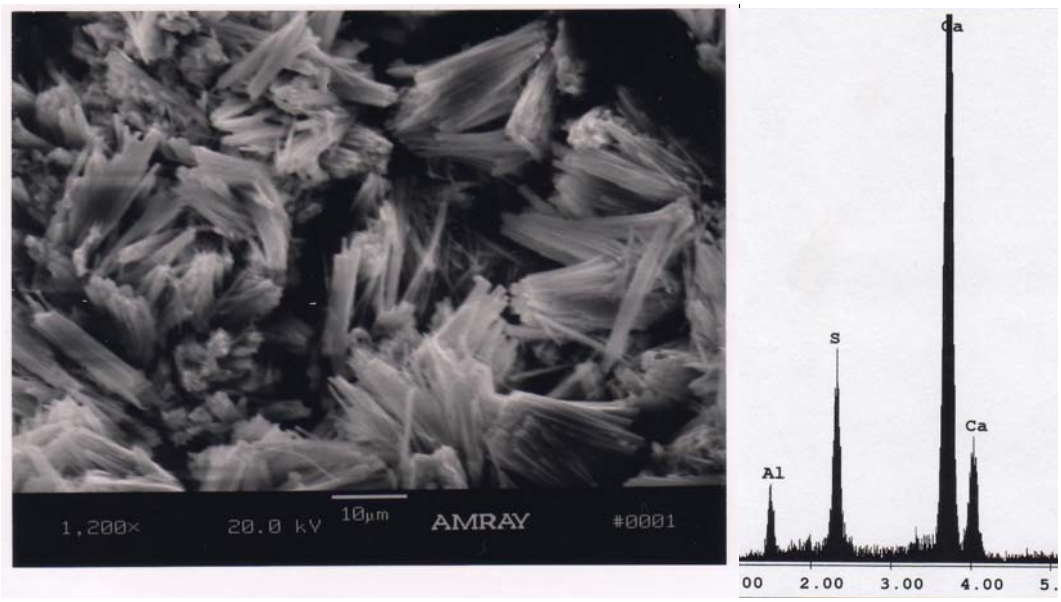


Figure 5.41: SEM and EDAX Analysis of Mortar Specimen in Exposure Condition 3 at Age of 540 Days, Showing Well-Developed Ettringite Crystals in the Cavities

*5.6.4 Mortar Samples in Exposure Condition 4A*

Based on the chemical composition and morphology of the material deposits between aggregate and cement, ettringite needles were observed using SEM equipped with EDAX. At 40 days, SEM and EDAX results revealed the presence of ettringite needles with reduced spectrum peaks. The reduced peaks were due to the presence of lots of calcium hydroxide crystals in the specimen. Figure 5.42 shows ettringite needles coupled with CH crystals for mortar specimens under field conditions. Figure 5.43 shows the EDAX analysis A is for the whole area and the EDAX analysis B is for the spot (CH crystal). Analysis of the whole figure reveals ettringite with a chemical composition of Al = 7.69% wt., Si = 1.93% wt., S = 16.02% wt., and Ca = 71.12% wt.

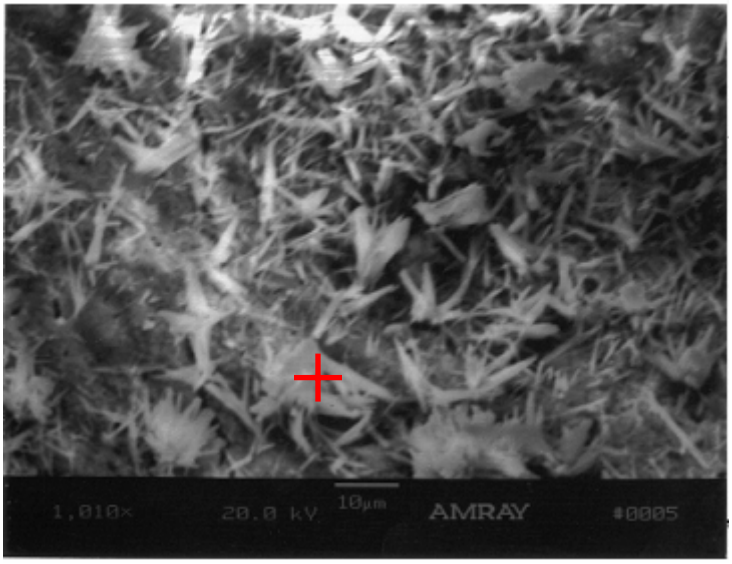


Figure 5.42: SEM Micrograph of Steam-Cured Mortar Specimen Under Field Conditions (C4A) at Age of 40 Days, Showing Ettringite Needles and CH Crystals Between Aggregate and Cement Paste

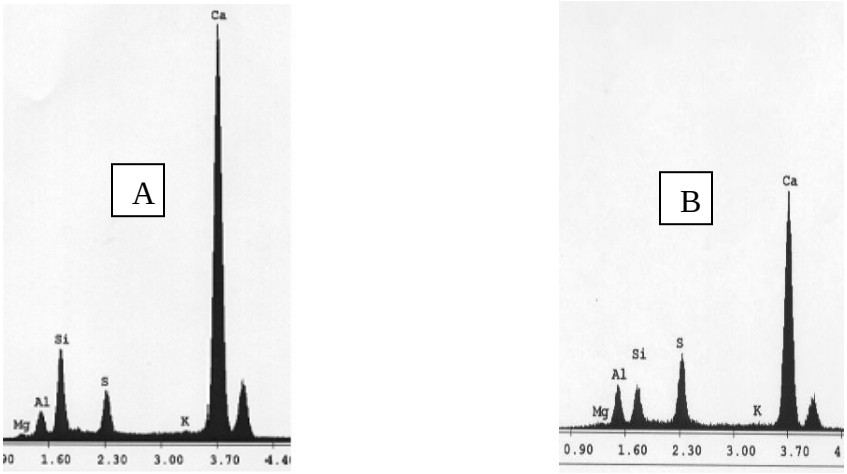


Figure 5.43: EDAX Analysis of Whole Area (A) and Spot B (CH Crystals)

At 100 days, concentrations of ettringite needles and clusters of CH crystals were found in the specimen. These massive ettringite crystals can be seen at low

magnifications. Figure 5.44 shows the SEM and EDAX analysis of the specimens. The EDAX analysis reveals ettringite with a chemical composition of Al = 3.71% wt., Si = 4.51% wt., S = 7.60% wt., and Ca = 79.71% wt.

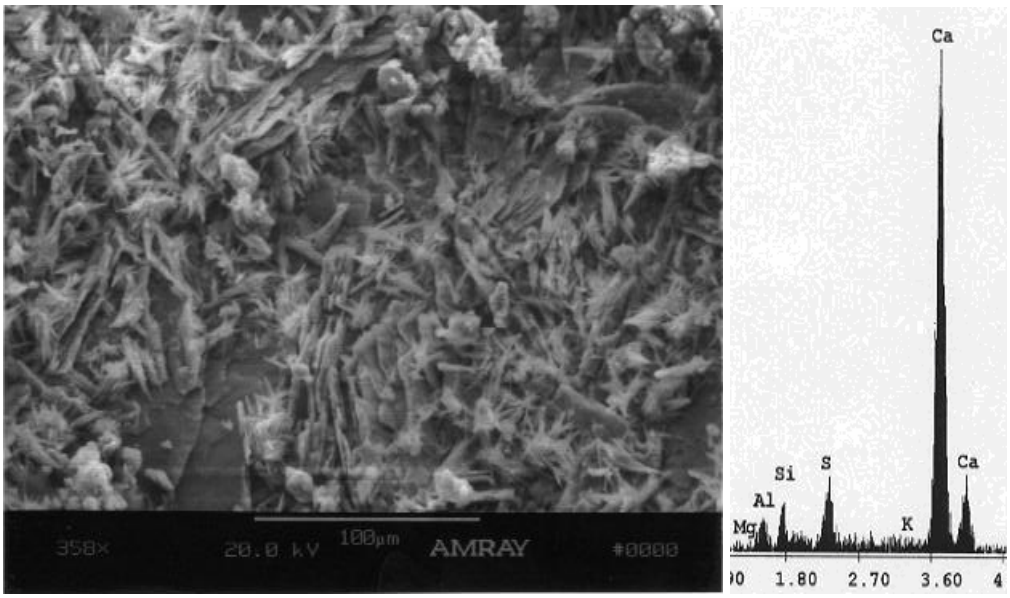


Figure 5.44: SEM and EDAX Analysis of Steam-Cured Mortar Specimen Under Field Conditions (C4A) at Age of 100 Days, Showing Ettringite Needles and CH Crystals on the Surface of An Aggregate

The SEM results at 240 days revealed calcium hydroxide crystal plates and little or no ettringite on the surface of an aggregate. The EDAX analysis confirmed the existence of calcium hydroxide crystals as shown in figure 5.45.

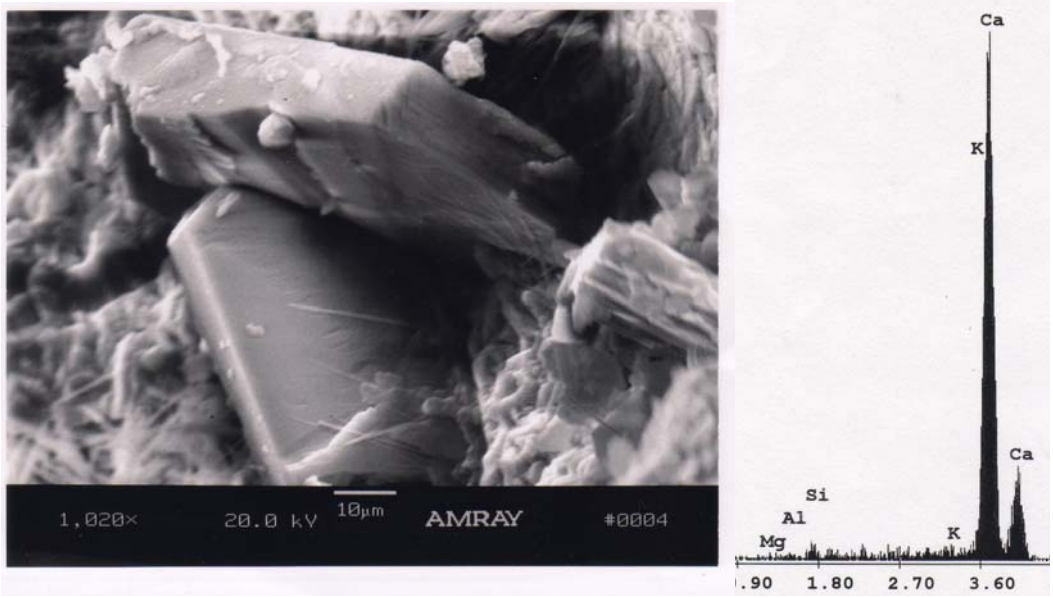


Figure 5.45: SEM and EDAX Analysis of Steam-Cured Mortar Specimen Under Field Conditions (4A) at Age of 240 Days, Showing CH Crystal Plates with Few Ettringite Needles on the Surface of An Aggregate

At 540 days, SEM examination found ettringite needles mixed with calcium hydroxide crystals throughout the whole area of the specimen. Figure 5.46 shows the SEM and EDAX analysis of the specimen. The EDAX analysis reveals ettringite with a chemical composition of Al = 5.63% wt., Si = 8.69% wt., S = 8.75% wt., and Ca = 74.38% wt.

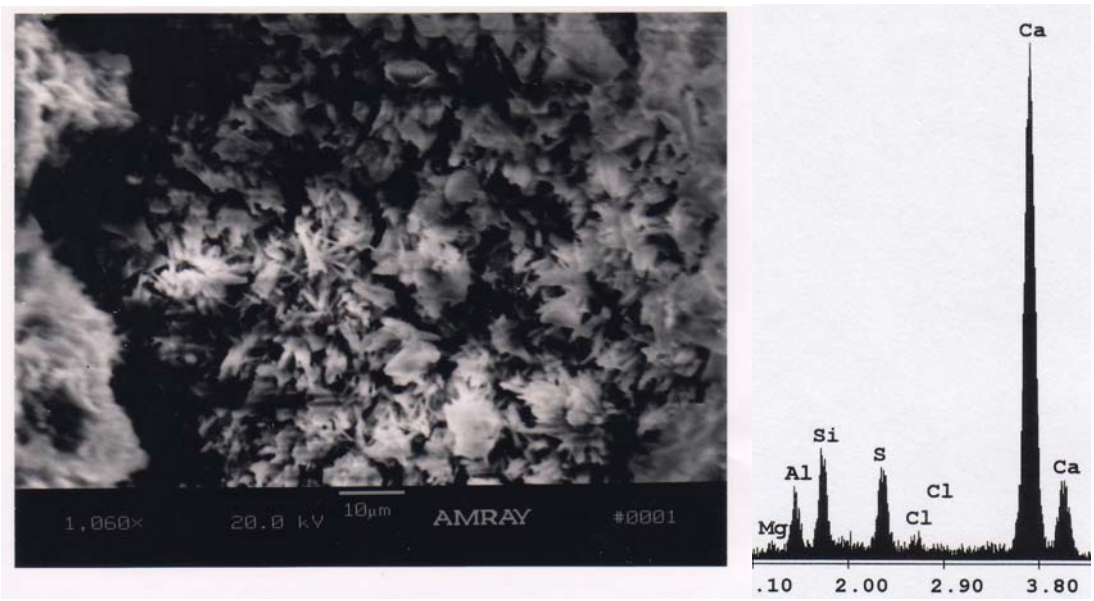


Figure 5.46: SEM and EDAX Analysis of Steam-Cured Mortar Specimen Under Field Conditions (4A) at Age of 540 Days, Showing Few Ettringite Needles Mixed with CH Crystals Covering the Sample

*5.6.5 Mortar Samples in Exposure Condition 4B*

Although the mortar samples were not steam-cured at high temperatures before being subjected to field conditions, ettringite needles and CH crystals were found from the SEM micrograph results after just 40 days of exposure. The ettringite needles were found around and within the air voids. The occurrences of needles were tentatively identified as ettringite, but no EDAX analysis could be obtained. No EDAX spectrum peaks were obtained because the conditions for maximum X-ray signals were not met due to very low counts. Figure 5.47 shows a SEM micrograph of the ettringite and CH crystals.


Figure 5.47: SEM Micrograph of Room Temperature Cured Mortar Specimen Under Field Conditions (C4B) at Age 40 Days, Showing Ettringite Needles and CH Crystals within Air Voids

At 100 days, no ettringite was found within the voids of the microstructure of the mortar sample. Most of the air voids were either concentrated with calcium hydroxide (CH) crystals or empty. Figure 5.48 shows the SEM and EDAX results of an air void filled with CH crystals. The EDAX confirms that the crystals within the air voids were CH and the chemical composition as Al = 0.00% wt., Si = 0.46% wt., S = 0.15% wt., and Ca = 97.81% wt. This clearly shows that CH crystals predominantly occupied the entire analysis void. Figure 5.49 shows the same air void at a higher magnification.

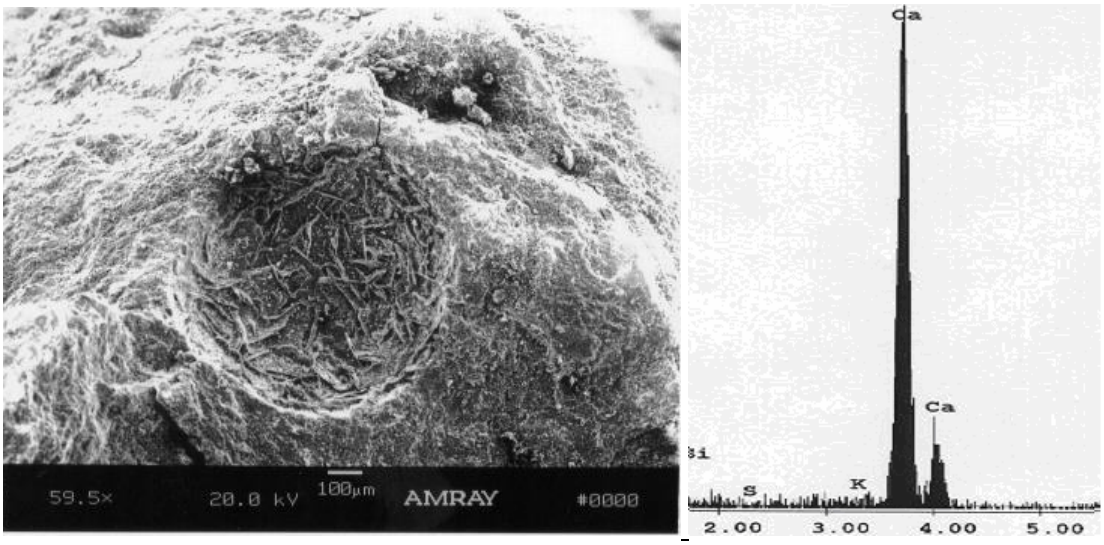


Figure 5.48: SEM and EDAX Analysis of Room Temperature Cured Mortar Specimen Under Field Conditions (C4B) at Age 100 Days, Showing CH Crystals Within Air Voids

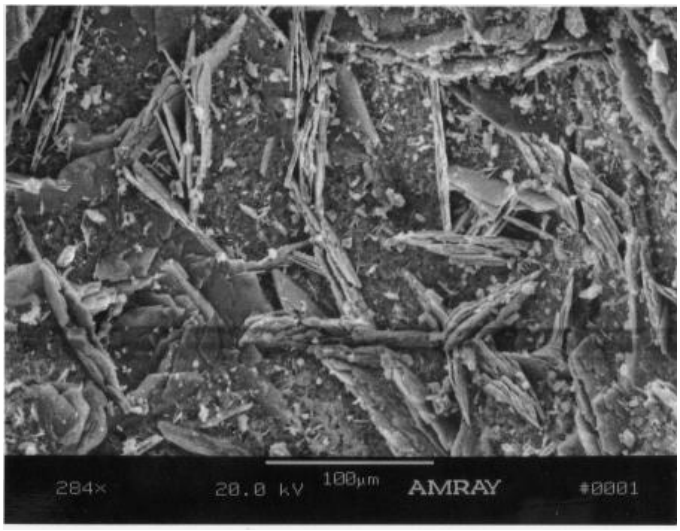


Figure 5.49: SEM Micrograph of Room Temperature Cured Mortar Specimen Under Field Conditions (C4B) at Age 100 Days, Showing CH Crystals within Air Voids at a Higher Magnification

The SEM micrograph results at 240 days support ettringite morphology within an air void, but could not be verified with the EDAX analysis. Figure 5.50 shows the SEM micrograph and EDAX at 240 days for the whole surface of the sample. The EDAX revealed the material deposits having a chemical composition as Al = 2.20% wt., Si = 5.75% wt., S = 1.96% wt., and Ca = 86.79% wt.

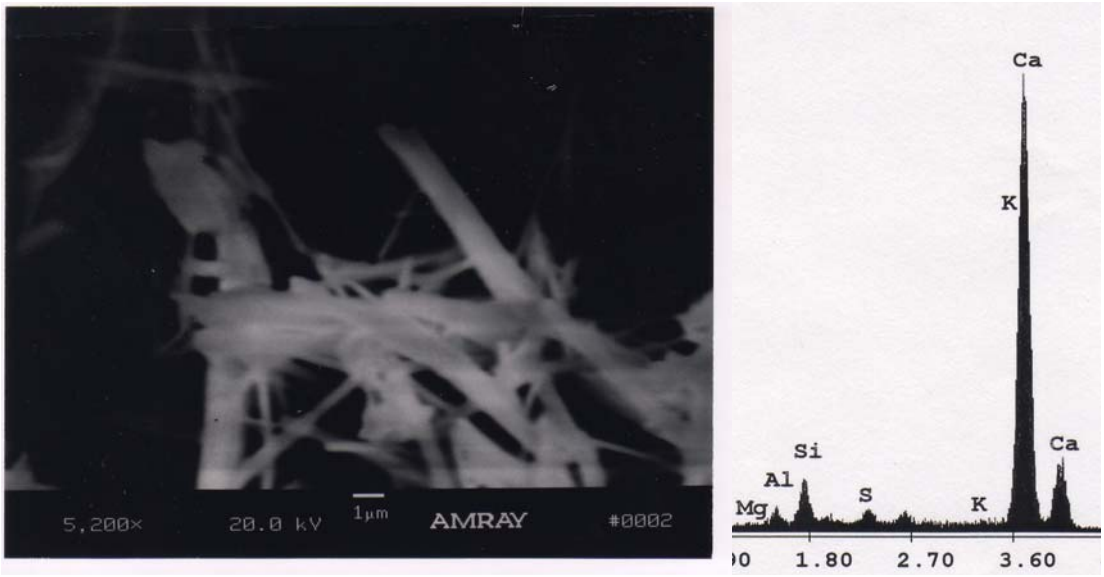


Figure 5.50: SEM Micrograph of Room Temperature Cured Mortar Specimens Under Field Conditions 4B at Age 240 Days, Showing Ettringite Morphology within Air Voids

At 540 days, SEM examinations revealed little or no ettringite in the mortar specimen under field condition 4B. The absence of ettringite can be influence by the constantly changing atmospheric conditions. The lack of the continuous presence of water affects the formation of ettringite in the mortar microstructure.

*5.7 X-ray Computed (X-ray CT) Analysis*

X-ray computed tomography (X-ray CT) was used to reveal any interior cracks within the microstructure of the mortar specimens. Figures 5.51 and 5.52 show computed tomography images of the mortar specimens after 40 days of storage in the different exposure conditions. The 2" mortar cubes were steam-cured and then subjected to the Duggan heat cycle prior to storage. This method did not reveal any interior cracks in the paste or around the aggregate particles of the specimen's microstructure. The X-ray computed tomography is a non-destructive test, and helps in monitoring the crack initiation and propagation over a period of time. This method did not reveal interior cracks in any of the tested mortar specimens.

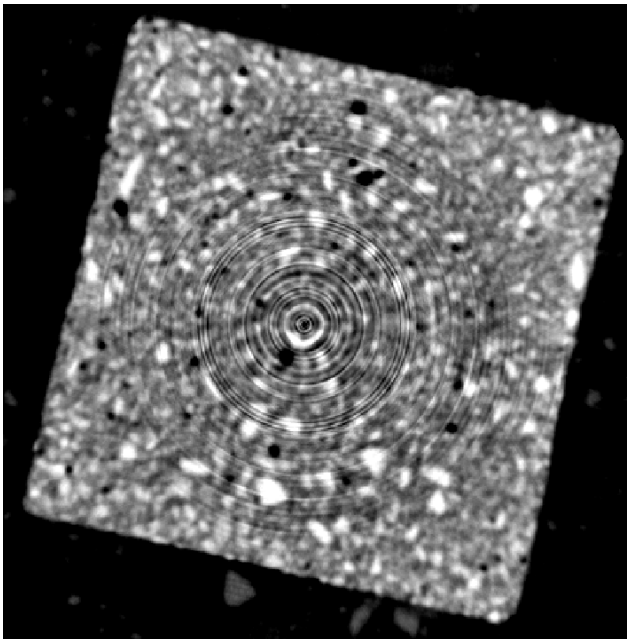

Figure 5.51: X-ray Computed Tomography Image of a Section Through a Mortar Cube at Age of 40 Days in Isothermal Water Bath, pH maintained at 12.5 – limewater

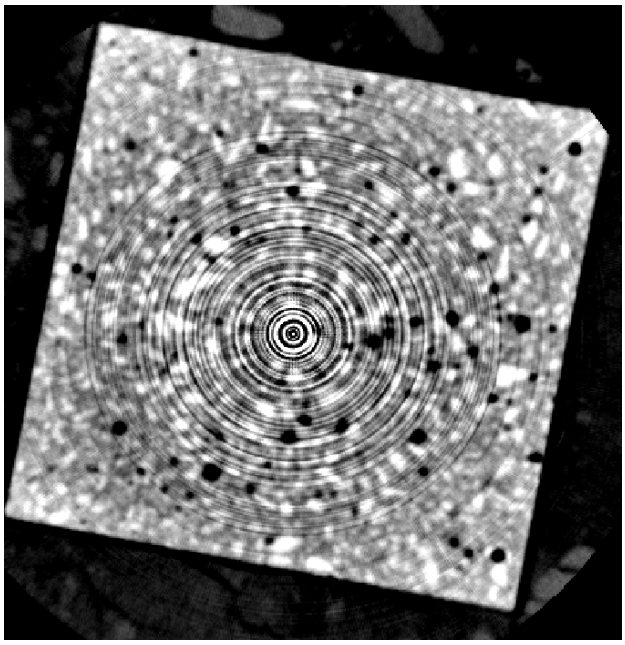

Figure 5.52: X-ray Computed Tomography Image of a Section Through a Mortar Cube Stored at Age of 40 Days in Moist Air Chamber, R.H maintained at 97%

*5.8 Summaries and Discussion of Mortar Samples (Control)*

The Portland cement type III used in this research study exceeds all the threshold values suggested by researchers. In 1994, Taylor outlined threshold values at 0.83% for equivalent $Na_2O$, 0.22% for $Na_2O$, 3.6% for $SO_3$ and 1.6 $\pm$ 0.2% for MgO. These criteria and subjection of the specimens to the Duggan heat cycle influenced the initiation of microcracks within a shorter period of time.

Expansion tests revealed that mortar samples stored in pH maintained at 12.5 - limewater exhibit the highest expansion during the first 100 days of storage after the Duggan heat cycle. Any differences in the expansion values of the mortar bars are attributed to the different exposure conditions. After 100 days, expansion values for

mortar bars in relative humidity at 97% increase significantly due to the potassium hygroscopic effect. In the relative humidity of 97%, the potassium continually extracts moisture which reacts to form more ettringite. There is constant leaching of potassium from the mortar bars into the limewater and plain water. Similar results were obtained by Shimada (2005). All mortar samples subjected to the Duggan heat cycle showed significant expansion for the period of storage, and the expansion continued. Also, all mortar samples subjected to the Duggan heat cycle exceeded 0.05% expansion value after 40 days of storage. The expansions at 730 days were 0.232%, 0.229% and 1.20% for the mortar bars stored in pH maintained at 12.5 – limewater, plain water and relative humidity of 97% respectively. The higher the expansion, the more severe is the observed cracking of the mortar bars. Expansions of mortar bars subjected to the Duggan heat cycle can be fitted using the Kolmogrov-Avrami-Johnson-Mehl equations (KAJM) (Kruger, 1993). Since the KAJM equations did not give a better fit for the experimental data (Ramadan, 2000), they were not used for data analysis. During this research study, linear regression analysis was carried out to best fit the experimental data.

Shrinkage or little expansion was observed in the mortar samples exposed to field conditions throughout the entire research project. Steam-cured mortar bars exposed to field conditions show less shrinkage but exhibit similar shrinkage patterns as room temperature-cured mortar bars under the same field conditions. The length change values at 720 days were -0.009% and -0.0166% for steam-cured and room temperature-cured mortar bars exposed to field exposures respectively.

Since the formation of ettringite requires the uptake of water, which results in weight gain of the specimen, mortar bars in pH maintained at 12.5 – limewater and plain water showed significant increase in weight after just a few days of storage. Weight changes of the mortar bars in relative humidity of 97% also revealed changes, especially between 37 and 41 days of storage. SEM examination was performed at the 40th day to determine the chemical composition within the microstructure of the specimen. The SEM results revealed ettringite and it is assumed that the sudden weight-change was attributed to the formation of delayed ettringite. Weight changes of the mortar bars under field conditions were irregular and showed little or no correlation with age throughout the entire research project. The weight-change of the mortar is influenced by the heat-curing and storage conditions. The expansion increases the capillary pore volume of the paste and the storage solution filling the increased volume results in a weight gain.

For the first 100 days of storage after the Duggan heat cycle, the expansion against weight-change of mortars in pH maintained at 12.5 - limewater and plain water showed a high positive linear correlation. It is assumed that expansion of the mortar bars is primarily due to the growth and formation of ettringite. Grattan-Bellew et al. obtained similar results; they concluded that there was a linear correlation between mass and expansion for mortar bars stored at 23$^{o}$C in limewater over a period of 17 to 59 days (1998). Shimada also suggested a linear relationship between the relative weight-change and the linear expansion coefficient, or the relative length-change (2005).

From the early compressive strength-tests, mortar cubes in relative humidity of 97% exhibit the highest results. Compressive strength at later stages revealed about a 25% increase for all exposure conditions. Compressive strength results increases with an increase in expansion under all the different exposure conditions. This suggests that the low expansion or shrinkage values exhibited by the mortar samples do not cause significant damage to the mortar microstructure. The mortar specimens exposed to field conditions exhibited higher strength than the specimens subjected to the Duggan heat cycle. Non heat-cured mortar specimens developed a denser microstructure, and thus higher strength than heat-cured mortar over time. These test results suggest that the Duggan heat cycle adversely affects the compressive strength of the control mortar samples. Several researchers indicated a strength reduction associated with high-curing temperatures (Ramadan, 2000, Ronne and Sellevold, 1994, Taylor, 1994).

The presence of alkalis greatly suppressed the dissolution of calcium hydroxide but enhanced the formation of ettringite. The alkali ions accelerate the formation of ettringite (Daerr et al., 1977, Wang et al., 1986 and Way et al., 1989). The hydroxide ions from the hydration of Portland cement result in a pore solution having a pH value of about 12.5 (Diamond, 1983). The concentration of alkalis being leached out was slightly higher in the pH maintained at 12.5 – limewater than the plain water storage conditions. The high concentration of $Ca^{2+}$ ions in the pH maintained at 12.5 – limewater storage condition also influences the formation of ettringite. This was confirmed by examinations of the mortar samples with the SEM equipped with EDAX. Researchers believed that formation of a reaction gel taking

place in concrete and mortar bars depends on the amount and availability of the $Ca^{2+}$ (Struble, 1987 and Kilgour, 1988).

The microstructural analysis of the control mortar specimens in pH maintained at 12.5 – limewater and plain water revealed lots of ettringite formation. Distinctive DEF ring cracks were observed in the samples in the pH maintained at 12.5 – limewater and plain water, usually at the aggregate paste interface. At 40 days of storage, mortar samples in limewater showed ettringite needles (> 10 μm) with patches of calcium hydroxide filling air voids and cracks. Mortar samples in plain water featured ettringite balls (> 100 μm) deposited in cavities. For the mortar samples in relative humidity of 97%, ettringite needles and CH crystals were found filling the cavities after 40 days. The SEM results show the morphology and crystal size of the ettringite varying for the different exposure conditions with time. The SEM results correlated to the expansion results showed that exposure conditions have a significant role in the expansion and formation of DEF. A summary table of the test results for the steam-cured mortar samples subjected to Duggan heat cycle is shown in table 5.8.

SEM studies of the mortar samples exposed to field conditions reveal the presences of ettringite. The steam-cured mortar samples with no Duggan heat cycle show abundant ettringite needles, and CH crystals between aggregate and cement paste. For the room temperature-cured mortar samples, ettringite needles were found after 40 days. The ettringite needles were not well-developed and there were few CH crystals within the air voids. The X-ray signal output from the EDAX could not be obtained to further verify the chemical composition of the deposits. The occurrences

of the gel deposits were tentatively identified as ettringite due to the shape and size revealed by the SEM micrograph. For room temperature-cured mortar samples in exposure field conditions, SEM examinations at 540 days discovered little or no ettringite. This is can be attributed to the ever changing atmospheric field conditions. The SEM examinations of the mortar specimens showed no evidence of ASR. The absence of ASR suggests that the materials and test parameters used in this research study were not conductive to the ASR deleterious mechanism. Results suggest that DEF is the mechanism responsible for the deterioration. Table 5.9 provides a summary of test results for the mortar samples subjected to field conditions.

X-ray CT image sections of the 2" mortar cubes did not reveal any interior cracks. Specimens that were under field conditions did not show any interior cracks regardless of the changing environmental conditions. Cracks were found by SEM to be filled only with ettringite crystals.

Table 5.8: Summary of Test Results of Control Mortar Samples – Steam-Cured and Subjected to Duggan Heat Cycle

| **Control Mortar Samples - Steam-Cured and Subjected to Duggan Heat Cycle** | | | | |
|---|---|---|---|---|
| | | Exp. Cond. 1 (Limewater) | Exp. Cond. 2 (Plain Water) | Exp. Cond. 3 (R.H at 97%) |
| Expansion | | Max. 0.26% | Max. 0.23% | Max. 1.20% |
| Weight Change | | Max. 12.16% | Max. 12.23% | Max. 10.87% |
| Compressive Strength (psi) | 28 Days | 5745 | 5475 | 6072 |
| | 365 Days | 7188 | 6708 | 7517 |
| | 540 Days | 7267 | 7517 | 8333 |
| Water Analysis (mmol/l) | pH | - | 8.33 - 12.26 | - |
| | Alkali | Max. 175 | Max. 142 | - |
| | $Ca^{2+}$ | - | Max. 139 | - |
| SEM/EDAX Analysis | 40 Days | Ettringite clusters and CH crystals | Ettringite Balls | Ettringite needles with CH crystals |
| | 100 Days | Ettringite clusters | Ettringite Balls | No ettringite |
| | 240 Days | Ettringite balls | Needle-Like ettringite crystals | Spherical ettringite balls |
| | 540 Days | Needle-like ettringite crystals | Clusters of needle-like ettringite crystals | Well-developed ettringite crystals |

Table 5.9: Summary of Test Results of Control Mortar Samples – Subjected to Field Conditions

| **Mortar Samples (Control) - Subjected to Field Conditions** | | | |
|---|---|---|---|
| | | Exp. Cond. 4A (Steam-Cured) | Exp. Cond. 4B (Room Temp.-Cured) |
| Length Change | | Max. -0.009% | Max. -0.017% |
| Weight Change | | Max. 0.28% | Max. -0.12% |
| Compressive Strength (psi) | 28 Days | 6280 | 6996 |
| | 365 Days | 8525 | 9200 |
| | 540 Days | 8467 | 10283 |
| SEM/EDAX Analysis | 40 Days | Ettringite needles | Few ettringite needles and CH crystals |
| | 100 Days | Ettringite needles and CH crystals | CH crystals |
| | 240 Days | CH crystals and no ettringite | Few ettringite |
| | 540 Days | Few ettringite needles and CH crystals | No ettringite |

# Chapter 6: Mortar Samples Made With High Potassium Content ($K_2O$) and DEF

## *6.1 Introduction*

The research study reported in this chapter focuses on the effects of an increase in potassium content, expressed as $K_2O$, in the mortar mixes and its association to DEF. Again, five (5) sets of mortar specimens were prepared according to the modified sample preparation method. As described earlier, only potassium carbonate was added to the batch mixes to increase the alkalinity. Some of the samples were steam-cured and others cured as before at room temperature in the laboratory. After steam-curing the samples were stored in water for six (6) days. Then they were subjected to the Duggan heat cycle, which took seven (7) days to complete prior to storage of specimens in their respective exposure conditions.

Again, 2" mortar cubes were tested for compressive strength after 28 days, 240 days and 540 days of storage. Scanning electron microscopy (SEM) and X-ray computed tomography (X-ray CT) testing were also performed to determine the cause of expansions, cracks and the chemical composition of the deposits within each specimen's microstructure.

The objectives were to study the effect of additional potassium on the expansion of mortar samples and to analyze its influence on the expansion, expansion rate, weight-change and DEF. SEM testing was conducted to identify the deterioration mechanism causing expansion and weight-change. The storage solution of exposure conditions 1 and 2 was also analyzed for leaching of alkali ions. X-ray

CT was used to analyze the internal microstructure for crack detection. All the test results are discussed and analyzed in this chapter.

## *6.2 Influence of Potassium Content and Exposure Conditions*

The specimens were all prepared with increased potassium content in order to study its influence in the expansions, weight-changes, and microstructures of the specimens. Again, expansion and weight change were periodically monitored. As suggested by Duggan, the expansion values at 21 days were compared to the threshold value of 0.05% as pass/fail criteria. SEM equipped with EDAX and X-ray CT testings were conducted at different times to investigate the mechanism responsible for the expansion.

## *6.3 Test Results of Mortar Samples Subjected to Duggan Heat Cycle*

For Phase 2, to accelerate the expansion, three mortar batch mixes were subjected to the Duggan heat cycle after one week of casting. All the mixes had an overall potassium content expressed as $K_2O$ of 1.5% by weight of cement added to the mixing water during batching. The potassium content influenced the amount of expansions exhibited in the mortar samples. The experimental results and tests performed are discussed and analyzed for the different exposure conditions in the following sections.

*6.3.1 Expansion Results*

*6.3.1.1 Length Change Measurements*

Five (5) mortar bars were used from each of the respective exposure conditions for length-change measurements. The mortar specimens made with 1.5% potassium content ($K_2O$) show higher expansions than the control specimens. After just five (5) days, mortar specimens in exposure conditions 1 and 2 exceeded the Duggan threshold value of 0.05% expansion. These results also confirmed that an increase in alkali content of the mortar specimens increases the potential for the mortar to expand. The rate of expansion of mortar bars increases significantly in all exposure conditions. Expansion values at 21 days of mortar specimens in exposure conditions 1, 2, and 3 were 0.117%, 0.200% and 0.055% respectively, which all exceeded the Duggan threshold value. The mortar bars in exposure condition 2 (plain water) showed higher expansion values than those in exposure condition 1 (limewater) throughout the research duration. This can be attributed to the extra calcium from the limewater which causes precipitation of ettringite. The precipitation of ettringite in the mortar bars close to the surface inhibits transport of solution into the microstructure of the mortar bars (Graf, 2007). The mortar bars in exposure condition 3 showed the highest expansion values. Within just 100 days, cracks become visible in the mortar bars stored in exposure condition 3. After 250 days, the mortar bars in exposure condition 3 showed the highest expansion values and rates. Mortar bars in exposure conditions 1 (pH maintained at 12.5) and 2 (plain water at room temperature) exhibit similar expansion patterns. Expansion values at 700 days were 0.241%, 0.436% and 0.608% for mortar bars in exposure conditions 1, 2 and 3

respectively. Figures 6.1 through 6.4 show the expansion values and rates of the mortar bars against age (days of storage after the Duggan heat cycle).

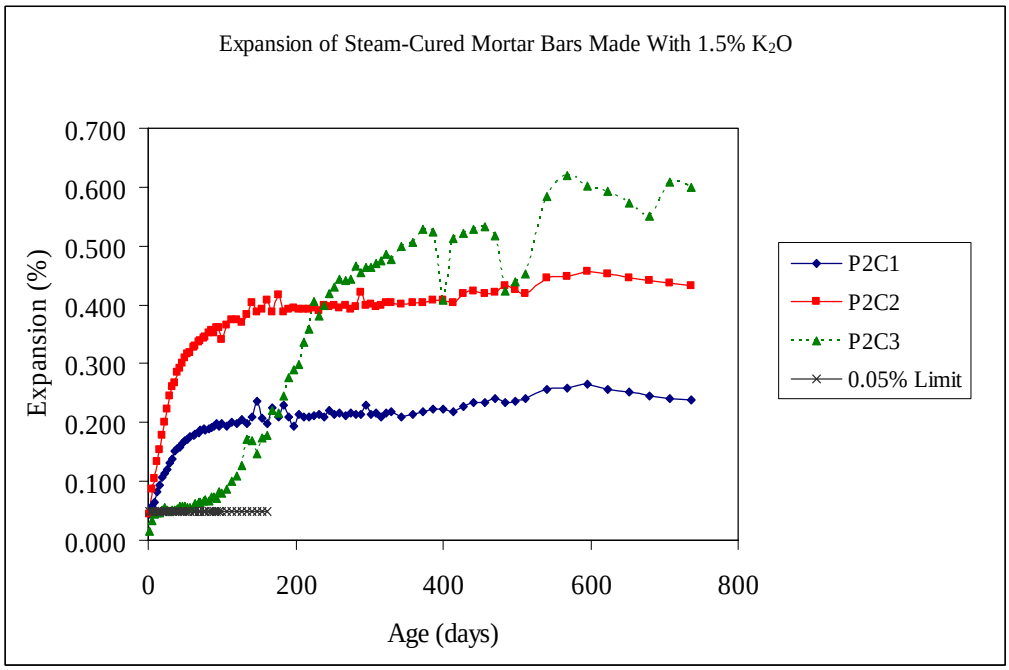


Figure 6.1: Expansion of Mortar Bars Made With 1.5% $K_2O$ Subjected to Duggan Heat Cycle and Stored Under Different Exposure Conditions

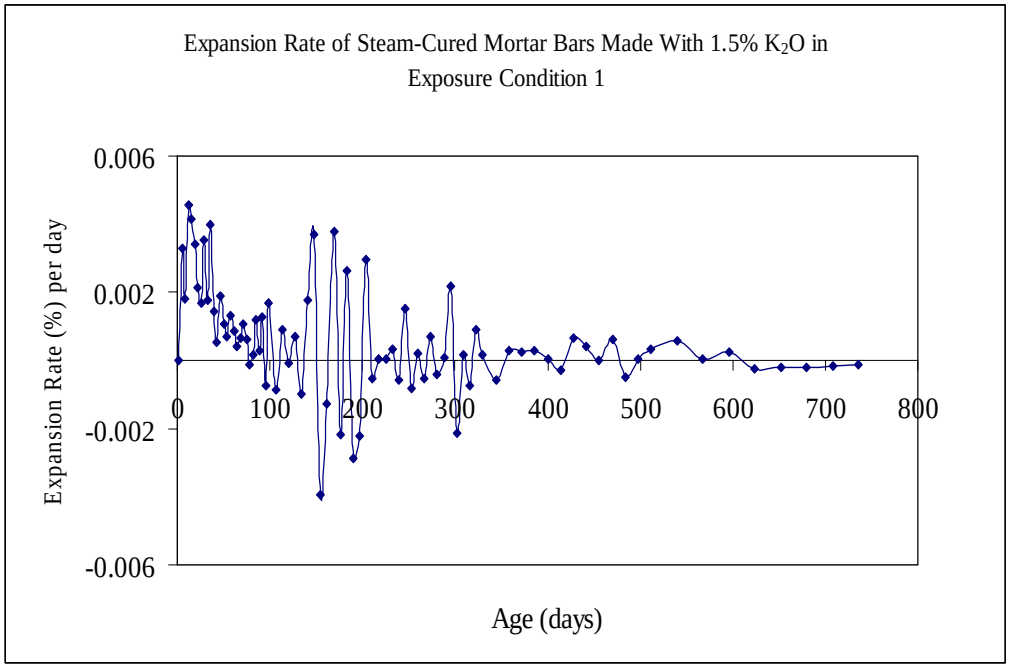


Figure 6.2: Expansion Rate of Mortar Bars Made With 1.5% $K_2O$ Subjected to Duggan Heat Cycle and Stored in Isothermal Water Bath, pH maintained at 12. 5 - limewater

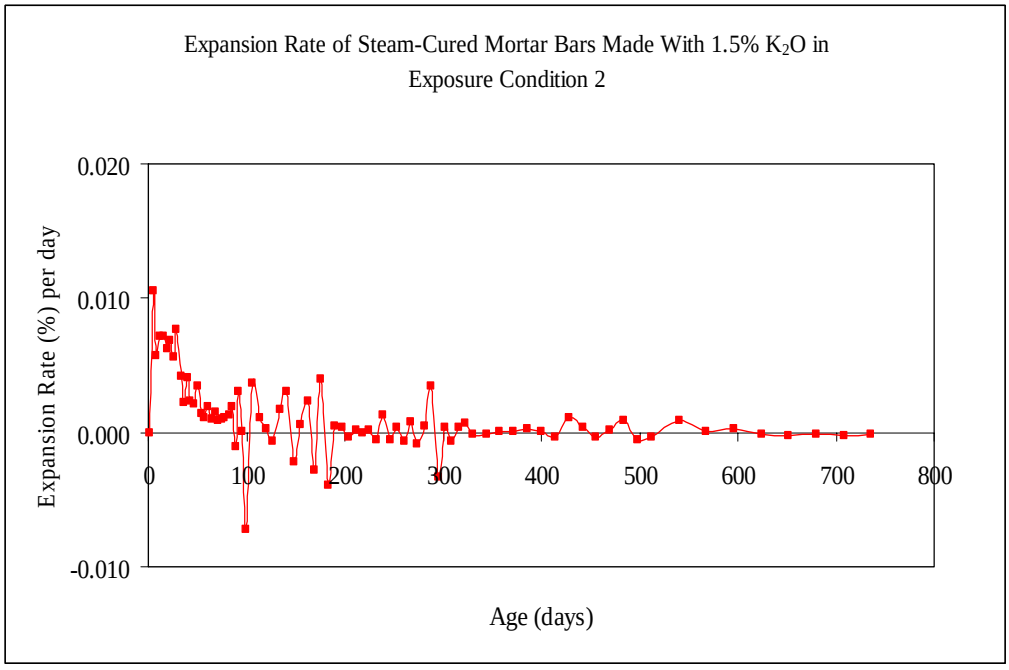


Figure 6.3: Expansion Rate of Mortar Bars Made With 1.5% $K_2O$ Subjected to Duggan Heat Cycle and Stored in Plain Water at Room Temperature

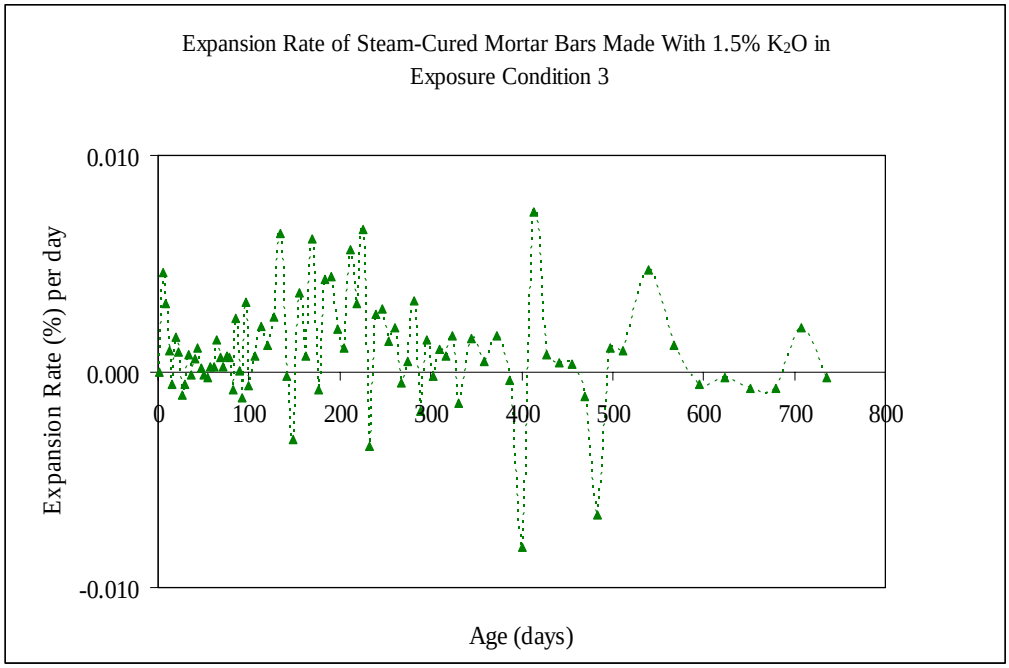


Figure 6.4: Expansion Rate of Mortar Bars Made With 1.5% $K_2O$ Subjected to Duggan Heat Cycle and Stored in Moist Air Chamber, R.H maintained at 97%

*6.3.1.2 Curve-Fitting Analysis*

Figures 6.5, 6.6, and 6.7 show the linear regression analysis curves of the experimental data. For best fit analysis of the data, two (2) linear regression curves were used for the experimental data. Mortar bars stored in exposure condition 2 (plain water at room temperature) show a higher linear correlation of expansion against age than with the other exposure conditions. Table 6.1 provides a summary of the regression equations used for analysis.

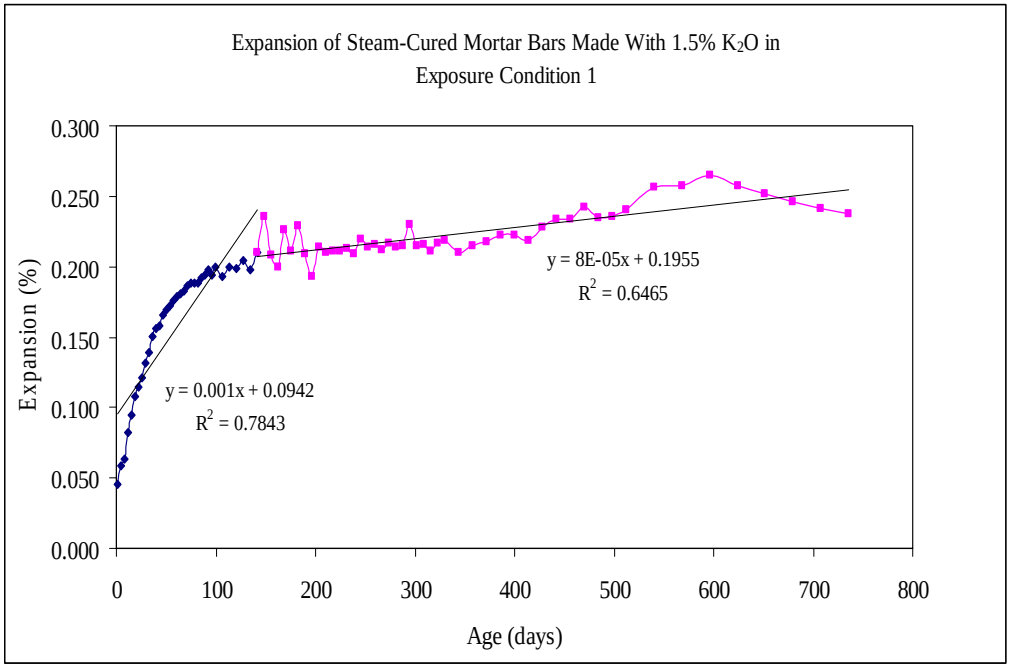


Figure 6.5: Expansion of Mortar Bars Made With 1.5% $K_2O$ Subjected to Duggan Heat Cycle and Stored in Isothermal Water Bath, pH maintained at 12.5 – limewater (Regression Curves)

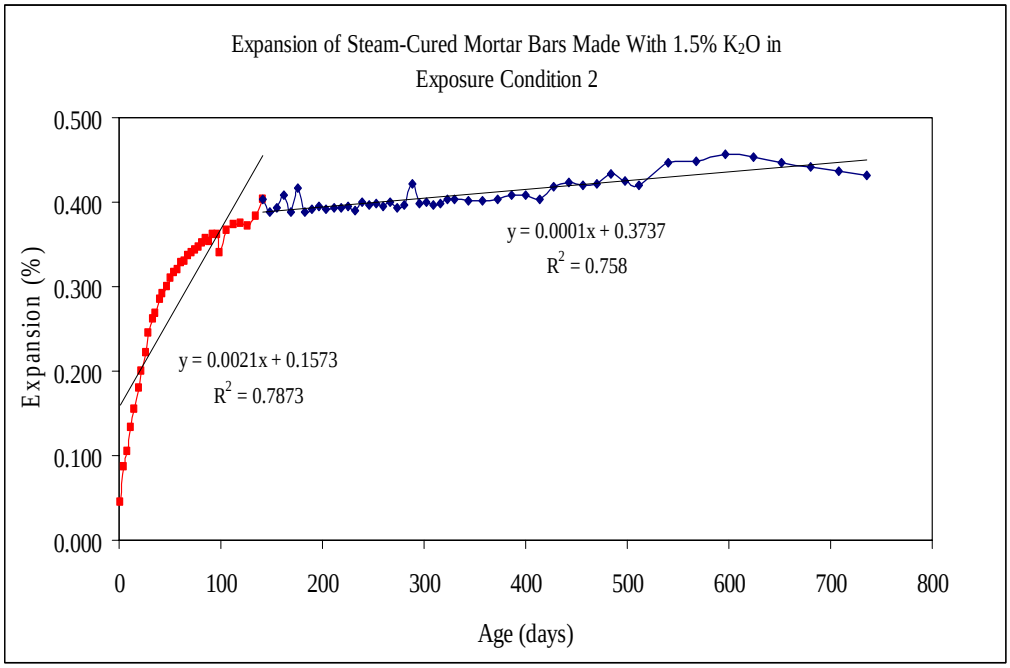


Figure 6.6: Expansion of Mortar Bars Made With 1.5% $K_2O$ Subjected to Duggan Heat Cycle and Stored in Plain Water at Room Temperatures (Regression Curves)

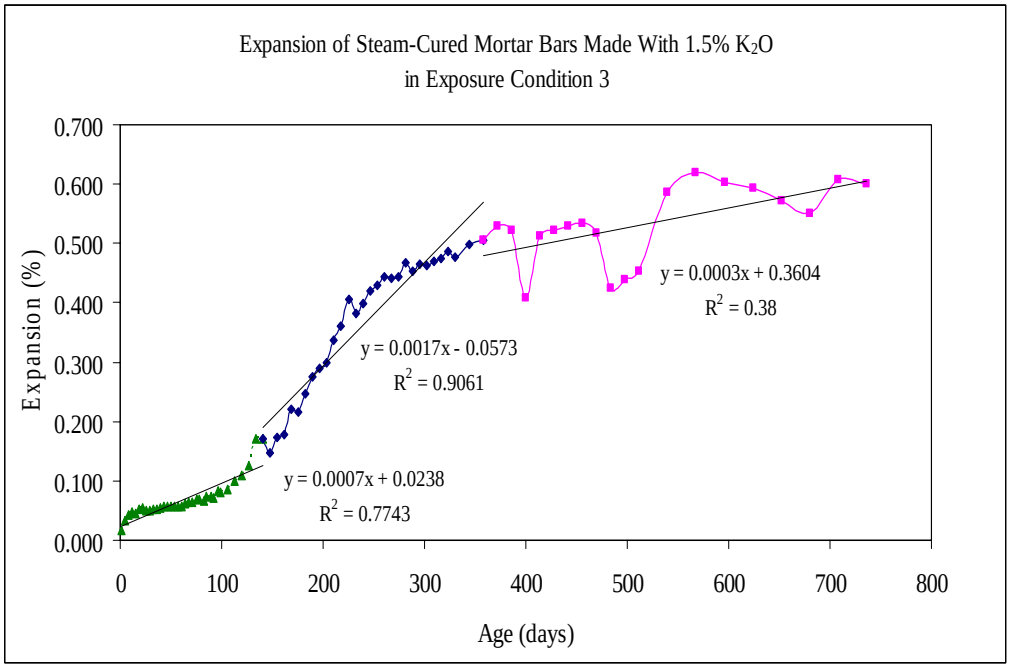


Figure 6.7: Expansion of Mortar Bars Made With 1.5% $K_2O$ Subjected to Duggan Heat Cycle and Stored in Moist Air Chamber, R.H maintained at 97% (Regression Curves)

Table 6.1: Linear Equations for Expansion vs. Age of Steam-Cured Mortar Bars Made With 1.5% $K_2O$ Subjected to Duggan Heat Cycle and Stored Under Different Exposure Conditions

| Phase 2 (Mortar with 1.5% $K_2O$ - Subjected to Duggan Heat Cycle) | | | | | |
|---|---|---|---|---|---|
| | | | | | |
| Exp. Cond. 1 | Max. Exp. 0.26% | Curve 1 | Day 1 - 141 | y = 0.0001x + 0.0942 | $R^2$ = 0.7843 |
| | | Curve 2 | Day 141 - 736 | y = 8E-05x + 0.1955 | $R^2$ = 0.6465 |
| | | | | | |
| Exp. Cond. 2 | Max. Exp. 0.46% | Curve 1 | Day 1 - 141 | y = 0.0021x + 0.1573 | $R^2$ = 0.7873 |
| | | Curve 2 | Day 141 - 736 | y = 0.0001x + 0.3737 | $R^2$ = 0.758 |
| | | | | | |
| Exp. Cond. 3 | Max. Exp. 0.62% | Curve 1 | Day 1 - 141 | y = 0.0007x + 0.0238 | $R^2$ = 0.7743 |
| | | Curve 2 | Day 141 - 358 | y = 0.0017x - 0.0573 | $R^2$ = 0.9061 |
| | | Curve 3 | Day 358 - 736 | y = 0.0003x + 0.3594 | $R^2$ = 0.3792 |
| | | | | | |

### *6.3.2 Weight Change Results*

#### *6.3.2.1 Weight Change Measurements*

Weight change of the mortar bars under different exposure conditions is shown in Figure 6.8. After just 1 day of storage, a significant weight-change of about 10% was observed in exposure conditions 1 and 2. It can be seen that all the specimens showed significant weight changes during the first 100 days of storage. The increase in weight-change can be attributed to increased capillary pore volume and the storage solution filling in the increased volume. The mortar bars in exposure conditions 1 and 2 posed similar weight change patterns throughout the entire research project. Weight changes of specimens in exposure condition 3 were the lowest, but increased at a steady rate during the time of storage. The increase in weight change continued for later stages after 100 days but at a much slower rate. Much of the weight gain can be attributed to substantial weight gain associated with large expansion exhibited by the mortar bars. The maximum weight changes observed were 12.79%, 12.91% and 10.34% in exposure conditions 1, 2 and 3 respectively.

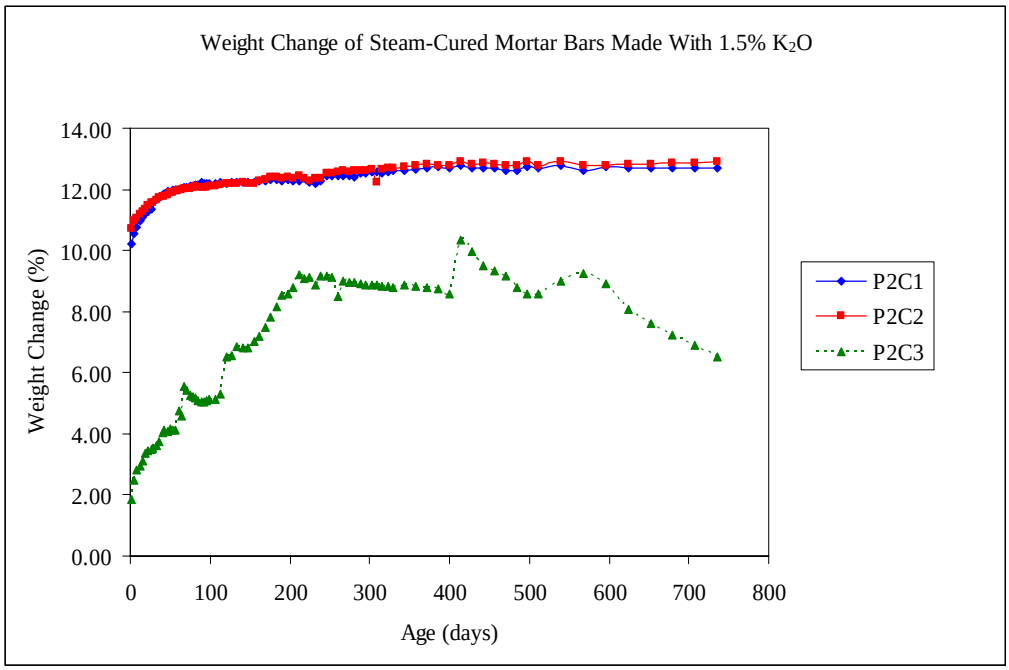


Figure 6.8: Weight Change of Mortar Bars Made With 1.5% $K_2O$ Subjected to Duggan Heat Cycle and Stored Under Different Exposure Conditions

*6.3.2.2 Curve-Fitting Analysis*

The best correlation coefficient for the weight change against age for the experimental data was obtained using linear regression curves. Figure 6.9 through 6.11 show linear regression curves fitted to the data. The experimental data for the first 100 days of storage was fitted with a linear regression curve which revealed a high linear correlation coefficient for all exposure conditions. Table 6.2 gives the regression equations used for the experimental data.

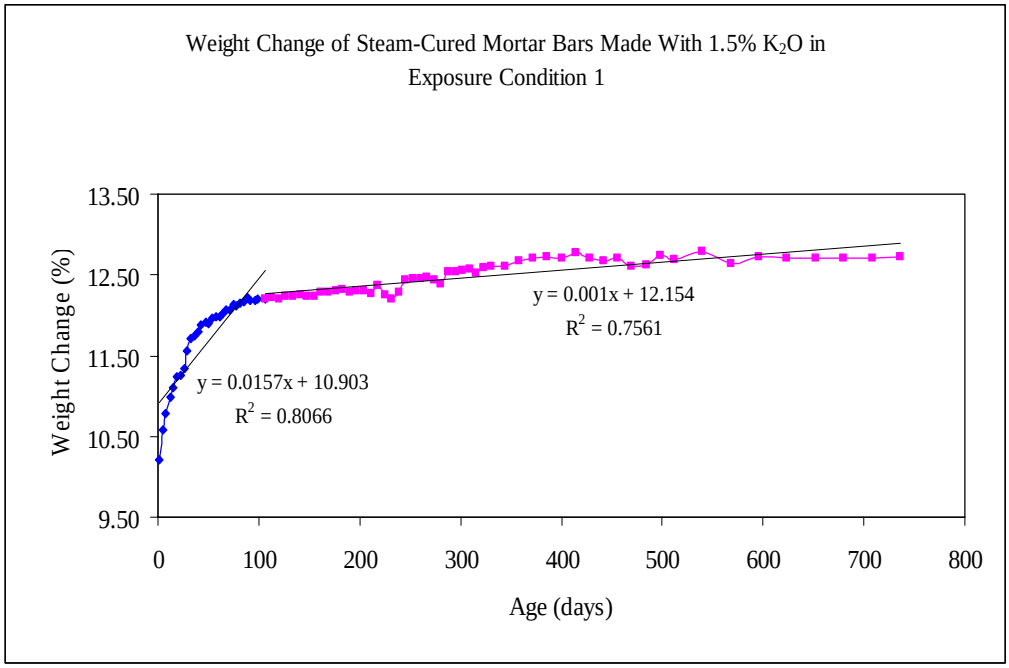


Figure 6.9: Weight Change of Mortar Bars Made With 1.5% $K_2O$ Subjected to Duggan Heat Cycle and Stored in Isothermal Water Bath, pH maintained at 12.5 - limewater (Regression Curves)

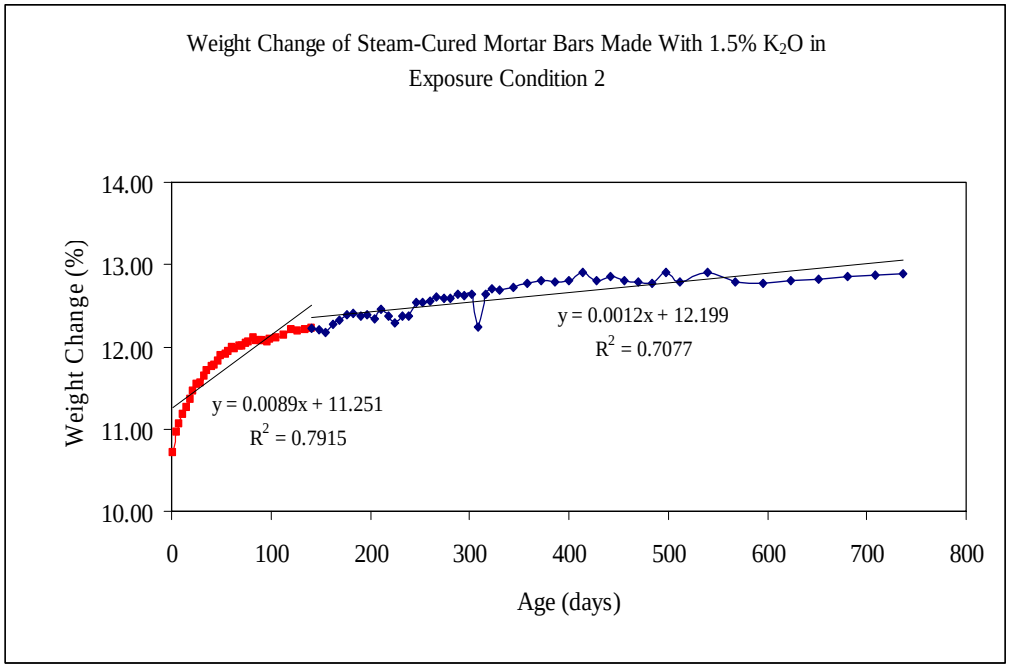


Figure 6.10: Weight Change of Mortar Bars Made With 1.5% $K_2O$ Subjected to Duggan Heat Cycle and Stored in Plain Water at Room Temperature (Regression Curves)

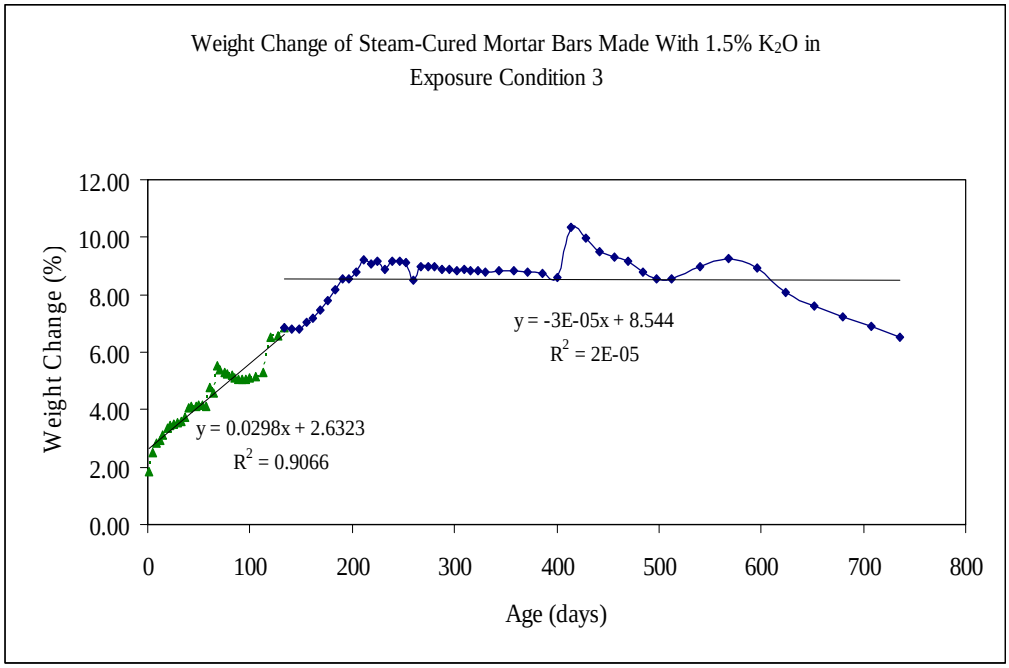


Figure 6.11: Weight Change of Mortar Bars Made With 1.5% $K_2O$ Subjected to Duggan Heat Cycle and Stored in Moist Air Chamber, R.H maintained at 97% (Regression Curves)

Table 6.2: Linear Equations for Weight Change vs. Age of Steam-Cured Mortar Bars With 1.5% $K_2O$ Subjected to Duggan Heat Cycle and Stored Under Different Exposure Conditions

| Phase 2 (Mortar Bars with 1.5% $K_2O$ - Subjected to Duggan Heat Cycle) | | | | | |
|---|---|---|---|---|---|
| | | | | | |
| Exp. Cond. 1 | Max. 12.79% | Curve 1 | Day 1 - 106 | y = 0.0157x + 10.903 | $R^2$ = 0.8066 |
| | | Curve 2 | Day 106 - 736 | y = 0.001x + 12.154 | $R^2$ = 0.7561 |
| | | | | | |
| Exp. Cond. 2 | Max. 12.91% | Curve 1 | Day 1 - 141 | y = 0.0089x + 11.251 | $R^2$ = 0.7915 |
| | | Curve 2 | Day 141 - 736 | y = 0.0012x + 12.199 | $R^2$ = 0.7077 |
| | | | | | |
| Exp. Cond. 3 | Max. 10.34% | Curve 1 | Day 1 - 134 | y = 0.0298x + 2.6323 | $R^2$ = 0.9066 |
| | | Curve 2 | Day 134 - 736 | y = -3E-05x + 8.544 | $R^2$ = 2E-05 |

*6.3.3 Expansion and Weight Change*

Mortar mixes with high alkali content show the expansion and weight change experimental data to be linearly correlated. The mortar bars mixed during this phase study have 1.5% $K_2O$ content and were stored under different exposure conditions after the Duggan heat cycle. Most of the mortar specimens in all the different exposure conditions showed a weight-change increase with an increase in expansion. Mortar bars in exposure conditions 1 and 2 acted in a similar manner. Figure 6.12 shows the expansion against weight-change data results.

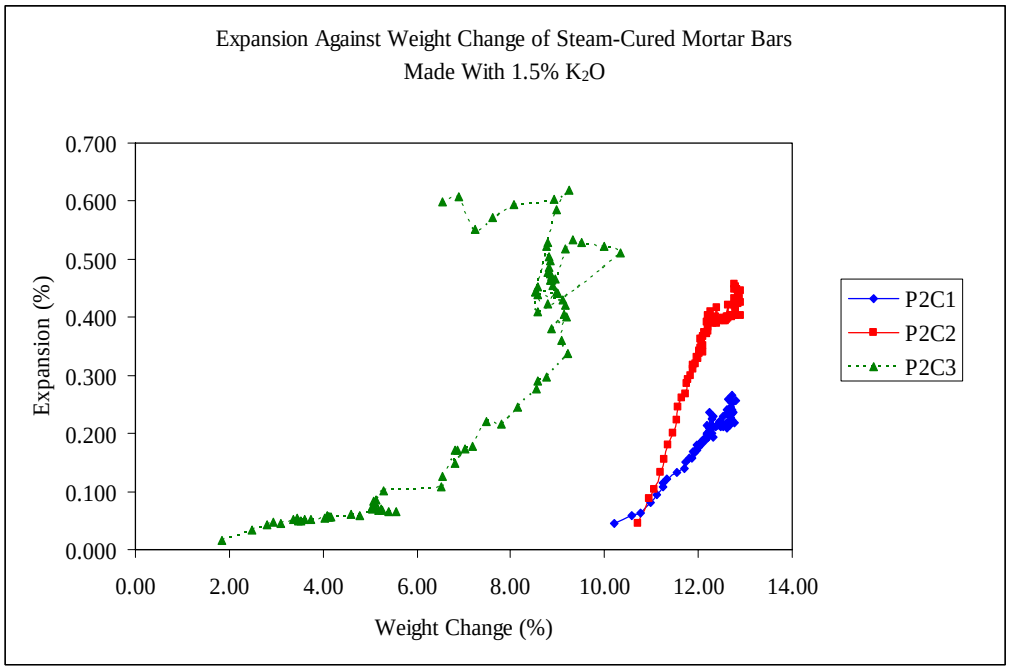


Figure 6.12: Expansion Against Weight Change of Mortar Bars Made With 1.5% $K_2O$ Subjected to Duggan Heat Cycle and Stored Under Different Conditions

The best correlation coefficient for the expansion against weight change of the mortar bars was obtained using linear regression analysis. Figures 6.13 through 6.15 show the linear and polynomial regression curves of the mortar bars for the different exposure conditions. The results revealed that a high positive linear correlation exists during the first 100 days of storage between expansion and weight-change of the mortar bars in all the exposure conditions. This can be attributed to the paste expansion which increases the capillary pore volume of the paste itself, and the storage solution filling the increased volume results in weight gain (Shimada, 2005). Table 6.3 provides the regression equations and coefficient for the different exposure conditions.

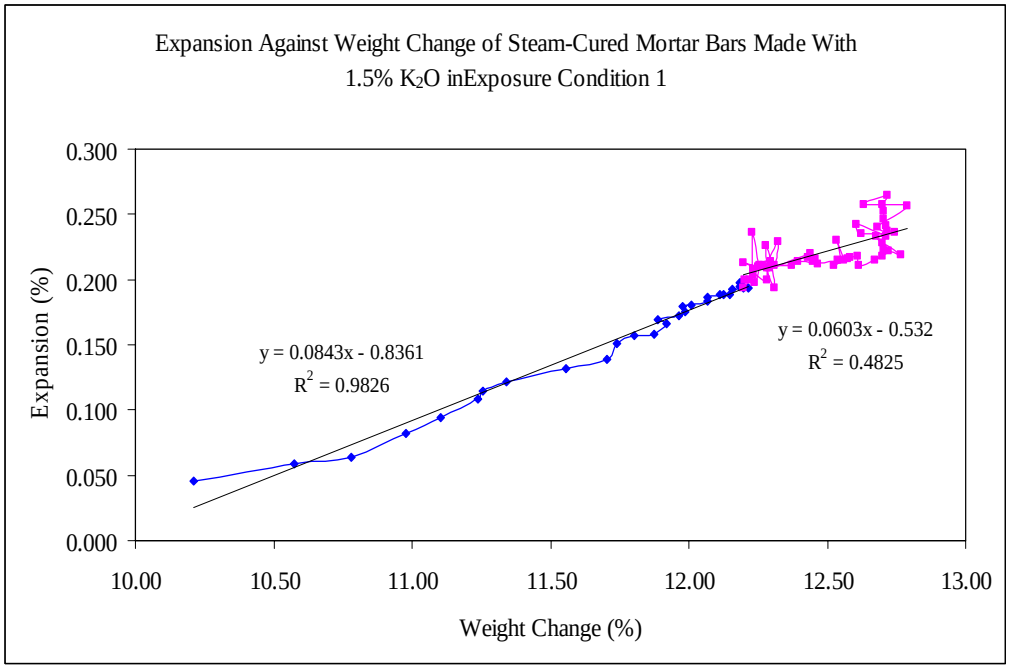


Figure 6.13: Expansion Against Weight Change of Mortar Bars Made With 1.5% $K_2O$ Subjected to Duggan Heat Cycle and Stored in Isothermal Water Bath, pH maintained at 12.5 - limewater (Regression Curves)

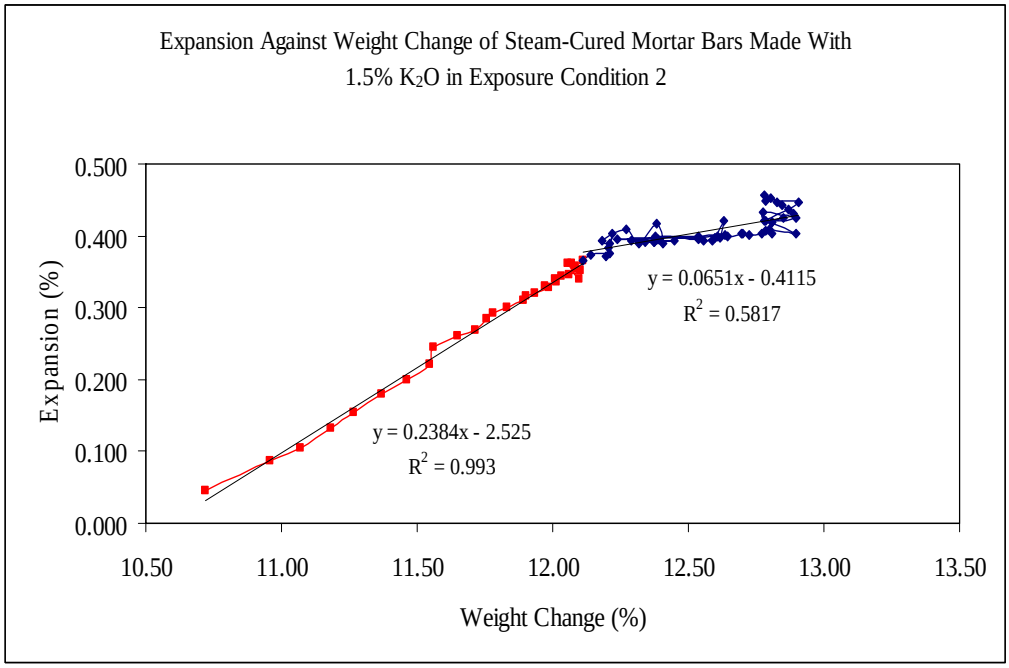


Figure 6.14: Expansion Against Weight Change of Mortar Bars Made With 1.5% $K_2O$ Subjected to Duggan Heat Cycle and Stored in Plain Water at Room Temperature (Regression Curves)

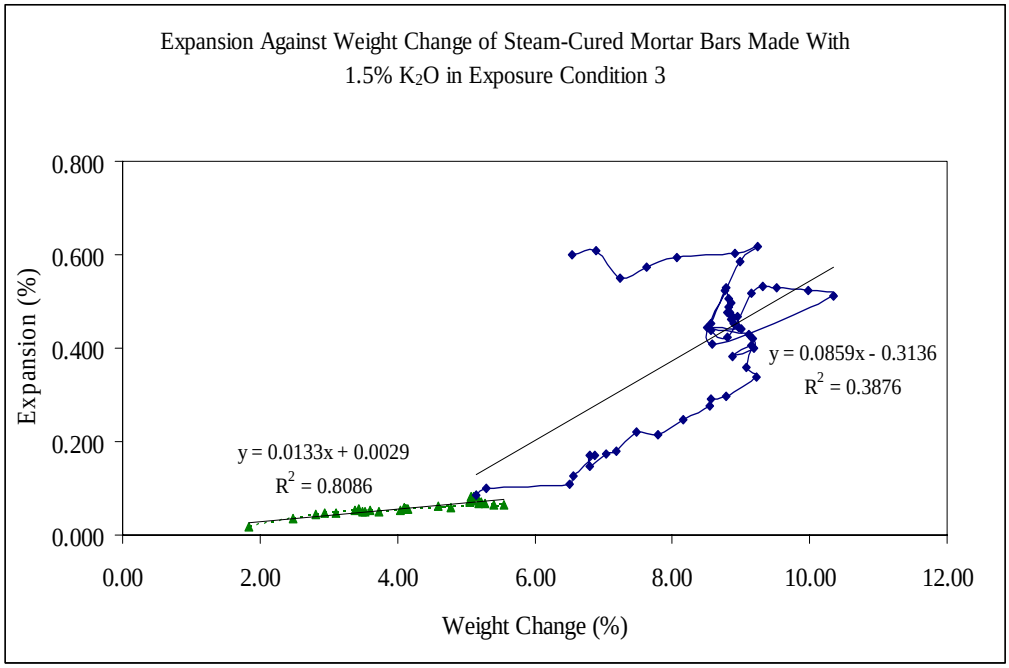


Figure 6.15: Expansion Against Weight Change of Mortar Bars Made With 1.5% $K_2O$ Subjected to Duggan Heat Cycle and Stored in Moist Air Chamber, R.H maintained at 97% (Regression Curves)

Table 6.3: Linear Equations for Expansion Against Weight Change of Steam-Cured Mortar Bars Made With 1.5% $K_2O$ Subjected to Duggan Heat cycle and Stored Under Different Exposure Conditions

| Phase 2 (Mortar Made With 1.5% $K_2O$ - Subjected to Duggan Heat Cycle) | | | | |
|---|---|---|---|---|
| | | | | |
| Exp. Cond. 1 | Curve 1 | Day 1 - 106 | y = 0.0843x - 0.8361 | $R^2$ = 0.9826 |
| | Curve 2 | Day 106 - 736 | y = 0.0603x - 0.532 | $R^2$ = 0.4825 |
| | | | | |
| Exp. Cond. 2 | Curve 1 | Day 1 - 106 | y = 0.2384x - 2.525 | $R^2$ = 0.993 |
| | Curve 2 | Day 106 - 736 | y = 0.0651x - 0.4115 | $R^2$ = 0.5817 |
| | | | | |
| Exp. Cond. 3 | Curve 1 | Day 1 - 106 | y = 0.0133x + 0.0029 | $R^2$ = 0.8086 |
| | Curve 2 | Day 106 - 736 | y = 0.0859x - 0.3136 | $R^2$ = 0.3875 |
| | | | | |

*6.3.4 Compressive Strength Results*

The compressive strength testing results after 28 days were 4590 psi, 4767 psi and 6692 psi for exposure conditions 1, 2 and 3 respectively. Compressive strength tests at later ages in all the exposure conditions showed an average increase of 25%. Mortar samples in relative humidity of 97% (Exp. Cond. 3) exhibited the highest average compressive strength throughout. Figure 6.16 shows the compressive strength tests of the mortar specimens with 1.5% $K_2O$ and subjected to the Duggan regime. The result of the average and standard deviation (Std) of the compressive strengths are shown in Table 6.4.

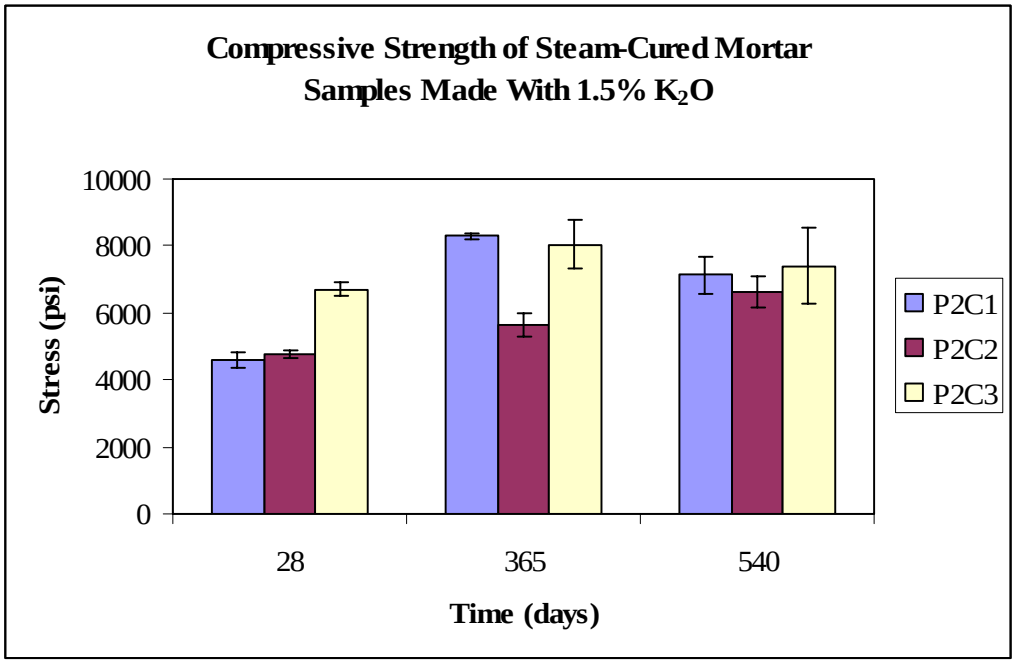


Figure 6.16: Compressive Strength Chart of Mortar Samples Made With 1.5% $K_2O$ Subjected to Duggan Heat Cycle and Stored Under Different Exposure Conditions

Table 6.4: Compressive Strength of Mortar Samples Made With 1.5% $K_2O$ Subjected to Duggan Heat Cycle and Stored Under Different Exposure Conditions

| | Average Compressive Strength (psi) | | |
|---|---|---|---|
| | 28 Days | 365 Days | 540 Days |
| | Std | Std | Std |
| P2C1 | 4590 | 8292 | 7133 |
| | 259 | 72 | 535 |
| P2C2 | 4767 | 5617 | 6642 |
| | 101 | 351 | 465 |
| P2C3 | 6692 | 8042 | 7400 |
| | 201 | 726 | 1131 |

*6.4 Field Samples Made With 1.5% $K_2O$ (No Duggan Heat Cycle)*

Two (2) batches of mortar with 1.5% $K_2O$ content were mixed and subjected to atmospheric conditions outside the laboratory. The first batch (P2C4A) was steam-cured, subsequently stored in water for six (6) days and the stored outside the laboratory exposed to environmental field conditions. The second batch (P2C4B) was cured in the laboratory at room temperature for 24 hours, and then stored under water for six (6) days prior to exposure to field conditions. In both mortar batches, no Duggan heat cycle was employed in the sample preparation. Only the potassium content was increased with other parameters kept constant. Expansion and weight change were monitored for almost two (2) years of storage.

*6.4.1 Length Change Results*

The maximum length-change measurements recorded for exposure conditions 4A and 4B were about 0.000% and 0.021% respectively. The length change of the mortar bars made with 1.5% $K_2O$ show similar patterns regardless of the pre-curing process. Exposure condition 4B shows less shrinkage than exposure condition 4A. The shrinkage rate of the mortar bars is highly influenced by the environmental conditions during periodically length and weight-change measurements. Figures 6.17 and 6.18 show the length-change and shrinkage rate of the mortar samples made with 1.5% $K_2O$ and stored under field conditions.

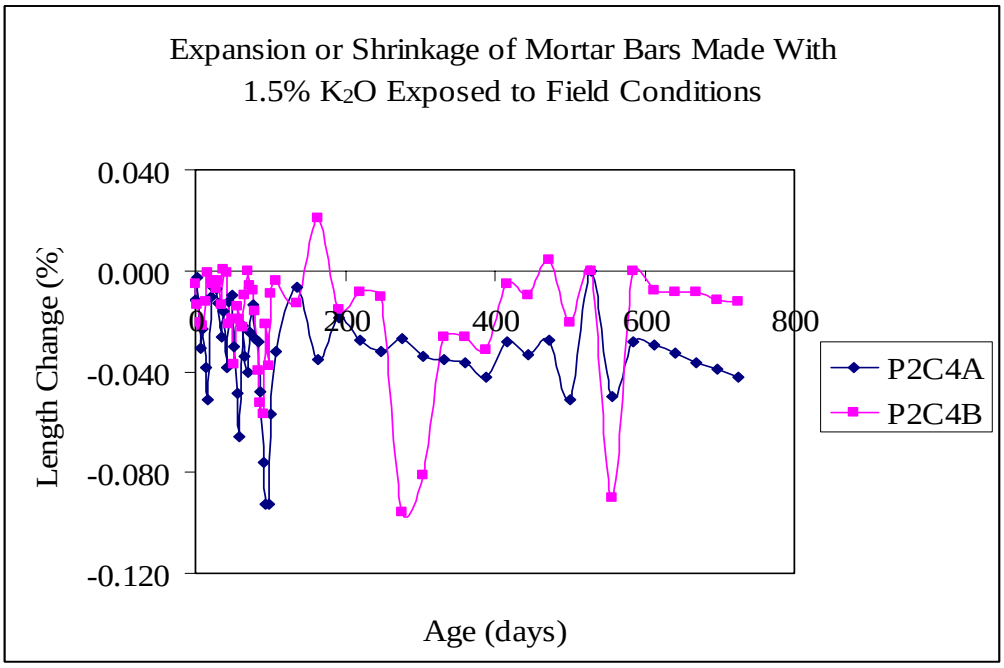


Figure 6.17: Length Change of Mortar Bars Made With 1.5% $K_2O$ Exposed to Field Conditions

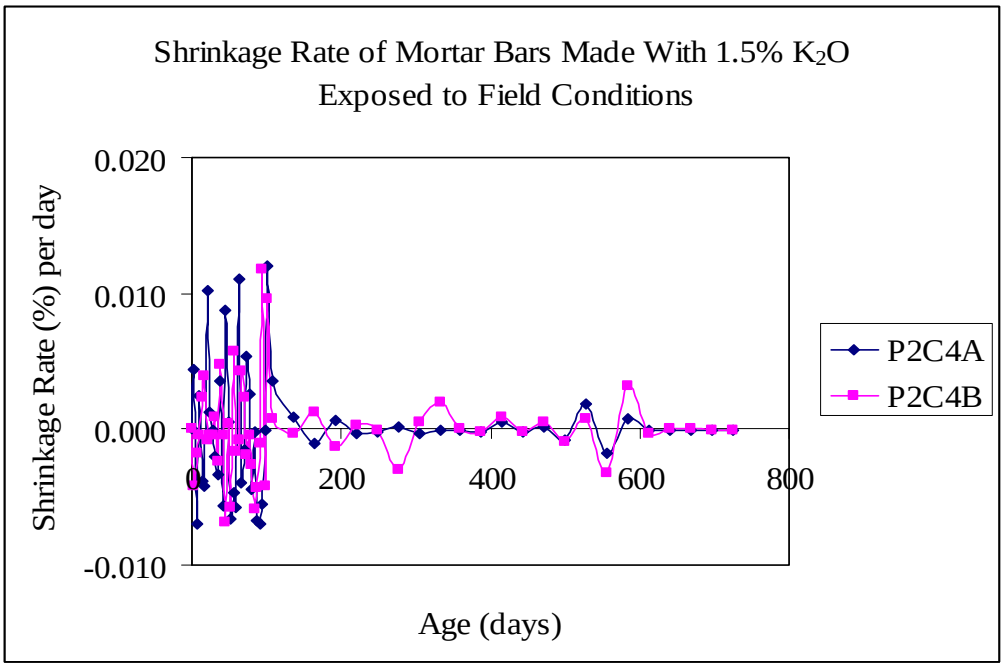


Figure 6.18: Shrinkage Rate of Mortar Bars Made With 1.5% $K_2O$ Exposed to Field Conditions

Figures 6.19 and 6.20 show the regression analysis curves of the field-exposed mortar samples made with 1.5% $K_2O$. The field-exposed mortar specimens showed no correlation between length-change and time. There were several changing parameters affecting the expansion or shrinkage of the mortar specimens. Table 6.5 provides the linear equations used for the best fit to the experimental data.

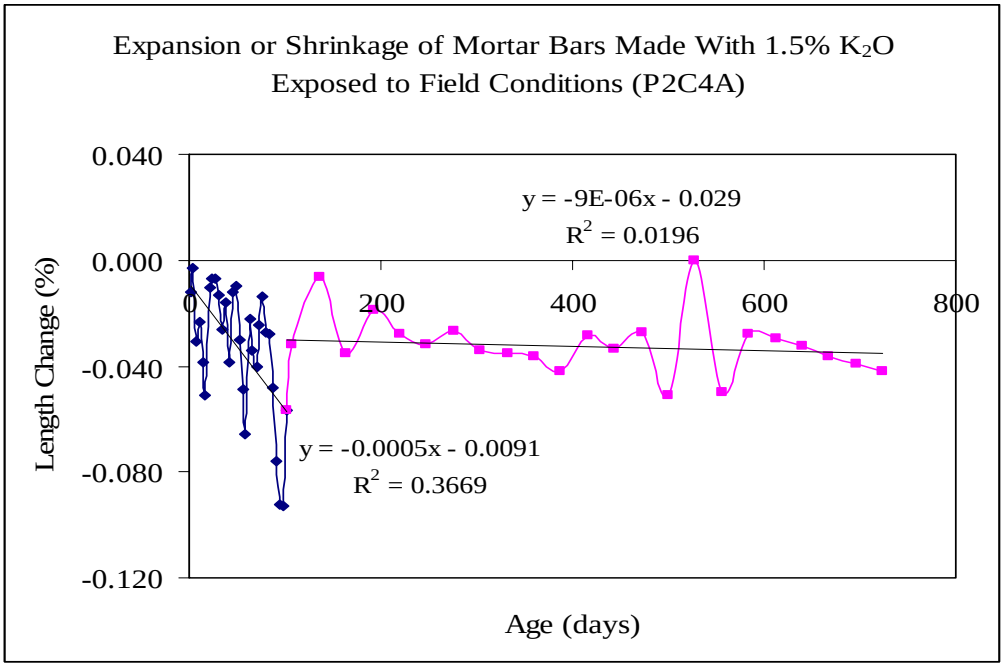


Figure 6.19: Length Change vs. Age of Steam-Cured Mortar Bars Made With 1.5% $K_2O$ and Stored Under Field Conditions (C4A) (Regression Curves)

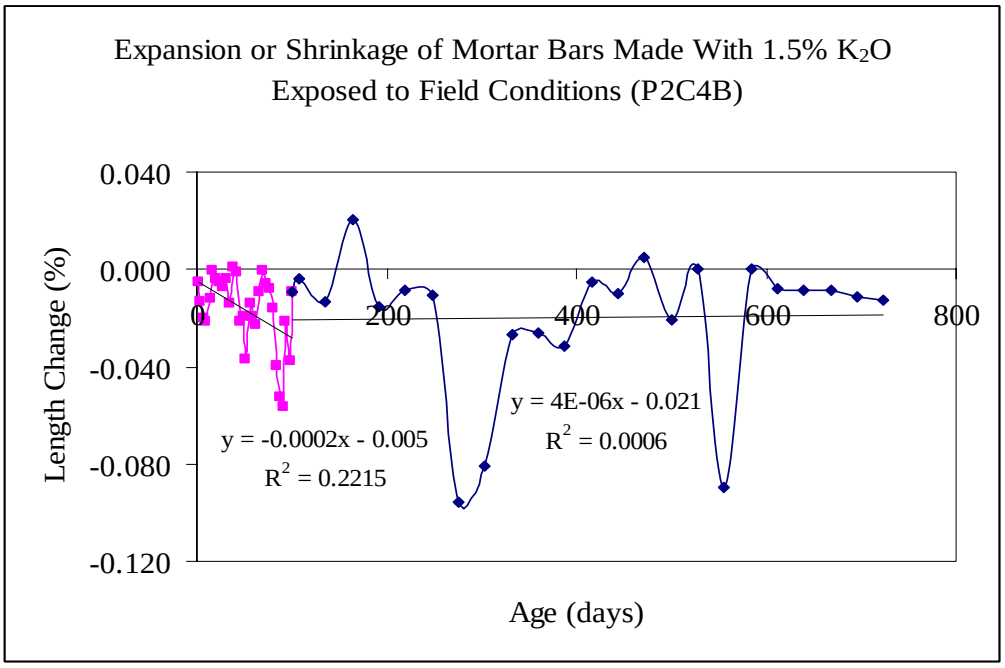


Figure 6.20: Length Change vs. Age of Room Temperature-Cured Mortar Bars Made With 1.5% $K_2O$ and Stored Under Field Conditions (C4B) (Regression Curves)

Table 6.5: Linear Equations for Length Change vs. Age of Mortar Bars Made With 1.5% $K_2O$ and Stored Under Field Conditions

| Phase 2 (Mortar Bars Made With 1.5% $K_2O$ Exposed to Field Conditions) | | | | |
|---|---|---|---|---|
| | | | | |
| Exp. Cond. 1 | Curve 1 | Day 1 - 101 | y = -0.0005x - 0.0091 | $R^2$ = 0.3669 |
| | Curve 2 | Day 101 - 724 | y = -9E-06x - 0.029 | $R^2$ = 0.0196 |
| | | | | |
| Exp. Cond. 2 | Curve 1 | Day 1 - 101 | y = -0.0002x - 0.005 | $R^2$ = 02215 |
| | Curve 2 | Day 101 - 724 | y = 4E-06x - 0.021 | $R^2$ = 0.0006 |
| | | | | |

*6.4.2 Weight Change Results*

Weight change measurements of the mortar samples made with 1.5% $K_2O$ content show a 5 to 6% decrease in mass for both sets of the field specimens. No weight-change pattern or trend could be outlined from the experimental data. The weight-change results decreased with time for the entire research. Figure 6.21 shows the weight change against age results of the field-exposed mortar samples.

Figures 6.22 and 6.23 provide the regression analysis curves of the data. There exists little or no correlation between weight changes against time. The field exposed mortar specimens exhibited shrinkage or low expansion and insufficient exposure to water resulted in little or no weight gain. Table 6.6 gives the regression equations used for the analysis.

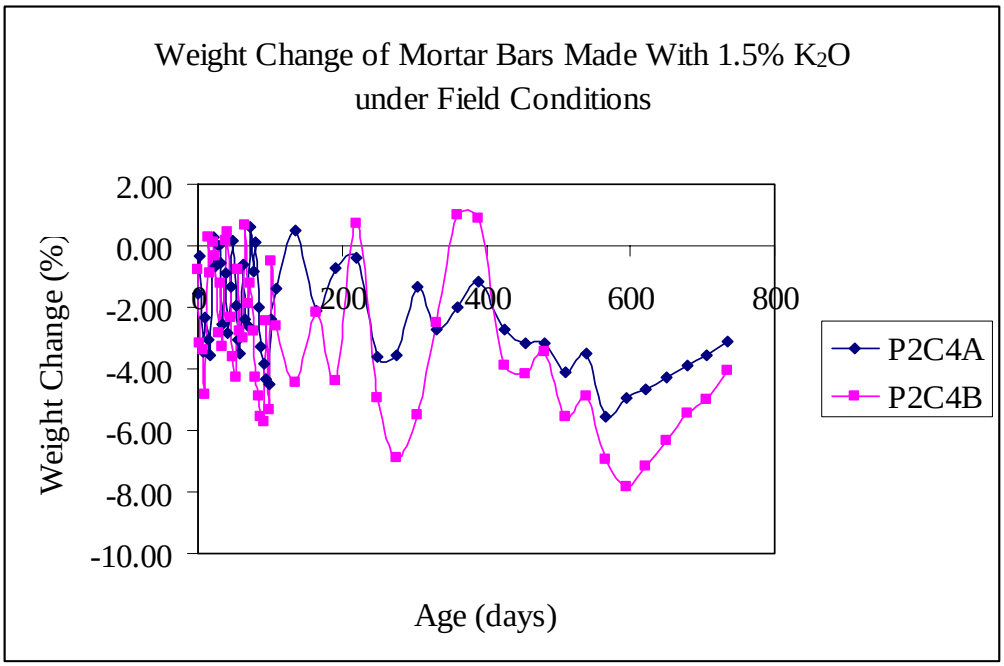


Figure 6.21: Weight Change of Mortar Bars Made With 1.5% $K_2O$ Exposed to Field Conditions

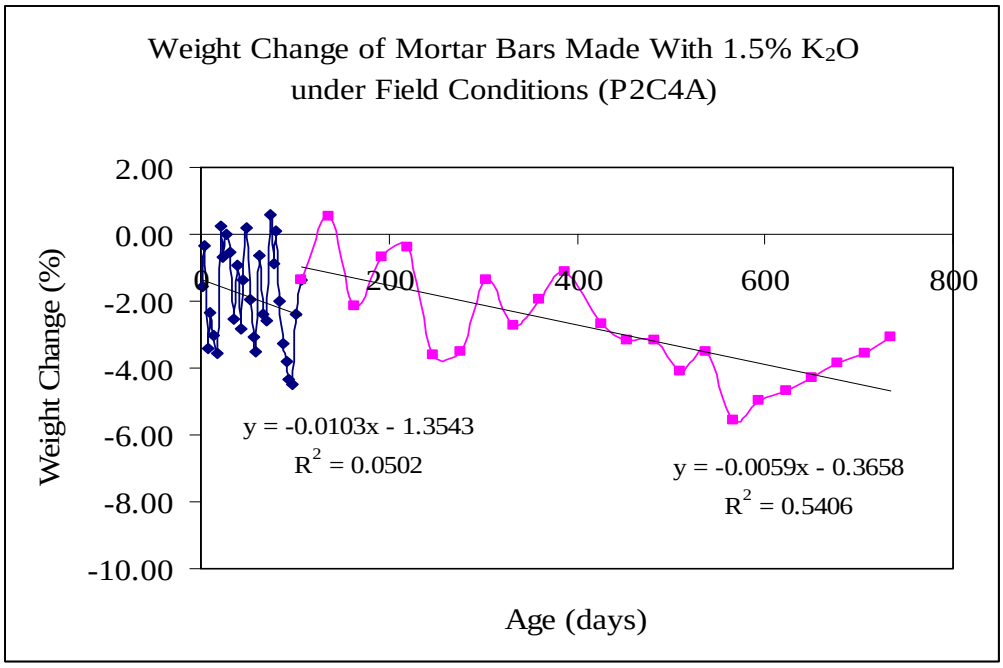


Figure 6.22: Weight Change vs. Age of Steam-Cured Mortar Bars Made With 1.5% $K_2O$ and Stored Under Field Conditions (C4A) (Regression Curves)

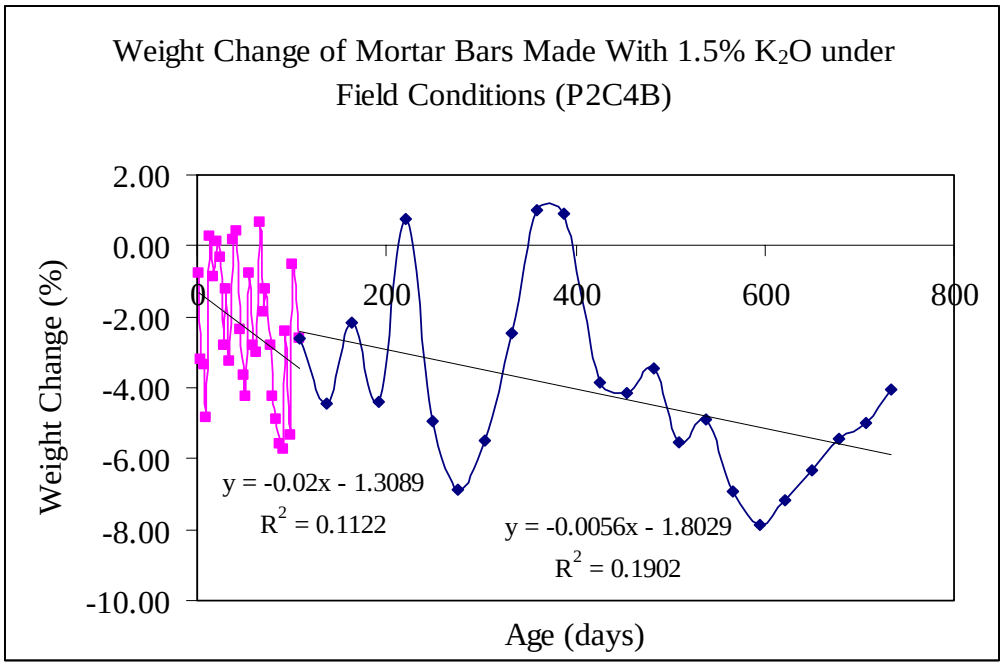


Figure 6.23: Weight Change vs. Age of Room Temperature-Cured Mortar Bars Made With 1.5% $K_2O$ and Stored Under Field Conditions (C4B) (Regression Curves)

Table 6.6: Linear Equations for Weight Change vs. Age of Mortar Bars Made With 1.5% $K_2O$ Stored Under Field Conditions

| Phase 2 (Mortar Samples Made With 1.5% $K_2O$ - Field Conditions) | | | | |
|---|---|---|---|---|
| | | | | |
| Exp. Cond. 4A | Curve 1 | Day 1 - 108 | y = -0.0103x - 1.3543 | $R^2$ = 0.0502 |
| | Curve 2 | Day 108 - 734 | y = -0.0059x - 0.3658 | $R^2$ = 0.5406 |
| | | | | |
| Exp. Cond. 4B | Curve 1 | Day 1 - 108 | y = -0.02x - 1.3089 | $R^2$ = 0.0365 |
| | Curve 2 | Day 100 - 734 | y = -0.00356x - 1.8029 | $R^2$ = 0.1902 |
| | | | | |

*6.4.3 Compressive Strength Results*

Compressive strength was checked at 28 days, 365 days, and 540 days for both field-exposed mortar samples. After 28 days of storage, the compressive strength testing of the room temperature-cured mortar cubes (Exp. Cond. 4B) exhibited an average of 5725 psi and the steam-cured specimens (Exp. Cond. 4A) exhibited an average of 5043 psi. Steam-curing contributes a major role in the early strength of mortar samples. The compressive strength results at 540 days were 8850 psi and 6692 psi for exposure conditions 4A and 4B respectively. Figure 5.24 shows the effect of steam-curing and high potassium content on the strength of the field exposure mortar samples. Table 6.2 gives the average and standard deviation of compressive strength results of the mortar specimens.

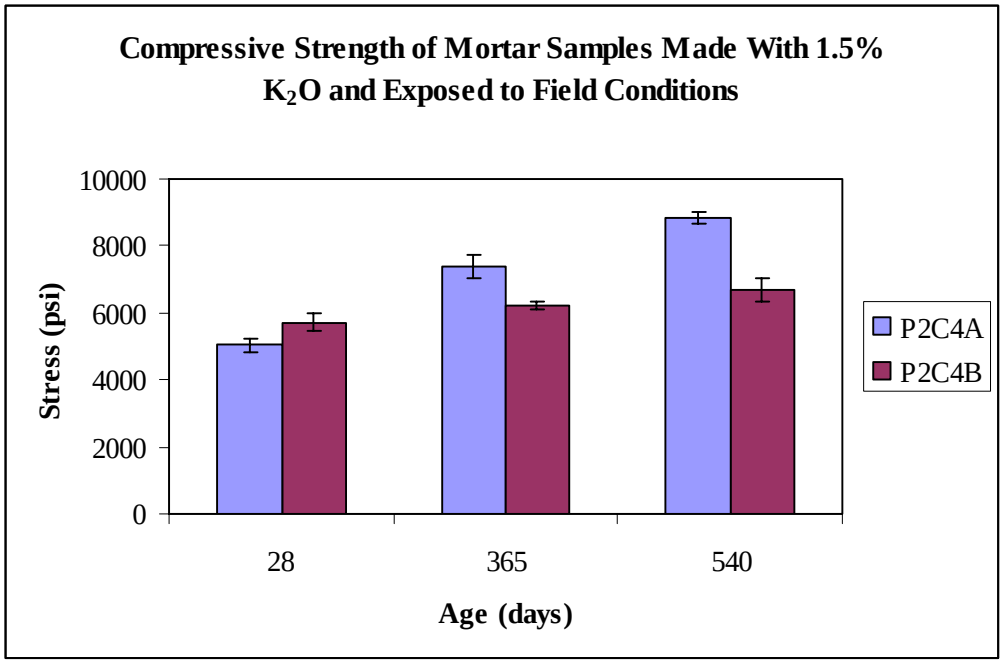


Figure 6.24: Compressive Strength Chart of Mortar Samples Made With 1.5% $K_2O$ and Exposed to Field Conditions

Table 6.7: Compressive Strength of Mortar Samples Made With 1.5% $K_2O$ and Exposed to Field Conditions

| | Average Compressive Strength (psi) | | |
|---|---|---|---|
| | 28 Days | 365 Days | 540 Days |
| | Std | Std | Std |
| P2C4A | 5043 | 7375 | 8850 |
| | 191 | 331 | 180 |
| P2C4B | 5725 | 6225 | 6692 |
| | 278 | 130 | 341 |

*6.5 Water Analysis Results of the Storage Solutions*

The mortar samples made with 1.5% potassium content ($K_2O$) were stored under similar conditions as the controls and the ion concentrations of their respective storage solutions were monitored. The pH value, Potassium ($K^+$), Sodium ($Na^+$) and Calcium ($Ca^{2+}$) ion concentrations were monitored periodically.

*6.5.1 Water Analysis of Exposure Condition 1*

The amount of alkali leached increased with time. A substantial amount of the alkalis were leached from the mortar samples during the first 100 days of storage. The highest recorded alkali concentration was 144.2 mmol/l. The alkalis content could apparently increase the solubility of ettringite and enhanced its formation (Wang et al. 1986). Figure 6.25 provides a plot of the results of the total amount of alkali leached against age (from the end of the Duggan heat cycle).

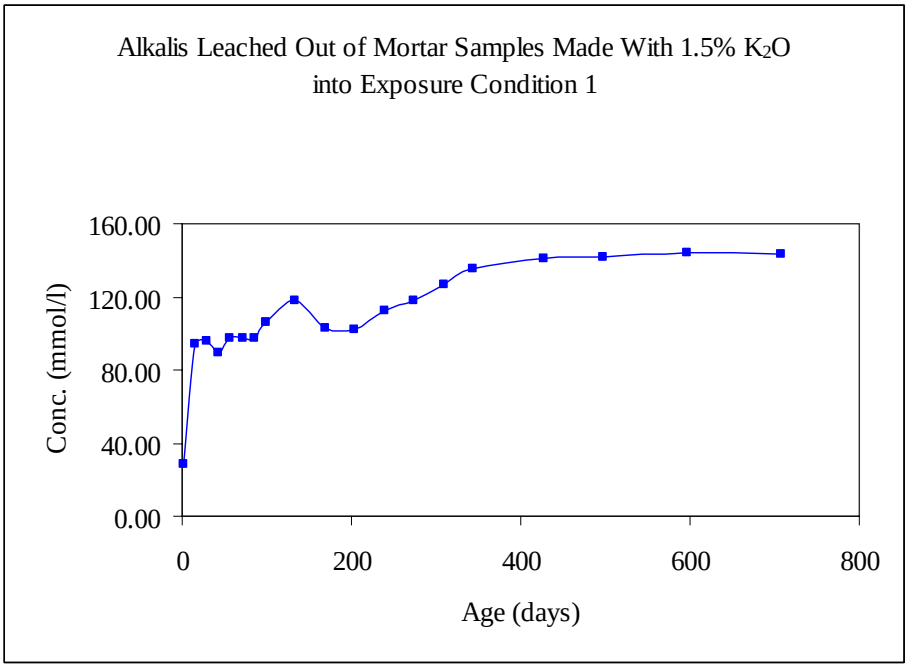


Figure 6.25: Alkalis Leaching from Mortar Samples Made With 1.5% $K_2O$ and Stored in Isothermal Water Bath, pH maintained at 12.5 - limewater

*6.5.2 Water Analysis of Exposure Condition 2*

The mortar samples made with 1.5%$K_2O$ and then stored in exposure condition 2 (water at room temperature) were monitored for pH value, $Na^+$, $K^+$ and $Ca^{2+}$ ion concentrations.

*6.5.2.1 Amount of Alkalis*

An increase in the amount of potassium content ($K_2O$) in the mortar mixes increases the amount of alkali being leached into the surrounding storage solution. The amount of alkali leached was higher in exposure condition 2 than 1. Figure 6.26 shows that the alkalis had been leached out of the mortar samples made with 1.5% $K_2O$ into the storage solution of exposure condition 2.

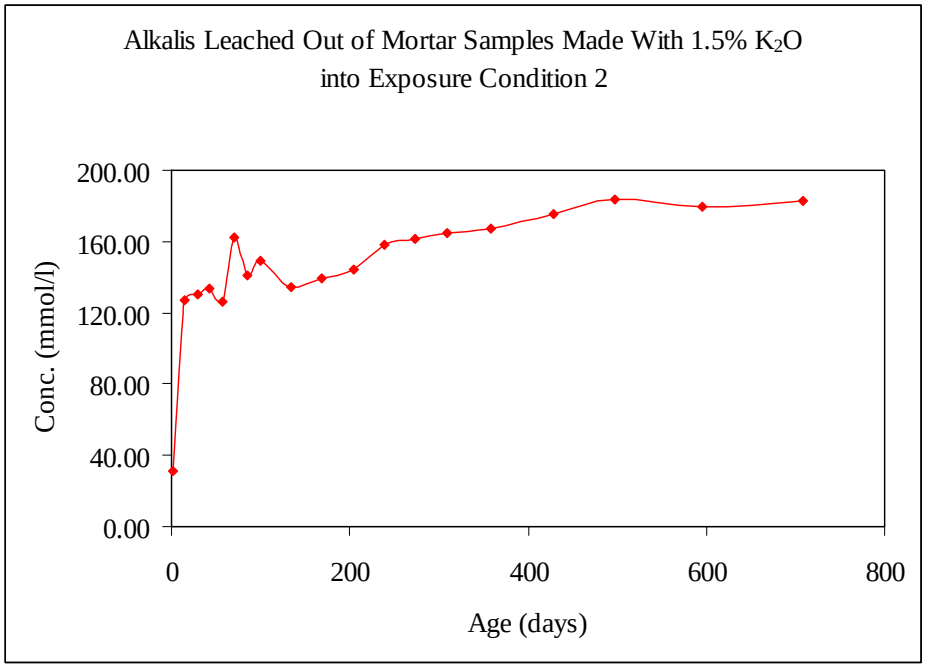


Figure 6.26: Alkali Leaching from Mortar Samples Made With 1.5% $K_2O$ and Stored in Plain Water at Room Temperature

*6.5.2.2 pH Value*

The pH value does change significantly with an increase in the potassium ($K_2O$) content of the mortar samples. This can be attributed to an increase in the hydroxide ion ($OH^-$) concentration in the solution containing high alkali mortar samples. Again, the pH values range from 11.10 to 12.23.

*6.5.2.3 Calcium Concentration*

The amount of calcium ions leached to the surrounding storage solution seems to be suppressed by the high alkali content of the mortar samples. Figure 6.27 shows the calcium concentration of the storage solution for exposure condition 2. The

highest amount of calcium leached was 108 mmol/l recorded after 400 days of storage in exposure condition 2 (plain water at room temperature).

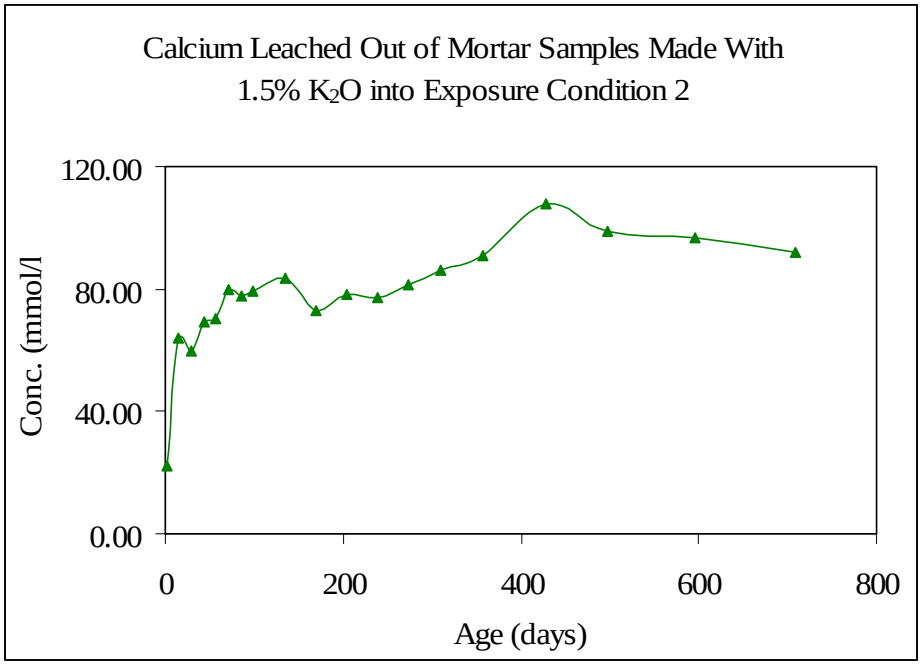


Figure 6.27: Calcium Leaching from Mortar Samples Made With 1.5% $K_2O$ and Stored in Plain Water at Room Temperature

*6.6 Microstructure Analysis Using SEM and EDAX*

For each SEM study, three sets of specimens from the samples were collected at different locations for testing. Prior to SEM examinations, specimens were carbon coated for accurate analysis. SEM equipped with EDAX was conducted for elemental analysis of the chemical composition of the gel within the microstructure of the specimens. The specimens were prepared as fractured surface samples for SEM examinations to show DEF in cracks, cavities and the interface between the cement paste and aggregates. High magnifications by SEM and EDAX elemental analysis

were used to identify the deterioration mechanism and differentiate between different morphologies of ettringite (DEF), alkali-aggregate reaction (AAR) and alkali-silica reaction (ASR) gel.

*6.6.1 Mortar Samples in Exposure Condition 1*

After 40 days of storage in water with pH maintained at 12.5 - limewater (Exp. Cond. 1), a fractured sample was collected for SEM study on the expanded mortar bars. Figure 6.28 shows well-developed spherical balls of ettringite gel identified with the SEM micrograph and EDAX chemical analysis. The EDAX results indicate ettringite having a chemical composition of Al = 5.02% wt., Si = 3.91% wt., S = 6.60% wt., and Ca = 82.79% wt. Also, calcium hydroxide crystals (CH) can be identified within the cavities and cement paste and aggregates of the specimens.

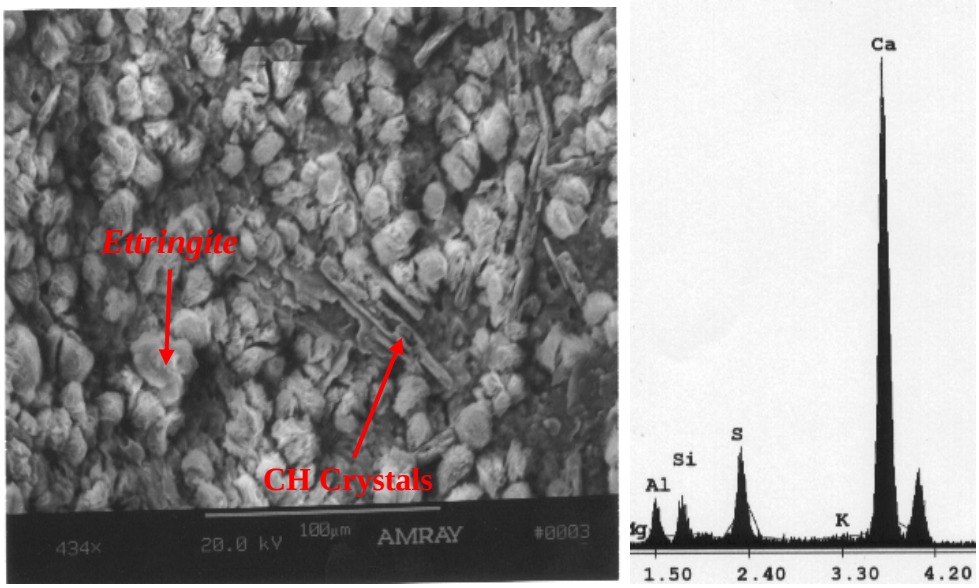


Figure 6.28: SEM and EDAX Analysis of Mortar Specimen Made With 1.5% $K_2O$ and Stored in Exposure Condition 1 at Age of 40 Days, Showing Ettringite Balls and CH Crystals Filling a Cavity

At 100 days, the SEM examinations showed developed ettringite balls filling a cavity similar to the results obtained at 40 days. Ettringite was also found in the interface between the cement paste and aggregate. Fewer amounts of calcium hydroxide crystals were found during the 100 days examinations. Figure 6.29 shows ettringite balls filling a cavity.

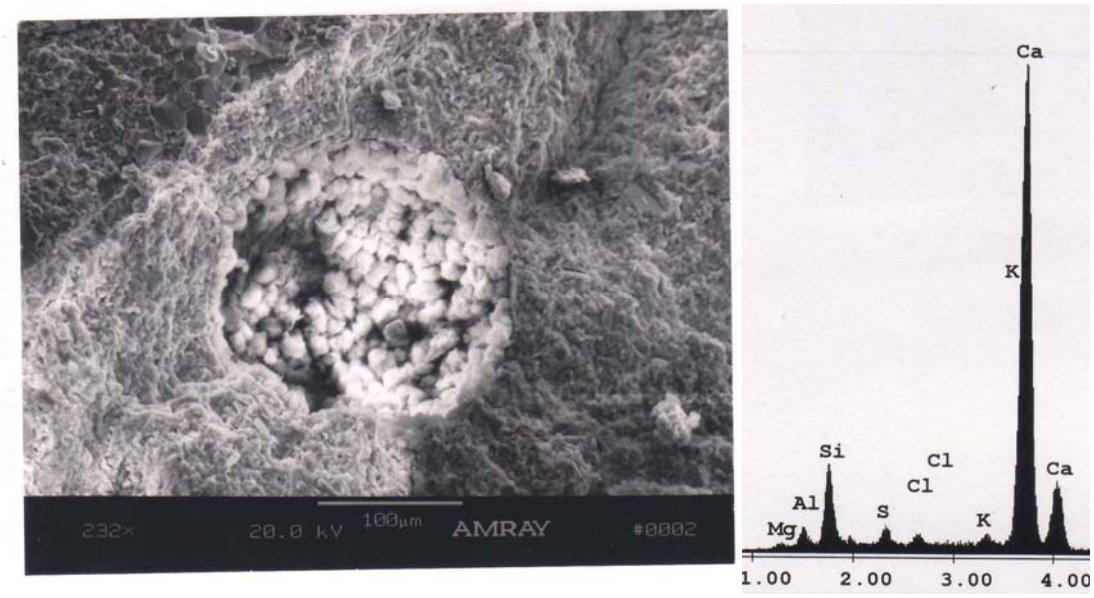


Figure 6.29: SEM and EDAX Analysis of Mortar Specimen Made With 1.5% $K_2O$ and Stored in Exposure Condition 1 at Age of 100 Days, Showing Ettringite Balls Filling a Cavity

Ettringite with calcium hydroxide crystals were discovered at the 240 days' SEM examinations. Ettringite rims ranging from 5 μm to > 10 μm, were found around a sand particle as shown in figure 6.30. The SEM micrograph showed many occurrences of ettringite that were growing in cavities and interfaces between aggregate particles in the mortar specimen.


Figure 6.30: SEM and EDAX Analysis of Mortar Specimen Made With 1.5% $K_2O$ and Stored in Exposure Condition 1 at Age of 240 Days, Showing Ettringite Rims Near a Sand Particle

Well-developed ettringite needles at random orientation were found at several locations on the mortar specimens after 540 days of storage. The ettringite did change from balls to needles at later stages. Most of the ettringite was discovered in cavities and air voids as shown in figure 6.31. EDAX elemental analysis was employed which revealed ettringite having a chemical composition of Al = 4.68% wt., Si =15.07% wt., S = 3.19% wt., and Ca = 63.92% wt.

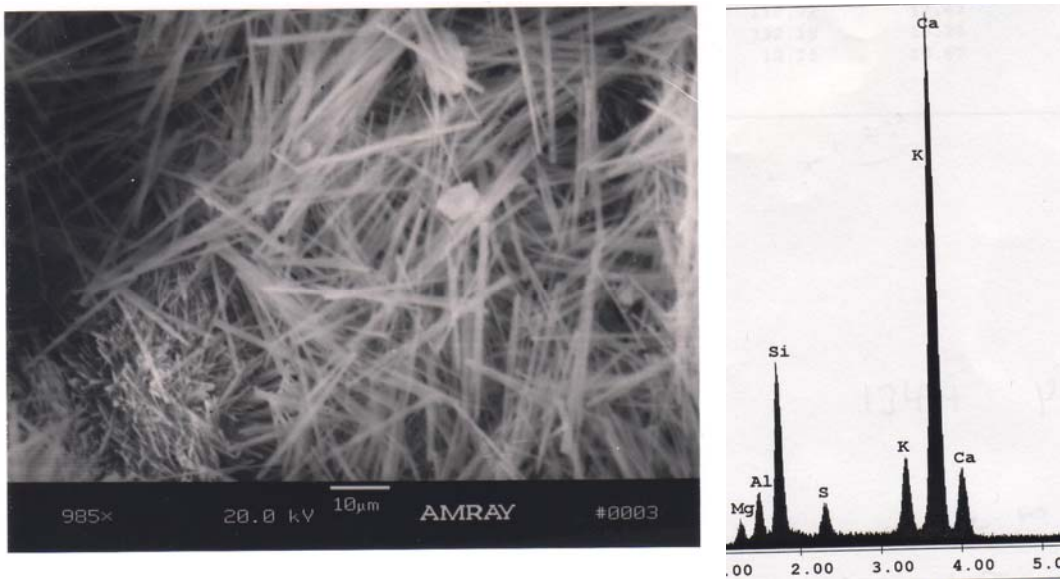


Figure 6.31: SEM and EDAX Analysis of Mortar Specimen Made With 1.5% $K_2O$ and Stored in Exposure Condition 1 at Age of 540 Days, Showing Developed Ettringite Needles Filling a Cavity

*6.6.2 Mortar Samples in Exposure Condition 2*

Well-developed ettringite gels could be identified all over the specimens at only 40 days of storage in plain water at room temperature (Exp. Cond. 1). Little clusters of CH and lots of spherical balls and needles loaded with ettringite were found in the air voids and cavities. The morphology of the ettringite did not change during the 100 days and the SEM micrographic and EDAX revealed similar features. Figure 6.32 provides the SEM and EDAX elemental analysis of the layer with ettringite deposits.


Figure 6.32: SEM and EDAX Analysis of Mortar Specimen Made With 1.5% $K_2O$ and Stored in Exposure Condition 2 at Age of 40 Days, Showing Ettringite Needles, Ettringite Spherical Balls and CH Clusters Filling Air Voids and Cavities

During the SEM examinations at 540 days, ettringite was found covering sand particles at several locations. EDAX elemental analysis was employed to reveal the chemical compositions of the ettringite. The EDAX results showed the ettringite with Al = 8.69% wt., Si = 2.12% wt., S = 19.36% wt., and Ca = 69.83% wt. which were consistent with ettringite composition. Figure 6.33 shows the SEM and EDAX analysis of an area around a sand particle covered with ettringite.

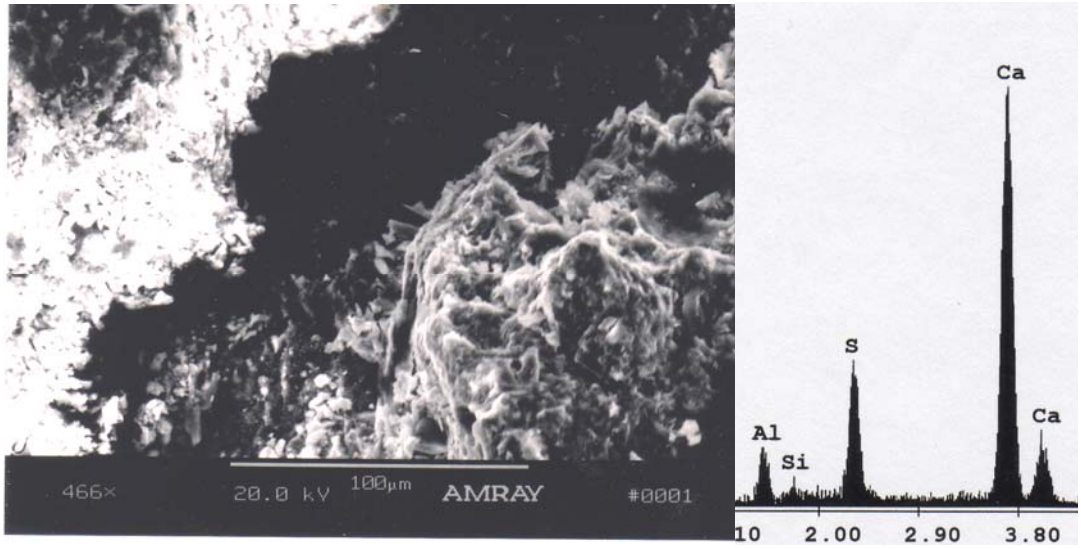


Figure 6.33: SEM and EDAX Analysis of Mortar Specimen Made With 1.5% $K_2O$ and Stored in Exposure Condition 2 at Age of 540 Days, Showing Ettringite Laminar Covering Sand Particles

*6.6.3 Mortar Samples in Exposure Condition 3*

At 40 days of storage under a relative humidity of 97% (Exp. Cond. 3), no ettringite could be found within the specimen. This might be attributed to high heating temperature during the Duggan heat cycle (85$^{o}$C), in which the ettringite crystals decomposed. This finding was consistent with previous research results, which indicates that ettringite crystals are not stable at high temperatures but reform when the temperature drops to normal and moist conditions exist. The EDAX revealed a high peak of potassium (K), which might be due to the high potassium content in the mortar mix. The SEM examination results at 100 days were similar to the 40 days' results. Figure 6.34 shows the EDAX results.

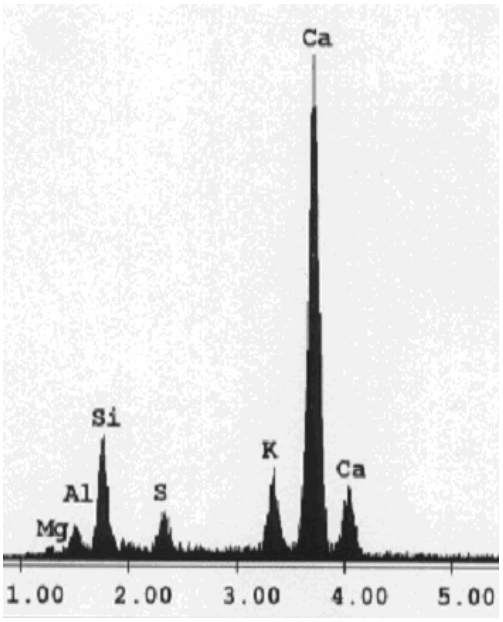


Figure 6.34: EDAX Analysis of Mortar Specimen Made With 1.5% $K_2O$ and Stored in Exposure Condition 3 at Age of 40 Days

The SEM results at 240 days revealed a cluster of ettringite needles filling the cavities and air voids throughout the examined specimen. The ettringite existed in the cavities and cracks and concentrated more in the interface between the aggregate particles and the cement paste matrix. Figure 6.35 shows the SEM and EDAX analysis of the whole area.

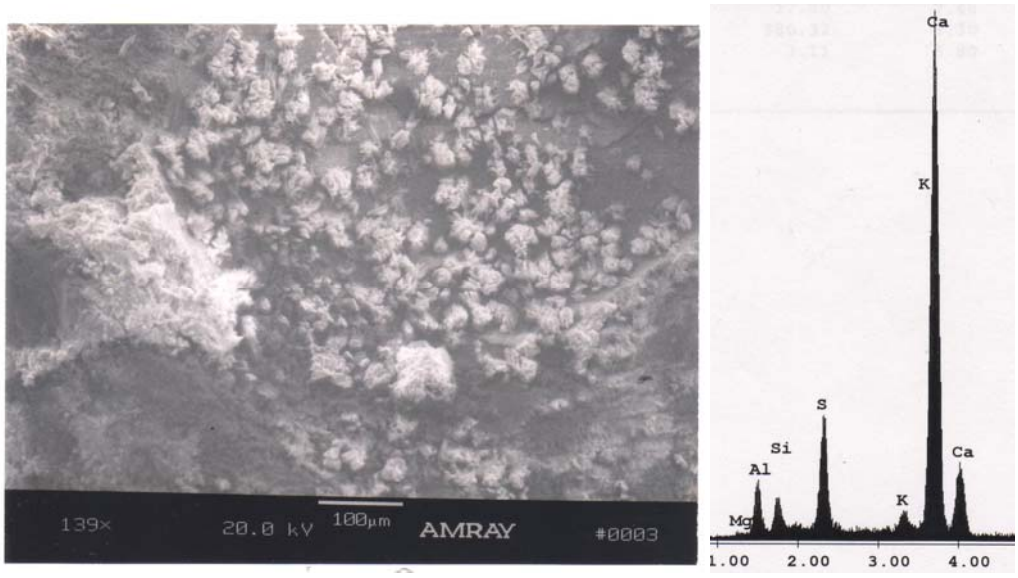


Figure 6.35: SEM and EDAX Analysis of Mortar Specimen Made With 1.5% $K_2O$ and Stored in Exposure Condition 3 at Age of 240 Days, Showing Clusters of Ettringite Needles Filling a Cavity

Figure 6.36 shows ettringite in a cavity at 540 days of storage in exposure condition 3 (R.H at 97%). Examination was conducted at a higher magnification to reveal the morphology of the ettringite. Well-developed ettringite found in the cavities was randomly oriented. Figure 6.37 shows the SEM micrographic and EDAX of the cavity at a higher magnification. The EDAX results showed the ettringite with Al = 7.68% wt., Si = 1.90% wt., S = 16.96% wt., and Ca = 69.82% wt.

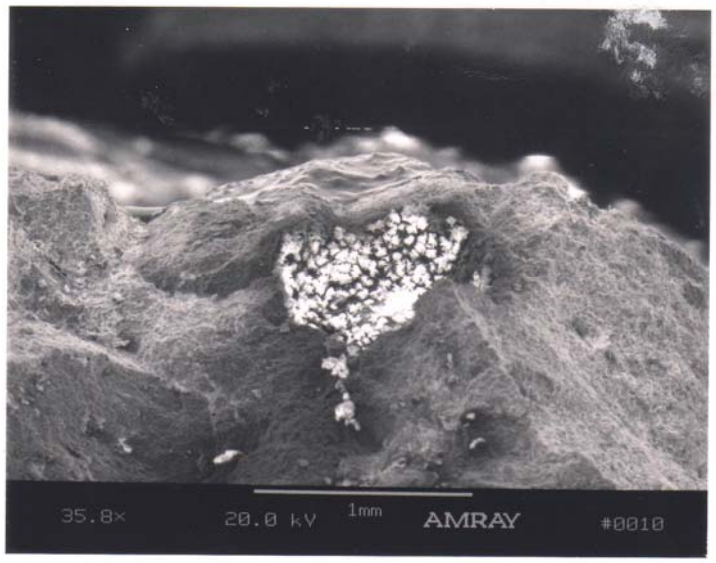


Figure 6.36: SEM Micrograph of Mortar Specimen Made With 1.5% $K_2O$ and Stored in Exposure Condition 3 at Age of 540 Days, Showing a Cavity Filled With Ettringite

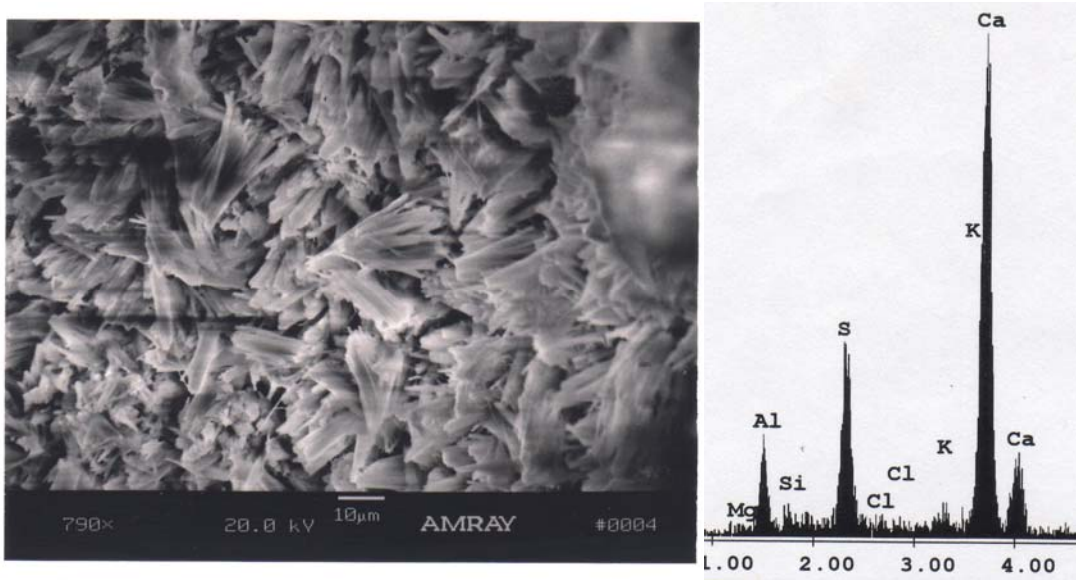


Figure 6.37: SEM and EDAX analysis of Mortar Specimen Made With 1.5% $K_2O$ and Stored in Exposure Condition 3 at Age of 540 Days, Showing a Cavity Filled With Ettringite at a Higher Magnification

*6.6.4 Mortar Samples in Exposure Condition 4A*

The mortar samples were steam-cured and stored in water at room temperature prior to storing in the field. The SEM and EDAX analyses showed neither ettringite nor its elemental composition peaks at 40 days. A prominently high potassium spectrum peak was observed, due to the high potassium content in the mix (1.5% $K_2O$ by weight of cement). Figure 6.38 shows the EDAX results.

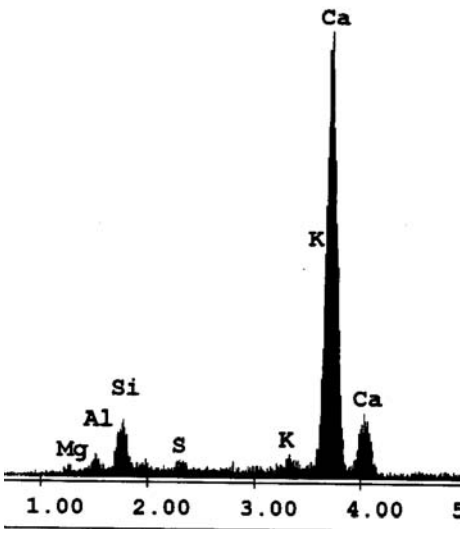


Figure 6.38: EDAX Analysis of Steam-Cured Mortar Specimen Made With 1.5% $K_2O$ and Stored Under Field Conditions (C4A) at Age of 40 Days

The SEM examinations at 100 days showed a mixture of ettringite needles and traces of calcium hydroxide crystals filling a cavity. The EDAX results showed the ettringite with Al = 4.82% wt., Si = 4.41% wt., S = 6.86% wt., and Ca = 81.29% wt. Figure 6.39 shows the SEM and EDAX of ettringite deposit after 100 days of storage in exposure condition 4A.

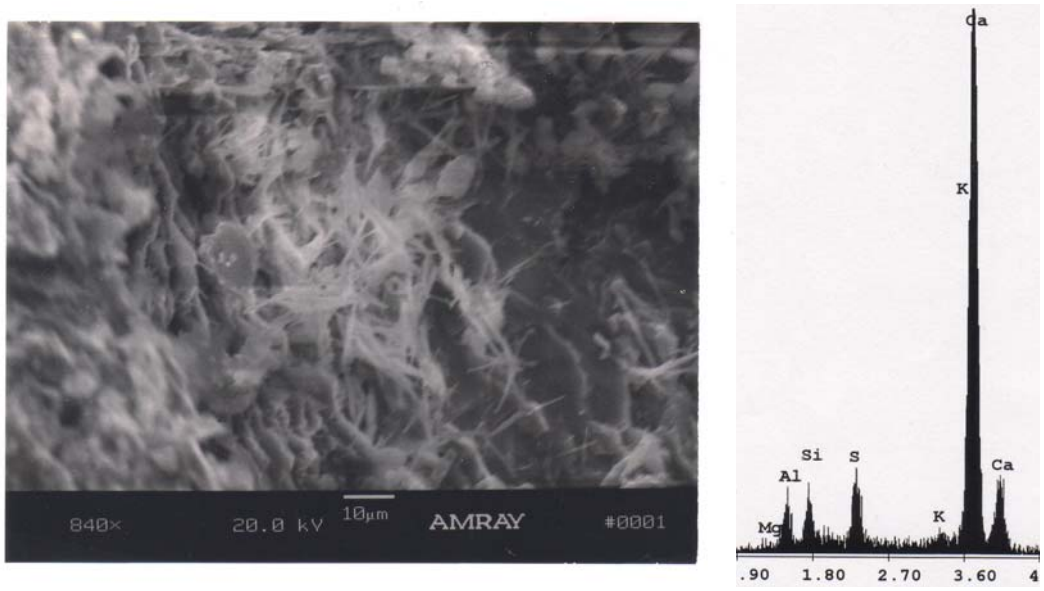


Figure 6.39: SEM and EDAX Analysis of Steam-Cured Mortar Specimen Made With 1.5% $K_2O$ and Stored Under Field Conditions (C4A) at Age of 100 Days, Showing Ettringite Needles Filling a Cavity

The EDAX and SEM micrograph examination results at 240 days of storage revealed clusters of ettringite with calcium hydroxide crystals covering the whole specimen as shown in figure 6.40. The characteristic composition of the ettringite includes Al = 4.85% wt., Si = 7.39% wt., S = 9.50% wt., and Ca = 73.50% wt.

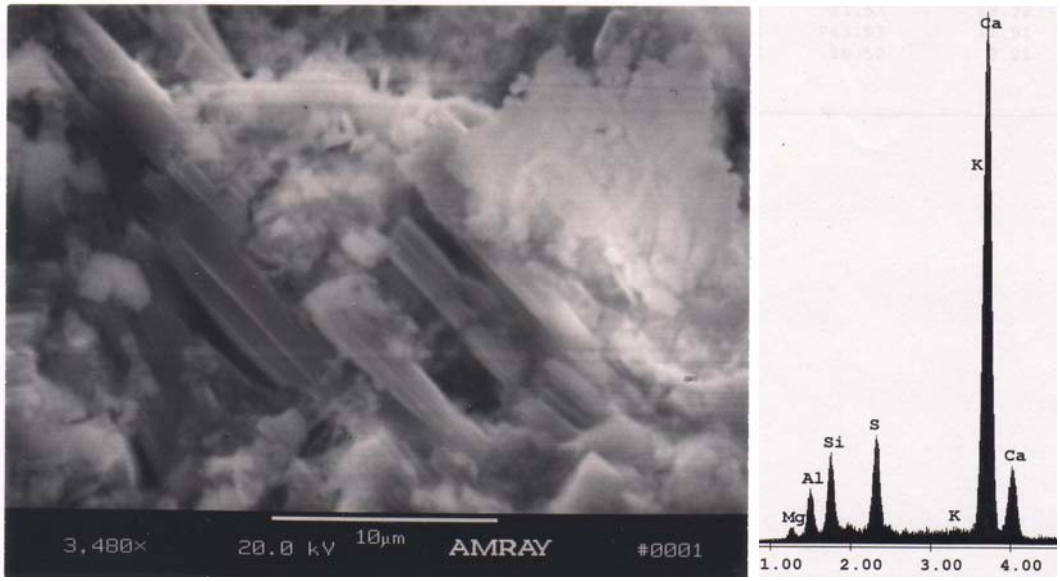


Figure 6.40: SEM and EDAX Analysis of Steam-Cured Mortar Specimen Made With 1.5% $K_2O$ and Stored Under Field Conditions (C4A) at Age of 240 Days Showing Ettringite with Calcium Hydroxide (CH) Crystals

Figure 6.41 showed SEM examinations at 540 days showing clusters of ettringite needles filling a cavity. Examination conducted at higher magnification revealed clusters or needles of ettringite mixed with calcium hydroxide crystals. The field exposure specimens are occasionally saturated with rain water or snow which apparently supports DEF. The EDAX results showed the ettringite with Al = 3.20% wt., Si = 9.19% wt., S = 4.08% wt., and Ca = 77.30% wt.

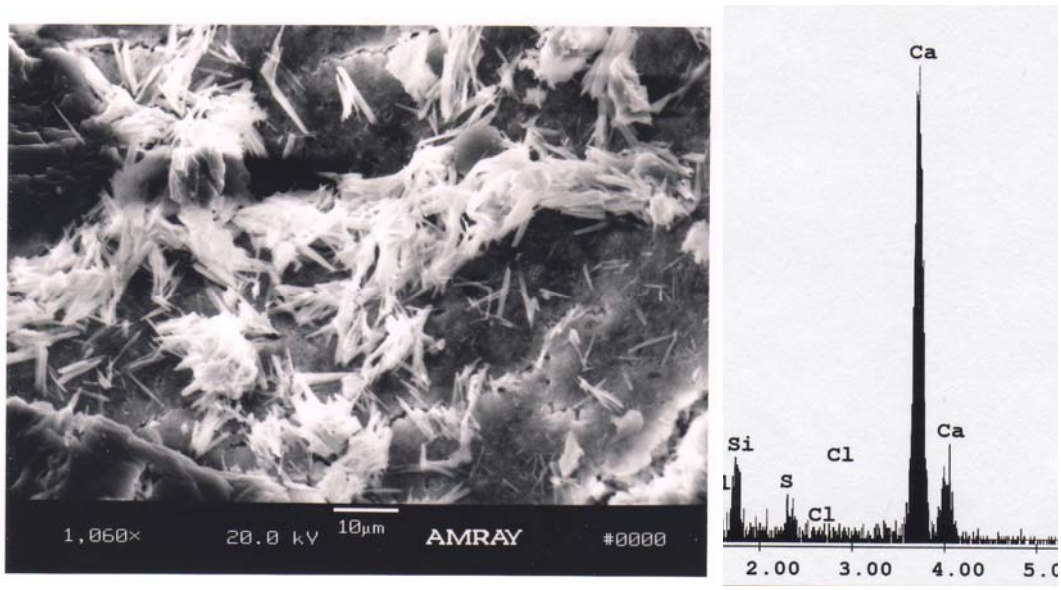


Figure 6.41: SEM and EDAX Analysis of Steam-Cured Mortar Specimen Made With 1.5% $K_2O$ and Stored Under Field Conditions (C4A) at Age of 540 Days Showing Ettringite Filling a Cavity

*6.6.5 Mortar Samples in Exposure Condition 4B*

At 40 days, SEM results revealed lots of ettringite around the voids and cavities of the specimen. The morphology is characteristic of ettringite deposits but could not be confirmed by EDAX due to low X-ray signals encountered during examination of specimens. Figures 6.42 and 6.43 provide SEM micrographs showing ettringite needles found at several locations.

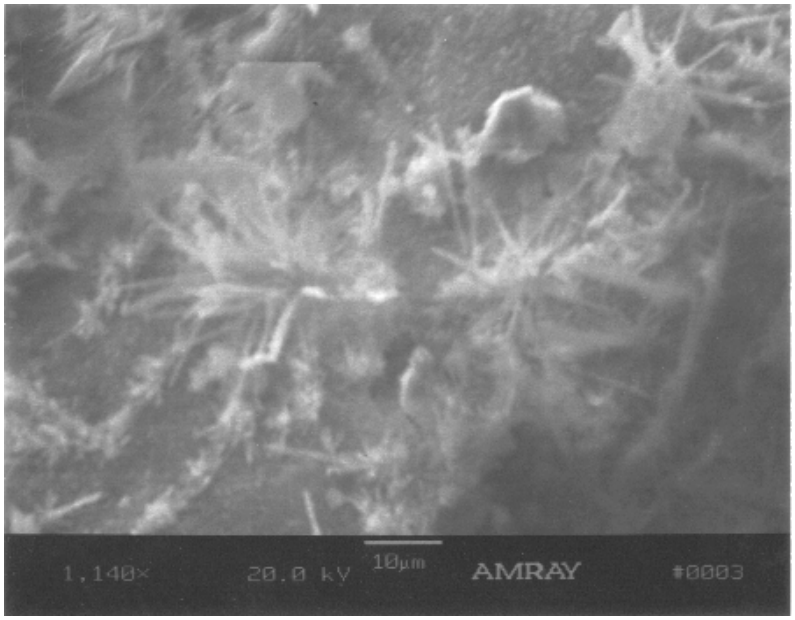


Figure 6.42: SEM Micrograph of Room Temperature-Cured Mortar Specimen Made With 1.5% $K_2O$ and Stored Under Field Conditions (C4B) at Age of 40 Days, Showing Ettringite Around Air Voids

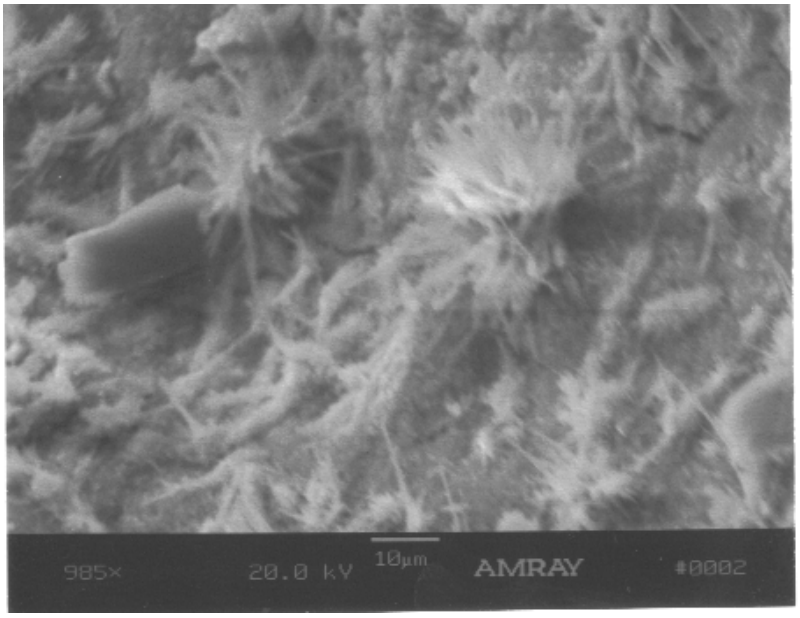


Figure 6.43: SEM Micrograph of Room Temperature-Cured Mortar Specimen Made With 1.5% $K_2O$ and Stored Under Field Conditions (C4B) at Age of 40 Days, Showing Ettringite Filling Cavities

Lots of ettringite needles are discovered during the 100 days' SEM examinations. Figure 6.44 show the SEM and EDAX analyses of the mortar specimens after 100 days of storage under field condition 4B. The presence of a high amount of silicon (Si) in the analysis revealed C-S-H gel, which converted to ettringite gel when soaking under water proceeded. The EDAX results showed the ettringite with Al = 5.50% wt., Si = 5.42% wt., S = 9.97% wt., and Ca = 75.58% wt.

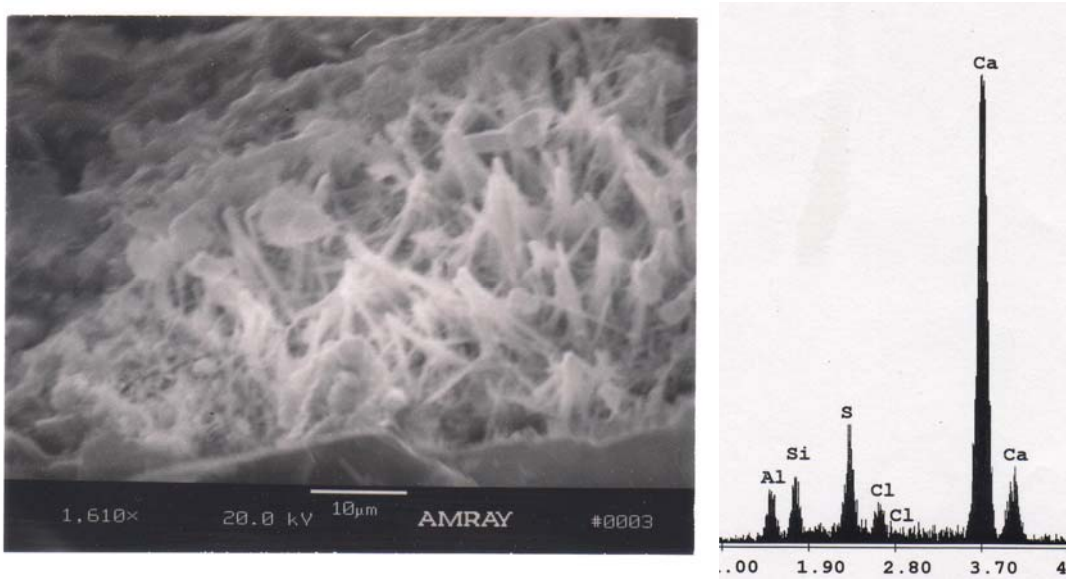


Figure 6.44: SEM and EDAX Analysis of Room Temperature-Cured Mortar Specimen Made With 1.5% $K_2O$ and Stored Under Field Conditions (C4B) at Age of 100 Days Showing Lots of Ettringite Needles

No ettringite was found during the 240 days SEM examinations. The SEM and EDAX results revealed only calcium hydroxide crystals. At 540 days, bubbles of ettringite balls that totally replaced the calcium hydroxide were found throughout the examined mortar specimen. Figure 6.45 shows deposits of ettringite balls filling an air void.

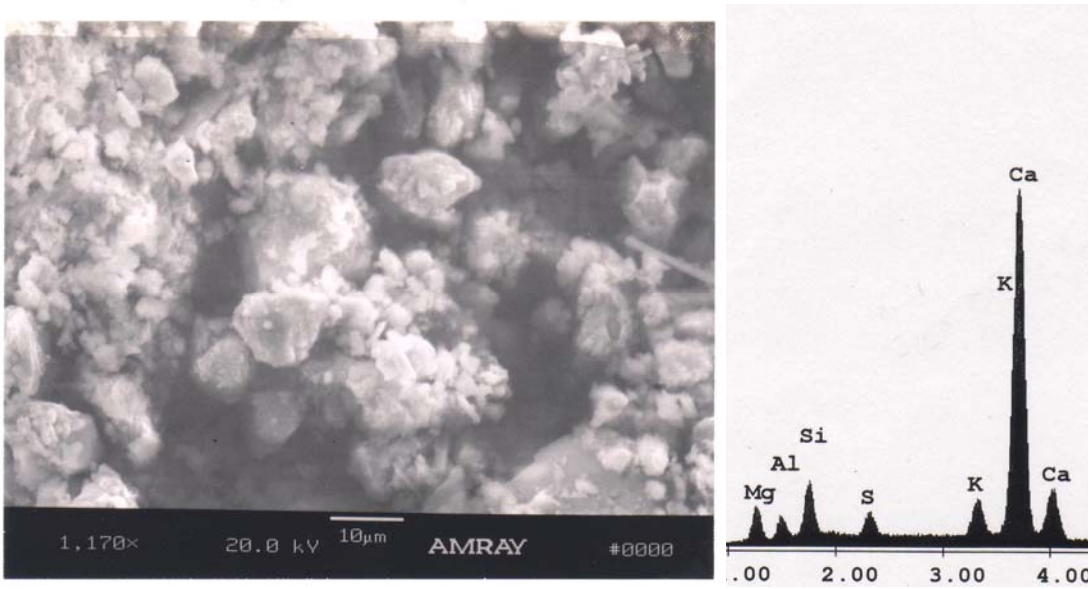


Figure 6.45: SEM and EDAX Analysis of Room Temperature-Cured Mortar Specimen Made With 1.5% $K_2O$ and Stored Under Field Conditions (C4B) at Age of 540 Days Showing Ettringite Balls

*6.7 X-ray Computed Tomography (X-ray CT) Analysis*

The X-ray computed tomography (X-ray CT) method is another technique that was used to reveal the interior cracks within the microstructure of the mortar specimens. The X-ray CT is a non-destructive method and the sample preparation method does not influence the results.

Figures 6.46 through 6.48 show computed tomography cross sectional images of the mortar specimens made with 1.5% $K_2O$ content after 40 days storage in the different exposure conditions. All the mortar specimens that were examined exhibited no visible interior cracks in the X-ray CT images.

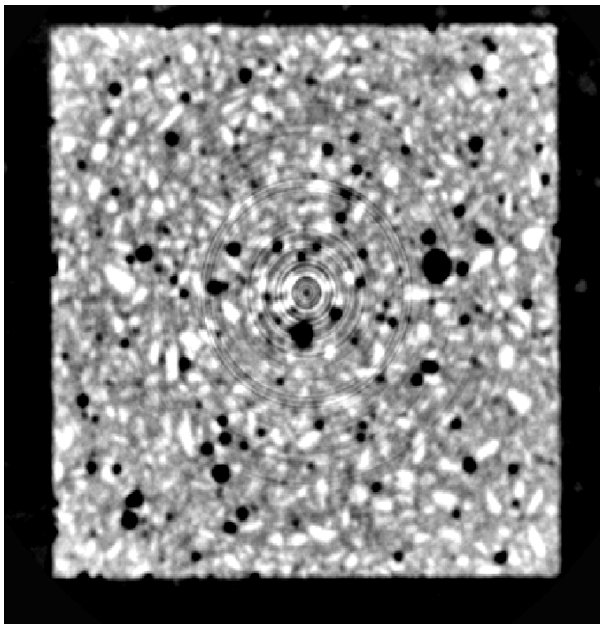

Figure 6.46: X-ray Computed Tomography Image of a Section Through a Mortar Cube Made With 1.5% $K_2O$ at Age of 40 Days in Plain Water at Room Temperature

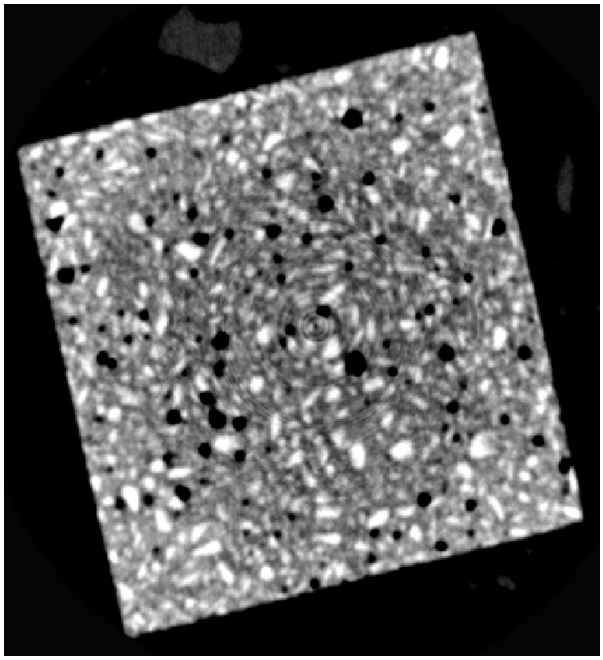

Figure 6.47: X-ray Computed Tomography Image of a Section Through a Mortar Cube Made With 1.5% $K_2O$ at Age of 40 Days in Moist Air Chamber, R.H maintained at 97%

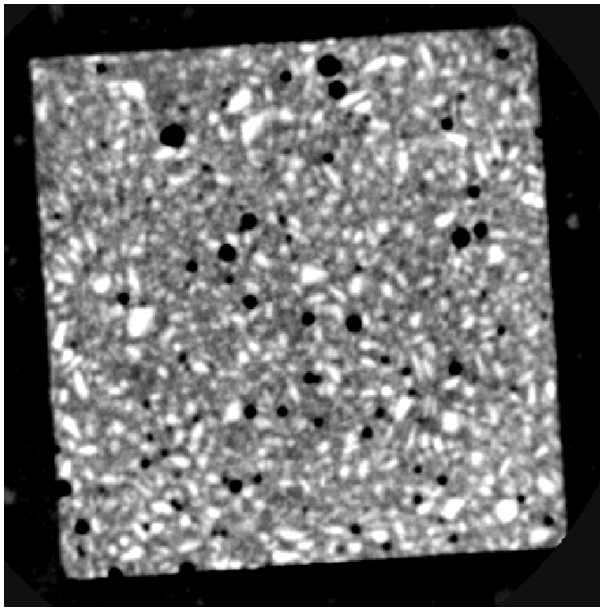

Figure 6.48: X-ray Computed Tomography Image of a Section Through a Room Temperature-Cured Mortar Cube Made With 1.5% $K_2O$ at Age of 40 Days Under Field Exposure Conditions

*6.8 Summaries and Discussion of Mortar Samples Made With 1.5% $K_2O$*

The mortar samples were prepared with high potassium ($K_2O$) content which increased the cement alkalis of the mortar batches. Potassium occurs as a minor constituent in Portland cement where it is usually found in the form of potassium sulfate (Pettifer, 1980). However, this possible effect is often obscured by the practice of not reporting sodium and potassium concentrations individually but rather as combined in the form of alkali (ASTM C-150). Stark and Bollman argued on the basis of an experimental relationship between ettringite crystalline size and pH that ettringite would not be stable at high alkali concentrations (1999). In 2000, Ramadan used a set of controlled concrete prisms and observed that expansion of concrete was correlated with potassium. The Duggan heat regime was employed to provide or

initiate microcracks within a short period of time in the laboratory-prepared mortar specimens.

All mortar bars subjected to the Duggan heat cycle showed expansion after three (3) days of storage. The mortar bars stored in the various exposure conditions exceeded the 21-day threshold expansion value of 0.05% suggested by Duggan. For the first 100 days, the expansion values of the mortar bars stored in limewater and plain water were higher than those stored in relative humidity maintained at 97%. The expansion rate of the mortar bars in relative humidity at 97% increases significantly after 250 days. This can be attributed to the potassium hygroscopic effect. The expansion results clearly indicated that expansion is accelerated by the increase in potassium content ($K_2O$). Mortar bars in pH maintained at 12.5 – limewater and plain water exhibited similar expansion patterns during the storage. The mortar bars in exposure condition 2 (plain water) showed higher expansion values than those in exposure condition 1 (limewater) throughout the research duration. This can be attributed to the extra calcium from the limewater which causes precipitation of ettringite. The precipitation of ettringite in the mortar bars close to the surface inhibits transport of solution into the microstructure of the mortar bars (Graf, 2007). This reduces the amount of water inside the microstructure of the mortar bars for absorption and formation of ettringite. The mortar bars exposed to field conditions that were not subjected to the Duggan heat regime showed shrinkage for the entire duration of the research study. There are several competing processes that can cause strains in the mortar bars.

Weight change of the mortar specimens in limewater and plain water was very significant. An increase in weight change up to 10% was revealed just after one (1) day of storage in the limewater and plain water exposure conditions. Weight change of the mortar specimens subjected to the Duggan heat show a steady increase with time. Weight change measurements of mortar bars in limewater and plain water posed similar patterns during the storage. Mortar bars in relative humidity of 97% exhibit the lowest weight change and this can be attributed to the lack of water uptake required for ettringite formation. There is a high correlation coefficient between weight change and time in the first 100 days for the steam-cured mortar bars subsequently subjected to the Duggan heat cycle. The weight change of the mortar field specimens was found to fluctuate and decreased with time. Overall, the mortar bars subjected to Duggan heat cycle showed a steady increase in weight change throughout the entire research.

For the first 100 days of storage, expansion against weight change of the mortar bars exhibited high positive linear correlations similar to the control mortar bars. These results were similar to those obtained by Grattan-Bellew et al (1998). Again, mortar bars in limewater and plain water posed similar patterns. According to Shimada, there exist three (3) separate weight-gain mechanisms which create paste expansion in mortar systems (1) Cement hydration, (2) Renewed ettringite formation and (3) Defect formation and increased capillary pore volume (2005).

Analysis of the 28-day compressive strength results suggested that an increase in potassium ($K_2O$) content in the mortar mix significantly reduced strength. The compressive strength results at 28 days were 4590 psi, 4767 psi and 6692 psi for

mortar specimens in limewater, plain water and relative humidity of 97% respectively. The mortar specimens subjected to the Duggan heat cycle and then exposed to a relative humidity of 97% exhibited the highest average strength. Compressive strength test results at later stages revealed an increase of up to 25% in all exposure conditions. Again, this suggests that the low expansion or shrinkage values exhibited by the mortar samples do not cause significant damage to the mortar microstructure. The mortar specimens under field conditions also showed an increase in compressive strength over time. The steam-cured mortar exhibited higher strength at later stages than the room-cured mortar specimens. The exposure condition enhanced and influenced the compressive strength of the mortar specimens.

Mortar samples made with higher potassium ($K_2O$) content showed higher alkali leaching and accelerated formation of ettringite. The alkali concentration was higher in the limewater than the plain water exposure conditions. Also, expansion values of mortar specimens in limewater were higher than those stored in plain water. However, since the cement and all other parameters were the same for both mortar sets, the expansion values can be attributed to the higher concentrations of potassium content and the amount of alkalis which had been leached into the storage solution.

Microstructural observation of the mortar specimens at different stages revealed significant amounts of ettringite balls or crystals filling the cracks and air voids. Calcium hydroxide crystals (CH) also were found within the cavities and cement paste of the mortar specimens. SEM results at 40 days, showed high peaks of potassium (K) but no ettringite was found in the mortar specimens stored in relative humidity of 97%. Ettringite deposits were discovered at 40 days' SEM examination

under the field exposure conditions but, due to the low X-ray signals encountered, no EDAX could be obtained. At 540 days, well-developed ettringite needles were found in mortar specimens stored in exposure condition 1. A summary of the test results for the steam-cured mortar samples made with 1.5% $K_2O$ and subjected to Duggan heat cycle is shown in Table 6.8.

Mortar specimens stored under field conditions also showed a significant amount of ettringite at later stages during the research. It can be concluded that ettringite can be found in non steam-cured mortar specimens. Ettringite or ettringite deposits were generally found in air voids, cavities, in the aggregate paste interface zone and in the paste matrix. The ettringite morphology changed over time in all the exposure conditions. The amount of damage due to ettringite formation is correlated with the expansion values. The highest expansion values showed the highest concentration of ettringite especially in the cavities. Table 6.9 provides a summary of test results for the mortar samples made with 1.5% $K_2O$ and subjected to field conditions.

The X-ray computed tomography (X-ray CT) imaging of the mortar cross sections showed no interior cracks within the microstructure. A better method or further enhancement of the process would be required to provide quantitative measures to analyze the observed cracks. Again, the only cracks revealed were with the SEM examinations and were found filled with ettringite. ASR was not found during the petrographic analysis of the specimens throughout the research study.

Table 6.8: Summary of Test Results of Mortar Samples Made with 1.5% $K_2O$ – Steam-Cured and Subjected to Duggan Heat Cycle

| **Mortar Samples (1.5% $K_2O$) - Steam-Cured and Subjected to Duggan Heat Cycle** | | | | |
|---|---|---|---|---|
| | | Exp. Cond. 1 (Limewater) | Exp. Cond. 2 (Plain Water) | Exp. Cond. 3 (R.H at 97%) |
| Expansion | | Max. 0.26% | Max. 0.46% | Max. 0.62% |
| Weight Change | | Max. 12.79% | Max. 12.91% | Max. 10.34% |
| Compressive Strength (psi) | 28 Days | 4590 | 4767 | 6692 |
| | 365 Days | 8292 | 5617 | 8042 |
| | 540 Days | 7133 | 6642 | 7400 |
| Water Analysis (mmol/l) | pH | - | 8.57 - 12.23 | - |
| | Alkali | Max. 144 | Max. 183 | - |
| | $Ca^{2+}$ | - | Max. 122 | - |
| SEM/EDAX Analysis | 40 Days | Ettringite balls and CH crystals | Ettringite spherical balls | No ettringite |
| | 100 Days | Ettringite balls | Ettringite spherical balls | No ettringite |
| | 240 Days | Ettringite rims | Ettringite spherical balls and CH crystals | Clusters of ettringite needles |
| | 540 Days | Ettringite needles | Ettringite laminar | Massive ettringite |

Table 6.9: Summary of Test Results of Mortar Samples Made with 1.5% $K_2O$ – Subjected to Field Conditions

| **Mortar Samples (1.5% $K_2O$) - Subjected to Field Conditions** | | | |
|---|---|---|---|
| | | Exp. Cond. 4A (Steam-Cured) | Exp. Cond. 4B (Room Temp.-Cured) |
| Length Change | | Max. 0.0000% | Max. 0.0206% |
| Weight Change | | Max. 0.59% | Max. 1.01% |
| Compressive Strength (psi) | 28 Days | 5043 | 5725 |
| | 365 Days | 7375 | 6225 |
| | 540 Days | 8850 | 6692 |
| SEM/EDAX Analysis | 40 Days | No ettringite | Lots of ettringite needles |
| | 100 Days | Ettringite needles and CH crystals | Lots of ettringite needles |
| | 240 Days | Ettringite needles and CH crystals | No ettringite |
| | 540 Days | Clusters of ettringite needles | Ettringite balls |

# Chapter 7: Concrete Samples (Control) and DEF

## *7.1 Introduction*

Delayed ettringite formation in concrete and its association with deleterious expansion is a controversial subject. This has led to a series of research projects through the years. These have been reviewed recently by researchers such as (Shimada, 2005, and Famy et al., 2001). This chapter emphasizes the use of concrete samples since heat dissipated during heat of hydration of cement is an important aspect of curing, with the size of the concrete member being a critical factor (Skalny and Locher, 1999). In 2002, Yan et al. demonstrated that high temperature rise induced by cement hydration in the core of massive concrete could result in the decomposition of primary ettringite and thus later expansion.

In this study, seven (7) sets of concrete samples were prepared according to the modified sample preparation method. The effect of Duggan versus Freeze-Thaw was also investigated in two (2) of the concrete sets which were subsequently stored in exposure condition 1 (pH maintained at 12.5 - limewater) for the duration of the research project. The deleterious effect due to DEF was monitored for the concrete specimens stored in four (4) different conditions. Again, Frederick Sand (manufactured sand) was used in all the batch mixes and, according to the Maryland State Highway Administration (MDSHA), the ASR result is 0.09%. The MDHSA classified the Frederick Sand to be of medium reactivity. Limestone ASTM # 57 stone was used for the coarse aggregate for the entire study. The Duggan heat cycle was used to initiate microcracks with a short period of time. Expansion and weight-change measurements were monitored for about two (2) years.

Compressive strength tests of the concrete samples were performed after 28 days, 365 days and 540 days of storage, for each exposure condition. Three (3) concrete cylinders from each exposure condition were tested, and the average result used. Also the effect of moisture content on the compressive strength of concrete specimens with potential of premature deterioration due to DEF was investigated. Scanning electron microscope (SEM) with X-ray analysis and Laser shearography (LAS) studies were performed on the concrete specimens. Laser shearography was employed to detect and monitor progress of any surface microcracks caused by Duggan or Freeze-Thaw cycles. The objectives were to study the effect of using a manufactured fine aggregate, limestone # 57, and different exposure conditions on leaching of ions, weight changes and the deleterious expansions associated with DEF. Expansions, weight-change, water analysis of storage solutions, SEM with EDAX, and laser shearography (LAS) results are presented and discussed in this chapter.

### *7.2 Influence of Exposure Conditions on DEF in Concrete*

Storage conditions were limited to four (4) in this research study. Most of the concrete samples were steam-cured before subjecting them to the Duggan heat cycle after seven (7) days. The concrete samples were then collected and stored in their respective exposure conditions. Length change, weight change, leaching of ions, SEM with EDAX and LAS were monitored for the entire storage of the concrete samples. Expansion and weight changes were monitored periodically. Expansion values at 21 days were compared to the threshold value of 0.05% expansion that was suggested by Duggan as pass/fail criteria. It should be noted that expansion and

expansion rate are affected by specimen size (Fu, 1996). The influence of the exposure condition plays a major role in the form and size of the ettringite found in mortar or concrete specimens. Exposure conditions with abundant moisture are ideal host of deleterious expansion associated with delayed ettringite formation. Ettringite formation requires a sufficient supply of water which is usually available in exposure conditions. SEM with EDAX analysis was employed to reveal the presence of ettringite and its ever-changing morphology. SEM examination results showed ASR in none of the examined samples. Therefore, it can be concluded that DEF in the mortar samples at different stages could be responsible for the expansion.

Curve fitting of the experimental data was obtained using linear regression curves. The linear regression curves are a better fit to the expansion data than the KAJM equation. Since, according to Ramadan, the KAJM equation does not give a better fit for the experimental data, it was not used (2000).

*7.3 Influence of Concrete Treatment and DEF*

Concrete prisms and cylinders were room-cured for 24 hours before subsequently storing them in a water bath for six (6) days. Duggan heat and Freeze-Thaw cycles were used to create microcracks in order to accelerate the expansion of the concrete specimens. The specimens were placed in exposure condition 1 (pH maintained at 12.5 – limewater) after the microcrack-inducing treatments. Gage studs were installed at the ends of the concrete prisms to facilitate length-change measurements. Length and weight change measurements were periodically employed

during the storage. Studies using SEM with X-ray analysis and Laser Shearography (LAS) were carried out to identify the DEF and its associated cracks.

### *7.4 Expansion Results*

Three (3) batch mixes of concrete samples were all subjected to the Duggan heat cycle after one (1) week of casting before storing them in different exposure conditions. Another additional two (2) sets of concrete samples were room temperature-cured in the laboratory before subjecting them to either Duggan or Freeze-Thaw cycles. After the treatments, the concrete samples were subsequently stored in exposure condition 1. The experimental results are discussed and analyses are presented herein.

#### *7.4.1 Expansion of Concrete Prisms Subjected to Different Exposure Conditions*

Five (5) concrete prisms from each exposure condition were used for each expansion measurement and the average expansion recorded. The expansions were measured according to ASTM C-490. The initial length measurements were taken after two (2) days of cooling after the Duggan heat cycle and before storage to the respective exposure conditions. All three sets of prisms showed expansion within three (3) days of storage in the different exposure conditions, and this continued for about 600 days. Expansion readings were then collected at specific intervals. Expansion values at 21 days were compared to the threshold value of 0.05% expansion suggested by Duggan as pass/fail criteria for concrete. The expansion values after 21 days of storage were 0.042%, 0.036% and -0.0304% for exposure

conditions 1, 2 and 3 respectively. The expansion rates were unique to each individual exposure condition. The concrete prisms in exposure conditions 1 and 2 exhibited extensive pattern cracking and expansion.

For up to about 400 days, concrete prisms stored in exposure condition 2 (plain tap water) exhibited slightly higher expansion values than those in exposure condition 1 (pH maintained at 12.5). This can be attributed to the extra calcium from the limewater in exposure condition 1 caused precipitation of ettringite close to the concrete surface that inhibited transport of solution into the microstructure (Graf, 2007). Any difference in the expansion behavior of the concrete prisms can be attributed to the difference in exposure conditions. At about 600 days of storage, the expansion values of the concrete prisms were 1.044%, 0.791% and -0.0135% for exposure conditions 1, 2 and 3 respectively. Concrete prisms in exposure condition 3 exhibited little or no expansion during the research study. This can be due to the lack of moisture required for expansion associated with DEF. A steady increase in expansion rate was observed in prisms in both exposure conditions 1 and 2. The highest rate of expansion was 0.0104% per day for prisms in exposure condition 1, 0.0063% per day for exposure condition 2 and 0.0136% per day for exposure condition 3. Expansion values and rates of the concrete prisms (control) are shown in Figures 7.1 through 7.4.

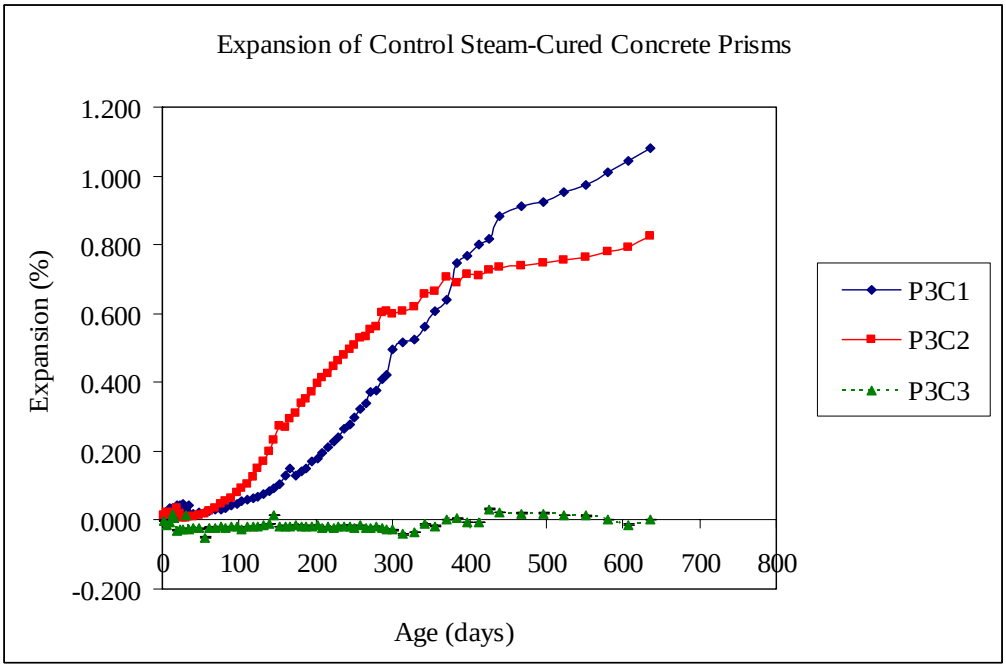


Figure 7.1: Expansion of Steam-Cured Concrete Prisms Subjected to Duggan Heat Cycle and Stored Under Different Exposure Conditions

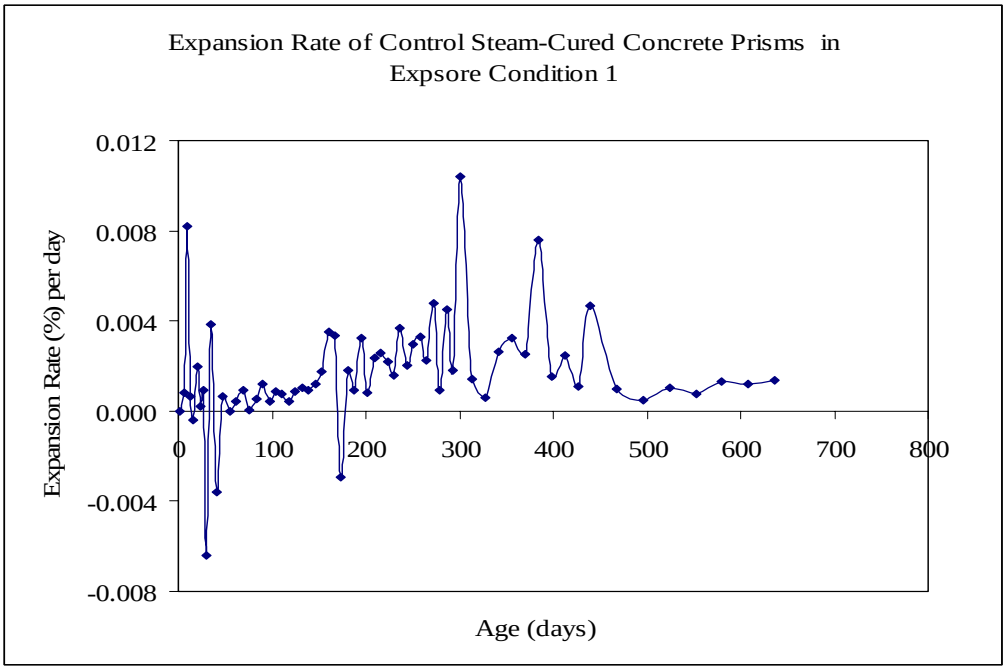


Figure 7.2: Expansion Rate of Steam-Cured Concrete Prisms Subjected to Duggan Heat Cycle and Stored in Isothermal Water Bath, pH maintained at 12.5 – limewater

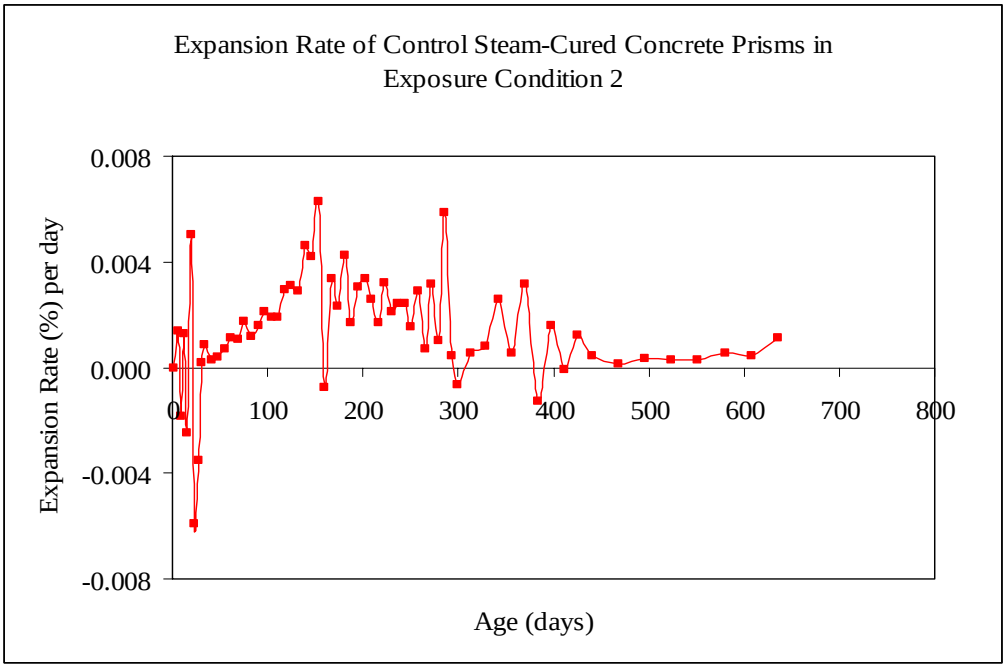


Figure 7.3: Expansion Rate of Steam-Cured Concrete Prisms Subjected to Duggan Heat Cycle and Stored in Plain Water at Room Temperature

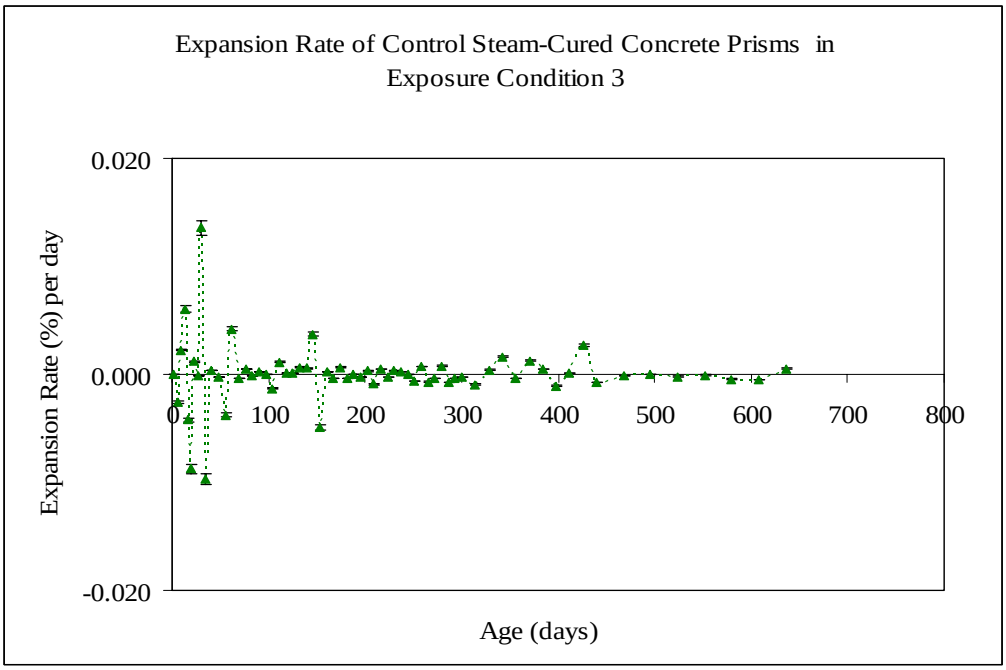


Figure 7.4: Expansion Rate of Steam-Cured Concrete Prisms Subjected to Duggan Heat Cycle and Stored in Moist Air Chamber, R.H maintained at 97%

The mean expansion data for the concrete samples are plotted as a function of time and curve-fitted to numerical equations. A series of linear equations were used to fit the experimental data. Two linear regression curves were used to fit the expansion data results obtained from length-change measurement of the prisms in exposure conditions 1 and 2. The cut-off points for the linear curves were determined based on the maximum correlation coefficient of the expansion values against time. Linear fits for each individual exposure condition are analyzed and plotted in Figures 7.5 through 7.7. Table 7.1 provides the linear regression equations used for the best fit of the experimental expansion data.

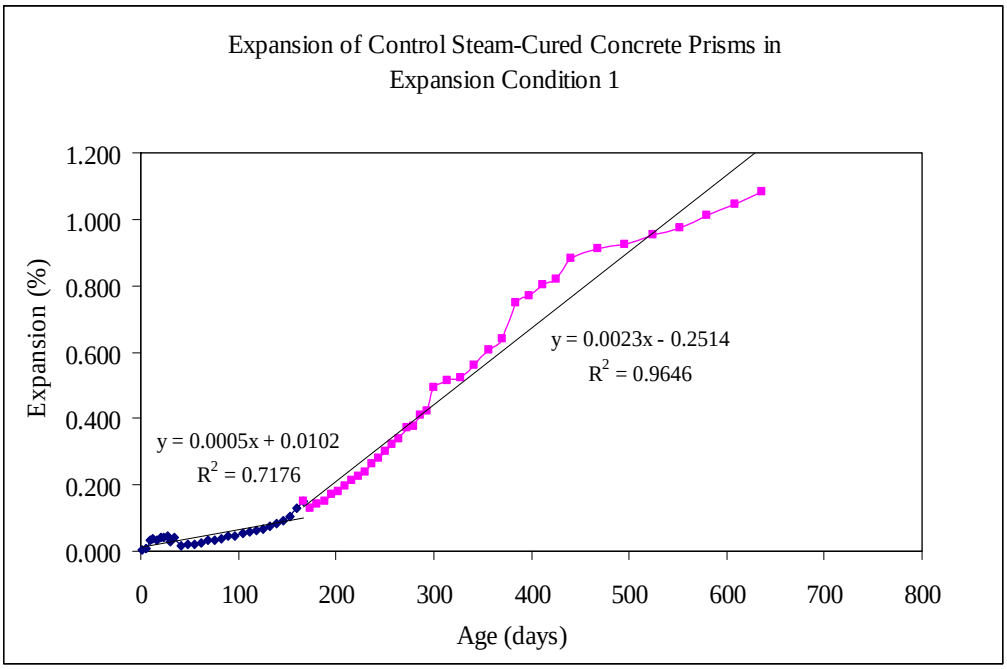


Figure 7.5: Expansion of Steam-Cured Concrete Prisms Subjected to Duggan Heat Cycle and Stored in Isothermal Water Bath, pH maintained at 12.5 – limewater (Regression Curves)

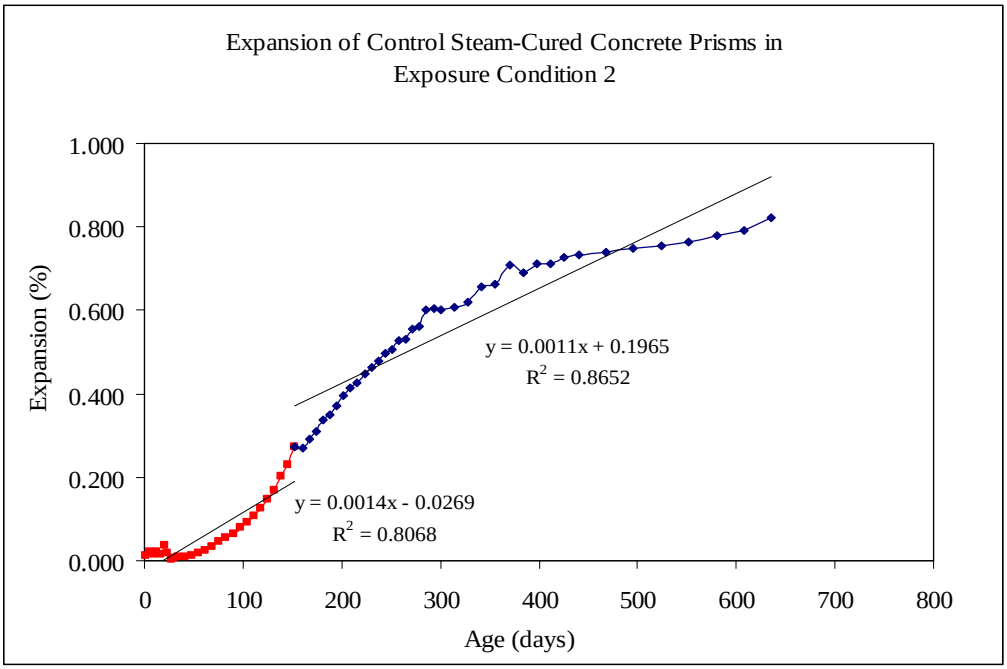


Figure 7.6: Expansion of Steam-Cured Concrete Prisms Subjected to Duggan Heat Cycle and Stored in Plain Water at Room Temperature (Regression Curves)

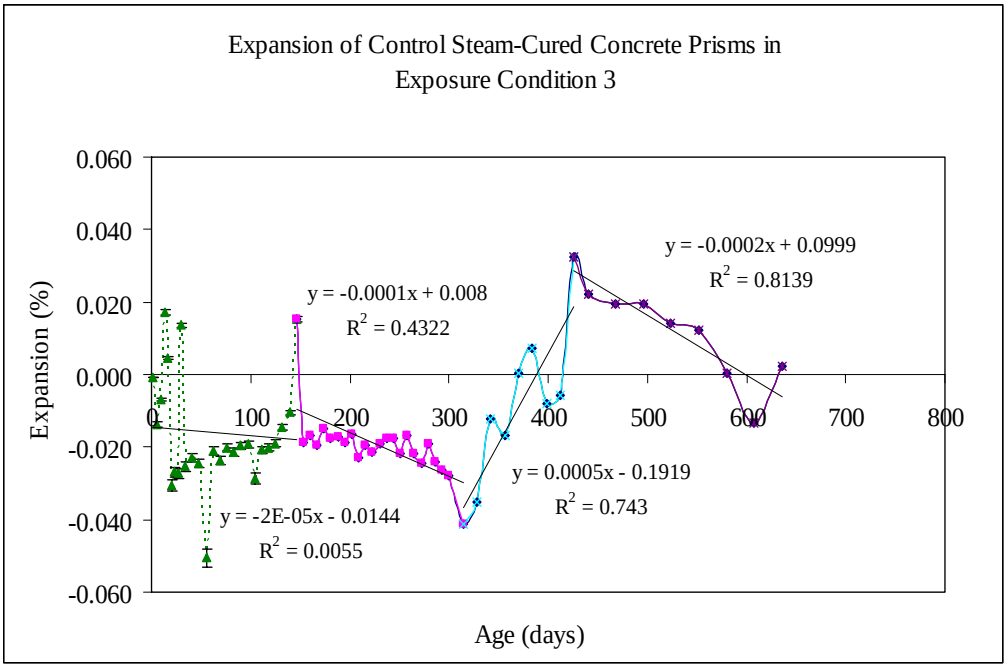


Figure 7.7: Expansion of Steam-Cured Concrete Prisms Subjected to Duggan Heat Cycle and Stored in a Moist Air Chamber, R.H maintained at 97% (Regression Curves)

Table 7.1: Linear Equations for Expansion vs. Age of Steam-Cured Concrete Prisms Subjected to Duggan Heat Cycle and Stored Under Different Exposure Conditions

| Phase 3 (Concrete Control Samples - Subjected to Duggan Heat Cycle) | | | | | |
|---|---|---|---|---|---|
| | | | | | |
| Exp. Cond. 1 | Max. Exp. 1.08% | Curve 1 | Day 1 - 167 | y = 0.0005x + 0.0102 | $R^2$ = 0.7176 |
| | | Curve 2 | Day 167 - 636 | y = 0.0023x - 0.2514 | $R^2$ = 0.9646 |
| | | | | | |
| Exp. Cond. 2 | Max. Exp. 0.82% | Curve 1 | Day 1 - 153 | y = 0.0014x - 0.0269 | $R^2$ = 0.8068 |
| | | Curve 2 | Day 153 - 636 | y = 0.0011x + 0.1965 | $R^2$ = 0.8652 |
| | | | | | |
| Exp. Cond. 3 | Max. Exp. 0.03% | Curve 1 | Day 1 - 146 | y = -2E-0.5x - 0.0144 | $R^2$ = 0.0055 |
| | | Curve 2 | Day 146 - 314 | y = -0.0001x + 0.008 | $R^2$ = 0.4322 |
| | | Curve 3 | Day 314 - 426 | y = 0.0005x - 0.1919 | $R^2$ = 0.743 |
| | | Curve 4 | Day 426 - 636 | y = -0.0002x + 0.0999 | $R^2$ = 0.8139 |
| | | | | | |

*7.4.2 Expansion of Concrete Prisms Subjected to Different Treatments*

The concrete prisms subjected to Duggan heat exhibit higher expansion values than with the Freeze-Thaw during the entire study. Expansion values at 21 days were 0.023% and 0.005% for Duggan heat and Freeze-Thaw treated concrete prisms respectively. Both sets of the concrete prisms showed less significant or no DEF-induced expansions for 400 days of storage in limewater. The reason is not very clear, but this may be attributed to the lack of high temperature curing during the early stages of concrete samples. Fu reported that concrete treatments such as freeze-thaw cycles appeared not to cause significant DEF-induced expansion (1996). The maximum expansion values exhibited were 0.1074% and 0.090% for the Duggan heat

and Freeze-Thaw treated concrete prisms respectively. The expansion values and expansion rate per day are shown in figures 7.8 and 7.9.

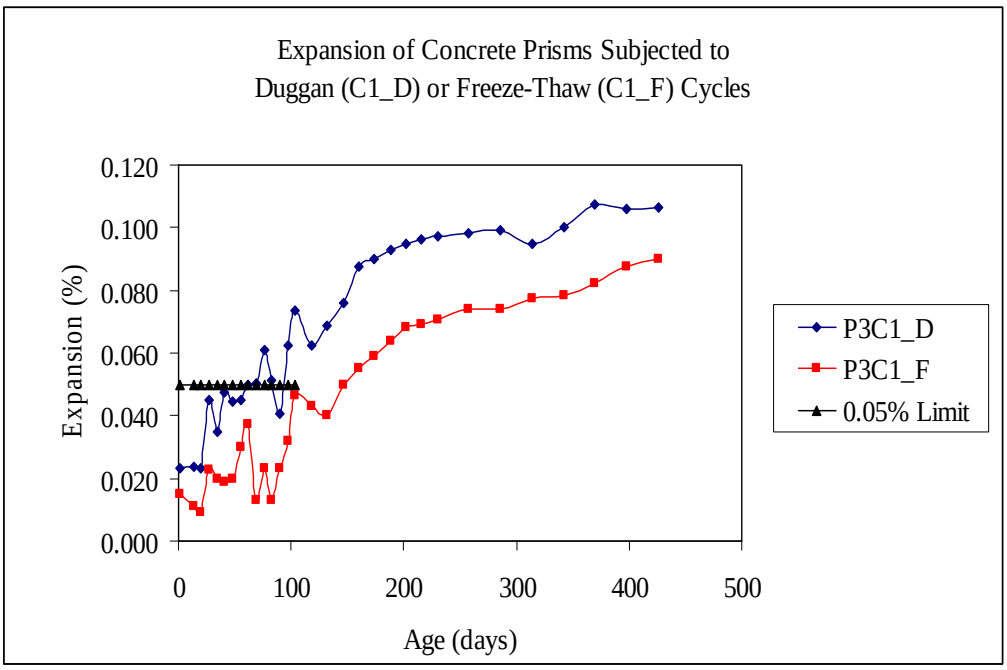


Figure 7.8: Expansion of Room Temperature-Cured Concrete Prisms Subjected to Different Treatments and Stored in Isothermal Water, pH maintained at 12.5 – limewater

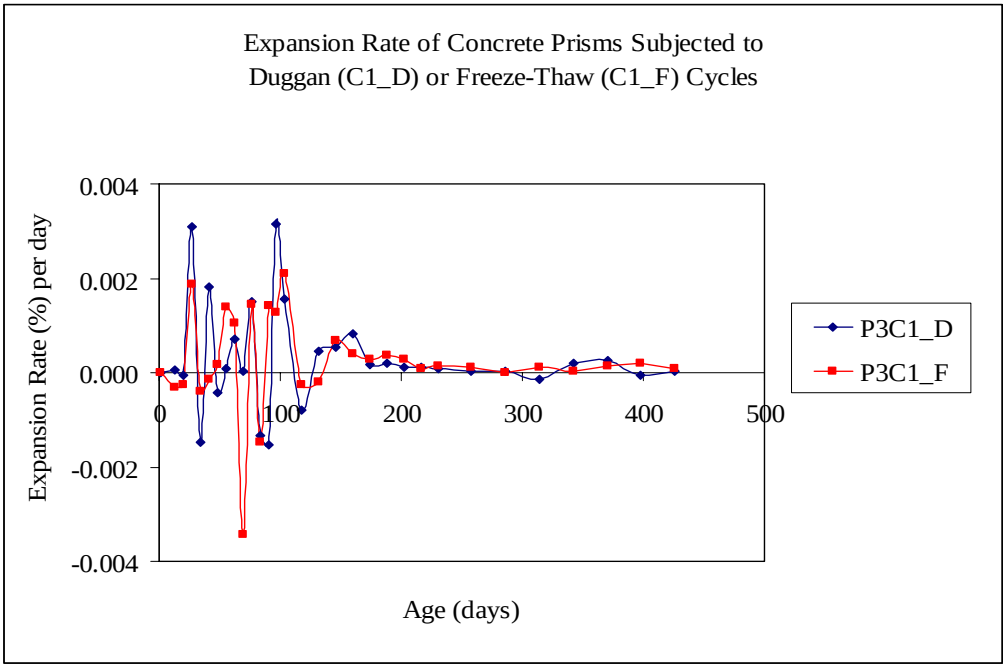


Figure 7.9: Expansion Rate of Room-Temperature-Cured Concrete Prisms Subjected to Different Treatments and Stored in Isothermal Water Bath, pH maintained at 12.5 - limewater

## *7.5 Weight Change Results*

### *7.5.1 Weight Change of Concrete Prisms Subjected to Different Exposure Conditions*

The pattern of weight change is quite similar for the concrete prisms stored in exposure conditions 1 and 2. Figure 7.10 shows the weight change against time measurements of the concrete prisms subjected to Duggan heat cycle and subsequently stored under exposure conditions.

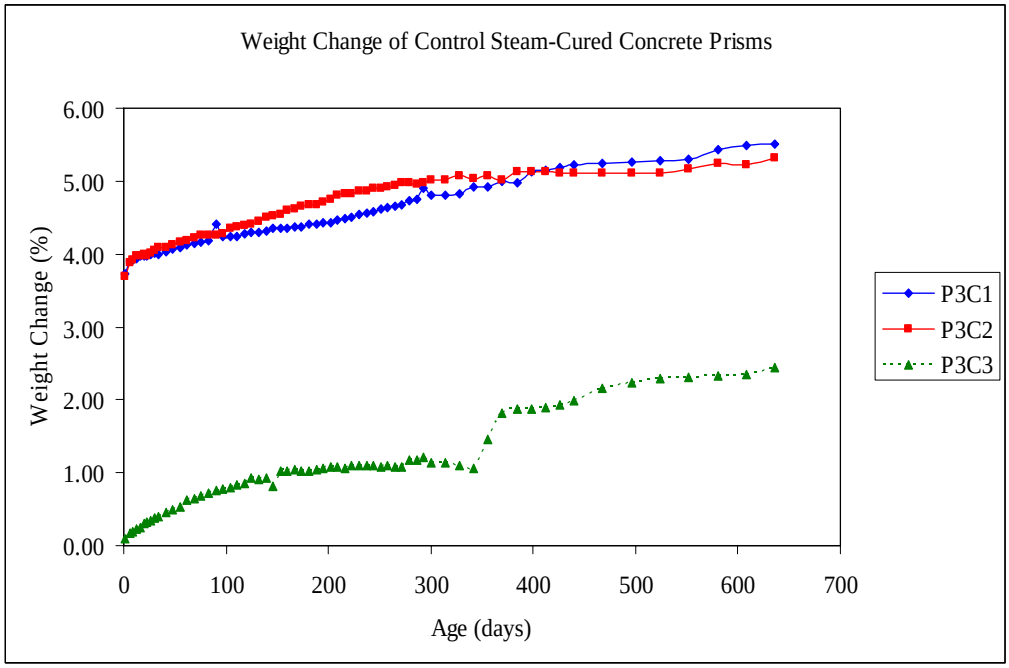


Figure 7.10: Weight Change of Steam-Cured Concrete Prisms Subjected to Duggan Heat Cycle and Stored Under Different Exposure Conditions

After one (1) day of storage, the weight changes of concrete prisms were 3.73%, 3.70% and 0.09% in exposure conditions 1, 2 and 3 respectively. Weight changes of concrete specimens showed rapid increases in the first 100 days of storage. Concrete prisms in exposure condition 3 (R.H maintained at 97%) showed less significant weight gain. Both exposure conditions 1 and 2 showed similar weight change patterns. After 100 days, the rate of weight change of the concrete prisms becomes slower in all exposure conditions. The weight-change measurements of the concrete prisms in exposure condition 3 showed a step pattern at around 350 days of storage. This can be attributed to weight gain due to moisture condensation which reacts to form more ettringite. The maximum weight changes exhibited by the

concrete prisms were 5.50%, 5.31% and 2.44% in exposure conditions 1, 2 and 3 respectively.

Linear regressions were employed to obtain the best fit for the experimental data of weight change against time for the concrete prisms. Two linear regression curves were used to best fit the weight-change data of the concrete prisms. A high linear correlation coefficient is revealed around the first 100 days of storage. Figures 7.11 through 7.13 show the linear regression curves while Table 7.2 provides the regression equations for the data.

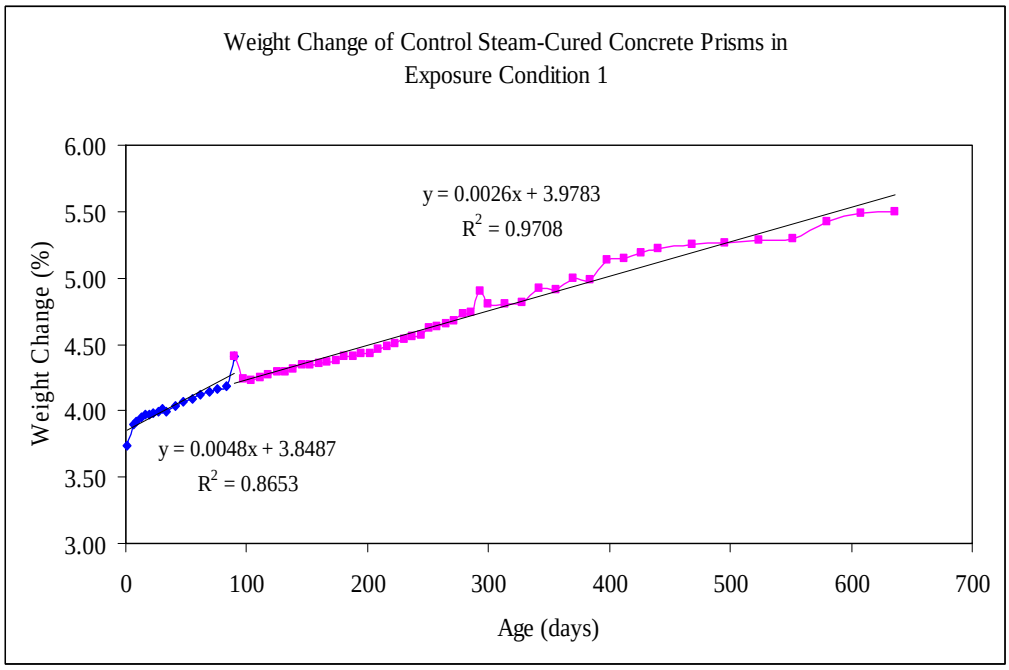


Figure 7.11: Weight Change of Steam Cured Concrete Prisms Subjected to Duggan Heat Cycle and Stored in Isothermal Water Bath, pH maintained at 12.5 - limewater (Regression Curves)

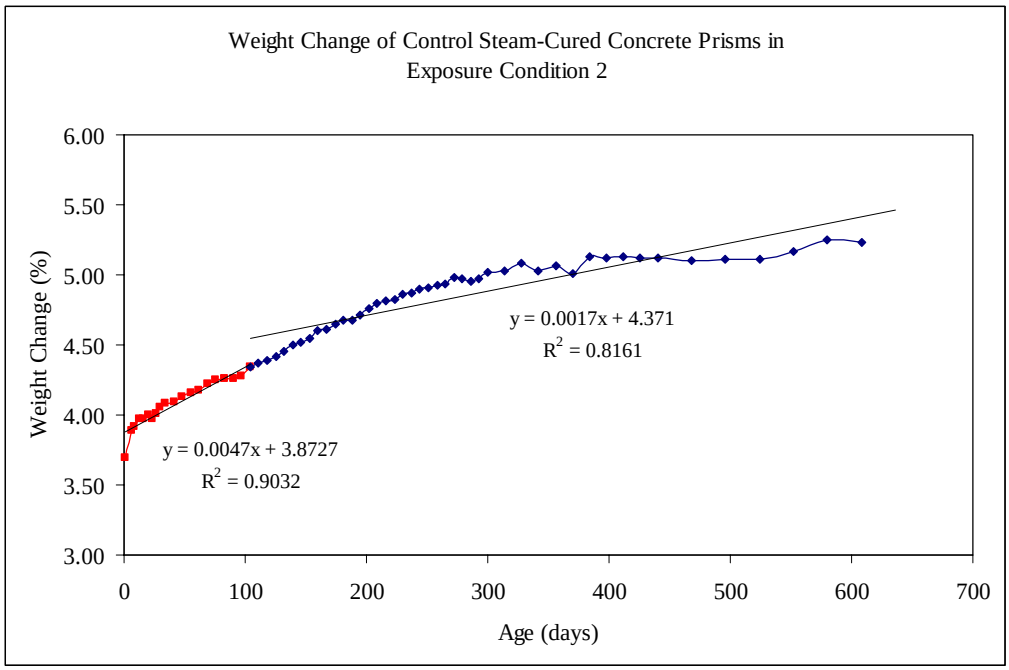


Figure 7.12: Weight Change of Steam-Cured Concrete Prisms Subjected to Duggan Heat Cycle and Stored in Plain Water at Room Temperature (Regression Curves)

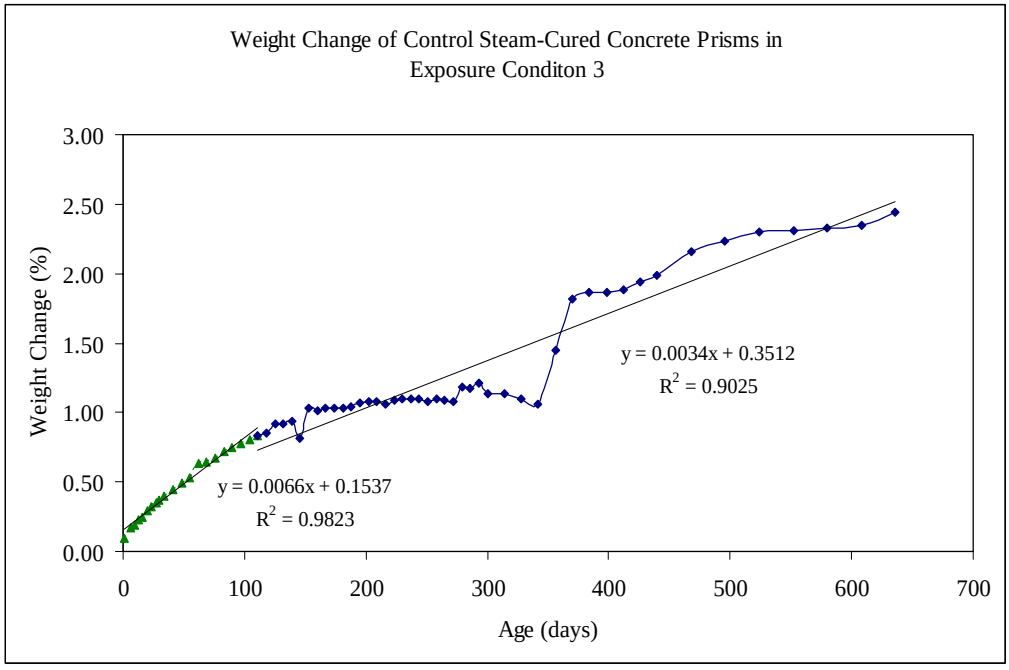


Figure 7.13: Weight Change of Steam-Cured Concrete Prisms Subjected to Duggan Heat Cycle and Stored in Moist Air Chamber, R.H maintained at 97% (Regression Curves)

Table 7.2: Linear Equations for Weight Change vs. Age of Steam-Cured Concrete Prisms Subjected to Duggan Heat Cycle and Stored Under Different Exposure Conditions

| Phase 3 (Concrete Control Samples - subjected to Duggan Heat Cycle) | | | | | |
|---|---|---|---|---|---|
| | | | | | |
| Exp. Cond. 1 | Max. 5.50% | Curve 1 | Day 1 - 90 | $y = 0.0048x + 3.8487$ | $R^2 = 0.8653$ |
| | | Curve 2 | Day 90 - 636 | $y = 0.0026x + 3.9783$ | $R^2 = 0.9708$ |
| | | | | | |
| Exp. Cond. 2 | Max. 5.31% | Curve 1 | Day 1 - 104 | $y = 0.0047x + 3.8727$ | $R^2 = 0.9032$ |
| | | Curve 2 | Day 104 - 636 | $y = 0.0017x + 4.371$ | $R^2 = 0.8161$ |
| | | | | | |
| Exp. Cond. 3 | Max. 2.44% | Curve 1 | Day 1 - 111 | $y = 0.0066x + 0.1537$ | $R^2 = 0.9823$ |
| | | Curve 2 | Day 111 - 636 | $y = 0.0034x + 0.3512$ | $R^2 = 0.9025$ |

*7.5.2 Weight Change of Concrete Prisms Subjected to Different Treatments*

The weight change measurements significantly increased after just one (1) day of storage for concrete prisms subjected to Duggan heat cycle and in exposure condition 1. The Duggan heat cycle was used to initiate microcrack which is intended to accelerate DEF, and associated deleterious expansion. The maximum weight change of the concrete prisms subjected to Duggan heat was 5.43% and occurred after about 40 days of storage. This can be attributed to ettringite formation and other weight-change mechanisms which influence concrete systems by introducing various structural defects. The Freeze-Thaw cycles treated concrete prisms exhibited less significant weight change throughout the study. This might be due to the lack of heat during the concrete treatment. Figure 7.14 shows the weight change of Duggan heat and Freeze-Thaw cycles treated concrete prisms. Figures 7.15

and 7.16 show the linear regression curves used for the best match of the experimental data. Table 7.3 provides the regression equations for the treated concrete prisms.

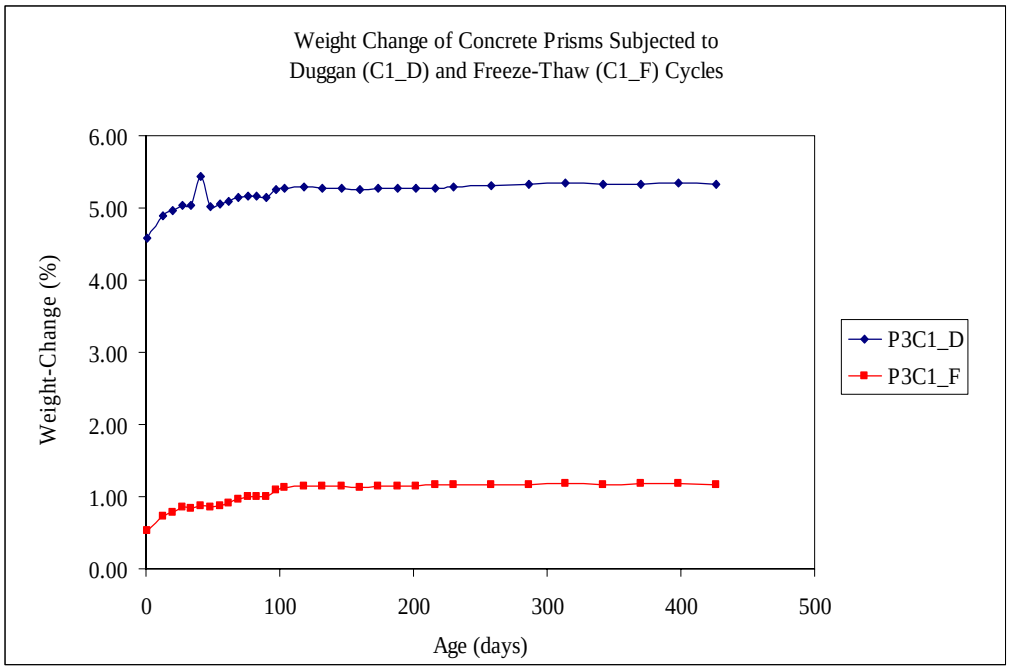


Figure 7.14: Weight Change of Room Temperature-Cured Concrete Prisms Subjected to Duggan Heat or Freeze-Thaw Cycles and Stored in Isothermal Water Bath, pH maintained at 12.5 - limewater

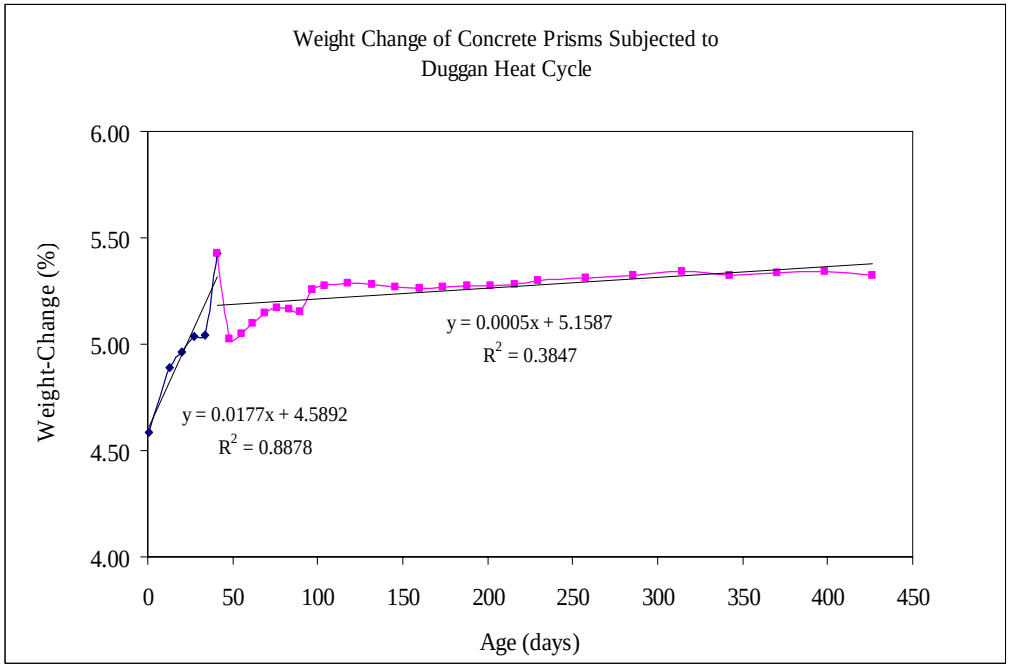


Figure 7.15: Weight Change of Room Temperature-Cured Concrete Prisms Subjected to Duggan Heat Cycles and Stored in Isothermal Water Bath, pH maintained at 12.5 – limewater (Regression Curves)

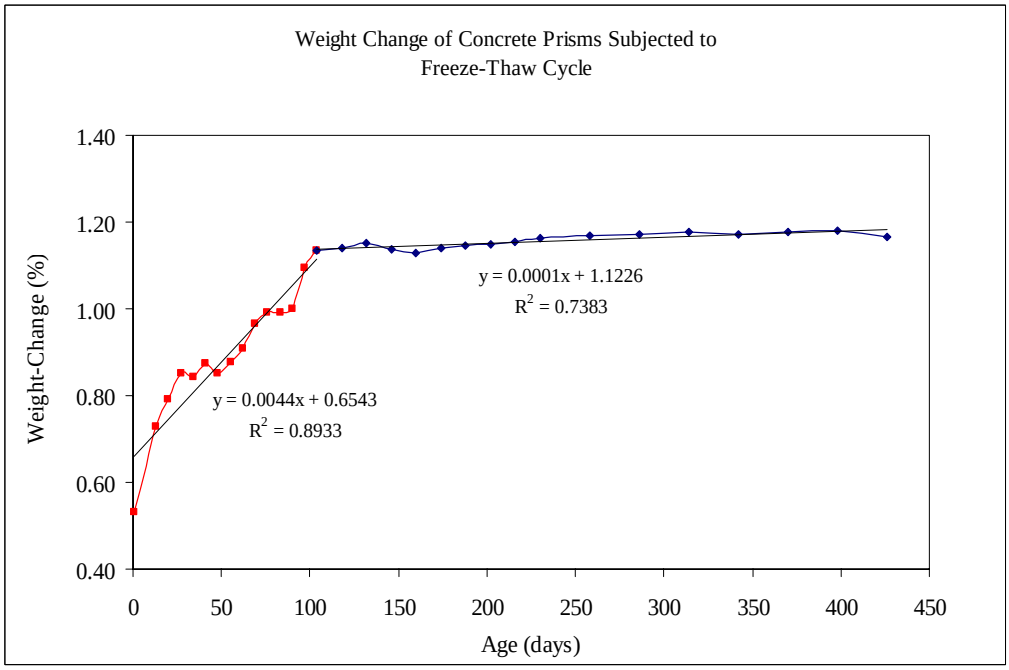


Figure 7.16: Weight Change of Room Temperature-Cured Concrete Prisms Subjected to Freeze-Thaw Cycles and Stored in Isothermal Water Bath, pH maintained at 12.5 - limewater (Regression Curves)

Table 7.3: Linear Equations for Weight Change vs. Age of Duggan Heat or Freeze-Thaw Cycles Treated Concrete Prisms and Stored in Isothermal Water Bath, pH maintained at 12.5 - limewater

| Phase 3 (Concrete Prisms - Subjected to Duggan or Freeze-Thaw Cycles) | | | | |
|---|---|---|---|---|
| | | | | |
| Duggan Heat Cycle | Curve 1 | Day 1 - 41 | $y = 0.0177x + 4.5892$ | $R^2 = 0.8878$ |
| | Curve 2 | Day 41 - 426 | $y = 0.0005x + 5.1587$ | $R^2 = 0.3847$ |
| | | | | |
| Freeze-Thaw Cycle | Curve 1 | Day 1 - 104 | $y = 0.0044x + 0.6543$ | $R^2 = 0.8933$ |
| | Curve 2 | Day 104 - 426 | $y = 0.0001x + 1.1226$ | $R^2 = 0.7383$ |
| | | | | |

## *7.6 Expansion and Weight Change*

### *7.6.1 Expansion and Weight Change of Concrete Prisms Subjected to Different Exposure Conditions*

Expansion and weight-change measurements were taken simultaneously to investigate if any correlation existed. Weight change during early stage of storage is mostly determined by the cement hydration behavior, leading not only to ettringite formation but also to the formation of various hydrated phases (Shimada, 2005). Figure 7.17 shows expansion against weight change of steam-cured concrete and subjected to Duggan heat cycle before subsequently being stored in different exposures.

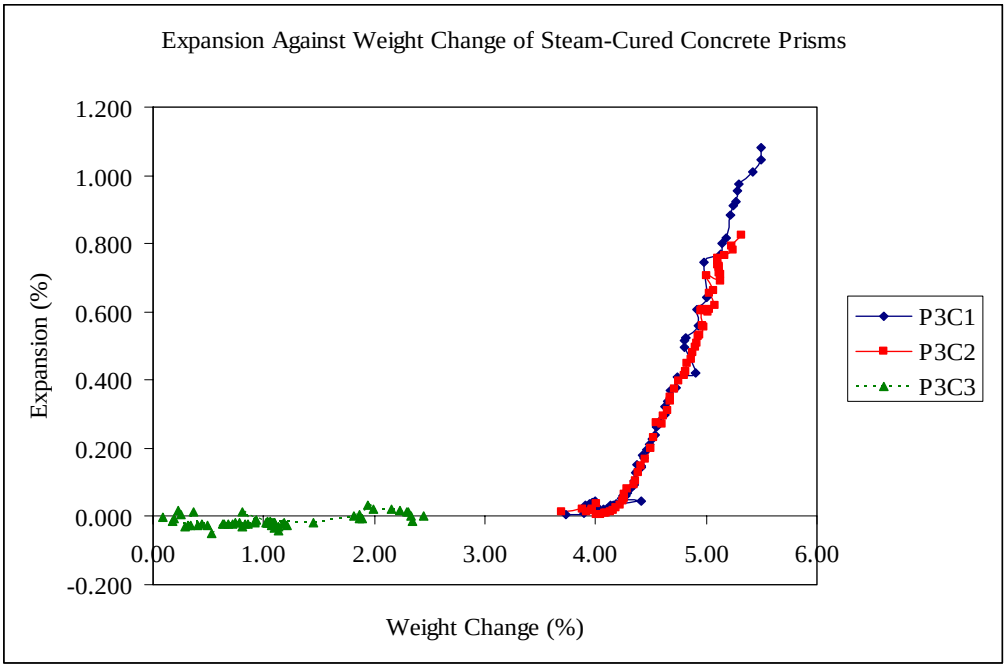


Figure 7.17: Expansion Against Weight Change of Steam-Cured Concrete Prisms Subjected to Duggan Heat Cycle and Stored Under Different Exposure Conditions

From the scatter plots of the expansion against weight change, it can be seem that only concrete prisms in exposure conditions 1 and 2 exhibit weight gain with increased expansion. The difference in weight-change patterns can be attributed to the different weight-change mechanisms taking place under the individual exposure conditions. Linear regression curves were applied to obtain correlation between the expansion and weight changes of the concrete prisms stored under different exposure conditions. Figures 7.18 through 7.20 show the linear curves of the concrete prisms results for the different exposure conditions. Table 7.4 shows the regression equations for the different exposure conditions. From 100 days up to 600 days of storage, a high positive linear correlation exists between expansion and weight

change of the concrete samples in exposure conditions 1 and 2. This can presumably be due to the weight change because of renewed ettringite formation and storage solution entering the microstructure through the structural defects. Observation results from the SEM and Laser Shearography (LAS) would be used to distinguish mechanisms in the microstructure of the concrete specimens responsible for concurrent increase in expansion and weight-change.

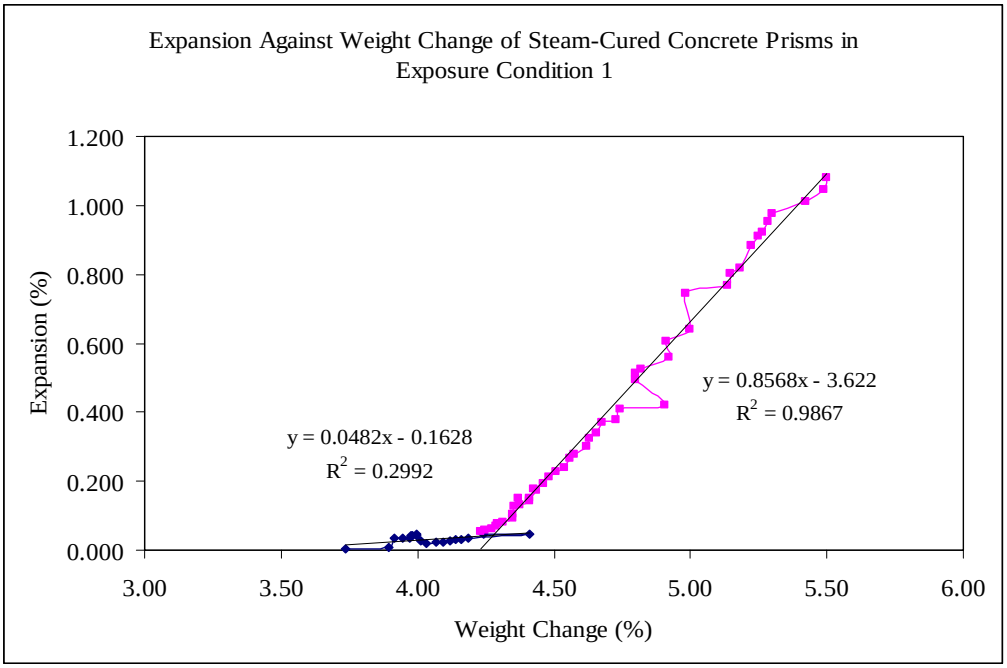


Figure 7.18: Expansion Against Weight Change of Steam-Cured Concrete Prisms Subjected to Duggan Heat Cycle and Stored in Isothermal Water Bath, pH maintained at 12.5 – limewater (Regression Curves)

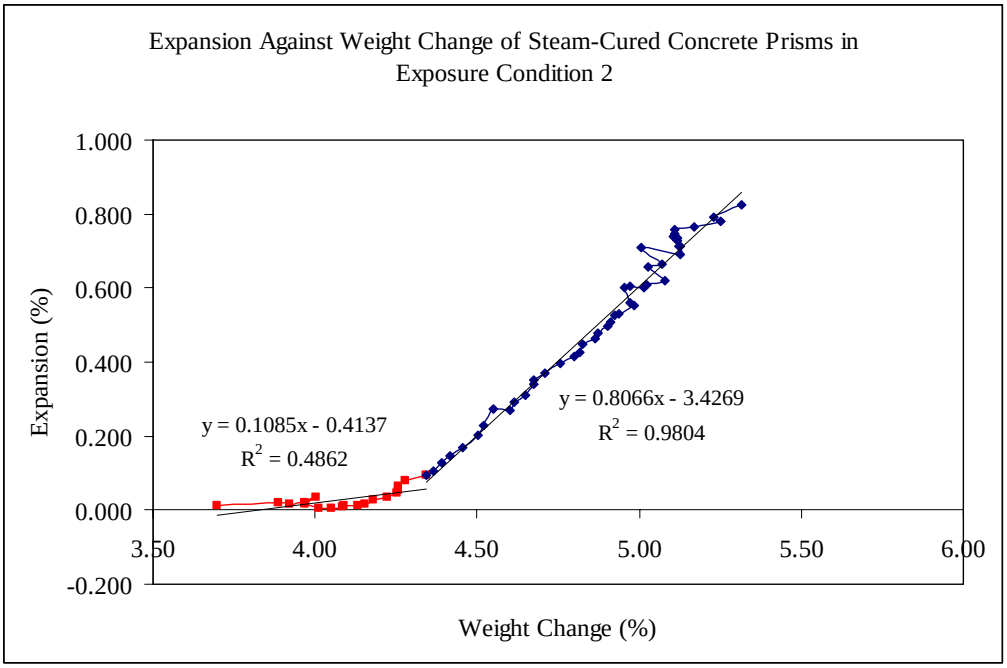


Figure 7.19: Expansion Against Weight-Change of Steam-Cured Concrete Prisms Subjected to Duggan Heat Cycle and Stored in Plain Water at Room Temperature (Regression Curves)

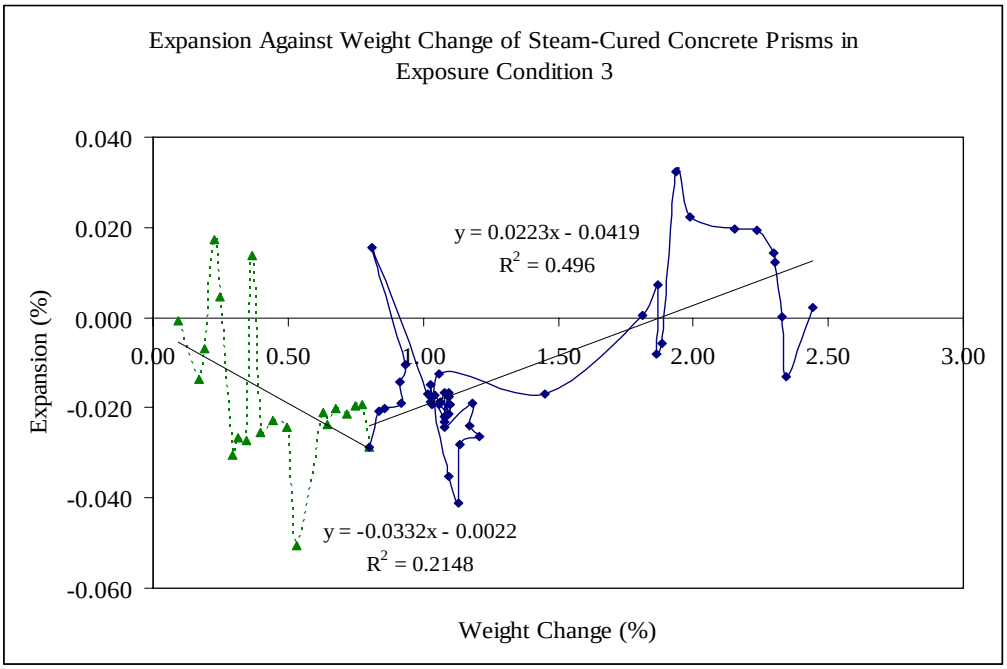


Figure 7.20: Expansion Against Weight Change of Steam-Cured Concrete Prisms Subjected to Duggan Heat Cycle and Stored in Moist Air Chamber, R.H maintained at 97% (Regression Curves)

Table 7.4: Linear Equations for Expansion vs. Weight Change of Steam-Cured Concrete Prisms Subjected to Duggan Heat Cycle and Stored Under Different Exposure Conditions

| Phase 3 (Concrete Control Samples - Subjected to Duggan Heat Cycle) | | | | |
|---|---|---|---|---|
| | | | | |
| Exp. Cond. 1 | Curve 1 | Day 1 - 104 | y = 0.0482x - 0.1628 | $R^2$ = 0.2992 |
| | Curve 2 | Day 104 - 636 | y = 0.8568x - 3.622 | $R^2$ = 0.9867 |
| | | | | |
| Exp. Cond. 2 | Curve 1 | Day 1 - 104 | y = 0.1085x - 0.4137 | $R^2$ = 0.4862 |
| | Curve 2 | Day 100 - 636 | y = 0.8066x - 3.4269 | $R^2$ = 0.9804 |
| | | | | |
| Exp. Cond. 3 | Curve 1 | Day 1 - 104 | y = 0.0332x - 0.0022 | $R^2$ = 0.2148 |
| | Curve 2 | Day 100 - 636 | y = 0.0223x - 0.0419 | $R^2$ = 0.496 |
| | | | | |

*7.6.2 Expansion and Weight Change of Concrete Prisms Subjected to Different Treatments*

Expansion against weight change analysis of Duggan heat or Freeze-Thaw cycles treated concrete samples exhibited no correlation for the duration of the study. Figures 7.21 and 22 showed expansion against weight-change data of the concrete samples.

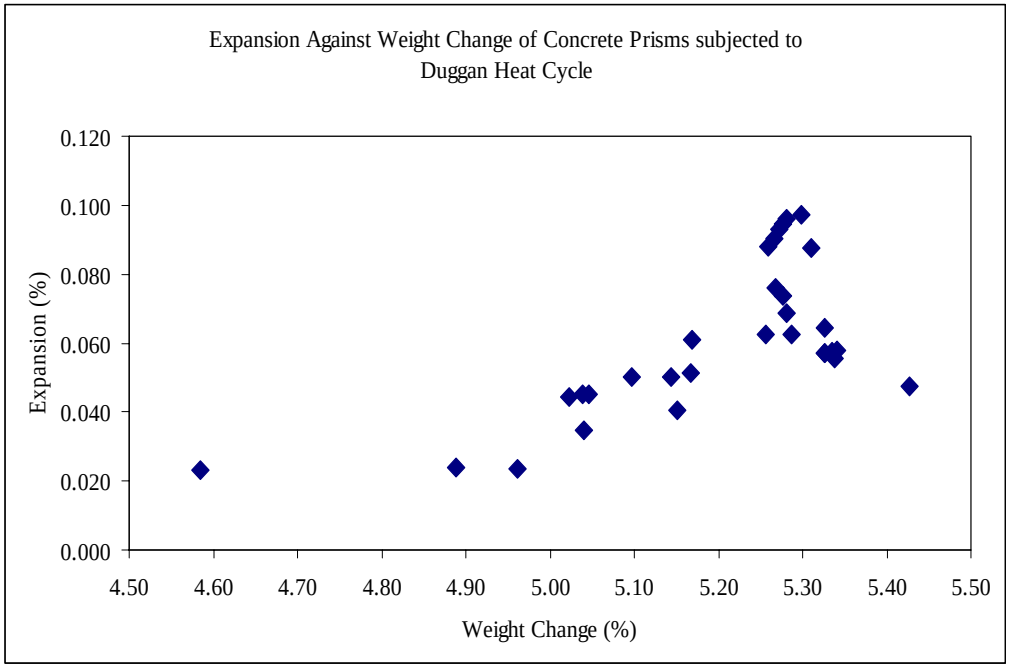


Figure 7.21: Expansion Against Weight Change of Room Temperature-Cured Concrete Prisms Subjected to Duggan Heat Cycles and Stored in Isothermal Water Bath, pH maintained at 12.5 - limewater

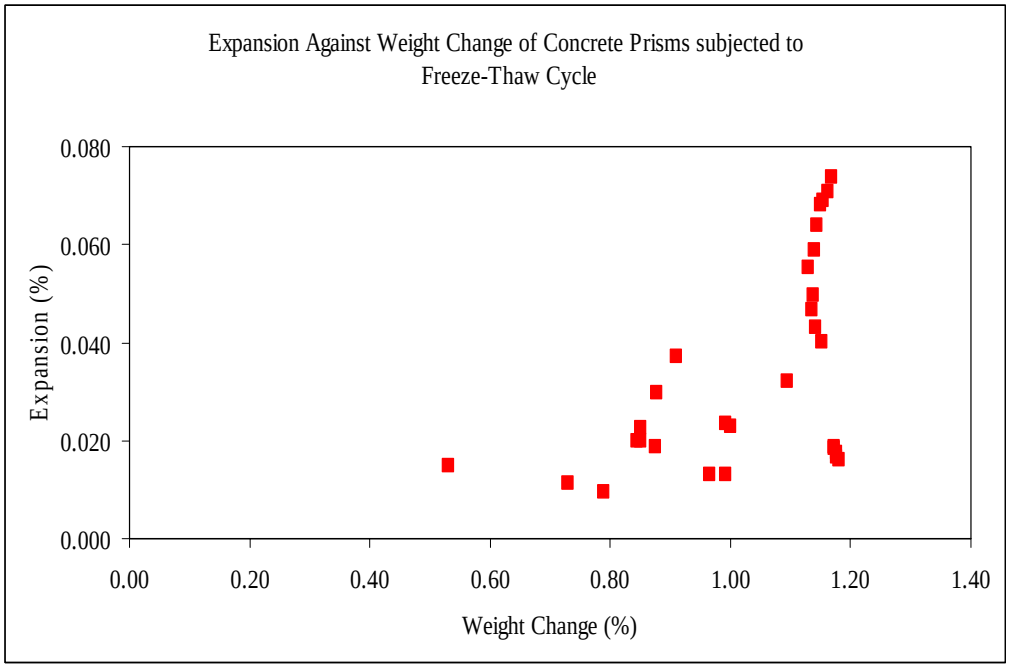


Figure 7.22: Expansion Against Weight Change of Room Temperature-Cured Concrete Samples Subjected to Freeze-Thaw Cycles and Stored in Isothermal Water Bath, pH maintained at 12.5 - limewater

## *7.7 Compressive Strength Results*

### *7.7.1 Effect of Exposure Conditions on Compressive Strength of Concrete Samples*

The compressive strength results of the heat-cured concrete specimens subjected to Duggan heat cycle and then stored under different exposure conditions is shown in figure 7.23. The compressive strength of the concrete cylinders was 5182 psi, 4792 psi and 5707 psi after 28 days of storage in exposure conditions 1, 2 and 3 respectively. At 540 days of compressive strength tests, exposure conditions 1 and 2 showed an 85% reduction in strength while exposure condition 3 revealed a 25% increase. These results postulated that heat-cured concrete, subsequently subjected to the Duggan heat cycle, has an adverse effect on the compressive strength. Much of the damage contributing to significant compressive strength reduction seems to be related to the damage variable caused by DEF. Table 7.5 provides the average compressive strength and standard deviations of the control concrete samples.

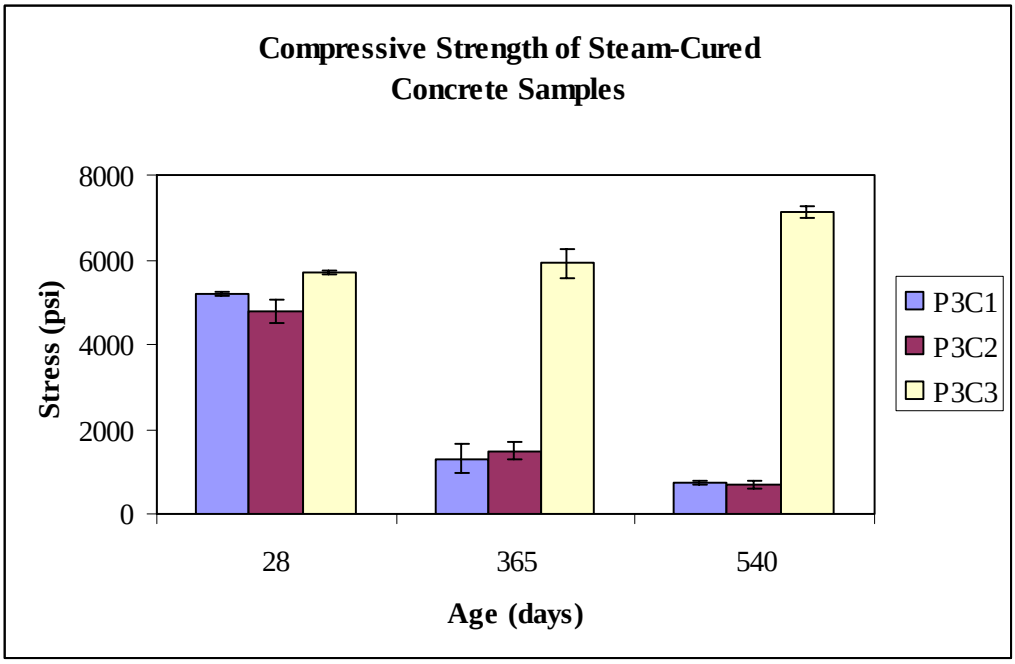


Figure 7.23: Compressive Strength Chart of Concrete Specimens Subjected to Duggan Heat Cycle and Stored Under Different Exposure Conditions

Table 7.5: Compressive Strength of Concrete Specimens Subjected to Duggan Heat Cycle and Stored Under Different Exposure Conditions

| | Average Compressive Strength (psi) | | |
|---|---|---|---|
| | 28 Days | 365 Days | 540 Days |
| | Std | Std | Std |
| P3C1 | 5182 | 1309 | 731 |
| | 45 | 340 | 39 |
| P3C2 | 4792 | 1488 | 684 |
| | 267 | 200 | 98 |
| P3C3 | 5707 | 5911 | 7116 |
| | 51 | 355 | 141 |

*7.7.2 Effect of Concrete Treatments on Compressive Strength of Concrete Samples*

Compressive strength testing was employed at 28 days, 240 days and 365 days for the Duggan or Freeze-Thaw cycles treated concrete samples. At 28 days, the compressive strength was 5917 psi for the Duggan heat cycle treated concrete samples and 6680 psi for the Freeze-Thaw cycle concrete samples. Compressive strength tests at later stages showed up to 25% increase in strength. The compressive strength after one (1) year was 7183 psi for the Duggan samples and 8050 psi for the Freeze-Thaw cycle treated concrete samples. Figure 7.24 shows the compressive strength of the concrete samples subjected to different treatment. Table 7.6 gives the average compressive strength and standard deviation of the test results.

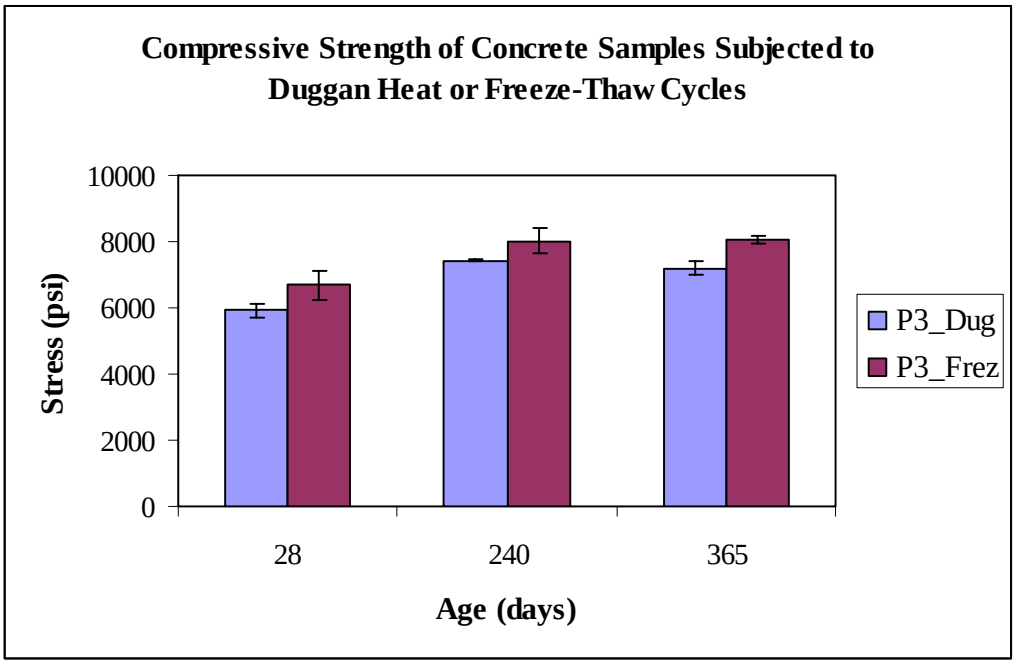


Figure 7.24: Compressive Strength Chart of Room Temperature-Cured Concrete Specimens Subjected to Duggan Heat or Freeze-Thaw Cycles and Stored in Isothermal Water Bath, pH maintained at 12.5 - limewater

Table 7.6: Compressive Strength of Room Temperature-Cured Concrete Samples Subjected to Duggan Heat or Freeze-Thaw Cycles and Stored in Isothermal Water Bath, pH maintained at 12.5 - limewater

| | Average Compressive Strength (psi) | | |
|---|---|---|---|
| | 28 Days | 240 Days | 365 Days |
| | Std | Std | Std |
| P3_Dug | 5917 | 7438 | 7183 |
| | 214 | 40 | 200 |
| P3_Frez | 6680 | 8014 | 8050 |
| | 441 | 377 | 98 |

*7.7.3 Effect of Moisture Content on Compressive Strength of Concrete Samples*

The concrete samples were room temperature-cured before subjecting them to the Duggan heat cycle, and before being stored subsequently in exposure condition 1, with tests employed at 40 days, 130 days and 300 days. A set of three (3) concrete cylinders were taken at each test period from the storage solution and dried at room temperature for about 12 days. The weight-change decreases about 2%, and this has a major influence on the compressive strength at early and later stages. The compressive strength at 40 days was 6168 psi for the moist concrete, and 7555 psi for the dry concrete. At 300 days, the compressive strength results were 7054 psi and 8902 psi for the moist and dry concrete cylinders respectively. These results reflect the effect of moisture content on the compressive strength of concrete. Figure 7.25 shows the compressive strength chart and Table 7.7 provides a summary of the test results.

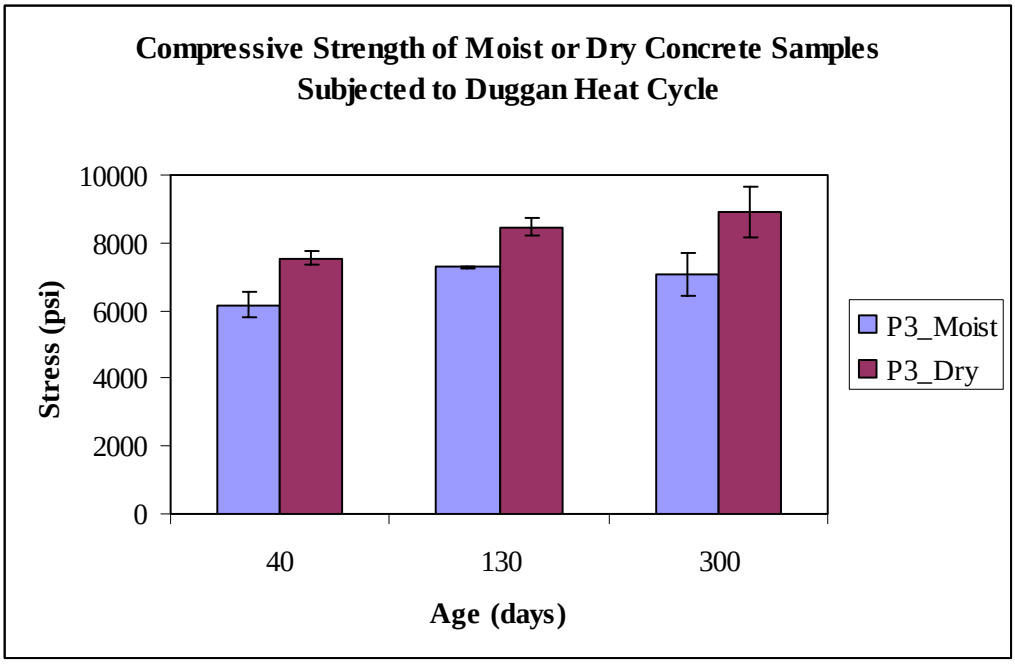


Figure 7.25: Compressive Strength Chart of Moist or Dry Room Temperature-Cured Concrete Samples Subjected to Duggan Heat Cycles and Stored in Isothermal Water Bath, pH maintained at 12.5 - limewater

Table 7.7: Compressive Strength of Moist or Dry Room Temperature-Cured Concrete Samples Subjected to Duggan Heat Cycles and Stored in Isothermal Water Bath, pH maintained at 12.5 – limewater

| | Average Compressive Strength (psi) | | |
|---|---|---|---|
| | 40 Days | 130 Days | 300 Days |
| | Std | Std | Std |
| P3_Moist | 6168 | 7271 | 7054 |
| | 385 | 47 | 619 |
| P3_Dry | 7555 | 8460 | 8902 |
| | 220 | 262 | 742 |

*7.8 Concrete Field Samples (No Duggan Heat Cycle)*

Two (2) sets of concrete mixes were prepared in the laboratory and then stored outside under atmospheric conditions. The first concrete batch (P3C4A) was steam-cured at 85$^{o}$C, then subsequently stored in water for six (6) days and stored outside the laboratory. The second concrete batch (P3C4B) was cured in the laboratory at room temperature for 24 hours, and then stored under water for six (6) days prior to exposure to field conditions. None of the batch mixes were subjected to the Duggan heat cycle.

*7.8.1 Length Change Results*

Figures 7.26 and 7.27 show the shrinkage and shrinkage rate of the concrete prisms prepared in the laboratory and then exposed to field conditions. Both sets of concrete samples showed shrinkage throughout the entire research study. The steam-cured concrete samples (Exp. Cond. 4A) exhibited shrinkage values lower than those cured at room temperature (Exp. Cond. 4B). The shrinkage and shrinkage rate increased with time for both sets of concrete samples. The maximum shrinkage at 600 days was about -0.0350% and -0.0378% for exposure conditions 4A and 4B respectively. Figures 7.28 and 7.29 showed the linear regression equations used to fit the experimental data. There exists little or no correlation between length-change and time of concrete sample stored under field conditions. Table 7.8 illustrates the linear equations for the best fit to the experimental data.

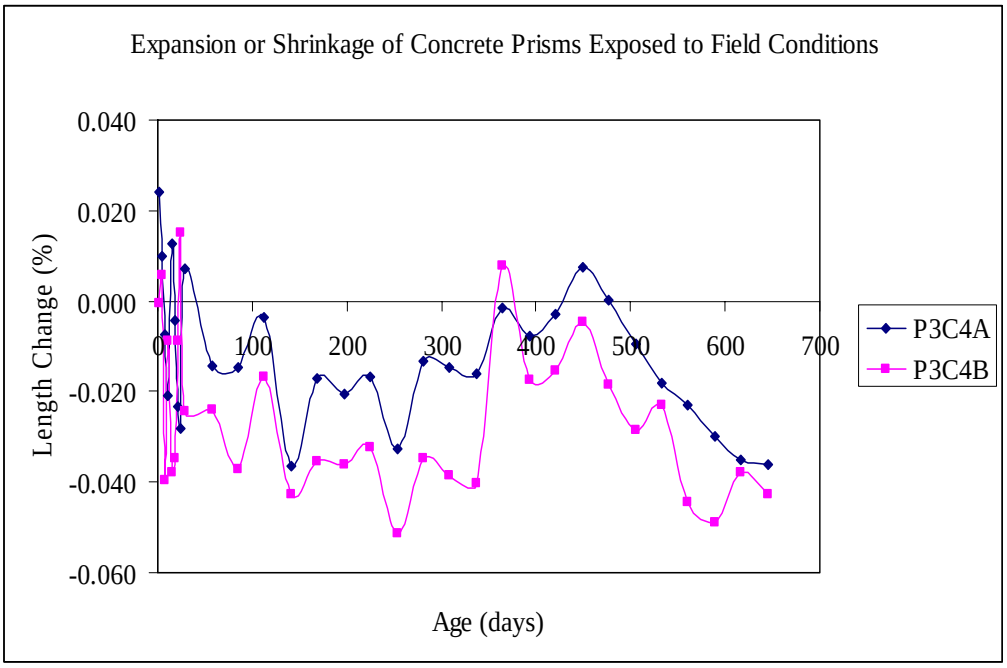


Figure 7.26: Length Change of Concrete Prisms Exposed to Field Conditions

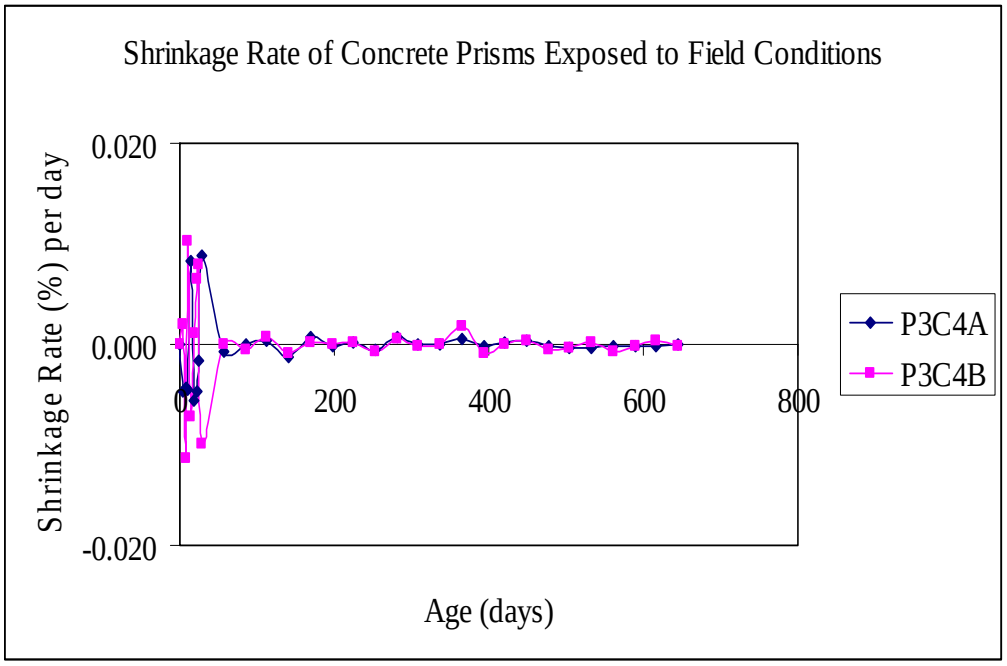


Figure 7.27: Shrinkage Rate of Concrete Prisms Exposed to Field Conditions

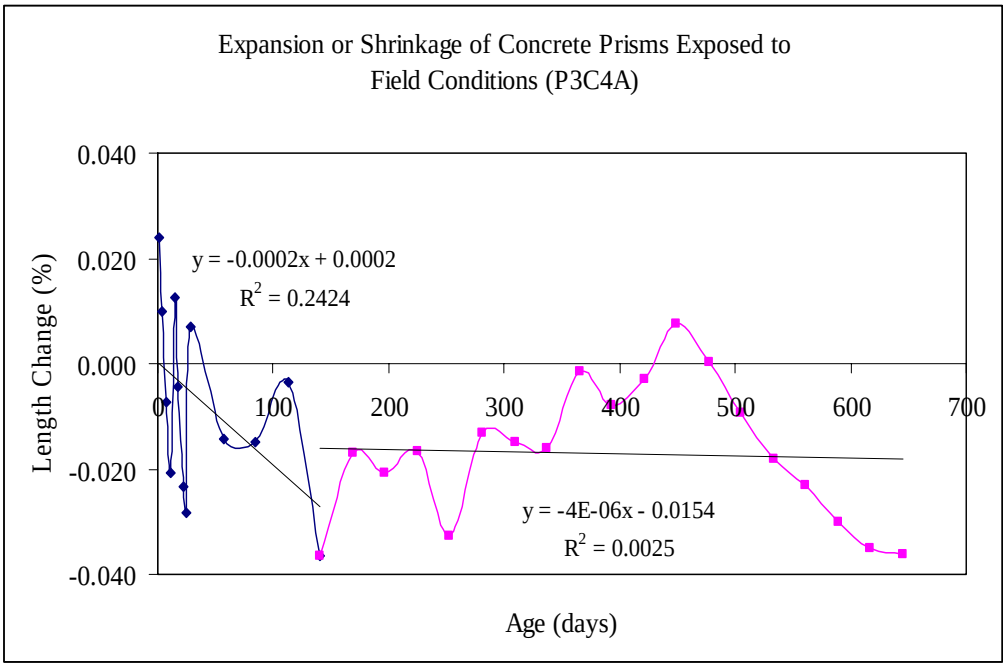


Figure 7.28: Length Change vs. Age of Steam-Cured Concrete Prisms and Stored Under Field Conditions (C4A) (Regression Curves)

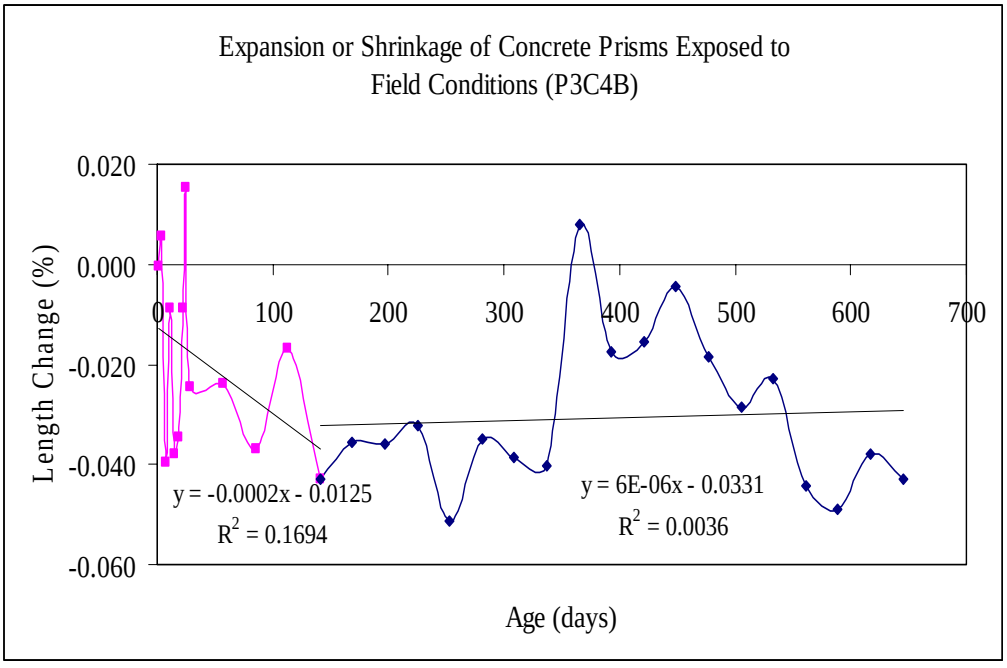


Figure 7.29: Length Change vs. Age of Room Temperature-Cured Concrete Prisms and Stored Under Field Conditions (C4B) (Regression Curves)

Table 7.8: Linear Equations for Length Change vs. Age of Concrete Prisms Stored Under Field Conditions

| Phase 3 (Concrete Control Samples Exposed to Field Conditions) | | | | |
|---|---|---|---|---|
| | | | | |
| Exp. Cond. 4A | Curve 1 | Day 1 - 141 | y = -0.0002x + 0.0002 | $R^2$ = 0.2424 |
| | Curve 2 | Day 141 - 645 | y = -4E-06x - 0.0154 | $R^2$ = 0.0025 |
| | | | | |
| Exp. Cond. 4B | Curve 1 | Day 1 - 141 | y = -0.0002x - 0.0125 | $R^2$ = 0.1694 |
| | Curve 2 | Day 141 - 645 | y = 6E-06x - 0.0331 | $R^2$ = 0.0036 |
| | | | | |

*7.8.2 Weight Change Results*

The weight changes of the field-exposed concrete samples were monitored for the duration of the research. Figure 7.30 shows the weight-change results for the field-exposed concrete samples. Both sets showed a decrease in weight over time. Concrete samples in exposure condition 4B exhibit a higher weight change than those in exposure condition 4A. These results revealed that the high shrinkage values affect the weight changes of the field samples. It can be seen that the weight fluctuates throughout with no defined pattern. This could be attributed to the various environmental changes occurring in the field.

Figures 7.31 and 7.32 provide the regression curves for the best fit for the weight-change against time data. From the linear and polynomial equations provided in Table 7.9, there exists little or no correlation between weight-change and time of the field-exposed concrete samples for the duration of the research study.

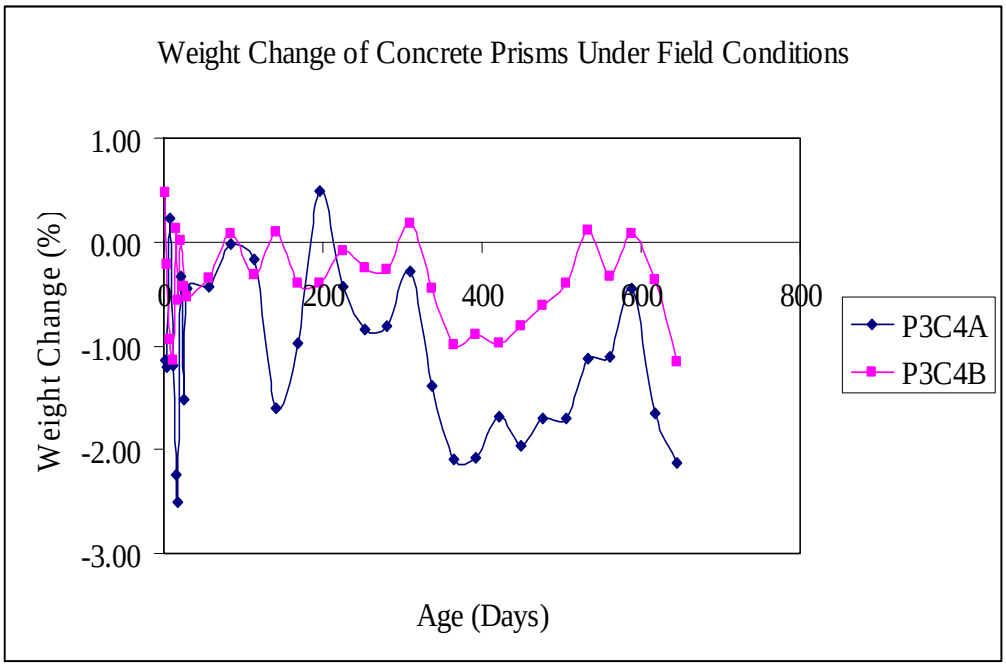


Figure 7.30: Weight Change of Concrete Prisms Exposed to Field Conditions

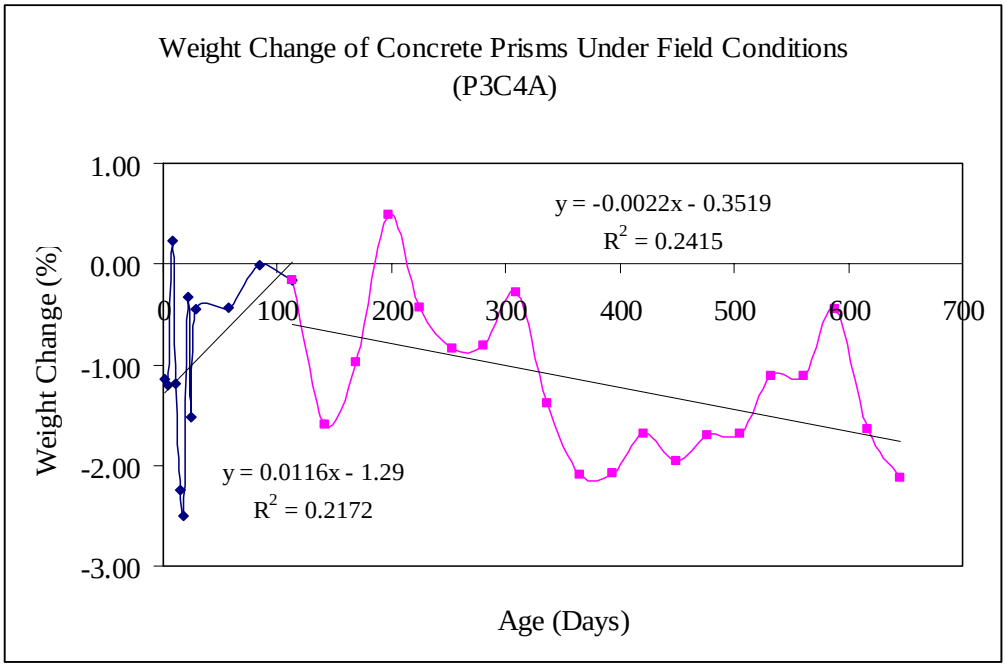


Figure 7.31: Weight Change vs. Age of Steam-Cured Concrete Prisms and Stored Under Field Conditions (C4A) (Regression Curves)

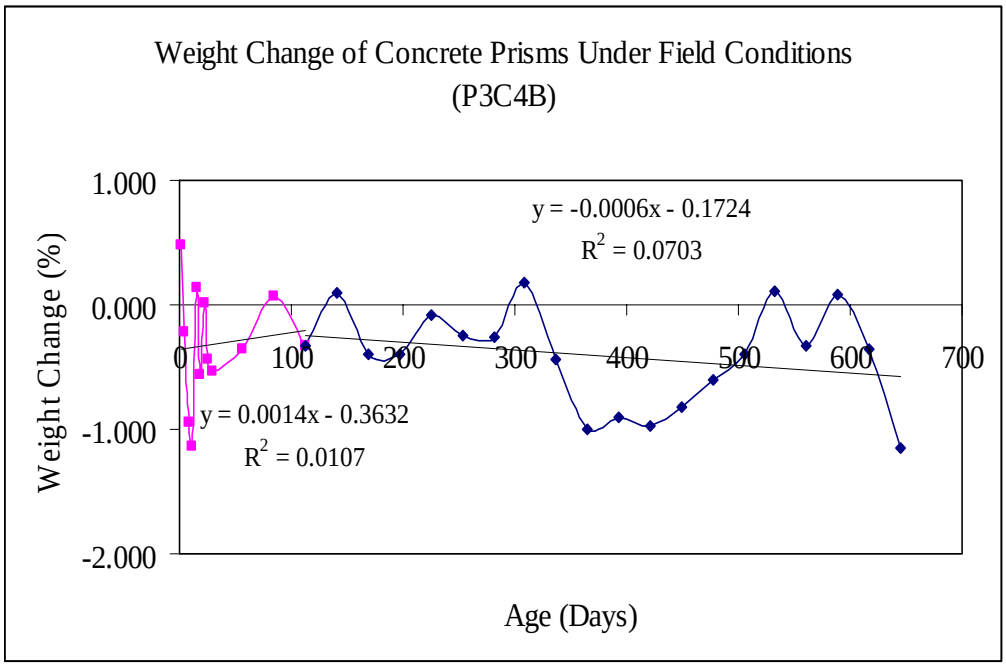


Figure 7.32: Weight Change vs. Age of Room Temperature-Cured Concrete Prisms and Stored Under Field Conditions (C4B) (Regression Curves)

Table 7.9: Linear Equations for Weight Change vs. Age of Concrete Prisms Stored Under Field Conditions

| Phase 3 (Concrete Control - Field Samples) | | | | |
|---|---|---|---|---|
| | | | | |
| Exp. Cond. 4A | Curve 1 | Day 1 - 113 | y = 0.0116x - 1.29 | $R^2$ = 0.2172 |
| | Curve 2 | Day 113 - 645 | y = -0.0022x -0.3519 | $R^2$ = 0.2415 |
| | | | | |
| Exp. Cond. 4B | Curve 1 | Day 1 - 113 | y = -0.0014x - 0.3632 | $R^2$ = 0.0107 |
| | Curve 2 | Day 113 - 645 | y = -0.0006x - 0.1724 | $R^2$ = 0.0703 |
| | | | | |

*7.8.3 Compressive Strength Results*

Compressive strength was checked at 28 days, 365 days and 540 days for both sets of field-exposed concrete samples. At 28 days, the average compressive strength was 4036 psi and 6118 psi for the room temperature-cured (P3C4B) and steam-cured at 85°C (P3C4A) respectively. There is a 35% and 70% increase in strength of the concrete specimens tested at later ages for exposure conditions P3C4A and P3C4B respectively. Figure 7.33 shows the compressive strength of the field-exposed concrete samples. The room temperature-cured concrete specimens have even higher compressive strength than those steam-cured at 85°C throughout. Table 7.10 shows the compressive strength results of the concrete samples subjected to field conditions.

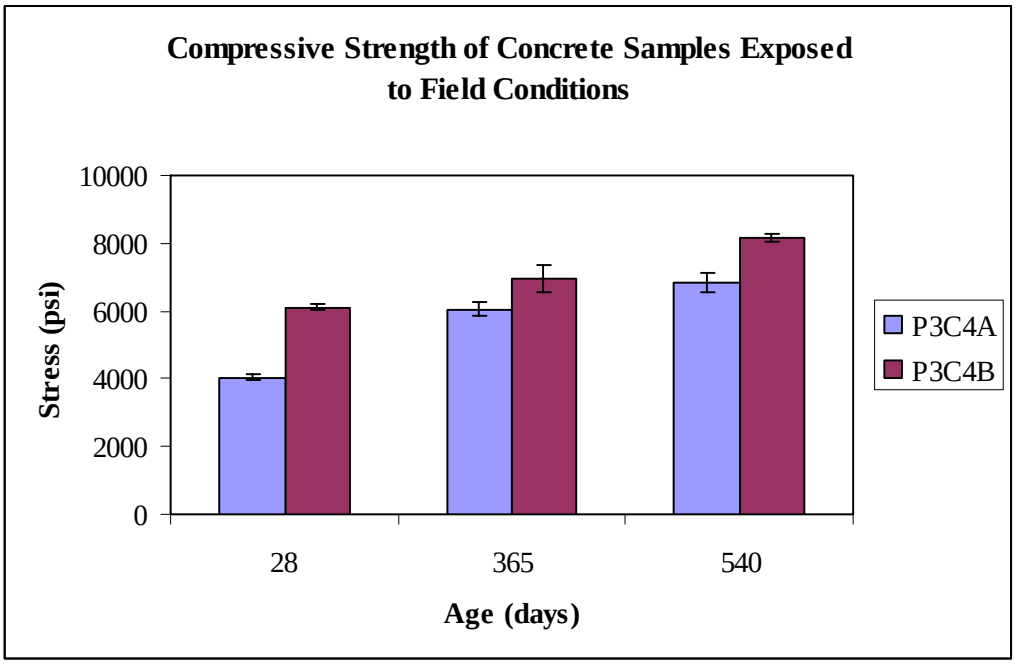


Figure 7.33: Compressive Strength of Concrete Samples Exposed to Field Conditions

Table 7.10: Compressive Strength of Concrete Samples Exposed to Field Conditions

| | Average Compressive Strength (psi) | | |
|---|---|---|---|
| | 28 Days | 365 Days | 540 Days |
| | Std | Std | Std |
| P3C4A | 4036 | 6054 | 6855 |
| | 74 | 185 | 299 |
| P3C4B | 6118 | 6953 | 8154 |
| | 104 | 427 | 105 |

*7.9 Water Analysis Results of Storage Solutions*

*7.9.1 Water Analysis of Exposure Conditions 1*

The storage solution was monitored for leaching of $Na^+$ (sodium) and $K^+$ (potassium) from the concrete samples. The storage solution was monitored periodically to determine the concentrations of the leached ions. The highest concentration of alkalis leached into the storage solution of exposure condition 1 (limewater) was about 304.4 mmol/l. The alkali concentrations in the storage solution increased with time during the storage period. Figure 7.34 shows the alkalis concentration against age for the concrete samples in exposure condition 1.

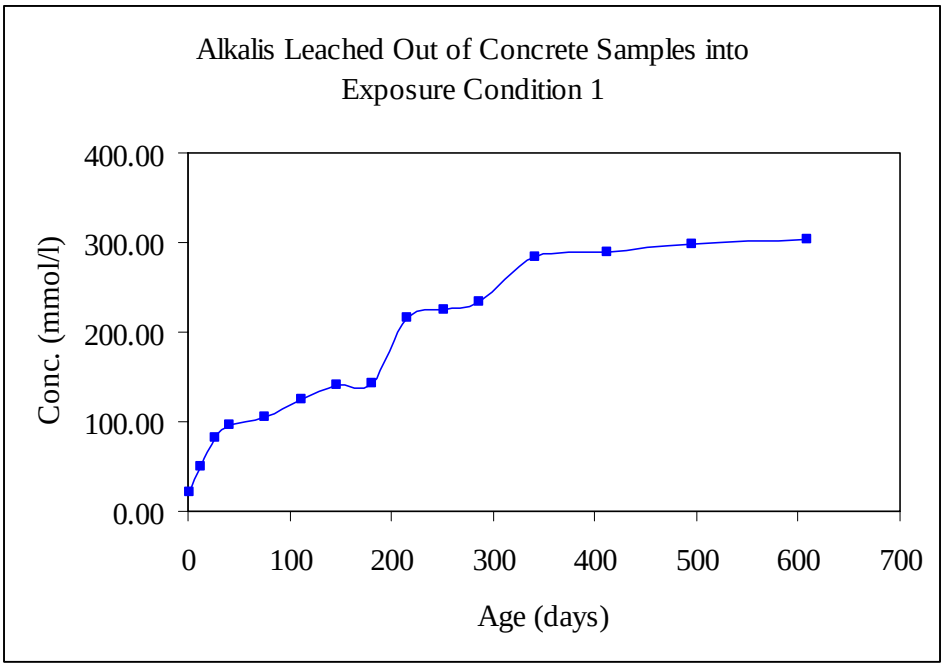


Figure 7.34: Alkalis Leaching from Concrete Samples Stored in Isothermal Water Bath, pH maintained at 12.5 - limewater

*7.9.2 Water Analysis of Exposure Condition 2*

The storage solutions of the concrete samples in exposure condition 2 (water at room temp.) were monitored for pH value, $Na^+$, $K^+$ and $Ca^{2+}$ ion concentrations

*7.9.2.1 Amount of Alkalis*

Figure 7.35 illustrates the alkalis leached from the concrete samples into the storage solution of exposure condition 2. Alkalis were continuously leached out from the concrete samples for the duration of the research. The amount of alkalis leached influence the rate of expansion of the concrete samples and formation of ettringite. However, Rivard observed that when excessive condensation of water takes place on

the specimen surfaces, alkalis are removed from the concrete and the rates of reaction and expansion were reduced (2003).

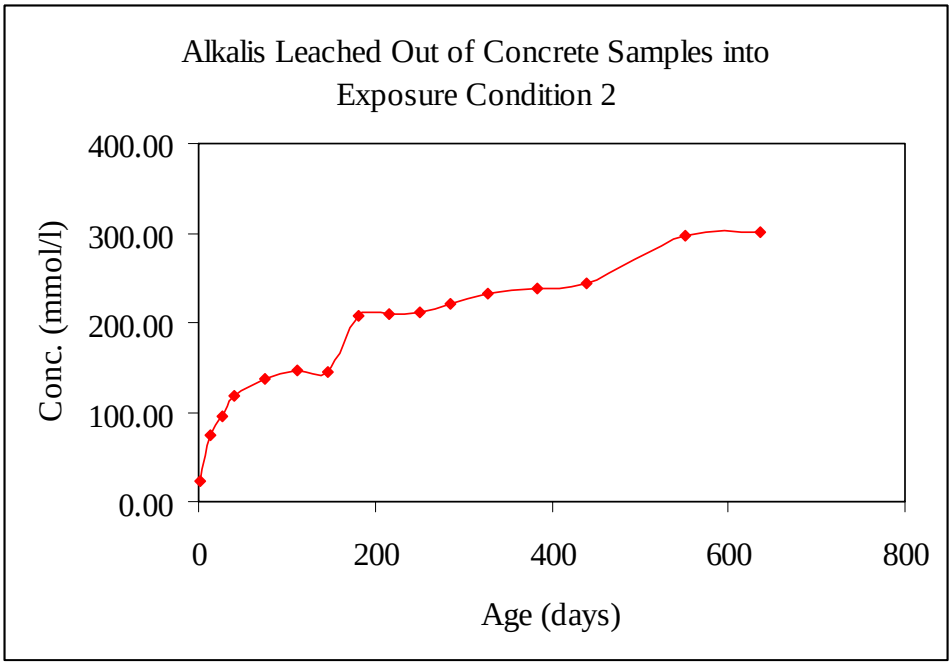


Figure 7.35: Alkalis Leaching from Concrete Samples Stored in Plain Water at Room Temperature

*7.9.2.2 pH Value*

The pH value of the storage solution was known to influence the characteristic and morphology of ettringite. The stability of ettringite is also affected by the pH value of the storage solution (Hampson and Bailey, 1982). The pH value of the storage solution ranges from 8.01 to 11.32.

*7.9.2.3 Calcium Concentration*

The calcium ($Ca^{2+}$) ions concentration of the storage solution seems to affect the porosity of the concrete samples. Their presence is essential for sodium and other ions to penetrate into the reacting grain of the pore structure of the concrete. Figure 7.36 gives the calcium concentration leached out from the concrete samples into the storage solution over time.

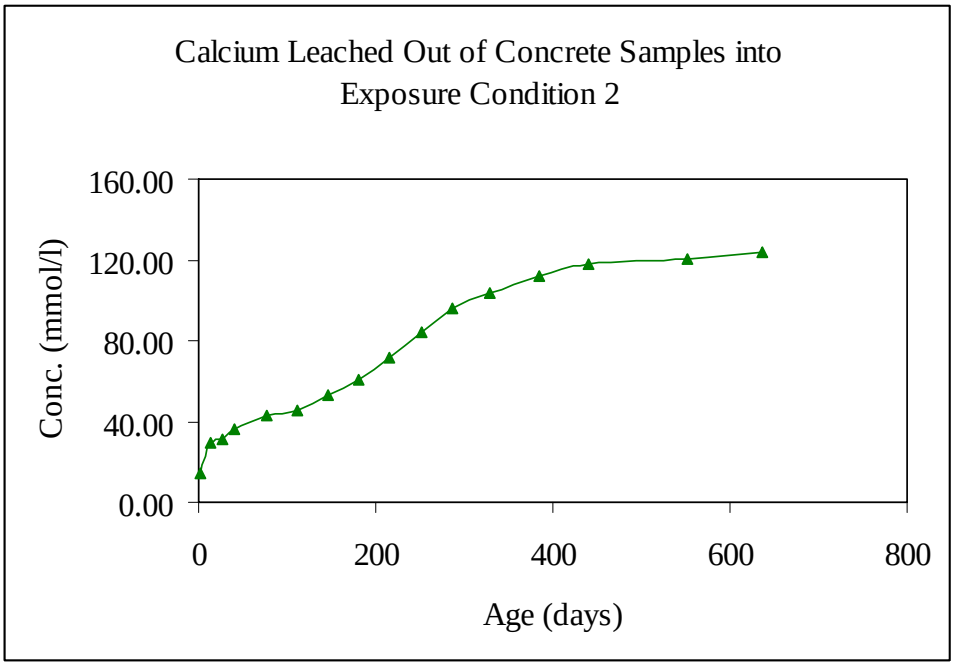


Figure 7.36: Calcium Leached from Concrete Samples Stored in Plain Water at Room Temperature

*7.10 Laser Shearography (LAS)*

Laser shearography is a nondestructive testing technique, and it was used to detect fine cracks with a spatial resolution < 10 microns. Fine cracks, which form because of various damage mechanisms including alkali-silicate reaction, delayed ettringite formation (DEF) or frost damage, eventually become visible, but it is important to detect them as soon as possible for possible mitigation (Livingston et al. 2006). Preliminary comparisons with digitized optical microscope image revealed the cracks that were 20 pixels wide in the laser shearography were not detectable in the optical micrographs, which has a resolution of about 10 microns per pixel. This implies that the laser shearography has a minimum detectable crack width < 10 microns. Laser shearography examinations were applied on the concrete prisms at distinct intervals to detect the onset of cracking and to measure its subsequent propagation. Each face of the 3" x 3" x 11.25" concrete prisms, except the end faces, were divided into three (3) equal sections and labeled for laser shearography work.

*7.10.1 Laser Shearography Analysis of Concrete Prisms Stored in Exposure Condition 1 (Isothermal Water Bath, pH maintained at 12.5 - Limewater)*

The laser shearography images showed no cracks before subjecting the concrete prisms to the Duggan heat cycle. Figure 7.37 is a laser shearography image of the concrete prism about seven (7) days after casting and before Duggan heat cycle treatment. No cracks are visible. Figure 7.38 shows the same concrete specimens after Duggan Heat cycle and subsequently being stored in exposure condition 1 (limewater) after 100 days. Storage in limewater is known to promote expansive stresses associated with DEF. Note that while the cracks can be clearly seen in the

shearography image, they are not visible using an optical microscopy, which has a resolution of 10 microns per pixel.

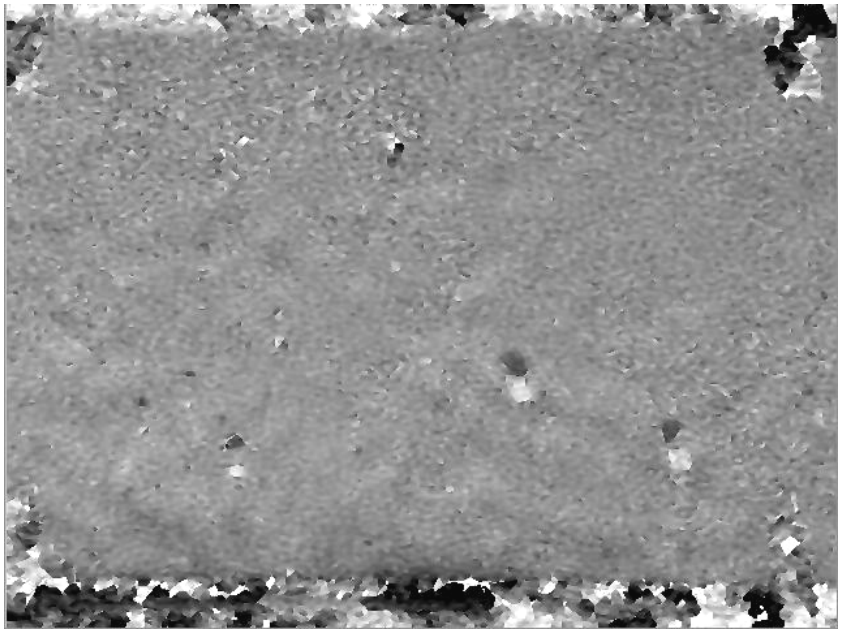

Figure 7.37: Shearography Image of Concrete Prism Surface 7 Days After Casting (Height = 7.6 cm ~ 3 in.)

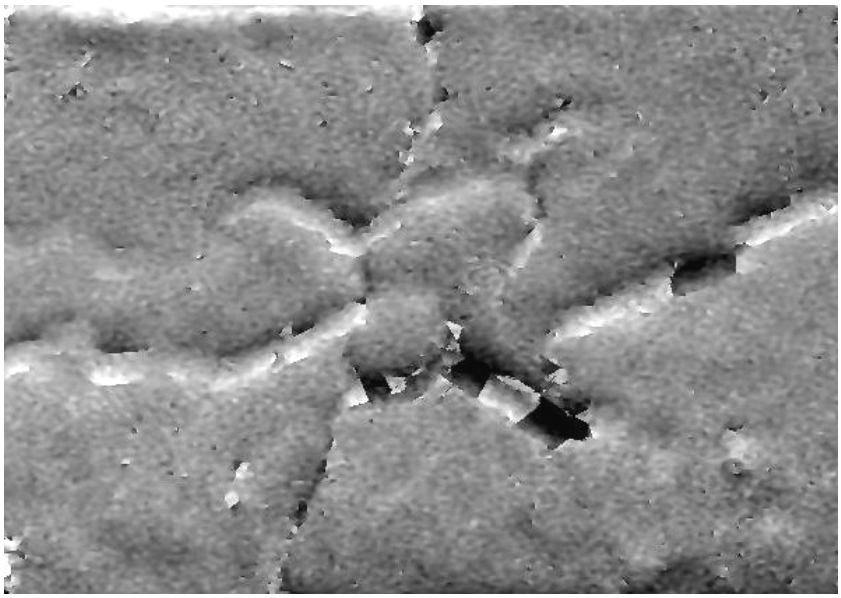

Figure 7.38: Shearography Image of Same Concrete Prism Surface at 100 Days in Isothermal Water Bath, pH maintained at 12.5 - limewater

The shearography images are then processed using advanced conventional image analysis software such as Image Pro Plus to obtain statistical data of the cracks which can provide insights into the mechanisms of cracking. Figure 7.39 shows an enhanced version of the laser shearography image of figure 7.38. This involved histogram stretching and edge detection algorithms to highlight the cracks.

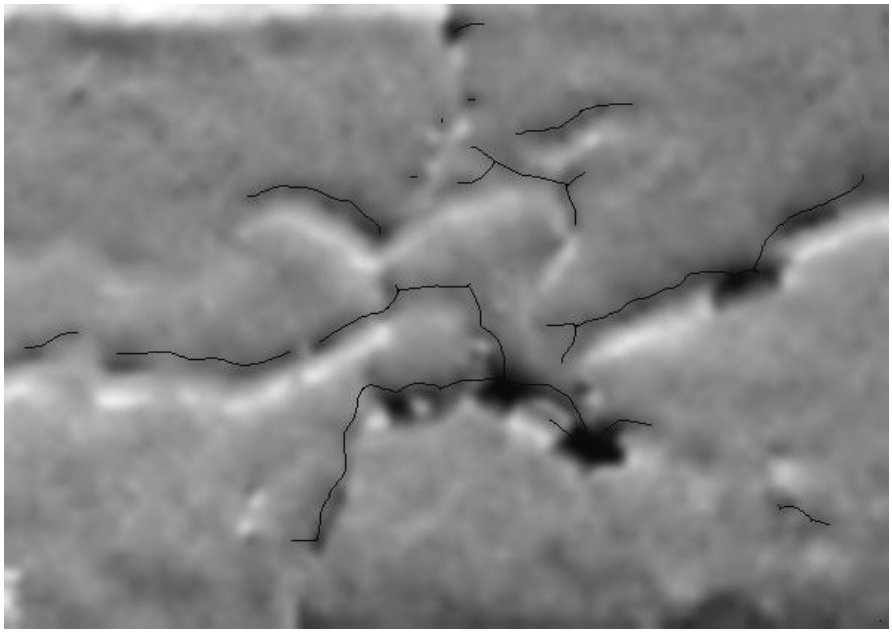

Figure 7.39: Enhanced Shearography Image of Concrete Prism Surface at 100 Days in Isothermal Water Bath, pH maintained at 12.5 - limewater

The cracks are highlighted with a bright color and the background removed for clarification of the image. The removal of the background is known as cropping. The laser shearography images were calibrated using the images' cross-sectional dimensions as a reference. A line is drawn alongside the height of the image and indicating the number of calibration units it represents. This reference line corresponded to 76.2mm (the height of the image). Then the corresponding pixel to

mm (p/m) ratio would be displayed. Consequently, the crack data is acquired and analyzed. Figure 7.40 shows the processed image using Image Pro Plus software.

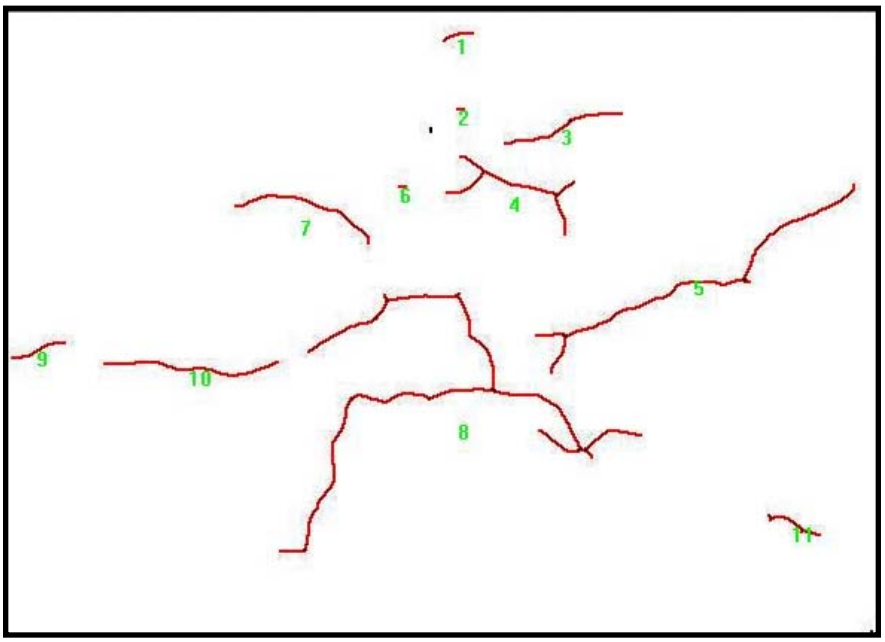


Figure 7.40: Shearography Image After Processing Using Image Pro Plus Software

Data from the shearography images processed by Image Pro Plus are analyzed and statistics of the individual cracks collected. Table 7.11 shows the measurement data sheet for face 2 section 2 of the concrete surface during the 100 days of laser shearography testing. Again, laser shearography was employed at 300 days to investigate the development of the cracks.

Table 7.11: Image Pro Plus Measurement Data Sheet for Face 2 Section 2 at 100 Days Laser Shearography Analysis

| Object # 22 | Area ($mm^2$) | Aspect Ratio | Angle | Perimeter (mm) | Size (length) mm |
|---|---|---|---|---|---|
| 1 | 0.0027 | 6.9662 | 76.2140 | 0.3328 | 0.1568 |
| 2 | 0.0007 | 3.4157 | 90.0000 | 0.0827 | 0.0376 |
| 3 | 0.0103 | 11.4976 | 71.6300 | 1.2731 | 0.6135 |
| 4 | 0.0178 | 3.3952 | 106.7316 | 2.1170 | 0.6388 |
| 5 | 0.0354 | 11.1150 | 63.3971 | 4.1601 | 1.7856 |
| 6 | 0.0007 | 3.4157 | 90.0000 | 0.0827 | 0.0376 |
| 7 | 0.0127 | 5.6247 | 105.0691 | 1.5711 | 0.7042 |
| 8 | 0.0713 | 1.4865 | 83.6659 | 7.8958 | 1.8524 |
| 9 | 0.0047 | 10.6160 | 69.5172 | 0.5862 | 0.2825 |
| 10 | 0.0145 | 14.4574 | 92.9505 | 1.8160 | 0.8785 |
| 11 | 0.0053 | 7.5494 | 112.9085 | 0.6099 | 0.2834 |
| **Total** | **0.1761** | | | **20.5274** | **7.2709** |

Figure 7.41 is a graph showing the number of cracks on each face of the concrete prisms. There is a 45% increase in crack density after 100 days of storage in exposure condition 1. Measurement of the crack size (length) also revealed an increase in crack propagation as shown in figure 7.42. The cracks showed significant increases in the end faces of the concrete prisms. The crack areas also increased which resulted in a significant increase of the concrete permeability.

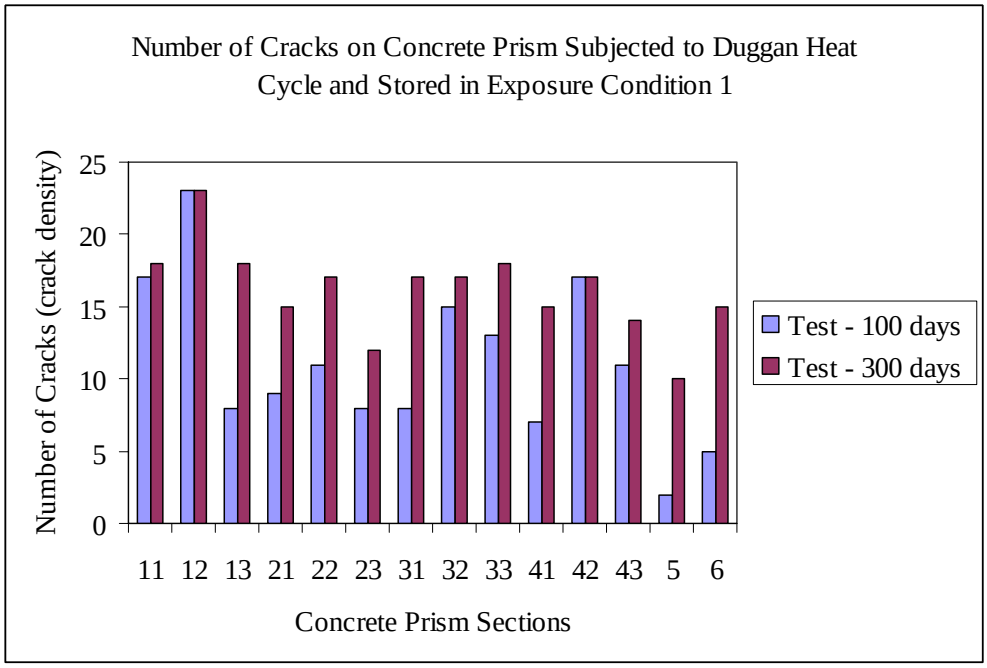


Figure 7.41: Number of Cracks on the Surfaces of Concrete Prism Subjected to Duggan Heat Cycle and Stored in Isothermal Water Bath, pH maintained at 12.5 - limewater

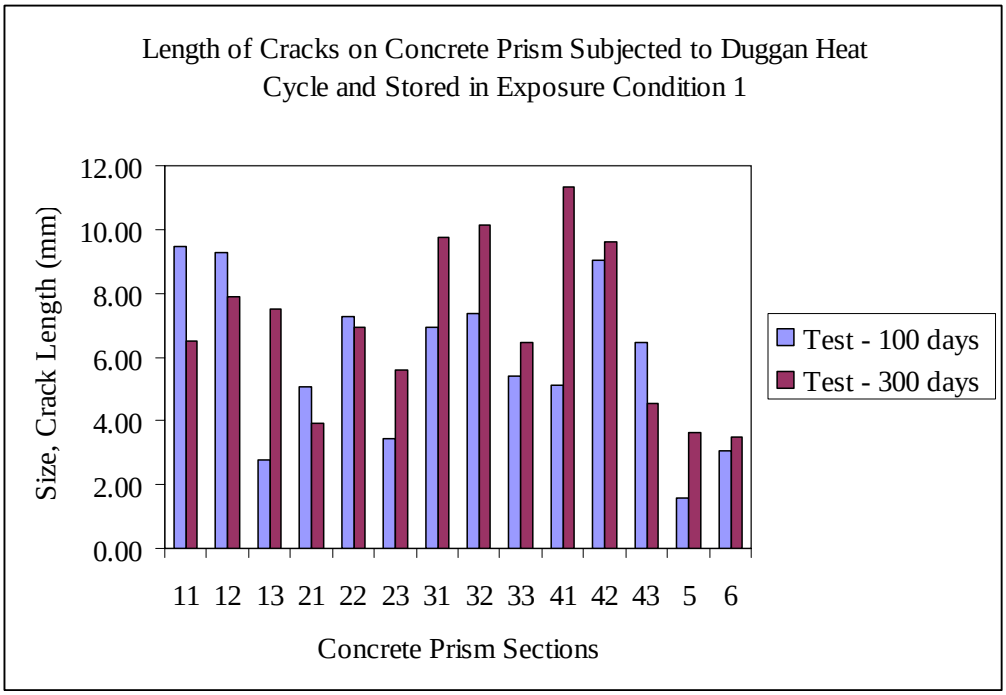


Figure 7.42: Size, Length of Cracks on Surfaces of Concrete Prism Subjected to Duggan Heat Cycle and Stored in Isothermal Water Bath, pH maintained at 12.5 - limewater

Later, the cracks on the concrete prism's surface formed macrocracks and a network of cracks visible to the unaided eye. Digital photo images of the cracks were captured at 750 days and the data analyzed as shown in figure 7.43. The cracks on the concrete prisms were again analyzed using the Image Pro Plus software. Table 7.12 gives the cracks data measurements at 750 days for each of the concrete surfaces.

Figure 7.43: Digital Photo Image of Concrete Prism at 750 Days in Isothermal Water Bath, maintained at 12.5 – limewater Showing Cracks

Table 7.12: Cracks Data Analysis at 750 days in Isothermal Water Bath, pH maintained at 12.5 - limewater

| P3C1 - 750 days (Digital Photo Images) | | | |
|---|---|---|---|
| **Face # Sec #** | **Crack Density** | **Crack Length (mm)** | **Area of Crack ($mm^2$)** |
| 11 | 4 | 5.503 | 0.171 |
| 12 | 8 | 5.3429 | 0.1992 |
| 13 | 7 | 4.2282 | 0.1015 |
| 21 | 7 | 4.5477 | 0.0992 |
| 22 | 11 | 8.5889 | 0.2277 |
| 23 | 4 | 5.2665 | 0.1340 |
| 31 | 6 | 7.9795 | 0.2424 |
| 32 | 17 | 9.4756 | 0.1750 |
| 33 | 11 | 7.8483 | 0.2087 |
| 41 | 13 | 9.4719 | 0.3847 |
| 42 | 12 | 7.6496 | 0.1755 |
| 43 | 8 | 7.1295 | 0.2170 |
| 5 | 5 | 3.4156 | 0.0685 |
| 6 | 2 | 2.4880 | 0.0474 |
| **Total** | **115** | **88.9354** | **2.4522** |

*7.10.2 Laser Shearography Analysis of Concrete Prisms Subjected to Different Treatments*

Laser shearography was used to provide insights into the mechanisms of cracking in concrete at early stages. Laser shearography images of the concrete prisms subjected to Duggan Heat or Freeze-Thaw cycles were collected at periodic intervals, and analyzed using Image Pro Plus software. No cracks were detected before subjecting the concrete prisms to either the Duggan heat or Freeze-Thaw cycles. Figures 7.44 and 7.45 show the laser shearography images before subjecting the concrete prisms to the Duggan Heat cycle and Freeze-Thaw cycle respectively.

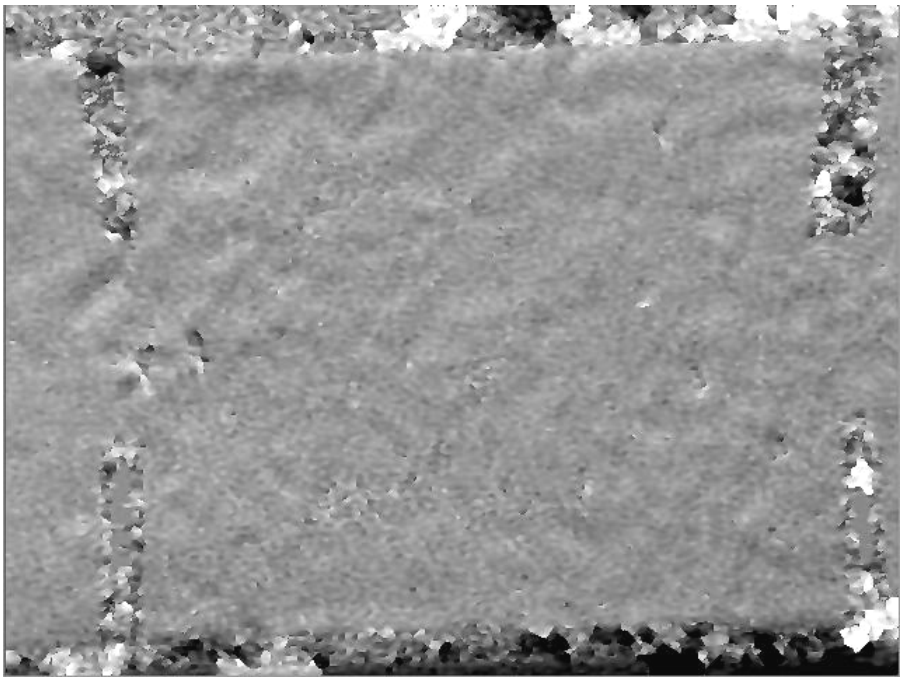

Figure 7.44: Laser Shearography Image of Concrete Prism Surface 7 Days After Casting and Before Duggan Heat Cycle Treatment (P3_Dug Face 2 Sec 2)

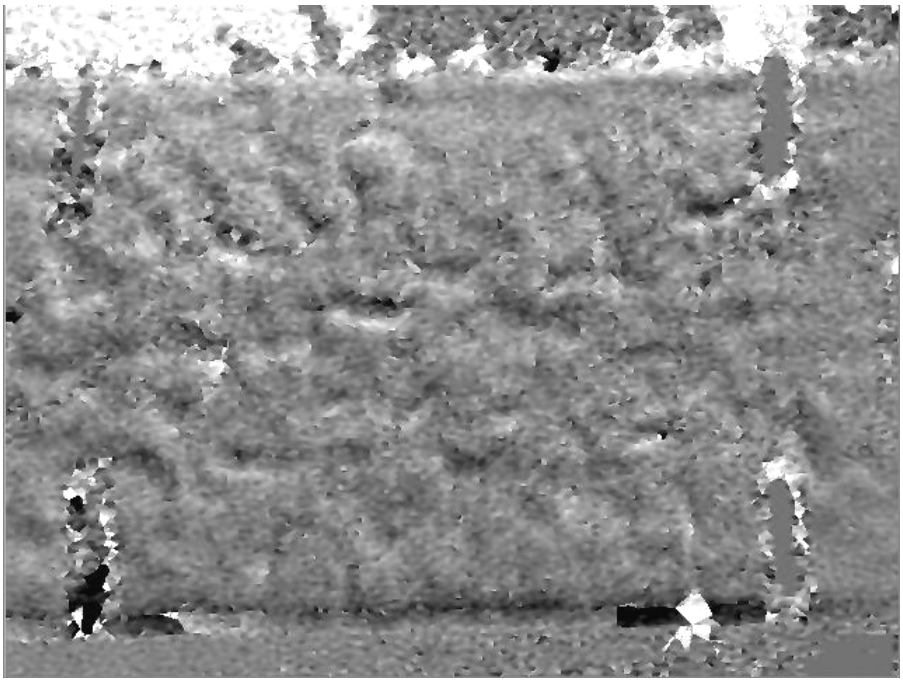

Figure 7.45: Laser Shearography Image of Concrete Prism Surface 7 Days After Casting and Before Freeze-Thaw Cycle Treatment (P3_Frez Face 1 Sec 2)

Cracks were found on the concrete prisms after subjecting them to either the Duggan Heat or Freeze-Thaw cycles treatment. The number of cracks and lengths on the surfaces of the concrete prism increases about 15% after the first 100 days of storage in limewater. Figures 7.46 and 7.47 show the processed laser shearography images by Image Pro Plus.

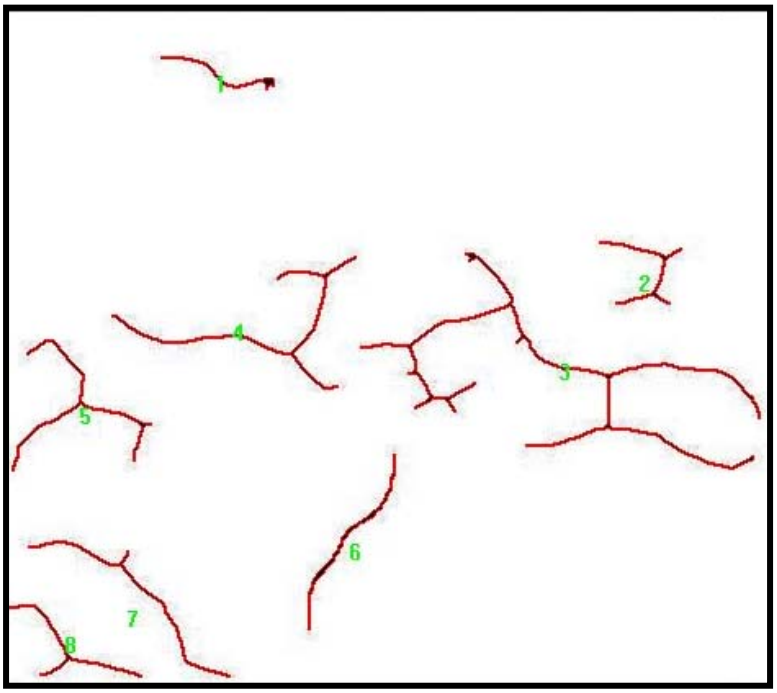


Figure 7.46: Processed Laser Shearography Image of Concrete Prism Surface After Duggan Heat Cycle Treatment and 100 Days Storage in Limewater

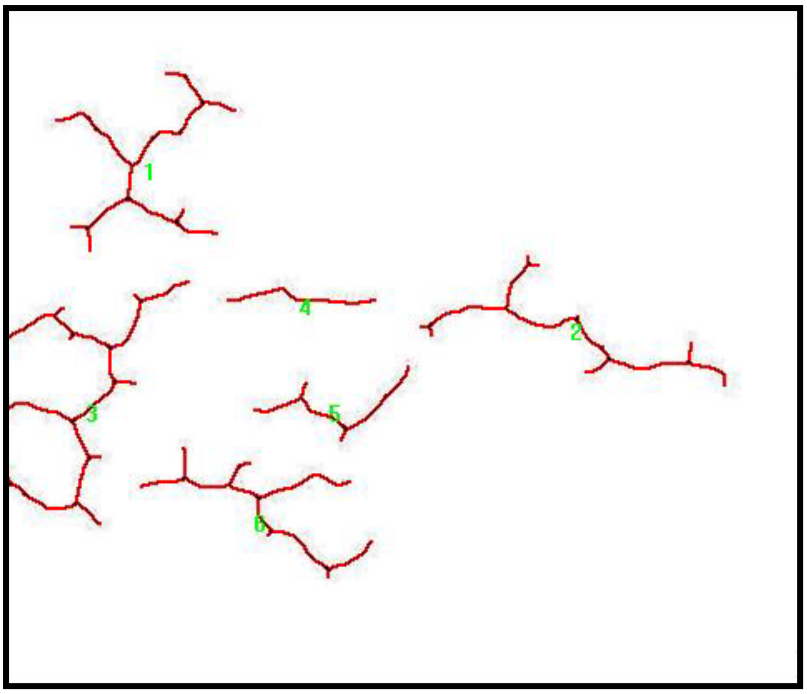


Figure 7.47: Processed Laser Shearography Image of Concrete Prism After Freeze-Thaw Cycle Treatment and 100 Days Storage in Limewater

Data collected from the Image Pro Plus analysis of the laser shearography images show more cracks in concrete samples subjected to the Freeze-Thaw cycle than the Duggan Heat. However, the Duggan heat treated concrete prism exhibited significantly higher expansion values. Table 7.13 and 7.14 provide the results from the laser shearography images of the concrete prisms subjected to different treatments.

Table 7.13: Image Pro Plus Measurement Data Sheet for Concrete Prism Subjected to Duggan Heat Cycle and Stored for 100 Days in Limewater

| **Duggan Heat Cycle** | | | |
|---|---|---|---|
| **Face # Sec #** | **Crack Density** | **Crack Length (mm)** | **Area of Crack ($mm^2$)** |
| 11 | 0 | 0.0000 | 0.0000 |
| 12 | 9 | 9.9022 | 0.2550 |
| 13 | 17 | 7.1329 | 0.1540 |
| 21 | 7 | 6.8349 | 0.1818 |
| 22 | 8 | 7.2684 | 0.2126 |
| 23 | 8 | 4.3138 | 0.0938 |
| 31 | 0 | 0.0000 | 0.0000 |
| 32 | 10 | 8.4636 | 0.1742 |
| 33 | 12 | 8.0354 | 0.1738 |
| 41 | 0 | 0.0000 | 0.0000 |
| 42 | 8 | 4.8304 | 0.1305 |
| 43 | 0 | 0.0000 | 0.0000 |
| 5 | 13 | 5.2951 | 0.1127 |
| 6 | 10 | 5.3009 | 0.1041 |
| **Total** | **102** | **67.3777** | **1.5924** |

Table 7.14: Image Pro Plus Measurement Data Sheet for Concrete Prism Subjected to Freeze-Thaw Cycle and Stored for 100 Days in Limewater

| **Freeze-Thaw Cycle** | | | |
|---|---|---|---|
| **Face # Sec #** | **Crack Density** | **Crack Length (mm)** | **Area of Crack ($mm^2$)** |
| 11 | 7 | 4.1585 | 0.1009 |
| 12 | 6 | 5.9778 | 0.1925 |
| 13 | 12 | 8.3554 | 0.1691 |
| 22 | 15 | 9.3836 | 0.2409 |
| 23 | 5 | 3.8547 | 0.0837 |
| 31 | 9 | 4.8448 | 0.1193 |
| 32 | 8 | 6.2908 | 0.1352 |
| 33 | 9 | 5.0142 | 0.1221 |
| 41 | 10 | 3.9577 | 0.1024 |
| 42 | 11 | 5.8851 | 0.1414 |
| 43 | 8 | 3.1870 | 0.0709 |
| 5 | 7 | 3.3347 | 0.0808 |
| 6 | 13 | 5.2339 | 0.1045 |
| **Total** | **120** | **69.4782** | **1.6640** |

*7.11 Microstructure Analysis Using SEM and EDAX*

The samples taken from the interior and exterior of the concrete samples were prepared as fractured surfaces and then coated with carbon. The SEM that was used to detect ettringite was equipped with an energy dispersive X-ray (EDAX) used to determine the chemical elemental components of the material deposits within the microstructure of the examined concrete specimens. Samples from each of the exposure conditions were examined to determine their influence in ettringite formation and morphology.

*7.11.1 SEM and EDAX Analysis of Concrete Specimens Stored in Different Exposure Conditions*

*7.11.1.1 Concrete Samples in Exposure Condition 1*

At 40 days of storage in isothermal water bath, pH maintained at 12.5 (Exp. Cond. 1), SEM examination showed plenty of ettringite balls covering the whole specimen. Spherical ettringite balls (> 10μm) were found growing in the cavities and in the interface between aggregate particles and the cement paste matrix in the concrete. At this early stage, the ettringite balls were well-developed and revealed an EDAX spectrum. Figure 7.48 shows the SEM micrograph and EDAX analysis of the ettringite balls filling the cavities and air voids. The EDAX analysis, a graph of intensity against x-ray energy, revealed ettringite having a chemical composition of Al = 4.35% wt., Si = 4.32% wt., S = 9.35% wt., and Ca = 80.80% wt.

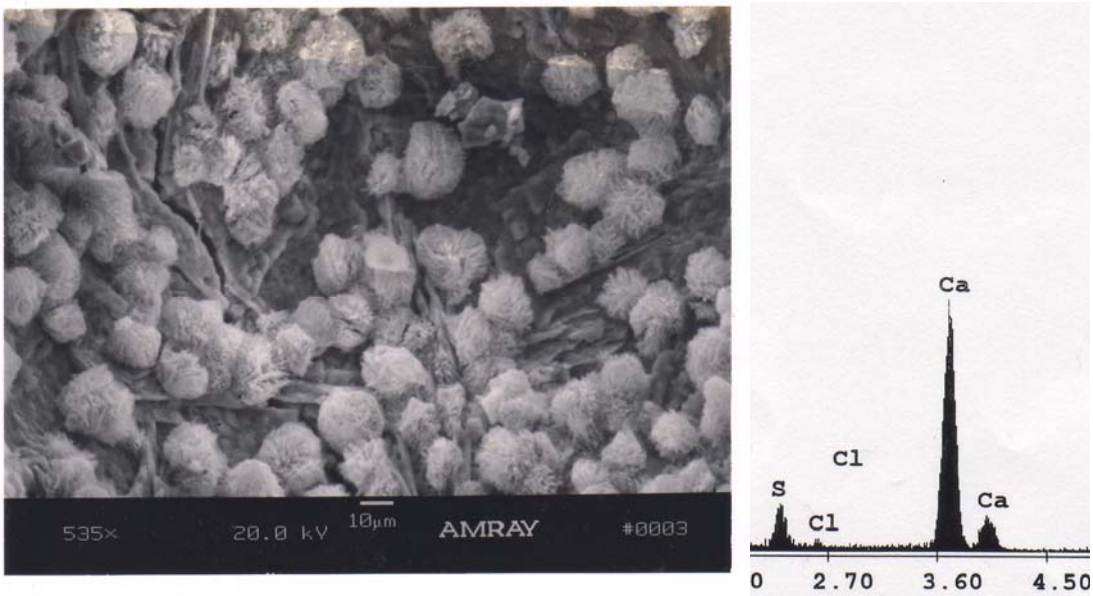


Figure 7.48: SEM and EDAX of Concrete Specimen in Exposure Condition 1 at Age of 40 Days, Showing Spherical Ettringite Balls Filing Cavities and Air Voids

SEM investigations at 100 days revealed clusters of ettringite needles filling the entire microstructure of the specimen as shown in Figure 7.49. The EDAX elemental composition analysis of the ettringite layer showed a chemical composition of Al = 0.62% wt., Si = 7.81% wt., S = 4.69% wt., and Ca = 76.07% wt. The high silicon (Si) peak presence in this analysis revealed the early presence of C-S-H gel, which was latter converted to ettringite, as water became predominantly available.

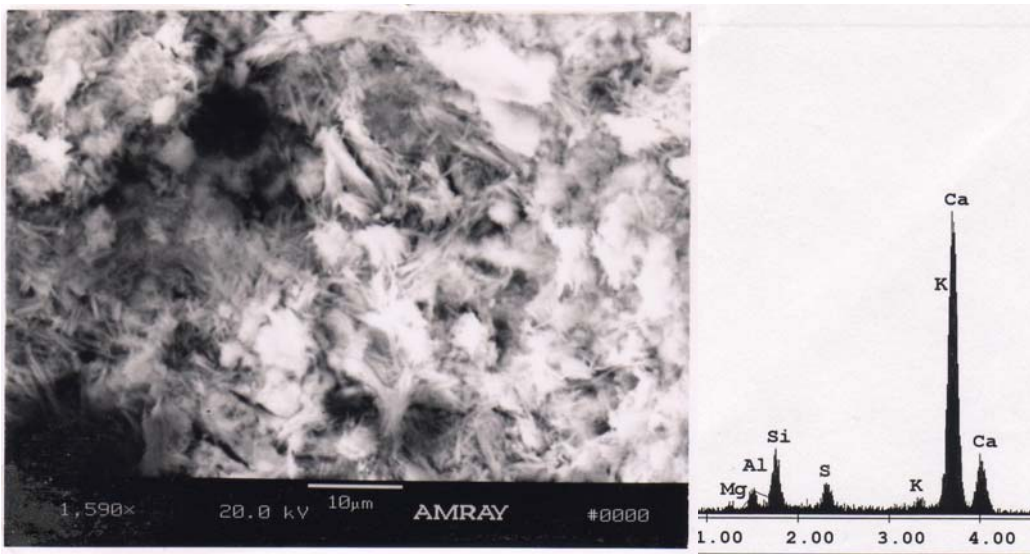


Figure 7.49: SEM and EDAX Analysis of Concrete Specimen in Exposure Condition 1 at Age of 100 Days, Showing Ettringite Needles Covering the Entire Specimen

Figure 7.50 shows the 240 days SEM results of the concrete specimen in exposure condition 1. Lots of randomly oriented ettringite needles were found at the interface between the aggregate particles and the cement paste matrix. The EDAX results revealed ettringite with chemical composition of Al = 3.00% wt., Si = 2.25% wt., S = 7.87% wt., and Ca = 83.21% wt.

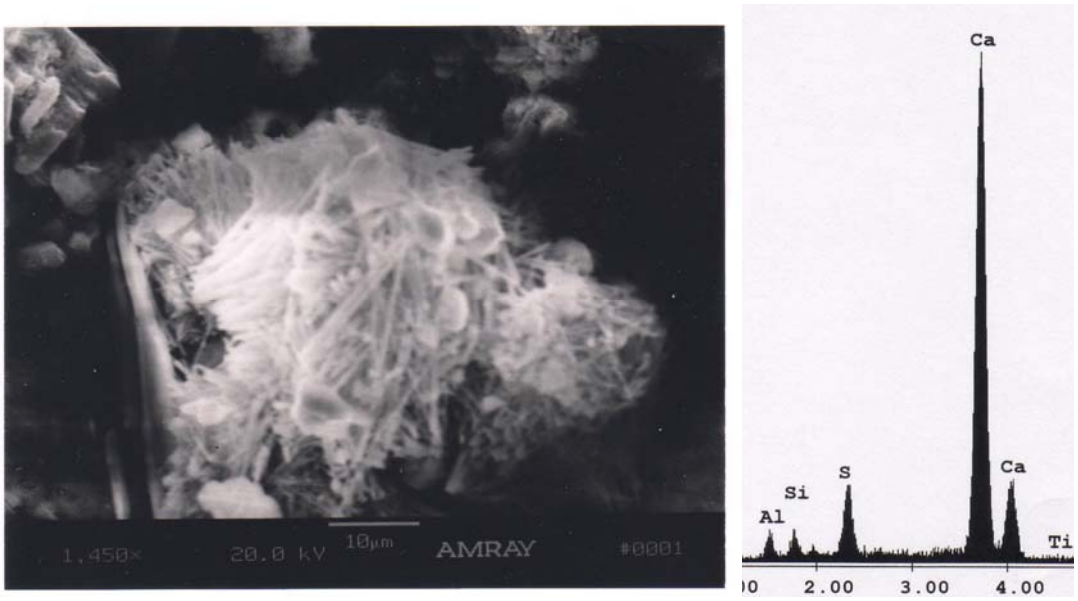


Figure 7.50: SEM and EDAX Analysis of Concrete Specimen in Exposure Condition 1 at Age of 240 Days, Showing Randomly Oriented Ettringite Needles Filling a Cavity

The SEM examinations at 540 days revealed lots of ettringite needle-like crystals covering the entire specimens. Most of the ettringite was found in air voids and interfaces between aggregates. The ettrringite undergoes physical transition from crystal balls into needle-like crystals, as time proceeded. SEM and EDAX analysis of the mortar specimens are shown in figure 7.51. The EDAX analysis of the ettringite needle-like crystals showed a chemical composition of Al = 5.26% wt., Si = 7.42% wt., S = 9.93% wt., and Ca = 75.88% wt.

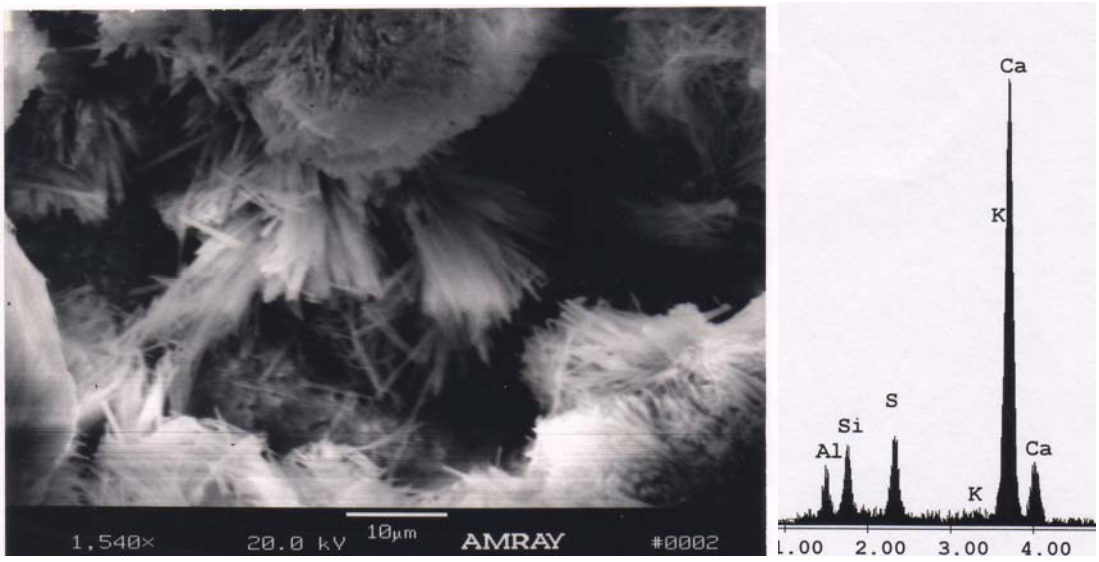


Figure 7.51: SEM and EDAX Analysis of Concrete Specimen in Exposure Condition 1 at Age of 540 Days, Showing Ettringite Needle-Like Crystals Filling an Air Void

*7.11.1.2 Concrete Samples in Exposure Condition 2*

Again, SEM and EDAX were used to determine or detect the chemical composition of deposits in the cracks and air voids within the microstructure of the concrete specimen. Ettringite spherical balls were found filling the air voids and cavities of the specimens. Figure 7.52 shows SEM and EDAX analysis of the examined concrete specimen, after 40 days of storage in exposure condition 2 (plain water at room temperature). Similar results were obtained at the 100 days SEM Examinations. The EDAX results indicate that the material deposits have a chemical composition of Al = 3.05% wt., Si = 1.38% wt., S = 8.11% wt., and Ca = 85.55% wt., which is characteristic of ettringite. The chemical composition from the EDAX analysis varies because of experimental errors and isomorphous substitutions of elements. Elements may substitute for one another, for instance Al for Si.

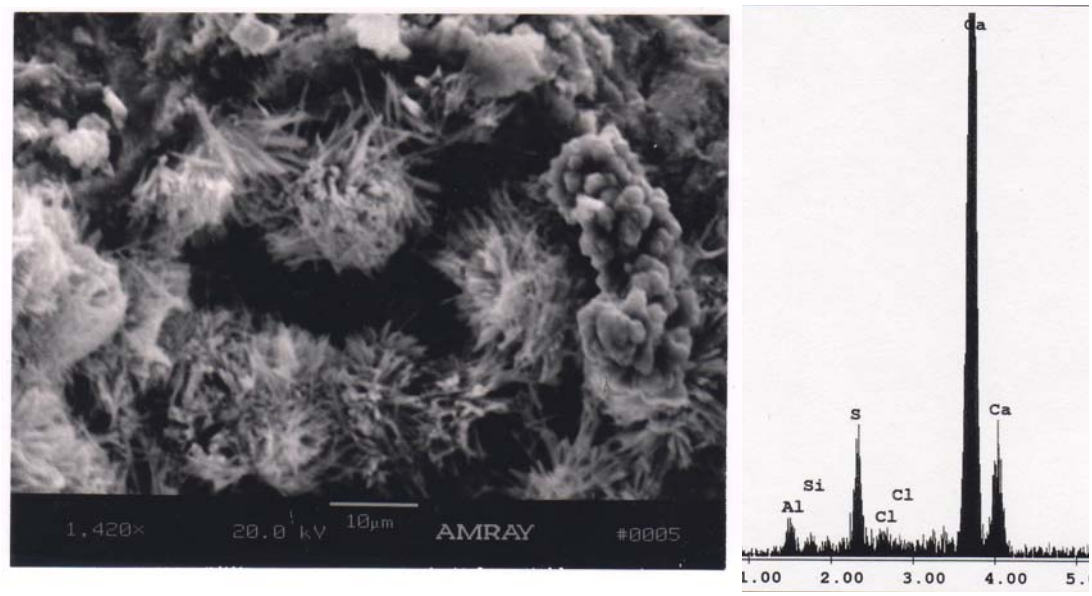


Figure 7.52: SEM and EDAX Analysis of Concrete Specimen in Exposure Condition 2 at Age of 40 Days, Showing Ettringite Balls Filling a Cavity

The SEM examinations at 240 days showed ettringite needles radiating from an air void. Ettringite also formed along interfaces between aggregate particles and the cement paste. Figure 7.53 shows the SEM micrograph and EDAX analysis of the material deposit in an air void of the examined concrete specimen. The EDAX elemental mapping of these materials matched with ettringite having a chemical composition of Al = 1.83% wt., S = 4.03% wt., and Ca = 94.14% wt. The relatively high percentage of Ca (94.14%) is due to the presence of calcium hydroxide crystals.


Figure 7.53: SEM and EDAX Analysis of Concrete Specimen in Exposure Condition 2 at Age of 240 Days, Showing Ettringite Needles Radiating from an Air Void

At 540 days, abundant ettringite needle-like crystals (>10μm) were found completely filling the cavities of the specimens. Ettringite in cracks through the paste and around aggregate particles was observed. The presence of the peripheral gap around the aggregate particles indicates volumetric change can be attributed to expansion of the paste relative to the aggregate particles. Some of the cracking occurred during the sample preparation. However, the cracks containing ettringite clearly occurred during the test. Figure 7.54 shows the SEM and EDAX analysis of ettringite needle-like crystal within the cement paste matrix. EDAX elemental mapping of these needle-like crystals matched with ettringite having a chemical composition of Al = 3.52%wt., Si = 3.16% wt., S = 7.37% wt., and Ca = 85.95% wt.

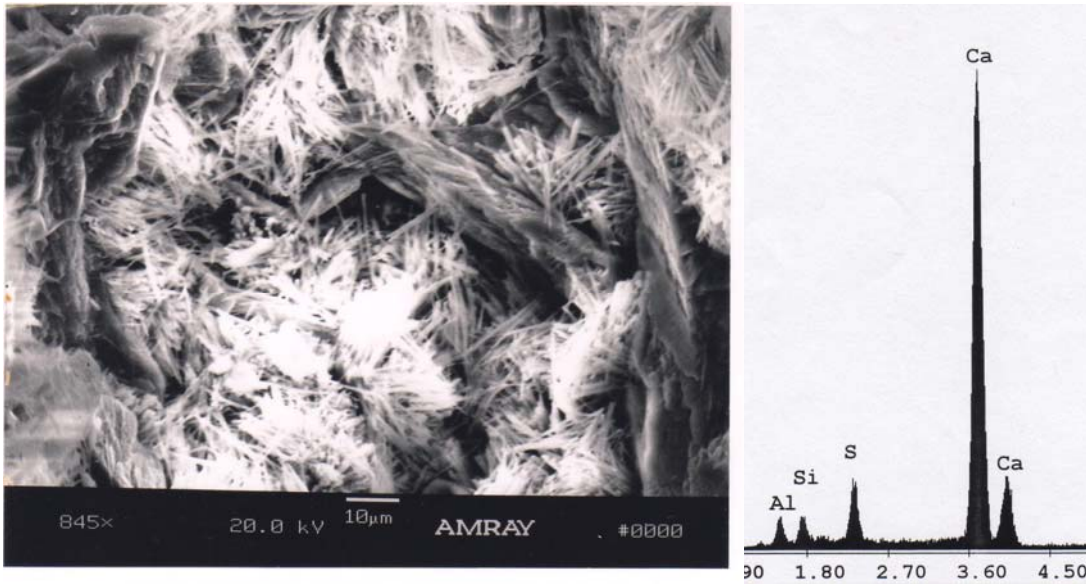


Figure 7.54: SEM and EDAX Analysis of Concrete Specimen in Exposure Condition 2 at Age of 540 Days, Showing Ettringite Needle-Like Crystals Filling the Cavities

*7.11.1.3 Concrete Samples in Exposure Condition 3*

Fractured specimens taken from representative concrete samples in exposure condition 3 revealed material deposits characteristic of ettringite, but no EDAX spectrum could be obtained. Figure 7.55 shows the SEM micrograph at 40 days. This type of material deposit was very common throughout the examined concrete specimens.


Figure 7.55: SEM Micrograph of Concrete Specimen in Exposure Condition 3 at 40 Days, Showing Probable Ettringite Needles and CH Crystals Filling a Cavity

At 100 days, SEM Examination revealed clusters of ettringite nuggets covering the entire concrete specimen. The ettringite occurred particularly in the cracks and cavities. The characteristic of these ettringite nuggets was obtained by EDAX analysis as shown in figure 7.56. The EDAX illustrated ettringite with a chemical composition of Al = 3.52%wt., Si = 3.16% wt., S = 7.37% wt., and Ca = 85.95% wt.

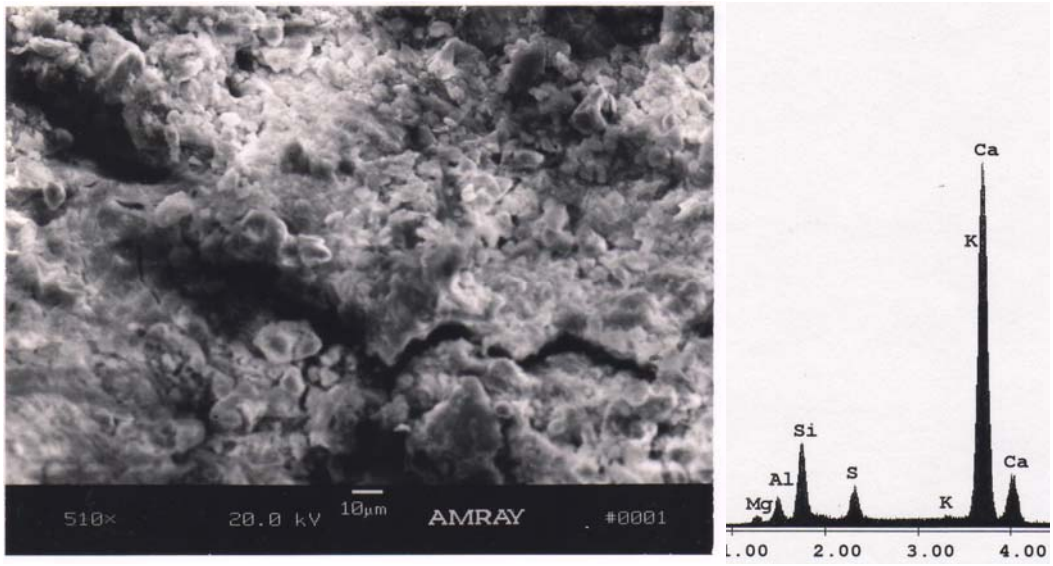


Figure 7.56: SEM and EDAX Analysis of Concrete Specimen in Exposure Condition 3 at Age of 100 Days, Showing Ettringite Nuggets Filling Cavities

No ettringite could be found during the 240 days SEM Examinations. The EDAX analysis showed deposits of calcium hydroxide crystals filling cavities and air voids. Figure 7.57 shows the SEM and EDAX analysis of the examined fractured concrete specimen stored in exposure condition 3. The EDAX of deposited material revealed a chemical composition of Al = 0.24%wt., Si = 8.63% wt., S = 1.98% wt., and Ca = 82.11% wt.

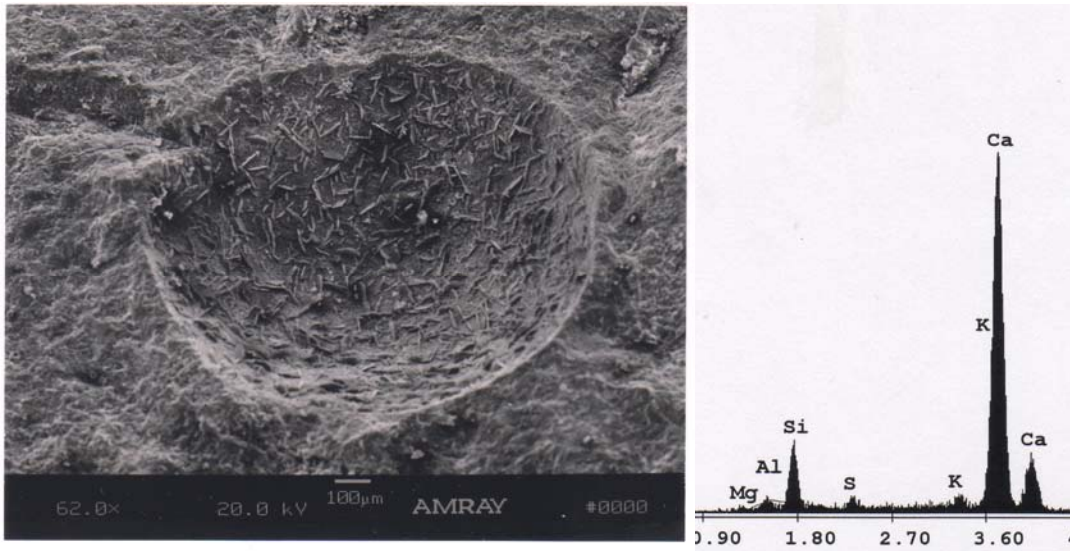


Figure 7.57: SEM and EDAX Analysis of Concrete Specimen in Exposure Condition 3 at Age of 240 Days, Showing Calcium Hydroxide (CH) Crystals in Cavities

Few ettringite crystals appeared in the 540 days' SEM examination filling an air void. Cement paste and aggregate interfaces were found empty of ettringite deposits. Figure 7.58 shows ettringite crystals filling an air void. The fluctuating and disappearing of ettringite in concrete samples in exposure condition 3 may be attributed to the lack of an abundant supply of water. The EDAX illustrated ettringite chemical composition that included 3.14% wt of Al, 2.77% wt of Si, 5.02% wt of S and 89.04% wt of Ca.

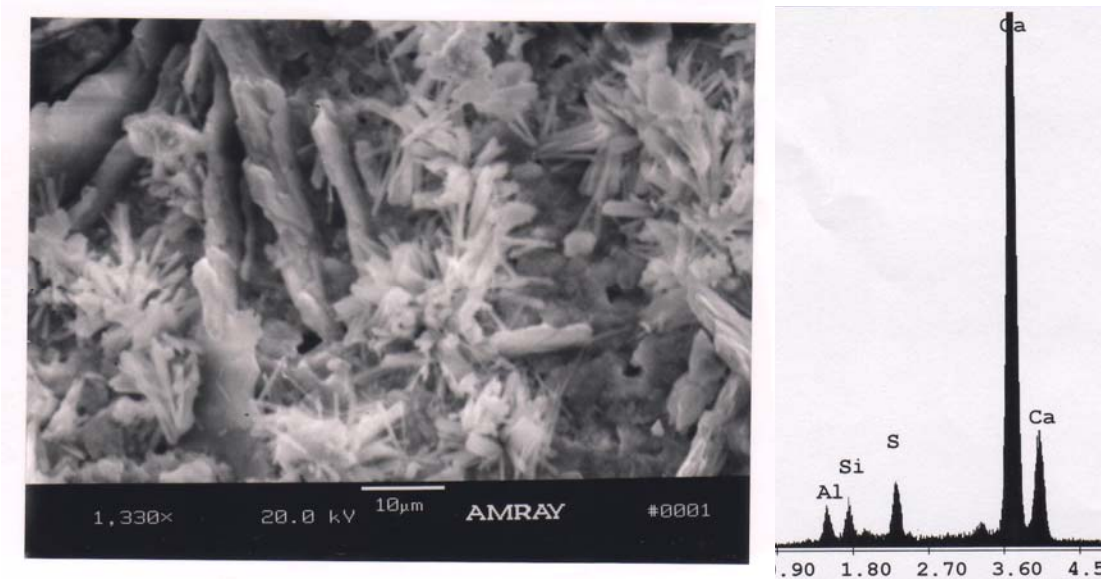


Figure 7.58: SEM and EDAX Analysis of Concrete Specimen in Exposure Condition 3 at Age of 540 Days, Showing Ettringite Crystals Filling an Air Void

*7.11.2 SEM and EDAX Analysis of Concrete Specimens Subjected to Different Treatments*

*7.11.2.1 Concrete Samples Subjected to Duggan Heat Cycle*

Concrete samples of this set were room temperature-cured and stored in water for six (6) days before being subjected to the Duggan heat cycle. Before the Duggan heat cycle, SEM examinations were carried out and revealed no ettringite. Ettringite started to appear immediately after the Duggan heat cycle. Ettringite needle-like crystals were found filling air voids of the concrete specimen. Figure 7.59 shows the SEM and EDAX analysis of the ettringite crystals filling an air void. The EDAX of the ettringite crystals revealed chemical composition of Al = 2.59%wt., Si = 0.72% wt., S = 3.62% wt., and Ca = 89.28% wt.

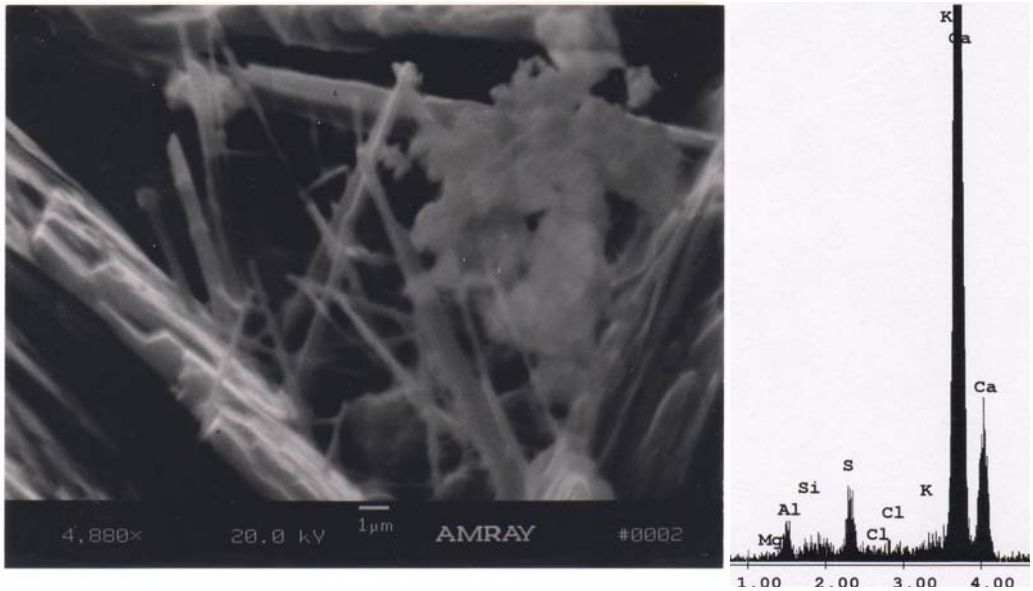


Figure 7.59: SEM and EDAX Analysis of Concrete Specimen Just after Duggan Heat Cycle Treatment Showing Ettringite Crystals Filling an Air Void

SEM examinations employed at 40 days showed both ettringite and calcium hydroxide (CH) crystals covering the whole concrete specimen. A cluster of calcium hydroxide crystal plates can be clearly observed in figure 7.60. The EDAX analysis was used to confirm the chemical characteristic of the deposits. The EDAX of the whole area revealed ettringite crystals with chemical composition of Al = 2.50%wt., Si = 5.17% wt., S = 5.13% wt., and Ca = 83.39% wt.

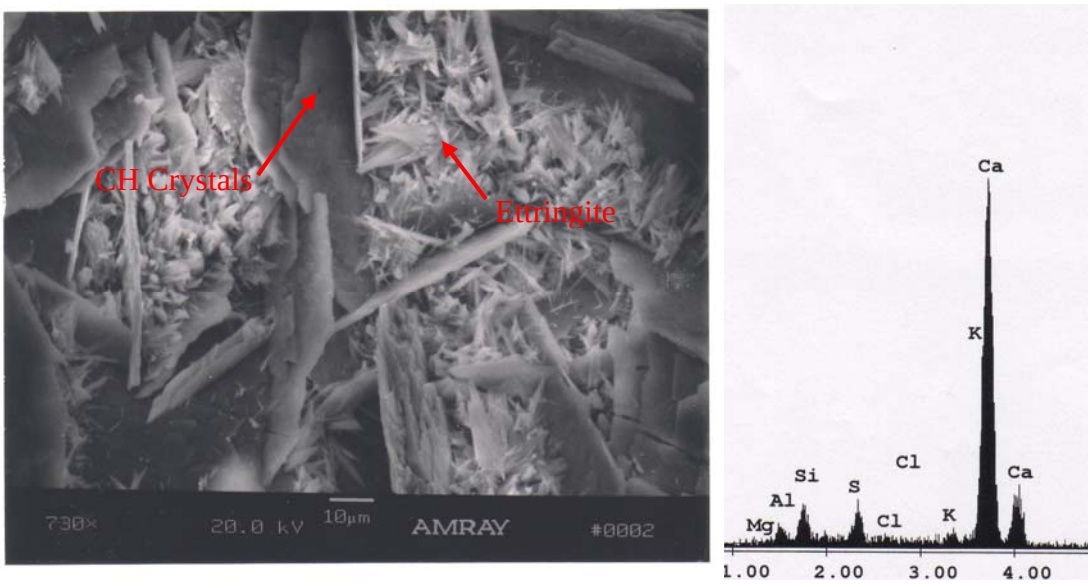


Figure 7.60: SEM and EDAX Analysis of Concrete Specimen Subjected to Duggan Heat Cycle Treatment and Stored in Exposure Condition 1 at Age of 40 Days, Showing Ettringite and CH Crystals

Bundles of ettringite were generally found in the 100 days SEM examinations of the concrete specimens subjected to Duggan heat cycle. Abundant amounts of ettringite were discovered within cavities and air voids. Figure 7.61 shows the SEM and EDAX analysis of the ettringite bundles.

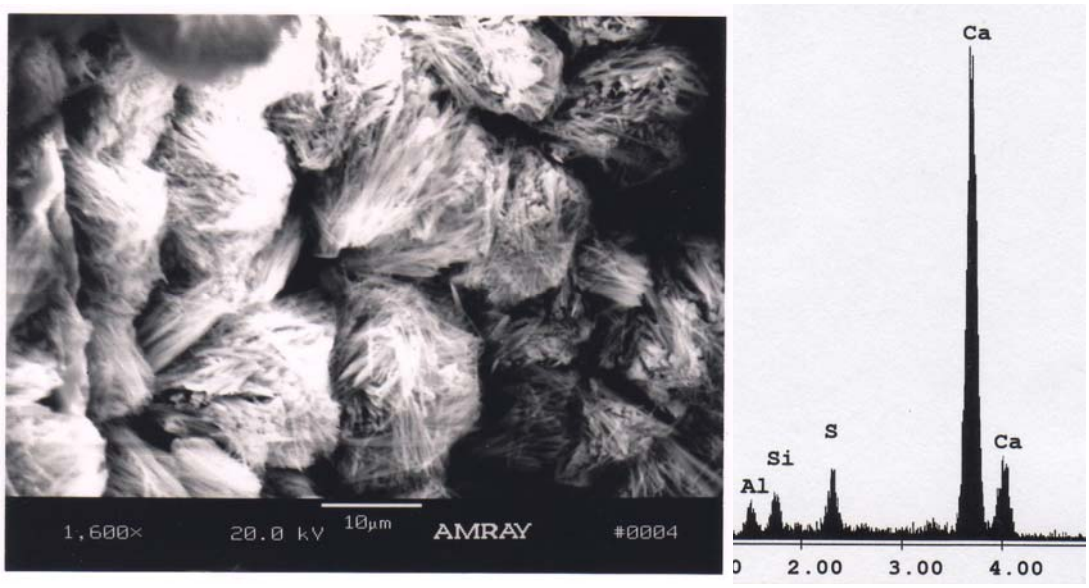


Figure 7.61: SEM and EDAX Analysis Concrete Specimens Subjected to Duggan Heat Cycle Treatment and Stored in Exposure Condition 1 at Age of 100 Days, Showing Ettringite Bundles

Ettringite traces or deposits were not found in the examined concrete specimens during the 240 days' SEM examination. The ettringite disappeared but later, at 365 days, it was discovered filling a void. The SEM micrograph with the EDAX analysis revealed materials with distinct characteristics of ettringite morphology filling the voids, as shown in figure 7.62. The EDAX of the materials within the void has ettringite crystals with chemical composition of Al = 3.42%wt., Si = 1.13% wt., S = 8.22% wt., and Ca = 87.23% wt.

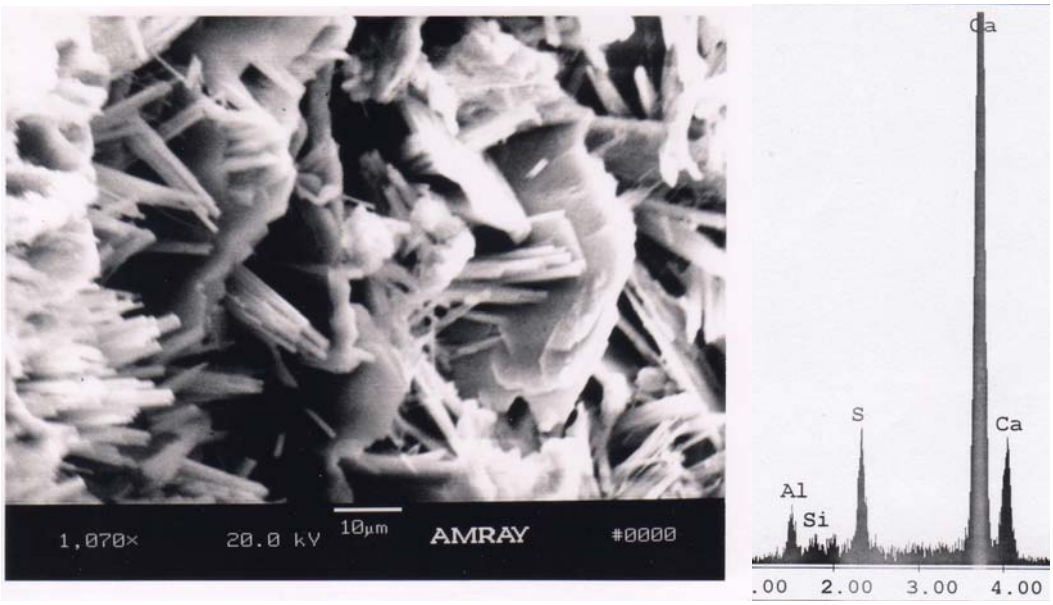


Figure 7.62: SEM and EDAX Analysis of Concrete Specimen Subjected to Duggan Heat Cycle Treatment and Stored in Exposure Condition 1 at Age of 365 Days, Showing Ettringite Crystals Filling an Air Void

*7.11.2.2 Concrete Samples Subjected to Freeze-Thaw Cycle*

These sets of concrete samples were cured at room temperature before subjecting them to Freeze-Thaw cycles after six (6) days of storage under water. Similar to the Duggan heat cycle treated concrete samples, no ettringite was discovered before treatment. SEM examinations after the Freeze-Thaw cycle revealed suspected ettringite mineral deposits within a void. Due to low count of the energy against intensity, no EDAX spectrum was available. Figure 7.63 shows the SEM micrograph of the suspected ettringite minerals. The probable identification of the suspected minerals is based on characteristics similar to ettringite in terms of morphology and experience examining concrete using SEM.

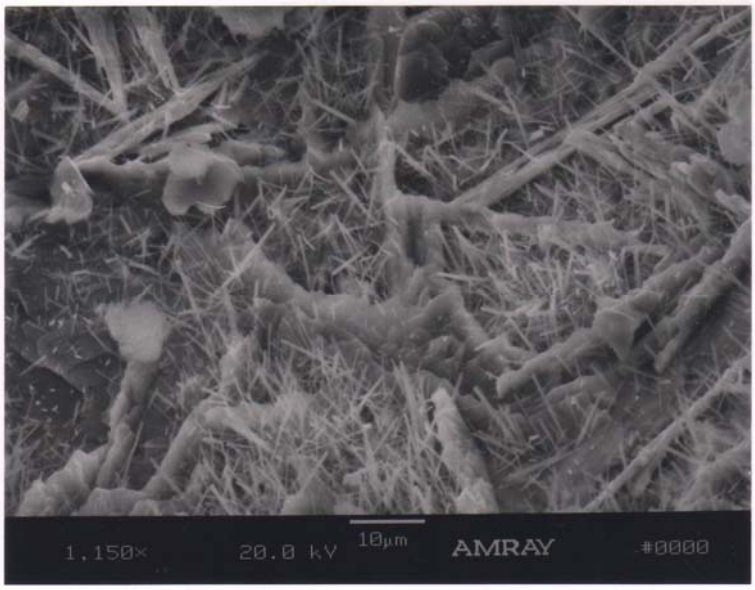


Figure 7.63: SEM Micrograph Analysis of Concrete Specimen Just after Freeze-Thaw Cycle Treatment Showing Probable Ettringite Deposits

Ettringite crystals and calcium hydroxide (CH) plates were discovered filling water voids during the 40 days' examinations. Figure 7.64 illustrated ettringite formation and CH plates filling water void. The EDAX analysis showed the chemical composition to be consistent with that of ettringite with Al = 2.77%wt., Si = 7.06% wt., S = 4.21% wt., and Ca = 85.47% wt.

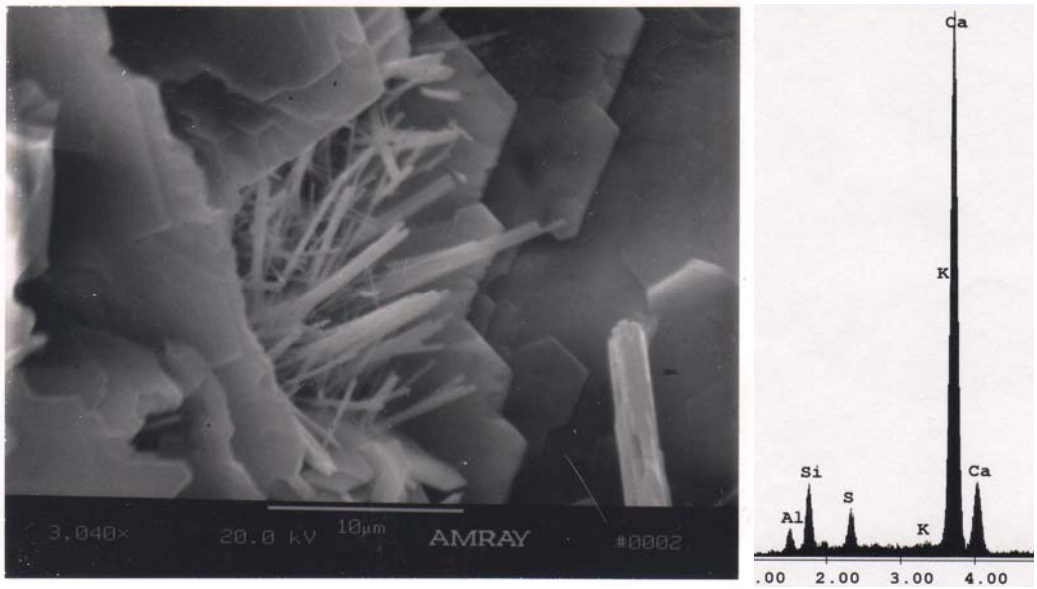


Figure 7.64: SEM and EDAX Analysis at of Concrete Specimen Subjected to Freeze-Thaw Cycles Treatment and Stored in Exposure Condition 1 at Age of 40 Days, Showing Ettringite and CH Plates Filling Water Void

Both the 100 days and 240 days' SEM examination results showed no ettringite. More calcium hydroxide (CH) plates were found filling water voids at 365 days' testing. The ettringite disappeared leaving behind huge amounts of CH plates filling the voids within the entire concrete specimen. Figure 7.65 shows calcium hydroxide plates filling water voids. This is confirmed by using the EDAX analysis.

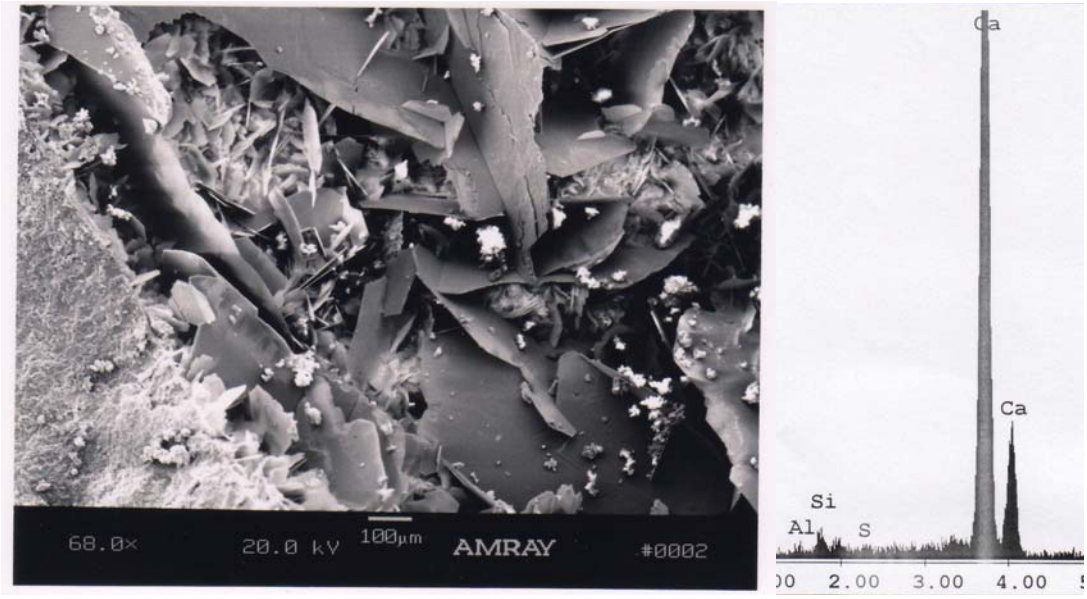


Figure 7.65: SEM and EDAX Analysis of Concrete Specimen Subjected to Freeze-Thaw Cycles Treatment and Stored in Exposure Condition 1at Age of 365 Days, Showing CH Plates Filling Water Voids

*7.11.3 SEM and EDAX Analysis of Concrete Specimens Subjected to Field Conditions*

*7.11.3.1 Concrete Samples in Exposure Condition 4A*

SEM results at 40 days showed little or no ettringite deposits in the cavities, air voids or aggregate interfaces of the concrete specimens. Further testing at 100 days under field exposure condition (P3C4A) revealed no ettringite. Ettringite needles filling cavities were found during the SEM examinations at 240 days. Eventually, well-developed ettringite gradually appeared as time proceeded. The chemical composition of the ettringite needles was Al = 6.83%wt., Si = 6.82% wt., S = 9.21% wt., and Ca = 71.83% wt. Similar observations were recorded during the SEM examinations at 540 days. Figure 7.66 shows SEM and EDAX analysis of the ettringite needle deposits inside cavities of the concrete specimen.

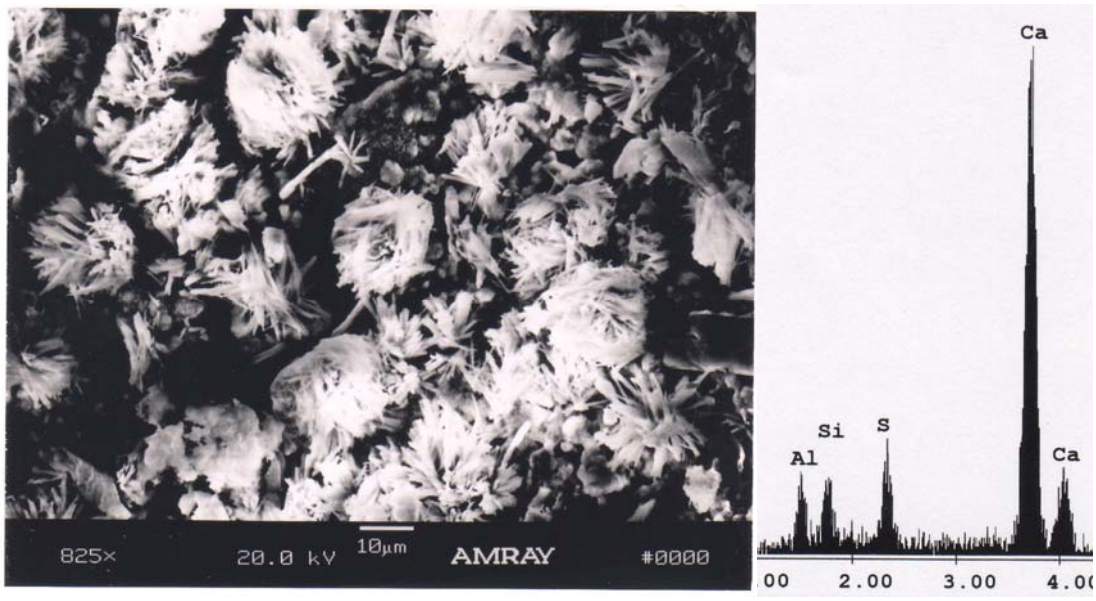


Figure 7.66: SEM and EDAX Analysis of Steam-Cured Concrete Specimen Under Field Conditions (C4A) at Age of 240 Days, Showing Ettringite Needles Filling Cavities

*7.11.3.2 Concrete Samples in Exposure Condition 4B*

The concrete samples were cured at room temperature before being subjected to field conditions and the SEM results at 40 days showed no ettringite deposits. Later SEM examinations at 100 days revealed lots of needle-like ettringite fillings within air voids. Figure 7.67 shows a SEM micrograph and EDAX analysis of the ettringite deposits within an air void. Ettringite was also found in aggregate pull-outs at various locations on the concrete specimen. The EDAX confirms that the deposits within the air voids were ettringite having chemical composition of Al = 2.89% wt., Si = 2.36% wt., S = 5.08% wt., and Ca = 83.28% wt.

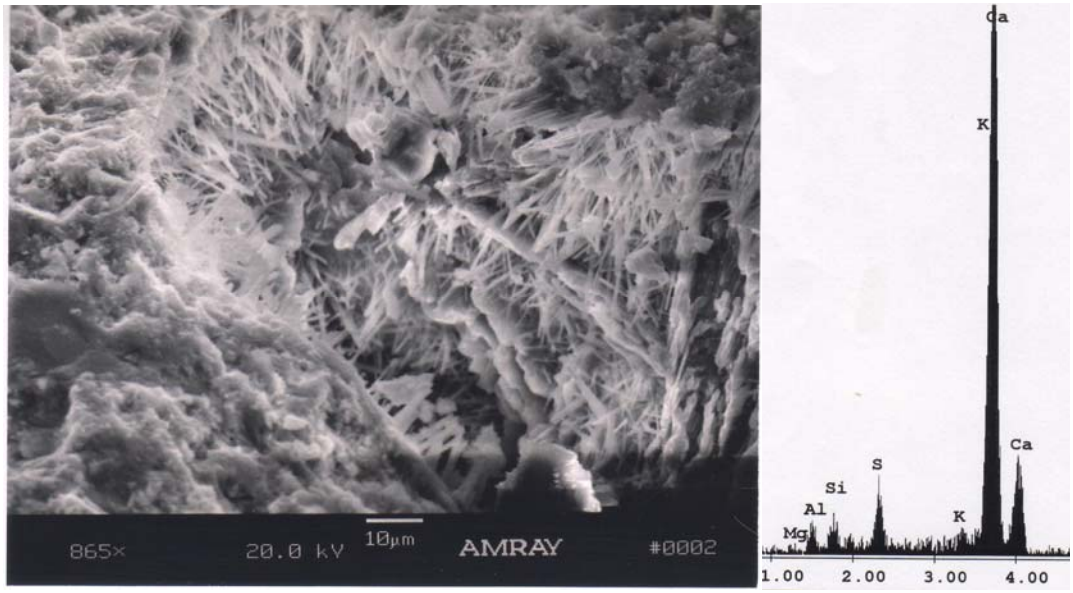


Figure 7.67: SEM and EDAX Analysis of Room Temperature-Cured Concrete Specimen Under Field Conditions (C4B) at Age 100 Days, Showing Ettringite Deposits Within an Air Void

At 540 days, SEM examinations revealed little or no ettringite in the mortar specimen under field condition 4B. The absence of ettringite may be attributed to the constantly changing atmospheric conditions which sometimes poses non-favorable ettringite formation. Most of the air voids were either concentrated with calcium hydroxide (CH) crystals or empty. Figure 7.68 shows the SEM micrograph of an air void filled with CH crystals. Due to low energy intensity count no EDAX spectrum could be established.


Figure 7.68: SEM Micrograph of Room Temperature-Cured Mortar Specimen Under Field Conditions (C4B) at Age 540 Days, Showing CH Crystals within Air Voids

*7.12 Summaries and Discussion of Concrete Samples (Control)*

Concrete design and construction practices during the 21st century are driven by strength rather than durability. However, due to the increase in repair orders and replacement costs of concrete structures, and a growing concern about sustainability of the concrete industry, more attention is now paid to the durability issues (Metha, 2006). In this research work, Portland cement type III and dolomite limestone aggregate - # 57 was used to study DEF. Some of the concrete samples were also subjected to the Duggan heat cycle to initiate microcracks and accelerate expansion. Others were subjected to Freeze-Thaw or stored under a field environment.

The concrete samples in limewater revealed the higher expansion values after 400 days of storage. This can be attributed to the fast expansion rate increase during

this interval onwards. According to Metha, there is a second stage of concrete damage process, which occurs at a slow rate at first and then proceeds rather too rapidly as the system becomes more permeable (2006). Then, the hydraulic pressure of the pore fluid in the saturated concrete rises due to the expansion and swelling of the massive ettringite crystals formed at this stage. The presence of massive ettringite crystals was confirmed by the SEM and EDAX analysis results at this stage. The expansion process of the concrete samples in limewater and plain water can be classified into two (2) stages. The correlation of expansion against time results revealed a high linear correlation for the first 160 days of storage in both exposure conditions.

Both sets of concrete samples subjected to either Duggan heat or Freeze-Thaw show some moderate expansions. The absence of steam-curing in the early stages of heat of cement hydration may influence the expansion and formation of ettringite. Both concrete sets showed similar expansion patterns which were subjected to different concrete treatments. Also, both concrete sets showed few surface microcracks as revealed by the laser shearography testing.

The control concrete samples in limewater and plain water exhibited similar weight change patterns. The weight change is mainly attributed to the storage solution imbibed to fill the structural defects (Shimada, 2005). This is also associated with large expansion of the concrete prisms. Little weight-change was observed in concrete samples stored in relative humidity maintained at 97%. From about 400 days of storage to the end, concrete samples in limewater showed the highest weight-change. This might be attributed to excessive weight-gain due to the formation of

massive ettringite crystals, discussed earlier. Again, a two-stage process was observed in the weight-change against time results of the control concrete samples. A high linear correlation coefficient is observed for the first 100 days of storage of the concrete prisms in all three exposure conditions.

The Duggan heat treated control concrete samples showed higher weight-change than the Freeze-Thaw concrete samples. The use of thermal heating cycles initiates or increases microcracks, which make the concrete system more permeable. This increases the capillary pore volume of the paste itself, and the storage solution filling the increased volume results in weight gain (Shimada, 2005).

The linear correlation of expansion against weight-change results of the control concrete showed little correlation for the 100 days of storage. These results were contrary to those obtained from the mortar samples. No linear correlation was observed in the Duggan heat or Freeze-Thaw treated concrete samples.

The effect of exposure conditions on the later age compressive strength of concrete specimens is different. The limewater and plain water exposed concrete samples revealed high significant expansion values accompanied by a drastic decrease in compressive strength at later stages. When the growing microcracks linked up with existing macrocracks and voids in the concrete, this weakens the microstructure and reduces the compressive strength. Totally immersed concrete samples in limewater showed reduction of up to 25% in compressive strength.

Length-change measurements of the field-exposed concrete specimens showed fluctuating expansion and shrinkage over time. This is characteristic of field-exposed specimens, due to a changing environment influencing too many variables.

Conversely this makes it difficult to attribute the damage to one particular mechanism. Likewise, the weight-change results pose similar patterns. Little or no correlation exists between weight-change and time for the duration of the research.

Unlike the control concrete specimens subjected to the Duggan heat cycle, the field-exposed concrete specimens showed an increase in compressive strength at later stages. For up to about two (2) years, examination of the concrete's exterior surface revealed no cracks visible to the unaided eye and no networks of cracks. Also, since no Duggan heat cycle heat was employed in field exposure concrete specimens, this might have contributed to an increase in compressive strength. Several researchers indicated a strength reduction associated with high curing temperatures (Ramadan, 2000, Ronne and Sellevold 1994, Taylor, 1994).

The amount of alkalis leached out from the concrete samples to the storage solutions increases with time. The high concentration of alkalis in the storage solution accelerates the formation of ettringite and its deleterious expansions. The alkalis concentrations of the storage solution correlated with the expansion showed an increase in expansion, with an increase in alkalis concentration. The high concentration of $Ca^{2+}$ ions can also contribute to the formation of ettringite. Researchers such as Struble and Kilgour believe that formation of reaction gel taking place in concrete and mortar bars depends on the amount and availability of the $Ca^{2+}$ (1987, 1988).

Analysis of the laser shearography images showed that both the Duggan heat and Freeze-Thaw initiate microcracks in the concrete prisms. The storage conditions further enhanced the propagation of the microcracks, which later form a network of

cracks leading to the concrete's deterioration. Duggan heat treated concrete samples showed higher expansion values than the Freeze-Thaw treated samples. The different concrete treatments influence the expansion values of the concrete samples.

The microstructural analysis of the control concrete specimens using SEM and EDAX revealed features characteristically associated with delayed ettringite formation as described by many other researchers. In 2000, Ramadan outlined these features to include the presence of peripheral cracks around aggregate particles, forming an intrinsic part of a network of cracks extending into the paste fully or partially filled with ettringite, discrete deposits of ettringite within the paste, and ettringite filled voids and cracks. Massive ettringite crystals were mainly found in air voids and cavities of the concrete specimens. The continuous availability of water to the cracked concrete specimens provided an ideal host for ettringite formation. The morphology of ettringite changes over time from small spherical ettringite balls to needle-like crystals, and finally to massive ettringite crystals. This was observed mainly in the concrete samples stored in limewater and plain water. Obviously, these massive ettringite crystals occupied wider spaces in the cavities, and thereby weaken the interface between the aggregate and cement paste. The lack of water in the relative humidity of 97% exposure condition might be attributed to the disappearance of ettringite at later stages. Calcium hydroxide (CH) crystals were found in the SEM examinations of concrete specimens in relative humidity of 97% and this might be from the un-reacted products produced during the hydration of Portland cement. According to Mehta, hydration reactions of Portland cement minerals produce a multiphase product consisting primarily of adhesive, poorly-crystalline, a C-S-H

phase, and some well-crystalline products including calcium hydroxide (CH) (2006). Table 7.15 provides the test results for the steam-cured concrete samples (control) and subjected to Duggan heat cycle before subsequently storing them in different exposure conditions. SEM and EDAX examinations of Freeze-Thaw treated concrete specimens revealed ettringite with calcium hydroxide plates throughout the research. The SEM results correlated to the expansion results showed that exposure conditions have a significant role in expansion and formation of DEF. Table 7.16 provides the test results for the room temperature-cured concrete samples subjected to different treatments prior to storing them in limewater.

The field-exposed concrete specimens showed ettringite needles which disappeared at later stages. Ettringite deposits were found in both sets of concrete specimens. SEM at later stages showed well-developed ettringite needles in the steam-cured concrete specimens exposed to field conditions. Table 7.17 provides the test results for the concrete samples subjected to field conditions.

Microscopic examinations, using SEM equipped with EDAX, of the concrete specimens show no evidence of ASR. The absence of ASR suggests that the materials and test parameters used in this research study were not conductive to any deleterious ASR mechanism. The results suggest that DEF is the mechanism responsible for the deterioration

Table 7.15: Summary of Test Results of Control Concrete Samples – Steam-Cured and Subjected to Duggan Heat Cycle

| **Concrete Samples (Control) - Steam-Cured and Subjected to Duggan Heat Cycle** | | | | |
|---|---|---|---|---|
| | | Exp. Cond. 1 (Limewater) | Exp. Cond. 2 (Plain Water) | Exp. Cond. 3 (R.H at 97%) |
| Expansion | | Max. 1.08% | Max. 0.82% | Max. 0.03% |
| Weight Change | | Max. 5.50% | Max. 5.31% | Max. 2.44% |
| Compressive Strength (psi) | 28 Days | 5182 | 4792 | 5707 |
| | 365 Days | 1309 | 1488 | 5911 |
| | 540 Days | 731 | 684 | 7116 |
| Water Analysis (mmol/l) | pH | - | 8.01 - 11.32 | - |
| | Alkali | Max. 304 | Max. 301 | - |
| | $Ca^{2+}$ | - | Max. 124 | - |
| SEM/EDAX Analysis | 40 Days | Spherical ettringite balls | Ettringite balls | Little ettringite |
| | 100 Days | Ettringite needles | Ettringite balls | Clusters of ettringite nuggets |
| | 240 Days | Random ettringite needles | ettringite needles | No ettringite |
| | 540 Days | Needle-like ettringite crystals | Needle-like ettringite crystals | Few ettringite crystals |

Table 7.16: Summary of Test Results of Room Temperature-Cured Concrete Samples – Subjected to Different Treatments

| **Room Temperature-Cured Concrete Samples - Subjected to Different Treatments** | | | |
|---|---|---|---|
| | | P3C1_D (Duggan Heat Cycle) | P3C1_F (Freeze-Thaw Cycle) |
| Expansion | | Max. 0.1074% | Max. 0.090% |
| Weight Change | | Max. 5.43% | Max. 1.18% |
| Compressive Strength (psi) | 28 Days | 5917 | 6680 |
| | 240 Days | 7438 | 8014 |
| | 365 Days | 7183 | 8050 |
| SEM/EDAX Analysis | Before treatment | No ettringite | No ettringite |
| | After treatment | Ettringite needle-like crystals | Probable ettringite |
| | 40 Days | Ettringite and CH crystals | Ettringite and CH crystals |
| | 100 Days | Bundles of ettringite | No ettringite |
| | 240 Days | Traces of ettringite | No ettringite |

Table 7.17: Summary of Test Results of Control Concrete Samples – Subjected to Field Conditions

| **Concrete Samples (Control) - Exposed to Field Conditions** | | | |
|---|---|---|---|
| | | Exp. Cond. 4A (Steam-Cured) | Exp. Cond. 4B (Room Temp.-Cured) |
| Length Change | | Max. 0.0240% | Max. 0.0152% |
| Weight Change | | Max. 0.49% | Max. 0.48% |
| Compressive Strength (psi) | 28 Days | 4036 | 6118 |
| | 365 Days | 6054 | 6953 |
| | 540 Days | 6855 | 8154 |
| SEM/EDAX Analysis | 40 Days | No ettringite | No ettringite |
| | 100 Days | No ettringite | Needle-like ettringite |
| | 240 Days | Ettringite needles | No ettringite |
| | 540 Days | Ettringite needles | CH crystals |

# Chapter 8: Concrete Samples Made With High Potassium Content ($K_2O$) and DEF

## *8.1 Introduction*

Delayed ettringite formation has a significant potential for serious premature deterioration in concrete. The objective of these experiments was to study the effect of adding additional potassium content ($K_2O$) to the concrete mixes and the formation of DEF and its associated deleterious expansion. The additional $K_2O$ increases the alkali content, which influences the chemical composition of the cement. This factor leads to disruption and damage to the microstructure, which can promote the formation of ettringite. In this study phase, seven (7) sets of concrete samples with 1.5% potassium content ($K_2O$) were prepared according to the modified sample preparation method. The effect of the Duggan Heat and Freeze-Thaw cycles were also investigated in two (2) of the concrete sets, which were subsequently stored in exposure condition 1 (pH maintained at 12.5 - limewater) for the duration of the research project. The deleterious effect due to DEF was monitored for the concrete specimens stored in four (4) different conditions. Concrete samples exposed to field conditions were also prepared. Expansion and weight-change measurements were monitored for about two (2) years.

The 4" x 8" concrete cylinders made with 1.5% $K_2O$ were prepared for compressive strength testing. Compressive strength was employed after storage of 28 days, 365 days and 540 days for each of the exposure conditions. Three (3) concrete cylinders were tested from each exposure condition, and the average result used. The scanning electron microscope (SEM) with X-ray analysis and Laser shearography

(LAS) studies were performed on the steam-cured concrete specimens. Laser shearography was employed to detect and monitor progress of any surface microcracks caused by the Duggan or Freeze-Thaw cycles. Leaching of ions from storage solutions in exposure conditions 1 and 2 was monitored. Expansions, weight-change, SEM with EDAX, and laser shearography (LAS) results are presented and discussed in this chapter.

## *8.2 Influence of Potassium Content and Exposure Conditions on Concrete*

All concrete samples were prepared with 1.5% $K_2O$, before subjecting them to different concrete treatments and subsequently storing them in their respective exposure conditions. Length-change, weight-change, SEM with EDAX and LAS were monitored for the entire storage time of the concrete samples. Leaching of ions was monitored in the storage solutions of exposure conditions 1 and 2. Expansion and weight changes were monitored periodically. Expansion values at 21 days were compared to the threshold value of 0.05% expansion that was suggested by Duggan as pass/fail criteria. The influence of exposure condition and alkali content played a major role in the amount of ettringite found in concrete specimens. SEM with EDAX analysis was employed to reveal the presence of ettringite and its ever-changing morphology. None of the SEM examination results showed ASR in any of the examined samples. Therefore, it can be concluded that DEF in the mortar samples at different stages could be responsible for the expansion.

Curve fitting of the experimental data was obtained using linear regression curves. The linear regression curves are a better fit to the expansion data than the

KAJM equation. Since, according to Ramadan the KAJM equation does not give a better fit for the experimental data, it was not used (2000).

*8.3 Influence of Potassium Content and Concrete Treatment*

Concrete samples made with 1.5% $K_2O$ were room-cured for 24 hours before subsequently storing them in a water bath for six (6) days then subjecting them to the Duggan heat or Freeze-Thaw cycles. The Duggan heat and Freeze-Thaw cycles were used to create microcracks in order to accelerate the expansion of the concrete specimens with 1.5% $K_2O$. Again, the specimens were placed in exposure condition 1 (pH maintained at 12.5 – limewater) after the microcrack initiation processes. Expansion values at 21 days were compared to the threshold value of 0.05% expansion that was suggested by Duggan as pass/fail criteria. Compressive strength test was employed using 4" x 8" cylinders at specific intervals, during the research duration. SEM equipped with EDAX was used to analyze the concrete microstructure, while Laser Shearography (LAS) was employed to study the early development of microcracks.

*8.4 Expansion Results*

*8.4.1 Expansion of Concrete Prisms Made With 1.5% $K_2O$ and Subjected to Different Exposure Conditions*

Only the concrete prisms made with 1.5% $K_2O$ and stored in exposure condition 1 exceeded the Duggan threshold value of 0.05% after 21 days. This suggested that the concrete samples in exposure condition 1 have the potential for damage due to DEF. The expansion values and rates against time for the concrete prisms made with 1.5% $K_2O$ subjected to the Duggan heat cycle before storing them under different exposure conditions are shown in figures 8.1 through 8.4.

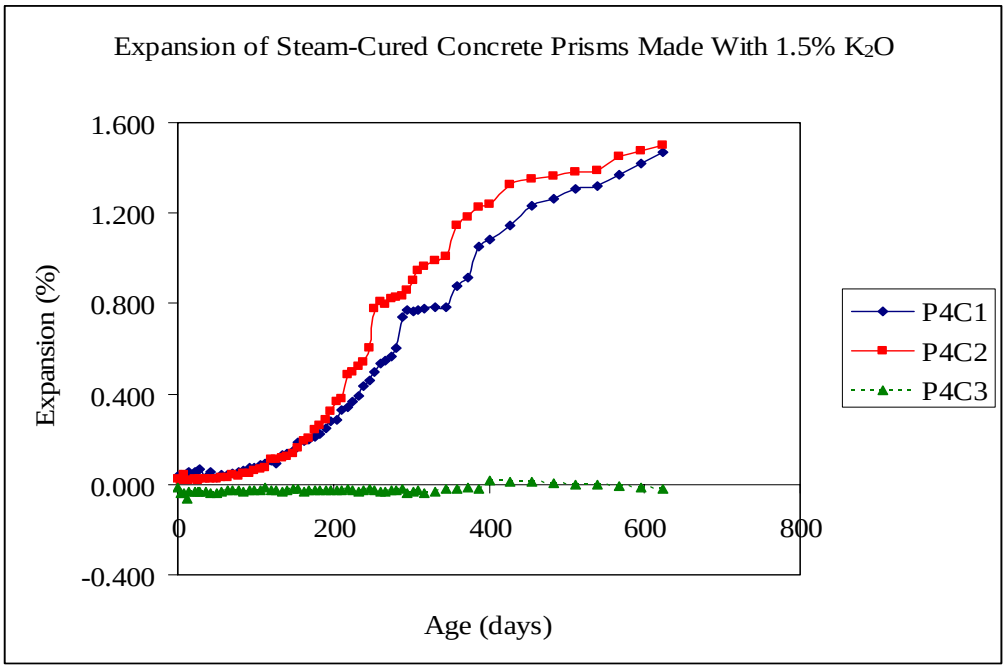


Figure 8.1: Expansion of Steam-Cured Concrete Prisms Made with 1.5% $K_2O$ Subjected to Duggan Heat Cycle and Stored Under Different Exposure Conditions

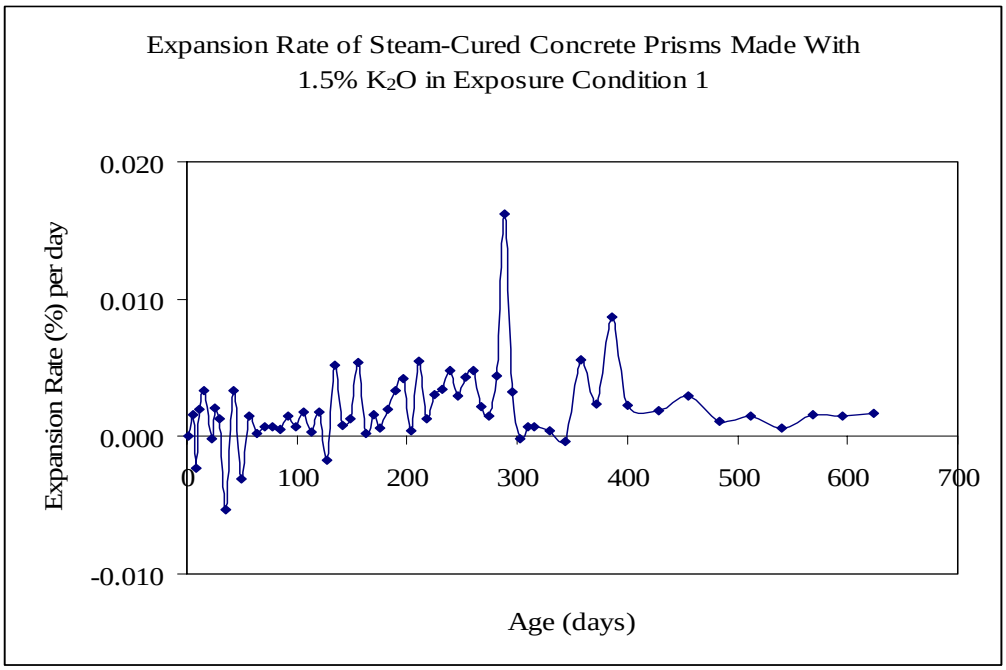


Figure 8.2: Expansion Rate of Steam-Cured Concrete Prisms Made with 1.5% $K_2O$ Subjected to Duggan Heat Cycle and Stored in Isothermal Water Bath, pH maintained at 12.5 - limewater

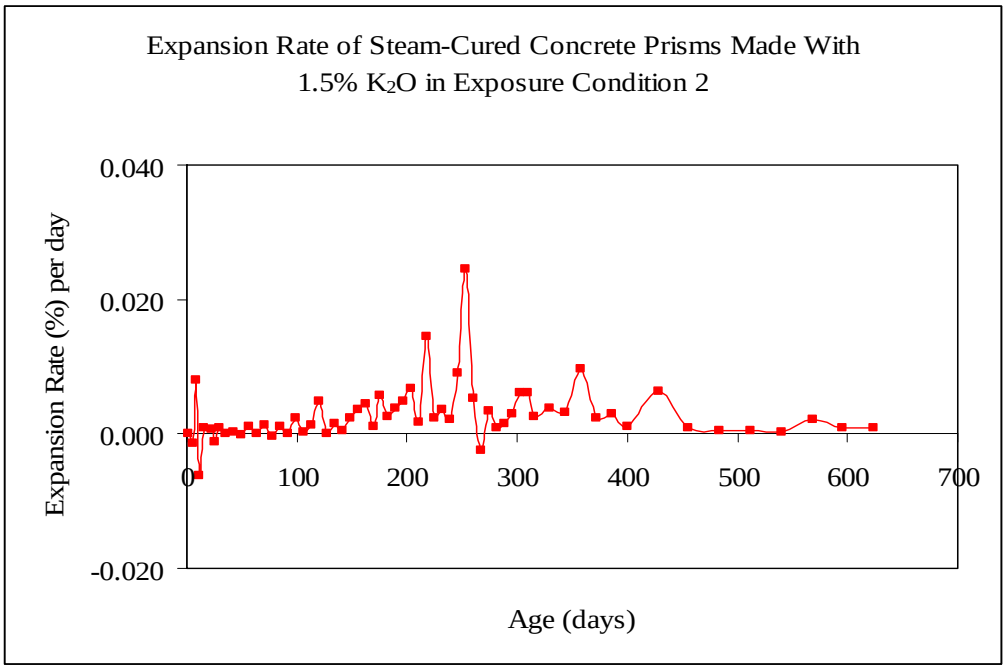


Figure 8.3: Expansion Rate of Steam-Cured Concrete Prisms Made With 1.5% $K_2O$ Subjected to Duggan Heat Cycle and Stored in Plain Water at Room Temperature

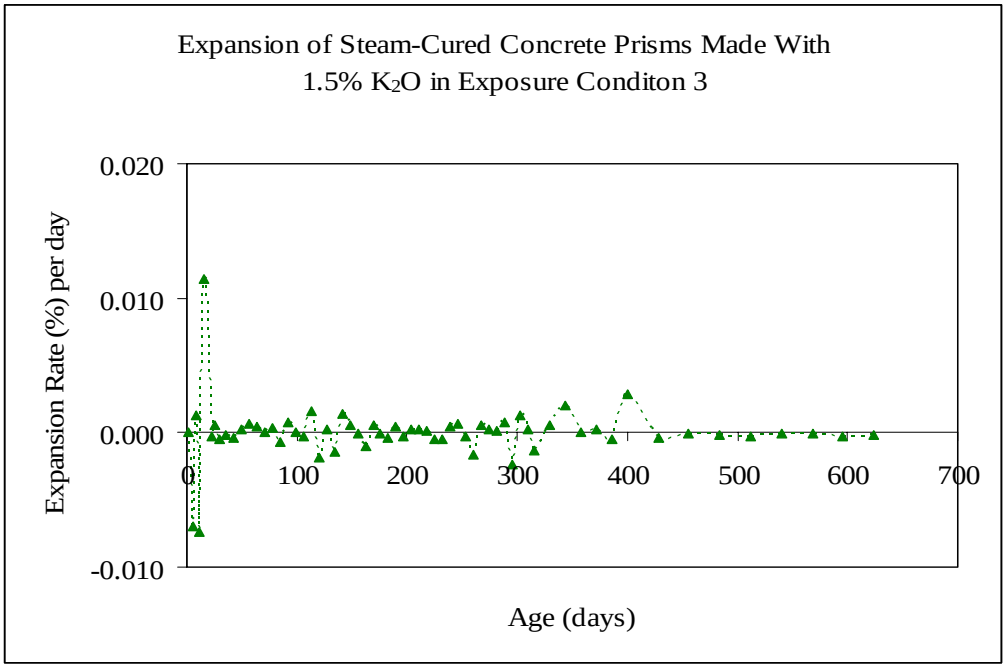


Figure 8.4: Expansion Rate of Steam-Cured Concrete Prisms Made With 1.5% $K_2O$ Subjected to Duggan Heat Cycle and Stored in Moist Air Chamber, R.H maintained at 97%

For up to about 300 days, the expansion of concrete prisms in exposure conditions 1 and 2 exhibited similar pattern. After 300 days, it could be seen that concrete prisms in exposure condition 2 exhibited higher expansion than those in exposure condition 1. This can be attributed to the extra calcium from the limewater in exposure condition 1 which can caused precipitation of ettringite. The ettringite precipitation can inhibits transport of solution into the microstructure retarding expansion of the concrete prisms. Lack of continuous supply of water can be attributed to the little or insignificant expansion exhibited by the concrete prisms in exposure condition 3. The maximum expansions were 1.470%, 1.501% and 0.0188% for concrete prisms in exposure conditions 1, 2 and 3 respectively. The expansion of the concrete prisms in all the exposure conditions will continue in the future. Isolated

cracks were observed on the concrete prisms in exposure conditions 1 and 2. As the expansion increases, the cracks become more developed forming a network of cracks as shown in figures 8.5 and 8.6.


Figure 8.5: Crack Pattern of Steam-Cured Concrete Prisms Made With 1.5% $K_2O$ Subjected to Duggan Heat Cycle and Stored in Limewater at Age of 500 Days

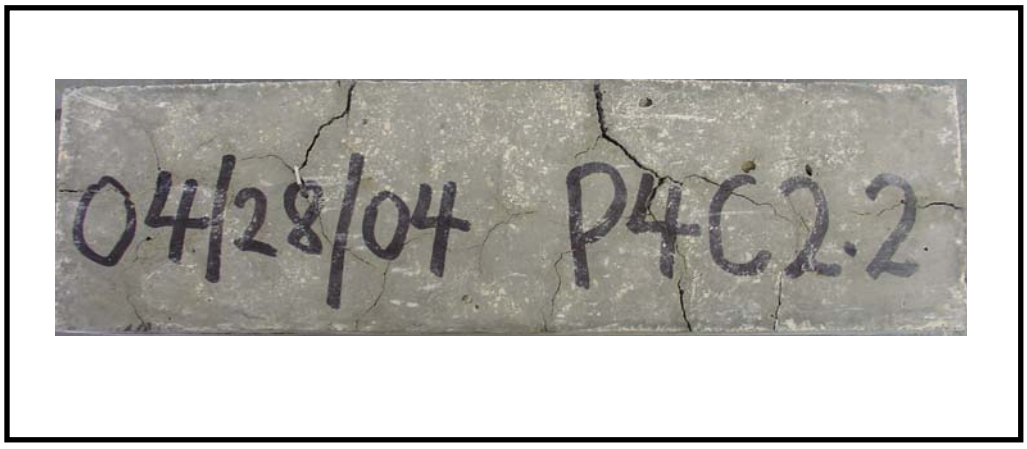


Figure 8.6: Crack Pattern of Steam-Cured Concrete Prisms Made With 1.5% $K_2O$ Subjected to Duggan Heat Cycle and Stored in Plain Water at Age of 500 Days

Linear regressions were applied to obtain the best fit for the experimental expansion data against time. Two linear regression curves were used to best fit the expansion data results obtained from length-change measurement of the concrete prisms. The cut-off points for the linear curves were determined based on the maximum correlation coefficient of the expansion values against time. The KAJM model equation was not used since it did not give a better fit for the experiment data (Ramadan, 2000 and Azzam, 2002). Figures 8.7 through 8.9 show linear regression curves for the experimental data of the concrete prisms stored in different conditions. Table 8.1 provides the linear regression equations and correlation coefficients used for the best fit of the experimental expansion data.

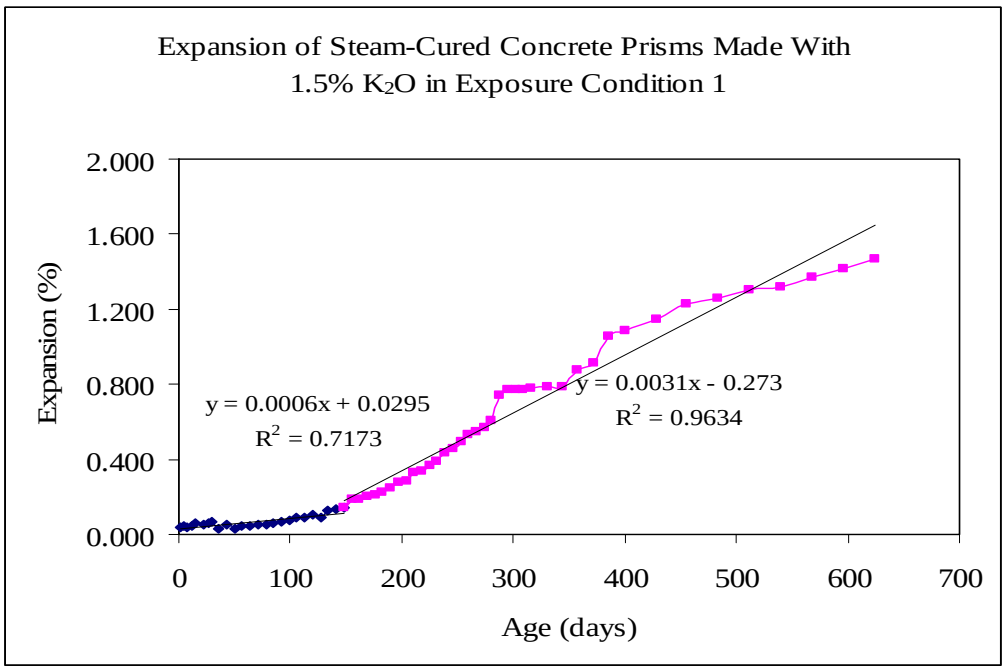


Figure 8.7: Expansion of Steam-Cured Concrete Prisms Made With 1.5% $K_2O$ Subjected to Duggan Heat Cycle and Stored in Water Bath, pH maintained at 12.5 – limewater (Regression Curves)

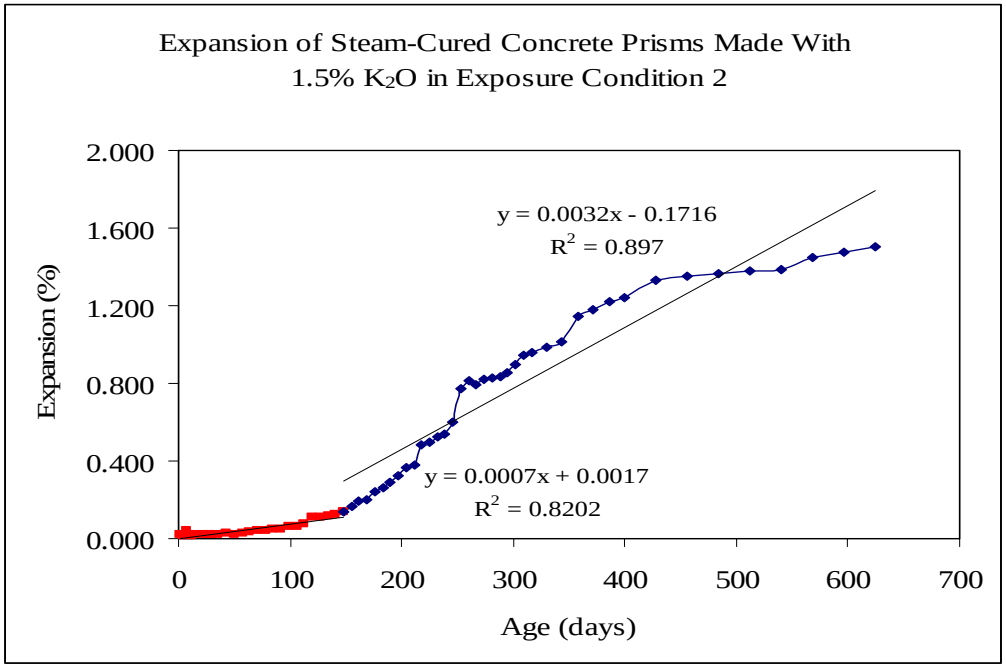


Figure 8.8: Expansion of Steam-Cured Concrete Prisms Made With 1.5% $K_2O$ Subjected to Duggan Heat Cycle and Stored in Plain Water at Room Temperature (Regression Curves)

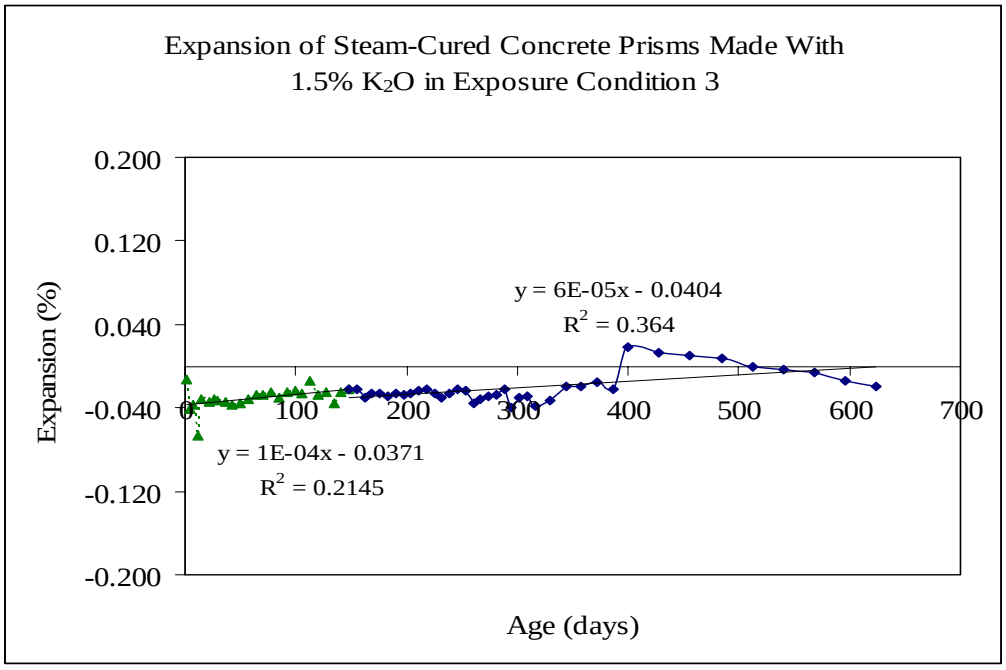


Figure 8.9: Expansion of Steam-Cured Concrete Prisms Made With 1.5% $K_2O$ Subjected to Duggan Heat Cycle and Stored in a Moist Air Chamber, R.H maintained at 97% (Regression Curves)

Table 8.1: Linear Equations for Expansion vs. Age of Steam-Cured Concrete Prisms Made With 1.5% $K_2O$ Subjected to Duggan Heat Cycle and Stored Under Different Exposure Conditions

| Phase 4 (Concrete Prisms Made With 1.5% $K_2O$ - Subjected to Duggan Heat Cycle) | | | | | |
|---|---|---|---|---|---|
| | | | | | |
| Exp. Cond. 1 | Max. Exp. 1.55% | Curve 1 | Day 1 - 148 | y = 0.0006x + 0.0295 | $R^2$ = 0.7173 |
| | | Curve 2 | Day 148 - 624 | y = 0.0027x - 0.0233 | $R^2$ = 0.9706 |
| | | | | | |
| Exp. Cond. 2 | Max. Exp. 1.50% | Curve 1 | Day 1 - 148 | y = 0.0007x + 0.0017 | $R^2$ = 0.8202 |
| | | Curve 2 | Day 148 - 624 | y = 0.0032x - 0.1716 | $R^2$ = 0.897 |
| | | | | | |
| Exp. Cond. 3 | Max. Exp. 0.02% | Curve 1 | Day 1 - 148 | y = 1E-04x - 0.0371 | $R^2$ = 0.2145 |
| | | Curve 2 | Day 148 - 624 | y = 6E-05x - 0.0404 | $R^2$ = 0.364 |
| | | | | | |

*8.4.2 Expansion of Concrete Prisms Made With 1.5% $K_2O$ and Subjected to Different Treatments*

Figures 8.10 and 8.11 illustrate the effect of concrete treatment in the expansion and the expansion rate of concrete made with 1.5% $K_2O$ and stored in exposure condition 1 (Isothermal Water Bath, pH maintained at 12.5 – limewater). The Duggan heat cycle treated concrete prisms exhibited higher expansion values than the Freeze-Thaw concrete prisms during the entire study. This can be attributed to the thermal heating and wetting cycles employed by the Duggan heat cycle. Fu reported that concrete treatments such as freeze-thaw cycles appeared not to cause significant DEF-induced expansion (1996). Expansion values at 21 days were 0.0350% and 0.0192% for the Duggan heat and Freeze-Thaw treated concrete prisms respectively. An increase in potassium content ($K_2O$) causes an increase in the

expansion of the concrete prisms. The expansion behaviors of both sets of concrete prisms are almost the same. The maximum expansion values exhibited were 0.1172% and 0.0984% for the Duggan heat and Freeze-Thaw treated concrete prisms respectively. The expansion values of the concrete prisms subjected to either Duggan heat or Freeze-Thaw cycle did not cause any significant damage due to DEF-induced expansions.

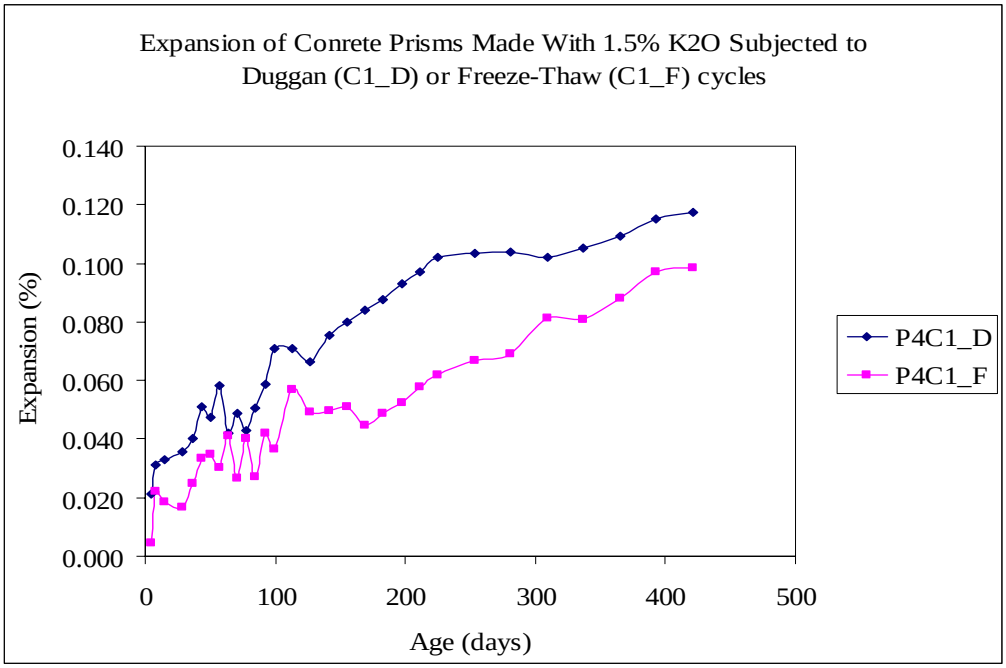


Figure 8.10: Expansion of Room Temperature-Cured Concrete Prisms Made With 1.5% $K_2O$ Subjected to Different Treatments and Stored in Isothermal Water Bath, pH maintained at 12.5 – limewater

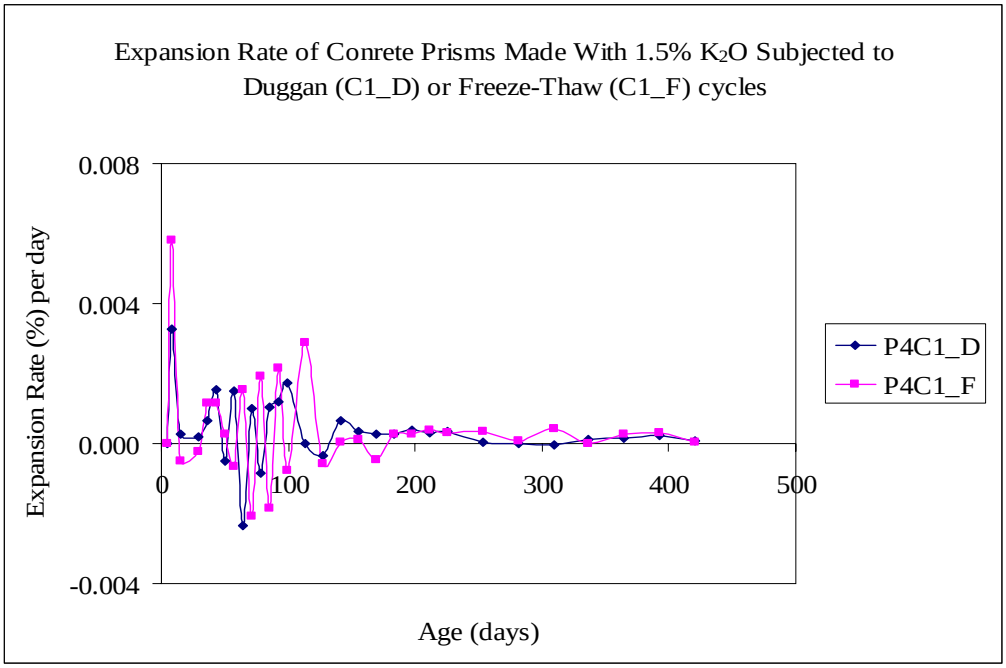


Figure 8.11: Expansion Rate of Room Temperature-Cured Concrete Prisms Made With 1.5% $K_2O$ Subjected to Different Treatments and Stored in Isothermal Water Bath, pH maintained at 12.5 - limewater

## *8.5 Weight Change Results*

### *8.5.1 Weight Change of Concrete Prisms Made With 1.5% $K_2O$ and Subjected to Different Exposure Conditions*

Figures 8.12 shows the weight-change of concrete prisms made with 1.5% $K_2O$ and stored in different exposure conditions. Weight change results of the concrete prisms in exposure conditions 1 and 2 showed a similar pattern. The weight change of the concrete prisms made with 1.5% $K_2O$ increased with time for all exposure conditions. Most of the weight change took place within about 100 days of storage in the respective exposure conditions. The maximum weight change observed in the concrete prisms was 4.98%, 5.42% and 2.15% for exposure conditions 1, 2 and 3 respectively.

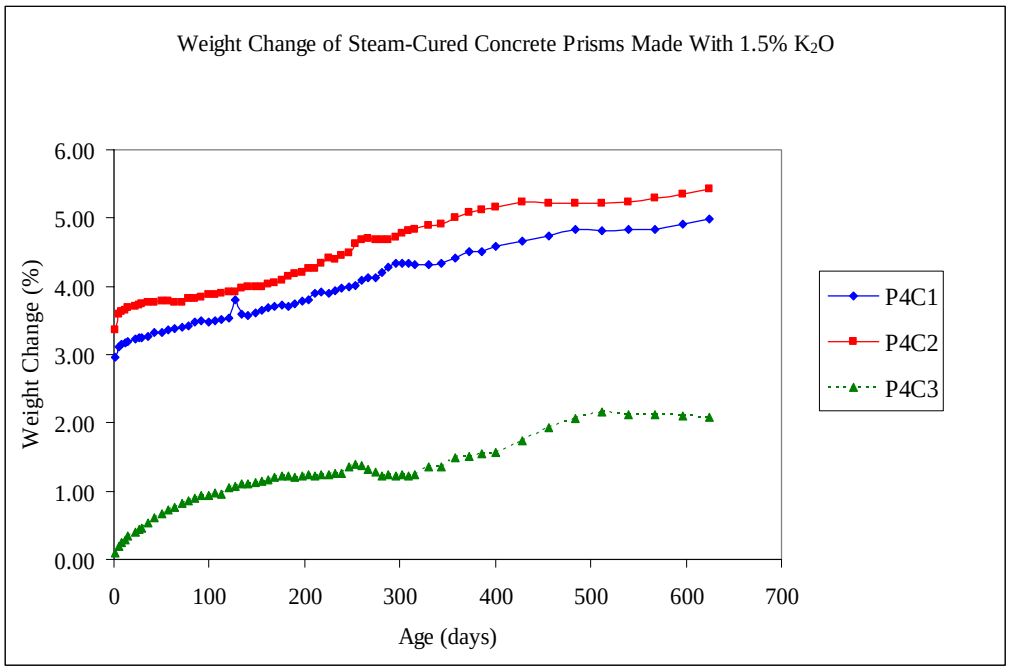


Figure 8.12: Weight Change of Steam-Cured Concrete Prisms Made With 1.5% $K_2O$ Subjected to Duggan Heat Cycle and Stored Under Different Exposure Conditions

Linear regressions were employed to obtain the best fit for the experimental data of weight change against time for the concrete prisms made with1.5% $K_2O$. Again, two linear regression curves were used to best fit the weight-change experimental results. A high linear correlation coefficient is revealed around the first 100 days of storage. Figures 8.13 through 8.15 show the linear regression curves while Table 8.2 provides a summary of the regression equations used for the experimental data.

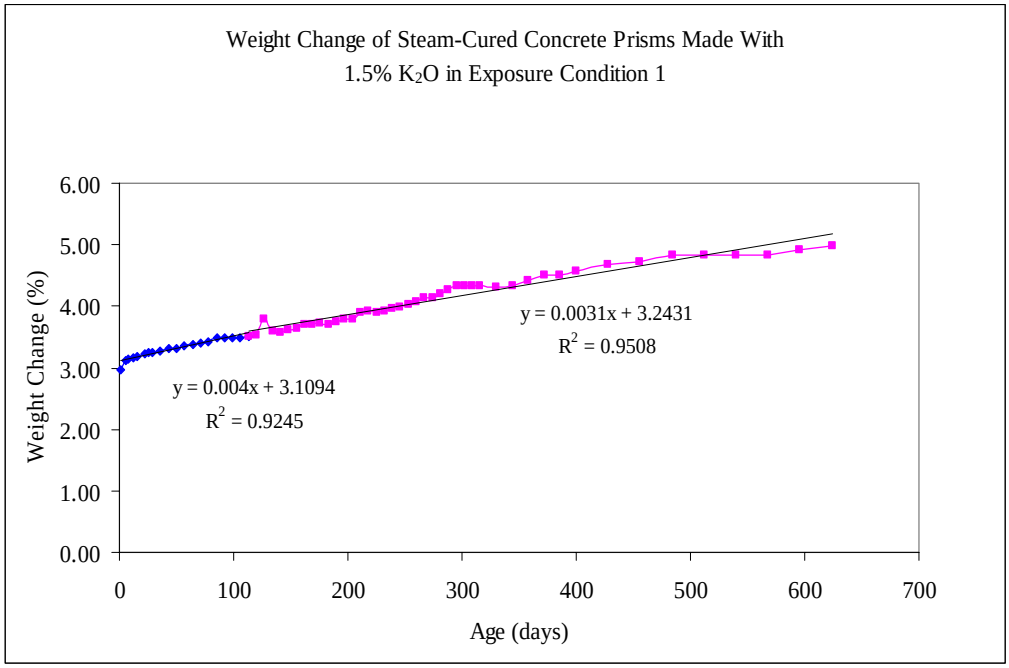


Figure 8.13: Weight Change of Steam-Cured Concrete Prisms Made With 1.5% $K_2O$ Subjected to Duggan Heat Cycle and Stored in Isothermal Water Bath, pH maintained at 12.5 - limewater (Regression Curves)

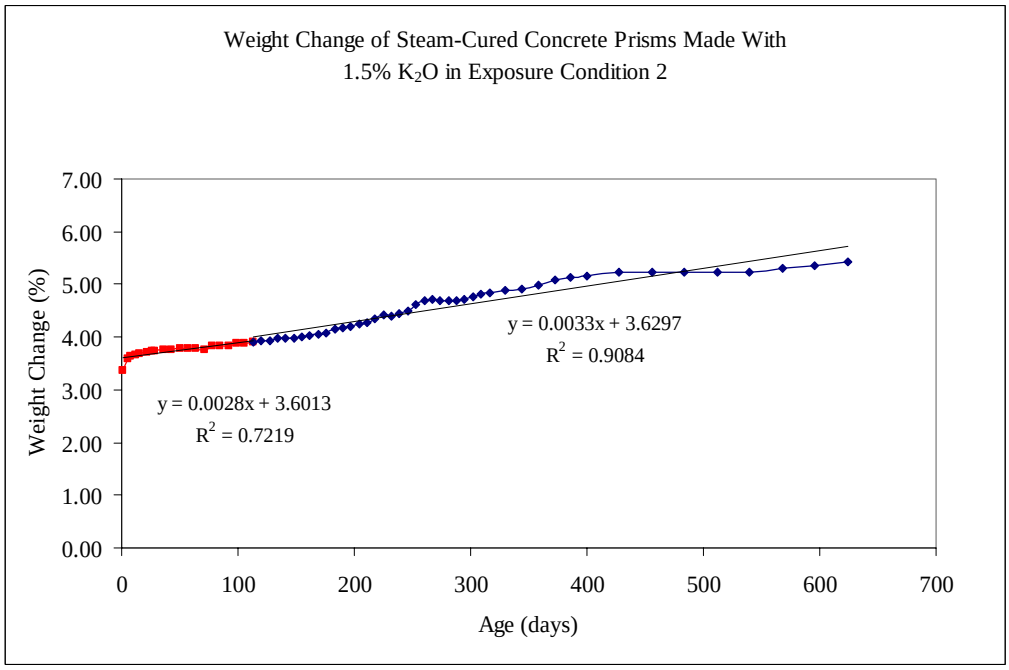


Figure 8.14: Weight Change of Steam-Cured Concrete Prisms Made With 1.5% $K_2O$ Subjected to Duggan Heat Cycle and Stored in Plain Water at Room Temperature (Regression Curves)

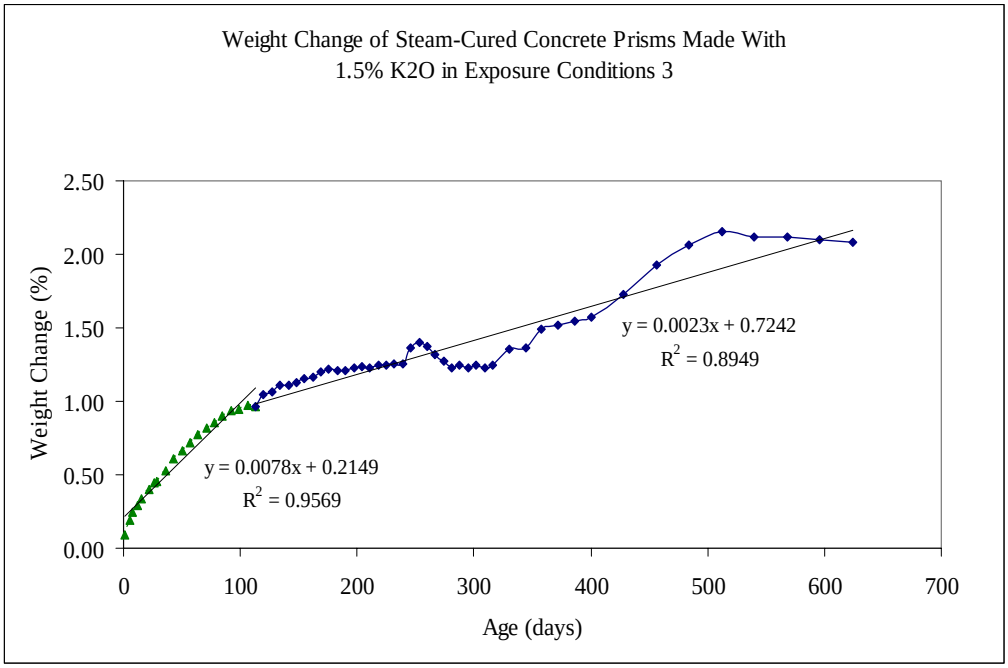


Figure 8.15: Weight Change of Steam-Cured Concrete Prisms Made With 1.5% $K_2O$ Subjected to Duggan Heat Cycle and Stored in Moist Air Chamber, R.H maintained at 97% (Regression Curves)

Table 8.2: Linear Equations for Weight Change vs. Age of Steam-Cured Concrete Prisms Made With 1.5% $K_2O$ Subjected to Duggan Heat Cycle Concrete Samples Stored Under Different Exposure Conditions

| Phase 4 (Concrete Samples Made With 1.5% $K_2O$ - Subjected to Duggan Heat Cycle) | | | | | |
|---|---|---|---|---|---|
| | | | | | |
| Exp. | Max. | Curve 1 | Day 1 - 113 | y = 0.004x + 3.1094 | $R^2$ = 0.9245 |
| Cond. 1 | 4.98% | Curve 2 | Day 113 - 624 | y = 0.0032x + 3.2177 | $R^2$ = 0.9524 |
| | | | | | |
| Exp. | Max. | Curve 1 | Day 1 - 113 | y = 0.0028x + 3.6013 | $R^2$ = 0.7219 |
| Cond. 2 | 5.42% | Curve 2 | Day 113 - 624 | y = 0.0035x + 3.6012 | $R^2$ = 0.9165 |
| | | | | | |
| Exp. | Max. | Curve 1 | Day 1 - 113 | y = 0.0078x + 0.2149 | $R^2$ = 0.9569 |
| Cond. 3 | 2.15% | Curve 2 | Day 113 - 624 | y = 0.0027x + 0.6476 | $R^2$ = 0.8795 |

*8.5.2 Weight Change of Concrete Prisms Made With 1.5% $K_2O$ and Subjected to Different Treatments*

The Duggan heat cycle treated concrete prisms exhibited significantly higher weight-change measurements than the Freeze-Thaw treated concrete prisms. The weight-change results were 4.78% and 0.77% after just one (1) day for the Duggan heat and Freeze-Thaw treated concrete prisms respectively. The Duggan heat and Freeze-Thaw cycles were used to initiate microcrack which is intended to accelerate DEF and associated deleterious expansion. This sudden increase in weight change for the Duggan heat cycle treated concrete prisms can be attributed to the structural defects introduced by the Duggan, which increases the capillary pore volume absorbing the storage solution. The maximum weight-change results observed in the concrete prisms for the test duration were 5.33% and 1.27% for the Duggan heat and Freeze-Thaw treated concrete prisms respectively. Figure 8.16 shows the weight change of Duggan heat and Freeze-Thaw cycles treated concrete prisms made with1.5% $K_2O$. Figures 8.17 and 8.18 show the linear regression curves used for the best match of the experimental data. A high correlation coefficient is observed for the first 100 days of storage. Table 8.3 provides the linear regression equations for the treated concrete prisms made with1.5% $K_2O$.

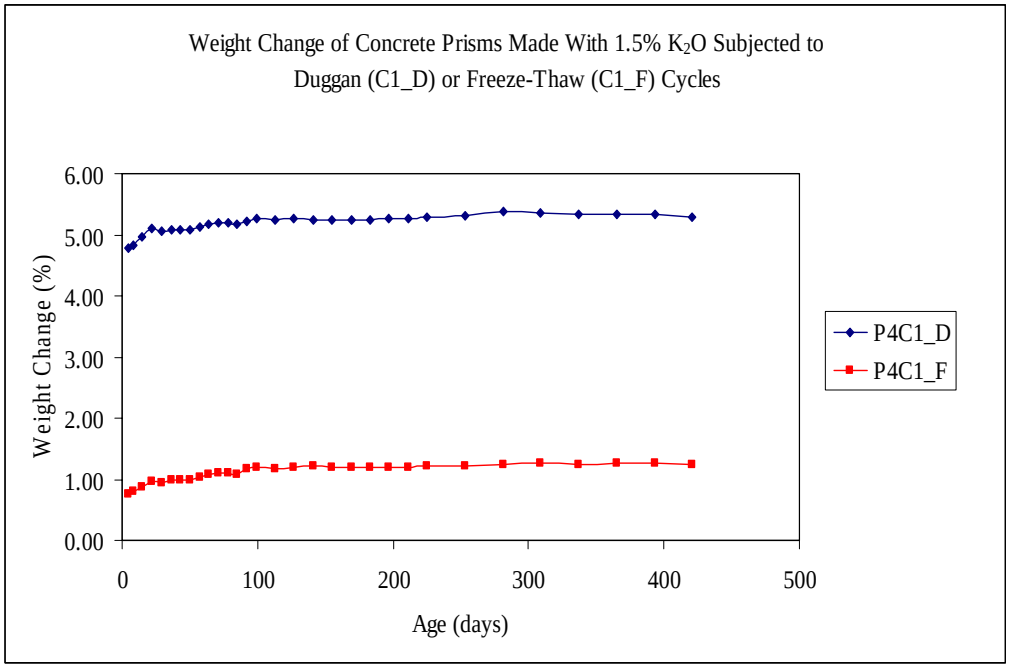


Figure 8.16: Weight Change of Room Temperature-Cured Concrete Prisms Made With 1.5% $K_2O$ Subjected to Different Treatments and Stored in Isothermal Water Bath, pH maintained at 12.5 - limewater

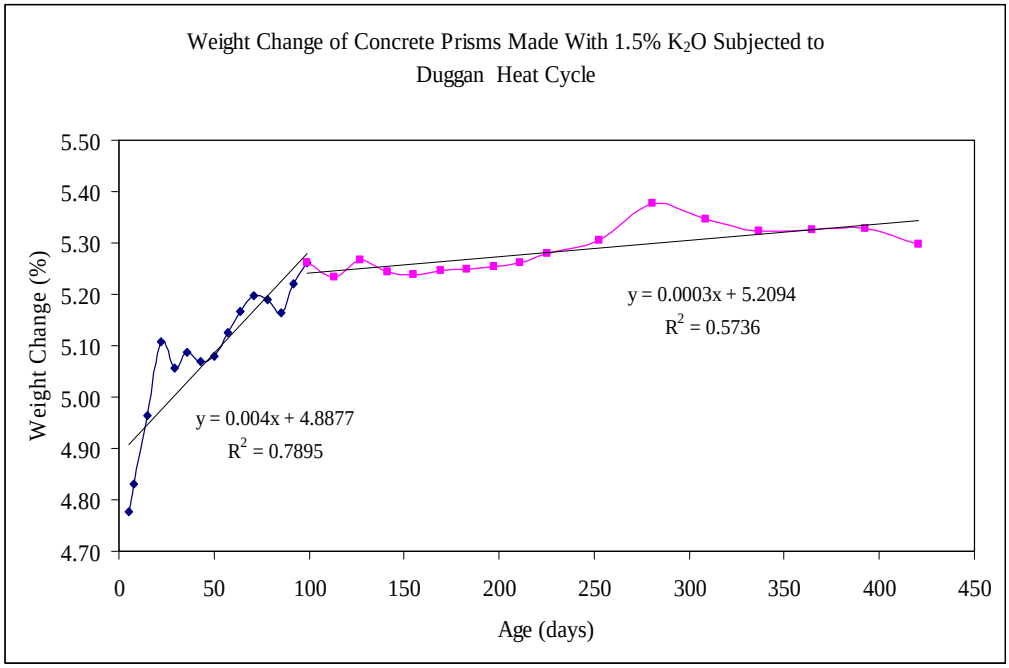


Figure 8.17: Weight Change of Room Temperature-Cured Concrete Prisms Made With 1.5% $K_2O$ Subjected to Duggan Heat Cycle and Stored in Limewater (Regression Curves)


Figure 8.18: Weight Change of Room Temperature-Cured Concrete Prisms Made With 1.5% $K_2O$ Subjected to Freeze-Thaw Cycles and Stored in Limewater (Regression Curves)

Table 8.3: Linear Equations for Weight Change vs. Age of Duggan Heat or Freeze-Thaw Treated Concrete Prisms Made With 1.5% $K_2O$ and Stored in Limewater

| Phase 4 (Concrete Prisms Made With 1.5% $K_2O$ - Duggan or Freeze-Thaw Cycles) | | | | |
|---|---|---|---|---|
| | | | | |
| Duggan Heat Cycle | Curve 1 | Day 1 - 99 | y = 0.004x + 4.8877 | $R^2$ = 0.7895 |
| | Curve 2 | Day 99 - 421 | y = 0.0003x + 5.2094 | $R^2$ = 0.5736 |
| | | | | |
| Freeze-Thaw Cycle | Curve 1 | Day 1 - 99 | y = 0.0039x + 0.8095 | $R^2$ = 0.9191 |
| | Curve 2 | Day 99 - 421 | y = 0.0003x + 1.1626 | $R^2$ = 0.8305 |
| | | | | |

*8.6 Expansion and Weight Change*

*8.6.1 Expansion and Weight Change of Concrete Prisms Made With 1.5% $K_2O$ and Subjected to Different Exposure Conditions*

Experimental data form the expansion and weight-change measurements were plotted to investigate if any correlation existed. Figure 8.19 shows expansion against weight change of steam-cured concrete made with 1.5% $K_2O$, and subjected to the Duggan heat cycle before subsequently being stored in different exposure conditions.

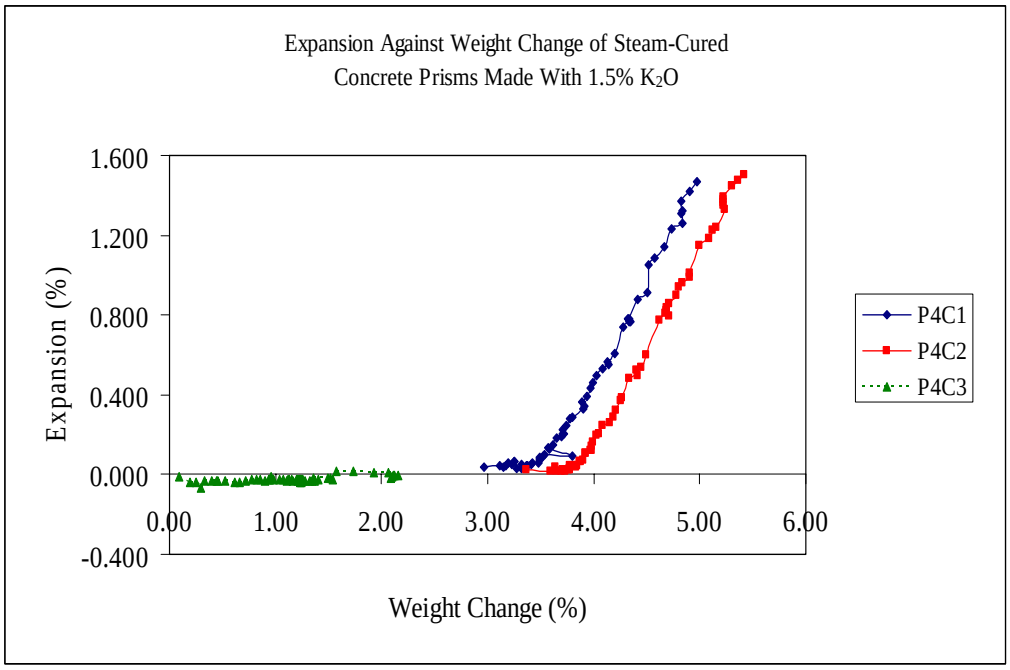


Figure 8.19: Expansion Against Weight Change of Steam-Cured Concrete Prisms Made With 1.5% $K_2O$ Subjected to Duggan Heat Cycle and Stored Under Different Exposure Conditions

Further analysis of the expansion against weight-change plots is performed using linear regression. It can be noted that exposure conditions 1 and 2 exhibited weight gain with increased expansion. Figure 8.20 through 8.22 illustrate the linear

regression curves of the expansion against weight-change experimental data. The results from exposure conditions 1 and 2 revealed a high positive linear correlation between expansion and weight change from about 120 days to the end. This may be attributed to the weight change due to renewed ettringite formation, which also caused paste expansion. SEM results found massive ettringite crystals in the microstructure of the concrete. Table 8.4 gives a summary of the linear regression equations used for the expansion against weight-change data.

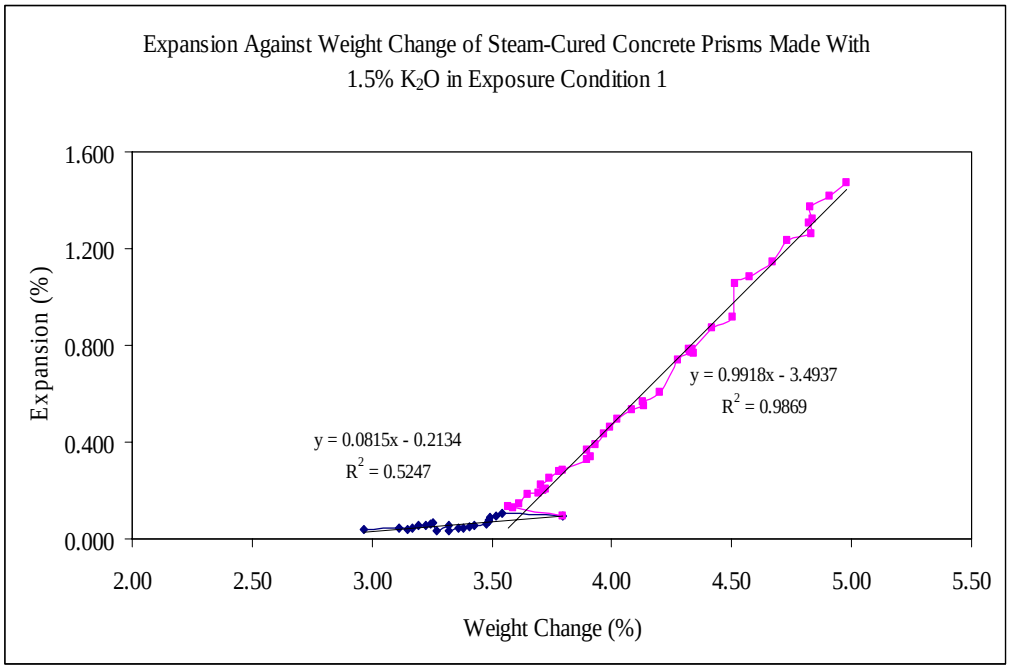


Figure 8.20: Expansion Against Weight Change of Steam-Cured Concrete Prisms Made With 1.5% $K_2O$ Subjected to Duggan Heat Cycle and Stored in Limewater (Regression Curves)

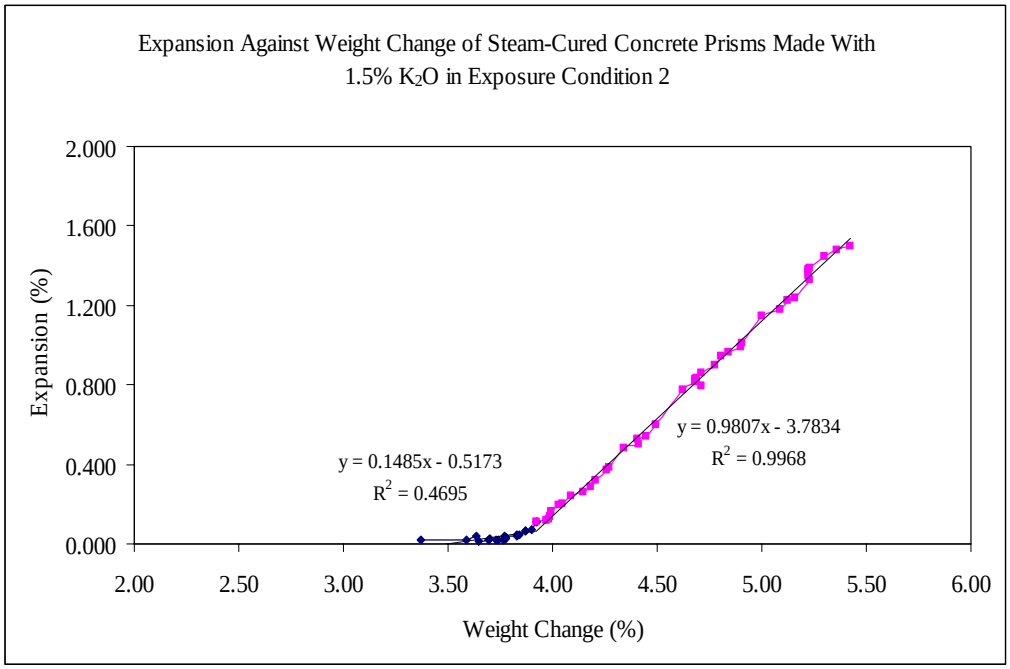


Figure 8.21: Expansion Against Weight-Change of Steam-Cured Concrete Prisms Made With 1.5% $K_2O$ Subjected to Duggan Heat Cycle and Stored in Plain Water at Room Temperature (Regression Curves)

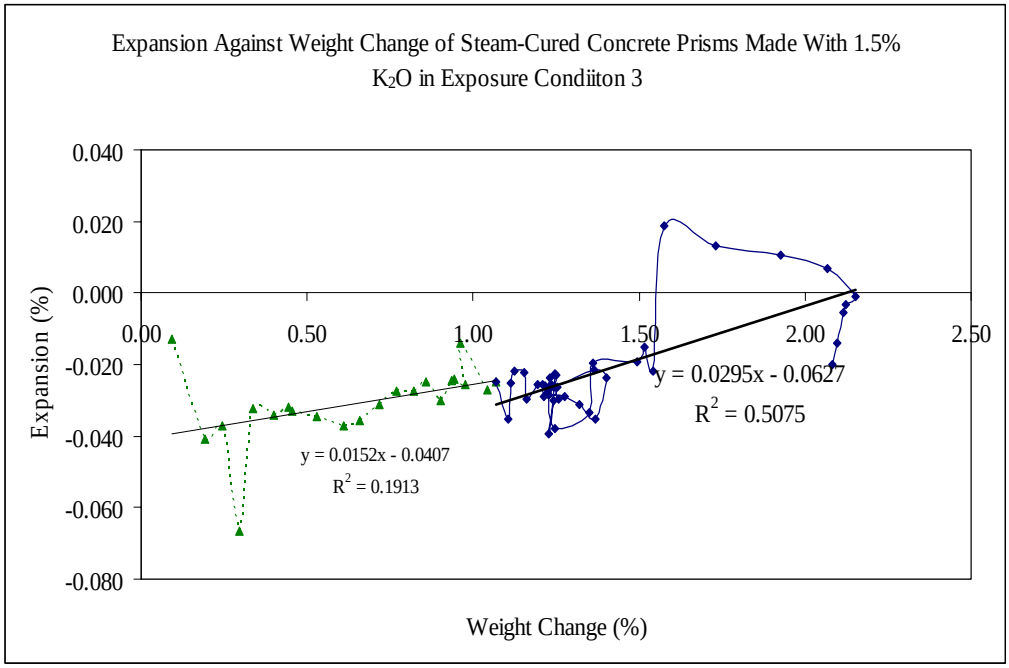


Figure 8.22: Expansion Against Weight Change of Steam-Cured Concrete Prisms Made With 1.5% $K_2O$ Subjected to Duggan Heat Cycle and Stored in Moist Air Chamber, R.H maintained at 97% (Regression Curves)

Table 8.4: Linear Equations for Expansion vs. Weight Change of Steam-Cured Concrete Prisms Made With 1.5% $K_2O$ Subjected to Duggan Heat Cycle and Stored Under Different Exposure Conditions

| Phase 4 (Concrete Prisms Made With 1.5% $K_2O$ - Subjected to Duggan Heat Cycle) | | | | |
|---|---|---|---|---|
| | | | | |
| Exp. Cond. 1 | Curve 1 | Day 1 - 127 | y = 0.0815x + 0.0662 | $R^2$ = 0.5247 |
| | Curve 2 | Day 104 - 624 | y = 0.8569x - 2.7557 | $R^2$ = 0.9848 |
| | | | | |
| Exp. Cond. 2 | Curve 1 | Day 1 - 127 | y = 0.1485x - 0.5173 | $R^2$ = 0.4695 |
| | Curve 2 | Day 104 - 624 | y = 0.9807x - 3.7834 | $R^2$ = 0.9968 |
| | | | | |
| Exp. Cond. 3 | Curve 1 | Day 1 - 127 | y = 0.0311x - 0.0549 | $R^2$ = 0.1184 |
| | Curve 2 | Day 104 - 624 | y = 0.0295x - 0.0627 | $R^2$ = 0.5075 |
| | | | | |

*8.6.2 Expansion and Weight Change of Concrete Prisms Made With 1.5% $K_2O$ and Subjected to Different Treatments*

Figures 8.23 and 24 showed expansion against weight-change data of the concrete prisms made with 1.5% $K_2O$ and subjected to the Duggan heat and Freeze-Thaw cycles respectively. Little or no correlation was discovered between the expansion and weight-change experimental results.

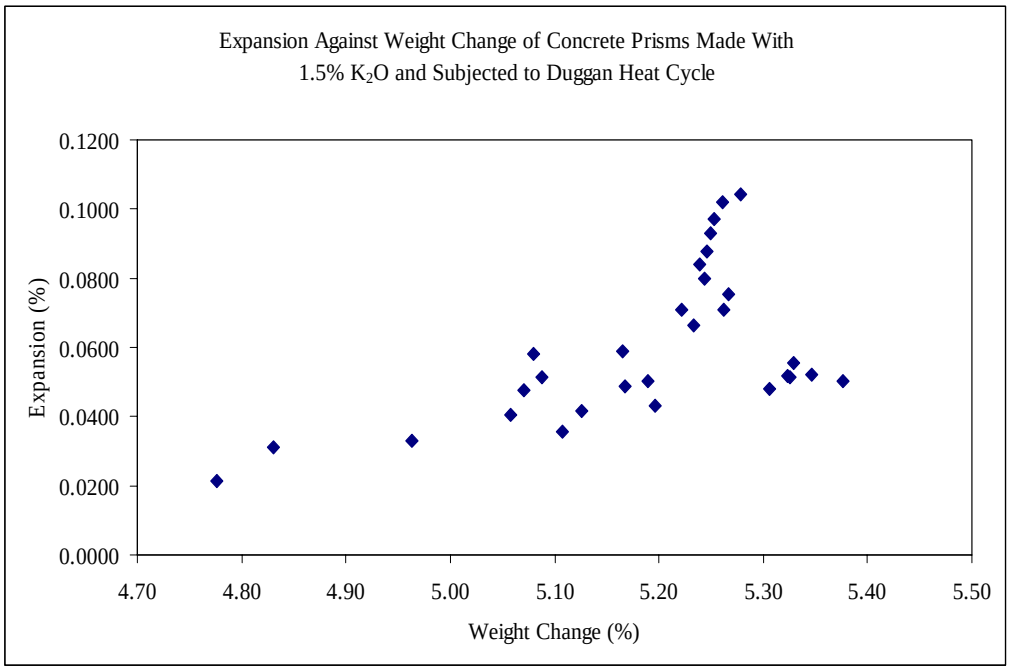


Figure 8.23: Expansion Against Weight Change of Room Temperature-Cured Concrete Prisms Made With 1.5% $K_2O$ Subjected to Duggan Heat Cycles and Stored in Limewater

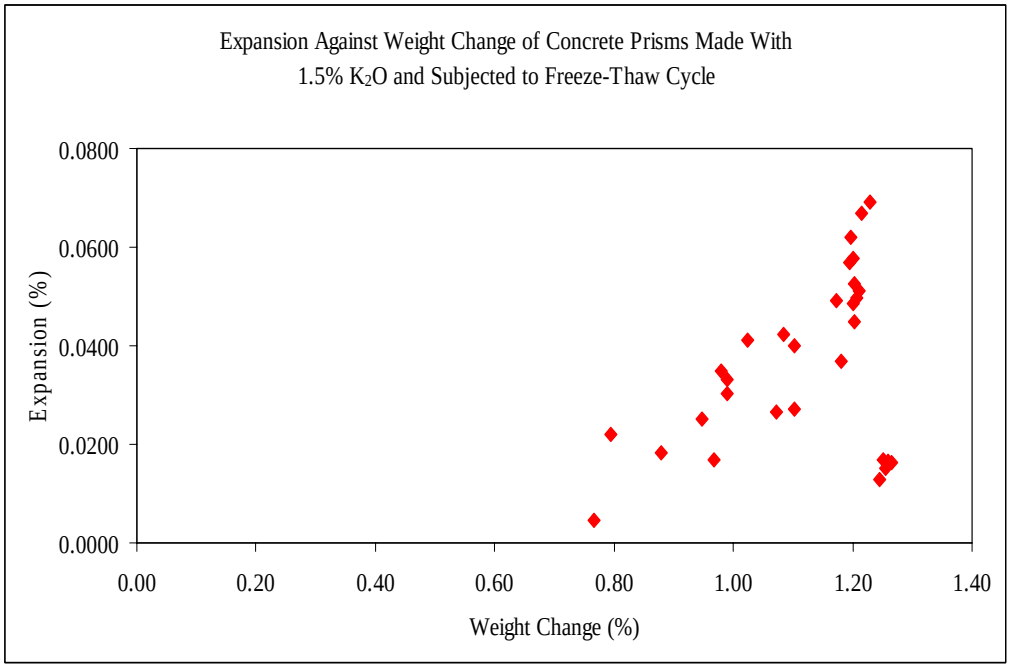


Figure 8.24: Expansion Against Weight Change of Room Temperature-Cured Concrete Prisms Made With 1.5% $K_2O$ Subjected to Freeze-Thaw Cycles and Stored in Limewater

## *8.7 Compressive Strength Results*

### *8.7.1 Effect of Exposure Conditions on Compressive Strength of Concrete Made With 1.5% $K_2O$*

The compressive strength of these concrete cylinders made with 1.5% $K_2O$ subjected to different exposure conditions is shown in figure 8.25. The concrete samples were steam-cured prior to subjecting them to the Duggan heat and subsequent storage in the different exposure conditions. After 28 days, the compressive strength of the concrete cylinders was 4521 psi, 4166 psi and 4885 psi for exposure conditions 1, 2 and 3 respectively. At 540 days of compressive strength tests, exposure conditions 1 and 2 showed up to 90% reduction while exposure condition 3 revealed a 25% increase. These results of compressive strength tests indicated that there is a reduction due to an increase in potassium content. In addition, the compressive strength of the concrete cylinders in exposure conditions 1 and 2 decreased with time. Much map cracking was found at later stages in the concrete cylinders in exposure conditions 1 and 2. This contributed to the low compressive strength results at later stages. SEM and EDAX analysis correlated with these results showed massive ettringite crystals found in the concrete at later ages. Table 8.5 provides the average compressive strength and standard deviations of the concrete samples made with 1.5% $K_2O$.

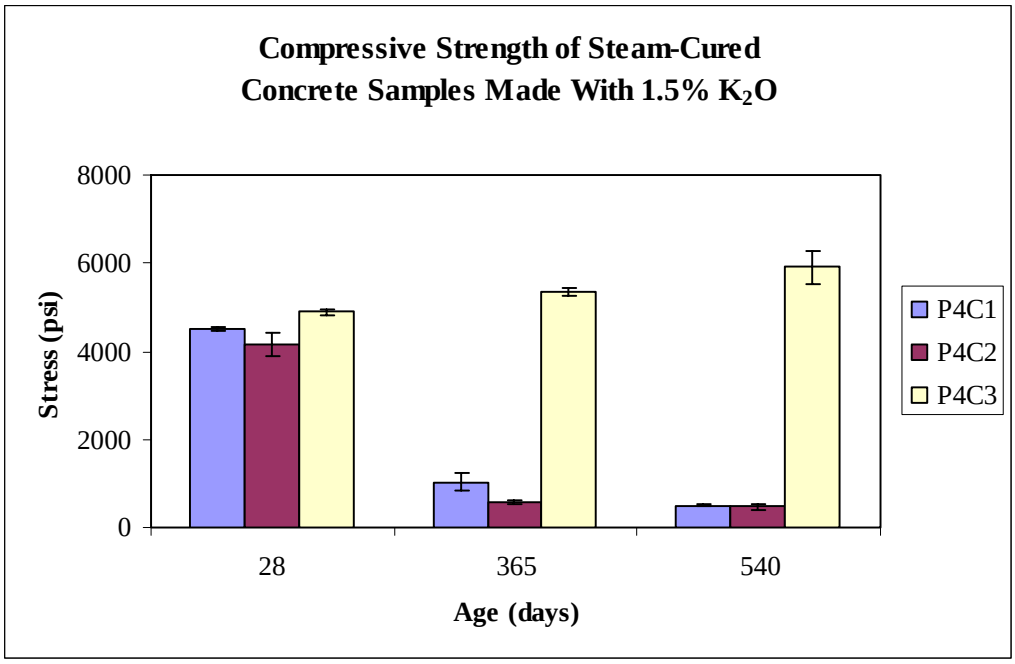


Figure 8.25: Compressive Strength Chart of Steam-Cured Concrete Samples Made With 1.5% $K_2O$ Subjected to Duggan Heat Cycle and Stored Under Different Exposure Conditions

Table 8.5: Compressive Strength of Steam-Cured Concrete Samples Made With 1.5% $K_2O$ Subjected to Duggan Heat Cycle and Stored Under Different Exposure Conditions

| | Average Compressive Strength (psi) | | |
|---|---|---|---|
| | 28 Days | 365 Days | 540 Days |
| | Std | Std | Std |
| P4C1 | 4521 | 1033 | 501 |
| | 46 | 195 | 24 |
| P4C2 | 4166 | 580 | 472 |
| | 268 | 35 | 66 |
| P4C3 | 4885 | 5349 | 5907 |
| | 63 | 70 | 366 |

*8.7.2 Effect of Concrete Treatments on Compressive Strength of Concrete Made With 1.5% $K_2O$*

Compressive strength was tested to determine the effect of different concrete treatments and the increase of potassium content to the durability of concrete. The concrete samples were room temperature-cured before subjecting them to either Duggan heat or Freeze-Thaw cycle and subsequently storing them in isothermal water bath, pH maintained at 12.5 – limewater. Compressive strength testing was employed at 28 days, 240 days and 365 days for the Duggan or Freeze-Thaw cycles treated concrete samples made with 1.5% $K_2O$. The compressive strength at 28 days was 4776 psi and 5022 psi for the Duggan heat and Freeze-Thaw cycles treated concrete respectively. Compressive strength results at one year were 5570psi and 6339 psi for the Duggan heat and Freeze-Thaw treated concrete respectively. These results indicated that the compressive strength of the concrete samples made with 1.5% $K_2O$ and then subjected to different treatments had higher strength at later ages. The measured compressive strengths of the Duggan heat and Free-Thaw cycles treated concrete made with 1.5% $K_2O$ are shown in figure 8.26. Table 8.6 illustrates the compressive strength and standard deviation of the test results.

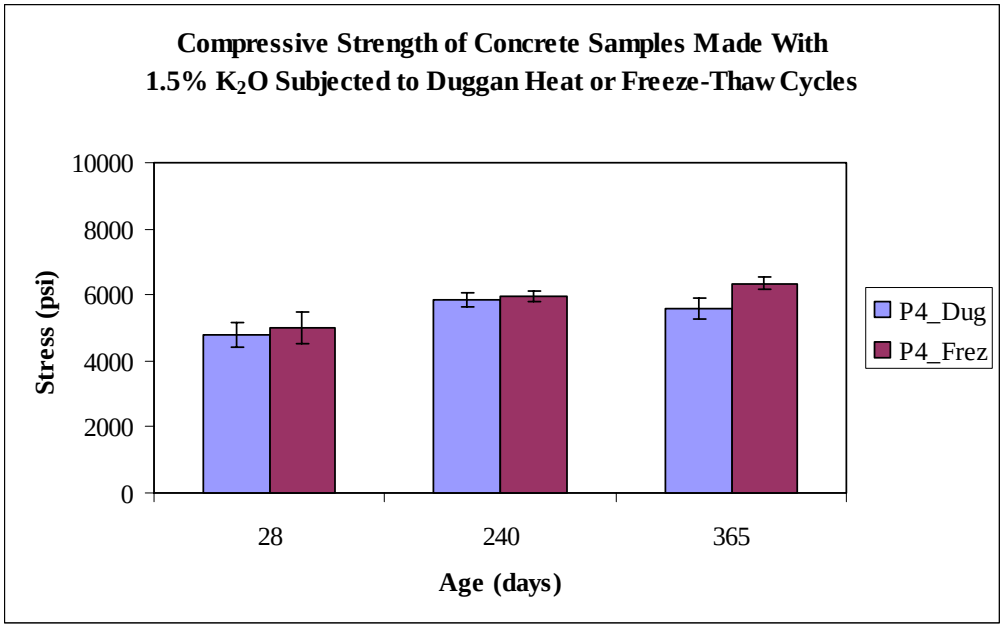


Figure 8.26: Compressive Strength Chart of Room Temperature-Cured Concrete Samples Made With 1.5% $K_2O$ Subjected to Duggan Heat or Freeze-Thaw Cycles and Stored in Limewater

Table 8.6: Compressive Strength of Concrete Samples Made With 1.5% $K_2O$ Subjected to Duggan Heat or Freeze-Thaw Cycles and Stored Limewater

| | Average Compressive Strength (psi) | | |
|---|---|---|---|
| | 28 Days | 240 Days | 365 Days |
| | Std | Std | Std |
| P4_Dug | 4776 | 5834 | 5570 |
| | 362 | 221 | 309 |
| P4_Frez | 5022 | 5959 | 6339 |
| | 479 | 180 | 193 |

*8.7.3 Effect of Moisture Content on Compressive Strength of Concrete Made With 1.5% $K_2O$*

Figure 8.27 shows the compressive strengths of the room temperature-cured concrete samples made with 1.5% $K_2O$, and subsequently subjected to the Duggan heat cycle before storing them in exposure condition 1. The compressive strengths were tested to determine the effect of moisture content on concrete samples subjected to Duggan heat cycle. The compressive strengths at 40 days were 4397 psi and 5797 psi for the moist and dry concrete cylinders. There was up to a 25% increase in the compressive strengths at later stages in both sets. Table 8.7 gives a summary of the compressive strengths and standard deviations of the tested concrete samples.

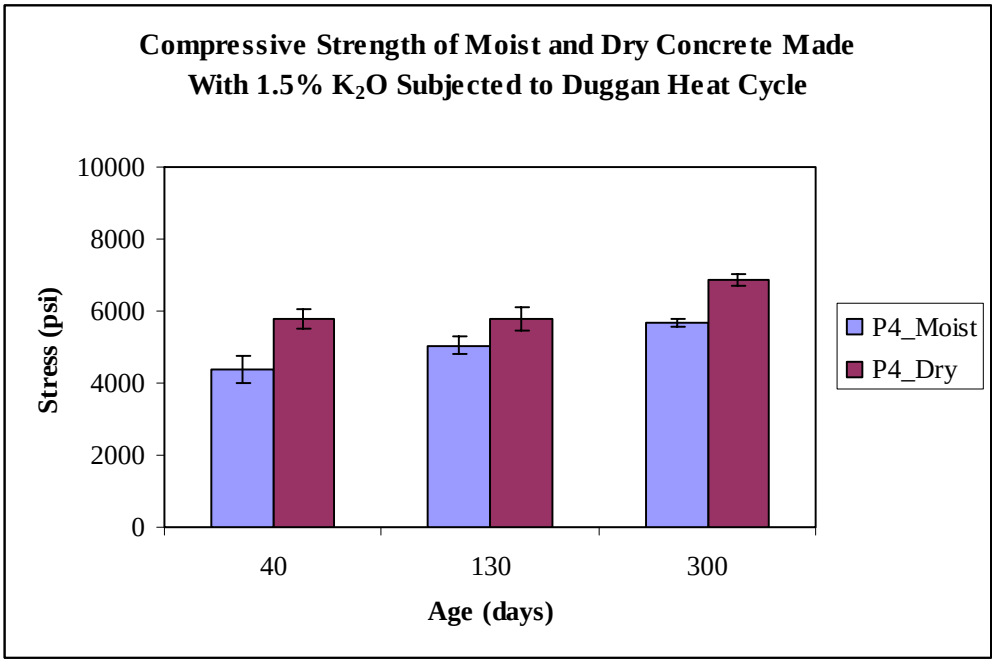


Figure 8.27: Compressive Strength Chart of Moist or Dry Room Temperature-Cured Concrete Samples Made With 1.5% $K_2O$ Subjected to Duggan Heat Cycles and Stored in Isothermal Water Bath, pH maintained at 12.5 - Limewater

Table 8.7: Compressive Strength of Moist or Dry Concrete Samples Made With 1.5% $K_2O$ Subjected to Duggan Heat Cycles and Stored in Limewater

| | Average Compressive Strength (psi) | | |
|---|---|---|---|
| | 40 Days | 130 Days | 300 Days |
| | Std | Std | Std |
| P4_Moist | 4397 | 5042 | 5685 |
| | 376 | 251 | 105 |
| P4_Dry | 5797 | 5780 | 6853 |
| | 278 | 307 | 153 |

*8.8 Concrete Field Samples Made With 1.5% $K_2O$ (No Duggan Heat Cycle)*

Again, two (2) sets of concrete mixes made with 1.5% $K_2O$ were prepared in laboratory and then stored outside under atmospheric conditions. The concrete samples were either steam-cured at 85$^{o}$C (P4C4A) or room temperature-cured (P4C4A). No Duggan heat cycle was employed in any of the concrete samples subjected to field conditions.

*8.8.1 Length Change Results*

The shrinkage values and shrinkage rates of the concrete prisms made with 1.5% $K_2O$ is shown in figures 8.28 and 8.29 respectively. The steam-cured concrete prisms (P4C4A) exhibited expansion during the entire research study. The highest expansion of the steam-cured concrete prisms was 0.0410% and occurred at about 280 days after subjecting the concrete samples to field conditions. The changes in environment such as humidity, ambient temperature, etc., influenced the test parameters of the field-exposed concrete samples. Cracking of the concrete samples

was not detected visually. Figures 8.30 and 8.31 illustrate the linear regression equations used for the best fit of the results. Linear regression analysis of the shrinkage values over time revealed no correlation. Table 8.8 gives the linear regression equations for the best fit to the experimental data.

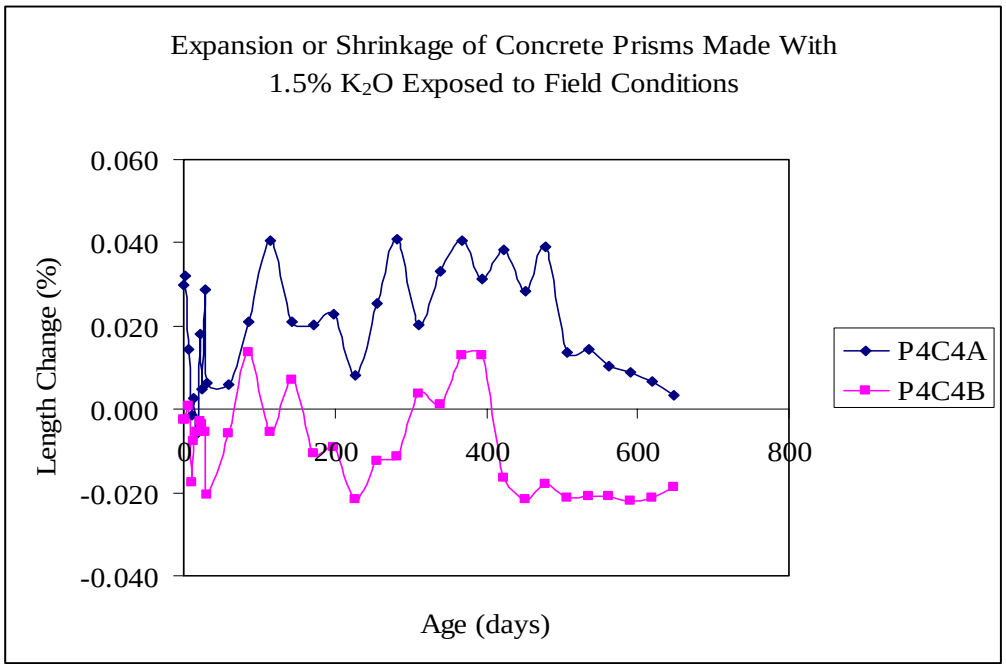


Figure 8.28: Length Change of Concrete Prisms Made With 1.5% $K_2O$ Exposed to Field Conditions

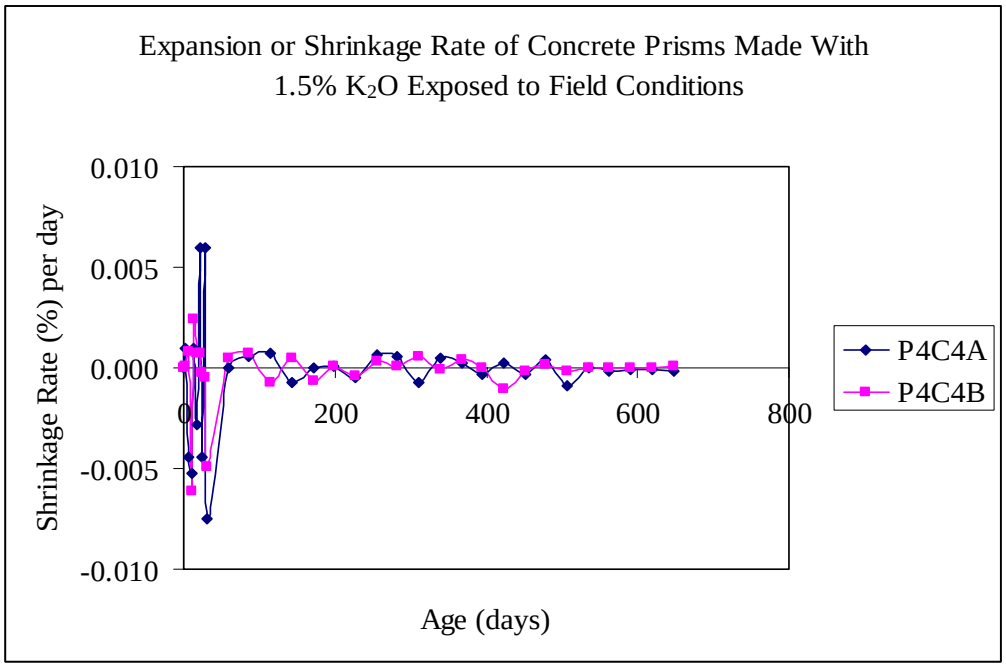


Figure 8.29: Shrinkage Rate of Concrete Prisms Made With 1.5% $K_2O$ Exposed to Field Conditions

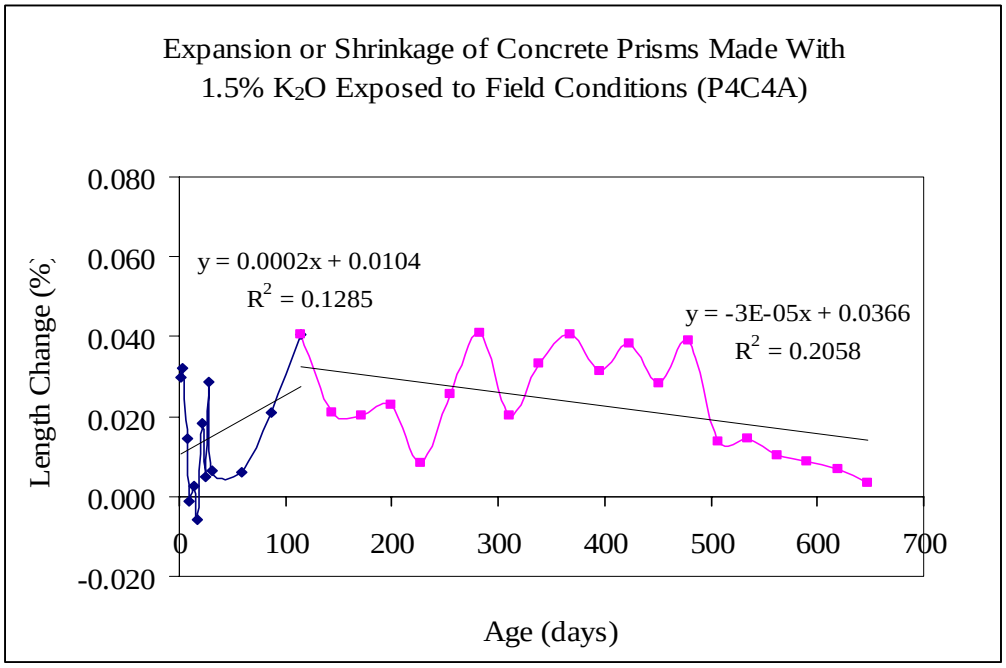


Figure 8.30: Length Change vs. Age of Steam-Cured Concrete Prisms Made With .5% $K_2O$ and Stored Under Field Conditions (C4A) (Regression Curves)

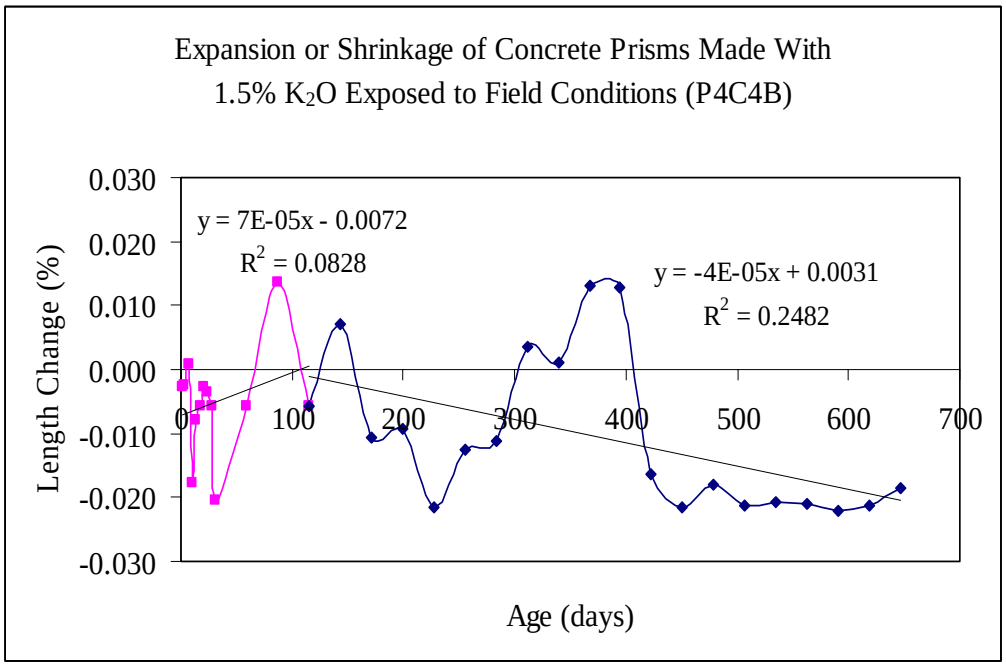


Figure 8.31: Length Change vs. Age of Room Temperature-Cured Concrete Samples Made With 1.5% $K_2O$ and Stored Under Field Conditions (C4B) (Regression Curves)

Table 8.8: Linear Equations for Length Change vs. Age of Concrete Prisms Made With 1.5% $K_2O$ Stored Under Field Conditions

| Phase 4 (Concrete Samples Made With 1.5% $K_2O$ and Exposed to Field Conditions) | | | | |
|---|---|---|---|---|
| | | | | |
| Exp. Cond. 4A | Curve 1 | Day 1 - 115 | y = 0.0002x + 0.0104 | $R^2$ = 0.1285 |
| | Curve 2 | Day 115 - 647 | y = -7E-05x + 0.041 | $R^2$ = 0.0762 |
| | | | | |
| Exp. Cond. 4B | Curve 1 | Day 1 - 115 | y = 7E-05x - 0.0072 | $R^2$ = 0.0828 |
| | Curve 2 | Day 115 - 647 | y = -6E-05x + 0.0033 | $R^2$ = 0.0502 |
| | | | | |

*8.8.2 Weight Change Results*

Figure 8.32 shows the weight-change results for the field-exposed concrete prisms made with 1.5% $K_2O$. Again, both sets of concrete prisms showed a decrease in weight change over time for the research duration. The room temperature-cured concrete prisms exhibited higher weight-change values than the steam-cured concrete prisms. The weight-change results were fitted with linear regression equations, and no correlation was observed. Figures 8.33 and 8.34 show the linear regression equation used for the analysis of experimental data. A summary of the linear regression equations is given in table 8.9.

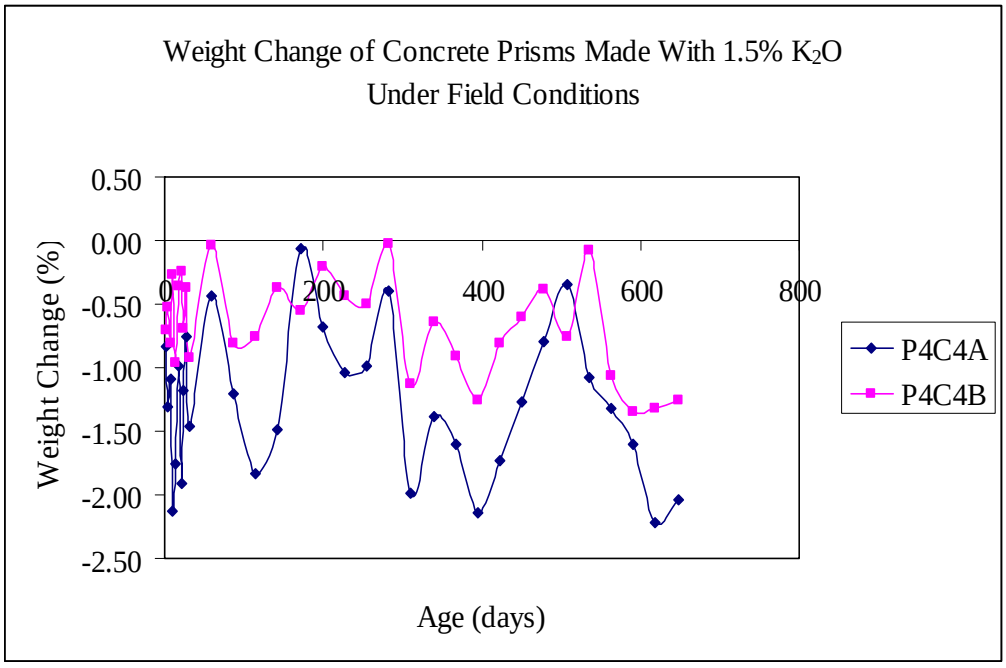


Figure 8.32: Weight Change of Concrete Prisms Made With 1.5% $K_2O$ Exposed to Field Conditions

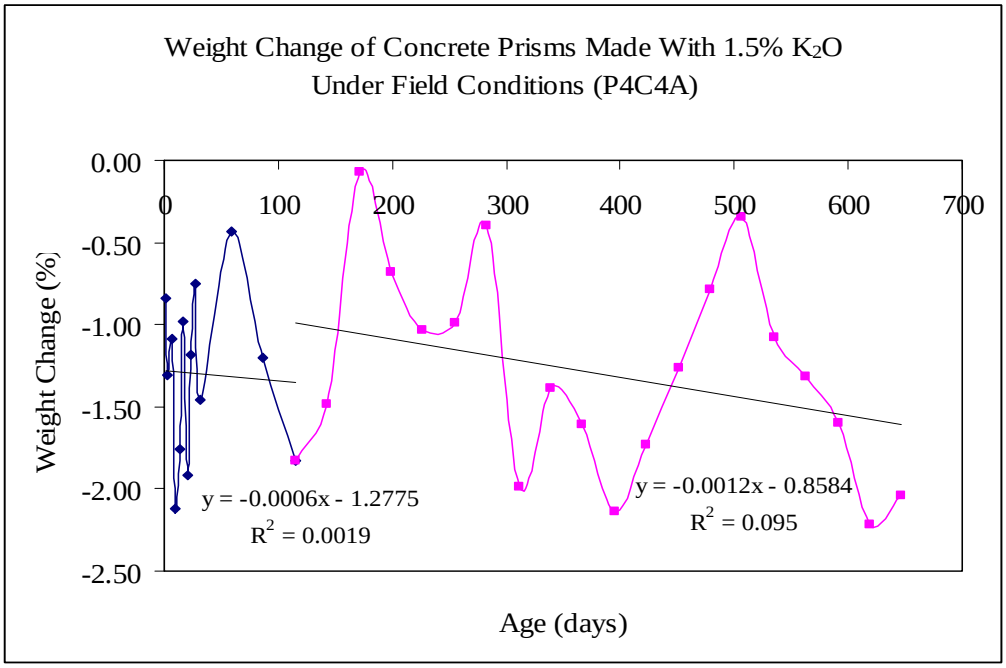


Figure 8.33: Weight Change vs. Age of Steam-Cured Concrete Prisms Made With 1.5% $K_2O$ and Stored Under Field Conditions (C4A) (Regression Curves)

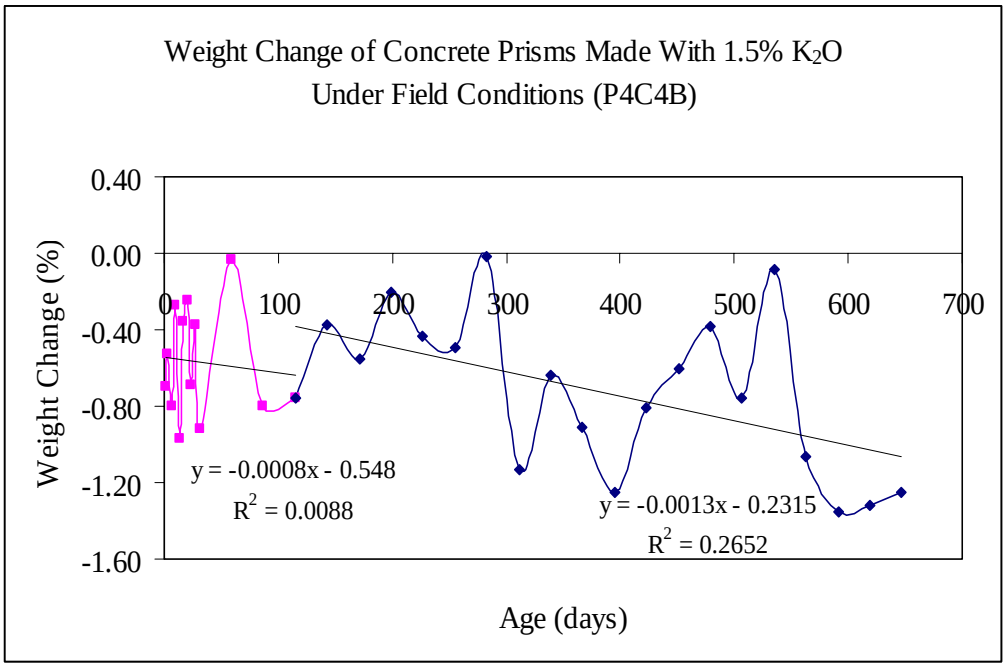


Figure 8.34: Weight Change vs. Age of Room Temperature-Cured Concrete Prisms Made With 1.5% $K_2O$ and Stored Under Field Conditions (C4B) (Regression Curves)

Table 8.9: Linear Equations for Weight Change vs. Age of Concrete Prisms Made With 1.5% $K_2O$ Stored Under Field Conditions

| Phase 4 (Concrete Field Samples Made With 1.5% $K_2O$) | | | | |
|---|---|---|---|---|
| | | | | |
| Exp. Cond. 4A | Curve 1 | Day 1 - 115 | y = -0.0006x - 1.2775 | $R^2$ = 0.0019 |
| | Curve 2 | Day 115 - 647 | y = -0.0012x - 0.8584 | $R^2$ = 0.095 |
| | | | | |
| Exp. Cond. 4B | Curve 1 | Day 1 - 115 | y = -0.0008x - 0.548 | $R^2$ = 0.0088 |
| | Curve 2 | Day 115 - 647 | y = -0.0013x - 0.2315 | $R^2$ = 0.2652 |
| | | | | |

*8.8.3 Compressive Strength Results*

Compressive strength was employed at 28 days, 365 days and 540 days for both sets of field-exposed concrete samples made with 1.5% $K_2O$. This was to determine the effect of increasing the potassium content ($K_2O$) to the durability of the concrete. The compressive strengths at 28 days were 4938 psi and 4776 psi for the steam-cured and room temperature-cured concrete samples respectively. Compressive strength tests carried out at later ages revealed an increase in strength for both sets of concrete samples subjected to field conditions. Figure 8.35 shows a bar chart of the compressive strengths of the concrete samples made with 1.5% $K_2O$, and table 8.10 provides a summary of the results.

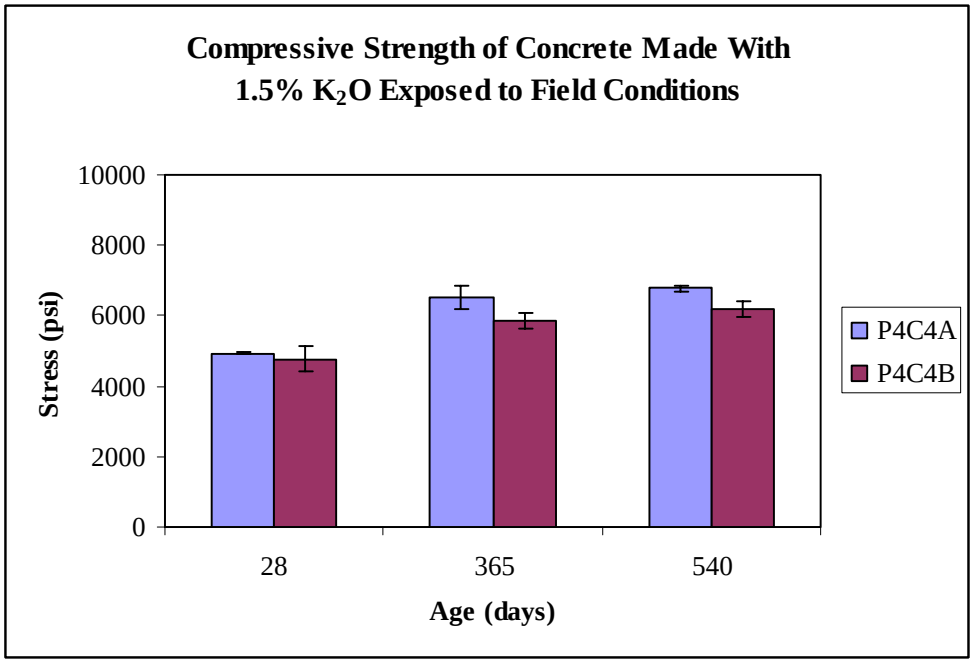


Figure 8.35: Compressive Strength Chart of Concrete Samples Made With 1.5% $K_2O$ Exposed to Field Conditions

Table 8.10: Compressive Strength of Concrete Samples Made With 1.5% $K_2O$ Exposed to Field Conditions

| | Average Compressive Strength (psi) | | |
|---|---|---|---|
| | 28 Days | 365 Days | 540 Days |
| | Std | Std | Std |
| P4C4A | 4938 | 6537 | 6781 |
| | 32 | 338 | 96 |
| P4C4B | 4776 | 5834 | 6180 |
| | 362 | 221 | 226 |

*8.9 Water Analysis Results of the Storage Solutions*

Again, water analysis was performed using ion selective electrodes (ISE) and an ISE meter to obtain readings of the ion concentrations in the storage solutions. Potassium ($K^+$), Sodium ($Na^+$) and Calcium ($Ca^{2+}$) ion concentrations in the storage solutions were monitored periodically for depletion of alkali content. The concrete prisms in storage solutions with high alkali concentration exhibited high expansion rates and values. These results correlated with the SEM examinations revealed that alkali leaching enhanced the formation of ettringite.

*8.9.1 Water Analysis of Exposure Condition 1*

Concrete samples made with 1.5% $K_2O$ were stored in isothermal water bath, pH maintained at 12.5 (exposure condition 1), and the leaching of $Na^+$ (sodium) and $K^+$ (potassium) into the storage solution was periodically monitored. The highest concentration of alkalis leached from the concrete samples was about 363 mmol/l for the test duration. A plateau seems to have been reached after 300 days of storage from the end of the Duggan heat cycle. Figure 8.36 shows the alkalis concentration against age for the concrete samples made with 1.5% $K_2O$ in exposure condition 1.

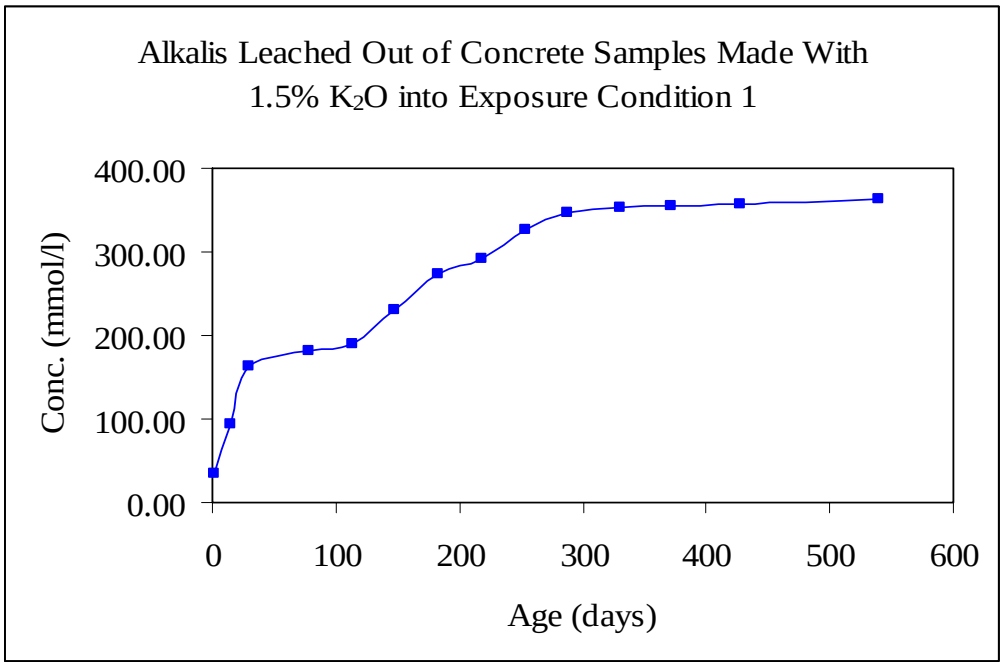


Figure 8.36: Alkalis Leaching from Concrete Samples Made With 1.5% $K_2O$ and Stored in Isothermal Water Bath, pH maintained at 12.5 - limewater

*8.9.2 Water Analysis of Exposure Condition 2*

The concrete samples made with 1.5% $K_2O$ and subsequently stored in exposure condition 2 (plain water at room temperature) are monitored for pH value, $Na^+$, $K^+$ and $Ca^{2+}$ ion concentrations. The presence of alkalis is believed to affect the solubilities of the reactants (e.g., $C_3A$, CH and $CSH_2$) in the $C_3A - CSH_2 - CH - H_2O$ system and hence the concentrations of the dissolved ions (e.g., $OH^-$, $SO_4^{2-}$, $Ca^{2+}$, etc.). The alkalis apparently could increase the formation of ettringite and decrease the solubility of calcium hydroxide (CH) (Daerr 1977, Wang et al., 1986 and Way et al., 1989).

*8.9.2.1 Amount of Alkalis*

Figure 8.37 shows the alkalis concentration leached from the concrete samples into the storage solution of exposure condition 2. The alkalis concentration of the storage solution increases with time. At 500 days of storage, the alkalis concentration was about 360 mmol/l. The expansion rates and values of the totally submerged concrete prisms increases with an increase in alkali concentration of the storage solutions.

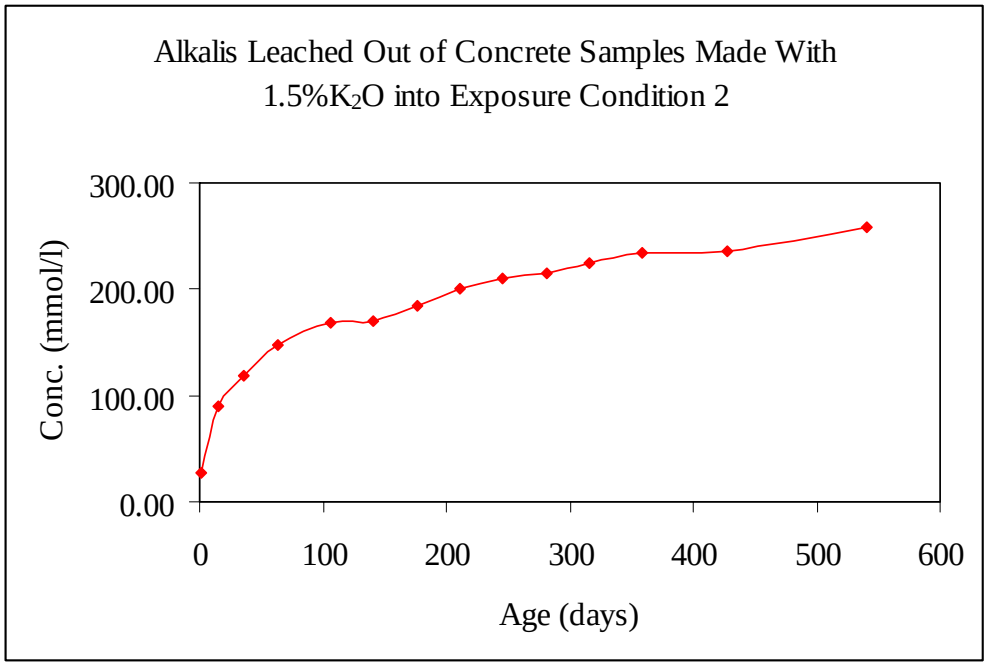


Figure 8.37: Alkalis Leaching from Concrete Samples Made With 1.5% $K_2O$ and Stored in Plain Water at Room Temperature

*8.9.2.2 pH Value*

Hampson and Bailey found that the pH value has effects on the morphology of ettringite (1982). It was concluded that at pH 11.5 to 11.8, sulphoaluminate forms as ettringite crystals and at pH 12.5 to 12.8, some non-crystalline materials may form

with a composition similar to ettringite. The pH value of the storage solution ranged from 9.01 to 11.57 for the test duration. A decrease in pH of the mortar system due to alkali leaching may favor the conversion from monosulfate to renewed ettringite (Shimada, 2005).

*8.9.2.3 Calcium Concentration*

The calcium concentration of the storage solution seems to plateau after the first 100 days of storage. The presence of the calcium hydroxide [$Ca(OH)_2$] ions is essential for sodium and other ions to penetrate into the reacting grain. This influences the expansion rate of the concrete samples. Figure 8.38 illustrates the calcium concentration of the storage solution for exposure condition 2.

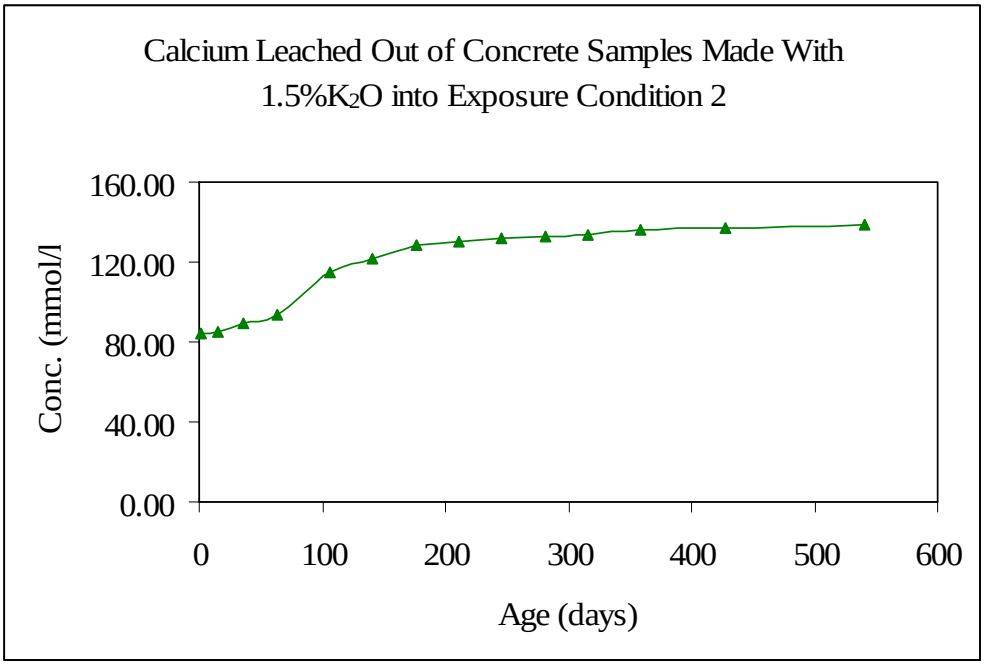


Figure 8.38: Calcium Leaching from Concrete Samples Made With 1.5% $K_2O$ and Stored in Plain Water at Room Temperature

*8.10 Laser Shearography (LAS)*

Concrete prisms made with 1.5% potassium content ($K_2O$) were prepared for laser shearography. This was done to determine the effect of increasing potassium content on the tendency for early shrinkage cracking in concrete specimens. Again, laser shearography images were collected at specific intervals to provide insights into the mechanisms of cracking.

*8.10.1 Laser Shearography Analysis of Concrete Prisms Made With 1.5% $K_2O$ and Stored in Exposure Condition 3*

A concrete prism was subjected to the Duggan heat cycle before subsequently storing it in exposure condition 3 (R.H at 97%). Few isolated cracks were found on the concrete's top face after the steam curing prior to the Duggan heat cycle. After subjecting the concrete prism to the Duggan heat cycle and storing in exposure condition 3, a significant amount of microcracks were revealed throughout the prism. The high potassium content ($K_2O$) of the concrete prism might also influence the formation of microcracks at the early stages. Figure 8.39 provides the laser shearography image of the concrete prism after the Duggan heat cycle. The laser shearography is processed using a series of algorithms with Image Pro Plus which enhanced the data acquisition. Figure 8.40 shows the processed laser shearography image shown in figure 8.39.

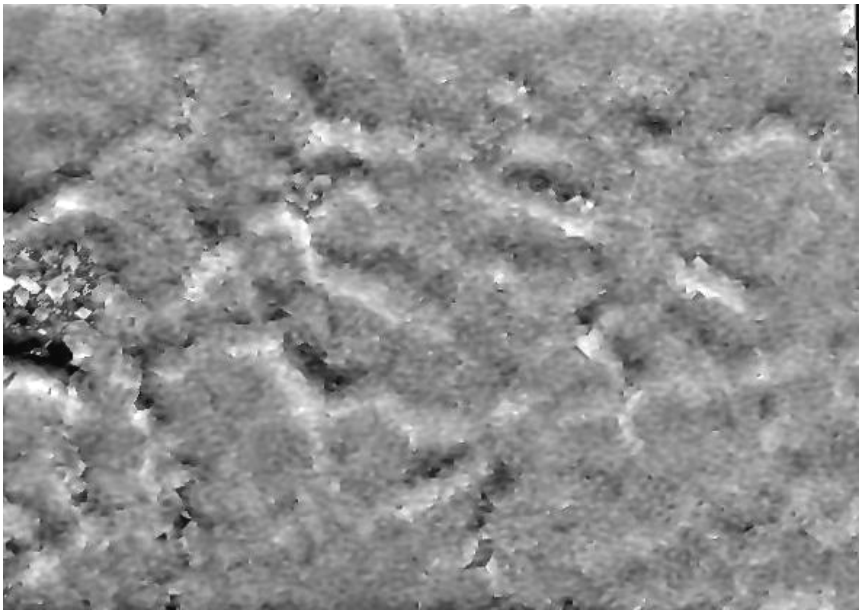

Figure 8.39: Shearography Image of Concrete Prism Surface Subjected to the Duggan Heat Cycle (Height = 7.6 cm ~ 3in.)

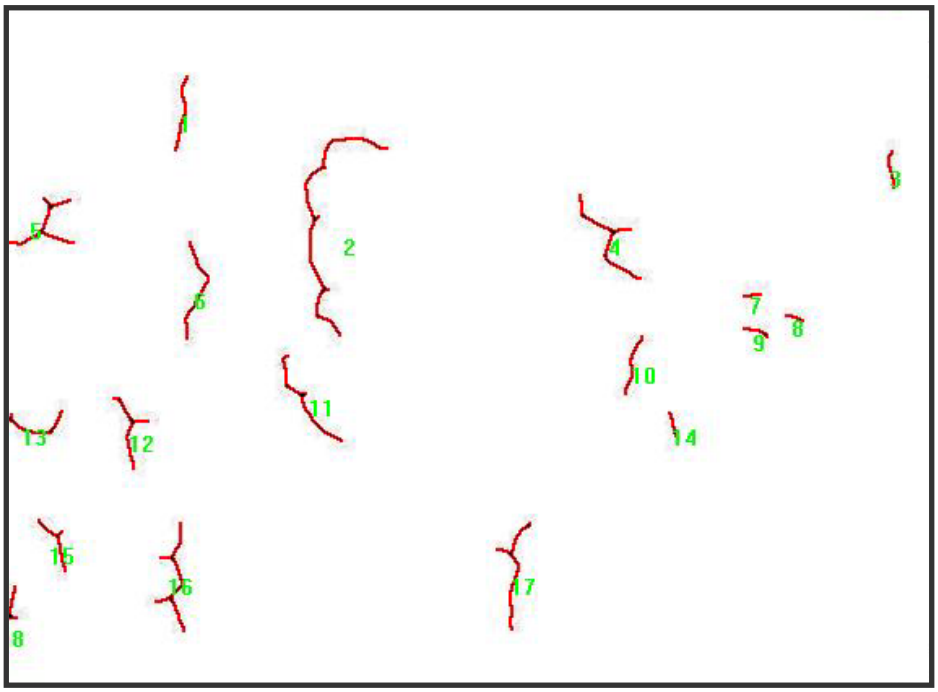


Figure 8.40: Processed Laser Shearography Image of Figure 8.39 (P4C3 Face 1 Sec 1)

The data for each of the faces was collected and analyzed. Spatial correlation was used to make a comparison between the laser shearography images over time. Laser shearography analysis was employed at later stages during the storage of the concrete prisms in exposure condition 3. Figure 8.41 illustrates a graph showing the density of cracks over time for the concrete prism. The cracks did not propagate at later stages, and this might due be to the lack of continuous access to water. Laser shearography tests at later stages showed few or no changes in the surface cracks density of the concrete prisms. Digital photo images were taken at about 600 days of storage, but no cracks could be captured.

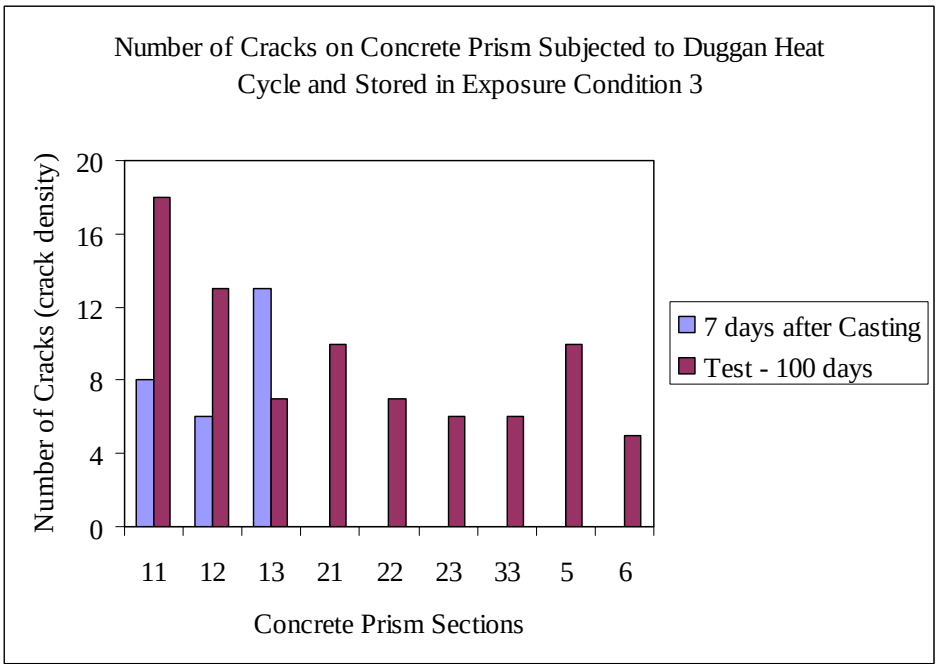


Figure 8.41: Number of Cracks on Surfaces of a Concrete Prism Made With 1.5% $K_2O$ Subjected to Duggan Heat Cycle and Stored in Exposure Condition 3

*8.10.2 Laser Shearography Analysis of Concrete Prisms Made With 1.5% $K_2O$ and Subjected to Different Treatments*

The concrete prisms made with 1.5% $K_2O$ were room temperature-cured in the laboratory and stored in limewater for six (6) days before treating them to either the Duggan heat or Freeze-Thaw cycles. No cracks were visible or identified by the laser shearography images before the concrete treatments. The concrete prisms show lots of cracks forming on the surfaces of the concrete prisms after the concrete treatments. This proves that the Duggan heat and Freeze-Thaw cycles do initiate microcracks in concrete. Figures 8.42 and 8.43 shows enhanced laser shearography images of the Duggan heat and Freeze-Thaw cycles treated concrete prisms respectively.

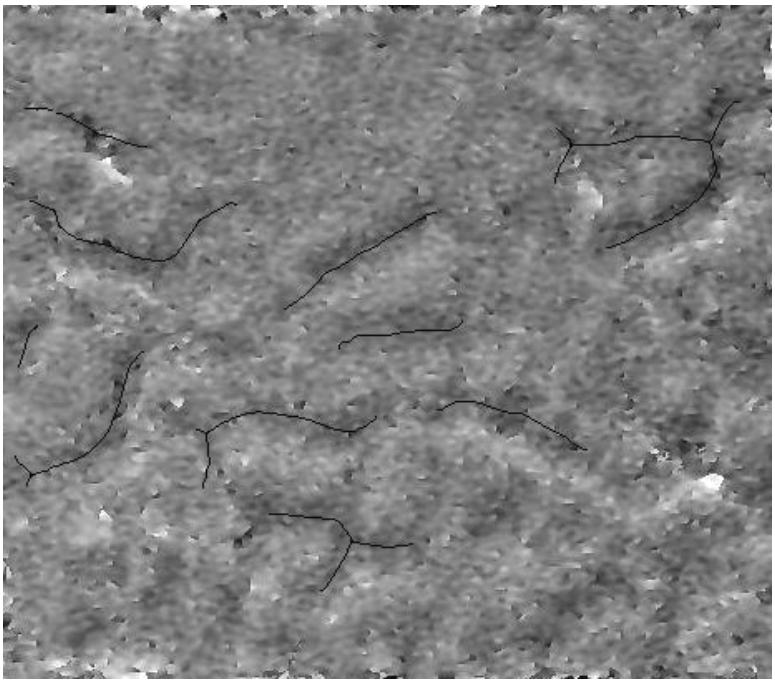

Figure 8.42: Enhanced Laser Shearography Image of Concrete Prism Surface After Duggan Heat Cycle Treatment (P4_Dug Face 2 Sec 2)

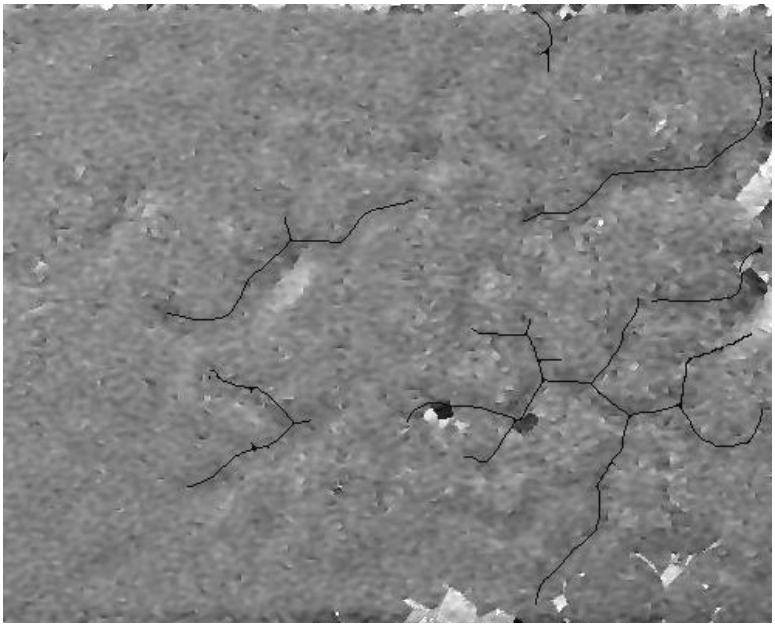

Figure 8.43: Enhanced Laser Shearography Image of Concrete Prism Surface After Freeze-Thaw Cycles Treatment (P4_Frez Face 1 Sec 1)

The Image Pro Plus results data showed the Duggan heat cycle treated concrete prism exhibited more cracked areas than the Freeze-Thaw treated concrete prism. This can be attributed to the higher expansion values exhibited by the concrete samples subjected to the Duggan heat cycle. There was a 50% increase in cracks for both sets of concrete prism after 100 days of storage in limewater. Tables 8.11 and 8.12 show the data results of the crack analysis on the concrete surfaces after 100 days in exposure condition 1 - limewater.

Table 8.11: Measurement Data Sheet for Concrete Prism Subjected to Duggan Heat Cycle and Stored for 100 Days in Limewater

| **Duggan Heat Cycle** | | | |
|---|---|---|---|
| **Face # Sec #** | **Crack Density** | **Crack Length (mm)** | **Area of Crack ($mm^2$)** |
| 11 | 7 | 6.8811 | 0.2516 |
| 12 | 10 | 7.7013 | 0.3034 |
| 13 | 11 | 8.5183 | 0.3105 |
| 21 | 13 | 8.2764 | 0.2570 |
| 22 | 8 | 9.4242 | 0.3513 |
| 23 | 12 | 6.2239 | 0.1924 |
| 31 | 0 | 0.0000 | 0.0000 |
| 32 | 10 | 6.9325 | 0.2696 |
| 33 | 10 | 7.0766 | 0.2811 |
| 41 | 6 | 4.6488 | 0.1608 |
| 42 | 0 | 0.0000 | 0.0000 |
| 43 | 0 | 0.0000 | 0.0000 |
| 5 | 9 | 5.7781 | 0.1607 |
| 6 | 11 | 6.6915 | 0.1901 |
| **Total** | **107** | **78.1528** | **2.7284** |

Table 8.12: Measurement Data Sheet for Concrete Prism Subjected to Freeze-Thaw Cycles and Stored for 100 Days in Limewater

| **Freeze-Thaw Cycle** | | | |
|---|---|---|---|
| **Face # Sec #** | **Crack Density** | **Crack Length (mm)** | **Area of Crack ($mm^2$)** |
| 11 | 6 | 7.0694 | 0.2377 |
| 12 | 9 | 6.9413 | 0.1955 |
| 13 | 8 | 4.3005 | 0.1046 |
| 22 | 8 | 6.6517 | 0.2567 |
| 23 | 15 | 7.2582 | 0.2203 |
| 32 | 20 | 10.7121 | 0.3040 |
| 33 | 17 | 8.2995 | 0.1916 |
| 41 | 13 | 9.4278 | 0.1967 |
| 42 | 12 | 9.1405 | 0.2208 |
| 43 | 21 | 12.4061 | 0.3878 |
| 5 | 7 | 5.6324 | 0.1301 |
| 6 | 8 | 4.7069 | 0.1510 |
| **Total** | **144** | **92.5466** | **2.5966** |

*8.11 Microstructure Analysis Using SEM and EDAX*

The SEM and EDAX analysis was used to determine the chemical composition of the mineral deposits, within the microstructure of the concrete samples made with 1.5% $K_2O$, which were subjected to different treatments and subsequently stored under different exposure conditions throughout the research. The samples were prepared as fractured surfaces and coated using carbon. Fracturing the concrete specimens using hammer introduces additional cracks, and the fractured surfaces cannot be used to study the crack patterns in the cement paste matrix or the cracking of the aggregate. Laser shearography (LAS), a nondestructive testing, was used to detect the cracks in the concrete. Representative concrete samples from each of the exposure conditions were tested to identify the deterioration mechanism and to differentiate between ettringite formation and morphology.

*8.11.1 SEM and EDAX Analysis of Concrete Specimens Stored in Different Exposure Conditions*

*8.11.1.1 Concrete Samples in Exposure Condition 1*

SEM examinations at 40 days of storage in water, pH maintained at 12.5 (Exp. Cond. 1), showed lots of ettringite spherical balls covering the whole specimen. Figure 8.44 shows an air void with ettringite balls. EDAX analysis revealed ettringite with chemical composition of Al = 2.05% wt., Si = 10.49% wt., S = 3.40% wt., and Ca = 79.41% wt.

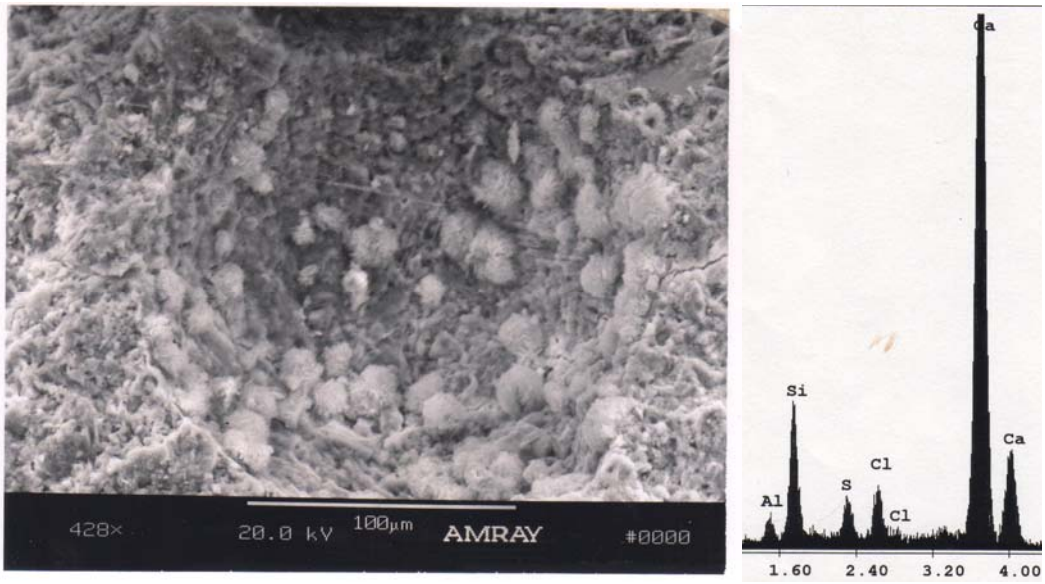


Figure 8.44: SEM and EDAX Analysis of Concrete Specimen Made With 1.5% $K_2O$ and Stored in Exposure Condition 1 at Age of 40 Days, Showing Ettringite Spherical Balls Filing an Air Void

Relatively large bundles of ettringite needles were discovered during the 100 days SEM investigation. The ettringite needles were randomly oriented filling the cavity and air voids of the concrete specimens. EDAX elemental analysis of the needles shows a typical composition and characteristics of ettringite. Figure 8.45 illustrates the SEM and EDAX analysis of the concrete specimen after 100 days of storage in exposure condition 1.

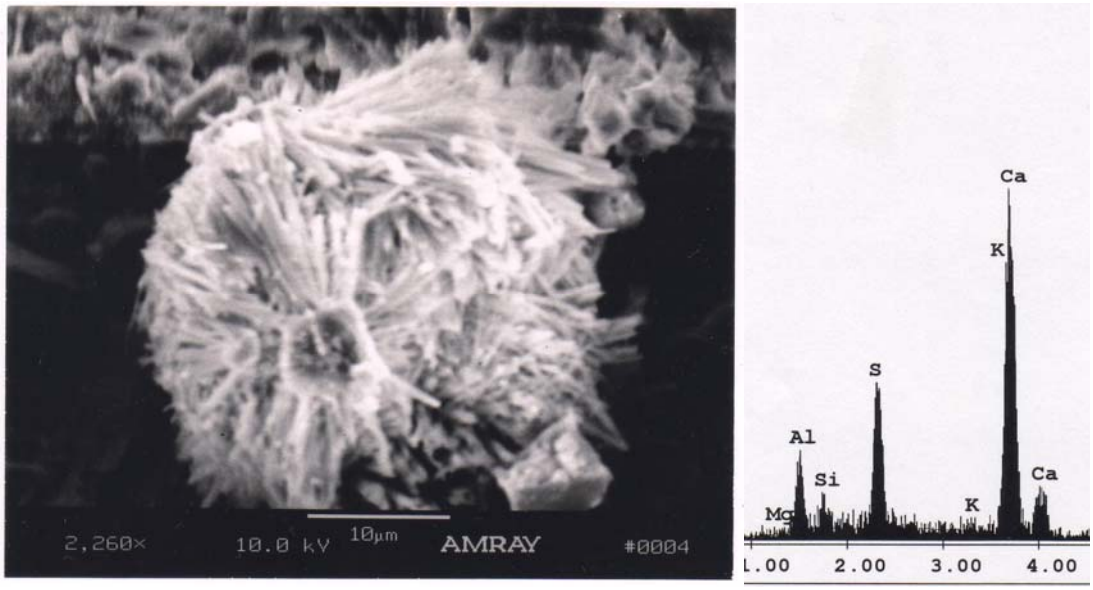


Figure 8.45: SEM and EDAX Analysis of Concrete Specimen Made With 1.5% $K_2O$ and Stored in Exposure Condition 1 at Age of 100 Days, Showing Bundles of Randomly Oriented Ettringite Needles Filling a Cavity

Figure 8.46 shows prismatic ettringite needles filling a cavity of the examined concrete specimen. The EDAX spectrum could not be obtained due to the low intensity of the ettringite deposits. Observation of the SEM micrograph revealed mineral deposits characteristic of ettringite morphology. Further SEM examinations of the same concrete specimens revealed ettringite deposits on sand and limestone aggregate particles.


Figure 8.46: SEM Micrograph of Concrete Specimen Made With 1.5% $K_2O$ and Stored in Exposure Condition 1 at Age of 240 Days, Showing Prismatic Ettringite Needles Filling a Cavity

Mineral deposits with characteristics of ettringite morphology were found filling air voids during the 540 days of SEM examinations. Further confirmation of mineral deposits using EDAX could not be obtained due to the low intensity spectrum. Figure 8.47 shows ettringite needles filling an air void.

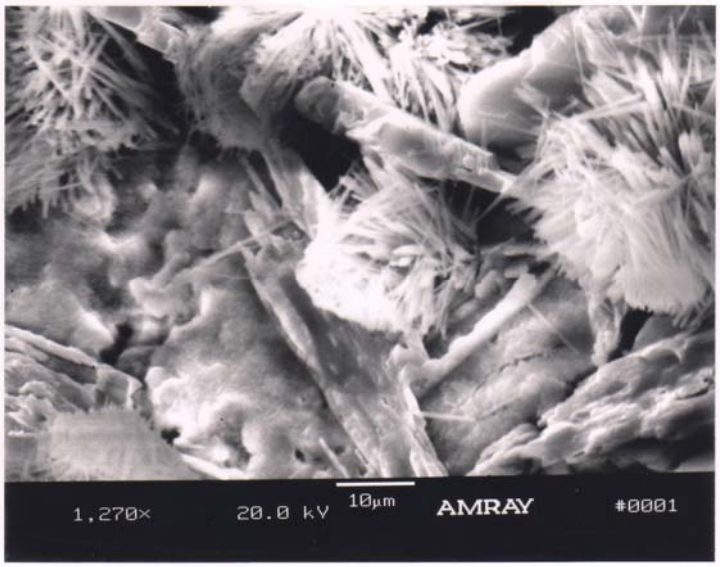


Figure 8.47: SEM Micrograph of Concrete Specimen Made With 1.5% $K_2O$ and Stored in Exposure Condition 1 at Age of 540 Days, Showing Ettringite Needles Filling an Air Void

*8.11.1.2 Concrete Samples in Exposure Condition 2*

No ettringite was found in the concrete specimens during the 40 and 100 days of SEM investigations. Ettringite needles were later discovered, during the 240 days' examinations, filling air voids and cavities of the concrete specimens. SEM and EDAX analysis of the microstructure showed ettringite needles with a few calcium hydroxide crystals filling a cavity, as shown in figure 8.48. The EDAX results indicate ettringite with a chemical composition of Al = 7.86% wt., Si = 4.73% wt., S = 17.71% wt., and Ca = 69.70% wt.

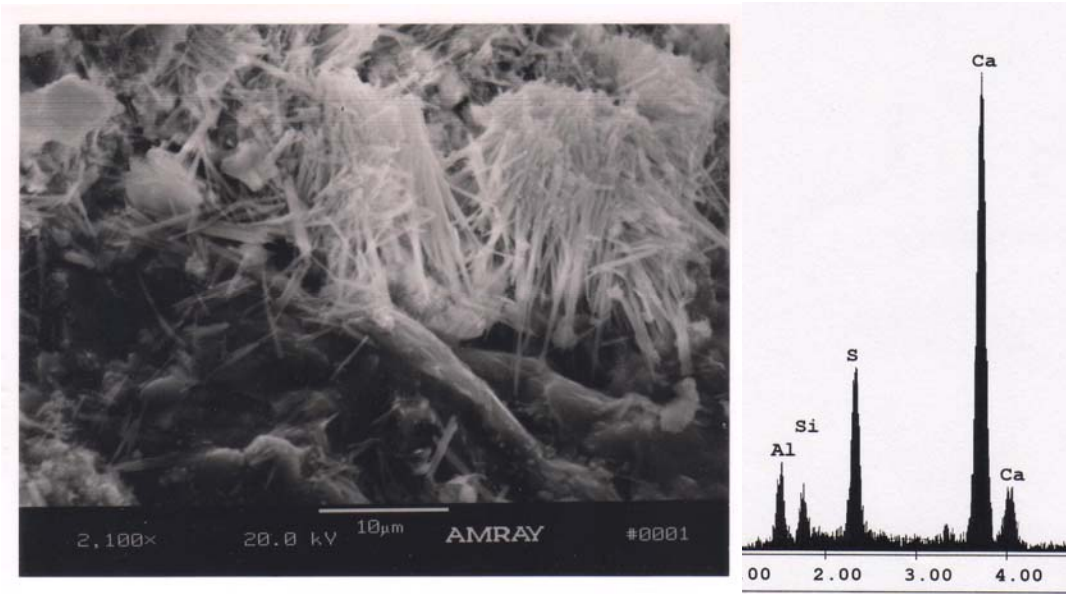


Figure 8.48: SEM and EDAX Analysis of Concrete Specimen Made With 1.5% $K_2O$ and Stored in Exposure Condition 2 at Age of 240 Days, Showing Ettringite Needles Filling a Cavity

The SEM examinations at 540 days showed lots of ettringite needles filling an air void. SEM investigations also found ettringite deposits in cracks between aggregate particles and the cement matrix at several locations. Figure 8.49 shows the SEM micrograph and EDAX analysis of the ettringite needles filling an air void. The EDAX elemental mapping of these materials matched with those of ettringite having a chemical composition of Al = 3.01% wt., Si = 8.82% wt., S = 4.54% wt., and Ca = 82.64% wt.

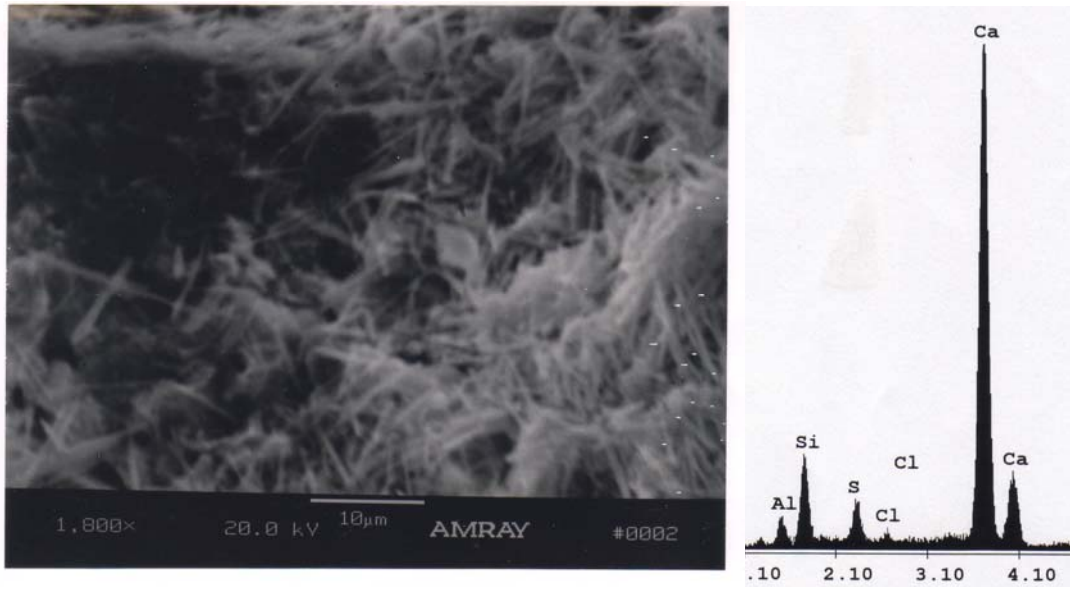


Figure 8.49: SEM and EDAX Analysis of Concrete Specimen Made With 1.5% $K_2O$ and Stored in Exposure Condition 2 at Age of 540 Days, Showing Ettringite Needles Filling an Air Void

*8.11.1.3 Concrete Samples in Exposure Condition 3*

Microstructural investigations at 40 days of the fractured concrete specimens taken from representative concrete samples in exposure condition 3 revealed no ettringite deposits. A SEM micrograph during the 100 days revealed material deposits characteristic of ettringite but no EDAX spectrum could be obtained. Figure 8.50 shows the SEM micrograph at 100 days. Similar material deposits are found at several locations within the microstructure of the concrete specimens.


Figure 8.50: SEM Micrograph of Concrete Specimen Made With 1.5% $K_2O$ and Stored in Exposure Condition 3 at 100 Days, Showing Probable Ettringite Needles Filling a Cavity

At 240 days, SEM Examination revealed a few clusters of ettringite needles covering the concrete specimen. Material deposits, probably ettringite, with massive calcium hydroxide (CH) crystals were discovered during the 540 days' SEM investigations of the specimen. Figure 8.51 shows ettringite with CH crystals covering the entire examined concrete specimen. The EDAX illustrated ettringite with chemical composition of Al = 2.47%wt., Si = 11.36% wt., S = 1.31% wt., and Ca = 80.82% wt. The high silicon (Si) peak in the analysis is because of contribution of background elements, cement paste (with much Al, Si) or cement hydration products (calcium silicate hydrate, C-S-H gel).

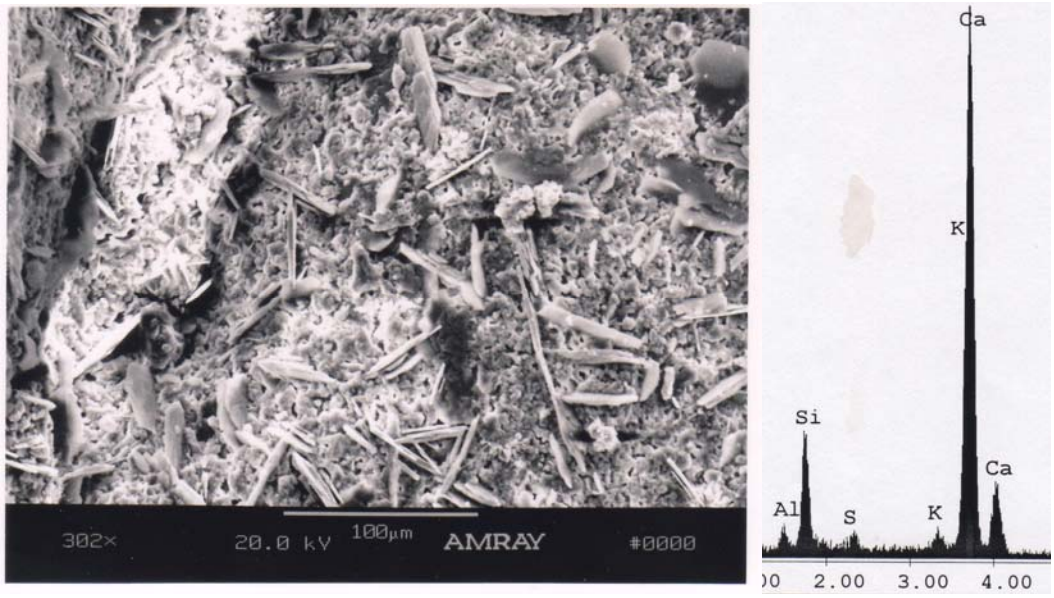


Figure 8.51: SEM and EDAX Analysis of Concrete Specimen Made With 1.5% $K_2O$ and Stored in Exposure Condition 3 at Age of 540 Days, Showing Ettringite Needles with CH Crystals Covering the Entire Specimen

### *8.11.2 SEM and EDAX Analysis of Concrete Samples Made With 1.5% $K_2O$ and Subjected to Different Treatments*

#### *8.11.2.1 Concrete Samples Subjected to Duggan Heat Cycle*

Concrete samples made with 1.5% $K_2O$ showed ettringite needles and calcium hydroxide (CH) crystals within the concrete microstructure, prior to subjecting them to the Duggan heat cycle. Figure 8.52 shows an air void filled with ettringite needles and CH crystals. The EDAX of the ettringite needles revealed a chemical composition of Al = 3.85%wt., Si = 8.85% wt., S = 4.49% wt., and Ca = 78.33% wt.


Figure 8.52: SEM and EDAX Analysis of Concrete Specimen Made With 1.5% $K_2O$ Before Being Subjected to Different Treatments Showing Ettringite Needles and CH Crystals Filling an Air Void

Immediately after the Duggan heat cycle, the SEM examinations found lots of randomly-oriented ettringite needles in the concrete specimen's microstructure. The Duggan heat cycle enhanced the formation of ettringite. The ettringite was found in cavities and at the interface between the aggregate particles and the cement paste matrix. Figure 8.53 shows the ettringite deposits in the paste matrix of the concrete specimens.


Figure 8.53: SEM and EDAX Analysis of Concrete Specimen Made With 1.5% $K_2O$ After Duggan Heat Cycle Treatment Showing Ettringite Deposits in the Cement Paste

Little ettringite was found in the concrete specimens during the 40 days SEM examinations. The ettringite was mixed with lots of CH crystals filling the cavities and water voids of the specimen. SEM examinations at 100 days after the Duggan heat cycle showed scattered ettringite needles with CH crystals covering the entire concrete specimen. The EDAX of the ettringite within the void showed chemical composition of Al = 3.42%wt., Si = 1.13% wt., S = 8.22% wt., and Ca = 87.23% wt. SEM examinations at 240 and 365 days revealed no ettringite in the specimen. Figure 8.54 shows the SEM and EDAX analysis of the ettringite mixed with CH crystals covering the concrete specimen.

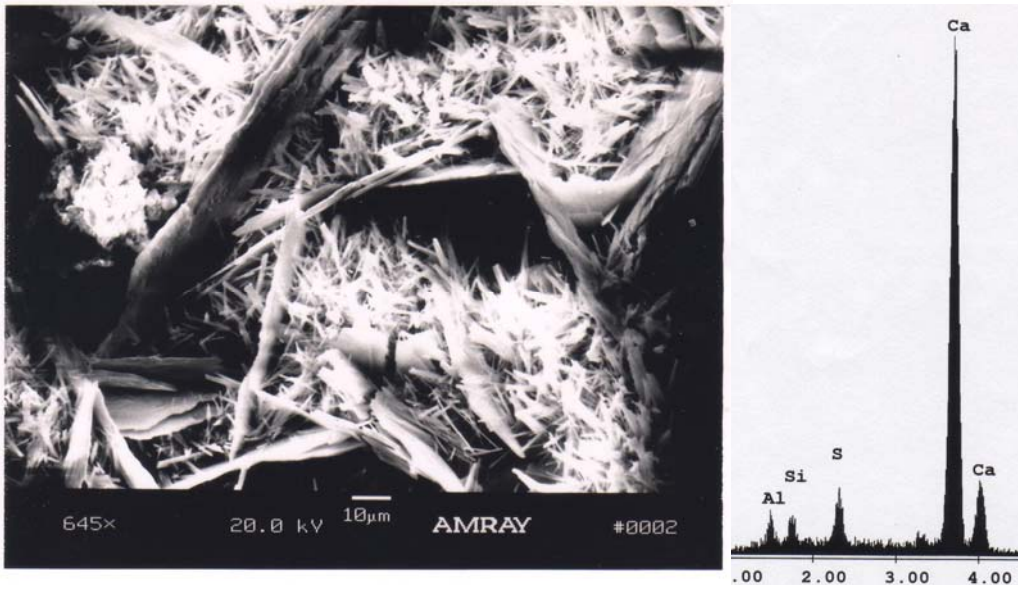


Figure 8.54: SEM and EDAX Analysis at Concrete Specimen Made With 1.5% $K_2O$ Subjected to Duggan Heat Cycle Treatment and Stored in Exposure Condition 1 at Age of 100 Days, Showing Ettringite Mixed with CH Crystals

*8.11.2.2 Concrete Samples Subjected to Freeze-Thaw Cycle*

SEM examinations after the Freeze-Thaw cycle revealed ettringite needles mixed with CH crystals filling cavities and air voids. The ettringite existed in the cavities and air voids, and concentrated more in the interface between the aggregate particles and the cement paste matrix. Figure 8.55 shows the ettringite deposits in the microstructure of the specimen. The EDAX analysis showed ettringite having chemical composition of Al = 3.49%wt., Si = 8.63% wt., S = 5.05% wt., and Ca = 75.08% wt.

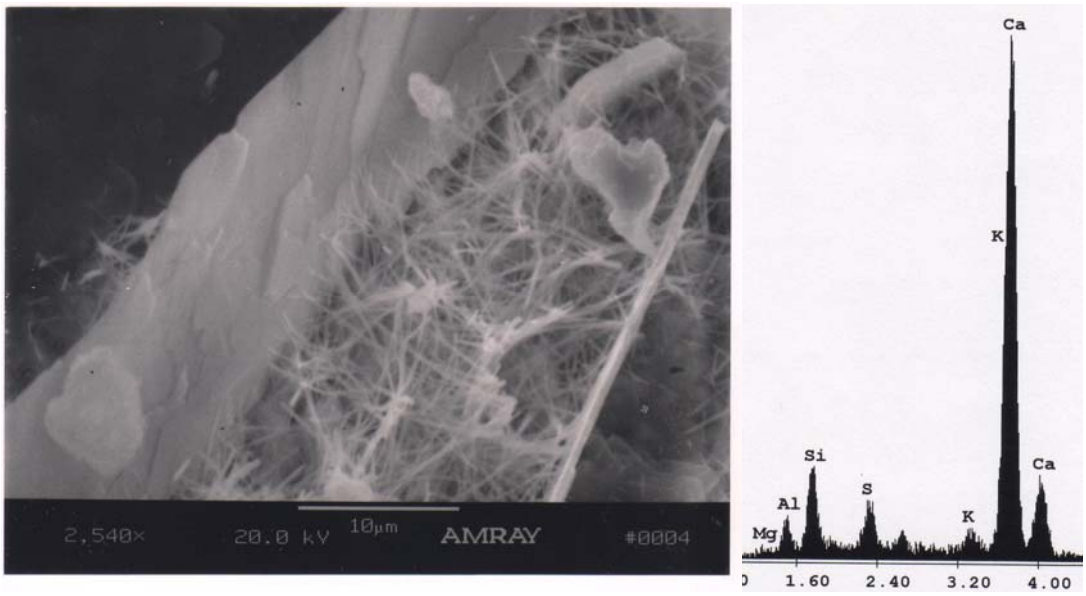


Figure 8.55: SEM and EDAX Analysis of Concrete Specimens Made With 1.5% $K_2O$ After Freeze-Thaw Cycles Treatment Showing Ettringite Needles and CH Crystals Filling an Air Void

Ettringite needles and calcium hydroxide (CH) crystals were discovered covering an aggregate pull-out during the 40 days examinations. Figure 8.56 illustrated ettringite formation and CH crystals on the aggregate pull-out. The EDAX analysis confirmed the elemental mappings consistent with ettringite.

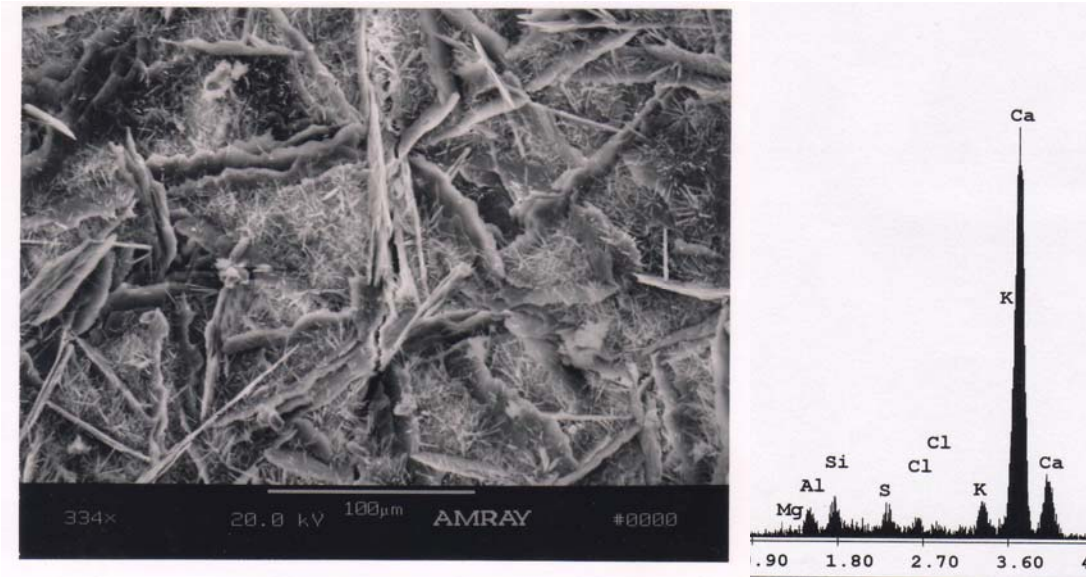


Figure 8.56: SEM and EDAX Analysis Concrete Specimen Made With 1.5% $K_2O$ Subjected to Freeze-Thaw Cycles Treatment and Stored in Exposure Condition 1 at Age of 40 Days, Showing Ettringite and CH Crystals Covering an Aggregate Pull-Out

Both of the SEM examination results at 100 days and 240 days showed no ettringite. Spherical ettringite balls were found during SEM examinations the 365 days filling the cavities of the concrete specimen as shown in figure 8.57. Ettringite was also present in the interface between the aggregate particle and cement paste. EDAX elemental analysis revealed the chemical compositions of the ettringite spherical balls were Al = 6.01%wt., Si = 1.05% wt., S = 10.52% wt., and Ca = 82.41% wt.

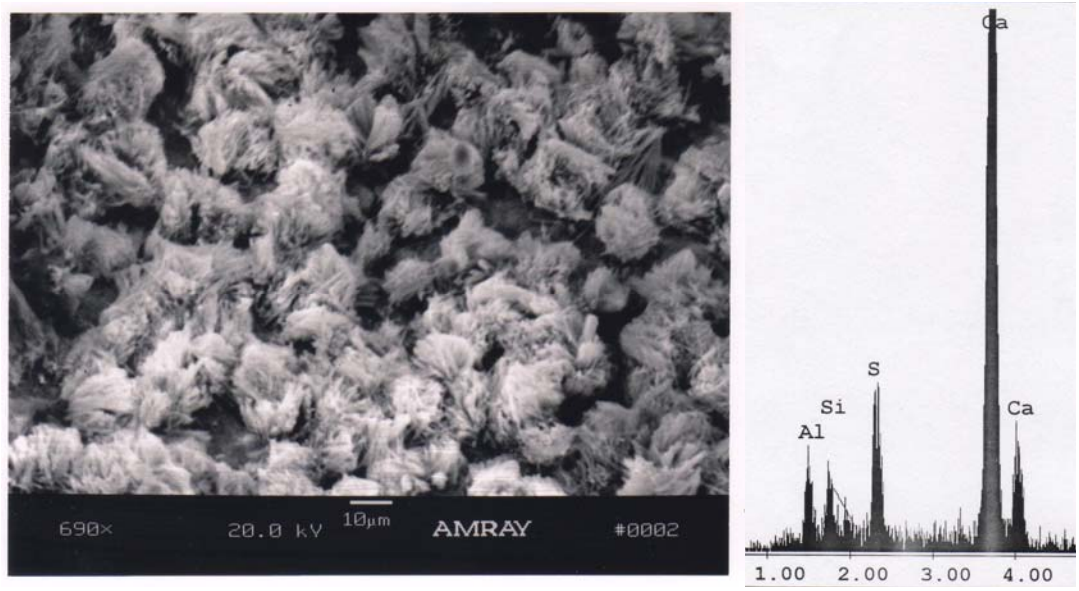


Figure 8.57: SEM and EDAX Analysis Concrete Specimen Made With 1.5% $K_2O$ Subjected to Freeze-Thaw Cycle Treatment and Stored in Exposure Condition 1 at Age of 365 Days, Showing Spherical Ettringite Balls Filling a Cavity

### *8.11.3 SEM and EDAX Analysis of Concrete Samples Made With 1.5% $K_2O$ and Subjected to Field Conditions*

#### *8.11.3.1 Concrete Samples in Exposure Condition 4A*

SEM results at 40 days showed few ettringite deposits in the cavities of the concrete specimens. Few isolated air voids filled with ettringite were also observed at a high magnification. Figure 8.58 shows few ettringite bundles in a cavity of about < 10 microns. EDAX elemental analysis of the deposits showed a typical composition of ettringite.

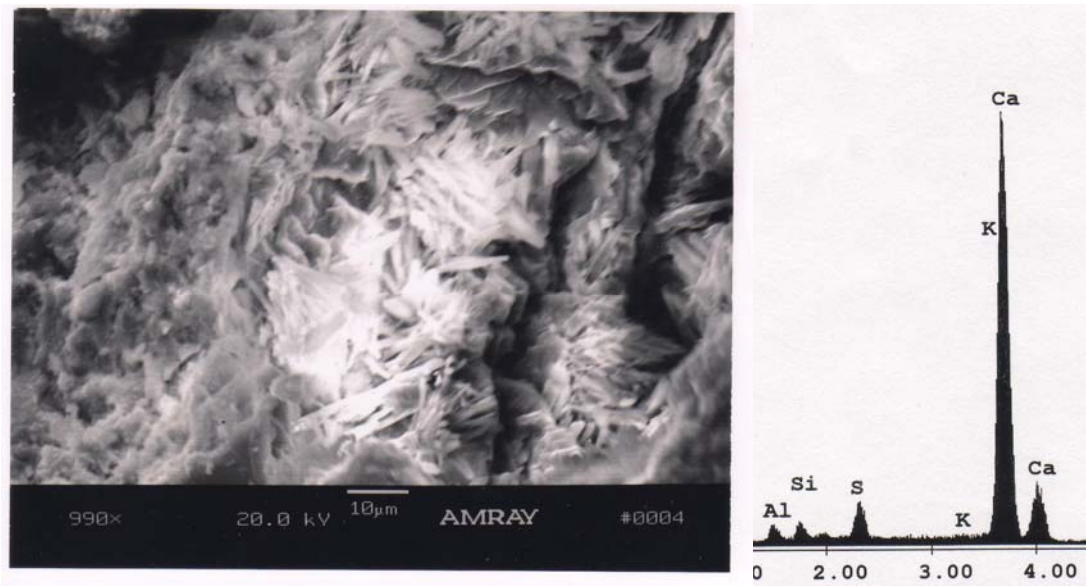


Figure 8.58: SEM and EDAX Analysis of Steam-Cured Concrete Specimen Made With 1.5% $K_2O$ and Stored Under Field Conditions (C4A) at Age of 40 Days, Showing Ettringite Bundles Filling a Cavity

Well-developed prismatic shaped ettringite was found during the 100 SEM examinations in the cavities. Ettringite was also found in the interface between the aggregate particles and cement paste matrix of the examined concrete specimens. Figure 8.59 shows the prismatic ettringite filling a cavity. The EDAX confirms that the deposits within the cavity were ettringite having a chemical composition of Al = 5.29% wt., Si = 0.68% wt., S = 10.45% wt., and Ca = 81.65% wt.

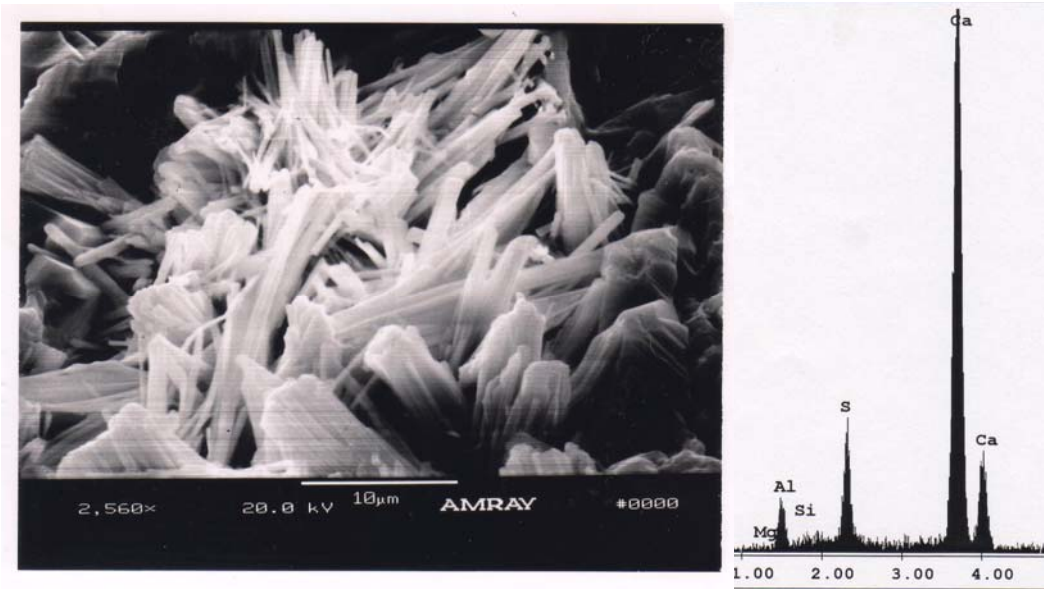


Figure 8.59: SEM and EDAX Analysis of Steam-Cured Concrete Specimens Made With 1.5% $K_2O$ and Stored Under Field Conditions (C4A) at Age of 100 Days, Showing Prismatic Ettringite Filling a Cavity

SEM examinations at 240 and 540 days showed large ettringite crystals in the concrete specimens. Lots of these ettringite crystals were found at various locations within the concrete specimen's microstructure. A very important finding was the transformation of ettringite from spherical ball to needles and then well-developed massive crystals at later stages. Figure 8.60 shows the ettringite crystals filling cavities and air voids of the specimen.

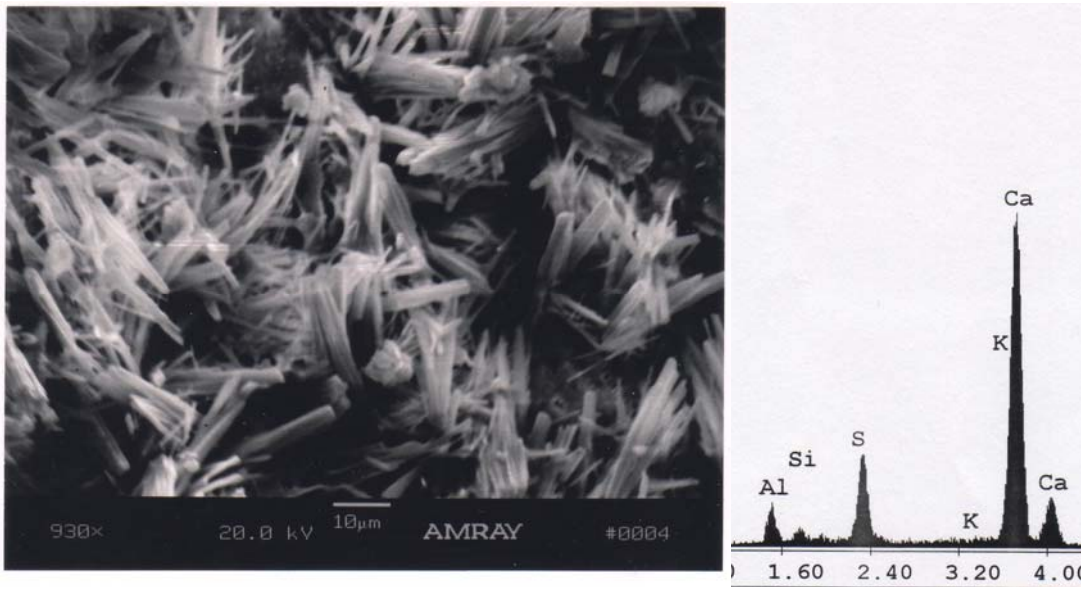


Figure 8.60: SEM and EDAX Analysis of Steam-Cured Concrete Specimen Made With 1.5% $K_2O$ and Stored Under Field Conditions (C4A) at Age of 540 Days, Showing Ettringite Crystals Filling Cavities and Air Voids

*8.11.3.2 Concrete Samples in Exposure Condition 4B*

Figure 8.61 shows ettringite needles with CH crystals covering the entire concrete specimen during the 40 days' SEM examinations. The EDAX revealed ettringite having a chemical composition of Al = 16.05% wt., Si = 5.19% wt., S = 24.02% wt., and Ca = 52.83% wt.


Figure8.61: SEM and EDAX Analysis of Room Temperature-Cured Concrete Specimen Made With 1.5% $K_2O$ and Stored Under Field Conditions (C4B) at Age 40 Days, Showing Ettringite Needles and CH Crystals Covering the Entire Concrete Specimen

Little or no ettringite was discovered in the concrete microstructure during the 100 or 240 days SEM examinations. The ettringite later reappeared during the 540 days SEM examinations. Figure 8.62 shows the ettringite needles mixed with CH crystals filling an air void.

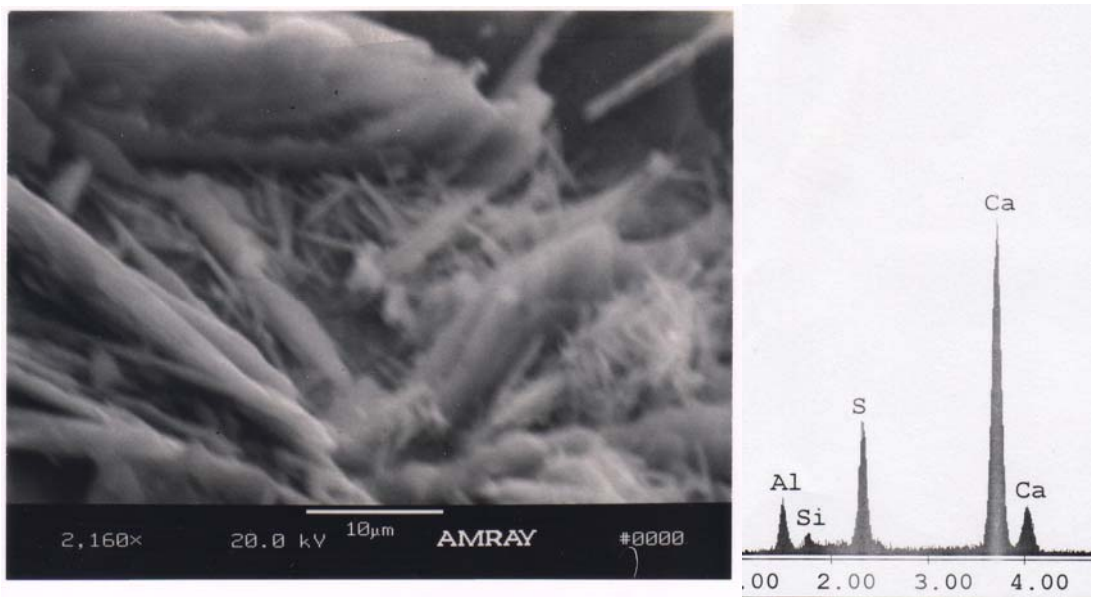


Figure 8.62: SEM and EDAX Analysis of Room Temperature-Cured Concrete Specimen Made With 1.5% $K_2O$ and Stored Under Field Conditions (C4B) at Age 540 Days, Showing Ettringite Needles and CH Crystals Filling an Air Void

*8.12 Summaries and Discussion of Concrete Samples Made With 1.5% $K_2O$*

In this research work, all the concrete samples made with 1.5% $K_2O$ exhibited excessive expansion and a significant reduction in strength. Changes in the cement manufacturing process for past decades produced cements with high alkali levels. As a consequence, this practice tended to raise the sulfate levels, which enhanced the formation of ettringite (Taylor, 1994). Portland cement type III and dolomite limestone aggregate - # 57 was used to study DEF and its associated deleterious expansions in concrete.

All the concrete prisms made with 1.5%$K_2O$ showed deleterious expansion except those stored in relative humidity of 97%. For up to about 300 days, the expansion of concrete prisms in limewater and plain water exhibited similar pattern.

After 300 days, it could be seen that concrete prisms in plain water exhibited higher expansion than those in limewater. This can be attributed to the extra calcium from the limewater in exposure condition 1 which can caused precipitation of ettringite. The ettringite precipitation inhibits transport of solution into the microstructure retarding expansion of the concrete prisms. Lack of continuous supply of water can be attributed to the little or insignificant expansion exhibited by the concrete prisms in relative humidity of 97%. The correlation of expansion against time results revealed a high linear correlation for the first 150 days of storage of the concrete prisms in limewater and plain water.

The early peak temperature of concrete samples influenced the expansion values of the concrete prisms at later ages. The expansion of concrete samples subjected to early peak temperature above 85$^{o}$C either increased or was broadly constant (Hobbs, 1999). An increase in potassium content ($K_2O$) causes an increase in the expansion of the concrete prisms. The expansion behaviors of both sets of concrete prisms are almost the same. Fu reported that concrete treatments such as freeze-thaw cycles appeared not to cause significant DEF-induced expansion (1996). For the research duration, the maximum expansion values were 0.1172% and 0.0984% for the Duggan heat and Freeze-Thaw treated concrete prisms. These expansion values were insignificant and therefore no visible cracks were observed on the outer surfaces of the concrete prisms.

The weight change due to water uptake and subsequent formation of DEF can indicate damage in the concrete samples. According to Shimada, weight gain during the early stage of storage is mostly determined by cement hydration behavior, leading

not only to ettringite formation but also to the formation of various hydrated phases (2005). This can be attributed to the significant weight change observed just after the Duggan heat, and submerging of the concrete prisms in either limewater or plain water. Concrete samples damaged during the Duggan heat cycle treatment will change its water uptake capability and a change in weight will result from the availability of water. Again, similar to the control concrete specimens, a high linear correlation coefficient was discovered for the first 100 days of storage in the limewater and plain water exposure conditions.

For the concrete samples made with 1.5% $K_2O$, the Duggan heat cycle treated samples showed much higher weight changes than the Freeze-Thaw samples. The use of thermal heating cycles at the early stages of fresh concrete damages the pore structure of the concrete and initiates structural defects.

Possible correlation of expansion against weight-change data was investigated and there existed little linear correlation for the first 100 days of storage in limewater and plain water. This is contrary to the results obtained for the expansion against weight-change results of the mortar samples. It can be noted that expansion and weight-change processes are influenced by the difference in the microstructure of the mortar and concrete samples. The expansion against weight change of the Duggan heat or Freeze-Thaw treated concrete samples made with 1.5% $K_2O$ showed no correlation.

The compressive strength of the concrete samples made with 1.5% $K_2O$ and stored in limewater and plain water showed a reduction of up to 75% at 365 days. In contrast, concrete samples in exposure conditions showed up to 10% increases in

compressive strength at 365 days testing. The room temperature-cured and subsequently Duggan heat or Freeze-Thaw cycles treated concrete samples revealed a 20% increase in compressive strength at later stages. Both the moist and dried tested concrete samples showed an increase in compressive strength. These results indicated that the compressive strength of steam-cured concrete specimens at later stages may increase or decrease depending on the early curing temperature and exposure conditions.

Only the field-exposed concrete prisms subjected to steam-curing (P4C4A) showed expansion for the research duration. The room temperature-cured concrete prisms showed minimal expansion and shrinkage for most time during the research. This showed that steam-curing can cause expansion in concrete exposed to field conditions. The field exposed concrete specimens showed an increase of up to 20% in compressive strength at later stages.

The presence of alkalis greatly influenced the rate of expansion of the concrete prisms and enhanced the formation of ettringite. The alkalis continuously leached from the concrete prisms, but were not lost to the defected pore structure with microcracks. Since the concrete samples were kept continuously in the storage solution, the alkali ions became trapped in the pore structure, and this caused further expansion damage. The amount of alkalis concentration leached from the concrete samples depended on the alkali content of the cement. Again, the high concentration of $Ca^{2+}$ ions in the limewater contributed to the formation of ettringite and this was confirmed with SEM and EDAX analysis.

Laser shearography is a nondestructive technique used to reveal fine cracks in concrete at early stages. The concrete prisms made with 1.5% $K_2O$, and stored in exposure condition 3 showed little or no changes in crack density or areas at later stages. The formation of microcracks in concrete is highly influenced by the curing methods and subsequent exposure conditions. The Duggan heat cycle treated concrete prisms exhibited more cracked areas than the Freeze-Thaw treated concrete prisms.

The SEM investigations of the concrete samples made with 1.5% $K_2O$ showed many occurrences of ettringite formation growing in the cavities, air voids, the interface between aggregate particles and the cement paste matrix. Well-developed ettringite crystals were discovered in concrete specimens subjected to the Duggan heat cycle, and subsequently stored in limewater and plain water during several test periods. Ettringite formation was found in varying amounts and forms in all samples. Different exposure conditions revealed ettringite with different morphologies. Expansion results correlated with SEM results showed that exposure condition contributes as the dominating role in the expansion and formation of DEF. Table 8.13 illustrates the test results for the steam-cured concrete samples made with 1.5% $K_2O$ and subjected to Duggan heat cycle before subsequently storing them in different exposure conditions. DEF and calcium hydroxide (CH) crystals were found in Freeze-Thaw treated concrete samples. It can be seen that the concrete samples made with 1.5% $K_2O$ produce not only higher expansion values but more ettringite crystals. Table 8.14 provides the test results for the room temperature-cured concrete samples made with 1.5% $K_2O$ and subjected to different treatments prior to storing them in

limewater. A network of cracks was observed in all the samples and this might have been introduced during the sample preparation. No signs of ASR were observed during the microstructural examinations of the concrete samples.

Thus, minimal expansion was observed in concrete samples exposed to field conditions but both sets showed ettringite within their microstructure. SEM results at 540 days of the steam-cured concrete samples stored under field conditions exhibited well-developed massive ettringite crystals. The SEM and EDAX analysis indicated that DEF was the primary cause of the expansion of the field exposed concrete samples. Table 8.15 provides the test results for the room temperature-cured concrete samples made with 1.5% $K_2O$ and subjected to different treatments prior to storing them in limewater.

Table 8.13: Summary of Test Results of Concrete Samples Made with 1.5% $K_2O$ – Steam-Cured and Subjected to Duggan Heat Cycle

| **Concrete Samples (1.5% $K_2O$) - Steam-Cured and Subjected to Duggan Heat Cycle** | | | | |
|---|---|---|---|---|
| | | Exp. Cond. 1 (Limewater) | Exp. Cond. 2 (Plain Water) | Exp. Cond. 3 (R.H at 97%) |
| Expansion | | Max. 1.55% | Max. 1.50% | Max. 0.02% |
| Weight Change | | Max. 4.98% | Max. 5.42% | Max. 2.15% |
| Compressive Strength (psi) | 28 Days | 4521 | 4166 | 4885 |
| | 365 Days | 1033 | 580 | 5349 |
| | 540 Days | 501 | 472 | 5907 |
| Water Analysis (mmol/l) | pH | - | 8.57 - 12.23 | - |
| | Alkali | Max. 363 | Max. 258 | - |
| | $Ca^{2+}$ | - | Max. 138 | - |
| SEM/EDAX Analysis | 40 Days | Spherical ettrinigte balls | No ettringite | No ettringite |
| | 100 Days | Ettringite needles | No ettringite | Probable ettringite |
| | 240 Days | Prismatic ettringite needles | Ettringite needles | Few clusters of ettringite |
| | 540 Days | Ettringite needles | Lots of ettringite needles | Little ettringite needles with CH crystals |

Table 8.14: Summary of Test Results of Room Temperature-Cured Concrete Samples Made with 1.5% $K_2O$ – Subjected to Different Treatments

| **Room Temperature-Cured Concrete Samples (1.5% $K_2O$) - Subjected to Different Treatments** | | | |
|---|---|---|---|
| | | P4C1_D (Duggan Heat Cycle) | P4C1_F (Freeze-Thaw Cycle) |
| Expansion | | Max. 0.1172% | Max. 0.0984% |
| Weight Change | | Max. 5.38% | Max. 1.27% |
| Compressive Strength (psi) | 28 Days | 4776 | 5022 |
| | 240 Days | 5834 | 5959 |
| | 365 Days | 5570 | 6339 |
| SEM/EDAX Analysis | Before treatment | Ettrinigite needles and CH crystals | No ettringite |
| | After treatment | Randomly-oriented ettringite needles | Ettringite needles and CH crystals |
| | 40 Days | Little ettringite | Ettringite and CH crystals |
| | 100 Days | Scattered ettringite needles | No ettringite |
| | 240 Days | No ettringite | No ettringite |

Table 8.15: Summary of Test Results of Concrete Samples Made with 1.5% $K_2O$ – Subjected to Field Conditions

| **Concrete Samples (1.5% $K_2O$) - Exposed to Field Conditions** | | | |
|---|---|---|---|
| | | Exp. Cond. 4A (Steam-Cured) | Exp. Cond. 4B (Room Temp.-Cured) |
| Length Change | | Max. 0.0410% | Max. 0.0136% |
| Weight Change | | Max. -0.07% | Max. -0.02% |
| Compressive Strength (psi) | 28 Days | 4938 | 4776 |
| | 365 Days | 6537 | 5834 |
| | 540 Days | 6781 | 6180 |
| SEM/EDAX Analysis | 40 Days | Few ettringite | Ettringite needles with CH crystals |
| | 100 Days | Prismatic shaped ettringite | Little or no ettringite |
| | 240 Days | Large ettringite crystals | Little or no ettringite |
| | 540 Days | Large ettringite crystals | Ettringite needles |

# Chapter 9: Analysis and Discussion of Results

## *9.1 Introduction*

Delayed ettringite formation (DEF) is mainly attributed to hardened mortar or concrete cured at elevated temperatures, and subsequently exposed to moisture. But in this research study, ettringite was found in samples subjected to no heat or thermal cycles. Generally, researchers paid little or no attention to investigating the influence of exposure conditions and their contribution to potential expansion and DEF of mortar and concrete samples. Researchers often measured dimensional changes mainly for expansion and performed scanning electron microscope (SEM) to analyze the elemental chemical composition of the deposits within the cracks, voids, cement paste and aggregate interface without any effective monitoring of the exposure conditions of the samples during storage. It is very important to monitor the exposure conditions since the C-S-H gel is responsible for DEF changes over time, and differently for different storage conditions (Famy, 2001). Monitoring the storage conditions, together with advanced material testing methods, can provide guidelines to mitigate or prevent delayed ettringite formation and its associated expansion, which causes the premature deterioration of mortar and concrete. In this chapter the results for all the mortar and concrete specimens that were presented in the previous chapters will be analyzed and discussed comprehensively.

*9.2 Summary*

In this research study, laboratory-prepared specimens were tested to investigate the mechanisms of delayed ettringite formation (DEF) and their associated expansions leading to the premature deterioration of mortar and concrete samples. A UMD/FHWA modified preparation method was used to enhance the length-change measurements of bars according to ASTM C490. The Duggan heat cycle was employed after seven (7) days of casting to initiate microcracks within a shorter period of time. The objectives of this study were: (1) to use applied advanced material testing methods on the complex processes of expansive cracking associated with DEF; (2) to investigate the effects of storage conditions and their influence on DEF pertaining to weight change, expansion/contraction, and damage variables; (3) to study by water analysis the potential of DEF in mortar specimens as a function of the alkali being leached into the storage solution; (4) to study the influence of potassium ($K_2O$) content on mortar expansion and its potential association with DEF; and (5) to investigate and explore the complexity of DEF at several stages.

Portland cement type III was used throughout the entire study which exceeds all the threshold values suggested by researchers. In 1994, Taylor outlined threshold values at 0.83% for equivalent $Na_2O$, 0.22% for $Na_2O$, 3.6% for $SO_3$ and 1.6 $\pm$ 0.2% for MgO. Manufactured Frederick Stone Sand conforming to ASTM C33 was used throughout the research. For the concrete batches, Calcitic Limestone ASTM # 57 was used for the coarse aggregate. The research study was conducted in four (4) phases. In phases one (1) and two (2), mortar samples were prepared in the laboratory to investigated damage attributed to DEF. Phase 1 served as the control

and was made with no additional potassium content ($K_2O$) while in phase 2 the mortar samples were made with additional $K_2O$. In phases 3 and 4 concrete samples were prepared for DEF and nondestructive testing such as Laser Shearography. SEM equipped with EDAX analysis were employed to explore the formation of DEF in mortar and concrete specimens. Laser Shearography testing was also employed to investigate the formation of cracks in the concrete samples. Again, phase 3 concrete served as the control, while phase 4 concrete samples were made with 1.5% $K_2O$. Increasing the potassium content ($K_2O$) by adding potassium carbonate ($K_2CO_3$) to the mixing water during batching increased the alkali concentration of the samples.

Another important factor, steam-curing at elevated temperatures, has been shown by many researchers to produce damage associated with DEF. The mortar and concrete samples were either steam-cured prior to being subjected to the Duggan heat regime or cured at room temperature in the laboratory. The Duggan heat cycle was used to initiate microcracks in order to accelerate DEF. At 21 days, the expansion results were compared to the threshold limit of 0.05% expansion, as suggested by Duggan as a pass-fail criterion for concrete. Some concrete batches were also subjected to Freeze-Thaw cycles prior to storage. Four different storage conditions were investigated in this research study: Isothermal water bath, pH maintained at 12.5 (limewater); plain water at room temperature; moist air chamber, R.H maintained at 97%; and field conditions.

## *9.3 Analysis and Discussion of Test Results*

### *9.3.1 Mortar Samples*

The mortar samples consisted of the control and mortar samples made with 1.5% potassium content ($K_2O$). The water to cement ratio, sand to cement ratio and fine aggregate were the same for all batches. The increased $K_2O$ of the mortar samples was obtained by adding potassium carbonate to the mixing water. This affected the workability of the mortar mix.

#### *9.3.1.1 Mortar Samples Subjected to Duggan Heat Cycle and DEF*

Expansion results of the mortar bars clearly showed that an increase in potassium content caused an increase in expansion rate. But the main factor critical to damage attributed to DEF was the exposure to moisture. The availability of moisture, probably from the storage solution or environmental agents, influenced the formation of ettringite. The expansion values did not necessarily depend on the amount of ettringite formed, but on the size of the crystals produced (Cohen, 1982). A summary of the expansion results for all the mortar bars exposed to different exposure conditions is shown in figure 9.1.

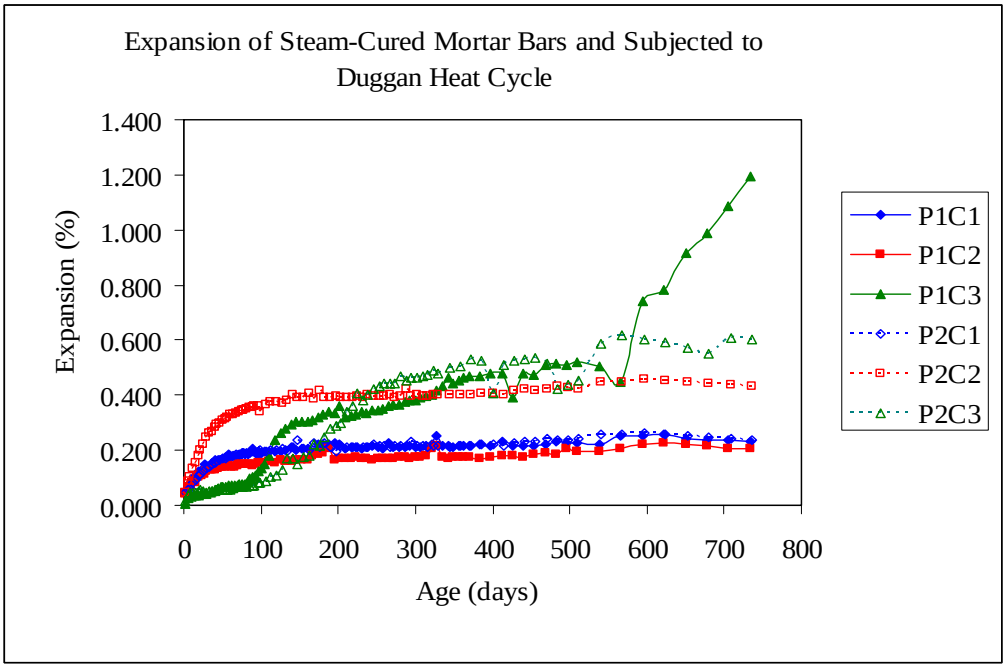


Figure 9.1: Expansion of all Steam-Cured Mortar Bars Subjected to Duggan Heat Cycle and Stored Under Different Exposure Conditions

The high expansion values exhibited by mortar bars in exposure condition 3 at later stages can be attributed to the potassium hygroscopic effect. The potassium continually extracts moisture which reacts to form more ettringite. The mortar bars in exposure condition 3 also exhibited local expansion areas near the ends. This can also contribute to the overall expansion of the mortar bars. Any differences in the mortar bars expansion can be attributed to the exposure conditions and alkali content. The effect of the high alkali content was very significant in the expansion rate of the mortar bars in exposure condition 2 (plain water at room temperature). The expansion rate and values of the mortar bars in exposure condition 1 were slightly depressed by the high calcium concentration in the storage solution. The extra calcium from the limewater in exposure condition 1 caused precipitation of ettringite

in the mortar bars close to the surface that inhibited transport of solution into the bars. After 120 days, the mortar bars in relative humidity of 97% exhibited faster expansion rate which may be attributed to an increase in moisture condensation in the pores. Similar results were found by Shimada (2005). The increased alkali content enhanced the increased the expansion of the totally submerged mortar bars. Researchers like Famy et al. earlier reported that the leaching of alkali into the storage water increases the releasing rate of sulfate ions from C-S-H (2001). According to Famy et al., the driving force for the release of sulphate from the lighter C-S-H into the pore solution increases with this difference, and thus this depends on the formation of ettringite which itself depends on the alkalinity of the pore fluid.

The steam-curing of the mortar samples and subsequently subjecting them to Duggan heat cycle prior to storing in different exposure conditions, introduced volumetric changes. The volumetric changes of the mortar samples are outlined by weight changes associated with paste expansion over time. Many researchers suggested this theory especially when the mortar samples are stored in water (Zhang, 2002 and Shimada, 2005). Figure 9.2 illustrates the weight change of the steam-cured mortar bars subjected to the Duggan heat cycle over time.

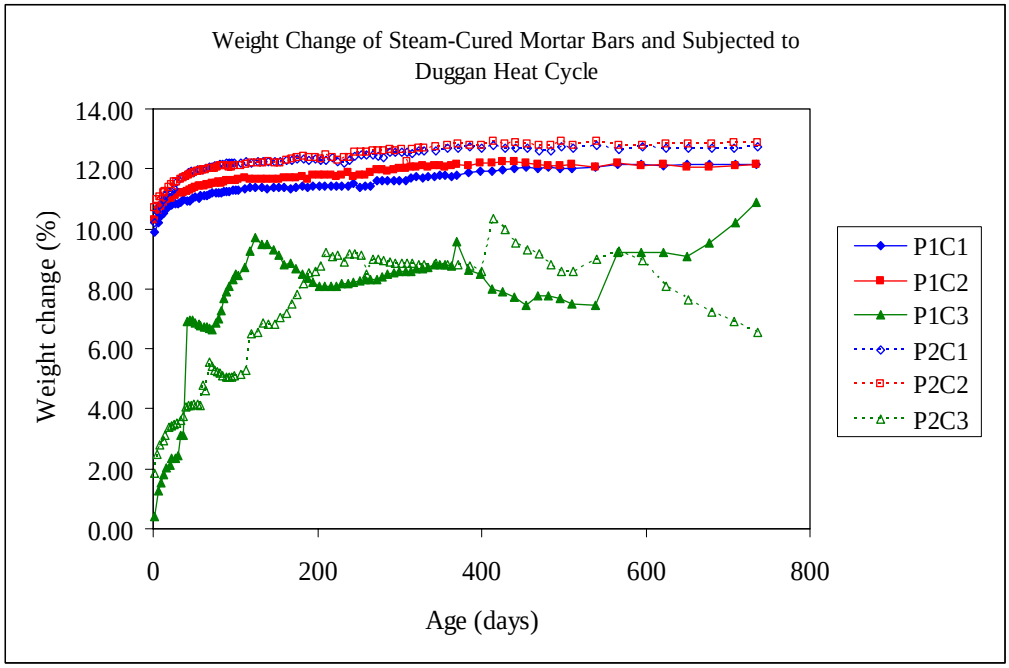


Figure 9.2: Weight Change of all Steam-Cured Mortar Bars Subjected to Duggan Heat Cycle and Stored Under Different Exposure Conditions

It can be seen that an increase in alkali content of the mortar samples is not very critical to weight-change behavior. Totally submerged mortar bars in exposure conditions 1 and 2 exhibited similar weight-change behaviors. Weight change against expansion results of the mortar bars show a high linear correlation for the first 100 days of storage in all the respective exposure conditions. This can be attributed to existing three (3) separate weight-change mechanisms taking place at the same time. According to Shimada, these are cement hydration, renewed ettringite formation and defect formation, and increased capillary pore volume (2005). Similar results were obtained by researchers such as Grattan-Bellew et al. (1998).

The effect of steam-curing and the Duggan heat cycle on the compressive strength was different for different exposure conditions, and the alkali level of the

mortar samples. The compressive strength of the mortar samples in exposure condition 2 (plain water at room temperature) tended to decrease with an increase in alkali level. However, both the control and mortar samples made with high potassium content showed an increase in compressive strength over time. This can be attributed to the low expansion or shrinkage values exhibited by the mortar samples over time causing little or no significant damage to the mortar microstructure. Figure 9.3 gives a summary of the compressive strength results of the mortar specimens.

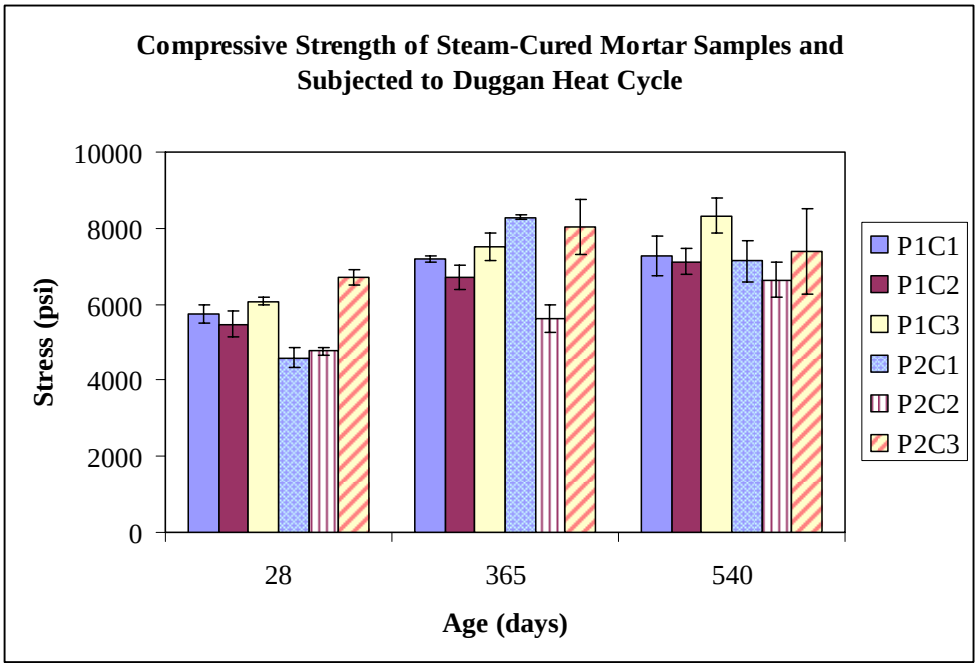


Figure 9.3: Compressive Strengths of all Steam-Cured Mortar Samples Subjected to Duggan Heat Cycle and Stored Under Different Exposure Conditions

Microstructural observations of the mortar specimens with SEM equipped with EDAX analysis revealed different ettringite characteristics and morphology for the different exposure conditions employed in this research project. The ettringite in the different exposure conditions change from spherical ettringite balls with calcium

hydroxide (CH) crystals, to clusters of ettringite needles to well-developed ettringite crystals at later stages. Ettringite was found in the interface between the cement paste and aggregate, and within cement paste in the cracks and air voids. These results are consistent with findings of other researchers such as (Diamond 1996, Zhang 1999, Famy, 2001 and Shimada, 2005). The form and crystal size of the ettringite found in the mortar specimens is highly influenced by the exposure conditions. Ettringite was found at all the examined stages in exposure conditions 1 and 2. But ettringite was predominant in exposure condition 3 only at later stages when high expansion values were exhibited by the mortar bars. Figure 9.4 shows ettringite crystals found in control mortar specimens in exposure condition 2 at 540 days. Figures 9.5 and 9.6 show the transition of clusters of ettringite needles to well-developed ettringite crystals. The large ettringite crystals required more space thereby exerted expansive forces and contributing to the damage of the mortar specimens' microstructure.

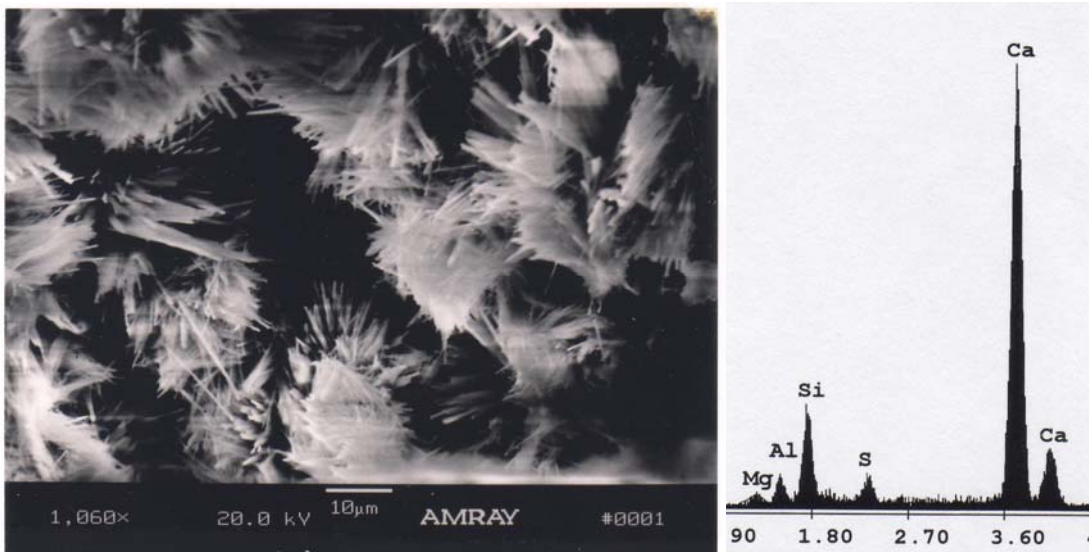


Figure 9.4: SEM and EDAX Analysis of Mortar Specimen in Exposure Condition 2 at Age of 540 Days, Showing Ettringite Crystals Filling the Cavities

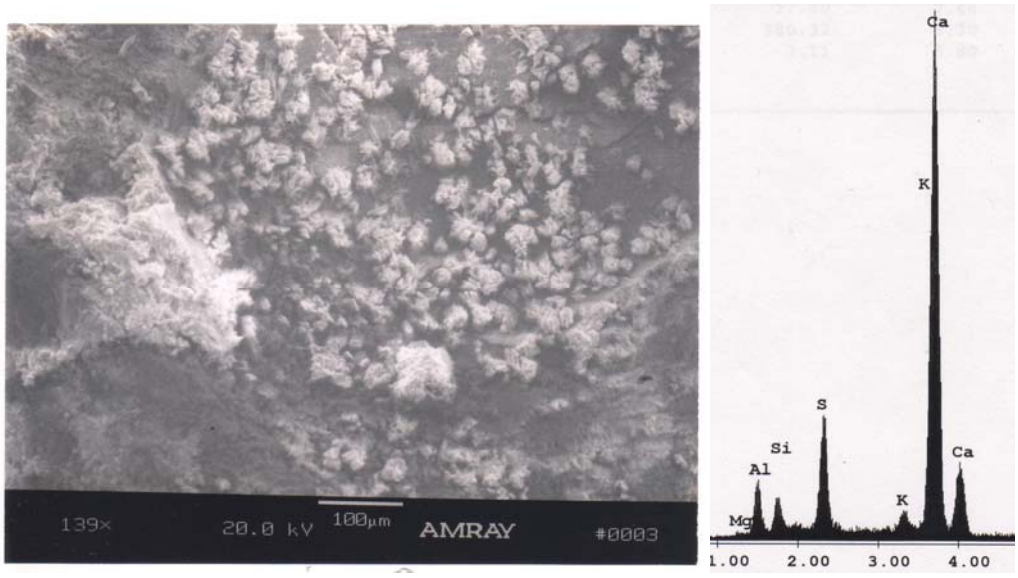


Figure 9.5: SEM and EDAX Analysis of Mortar Specimen Made With 1.5% $K_2O$ and Stored in Exposure Condition 3 at Age of 240 Days, Showing Clusters of Ettringite Needles Filling a Cavity

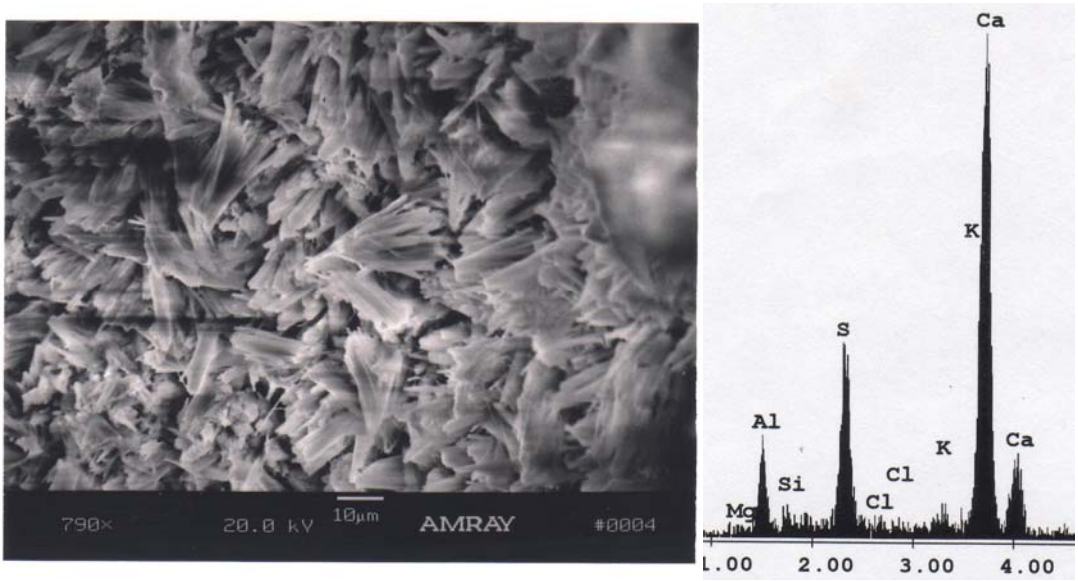


Figure 9.6: SEM and EDAX Analysis of Mortar Specimen Made With 1.5% $K_2O$ and Stored in Exposure Condition 3 at Age of 540 Days, Showing Well-Developed Ettringite Crystals Filling the Cavities

*9.3.1.2 Mortar Samples Subjected to Field Conditions and DEF*

Both sets of mortar specimens showed shrinkage for most of the storage period. Minimal expansion values caused by varying moisture conditions influenced by the environment were exhibited in the mortar samples. The little expansion values exhibited by the mortar bars caused little or no damage to the microstructure. Figure 9.7 illustrates the length-change measurements of the control and mortar bars made with 1.5% $K_2O$.

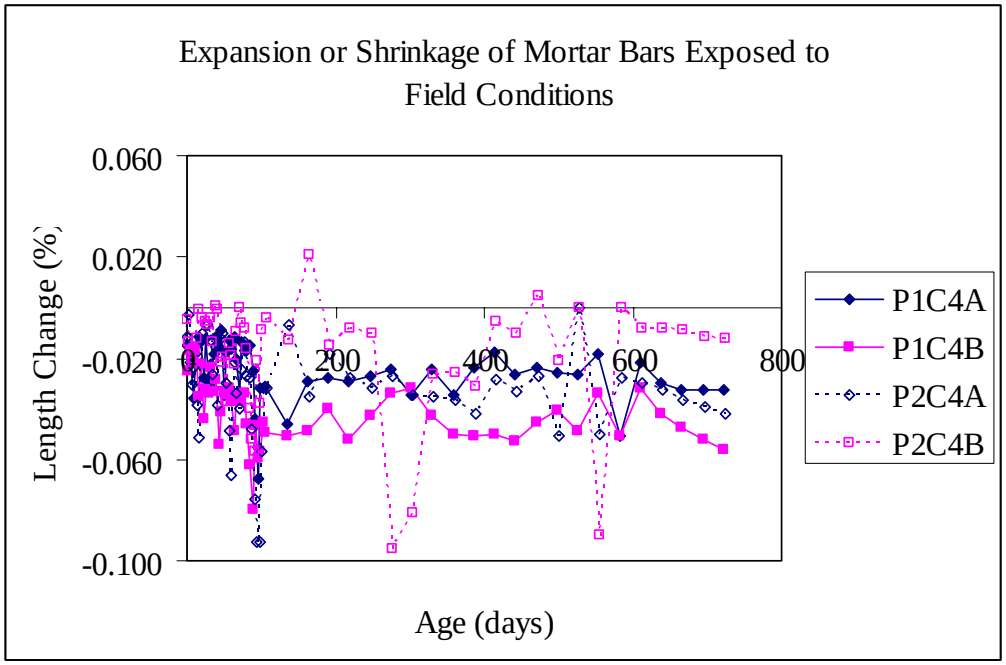


Figure 9.7: Length-Change of all Mortar Bars Exposed to Field Conditions

Weight-change measurements of the mortar samples subjected to field conditions decreased over time. This might be due to the high shrinkage caused by intensive drying from the sun. The intensive drying introduced stress which caused

changes in the microstructure. Figure 9.8 shows the weight-change measurements of the mortar bars subjected to field conditions.

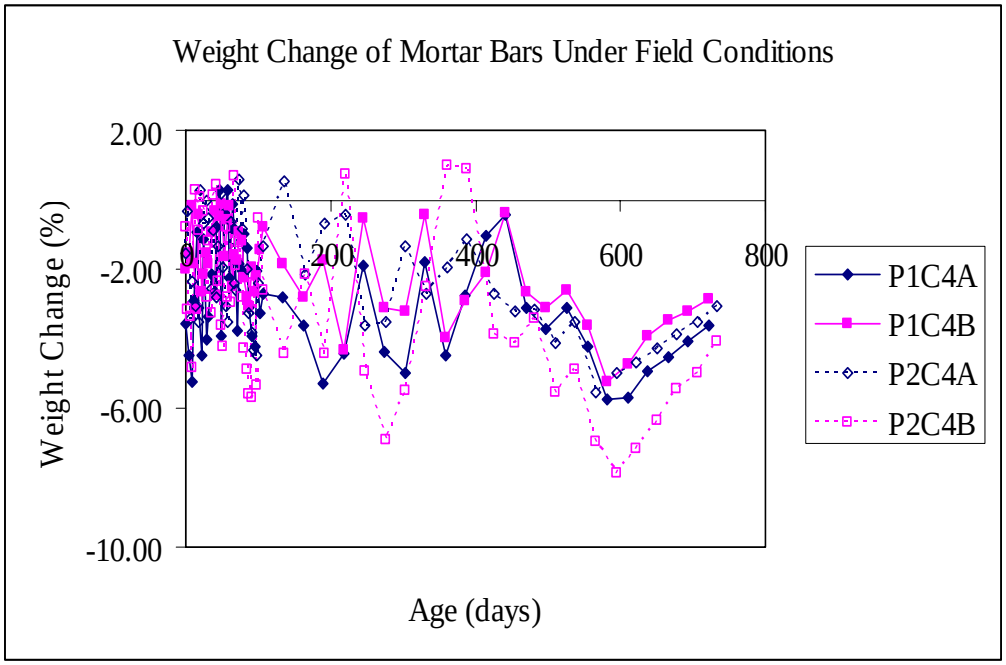


Figure 9.8: Weight-Change of all Mortar Bars Exposed to Field Conditions

The compressive strength of the field-exposed concrete specimens at later age is different for different mortars. Minimal expansion exhibited by the mortar samples caused little or no significant damage to the microstructure to warrant a loss in compressive strength. The room temperature-cured control mortar specimens subjected to field conditions showed an increased up to 35% in compressive strength at later age. A slight reduction in strength is observed in mortar specimens made with high potassium content. Figure 9.9 shows the compressive strength results of the mortar specimens subjected to field conditions.

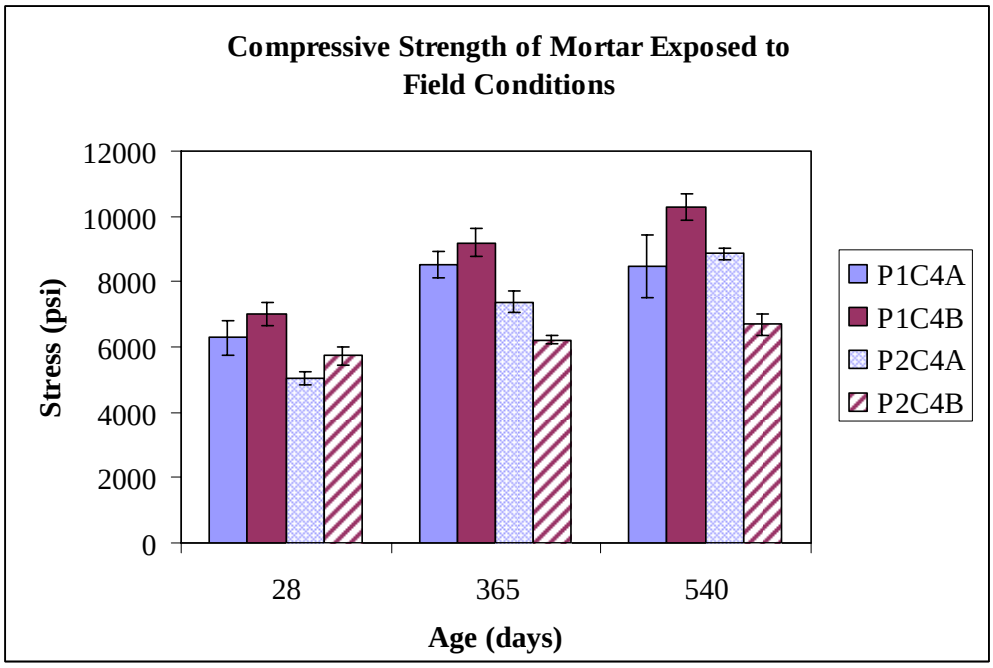


Figure 9.9: Compressive Strength Results of all Mortar Samples Subjected to Field Conditions

SEM and EDAX analysis at several stages revealed ettringite formation in the microstructure of the mortar samples. The SEM micrograph shows typical ettringite formation and characteristics in the air voids, cavities and in the interface between cement paste and aggregate of the mortar specimens. Although the mortar bars exhibit minimal expansion or shrinkage at most, DEF was found in the microstructure. DEF-related damage can also occur in no heat-treated mortar, which is exposed only to normal climatic conditions in the field (Stark and Bollman, 199). Figure 9.10 shows ettringite needles filling air voids and cavities of a mortar specimen.

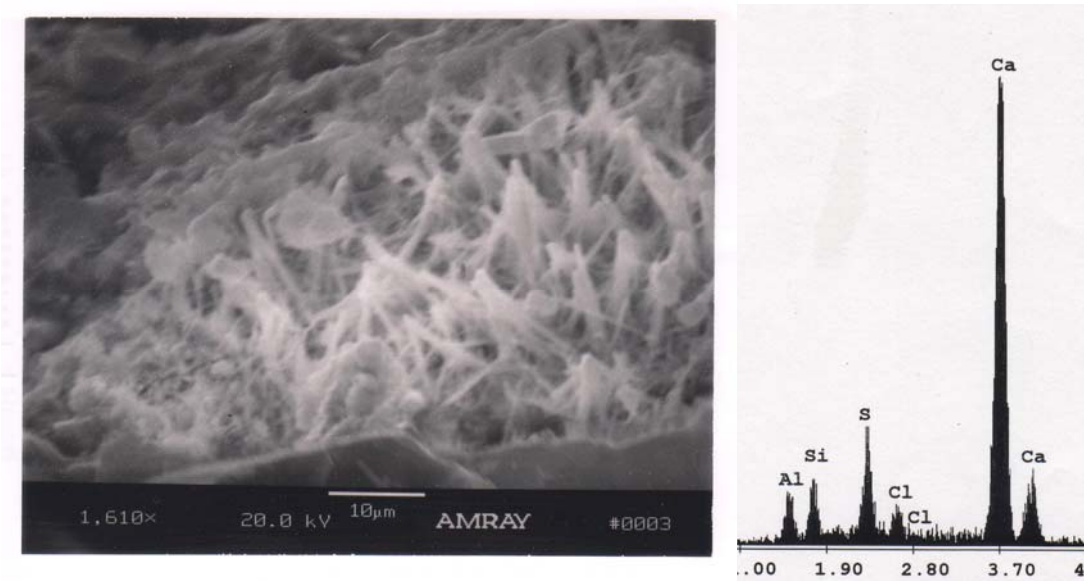


Figure 9.10: SEM and EDAX Analysis of Mortar Specimen Under Field Conditions (Exp. Cond. 4B) at Age of 100 Days, Showing Lots of Ettringite Needles Filling Cavities and Air Voids

*9.3.2 Concrete Samples*

Two (2) phases of concrete samples were prepared to investigate DEF in hardened concrete. The concrete samples were either steam-cured or at room temperature-cured prior to subsequent treatment to initiate microcracks. Steam-curing is a well-known factor used by researchers in producing DEF-related damage. Furthermore, the Duggan heat cycle and Freeze-Thaw cycles were used to initiate microcracks in a short period of time.

*9.3.2.1 Concrete Samples Subjected to Duggan Heat Cycle and DEF*

The effects of potassium content and exposure condition were investigated to explore DEF-related damage in concrete. The expansion values and rates of the concrete prisms increased with an increased in potassium content. These results

agree with researchers' results (Kelham 1996, Ramadan 2000 and Azzam 2002). This was not very significant in exposure condition 3 because the concrete prisms were not totally submerged under water. For up to 220 days, control and concrete prisms made with 1.5% $K_2O$ exhibited similar expansion rates. The amount of alkali concentration leached out from the concrete samples was also identical during this period. As the storage continues, the concrete prisms with high potassium content exhibited faster expansion rates. The exposure conditions of the concrete prisms after the Duggan heat cycle were found to be very critical to DEF and its associated expansion.

Duggan suggested a threshold value of 0.05% expansion at 21 days as a pass or fail criterion for concrete. It should be noted that the Duggan threshold values in used only for comparison purposes. Since it has been observed that the sample size affects the time to the start of expansion, for the same concrete smaller samples expanded much earlier than larger ones (Heinz et al., 1987 and 1989). None of the control concrete samples subjected to the Duggan heat cycle showed expansion of 0.05% at 21 days. Based on these results, this expansion of 0.05% at 21 days is not sufficient to predict the premature deterioration of concrete due to DEF. The changing concrete microstructure due to structural defects at early stages can be very influential to the overall durability of the concrete at later stages. Concrete dimensions also affect the expansion rates and values (Fu, 1996 and Ramadan, 2000). However, the Duggan expansion threshold value needs to be revised to include concrete under different exposure conditions, before any such limit can be established. Figure 9.11 shows the expansion of the control and concrete prism made

with 1.5% $K_2O$ subjected to the Duggan heat cycle, and stored in different exposure conditions.

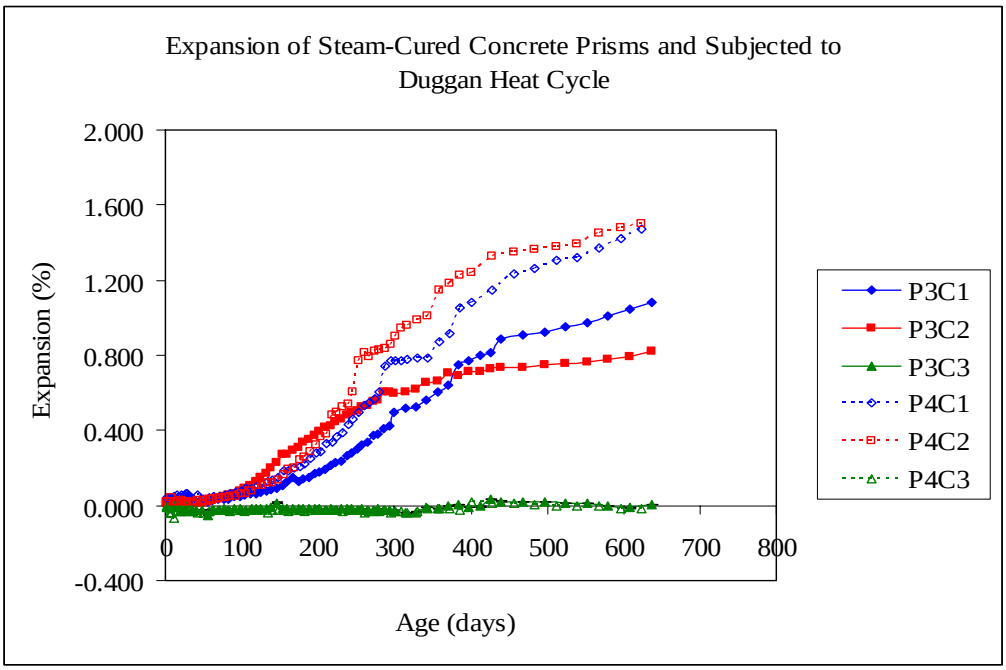


Figure 9.11: Expansion of all Steam-Cured Concrete Prisms Subjected to Duggan Heat Cycle and Stored Under Different Exposure Conditions

The concrete prisms with high potassium content exhibited slightly smaller weight changes than the control. This can be attributed to the high alkali level associated with fast expansion rates of the concrete prism causing significant damage to the microstructure. As the concrete expands faster, the microstructure disintegrates, and its pore structure loses capacity to hold water. However, this becomes very favorable for ettringite formation. The weight change was higher in the totally submerged concrete prisms, and was due to the ettringite formation and excess water trapped in the cracks. This was confirmed with the SEM and EDAX analysis

results. Figure 9.12 illustrates the weight change of control and concrete prisms made with 1.5% $K_2O$ subjected to the Duggan heat cycle and stored in different conditions.

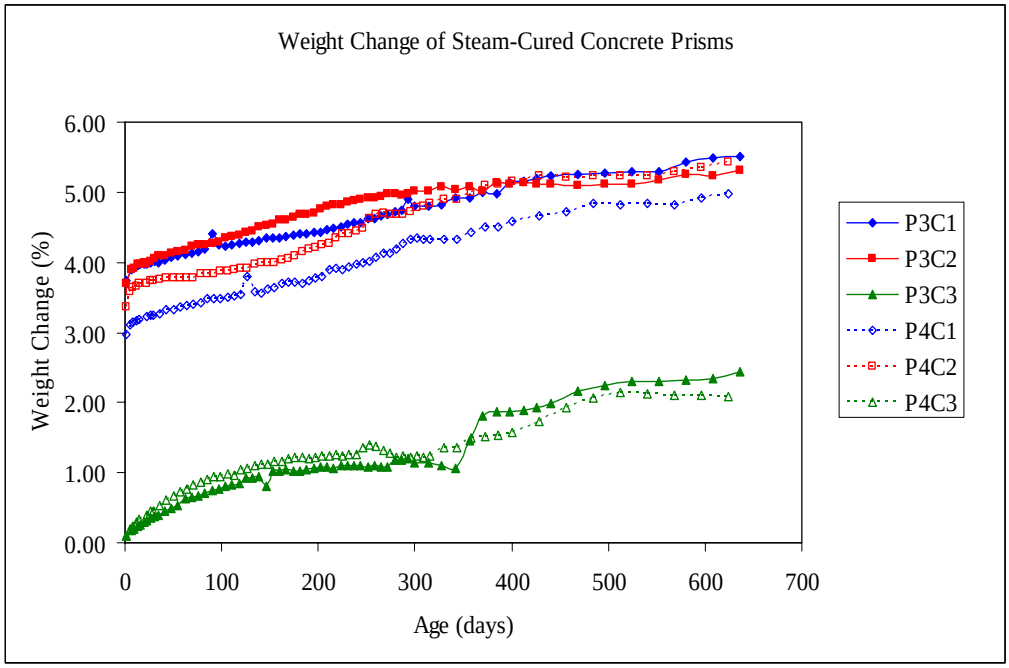


Figure 9.12: Weight Change of all Concrete Prisms Subjected to Duggan Heat Cycle and Stored Under Different Exposure Conditions

Expansion against weight change of the steam-cured concrete prisms subjected to the Duggan heat cycle showed little or no linear correlation for the first 100 days. However, a high linear correlation was observed from 100 days to the end for concrete prisms in exposure conditions 1 and 2.

The concrete samples kept submerged under water showed a decrease in compressive strength at later stages. Also, the results showed that an increase in potassium content caused a decrease in compressive strength of the concrete samples. Similar results were found by other researchers (Ronne and Sellevold, 1994, Taylor,

1994, Ramadan, 2000 and Azzam, 2002). These results are shown in figure 9.13. The effect of moisture content on compressive strength of concrete samples was investigated. Concrete may experience a wide variety of moisture conditions, ranging from the fully saturated in the case of submerged structures, to the almost fully dry in some buildings. Concrete samples that were dried in the laboratory for about 10 days before testing exhibited higher compressive strength than the moisture-saturated concrete samples. It was also discovered that the curing method employed at the early stages of the fresh concrete influenced the compressive strength at later stages. The room temperature-cured concrete samples prior to being subjected to the Duggan heat cycle were found to exhibit higher compressive strength than the steam-cured samples at later age.

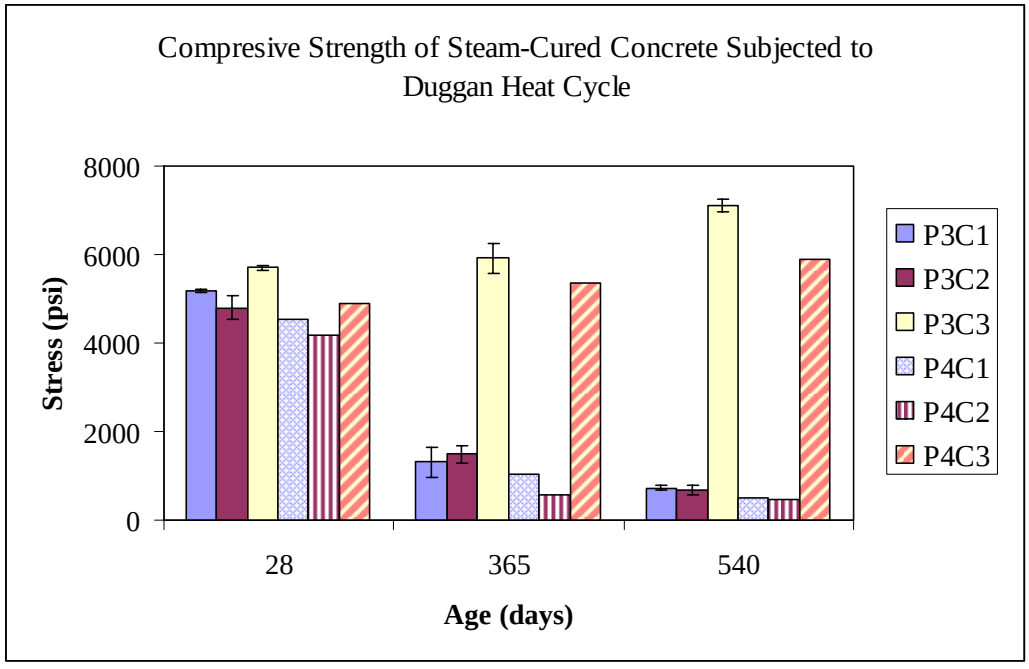


Figure 9.13: Compressive Strength Results of all Steam-Cured Concrete Samples Subjected to Duggan Heat Cycle and Stored Under Different Exposure Conditions

Using SEM equipped with EDAX analysis is essential in the investigation of DEF-related damage in concrete. The SEM micrograph identifies the characteristics while the EDAX analysis outlined the elemental chemical composition of mineral deposits within the microstructure of the concrete specimens. The examined concrete specimens showed different ettringite morphology for the different exposure conditions. SEM investigations of the totally submerged concrete prisms revealed ettringite occurrences that varied from a spherical ball, to needles to well-developed crystals over time. The SEM results of the concrete prisms in exposure condition 3 showed less ettringite with calcium hydroxide (CH) crystals. The concrete samples in the totally submerged storage conditions revealed CH crystals in the early stages. The CH crystals were gradually replaced by ettringite needles, which later changed to well-developed ettringite crystals. These large ettringite crystals occupied more space and contribute to the overall expansion of the concrete specimen. These types of ettringite in the concrete microstructure were found within the cement paste, in the cracks, inside the air voids, and in the interface between the cement paste and the aggregates. A correlation exists between ettringite formation, and extensive cracking in the concrete prisms. The crack network became extensive as the sizes of ettringite crystals grew. This was confirmed with the Laser Shearography image analysis. Accelerated expansion values were also noted during this period. Leaching of alkali ions from the concrete samples into the storage solutions was very substantial in exposure conditions 1 and 2. In addition, leaching led to decreasing the concentration of pH of the concrete pore structure, and thereby promoted the release of sulfate ions from the C-S-H gel, which favored ettringite formation. Alkali-Silica Reaction

(ASR) gel was absent in all the examined concrete specimens. Therefore, during this research study, all damage to the concrete samples is attributed to DEF. Figures 9.14 and 9.15 show ettringite formation in concrete samples subjected to the Duggan heat cycle, and stored under different exposure conditions.

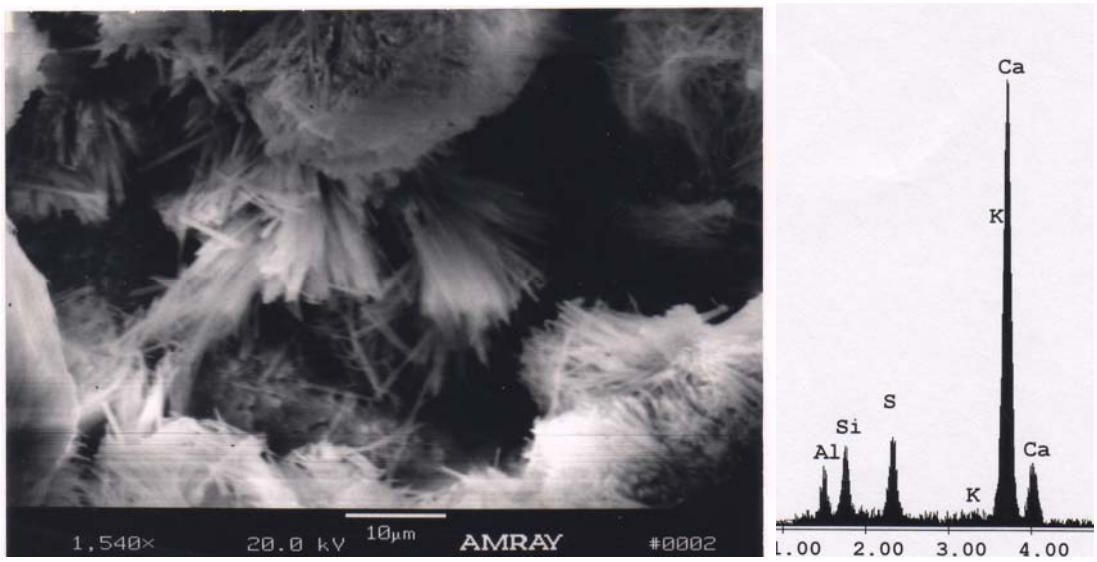


Figure 9.14: SEM and EDAX Analysis of Concrete Specimen in Exposure Condition 1 at Age of 540 Days, Showing Ettringite Needle-Like Crystals Filling an Air Void

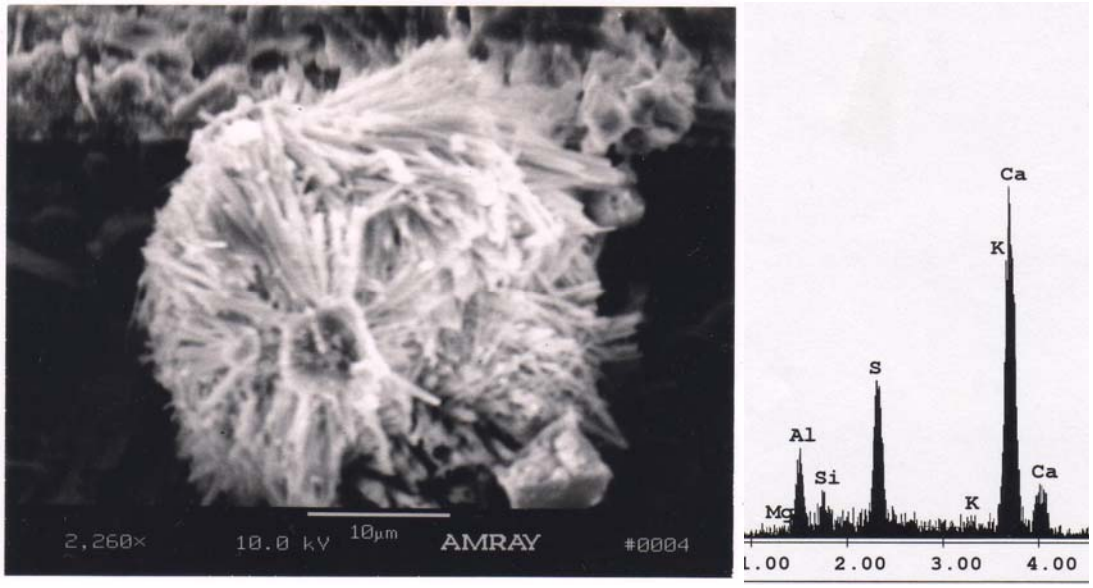


Figure 9.15: SEM and EDAX Analysis of Concrete Specimen Made With 1.5% $K_2O$ and Stored in Exposure Condition 1 at Age of 100 Days, Showing Bundles of Randomly Oriented Ettringite Needles Filling a Cavity

*9.3.2.2 Influence of Concrete Treatments and DEF*

Concrete samples were room temperature-cured before subjecting them to either the Duggan heat or Freeze-Thaw cycles, and subsequently storing them in isothermal water bath, pH maintained at 12.5 (limewater). The overall maximum expansion values of the concrete prisms were less 1.0% for entire research duration. Therefore, the both concrete samples showed no significant damage associated with DEF-induced expansion. Also, no visible cracks were observed on the concrete surfaces for up to 400 days of storage. The steam-curing method accelerated the expansion and formation of ettringite at a later age of the concrete samples. The steam-curing also increased cracking; this facilitated water movement into the pore structure of the specimen. Figure 9.16 illustrates the expansion of the room

temperature-cured concrete prisms subjected to either the Duggan heat or Freeze-Thaw cycles.

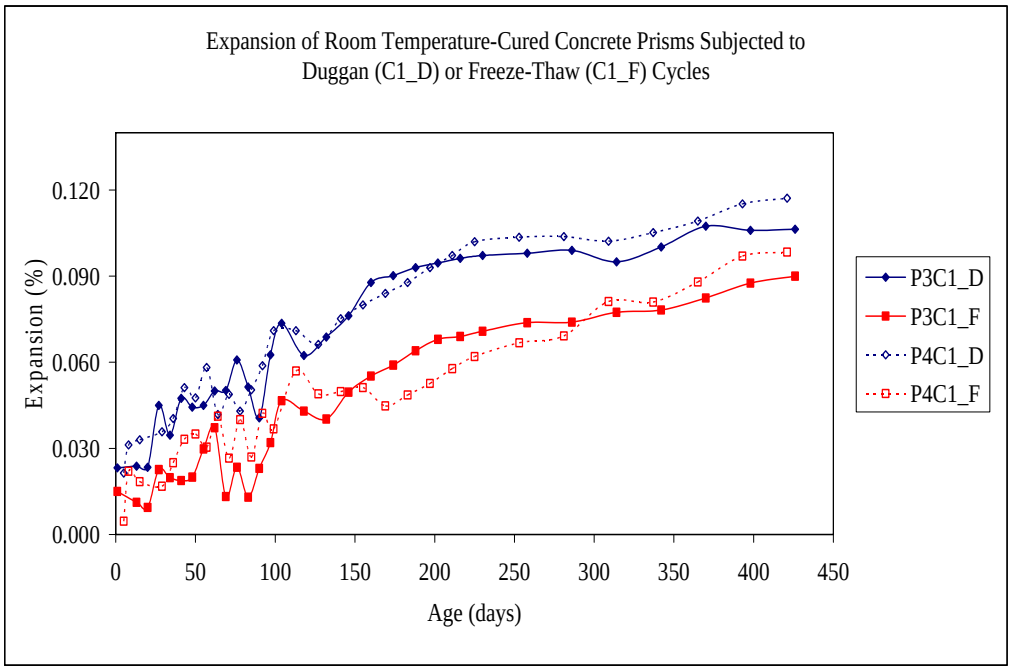


Figure 9.16: Expansion of all Room Temperature-Cured Concrete Prisms Subjected to Different Treatments and Stored in Limewater

The Freeze-Thaw cycles treated concrete prisms exhibited less significant weight change. This might be due to a smaller amount of ettringite found in the microstructure of the Freeze-Thaw treated concrete prisms. The weight-change measurements of the concrete prisms plateau over time. The SEM results correlated with the expansion showed minimal weight change in the concrete prisms with less occurrences of ettringite at later ages. An abundant amount of ettringite crystals were found only in the Duggan heat cycle treated concrete prisms. Figure 9.17 shows the

weight change of the room temperature-cured concrete prisms subjected to either the Duggan heat or Freeze-Thaw cycles.

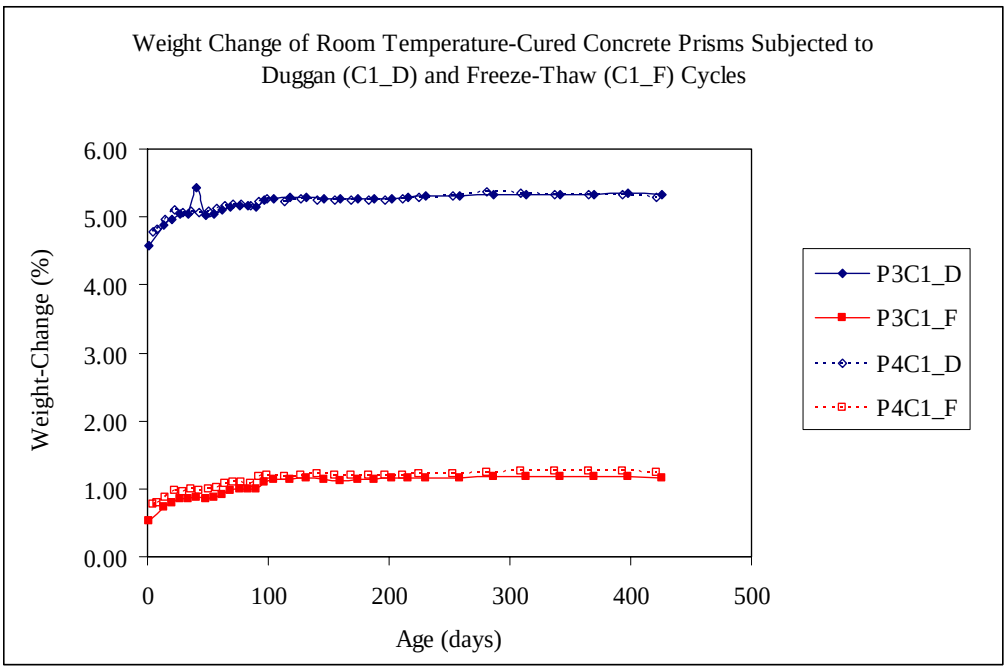


Figure 9.17: Weight Change of all Room Temperature-Cured Concrete Prisms Subjected to Different Treatments and Stored in Limewater

The effect of concrete treatment and potassium content on the compressive strength of concrete specimens was investigated. Earlier results showed that an increase in potassium content drastically decreased the compressive strength of the concrete specimens. However, both sets of the room temperature-cured concrete specimens revealed an increase in compressive strength at later ages. This further suggests that there are problems associated with steam-curing which have an adverse influence on the compressive strength of concrete samples. Figure 9.18 shows the

compressive strength of the room temperature-cured concrete specimens subjected to the Duggan heat or Freeze-Thaw cycles.

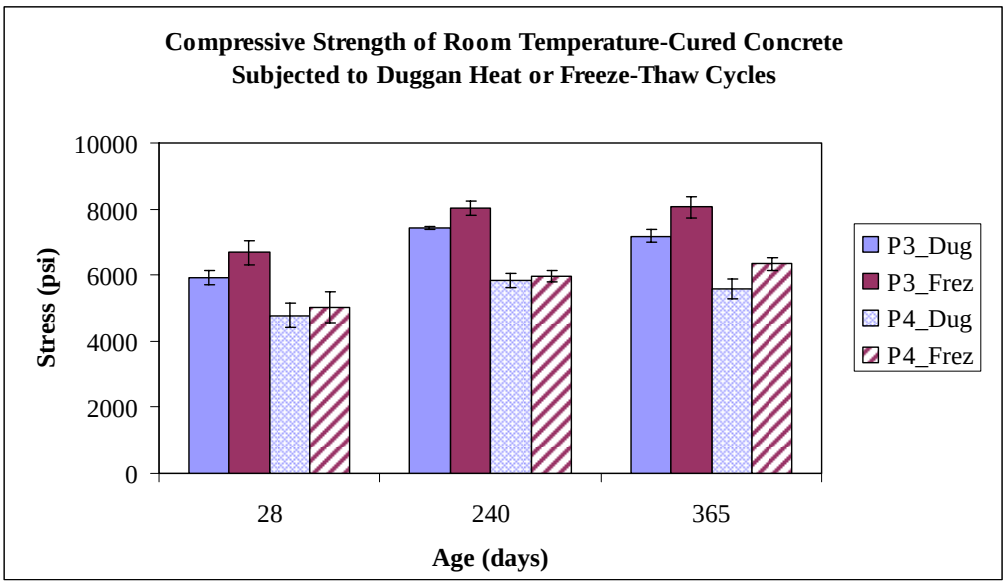


Figure 9.18: Compressive Strength Results of all Room Temperature-Cured Concrete Samples Subjected to Different Treatments and Stored in Limewater

Laser shearography image analysis showed that most of the microcracks formed in the concrete specimens were due to different concrete treatments employed at early ages of the concrete. Laser shearography analysis revealed the Duggan heat cycle treated concrete prisms exhibited more cracked areas than the Freeze-Thaw treated concrete prisms. The amount of microcracks formed at the early age of the concrete specimens played important roles in the durability of the specimens. The microcracks influenced the permeability of the concrete pore structure, and this led to an increase in the expansion rate of the concrete specimens. Therefore, it is of great importance to cure concrete properly in order to minimize or eliminate structural

defects leading to premature deterioration of the concrete specimen. A correlation exists between the SEM results and the Laser Shearography image analysis. The amount and size of the ettringite crystals found in the concrete specimens did not increase significantly or disappeared at later stages. It can be postulated that since the growth of ettringite was minimal, this might have retarded the rate of expansion of the concrete prism. SEM investigations of the Freeze-Thaw cycles treated concrete specimens showed few ettringite and calcium hydroxide (CH) plates at several stages during the storage period. Figures 9.19 and 9.20 show SEM and EDAX analysis of room temperature-cured concrete specimens subjected to either the Duggan heat or Freeze-Thaw cycles respectively.

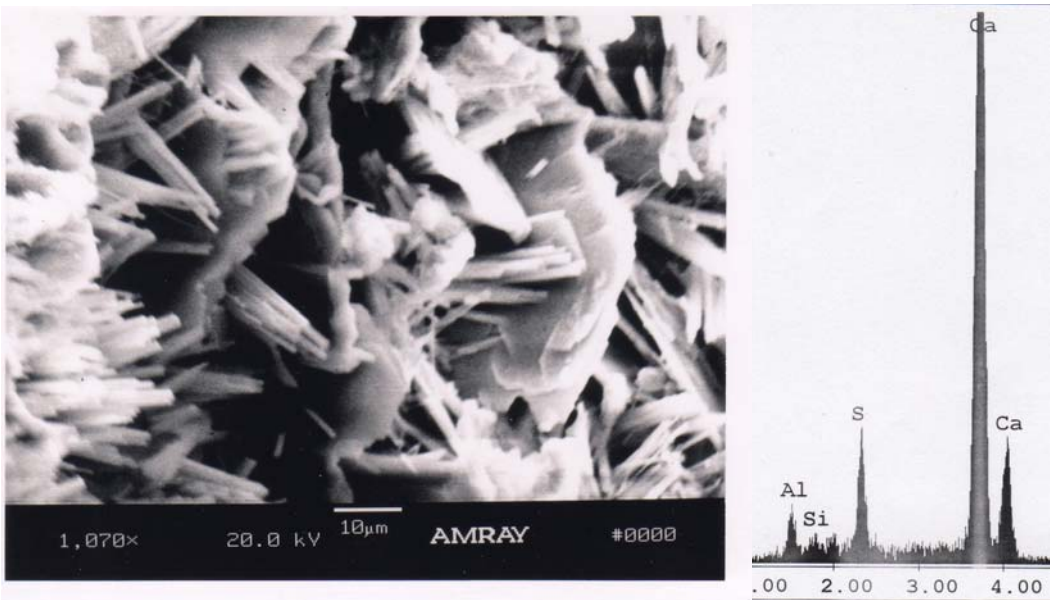


Figure 9.19: SEM and EDAX Analysis of Room Temperature-Cured Concrete Specimen Subjected to Duggan Heat Cycle and Stored in Limewater at Age of 365 Days, Showing Ettringite Crystals Filling an Air Void

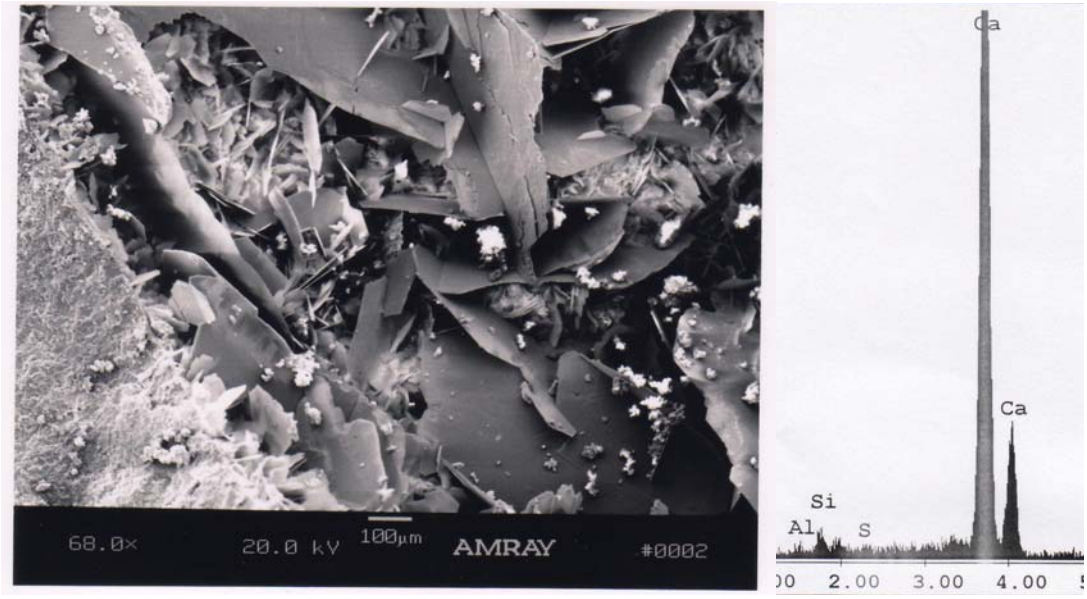


Figure 9.20: SEM and EDAX Analysis of Room Temperature-Cured Concrete Specimen Subjected to Freeze-Thaw Cycles and Stored in Limewater at Age of 365 Days, Showing CH Plates Filling Water Voids

*9.3.2.3 Concrete Samples Subjected to Field Conditions and DEF*

Concrete samples were prepared in the laboratory and subsequently exposed to field conditions to explore DEF and its associated expansion. None of the concrete prisms showed a significant expansion regardless of the curing method employed. This is characteristic of field-exposed specimens due to the ever changing environmental conditions. Long-term tests will be required in order to correlate the field results, if any, with the laboratory stored specimens. The expansion and weight change of the field-exposed concrete specimens fluctuated over time. Only the concrete prisms made with high potassium content showed expansion over time. Figures 9.21 and 9.22 show expansion and weight change results of the field exposed concrete prisms respectively.

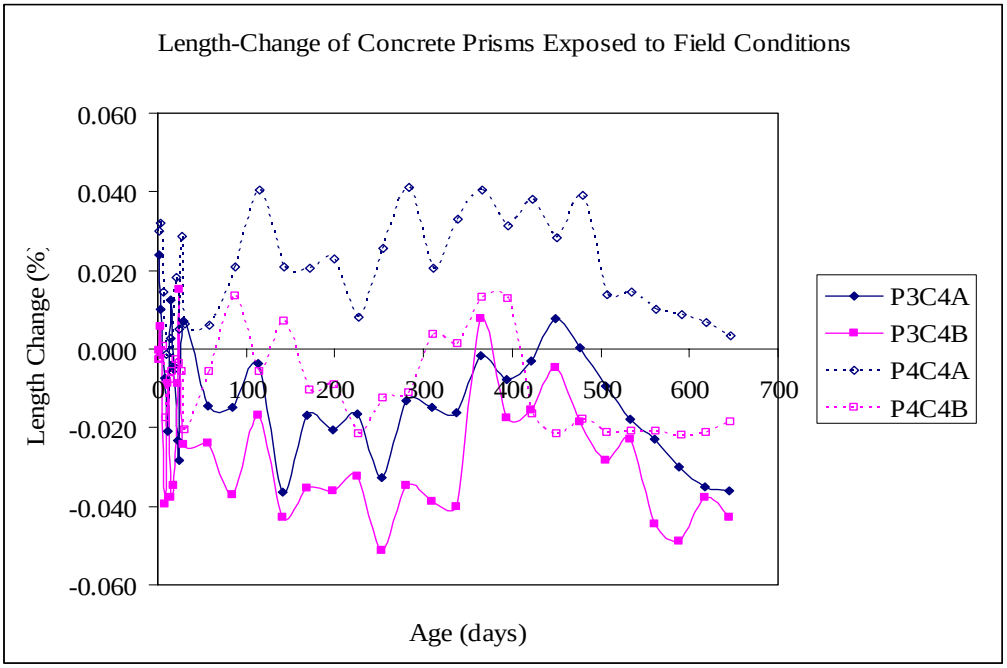


Figure 9.21: Length-Change of all Concrete Prisms Exposed to Field Conditions

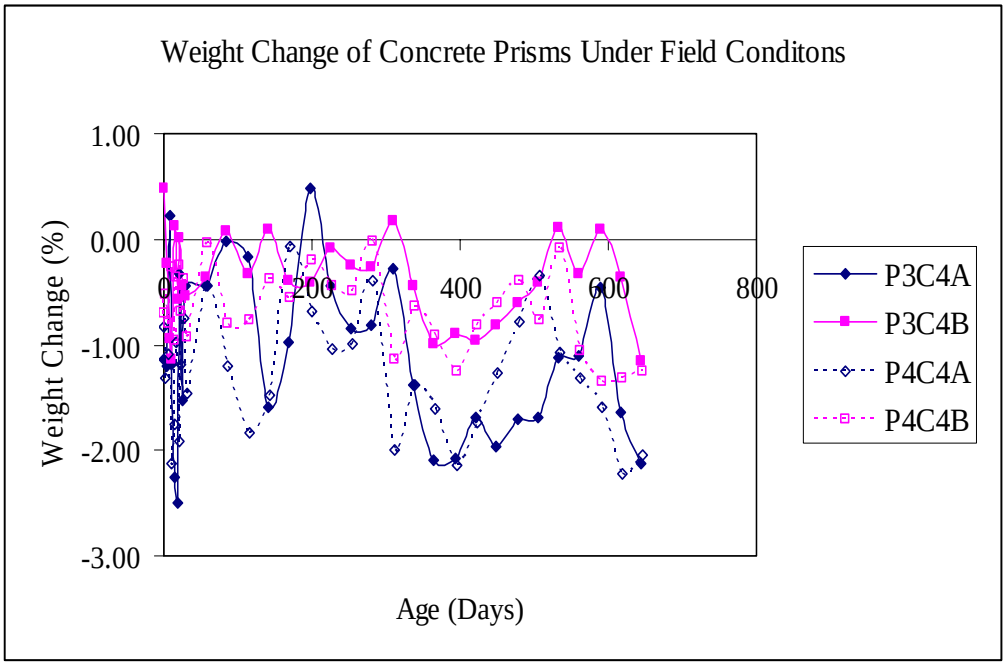


Figure 9.22: Weight-Change of all Concrete Prisms Exposed to Field Conditions

The field-exposed concrete specimens showed an increase of up to 20% in compressive strength at later age. These results suggest that steam-curing and the cement composition of the concrete specimens are critical to the compressive strength. The effect of an increase in potassium content on the compressive strength of field-exposed concrete did not show any trend. Figure 9.23 shows the compressive strength of the field-exposed concrete specimens.

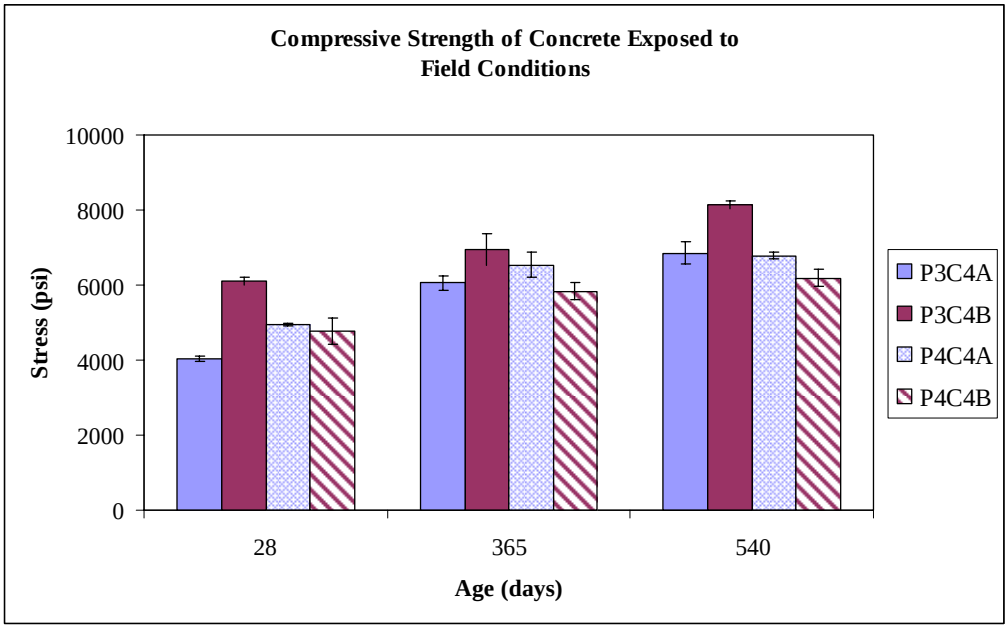


Figure 9.23: Compressive Strength Results of all Concrete Samples Subjected to Field Conditions

SEM investigations found DEF in the concrete prisms exposed to field conditions. However, the amount and size of the ettringite crystals were not as large as those in the totally submerged concrete prisms. SEM results correlated with expansion revealed that ettringite can occur without deleterious expansion. Any damage exhibited by the concrete samples was attributed to mineral deposits, mainly

DEF, found in their microstructures. Figures 9.24 and 9.25 show SEM and EDAX analysis of concrete specimens subjected to field conditions.

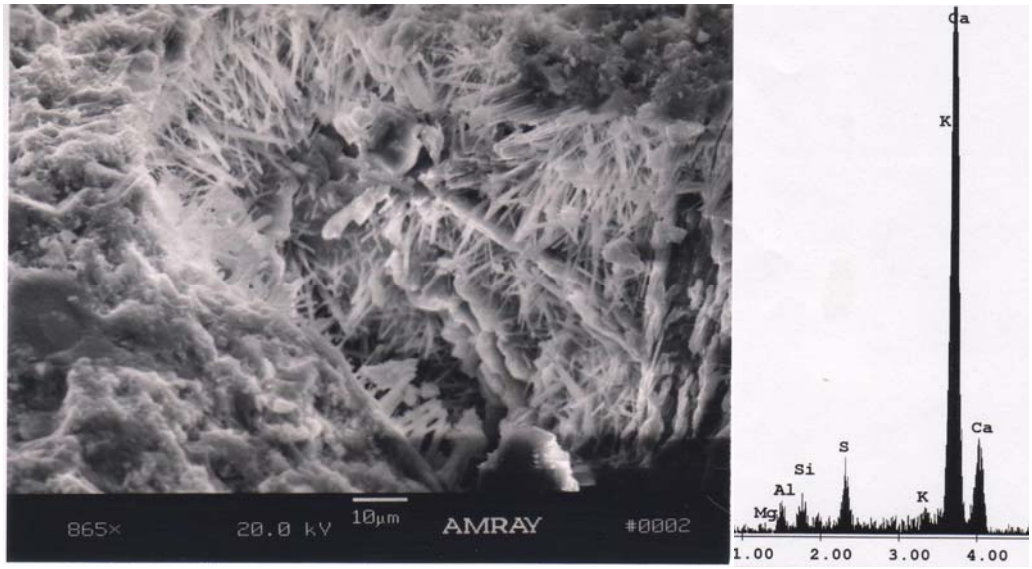


Figure 9.24: SEM and EDAX Analysis of Room Temperature-Cured Concrete Specimen Under Field Conditions (C4B) at Age of 40 Days, Showing Ettringite Deposits Within an Air Void

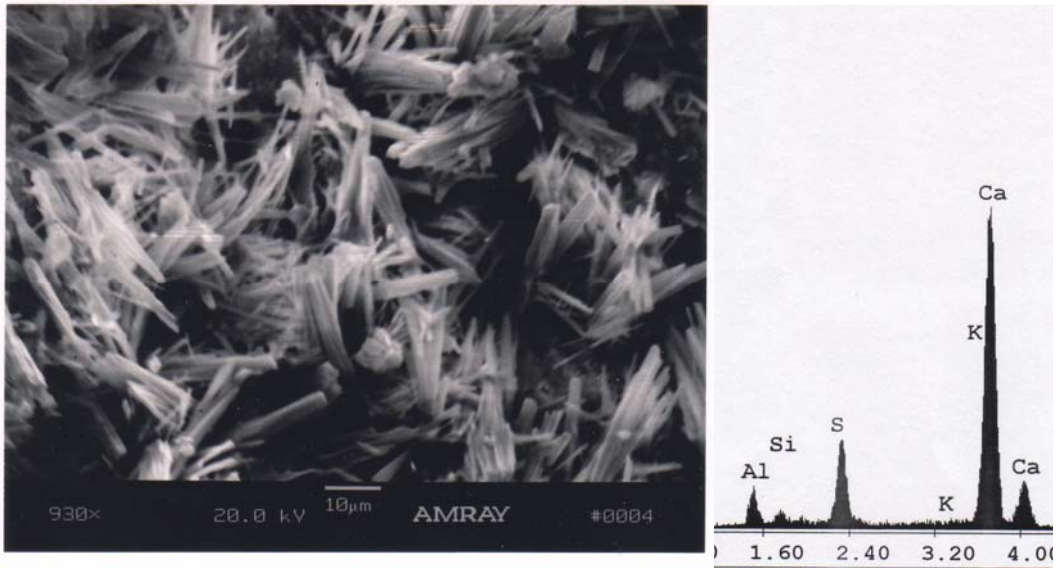


Figure 9.25: SEM and EDAX Analysis of Steam-Cured Concrete Specimen Made With 1.5% $K_2O$ and Stored Under Field Conditions (C4A) at Age of 540 Days, Showing Ettringite Crystals Filling Cavities and Air Voids

# Chapter 10: Conclusions and Recommendations

## *10.1 Introduction*

Delayed ettringite formation (DEF) and its associated deleterious expansions in mortar and concrete samples were mainly affected by the storage conditions and cement composition. Increasing the alkali level by adding potassium carbonate to the mixing water increased the sulfate concentration which in turn induced the precipitation of ettringite. The ettringite morphology changed over time for all the different exposure conditions. DEF was also found in concrete samples subjected to no heat or thermal cycles during the entire research study. Limiting the amount of microcracking present at the early stages of fresh concrete is very essential in DEF mitigation and enhancement of concrete durability. These experiments have shown that significant expansions of mortar and concrete, and the occurrence of DEF are correlated over time. However, it is not possible to conclude that DEF causes the expansion. At a macroscopic level, both processes require abundant moisture. Nevertheless, the actual damage takes place on a microscopic level. Throughout the entire research, at several intervals no ASR was discovered in any of the examined mortar and concrete specimens.

*10.2 Conclusions*

Based on the results of this research, the following conclusions were obtained:

1. The rate of expansion of the mortar and concrete samples increased with an increase in potassium content ($K_2O$) of the specimens.
2. High temperature-curing regimes were found to enhance DEF but were not the critical factors required for DEF. DEF was found even in mortar and concrete specimens that were not subjected to heat cycles.
3. Microstructural observations, which included the use of Scanning Electron Microscopy (SEM) equipped with energy dispersive analysis X-ray (EDAX), of the expanded mortar and concrete specimens at several stages, revealed delayed ettringite formation without detecting any sign of ASR.
4. SEM results correlated with expansion results showed that the exposure conditions of the mortar and concrete specimens played a dominating role in the expansion and the formation of DEF.
5. SEM investigations also revealed that calcium hydroxide (CH) crystals were gradually replaced by ettringite needles, which later proceeded to well-developed crystals.
6. Mortar and concrete specimens that showed deleterious expansion exhibited a lot of ettringite.
7. DEF damage in mortar and concrete specimens became very significant, when large ettringite crystals were found in the cracks of the matrix. However, this does not exclude the contribution of cement paste expansion to the overall expansion.

8. Curing at elevated temperatures followed by severe thermal drying and wetting processes such as the Duggan heat cycle promoted mortar and concrete deterioration due to DEF.
9. The leaching of alkalis from the mortar and concrete specimens into the storage solutions increased the rate of expansion, hence promoting the formation of ettringite.
10. During the first 100 days of storage, the expansion of the mortar bars showed high linear correlations with weight-change for the totally submerged specimens in exposure conditions 1 and 2. Even with an increase in alkali content, the expansion against weight-change measurements still showed a linear correlation.
11. About 80 to 90% of the weight-change of the concrete prisms occurred during the first 100 days of storage in exposure conditions 1 and 2.
12. DEF-related damage can also be monitored by weight change of the specimens instead of length change measurements (See item 11).
13. Curing method employed during preparation of mortar and concrete samples affected the behavior at later age. Regardless of exposure conditions, Duggan heat cycle treated concrete prisms expanded higher than Freeze-Thaw cycles treated concrete prisms.
14. The threshold expansion value of 0.05% at 20 days suggested by Duggan needs to be revised to address sample size and samples from existing structures. In this research, concrete samples did not reach the threshold value

at the suggested time but revealed deleterious expansion and DEF after several months.

15. The effect of heat-curing, potassium content and the Duggan heat cycle on the later age compressive strength of mortar and concrete specimens was different for different exposure conditions. For some, it may decrease their later age compressive strength but, for others, it may increase the strength.
16. The concrete specimens were tested moist and surface-dry. The compressive strength was very sensitive to the moisture conditions of the tested concrete specimens. The compressive strength of the surface-dry concrete specimens was about 20% higher than the moist-saturated concrete specimens.
17. Laser shearography image analysis can be used to detect cracks' growth over time in concrete specimens damaged by DEF. Laser shearography has a minimum detectable crack width < 10 microns.
18. Laser shearography image analysis showed that ettringite in the pre-existing cracks led to lengthening and widening of these cracks after continuous exposure to water.
19. In this research, the laboratory-prepared, and subsequently field exposed specimens, showed no significant expansion and weight change caused by DEF.

*10.3 Recommendations for Further Work*

1. Investigate the use of other crushed stone sands with higher ASR reactivity.
2. Study the use of synchrotron radiation to quantify ettringite distribution in mortar and concrete samples at different expansion stages.
3. Since premature deterioration due to DEF is yet to be fully understood, explore studies to mitigate the problem.
4. The role of coarse aggregate on DEF, if any, should be investigated.
5. Long-term tests using concrete prisms are needed for any correlation to be established between laboratory and field concretes.
6. Further investigation including sample sizes of concrete from existing structures is required to establish Duggan threshold limits.

# References


ASTM, 2001 Annual Book of Standards. Volume 04.02 Concrete and Aggregate. American Society for Testing and Materials, Philadelphia.

ASTM, 2001 Annual Book of Standards. Volume 04.01 Cement; Lime; Gypsum. American Society for Testing and Materials, Philadelphia.

ASTM, 2002 Annual Book of Standards. Volume 11.03 Atmospheric Analysis; Occupational Health and Safety; Protective Clothing. American Society for Testing and Materials, Philadelphia.

Atkins, N. H., 1997, "Highway Materials, Soils and Concrete," 3rd Edition, Ed Francis, Ed., pp. 280 – 289.

Amde, A.M., Azzam, A., Sabnis, G. and Livingston, R. A., October 11-13, 2006, "The Effects of Mix Water Conditioner on Internal Sulfate Attack in Concrete," Seventh International Congress on Advances in Civil Engineering (ACE 2006), Istanbul, Turkey (under review).

Amde, A.M., Ceary, M. and Livingston, R,A., January 6-8, 2005a, "Investigation Of Maryland Bridges For DEF And ASR," International Conference on Advances in Concrete Composites and Structures, ICACS- 2005, editors: N. Lakshmanan, S. Gopalakrishnan and H.G. Sreenath, Chennai, India, pp. 809-816.

Amde, A.M., Azzam, A. and Livingston, 2005b, "Mitigation of Delayed Ettringite Formation Using Class F Fly Ash and Mix Water Conditioner," 30th Conference on Our World in Concrete and Structures–Engaging the Future, editors: C.T.Tam, K.C.G. Ong and T.H. Tan, CI-Premier PTE LTD, Vol. XXIV (ISBN 981-05-3546-5), pp. 191-198.

Amde, A.M., Williams, K. and Livingston, R.A., 2005c "Influence of Fine Aggregate Lithology on Delayed Ettringite Formation in High Early Strength Concrete," High-Performance Cement-Based Concrete Composites, J. Biernacki, S. Shah, N. Lakshmanan and S. Gopalakrishnan, editors, Materials Science of Concrete Special Volume, the American Ceramic Society, Westerville, Ohio, pp. 199-209.

Amde, A.M., December 2004a, "UMD/FHWA Studies on Delayed Ettringite Formation," International Conference on Advances in Concrete and Construction (ICACC2004), Hyderabad, India.

Amde, A.M., Ceary, M. and Livingston, R., April 18-21, 2004b, "Measurement of Expansion Associated with Delayed Ettringite formation," 106th Annual meeting & Exposition of the American Ceramic Society, Indianapolis, U.S.A.

Amde, A.M., Livingston, R.A. and Azzam, A., September 2003a, "Influence of Alkali Content and Development of Accelerated Test Method for Delayed Ettringite Formation," Proceedings of International Innovative World of Concrete Conference, Pune, India

Amde, A.M., Livingston, R.A. and Azzam, A., September 2003b, "Characterization of Damage and Development of Accelerated Test Method for Delayed Ettringite Formation," International Symposium on the Innovative World of Concrete, Pune, India.

Azzam, A., 2002, "Delayed Ettringite Formation, the influence of aggregate types, curing conditions, exposure conditions, alkali content, fly ash and mix water conditioner (MWC)," Ph.D Dissertation, University of Maryland, College Park, USA.

Azzam, A., Amde, A.M. and Livingston, R.A., "Delayed Ettringite Formation, the Influence of Aggregate Type and Curing Conditions," J. of Materials in Civil Eng., ASCE (under review).

Abo-El-Enein, S. A., Hanafi, S., Hekal, E. E., 1988, "Thermal and Physiochemical Studies on Ettringite II: dehydration and thermal stability," Cemento, Vol. 85, No.2, pp. 121-132.

Abo-El-Enein, S. A., Abo-Nuaimi, K. Kh., Marusin, S. L., and El-Hemaly, S. A.S., 1984, "Hydration Kinetics and Microstructure of Ettringite," Proc. 6th Conf. on Cement Microscopy, Int. Cement Microscopy Assoc., Duncanville, TX, pp. 219-231.

Attiogbe, E. K., Wells, J. A., and Rizkalla, S. H., Sept. 1990, "Evaluation of Duggan Concrete Core Expansion Test," Research Report, Sponsored by Canadian National Railway and Transport Institute, University of Manitoba, Winnipeg, Canada.

BioImaging research Inc. (BIR), 1998, "ACTIS 600/420 Real-Time Radiography/Digital Radiography/Tomography," Report, Bio-Imaging Research, Inc. (BIR), Lincolnshire, IL, 1998.

Bentur, A. and Berger, R. L., 1979, "Chemical Composition of C-S-H Gel Formed in the Hydration of Calcium Silicate Pastes," Journal of The American Ceramic Society, Vol. 62, pp. 117-120

Candlot, E. 1890, “Properties des ciments et des liants hydrauliques,” Bull. Soc. Encour. Ind. Natn., pp. 682-685.

Ceesay, J., Amde, A.M., Azam, A.,Livingston, R,A., and Newman, J, W., September 19-21, 2007, “Investigation of Modifications to the Duggan Test for Delayed Ettringite Formation,” The First International Conference on Recent Advances in Concrete Technology, Washington, DC (accepted).

Chamberline, W. H., Brewer, H. W., and Shiderler, J. J., August 1952, “Compressive Strength of Steam-Cured Concrete,” Report C-621, Bureau of Reclamation, U.S. Dept. of the Interior, Denver.

Chandra, S., Berntsson, L., Nov-Dec, 1988, “Deterioration of Concrete in Swimming Pool in the South of Sweden,” ACI Materials Journal, American Concr. Inst., Vol.85, N6, pp. 489-494.

Chatterji, S., Thaulow, N., Jensen, A. D., and Christiansen, P., 1987, “Mechanisms of Accelerating Effects of NaCl and $Ca(OH)_2$ on Alkali-Silica Reaction,” Proceedings 7th International Conference on Alkali-Aggregate Reaction, Ottawa, pp. 115-124.

Cody, R., Cody, A., Spry, P., Hyomin, L. (2001), “Reduction of Concrete Deterioration by Ettringite Using Crystal Growth Inhibition Techniques,” Iowa Department of Transportation, TR-431.

Cohen, M. D. 1982, “Microstructural Analysis of Ettringite Formation,” Scanning Electron Microscopy Assoc., Duncanville, TX, pp. 204-224.

Cohen, M. D. and Richards, C. W., 1982, “Effects of the Particle Sizes of Expansive Clinker on Strength – Expansion Characteristics of Type K Expansive Cements,” Cement and Concrete Research, Vol. 12, No. 6 pp.717-725.

Cohen, M. D., 1983, “Modeling of Expansive Cement,” Cement and Concrete Research, Vol. 13, pp. 519-528.

Cohen, M. D., Campbell, E. and Fowle, W., 1985, “Kinetics and Morphology of Ettringite Formation,” Proc. 7th Int. Conf. Cem. Microsc., Ed. James Bayles, pp. 360-381.

Collepardi, M., January 1999, “Damage by Delayed Ettringite Formation – A Holistic Approach and New Hypothesis,” Concrete International, Vol. 21, No. 1, pp. 69-74.

Collepardi, M., Baladini, G., Pauri, M., and Corradi, M., 1987, “Tricalcium Aluminate Hydration in the Presence of Lime, Gypsum or Sodium Sulfate,” Cement and Concrete Research, Vol. 8, No. 5, pp.571-580.

Damidot, D. and Glasser, F. P., 1993, "Thermodynamic Investigation of the CaO-$Al_2O_3$-$CaSo_4$-$H_2O$ System at 50°C and 85°C," Cement and Concrete Research, Vol. 23, pp. 221-238.

Dana, E. S., 1932, "A Textbook of Mineralogy," Wiley and Sons, New York.

Day, R. L., 1992, "The Effect of Secondary Ettringite Formation on the Durability of Concrete," A Literature Analysis of Portland Cement Association. Skokie, IL.

Daerr, G. M., Punzet, M., Ludwig, U., 1977 "On the Chemical and Thermal Stability of Ettringite on Dehydration I," Cem. Summ. Contrib. Semin., pp. 42-45.

Dean, J. A., 1999, "Lange's Handbook of Chemistry," 15th Edition, pp. 5.18.

Deng, M. and Tang, M., 1994, "Formation and Expansion of Ettringite Crystals," Cement and Concrete Research, Vol. 24, pp. 119-126.

Derucher, K. N., Korfiatis, G. P., Ezeldin, A.S., 1998, "Materials For Civil and Highway Engineers," 4th Edition, pp. 81- 90.

Diamond, S., 1983, "Alkaline Reactions in Concrete Pore Solution Effects," Proceedings 6th International Conference on Alkalis in Concrete, pp.155-166.

Diamond, S., 1996, "Delayed Ettringite Formation – Processes and Problems," Cem. Concr. Composites, Vol. 18, pp.205-215.

Diamond, S., 1989, "ASR-Another Look At Mechanisms," Proceedings 8th International Conference on Alkali-Aggregate Reaction, Kyoto, Japan, pp. 83-94.

Diamond, S., 1987, "Cement Paste Microstructure in Concrete," Proc. of Material Research Society, Vol. 85, pp.21-31.

Diamond, S., Olek, J. and Wang, Y., 1998, "The Occurrence of Two-Tone Structures in Room Temperature Cured Cement Pastes," Cem. Concr. Res., Vol. 28, No. 9, pp. 1237-1243.

Diamond, S., and Ong, S., 1994, "Combined Effects of Alkali Silica Reaction and Secondary Ettringite Deposition in Steam Cured Mortars," In Cement Technology, American Ceramic Society, Westerville, Ohio, pp. 79 – 90.

Duggan, R. and Scott, F., 1989, "New Test for Deleterious Expansion in Concrete," Alkali-Aggregate Reaction. 8th International Conference, Elsevier Applied Science, New York, pp. 403-408.

Divet, L., and Randriambolona, R., 1998, “Delayed Ettringite Formation: The Effect of Temperature and Basicity on the Interaction of Sulphate and C-S-H Phase,” Cem. Concr. Res., Vol. 28, pp. 357-363.

El-Sayed, H. A., El-Wahed, M. G. Abd, Ali, A. H., July 1987, “Some Aspects of the Corrosion of Reinforcing Steel in Concrete Marine Atmospheres,” Durability of Building Materials, Vol.5, N1, pp. 13-25.

Eriksson, B. E. and Tepponen, P., 1985, “Heat Treatment as the Cause of Concrete Failure,” Betonintuote, Vol. 2.

Famy, C., Scrivener, K. L., Brough, A.R., Atkinson, A., 2001, “Influence of the Storage Conditions in the Dimensional Changes of Heat-Cured Mortars,” Cem. Concr. Res. Vol. 31, pp. 795-803.

Famy, C., 1999, “Expansion of Heat-Cured Mortars,” Ph.D. Thesis, Purdue University, USA.

Farsky, R., Basavarajaiah B. S. Jan. 1971 “Some Studies of Steam Curing of Cement Mortar,” Indian Concrete Journal, Vol. 45, No. 1, pp. 35-41.

Fu, Y., 1996, “Delayed Ettringite Formation in Portland Cement Products,” Ph.D. Thesis, University of Ottawa, Ottawa, Canada.

Fu, Y., and Beaudoin, J. J., 1996, “Mechanism of Delayed Ettringite Formation in Portland Cement Systems,” ACI Materials Journal, Vol. 93, No. 4, pp. 327-333.

Fu, Y. and Beaudoin, J. J., 1996, “Microcracking as Precursor to Delayed Ettringite Formation in Cement Systems,” Cem. Concr. Res., Vol. 26, No. 10, pp. 1493-1498.

Fu, Y. and Beaudoin, J. J., 1996, “On the Distinction Between Delayed and Secondary Ettringite Formation in Concrete,” Cem. Concr. Res., Vol. 26, No. 6, pp. 979-980.

Fu, Y. and Beaudoin, J. J., 1996, “Expansion of Portland Cement Mortar due to Internal Sulfate Attack,” Cem. Concr. Res., Vol. 27, No. 9, pp. 1299-1306.

Fu, Y., Xie, P., Gu, P., and Beaudoin, J. J., 1995 “Kinetic Study of Delayed Ettringite Formation in Cement Systems,” Cem. Concr. Res., Vol. 25, No. 1, pp. 63-70.

Fu, Y., Xie, P., Gu, P., and Beaudoin, J. J., 1993, “Preferred Nucleation of Secondary Ettringite in Pre-existing Cracks of Steam-cured Cement Paste,” Cement and Concrete Research, Vol. 24, No. 6, pp. 1015-1024.

Fu, Y., Xie, P., Gu, P., and Beaudoin, J. J., 1994, "Significance of Pre-existing Cracks on Nucleation of Secondary Ettringite in Steam Cured Cement Paste," Journ. Mat. Sci. Let., Vol. 12, pp. 1864-1865.

Gartner, E. M., Young, J. F., Damidot, D. A., and Jawed, I., 2002, "Structure and Performance of Cements," 2nd Edition, J. Bensted and P. Barnes, Ed., pp.57-113.

Gillott, J. E., Grobowski, E., Jones, T. N., Quinn, T., Scott, J. F., and Duggan, C. R., May 1989, "Mechanism of Expansion in Rapid Test Method for Alkali-Aggregate Reaction," Progress Report # 1, Dept. of Civil Engineering, University of Calgary, Calgary, Canada.

Ghorab, H. Y., Heinz, D., Ludwig, U., Meskendal, T., Wolter, A., 1980, "On the Stability of Calcium Aluminates Sulphate Hydrates in Pure Systems in Cements," 7th Intnl. Congr. Chem. Cem., Vol. IV, 496-503.

Ghorab, H. Y., Kishar, E. A., Jan. 1985, "Studies on the Stability of the Calcium Sulfoaluminate Hydrate: Part I: Effect of Temperature on the Stability of Ettringite in Pure Water," Cem. Concr. Res. Vol. 15, No. 1, pp. 93-99.

Ghorab, H. Y., Kishar, E. A., 1986, "The Stability of Calcium Sulfoaluminate Hydrate in Aqueous Solutions," Proc. 8th International Congress Chem. Cement, Rio de Janeiro, Vol. V., pp. 104-109.

Ghorab, H. Y. and Abou El Fetouh, S. H., 1985, "New Approach to the Hydration Reaction of the Tricalcium Aluminate with Gypsum at 30°C, Part I: Effect of Lime," Zement-kalk-Gips, Vol. 38, No. 5, pp. 267-270.

Grabowski, E., Czamecki, B., Gillott, J. E., Duggan, C. R. and Scott, J. F., 1992, "Rapid Test of Concrete Expansivity due to Internal Sulfate Attack," ACI Material Journal, Vol. 85, No. 5, pp.385-469.

Graf, L. A., 2007, "Effect of Relative Humidity on Expansion and Microstructure of Heat-Cured Mortars," PCA Serial No. SN2945, Portland Cement Association, Skokie, Illinois, USA.

Grattan-Bellew, P. E & Beaudoin, J. J., 1998, "Delayed Ettringite Formation; Effect of Clinker Particle Size and Composition on Expansion of Mortar Bars," Material Science of Concrete – The Sidney Diamond Symposium, Hawaii, pp. 295-307.

Grattan-Bellew, P. E & Lefebvre, P. V., 1986, "Effect of Confinement on Deterioration of Concrete Made with Alkali-Aggregate Reactions," Ottawa, Canada, pp. 280-285.

Gress, D., "Early Distress of Concrete Pavements," Federal Highway Administration, Publication No. FHWA-SA-97-045-53.

Hampson, C. J. and Bailey, J. E. Nov. 1982, "On the Structure of Some Precipitated Calcium Aluminsulphate Hydrates," Journ. of Materials Science, Vol. 71, No. 11, pp. 3341-3346.

Hanson, J. A., Jan. 1963, "Optimum Steam Procedures in Precasting Plants," Journal of American Concrete Institute, Vol. 60, pp. 1-25.

Heinz, D., and Ludwig, U., 1987, "Mechanism of Secondary Ettringite Formation in Mortars and Concretes Subjected to Heat Treatment," Concrete Durability ACI SP 100 Vol. 2 American Concrete Institute. Farmington Hills, MI, pp. 2059-2071.

Heinz, D., Ludwig, U., and Rudinger, I., 1989, "Delayed Ettringite Formation in Heat–Treated Mortar and Concretes," Concrete Precasting Plant and Technology, Vol.11, pp. 56-61.

Heinz, D., and Ludwig, U., 1986, "Mechanisms of Subsequent Ettringite Formation in Mortar and Concretes After Heat Treatment," 8th Int. Cong. Chem. Cem. Secretaria General de 8th CIQC, Rio de Janeiro, Vol. V, pp. 189-194.

Hekal, E. E., Abo El-Enein, S. A. 1986, "Effect of Compression on Microstructure and Thermal Stability of Ettringite," Proc. Intnl. Conf. On Cement Microscopy, 8th, Int. Cement Microscopy Assoc. Duncanville, TX. pp. 227-243.

Hime, W. G., 1996, "Clinker Sulfate: A Cause for Distress and a Need for Specification," Concrete for Environment Enhancement and Protection, Edited by R. K. Dhir and T.D Dyer, Published by E & F.N. Spon, London. UK., pp. 387-395.

Hime, W., July-August, 1996, "Delayed Ettringite Formation – A Concern for Precast Concrete," PCI Journal, pp. 26-30.

Hime, W. G., and Marusin. S. L., 1999, "Ettringite: The Sometimes Host of Destruction," SP-177, B. Erlin, (ed.), American Concrete Institute, Farmington Hills, MI.

Hunter, D., 1989, "The Geochemistry of Lime-induced Heave in Sulfate Bearing Clay Soils," Ph.D. Thesis, University of Nevada, Reno.

Idorn, G. M., 1968, "The Effect of Hydration Temperature on the Products of Portland Cement," Proceedings of the 5th International Symposium on the Chemistry of Cement, Tokyo, Japan, Vol. III, pp. 411.

Johansen, V., Thaulow, N., and Skalny, J., 1993, "Simultaneous Presence of Alkali-Silica Gel and Ettringite in Concrete," Advances in Cem. Res., Vol. 5, No. 17, pp. 23-29.

Jones, F. E., 1939, "The Quaternary System $CaO$-$Al_2O_3$-$CaSO_4$-$H_2O$ at 25°C," Trans. Faraday Soc. Vol. 35, pp.1484

Kalousek, G. L., 1941, "Sulphoaluminates of Calcium as Stable and Metastable Phases," Ph.D. Thesis, University of Maryland.

Kalousek, G. L., and Adams, M., Sept. 1951, "Hydration Products Formed in Cement Pastes at 25 to 150°C," ACI Journal. Proceedings, No. 48-7, pp. 77.

Kasdan, K. S., Sept. 27, 2003 "Sulfate Attack to Concrete – A Technical Perspective," http://www.kbla.com/articles.

Kelham, S., 1999, "Influence of Cement Composition on Volume Stability of Mortar," Ettringite: The Sometimes Host of Destruction, SP-177, B. Erlin, (ed.), American Concrete Institute, Farmington Hills, MI, pp. 141-158.

Kennerly, R. A., 1965, "Ettringite Formation in Dam Gallery," ACI Journal, pp. 559-576.

Ketcham, A., Denison, C. and Carlson, W. D., 1997, "Three-dimensional Quantitative Textural Analysis of Metamorphic Rocks Using High-Resolution Computed X-ray Tomography: Part I. Methods and Techniques," Journal of Metamorphic Geology, Vol. 15, pp. 29-44.

Kilgour, C. L., 1988, "Composition and Properties of Indian Fly Ashes," Ph.D. Thesis, Purdue University.

Kjellsen, K. O., 1996, "Heat Curing and Post-Heat Curing Regimes of High-Performance Concrete: Influence of Microstructure and C-S-H Composition," Cement and Concrete Research, Vol. 26, No. 2, pp. 295-307.

Kjellsen, K. O. and Detwiler, R. J., 1992, Cem. Concr. Res., Vol. 22, pp. 112-120.

Klemm, W. A., and Adams, L. D., 1990, "Investigation of the Formation of Carboaluminates," ASTM Special Tech. Publ., V-STP, No. 1064, pp. 60-72.

Klieger, P., June 1958 "Effect of Mixing and Curing Temperature on Concrete Strength," Journal of American Concrete Institute, Vol. 54, No. 12.

Klieger, P., March 1958 "Early High-Strength Concrete for Prestressing," Portland Cement Association, Research Bulletin RX91.

Klingner, R.E., Fowler, T.J., et al. 2002, "Nondestructive Testing of Prestressed Bridge Girders with Distributed Damage," University of Texas, Center for Transportation Research, CTR 1857-2.

Klingner, R.E., Fowler, T.J., et al. 2004a, "Mitigation Techniques for In-Service Structures with Premature Concrete Deterioration: A Literature Review," University of Texas, Center for Transportation Research, CTR 4069-1.

Klingner, R.E., Fowler, T.J., et al. 2004b, "Mitigation Techniques for In-Service Structures with Premature Concrete Deterioration: Development and Verification of New Test Methods," University of Texas, Center for Transportation Research, CTR 4069-2.

Klingner, R.E., Fowler, T.J., et al. 2004c, "Mitigation Techniques for In-Service Structures with Premature Concrete Deterioration: Synthesis Report," University of Texas, Center for Transportation Research, CTR 4069-3.

Kruger, P. 1993, "On the Relation between Non-isothermal and Isothermal Kolmogorov-Avrami-Johnson-Mehl Crystallization Kinetics," Journal of Physical Chemistry of Solids, Vol. 34, No. 11, pp. 1549-1555.

Kuzel, H. J. and Strohbauch, G., Aug. 1989, "Reactions Associated with the Action of $CO_2$ on Heat Treated Hardened Cement Pastes," ZKG International, No. 42, pp. 413-418.

Kuzel, H. J., 1996, "Initial Hydration Reactions and Mechanism of Delayed Ettringite Formation in Portland Cement," Cement and Concrete Composites, Vol. 18, pp. 195-203.

Kuzel, H. J., Pollmann, H., 1991, "Hydration of $C_3A$ in the Presence of $Ca(OH)_2$, $CaSO_4.2H_2O$ and $CaCO_3$," Cement and Concrete Research, Vol. 21, pp. 885-895.

Kuzel, H. J. Mayer, H., 1993, "Mechanism of Ettringite and Monosulfate Formation in Cement and Concrete in the Presence of $CO_2$," Proceedings of the 15th International Conference on Cement Microscopy, Dallas, 1993, International Cement Microscopy Association, Duncanville, Texas, 1993, pp. 191-203.

Kuzel, H. J., 1993, "Formation of AFm and AFt Phases in Hydrating Portland Cements," Virginia, 1994, International Cement Microscopy Association, Duncanville, Texas, 1993, pp. 125-136.

Lachaud, R., March 1979, "Thaumasite and Ettringite in Building Materials," Annales de I'Institut Technique du Batiment et des Travaux Publics, No. 370, pp. 1-7.

Lawrence, B. L., Myers, J. J., and Carrassquillo, R. L., 1999, "Premature Concrete Deterioration in Texas Department of Transportation Precast Elements," Ettringite: The Sometimes Host of Destruction, SP-177, B. Erlin, (ed.), American Concrete Institute, Farmington Hills, MI, pp. 141-158.

Lawrence, C. D., 1998, "Physiochemical and Mechanical Properties of Portland Cements," Lea's Chemistry of Cement and Concrete, 4th Editions, Arnold Publisher, Edited by P.C. Hewlett, pp. 343-419.

Lawrence, C. D., 1995, "Mortar Expansions Due to Delayed Ettringite Formation – Effects of Curing and Temperature," Cem. Concr. Res., Vol. 25, No. 4, pp.903-914.

Lawrence, C. D., 1993, "Laboratory Studies of Concrete Expansion Arising from Delayed Ettringite Formation," BCA Publications C/16, 147 pp. British Association. Crowthome, Berks, UK.

Lawrence, C. D., Dalziel, J. A., and Hobbs, D. W., May, 1990, "Sulphate Attack Arising from Delayed Ettringite Formation," Interim Technical Note, 12, British Cement Association, Wexham Springs, Slough, U.K

Lerch, W., Ashton, F. W., and Bogue, R. H., 1929, "Sulphoaluminates of Calcium," Journ. of Res. of the National Bureau of Standards, Vol. 2, No. 4, pp. 715.

Lerch, W. and Ford, C. L., 1948, "Long-Time Study of Cement Performance in Concrete - Chapter 3. Chemical and Physical Testing of Cements," Journ. Amer. Concr. Inst., Proceedings, Vol. 44, pp. 743-795.

Lewis, M. C., Scrivener, K. L., and Kelham, S., 1994, "Heat Cured and Delayed Ettringite Formation," Mat. Res. Soc. Symp. Proc. No. 370, pp. 67-77.

Lewis, M. C., 1996, "Heat Curing and Delayed Ettringite Formation in Concretes," Ph.D. Thesis, University of London.

Lewis, M. C., and Scrivener, K. L., 1997, "A Microstructural and Microanalytical Study of Heat Cured Mortars and Delayed Ettringite Formation," Proc. Int. Congr. Chem. Cem., 10th Gothenburg, Vol. 4, pp. 409-416.

Lieber, W., 1963, "Ettringite Formation at Elevated Temperatures," Cement Kalk-Gips, Vol. 9, pp. 364-365.

Livingston, R. A., Newman, J., Ceesay, J., Amde, A. M., and Wallace, D., June 2006, "Laser Shearography for Detection of Fine Cracks in Concrete and Masonry," Forde, M (Ed) Structures and Faults-2006, Edinburg, UK.

Livingston, R. A., Newman, J., Ceesay, J., Amde, A. M., and Wallace, D., June 2006, "Development of a Portable Laser Shearography for Crack Detection in Bridges," Al_Qadi and Washer, G. A (Eds), NDE Conference on Civil Engineering, American Society for Nondestructive Testing, St. Louis, MO, pp. 262-268.

Livingston, R. A., Ceary, M. & Amde, A. M., 2002, "Statistical Sampling Design for a Field Survey of Delayed-Ettringite-Formation Damage in Bridges," in Structural Materials Technology V: An NDT Conference (eds. Washer, G. A. & Alampalli, S.), 411-420, ASNT, Cincinnati, OH, U.S.A.

Livingston, R. A. & Amde, A. M., 2001a, "Nondestructive Test Field Survey for Assessing the Extent of Ettringite-related Damage in Concrete Bridges," in Nondestructive Characterization of Materials X (eds. Green, R. E., Kishi, T., Saito, T., Takeda, N. & Djordjevic, B. B.), 167-174, Elsevier Science Ltd., Oxford, U.K.

Livingston, R.A., Amde, A.M. and Ramadan, E., 2001b, "Characterization of Damage in Portland Cement Concrete Associated with DEF," Proc. of the 6th Int. Conf. CONCREEP 6 @ MIT (eds. Ulm, Bazant, and Wittmann), pp. 463 – 468, Elsevier, Cambridge, U.K.

Livingston, R. A., and Amde, A. M., and Wallace, D., June 28, 2000, "Nondestructive Test Field Survey for Assessing the Extent of Ettringite-Related Damage in Concrete Bridges," Presented at 10th International Symposium on the Destructive of Materials, Karuizawa, Japan.

Livingston, R. A., 1998, "Notes on Kolmogorov-Arvrami-Johnson-Mehl Analysis of Modified Duggan Test Data," unplished draft, Nov. 4, Turner Fairbank Highway Research Center, FHWA.

Ludwig, U., 1991, "Problems of Ettringite Formation in Heat Treated Mortars and Concretes," 11th International Building Materials and Silicate Conference, EMS European Media Service, Witzmannsberg, Germany, pp. 164-177.

Macleod, G., Hall, A. J. and Hagleitner, K., 1977, "An Applied Mineralogical Investigation of Concrete Degradation in Major Concrete Road Bridge," Mineral. Mag., Vol.55, N377, pp. 637-644.

Marusin, S. L., 1995, "Deterioration of Railway Ties in the USA," CANMET/ACI Intl. Workshop on AAR in Concr., Nova Scotia, Canada, pp. 243-255.

Marusin, S. L., March 28 - April 1, 1993, "SEM Studies of DEF in Hardened Concrete," Proceeding of the Fifteenth International Conference on Cement Microscopy, Dallas, Texas, pp. 289-299.

Marusin, S. L., 1993, "SEM Studies of Concrete Failures Caused by Delayed Ettringite Formation," Proceeding of the 4th Euroseminar on Microscopy Applied to Building Material, Visby, Sweden.

Marusin, S. L., 1995, "Sample Preparation – the Key to SEM Studies of Failed Concrete," Cement Concrete Composites, Vol. 17, No. 4, pp. 311-318.

Mather, B., 1984, "Discussion of Paper Theories of Expansion in Sulfoaluminate-Type Expansive Cements: Schools of Thought," by M.D. Cohen, Cement and Concrete Research, Vol. 14, No. 4, pp. 603-609.

McMorris, N., Tanesi, J., Livingston, R,A., Ceesay, J., and Amde, A.,September 19-21, 2007, "Quantification of Delayed Ettringite Formation Damage in Laboratory Specimens using the Ultrasonic Quality Factor," The First International Conference on Recent Advances in Concrete Technology, Washington, DC (accepted).

Mehta, P. K., May 2006, "Durability of Concrete – The Zigzag Course of Progress," CANMET, Durability Meeting, Montreal, Canada, SP-234-1, pp. 1-16.

Mehta, P. K., 1969, "Morphology of Calcium Sulphoaluminate Hydrates," Journ. Amer. Ceram. Soc., Vol. 52, No. 9, pp.521-522.

Mehta, P. K., and Moteiro, P. J. M., "Concrete: Structure, Properties, and Materials," Second edition, Prentice Hall, 1993.

Mehta, P.K., 1973 "Mechanism of Expansion Associated with Ettringite Formation," Cement and Concrete Research, Vol. 3, No. 1, pp. 1-6.

Mehta, P. K., 1973 "Effect of Lime on Hydration of Pastes Containing Gypsum and Calcium Aluminates or Calcium Sulfoaluminate," Journ. Amer. Ceram. Soc., Vol. 56, No. 6 pp. 315.

Mehta, P. K. and Hu. F., 1978, "Further Evidence for Expansion of Ettringite by Water Adsorption," Journ. Ameri. Ceramic Soc., Vol. 61, pp. 179-181.

Mielenz, R. C., Maursin, S. L., Hime, W. G., and Jugovic, Z. T., December 1995, "Investigation of Prestressed Concrete Railway Tie Distress," Concrete International, Vol. 17, No.12, pp. 62-68.

Midley, H. G., and Pettifer, K., 1971, "The Microstructure of Hydrated Supersulfated Cement," Cement and Concrete Research, Vol. 1, No. 1, pp. 101.

Miller, F. M., and Tang, F. J., 1996, "The Distribution of Sulfur in Present-Day Clinkers of Variable Sulfur Content," Cement and Concrete Research, Vol. 26, pp.1821-1829.

Mouret, M., Bascoul, A and Escadeillas, G., 1999, "Microstructural Features of Concrete in Relation to Initial Temperature – SEM and ESEM Characterization," Cement and Concrete Research, Vol. 29, pp. 369-375.

Oberholster, R. E., Maree, N., and Brand, J. H. D., 1992, "Cracked Prestressed Concrete Railway sleepers: Alkali-Silicate Reaction or Delayed Ettringite Formation," pp. 739-749, 9th Int. Conf. Alkali-Aggregate Reaction, Vol. II, The Concrete Society, London.

Odler, I., 1980, "Interactions Between Gypsum and the C-S-H Phase Formed in $C_3S$ Hydration," 7th Int. Cong. Chem. Cem, Vol. IV, Editions Septima, Paris, pp. 493-495.

Odler, I., Abdul-Manula, and Zhongya, L., 1987, "Effect of Hydration Temperature on Cement Paste Microstructure," in Microstructural Development During Hydration of Cements, L. J. Strudl and P. W. Brown, Eds., Mat. Res. Soc. Symp. Proc, Vol. 85, pp. 139-144.

Odler, I., and Chen, Yaoxin, 1996, "On the Delayed Expansion of Heat Cured Portland Cement Pastes and Concretes," Cem. Concr. Composites, Vol. 18, pp. 181-185.

Ogawa, K. and Roy, D. M., 1982, "$C_4A_3S$ Hydration, Ettringite Formation, and Its Expansion Mechanism: II. Microstructure Observation of Expansion," Cement and Concrete Research, Vol. 12, No. 4, pp. 577-585.

Ozol, M, A., and Strand, Walter III., June 2002, "Delayed Ettringite Formation at Brewer Stadium, Boone, North Carolina," Cement, Concrete Aggregates, CCAGDP, Vol. 22, No. 1, pp. 24-34.

Oztekin, E., 1984, Cimento Bull, Vol. 21, pp. 3-13.

Pauri, M. and Collepardi, M., 1989, "Thermo-Hygrometrical Stability of Thaumasite and Ettringite," II cement, No.86, pp. 177-184.

Pettifer, K., and Nixon, P. J., 1980, "Alkali Metal Sulfate-A factor Common to Both Alkali Aggregate Reaction and Sulfate Attack on Concrete," Cement and Concrete Research, Vol. 10, pp. 173-181.

Petrov, N., Thibault, M., and Tagnit-Hamou, A., May 2006, "Expansion Due to DEF in Normally-Cured Concrete Heated by Cement Hydration," CANMET, Durability Meeting, Montreal, Canada, SP-234-16, pp. 239-249.

Possetti, V. A., Chiocchil, G. and Paolini, A. E., 1982, "Expansive Properties of the Mixture $C_4AH_{12}.2Cl$. An Hypothesis on the Expansion Mechanism," Cement and Concrete Research, Vol. 12, No. 4, pp. 577-585.

Powers, T. C., Copeland, L. E., Hayes, J. C. and Mann, H. M. 1954, "Permeability of Portland Cement Paste," ACI Journal Proceedings, Vol. 51, No. 3, pp. 267-285.

Ramadan, E., 2000, "Experimental and Theoretical Study of Delayed Ettringite Damage in Concrete," Ph.D. Thesis, University of Maryland, College Park, USA.

Ramadan, E., Amde, A.M. and Livingston, R.A., "Effect of Potassium on Delayed Ettringite Formation" Journal of Materials in Civil Engineering, ASCE (under review).

Rivard, P., Berube, M, A., Ollivier, J, P., and Ballivy, G., 2003, "Alkali Mass Balance During the Accelerated Concrete Prism Test for Alkali-Aggregate Reactivity," Cement and Concrete Research, Vol. 33, pp. 1147-1153.

Ronne, M., and Hammer, T. A., 1999, "Delayed Ettringite Formation (DEF) in Structural Lightweight Aggregate Concrete: Effect of Curing Temperature, Moisture, and Silica Fume Content," Cem. Concrete, and Aggregates, CCAGDP, Vol. 21, No. 2, pp. 202-211.

Rome, M., and Sellevold, E. J., 1994, "LIGTCON.DP2 Material Properties. Report 2.3 Effect of Hydration Generated Temperature-Literature Survey," SINTEF report STF70 A978424. Trondheim. Norway, (in Norwegian).

Sagrera, J. L., May 1972, "Study on the Durability of Sulphate Application of Le Chatelier-Anstett Method to an Ordinary Portland Cement," Cement and Concrete Research, Vol. 2, No. 3, pp. 253-260.

Satava, V. and Veprek, O., 1975, "Thermal Decomposition of Ettringite under Hydrothermal Conditions," Journ. American Cerem. Soc., Vol. 58, No. 7-8, pp. 357-359.

Saul, A. G. A., March 1951, "Principals Underlying the Steam Curing of Concrete at Atmospheric Pressure," Magazine of Concrete Research, Vol. 2, No.6, pp. 127-140.

Schlorholtz, S., and Bergeson, K. L., 1993, "Evaluation of the Chemical Stability Durability of Iowa Fly Ash Concrete," final report, Iowa Department of Transportation project HR-327, ERI project 3295, ISU-ERI Ames 93-411.

Schlorholtz, S., and Amenson, J., 1995, "Evaluation of Microcracking and Chemical Deterioration in Concrete Pavements," final report, Iowa Department of Transportation project HR-358, Engineering Research Institute, Iowa State University.

Schwiete, H. E., Lucwing, V., and Jager, P., 1966, "Investigations in the Systems $3CaO.Al_2O$-$CaSO_4$-$CaO$-$H_2O$," Symposium on Structure of Portland Cement Paste and Concrete," Highway Research Board, Special Report 90, pp. 353.

Scrivener, K. L., 1984, "The Development of Microstructure During the Hydration of Portland Cement," Ph.D. Dissertation, University of London.

Scrivener, K. L., and Damidot, D., and Famy, C., 1999, "Possible Mechanisms of Expansion of Concrete Exposed to Elevated Temperatures During Curing (Also Know as DEF) and Implications for Avoidance of Field Problems," Cement, Concrete, and Aggregates, CCAGDP, Vol. 21, No. 1, pp. 93-101.

Scrivener, K. L., and Pratt, P. L., 1984, "Microstructural Studies of the Hydration of $C_3A$ and $C_4AF$ Independently and in Cement Paste," Br. Ceram. Proc., Vol. 35, pp. 207.

Scrivener, K. L., 1992, "The Effect of Heat Treatment on Inner Product C.S.H," Cement and Concrete Research, Vol. 22, pp. 1224-1226.

Scrivener, K. L., and Taylor, H. F. W., 1993, "Delayed Ettringite Formation: A Microstructural And Microanalytical Study," Adv. Cem. Res., Vol. 5, pp.139.

Seligmann, P. and Greening, N. R., 1964, "Studies of Early Hydration Reactions of Portland Cement by X-Ray Diffraction," Highway Research Record, No. 62.

Shayan, A. and Quick, G. W., 1992, "Microscopic Features of Cracked and Uncracked Concrete Railway Sleepers," ACI Material Journal, Vol. 89, pp. 348-361.

Shayan, A. and Ivanusec, I. 1996, "An Experimental Clarification of the Association of Delayed Ettringite Formation with Alkali Aggregate Reaction," Cem. Concr. Comp., Vol. 18, pp. 161-170.

Shayan, A. and Quick, G., 1989, "Microstructure and Composition of AAR Products in Conventional Standard and New Accelerated Testing," In Proc. Of the 8$^{th}$ Int. Conf. on Alkali-Aggregate Reaction, Kyoto, Japan, pp. 475-482.

Shayan, A., 1995, "Behavior of Precast Prestressed Concrete Railway Sleepers Affected by AAR," Real World Concrete, N. R. Swamy Symposium, pp. 35-56.

Shimada, Y., 2005, "Chemical Path of Ettringite Formation in Heat-Cured Mortar and Its Relationship To Expansion," Ph.D. Thesis, Northwestern University, Evanston, IL, USA.

Siedel, H., Hempel, S. and Hempel, R., 1993, "Secondary Ettringite Formation in Heat Treated Portland Cement Concrete: Influence of Different W/C Ratios and Heat Treatment Temperatures," Cem. Concr. Res. Vol. 23, No. 2, pp. 453-461.

Skalny, J. P. and Locher, F., June 199, "Curing Practices and Internal Sulfate Attack – The European Experience," Cement, Concrete and Aggregates, Vol. 21, No. 1, pp. 59-63.

Skolinskaya, N. N., Krasil' nokov, K. G., Nikitina, L. V., Varlamov, V. P., 1975, "Changes in Crystal Structure of Ettringite on Dehydration II," Cement and Concrete Research, Vol. 5, No. 5, pp. 419-31.

Skolinskaya, N. N., Krasil' nokov, K. G., 1975, "Changes in Crystal Structure of Ettringite on Dehydration I," Cement Concrete Research, Vol. 5, No. 4, pp.381-393.

Stark, J. and Bollmann, K. 1999, "Laboratory and Field Examination of Ettringite Formation in Pavement Concrete,"Ettringite: -The Sometimes Host of Destruction, SP-177, B. Erlin, (ed.), American Concrete Institute, Farmington Hills, MI, pp. 183-198.

Struble, L. J., 1987, "The Influence of Cement Pore Solution on Alkali Silica Reaction," Ph.D. Thesis, Purdue University, U.S.A.

Sylla, H. M., 1988, "Reactionen im Zementstein durch Warmbelehandlung," Beton, Vol. 38, pp. 449-454.

Taylor, H. F. W., 1994, "Delayed Ettringite Formation, Advances in Cement and Concrete," Proceedings, Engineering Foundation Conference, Durham, New Hampshire.

Taylor, H. F. W., 1997, "Cement Chemistry," 2nd Edition, Thomas Telford, Ed.

Tepponen, P. and Eriksson, B. E., 1987, "Damages in Concrete Railroad Sleepers in Finland," Nordic Concr. Res., No. 6, pp. 199-209.

Thaulow, N., Johansen, V. and Hjorth Jacobsen, V., 1996, "What caused Delayed Ettringite Formation?," Ramboll Bulletin No. 60, pp. 8.

Thermo Orion, 2001, "Ion Selective Electrode – Instruction Manual, $Ka^{+}$, $Na^{+}$ and $Ca^{2+}$," pp. 3-13.

Verbeck, G. J. and Foster, C. W., 1950, Proceedings American Soc. Test. Mat., Vol. 50, pp. 1235.

Verbeck, G. J. and Helmuth, R.H., 1968, Proceedings 5th Intl. Conf. Chem. Cem., Tokyo, pp. 1-32.

Vitousova, L., April 1991, "Concrete Sleepers in CSD Tracks," International Symposium on Precast Concrete Sleeper, Madrid pp. 253-264.

Volkwein, A. and Springenschmid, R., Sept. 5, 1981, "Corrosion of Reinforcement in Concrete Bridges at Different Ages due to Carbonation and Chloride Penetration," 2nd Intnl. conf. on durability of Building Materials and Components," 14 – 16, Publ. By NBS, Washington D.C., pp. 119-209.

Wang, S., Ji, S., Lui, and Hu, K., 1986, "Effect of Alkali on Expansion of Sulphoaluminate Cement," J. Chinese Cera. Soc., Vol. 14, No. 3, pp. 285-292.

Way, S., J., Shayan, A., Sept. 1989, "Early Hydration of Portland Cement in Water and Sodium Hydroxide solutions, Compositions of Solutions and Nature of Solid Pastes," Cement and Concrete Research, Vol. 19, No. 5, pp. 759-769.

Wells, J. A., Attiogbe, E. K., and Rizkalla, S. H., 1990, "Deleterious Expansion of Cement Paste Subjected to Wet Dry Cycle," Reprint.

Xie, P. and Beaudoin, J. J., 1992, "Mechanism of Sulfate Expansion II. Validation of Thermodynamic Theory," Cement and Concrete Research, Vol. 25, pp. 845-854.

Yan, P., Peng, J., and Qin, X., 2002, "Behaviour and the Controlling Factor of Delayed Ettringite Formation in Shrinkage-compensating Massive Concrete," Magazine of Concrete Research, Vol. 54, No. 5, pp. 315-320.

Yang, R., and Lawrence, C. D., 1995, "Mortar Expansions due to Delayed Ettringite Formation. Effects of Curing Period and Temperature," Cement and Concrete Research, Vol. 25, pp. 903-910.

Yang, R., Lawrence, C. D., and Sharp, J. H., 1996, "Delayed Ettringite Formation in 4-Year Old Cement Pastes," Cem. Concr. Res., Vol. 26, No. 11, pp. 1649-1659.

Zhang, F., Zhou, Z and Lou, Z., 1980, "Solubility Product and Stability of Ettringite," 7th Intnl. Congress Chem. Cem. Vol. 2, Paris, II/88-II/93.